Palaeoenvironmental and biotic change through the Lower Jurassic in Bulgaria

Autumn Charlotte Pugh

Submitted in accordance with the requirements for the degree of

Doctor of Philosophy

The University of Leeds

Earth Surface Science Institute

School of Earth and Environment

November, 2018

The candidate confirms that the work submitted is his/her own and that appropriate credit has been given where reference has been made to the work of others.

II

Acknowledgements

Many people deserve thanks for the help they have given me during this project. Firstly, thank you to my supervisors Cris Little, Rob Newton, Paul Wignall, Lubomir Metodiev, Ivan Savov and Jim Riding. I would also like to thank external collaborators Emanuela Mattioli, Chris Korte, Lawrence Percival and Chris Vane for giving their time to run my samples.

Completion of my fieldwork in Bulgaria would have been impossible without the dedicated support and assistance of Lubo, Docho and Laki. Thank you all for the encouragement, optimism, rakia and tireless efforts in teaching me Bulgarian.

I would like to express my sincerest gratitude to the technical assistance provided by several people at the University of Leeds, namely Linda Forbes, Harri Wyn Williams, Gary Keech, Andy Connelly and Stephen Reid.

To all of my officemates and fieldtrip companions over the years, thank you for your advice, humour and friendship. In particular thank you to James Witts, Tom Fletcher, Adam Woodhouse, Beth Allen, Andy Mair, Emma James, Luke Faggetter, Carl Spence-Jones, Jed Atkinson, Amicia Lee, Laura Gregory, Michelle Shiers, Tim Cullen, Mike Shotton, Katie Farrell and Will Foster. Special thanks goes to my closest friends Evie Barratt, Lucy Atkinson and Kathy Doyle, whose support and friendship has been invaluable.

Thank you especially to James, whose support has been unwavering. Thank you for everything.

Finally, I would like to thank my family, who have always supported me and encouraged me in everything I have done. With special thanks to my gran, whose thoughtful advice on working hard is with me daily.

Abstract

The early Toarcian was a time of widespread environmental and biotic changes linked to the eruption of the Karoo-Ferrar large igneous province (LIP). Despite the purported global nature of these changes, the majority of the data come from western European sections, with a particular focus on settings in which the early Toarcian Oceanic Anoxic Event (T-OAE) was clearly expressed. This thesis examines a series of Lower Jurassic successions in northwest Bulgaria that were deposited on an open-ocean facing carbonate shelf in the northwest Tethys Ocean. The Bulgarian $\delta^{13}C$ and $\delta^{18}O$ profiles show similar trends through the Lower Jurassic to coeval European sections, suggesting that seawater in the Moesian Basin was recording global palaeoceanographic conditions. The carbon isotope record reveals a broad positive carbon isotope excursion (CIE) of 3 ‰ in $\delta^{13}C_{bel}$ through the early Toarcian, interrupted by a negative CIE of 3.5 ‰ in $\delta^{13}C_{org}$. Rapid warming of seawater temperatures and increased influx of freshwater into the basin through the early Toarcian is indicated in $\delta^{18}O_{bel}$. Such changes are attributed to the eruption of the Karoo-Ferrar LIP, reflected in the Moesian Basin by an enrichment in Mercury (Hg) recorded as a shift in sedimentary Hg/TOC values, synchronous with the negative CIE. A biotic crisis is recorded amongst bivalves in Bulgaria for the first time. Although a significant loss amongst bivalves during the early Toarcian often coincides with the spread of anoxia elsewhere, this link is not clearly seen in Bulgaria. Framboid analysis and a lack of laminated sediments during the early Toarcian indicate oxygen-deficiency as an unlikely driver of the biotic crisis. Rapid warming of seawater temperatures are tentatively suggested as a key driving mechanism in this central Tethyan region.

Table of Contents

List of Tables

List of Figures

Abbreviations

BGS	British Geological Survey
CIE	Carbon isotope excursion
EES	European Epicontinental Seaway
ETME	Early Toarcian Mass Extinction
Hg	Mercury
LIP	Large Igneous Province
Ma	Million years ago
Myr	Million years
Pl-To	Pliensbachian – Toarcian
POC	Percentage of carbon
TC	Total Carbon
T-OAE	Toarcian Oceanic Anoxic Event
TOC	Total Organic Carbon
TIMS	Thermal Ionisation Mass Spectrometer
SOEE	School of Earth and Environment
VPDB	Vienna Pee-Dee Belemnite

Chapter 1 Introduction

1.1 Thesis rationale

Throughout the Phanerozoic, five first order mass extinction events have been identified, as well as number of smaller second order ones (Sepkoski and Raup, 1986; Raup, 1994; Hallam and Wignall, 1997; Bond and Grasby, 2017). Second order events are less well understood, they are often restricted to a specific environment or biogeographic realm and are characterised by much lower extinction rates (Harries and Little, 1999).

Currently there are a wide variety of causal factors and mechanisms invoked to explain mass extinction events and a 'Volcanic Greenhouse Scenario' is often considered for Late Palaeozoic and Mesozoic extinctions (Wignall, 2005). This scenario postulates the eruption of large igneous provinces (LIPs) was the key driving mechanism for many extinctions in Earth history, with volcanic activity leading to a synergistic suite of events including global warming, marine anoxia, and ocean acidification (Pálfy and Smith, 2000; Wignall, 2001; Courtillot and Renne, 2003; Wignall, 2005; Bond and Wignall, 2014).

The early Toarcian (183.8-174.1 Ma), in the Lower Jurassic, is characterised by LIP volcanism in the Karoo-Ferrar province, rapid global warming, significant perturbations in the global carbon cycle, the development of widespread anoxia known as the early Toarcian Oceanic Anoxic Event (T-OAE) and a biotic crisis in the marine realm known as the early Toarcian Mass Extinction (ETME) (e.g. Jenkyns, 1988; Little, 1995; Hallam and Wignall, 1997; Jenkyns and Clayton, 1997; Pálfy and Smith, 2000; Hesselbo et al., 2000; Pálfy et al., 2001; Wignall, 2001; Jenkyns, 2003; Suan et al., 2008; Jenkyns, 2010; Gómez and Goy, 2011; Suan et al., 2015; Vörös et al., 2016).

The ETME is a second-order extinction event, recorded in detail from marine invertebrates of northwest Europe (Hallam, 1986; Hallam, 1987; Little, 1995; Caswell et al., 2009; Danise et al., 2013). There are relatively few studies on the ETME outside of Europe, with studies from Argentina (Aberhan and Fürsich, 1996; Aberhan and Fürsich, 2000; Aberhan and Baumiller, 2003), North America (Caruthers et al., 2014; Martindale and Aberhan, 2017) and Siberia (Zakharov et al., 2006) being amongst the few examples.

There is no consensus on the prominent kill mechanisms for the ETME although global warming (Gómez et al., 2008; Gómez and Arias, 2010; Gómez

and Goy, 2011) and anoxia (e.g. Aberhan and Baumiller, 2003; Wignall et al., 2005; Danise et al., 2015) are often accorded a role. Much of the ongoing debate surrounding the potential drivers of the ETME is linked to the development, or lack of, anoxia in epicontinental basins. Many of the studies from northern Europe, Argentina and Chile link a biotic crisis to the onset of oxygen depleted organic rich, laminated mudstones (Aberhan and Fürsich, 2000; Aberhan and Baumiller, 2003; Wignall et al., 2005; Martindale and Aberhan, 2017). However, studies of marine invertebrates from southern Europe, recognise biotic crises, even though organic-rich lithologies are often thin, condensed or even absent, and average total organic carbon (TOC) values are lower. This is the case in the Tethys from sections in Portugal (Suan et al., 2008), Spain (Rodríguez-Tovar and Reolid, 2013; Rodríguez-Tovar et al., 2017) and Morocco (Bodin et al., 2010; Brame et al., 2018). Gómez and Goy (2011) have suggested that temperature played a more significant role in the early Toarcian mass extinction biotic crises, from settings in which evidence for anoxia is not apparent. A more detailed palaeogeographic understanding of faunal and environmental change is required to better understand this event in Tethyan realms. It is particularly important to focus on basins in which anoxia is not clearly developed to evaluate a combination of biotic and palaeoenvironmental change to provide further insights into the main driving mechanisms behind this biotic crisis.

Prior to the early Toarcian interval (during the Sinemurian and Pliensbachian) palaeoenvironmental and biotic changes have received significantly less attention. Recent studies have started to highlight significant and global palaeoenvironmental change during this time, including perturbations in the carbon cycle and fluctuating seawater temperatures (Korte and Hesselbo, 2011). It is important to understand biotic and environmental change through the Lower Jurassic to provide a longer term context of changes leading up to the ETME.

The early Toarcian has been intensively studied in NW Europe with detailed and extensive litho-, bio- and chemostratigraphical records from this part of the Tethys Ocean, where the oceanic anoxia is clearly expressed. While new studies continue to look at trends in TOC and redox-sensitive elements to re-confirm scenarios of widespread ocean deoxygenation and increased weathering during the T-OAE (Bougeault et al., 2017; Thibault et al., 2017; Caswell and Frid, 2017; Correia et al., 2017; Them et al., 2017; Suan et al., 2018; Fonseca et al., 2018; Izumi et al., 2018; Fantasia et al., 2018a,b; Xu et al., 2018a; Ruebsam et al., 2018), fewer studies focus on sections where the

manifestation of oceanic anoxia is weak (Miguez-Salas et al., 2017; Han et al., 2018; Rosales et al., 2018). Additionally, many studies focus on the OAE or extinction event independently, rather than simultaneously. It is important to study both oceanic and extinction events from the same setting to understand the causal mechanisms for the extinction. The documentation of the biotic change and palaeoenvironmental conditions in areas away from the interiors of the European Epicontinental Seaway (EES), such as from a shallower marine carbonate setting close to the open ocean, can shed further light on the spatial nature of changes during this time, contributing to a more complete understanding across the epicontinental Tethys and global implications.

Although the ETME has been documented globally, there remains a rather limited dataset of biotic changes during this time, particularly when compared to other mass extinction events through the Phanerozoic. Although the extinction itself is not on the same order as 'the big five' mass extinction events, the characteristic situation of global warming, a prominent negative carbon isotope excursion and mass extinction are clearly recorded. Therefore, the study of the environmental and biotic response (both locally and globally) to a carbon-forced greenhouse warming event can also help elucidate the mechanisms at play in the modern day crisis, both biological and environmental, brought about by anthropogenic climate change (Payne and Clapham, 2012). The injection of large amounts of CO_2 into the atmosphere during the early Toarcian is potentially analogous to modern day CO_2 build up, though the rate of CO_2 input in the modern day is at least 400 times faster (Saunders and Reichow, 2009). Several environmental conditions observed during the early Toarcian have already begun to manifest in the oceans today, including increased sea surface temperature and Oxygen Minimum Zones (OMZ's) (Stramma et al., 2008; Hoegh-Guldberg, 2012; Doney et al., 2012). Hence, events in the early Toarcian can play as analogues for modern day carbon release scenarios.

1.2 Aims and objectives

This thesis aims to examine a series of Lower Jurassic successions in the Balkan Mountains of Bulgaria, with particular focus on the Pliensbachian-Toarcian sedimentary record. These sedimentary successions were deposited on an open-ocean facing carbonate shelf in the Moesian Basin, located in the eastern epicontinental Tethys. The key aim of this thesis is to assess the timing and nature of palaeoenvironmental and climatic changes in Moesian Basin and

how they link to biotic change recorded in marine benthos through the Lower Jurassic.

A suite of geochemical and sedimentological techniques can be utilised to assess palaeoenvironmental change. Inorganic and organic carbon isotopes provide an insight into the carbon cycle and oxygen isotope records can be used as a proxy for past seawater temperatures. Mercury (Hg) is used as a potential tracer for volcanism in sedimentary successions. Framboid analysis assesses the changing redox regimes within the basin, size distribution of pyrite framboid populations is used as a paleoproxy to indicate the presence of euxinic, dysoxic or oxic conditions. This is used in conjunction with sedimentological evidence (e.g. evidence for bioturbation or lamination) and biotic evidence (e.g. abundance of opportunistic taxa adapted to low-oxygen conditions) as further indicators of oxygen levels within the basin.

This thesis aims to provide a detailed record of bivalve occurrences through the Sinemurian-Toarcian interval. This record will allow the distribution of bivalves within the basin to be assessed and evaluation of any extinction intervals present, which might be a part of the early Toarcian mass extinction event and can add significant new data to the extinction record globally. The bivalve record can then be assessed alongside palaeoenvironmental changes to evaluate potential causative mechanisms for the biotic crisis.

To understand timings of the extinction and palaeoenvironmental perturbations, the published ammonite biostratigraphy is integrated with new calcareous nannofossil biostratigraphy, and chemostratigraphy using strontium and carbon isotopes, to provide a more robust age model for Toarcian sections in the Moesian Basin. This is then used to understand stratigraphic gaps and condensation in the Toarcian record.

This thesis aims to answer the following questions:

1. Can additional biostratigraphic and chemostratigraphic work help improve the age control of any Lower Jurassic successions in Bulgaria?
2. What environmental perturbations in the carbon cycle and changes in seawater palaeotemperature are recorded in the Lower Jurassic of the Moesian Basin?
3. Is the T-OAE expressed in the Moesian Basin? How does the expression of the T-OAE contribute to understanding the spatiotemporal nature and intensity of anoxia across the EES?

4. Is there evidence for Karoo-Ferrar volcanic activity in the Moesian Basin?
5. Is there evidence for the ETME in the Moesian Basin? If so, what do the linked records of environmental, carbon cycle and faunal change, and volcanic activity tell us about the causal mechanisms for the extinction?

1.3 Thesis outline

To answer the proposed research questions, this thesis is divided into seven chapters. Chapter 1 highlights the current understanding of the ETME and T-OAE and highlights current gaps in the field. It also reviews past studies of the Lower Jurassic in Bulgaria. Chapter 2 provides a detailed review of the methods and materials used throughout this project. Chapter 3 introduces the stratigraphic sections used in this study, with an overview of lithological changes during the Lower Jurassic. Additional biostratigraphic and chemostratigraphic ages are provided for some sections to improve dating. Chapter 4 presents long-term changes in the carbon cycle and uses oxygen isotopes as a palaeoproxy for temperature changes through the upper Sinemurian-Toarcian of the Lower Jurassic, using diagenetically screened belemnite calcite. Chapter 5 assesses the presence of the T-OAE in Bulgarian records, documenting changes in organic carbon isotopes, total organic isotopes and mercury enrichments, and evaluates if anoxia developed in the Moesian Basin. These changes are then discussed relative to global records, particularly across Europe, to highlight aspects of spatial variability. Chapter 6 presents a detailed study of bivalve occurrences through the Lower Jurassic, to provide evidence of the early Toarcian Mass Extinction. This chapter then uses data from previous chapters to scrutinise possible causative mechanisms for the extinction. Finally, Chapter 7 provides a summary of the major findings of this work and recommendations are then made for the direction of future studies in Bulgaria.

1.4 The Early Jurassic

The Early Jurassic period (201.4 - 174.1 Ma) (Figure 1.1), is marked by multiple periods of global climatic and palaeoceanographic change, perturbed global geochemical cycles and biotic crisis. These events are documented throughout the Early Jurassic, with the most severe and biotically damaging changes recorded nearer the end of the Early Jurassic, within the early Toarcian. At this time a period of volcanic-driven global warming led to the development of the early Toarcian Oceanic Anoxic Event (T-OAE) and the early Toarcian Mass Extinction (ETME).

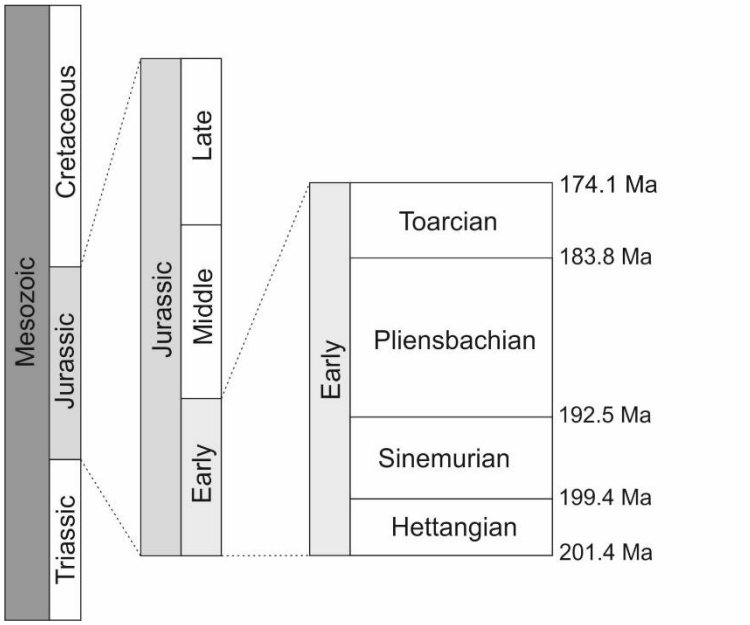

Figure 1.1 The Early Jurassic Timescale with basal-age for each stage (stage boundary ages after Ruhl et al., 2016).

During the Early Jurassic the Earth's landmasses, that comprised the super-continent Pangaea, were undergoing a large scale tectonic plate reorganisation (Figure 1.2). Rifting phases, that initiated in the Late Triassic, continued through the Early Jurassic and resulted in the formation of the two large continental landmasses: Laurasia and Gondwana (Golonka and Ford, 2000; Golonka, 2007). Associated with this rifting, was the eruption of the Karroo-Ferrar Large Igneous Province (LIP) in southern Gondwana (Jourdan et al., 2008) (Figure 1.2).The oceans surrounding these supercontinental landmasses comprised the Panthalassa Ocean and the Tethys Ocean. The large landmasses were often surrounded by shallow seas, including the broad epicontinental shelf-sea with

island land masses that opened up in the north western (NW) Tethys Ocean (Thierry, 2000). The epicontinental sea in the NW Tethys is often termed the European Epicontinental Seas (EES) or epicontinental Tethys and comprises most of present day Europe The landmasses were connected by narrow seaways that provided connections between the oceans during the Early Jurassic. To the west of the EES, the Hispanic, connected the Panthalassic ocean to the western EES. The Hispanic corridor is argued to have opened during the late Pliensbachian (*margaritatus* Zone), which allowed Panthalassan bivalves to migrate into the north-west EES (Aberhan, 2001).

The EES is often split into palaeobiogeographic realms, with the Boreal realm occurring to the north and the Tethyan realm to the south (Figure 1.2). The southern edge of the Tethyan realm can also be called the Mediterranean realm. Most faunal realms, also called provinces, do not develop until later in the Early Jurassic during the Pliensbachian, which is recognised as a time of marked provincialism in the marine realms, notably between the Boreal and Mediterranean realms (Neumayr, 1883; Uhlig, 1911; Westermann, 2000; Dommergues et al., 2009; Damborenea, 2017). There is slight variability of transition between biotic realms depending on which groups are being studied (Liu, 1995; Dommergues et al., 2008).

In the case of ammonites, the two main realms (Boreal and Tethyan) were originally described by Neumayr (1885) and Arkell (1956). Recognition of other ammonite realms outside the EES (Dommergues et al., 2009) have also been reported globally, from North America (Imlay, 1965) and New Zealand (Marwick, 1953; Stevens, 1967). In the case of bivalves, the first attempt to identify paleobiogeographic units based on bivalve distributions through the Jurassic was made by Hallam, (1977). A recent study by Damborenea (2017), builds on the work of Liu (1995) and Liu et al. (1998) to give a worldwide synthesis of the global biogeographic patterns of bivalves from the Early to Late Jurassic. Three first order realms are recognised through the Lower Jurassic: Boreal, Tethyan and Austral realms, characterised by the degree of endemism, relative diversity and palaeobiogeographic affinities of bivalve genera. In the EES, transitional zones are recorded between the Boreal and Tethyan realms Liu, (1995). Despite a more comprehensive understanding of the global distribution of bivalves through the Lower Jurassic, the eastern edge of the EES remains poorly understood. Patterns of Lower Jurassic bivalve distributions provide important insight into changing palaeogeography during this time.

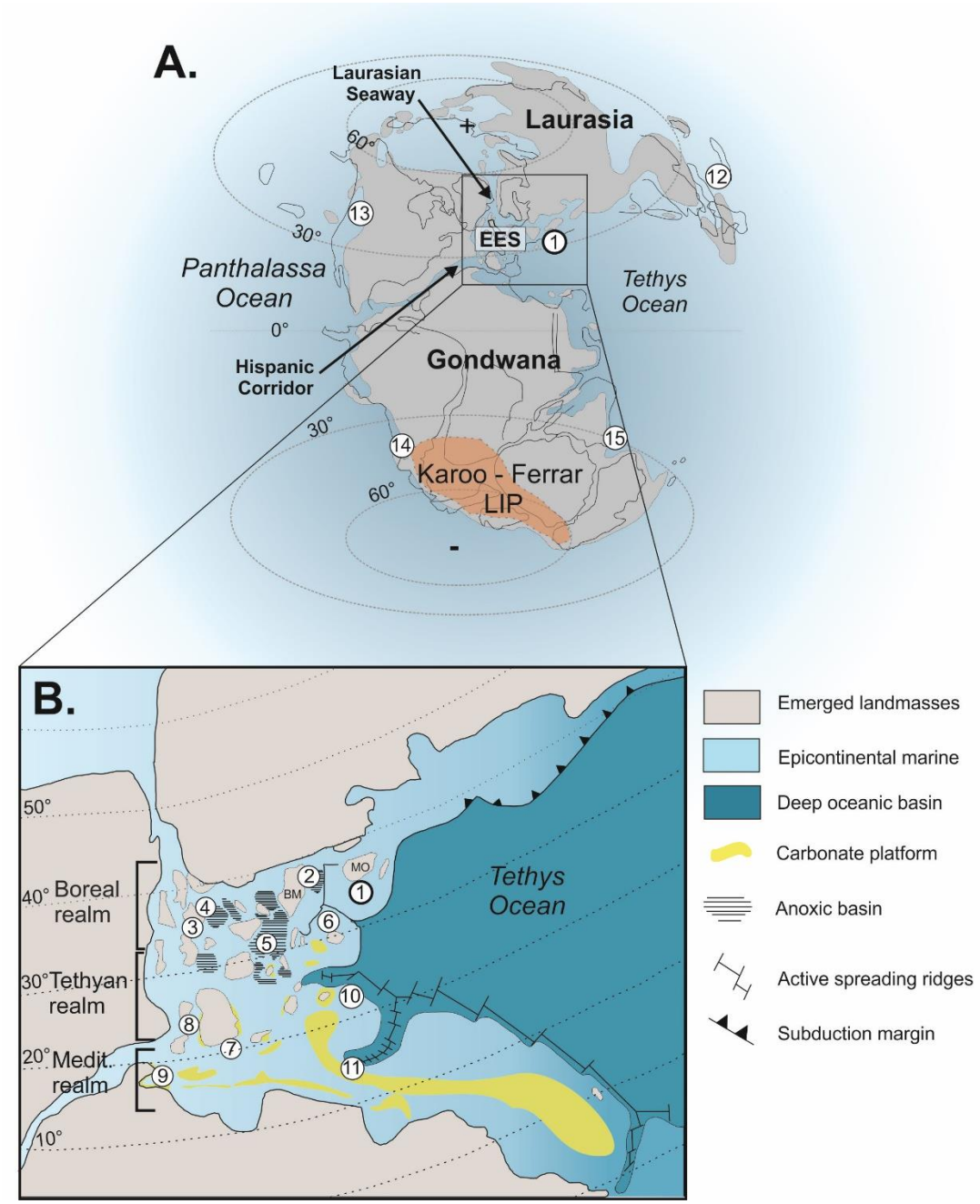

Figure 1.2 Palaeogeography and location maps. A. Early Jurassic global palaeogeography (~180 Ma), modified after Dera et al. (2009) and Suan et al. (2018). The Karoo-Ferrar LIP is shown in orange. B. A more detailed map showing the European Epicontinental Seas (EES). Location of the Moesian Basin (bold circle) and other areas discussed in the text with regard to the early Toarcian (Lower Jurassic) palaeogeography. Map modified. Localities: 1- Moesian Basin (Bulgaria, this study), 2- Carpathians (northwest Slovakia), 3- Mochras borehole (Cardigan Bay, Wales, UK), 4- Cleveland Basin (Yorkshire Coast, UK), 5- Paris Basin (France) 6- Mecsek Basin (Hungary), 7- Iberian Margin (south Spain), 8- Lusitanian Basin (Portugal), 9- Middle Atlas (Morocco), 10- Umbria-Marche Basin (Italy), 11- Pindos Margin (Greece), 12- Sakuraguchi (Japan), 13- Western Canada Sedimentary Basin (Alberta, Canada) 14- Neuquén Basin (Argentina), 15- Tethys Himalaya (south Tibet). Medit.=Mediterranean. BM=Bohemian Massif. Mo=Moesian Platform.

1.4.1 Hettangian

The Hettangian represents the first stage of the Early Jurassic Period (Figure 1.1) and its base is defined by the first occurrence of the ammonite *Plisoceras spelae* (e.g. Hillebrandt et al., 2013). During this period the world's biotas were recovering from the end-Triassic mass extinction, which had resulted in the loss of 24.3% of marine families (Hallam and Wignall, 1997). This extinction is thought to have been the result of acidification, anoxia, sea-level changes and rapid global warming caused by the impacts of the magmatism at the Central Atlantic Magmatic Province (CAMP) (e.g. Hallam, 1960; Benton, 1995; Hallam and Wignall, 1999; Pálfy et al., 2001; Wignall, 2001; Jenkyns et al., 2002; Greene et al., 2012). The end-Triassic extinction event severely affected ammonoid populations, consequently allowing for the successful diversification of ammonites through the Jurassic (Hallam and Wignall, 1997). The resulting abundance of ammonites, with fast turn-over rates allowed for globally correlated biostratigraphic schemes to be developed for the Jurassic (Page, 2003).

1.4.2 Sinemurian

The Sinemurian represents the second stage of the Early Jurassic period that spans from 199.4 Ma to 192.5 Ma (Figure 1.1). The Global Stratotype Section (GSSP), defining the base of the Sinemurian is found in Somerset, southwest UK (Bloos et al., 2002). The Sinemurian as identified through the first appearance of the genera *Vermiceras* and Metophioceras (Bloos et al., 2002). Throughout Europe a stratigraphical gap is often present at the Hettangian and Sinemurian boundary (Bloos et al., 2002). Throughout the Sinemurian the EES covered most of Europe and a global transgression is recorded during the early Sinemurian (Hallam, 2001). This study covers the later stage of the Sinemurian, particularly towards the Sinemurian-Pliensbachian boundary.

The Sinemurian–Pliensbachian boundary event (SPBE) is marked by a clear negative shift of around 2–4 ‰ in the carbon-isotope composition ($\delta^{13}C$) of belemnite calcite, bulk shallow-water carbonate, and organic matter, with most negative values reached at the Sinemurian-Pliensbachian boundary (Jenkyns et al., 2002; Korte and Hesselbo, 2011; Franceschi et al., 2014; Peti et al., 2017). Although commonly recognised in the EES, the commonality between the terrestrial and marine records can be used to infer shifts of global significance (e.g. Koch et al., 1992; Gröcke et al., 1999; Hesselbo et al., 2000a; Hesselbo et

al., 2007) and represents a perturbation of the global exogenic carbon cycle (Korte and Hesselbo, 2011).

The cause of the CIE has been suggested to have resulted from the release of isotopically depleted carbon into the ocean–atmosphere system, from either a volcanic contribution, as proposed by Ruhl et al. (2016). Alternatively, the release of methane has been proposed, similarly to the negative carbon isotope excursion in the Toarcian (Hesselbo et al., 2000a; Hesselbo et al., 2007; Hesselbo and Pienkowski, 2011; Suan et al., 2011).

Alongside changes in the carbon cycle, a weak positive oxygen isotope shift is recorded from the epicontinental Tethys in the Cleveland Basin (Yorkshire, UK) and the Lusitanian Basin (Portugal) (Hesselbo et al., 2000b; Duarte et al., 2014), albeit these shifts in oxygen isotopes are not globally recognised (Jenkyns et al., 2002; Rosales et al., 2004). It has been argued that the trend towards heavier $\delta^{18}O$ values during the SPBE recorded from the Yorkshire Coast is likely of local significance, associated with transgressive sea-level, caused as a result of bottom water cooling during a distinct increase in atmospheric CO_2 (Korte and Hesselbo, 2011).

1.4.3 Pliensbachian

Biotic records for the Pliensbachian suggest ecological systems during this time were relatively stable. With respect to bivalve diversities, spatial and temporal distribution of bivalve taxa in multiple basins through the Pliensbachian stage, including the Lusitanian Basin (Portugal) and the Balkan Mountains in Serbia, are thought to be representative of high bivalve diversities across the European province during this time (Radulović, 2013; Paredes, 2014).

Geochemical records from the Pliensbachian show periods of palaeoclimatic change with discrete disturbances in the global biochemical cycles. The early/late Pliensbachian boundary *(ibex*/d*avoei* Zone) is characterised as a warming interval, with relatively humid conditions and a short-lived minor positive $\delta^{13}C$ perturbation (). Studies focussed in the Boreal realm, such as the Paris Basin (France) and Mochras (Cardigan Bay, UK), record a negative CIE around the *davoei* Zone in $\delta^{13}C_{carb}$ and $\delta^{13}C_{org}$ with an amplitude of ~1-2 ‰ (van de Schootbrugge et al., 2005; Peti et al., 2017).

The end of the Pliensbachian is also marked by significant positive and negative shifts in both carbon and oxygen isotopes, termed the ‘late Pliensbachian Event’ (LBE) (). A positive carbon isotope excursion recording a ~2 ‰ shift, within the late Pliensbachian m*argaritatus* Zone, is recorded in biogenic carbonates,

marine and terrestrial organic matter and in fossil wood, arguing for a global perturbation of the carbon cycle (Jenkyns and Clayton, 1986; van de Schootbrugge et al., 2005; Suan et al., 2010; Korte and Hesselbo, 2011; Silva et al., 2011; Silva and Duarte, 2015).The duration of the negative CIE has an astrochronologically defined duration of ~ 0.6 Myr (Ruhl et al., 2016). The positive CIE is contemporaneous with the deposition of organic-rich sediments, termed Organic Matter Preservation Intervals (OMPI) (Silva et al., 2011). These organic-rich facies were deposited under fluctuating dysoxic, anoxic and occasionally euxinic conditions (Silva and Duarte, 2015). In the Lusitanian Basin (Portugal), such intervals coincide with the formation of black shale (Silva et al., 2011). These basin-wide black shales, corresponding to widespread mucilage and microbial outbreaks, were driven by extreme climate warming coupled with high oceanic productivity and intermittently stratified epeiric seas (Silva et al., 2015). The positive CIE recorded during the late Pliensbachian (*margaritatus* Zone) is commonly attributed to the widespread preservation of organic matter, leading to enhanced carbon burial, under these low-oxygen conditions (Hesselbo and Jenkyns, 1995; Suan et al., 2010; Korte and Hesselbo, 2011; Silva et al., 2011; Silva and Duarte, 2015).

The $\delta^{18}O$ records for the late Pliensbachian event are characterised by ~2 ‰ positive shift, coinciding with the changes in the $\delta^{13}C$ record. These $\delta^{18}O$ data provide evidence for a cooling event, and records mainly come from the European realm and are documented in belemnite rostra (Rosales et al., 2004; Dera et al., 2009; Korte and Hesselbo, 2011; Martinez and Dera, 2015), as well as in brachiopod and bivalve shells (Suan et al., 2010; Korte and Hesselbo, 2011). The ~2 ‰ amplitude of the change in oxygen isotope values is equivalent to a seawater temperature change of ~8°C, if this variation is attributed to temperature alone, marginally less if continental ice is postulated (Dera et al., 2009). Evidence for significant global cooling during the late Pliensbachian has come from the occurrence of glendonites (predominantly cold-water calcite pseudomorphs) found in Serbia and ice rafted debris (Kaplan, 1978; Price, 1999; Rogov and Zakharov, 2010; Bougeault et al., 2017). However, the presence of continental ice sheets during this time and associated glacioeustatic effects are still debated (Dera et al., 2007).

Following the late Pliensbachian positive CIE in the *margaritatus* Zone, a minor negative excursion in $\delta^{13}C$ is recorded in the subsequent *spinatum* Zone, which has been suggested to correspond with negative CIE records at the Pl-To boundary (Rosales et al., 2005; Korte and Hesselbo, 2011; Martinez and Dera, 2015; Silva and Duarte, 2015; Peti et al., 2017).

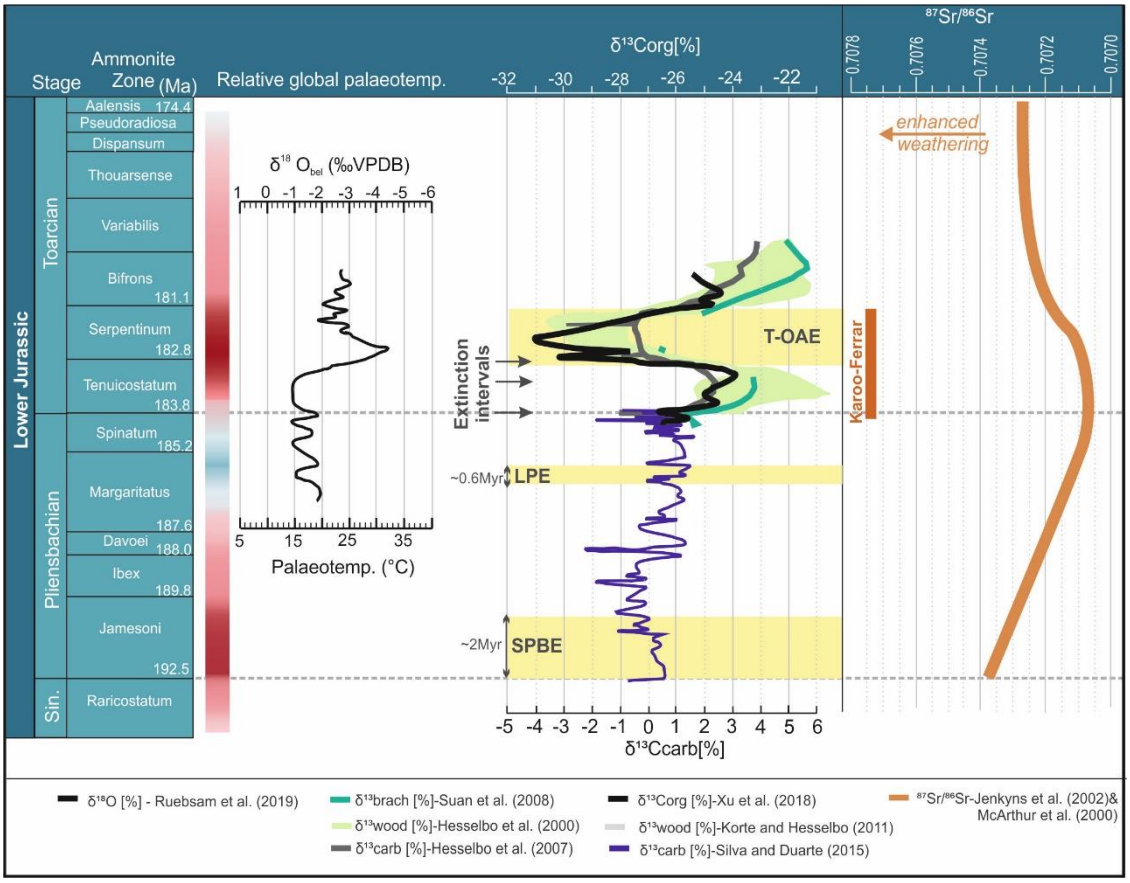

Figure 1.3 Compilation of generalised trends in carbon isotopes and strontium isotopes, relative global palaeotemperatures, major biotic or palaeoenvironmental events recorded during the Lower Jurassic Series from the upper Sinemurian, to the Toarcian. Ammonite Zones are given under the NW Europe biostratigraphy based on Page, (2003). Absolute ages based on Kent and Olsen (2008); Schaltegger et al. (2008); Suan et al. (2008); Ruhl et al. (2010); Schoene et al. (2010), Guex et al. (2012a, 2012b), Blackburn et al. (2013), Boulila et al. (2014), Huang and Hesselbo (2014), Hüsing et al. (2014); Ruebsam et al. (2014, 2015); Sell et al. (2014). Radiometric, astrochronological or biostratigraphical uncertainty for absolute ages are reported in Ruhl et al. (2016). The Sr isotope ($^{87}Sr/^{86}Sr$) trend is derived from McArthur et al. (2000) and Jenkyns et al. (2002). The carbon isotope trends are shown for the upper Sinemurian to middle Toarcian using only European datasets. The relative palaeotemperatures are derived from the oxygen isotope records from Ruebsam et al. (2019). SPBE: Sinemurian-Pliensbachian Boundary Event; LPE: late Pliensbachian event; T-OAE: early Toarcian Oceanic Anoxic Event. The extinction interval coincides with the ETME (early Toarcian mass extinction) with black arrows highlighting the extinction pulses (e.g. Caswell et al., 2009).

1.4.4 Toarcian

The Lower Jurassic Toarcian stage is an important part of Mesozoic history, seeing a multitude of integrated and complex changes in atmospheric, oceanographic and biotic systems. The onset of the Karoo-Ferrar large Igneous Province (LIP) caused a subsequent cascade (Figure 1.4) of environmental and biotic perturbations (Pálfy and Smith, 2000; Cohen and Coe, 2007; Dera et al., 2010; Bond and Wignall, 2014; Burgess et al., 2015).

1.4.4.1 LIP volcanism

The Karoo-Ferrar LIP is a flood basalt province that was situated in southern Gondwana (Figure 1.2) and arguably records one of the largest continental flood basalt outpourings of the Phanerozoic (Courtillot and Renne, 2003). Despite vastly improved radio-isotopic dating, the precise timing of the emplacement of Karoo-Ferrar is difficult, due to uncertainties associated with radiometric dating and poor bio- and chemostratigraphic control on strata interbedded with the volcanic deposits (e.g. Sell et al., 2014; Burgess et al., 2015). Recently, a combined study using bio- (ammonite, foraminiferan), chemo- (carbon-isotope) and magnetostratigraphy to construct a framework for the entire Toarcian Stage has successfully correlated the major eruption phase of the Karoo-Ferrar lavas with climatic and environmental perturbations occurring at both the Pliensbachian-Toarcian boundary and the early Toarcian T-OAE interval in the northern Boreal realm (Xu et al., 2018b).

Mercury (Hg) concentrations have recently been used as a global-scale proxy for increased volcanic activity in the early Toarcian (Percival et al., 2015). This study uses mercury/TOC ratios as an indicator of enhanced atmospheric Hg availability, sourced uniquely from volcanism. Other studies have suggested the use of Hg- chemostratigraphy as an efficient tool for tracing distal volcanism and LIP activity during major palaeoenvironmental perturbations (Sanei et al., 2012; Sial et al., 2013; Blum et al., 2014; Grasby et al., 2016; Font et al., 2016; Thibodeau et al., 2016; Percival et al., 2017; Jones et al., 2017; Gong et al., 2017; Them et al., 2019).

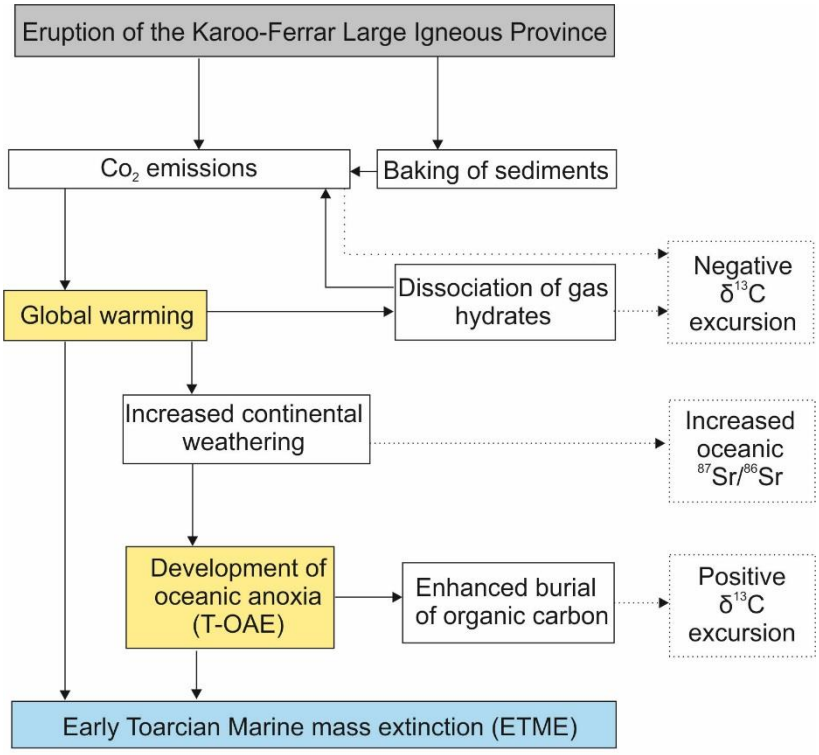

Figure 1.4 Chain of cause and effect for Toarcian environmental change including the T-OAE and ETME. Yellow boxes – proposed kill mechanisms for the ETME. Modified after Wignall (2001, 2011, 2015) and Bond and Wignall, (2014).

1.4.4.2 Warming

The Early Jurassic is characterised by greenhouse conditions with severe global warming recorded through the early Toarcian. The main line of evidence for rapid global warming through the early Toarcian is through a shift to negative $\delta^{18}O$ values. Oxygen isotopes can be used as a proxy for palaeotemperature record as the oxygen isotope compositions of calcite shells show temperature dependant fractionation (Urey et al., 1951). Oxygen isotopes are often used to indicate past seawater temperatures as biogenic calcite precipitated from warmer oceans is enriched in $\delta^{16}O$ whilst in cooler oceans are depleted in $\delta^{16}O$ (Veizer et al., 1999). Changes in the oxygen isotopic composition of calcite shells can also reflect changes in seawater $\delta^{18}O$, pH and salinity (e.g. Veizer et al., 1999).

The occurrence of important variations in the $\delta^{18}O$ values, and hence in the palaeotemperature of the oceans during the latest Pliensbachian– early Toarcian, has been documented by many authors in several parts of western Europe (Chandler et al., 1992; Saelen et al., 1996; McArthur et al., 2000; Röhl

et al., 2001; Schmid-Röhl et al., 2002; Jenkyns, 2003; Rosales et al., 2004; Gómez et al., 2008; Mattioli et al., 2008; Dera et al., 2009; Gómez and Arias, 2010; Joral et al., 2011; Dera et al., 2011), eastern Europe (Metodiev and Koleva-Rekalova, 2008), north Siberia and the Arctic Region (Zakharov et al., 2006). The first step of progressive seawater warming, which can be observed in all the studied European sections, started at the early Toarcian t*enuicostatum* Zone, with a significant shift to negative $\delta^{18}O$ in the f*alciferum* Zone (Korte et al., 2015). The $\delta^{18}O$ records show a close correlation in the evolution of seawater palaeotemperature across Europe, with a global temperature rise of ~5–8 °C (Chandler et al., 1992; Bailey et al., 2003; Rosales et al., 2004; McElwain et al., 2005; Gómez et al., 2008; Joral et al., 2011; Dera et al., 2011).

At the end of the Toarcian, at the Toarcian-Aalenian boundary, a positive $\delta^{18}O$ shift of ~2.5 ‰ in biogenic calcite has been recorded from European sections including Portugal, Germany and Scotland (Korte et al., 2015). This perturbation has been suggested to reflect a cooling of seawater temperatures, of up to 10 °C over a period of about 0.5 Myr (Korte et al., 2015).

1.4.4.3 Increased hydrological cycle

Global warming during the early Toarcian led to an increased hydrological cycle and subsequently increased continental weathering. Several independent parameters support the notion of increased continental weathering and run-off from the late *tenuicostatum* Zone to mid e*xaratum* Zone. One is an abrupt rise in osmium-isotope ratios ($^{187}Os/^{188}Os$) (Cohen et al., 2004a; Percival et al., 2016). Another is the gradual rise in the strontium-isotope ratios ($^{87}Sr/^{86}Sr$) recorded in belemnite calcite (Jones et al., 1994a; McArthur et al., 2000; Jones and Jenkyns 2001). Both of these geochemical tracers indicate enhanced flux into the oceans of radiogenic isotopes derived from continental crustal rocks. This effect is in accord with the assumption that the $\delta^{18}O$ values of belemnites could have been affected by freshwater input, as suggested before for this interval of time (Jenkyns, 1988; Saelen et al., 1996; Bjerrum et al., 2001). Jenkyns (1999) recorded an accelerated hydrological cycle during the early Toarcian, with increased continental weathering and flux of nutrients to the oceans and intensified wind-driven upwelling, together driving increased marine organic productivity and carbon burial.

The abrupt shift to more radiogenic values during the early Toarcian means that the well-defined $^{87}Sr/^{86}Sr$ curve through the Lower Jurassic can be used as a chemostratigraphic tool for Strontium Isotope Stratigraphy (SIS) (McArthur et

al., 2000). The Sr of marine $^{87}Sr/^{86}Sr$ rose and fell repeatedly during the Phanerozoic (Veizer and Compston, 1974). The $^{87}Sr/^{86}Sr$ profile of these fluctuations is since improved and is now relatively well-established, particularly for the Lower Jurassic (Jones et al., 1994b; McArthur et al., 2000).

Strontium is a radiogenic isotope that is part of the Rubidium-Strontium (Rb-Sr) system. Rb and Sr are trace elements in the Earth and ^{87}Rb decays to ^{87}Sr over time. Rb is an incompatible element, which results in it being strongly enriched in the continental crust and depleted in the mantle and oceanic crust. Therefore, the contrasting Sr isotope fluxes that comprise the $^{87}Sr/^{86}Sr$ profile for the Early Jurassic, result as a consequence from the extraction of continental crust from the primitive mantle. This crust extraction and the old nature of resulted in the development of radiogenic $^{87}Sr/^{86}Sr$ reservoir (Jones and Jenkyns, 2001).

Variation of seawater $^{87}Sr/^{86}Sr$ as a function of geological time is widely applied to date and to correlate stratigraphic horizons between sedimentary sections (McArthur et al., 2000; McArthur et al., 2016). Modern seawater $^{87}Sr/^{86}Sr$ is primarily determined by competing fluxes from continental weathering via river runoff (high $^{87}Sr/^{86}Sr$ values) and seafloor hydrothermal vents, after seawater leaching of mid-ocean ridge basalts (with low $^{87}Sr/^{86}Sr$ values of ~0.703 (Palmer and Edmond, 1989; Vance et al., 2009).

To use $^{87}Sr/^{86}Sr$ as a chemostratigraphic tool, some assumptions have to be made. One assumption is the mixing time of the oceans with respect to Sr is significantly shorter (1 Kyr) compared to its residence time (~3 Myr) (Palmer and Edmond, 1989; Pearce et al., 2015). This means that oceans are thoroughly mixed and homogeneous with respect to $^{87}Sr/^{86}Sr$ on time scales that are short relative to the rates of input and output of Sr. Another assumption is that the primary seawater isotopic signal is well-preserved in the diagenetically least-altered marine carbonate, providing the true $^{87}Sr/^{86}Sr$ values of the coeval ocean (McArthur et al., 2000).

1.4.4.4 The Early Toarcian Oceanic Anoxic Event (T-OAE)

The development or organic-rich 'black shales'

The deposition of organic-rich laminated mudrocks is a well-known feature of sedimentological records during the early Toarcian. These particular mudrocks are often referred to as black shales. Black shales are defined as 'a black/dark grey mudstone rich in organic carbon (>5 wt%) generally formed in anoxic marine bottom waters' (Kearey, 2001). For the early Toarcian, authors have

variable definitions on what constitutes a black shale, with some views that the term has been over-used and stretched (McArthur et al., 2008). Authors have used the term black shale to record sediments with <2 wt% TOC (Jenkyns, 1988), whereas Neuendorf (2005) defines a black shale as 'a shale interval on the basis of sediment lamination' rather than a TOC content higher than 5 wt%.

These organic rich (i.e. black) shale facies are particularly abundant and widespread in the European Boreal realm and classic examples include the Posidonia shales of southern Germany, the Schistes Cartons of southern France and the Jet Rock of the Yorkshire Coast (Röhl et al., 2001; Suan et al., 2013). The deposition of this facies is often associated with periods of transgressive sea-level, such is the case with the depositions of the Jet Rock (Yorkshire Coast, UK) (Jenkyns, 1999). The TOC content is particularly high within the north-west European black shales with values of up to 14 wt% (Röhl et al., 2001).

However, there are many localities where these organic-rich lithologies are often thinner, condensed or even absent, and associated with lower TOC values. This is seen in: the southern Tethys, from sections in Portugal (Suan et al., 2008) and Spain (Rodríguez-Tovar and Uchmann, 2010; Rodríguez-Tovar and Reolid, 2013); Italy (Sabatino, 2013); the northern margin of Gondwana in Oman (Immenhauser et al., 1998), Morocco (Bodin et al., 2016; Brame et al., 2018) and Algeria (Reolid et al., 2012; Reolid et al., 2014) and areas of the Panthalassic Ocean in Canada (Caruthers et al., 2011) and Japan (Gröcke et al., 2011).

Oceanic anoxia

Development of these organic-rich sediments are often recognised to be an indication of expanded and intensified OMZs during intervals in time referred to as oceanic anoxic events, or OAEs (Schlanger and Jenkyns, 1976; Jenkyns, 2010). OAEs are palaeoceanographic phenomena that have occurred multiple times in the past and are known most famously in the Mesozoic. Three major OAEs have been identified during the Mesozoic: at the Cenomanian-Turonian boundary (~94 Ma), in the early Aptian (~120 Ma), and in the early Toarcian (~183 Ma) (Jenkyns, 2010).

The early Toarcian Oceanic Anoxic Event (T-OAE) is commonly used to refer to the time in which parts of the Tethys and Panthalassic Oceans were anoxic or euxinic. As with many OAEs, there are significant remaining questions as to how widespread anoxia was and in what basinal setting deoxygenation was

favoured (e.g. Pancost et al., 2004; Monteiro et al., 2012; Owens et al., 2013). To address these questions a detailed understanding of how OAEs are globally distributed is necessary. Thought by some authors to have a regional nature, the term, Regional Anoxic Event (RAE) was proposed to describe the event that generated the presence of laminated black shales during the early to middle Toarcian in the Boreal realm (McArthur et al., 2007; McArthur et al., 2008). However, evidence of anoxia, characteristically documented by the occurrence of black shales, is recognised to be more globally widespread and the phenomena has been documented outside the more characteristic epicontinental deposits, but also from open oceanic settings (Jenkyns, 1988; Gröcke et al., 2011).

Although black shale facies, associated with the T-OAE are recognised globally, the expression of the early T-OAE has a wide geographic variability which is reflected in terms of organic matter content and degree of oxygenation of bottom waters. In addition to a ‘patchy’ distribution of anoxic conditions in Early Jurassic oceans, for the basins in which anoxic conditions are recognized, it is widely accepted that anoxia was not prevalent for the entire duration, with either low oxygen, rather than anoxic conditions or temporary oxygenation of seafloor bottoms (Schmid-Röhl et al., 2002). Specific biofacies commonly associated with the deposition of organic-rich mudrocks from this time, represent benthic colonization events under low oxygen conditions, indicating temporary oxygenation of the sea-floor, rather than permanent anoxia (Röhl et al., 2001; Caswell et al., 2009; Martindale and Aberhan, 2017).

The link between two key global phenomena occurring during the early Toarcian, global warming and anoxia during the T-OAE are widely accepted (Wignall and Twitchett, 2002). The most likely cause-and-effect is rising temperature, typically resulting in high humidity, which in turn causes increased run-off from the continents, due to extra rainfall and thus excesses in the supply of terrestrial nutrients to the sea. The abundant nutrients cause plankton populations to increase. This results in an increase in planktonic matter on the sea floor over time, which led to the development of oxygen depleted conditions through organic-matter (OM) oxidation (Jenkyns, 2010), causing eutrophication of sea shelves (Jenkyns et al. 2002.; Jenkyns, 1999; Pálfy and Smith, 2000; Cohen et al., 2004b).

To establish the presence and extent of marine oxygen depletion in different basinal settings, as recognition of the T-OAE, indirect methods such as recording organic-rich facies, carbon isotope excursions, and biological turnover are commonly used. Low oxygen conditions been recorded using the presence

and size of framboids in early Toarcian successions (Suan et al., 2018). Framboids are spherical or sub-spherical aggregates of pyrite microcrysts which are equant and equidimensional (Butler and Rickard, 2000).

The quantitative framework measuring size distribution of pyrite framboids in different modern environments (Wilkin et al., 1996) can be applied to ancient environments as a redox proxy to determine euxinic and dysoxic settings. This can be used in conjunction with sedimentological analysis, such as evidence of bioturbation or lamination to indicate redox conditions (Wignall and Newton, 1998; Nielsen and Shen, 2004; Wignall et al., 2005; Bond and Wignall, 2010; Liao et al., 2010; Song et al., 2012). In euxinic settings, when free H_2S is present, then framboids can also develop in the water column (wilkin et al., 1996). The formation of framboids in euxinic settings is controlled by ambient buoyancy which is reached at ~ 5-6 μm (Wilkin et al., 1996). When framboids reach 5-6 μm in diameter before they sink below the iron reduction zone and stop growing (Wilkin et al., 1996). Therefore, euxinic conditions will produce a distinct size distribution characterised by a small range of very small (<5-6 μm diameter) pyrite framboids (Wilkin et al., 1996).

However, it is worth noting that the same factor would also control pyrite growth and size in a ferruginous water column (e.g. Hammarlund et al., 2012) and therefore this proxy cannot be used to differentiate between euxinic or ferruginous conditions in the water column. Differences can be determined between framboid populations developed in a euxinic or dysoxic environments. In dysoxic settings, where the seafloor is weakly oxygenated, pyrite framboids grow in the surficial sediments, where their size is limited by the local availability of reactants, rather than their neutral buoyancy, allowing for larger framboids over a wider range of sizes to form (Wilkin et al., 1996). Oxic settings are indicated by a lack of framboids and rare pyrite crystals.

1.4.4.5 Changes to the carbon cycle

Early Toarcian positive CIE

The changes in the carbon isotope composition of organic matter and carbonate in terrestrial and marine sediments over time indicate that the Toarcian was subject to abrupt and substantial disturbances to the global carbon cycle (Hesselbo et al., 2000; Schouten, 2000; Jenkyns et al., 2002; Cohen et al., 2004a; Kemp et al., 2005; Hesselbo et al., 2007; Hermoso et al., 2009; Al-Suwaidi et al., 2010; Newton et al., 2011; Gill et al., 2011; French et al., 2014;

Percival et al., 2016; Al-Suwaidi et al., 2016; Xu et al., 2017; Xu et al., 2018; Suan et al., 2018; Ruebsam et al., 2019).

Carbon isotope changes through the early Toarcian are marked by an overarching long-term positive excursion, punctuated by a sudden and discrete shorter-term negative excursion (e.g. Hesselbo et al., 2000;. Jenkyns et al., 2002; Kemp et al., 2005; Hermoso et al., 2009).

The overarching shift to heavier $\delta^{13}C$ ratios, has been recorded in biogenic calcite, organic carbon and wood. The later part of this overarching positive excursion, occurring after the interruption from the negative CIE, records a shift of ~2-3.5 ‰ in $\delta^{13}C$ marine carbonate (Jenkyns, 1988). This positive excursion, has been attributed to the removal of isotopically light carbon from the oceans through enhanced burial of organic matter though the deposition of black shales in anoxic seas (e.g. Wignall et al., 2005) or the response of water masses to rapid burial of large amounts of organic carbon, which lead to an enrichment of ^{13}C in the sediments (Jenkyns and Clayton, 1986; Jenkyns and Clayton, 1997; Schouten, 2000).

Early Toarcian negative CIE

The large negative CIE has been recognized in organic carbon, carbonate carbon, and fossil wood at several geographic locations in the Boreal realm (Jenkyns et al., 2002.; Jenkyns and Clayton, 1997; Hesselbo, Gröcke et al., 2000; Schouten, 2000; Röhl et al., 2001; Cohen et al., 2004a; Kemp et al., 2005), the Tethyan realm (Hesselbo et al., 2007; Hermoso et al., 2009; Bodin et al., 2010; Hesselbo and Pienkowski, 2011; Hermoso et al., 2012; Kafousia et al., 2014), in Argentina (Al-Suwaidi et al., 2010; Al-Suwaidi et al., 2016), the Arctic (Suan et al., 2011), North America (Caruthers et al., 2011; Caruthers et al., 2014; Them et al., 2017), Japan (Gröcke R. et al., 2011; Kemp and Izumi, 2014), China (Xu et al., 2017) and Tibet (Fu et al., 2016; Han et al., 2018). Interestingly, the negative CIE is not well documented in marine calcite, particularly belemnite calcite (van de Schootbrugge et al., 2005), a discrepancy that is still not fully understood (Kemp et al., 2005), and has been suggested to record a habitat response of belemnites to anoxic conditions (Ullmann et al., 2014).

The negative CIE, recording a clear shift to lighter $\delta^{13}C$ values, reaches a minimum in the f*alciferum* Zone. Although a clear negative CIE is widely accepted, the magnitude of the negative CIE is contested. An excursion of up to ~5 ‰ in the $\delta^{13}C$ record of marine organic matter, ~8 ‰ in wood, ~2 to 3.5 ‰ in

negative $\delta^{13}C$ marine carbonate and −3 to −4 ‰ indicated by biomarkers (e.g. Schouten, 2000; Hesselbo et al., 2007; French et al., 2014; Suan et al., 2015).

High resolution studies of the negative CIE have a stepped nature to the negatively shifting values on the falling limb of the CIE, superimposed onto a more protracted decrease. These small scale CIEs, with recorded oscillations of ~1 to 2.5 ‰, have been recorded globally, predominantly from the EES (Jenkyns et al., 2001; Kemp et al., 2005; Hesselbo and Pienkowski, 2011; Hermoso et al., 2012; Ruebsam et al., 2014; Bodin et al., 2016; Ruebsam et al., 2019) but more recently from outside Europe, in North America (Eastern Panthalassa Ocean) (Them et al., 2017) and Argentina (Al-Suwaidi et al., 2016). These small-scale CIEs have been interpreted to represent discrete methane clathrate destabilization events tied to astronomically forced changes to the global climate (Kemp et al., 2005; Hesselbo and Pienkowski, 2011; Hermoso et al., 2012).

The duration of the negative CIE also remains debated (Kemp et al., 2005; Gröcke et al., 2011; Huang and Hesselbo, 2014; Boulila and Hinnov, 2015; Ruebsam et al., 2019). Durations estimated from cyclostratigraphy, argued to represent a minimum duration (McArthur et al., 2016) range from 120-930 Kyr (Suan et al., 2008; Sabatino et al., 2009; Ikeda and Hori, 2014; Boulila et al., 2014; Huang and Hesselbo, 2014; Ruebsam et al., 2014). Estimates of duration based on $^{87}Sr/^{86}Sr$ suggest a longer duration of around 2.4 Myr (McArthur et al., 2016). The variability in estimated durations of the CIE could suggest the event is not synchronous and so not of equal duration everywhere (Neumeister et al., 2015).

A number of hypotheses have been proposed as the cause of the global negative CIE. The first involves an overturning or upwelling of a stratified water mass (‘Kuspert model’), whereby isotopically light dissolved inorganic carbon (DIC) is recycled from lower levels of salinity-stratified water masses into the photic zone (Kuspert, 1982). The second involves the rapid large scale dissociation of methane from gas hydrates and /or from permafrost melting, with a consequent release of light carbon (Hesselbo et al., 2000; Kemp et al., 2005; Hesselbo et al., 2007; Suan et al., 2011; Hermoso and Pellenard, 2014). Finally, a magma-intrusion hypothesis whereby an injection of isotopically light carbon from the release of thermogenic methane occurred as a result of the intrusion of Toarcian-aged Karoo-Ferrar dolerites into Gondwanan coals by (McElwain et al., 2005; Svensen et al., 2007a).

The global record of the characteristic shifts in the carbon isotope ratios, including records from shallow-water carbonates, provides a stratigraphic tool in

platform carbonates that typically lack useful fossils such as ammonites and coccoliths (Woodfine et al., 2008; Sabatino, 2013). The global nature of the curve confirms the utility of the early Toarcian negative CIE as a global chemostratigraphic marker (Them et al., 2017).

Pl-To boundary negative CIE

The Pliensbachian– Toarcian (Pl-To) boundary was marked with a ~ 2 to 3 ‰ negative carbon-isotope excursion in marine carbonate, organic matter and fossil wood, documented in the Boreal realm, from the Yorkshire Coast (UK) (Littler et al., 2010), the Paris Basin (Peti et al., 2017) and the southern Tethyan realm from Portugal, Morocco and Greece (Hesselbo et al., 2007; Bodin et al., 2010; Kafousia et al., 2014; Pittet et al., 2014). A recent study from Ruebsam et al. (2019) reveals up to three negative CIE shifts, as part of the minor Pl-To negative CIE, with magnitudes between −1 to−3 ‰ can be distinguished. Studies outside Europe, argue further for the global nature to the Pl-To negative CIE, with carbon isotope records from South and North America as well as from Asia (Gröcke et al., 2011; Caruthers et al., 2014;Fantasia et al.,2018). This prominent negative CIE, recorded in both biogenic and abiotic calcite, is indicative of a global scale carbon-cycle perturbation and demonstrates the potential importance of the $\delta^{13}C$ excursion as a chemostratigraphical marker for the Pl-To boundary. The causes of the Pl-To CIE are not well constrained. The more positive $\delta^{18}O$ isotope in the Yorkshire Coast Cleveland Basin suggest deepening is responsible for colder bottom waters (Korte and Hesselbo, 2011), although brachiopod $\delta^{18}O$ records from Portugal show a lightening of oxygen isotopes, which might reflect global, rather than local changes (Suan et al., 2010). Ruebsam et al. (2019) further argues the negative shift in $\delta^{18}O$ at the Pl-To boundary is attributed to both elevated sea surface temperatures and a strong ice mass related signal due to the inflow of ^{18}O-depleted freshwater from ice-cap melting and salinity reduction of oceanic surface waters.

1.4.4.6 The early Toarcian mass extinction event (ETME)

Towards the end of the Early Jurassic, marine biota suffered a crisis. Although not one of the ‘Big 5’ mass extinction events of the Phanerozoic, the early Toarcian mass extinction event (ETME), classed as a second-order extinction event, and is considered to be one of the most significant extinction events of the Mesozoic (Figure 1.5). On the whole, the ETME did not cause extensive changes in the composition of marine communities. Although many faunal

groups suffered losses during the extinction, none were of a catastrophic nature that required ecosystem re-structuring, with the ‘Modern evolutionary faunas’ dominating ecosystems prior and post extinction (Sepkopski, 2002).

The mass extinction led to significant taxonomic loss of marine faunas, an estimated of loss up to 26% of genera (Sepkopski 1989,1996). The benthic invertebrate macrofauna were particularly hard hit during the ETME, with species extinction intensity of 90% documented in NW Europe (Little and Benton, 1995; Harries and Little, 1999).

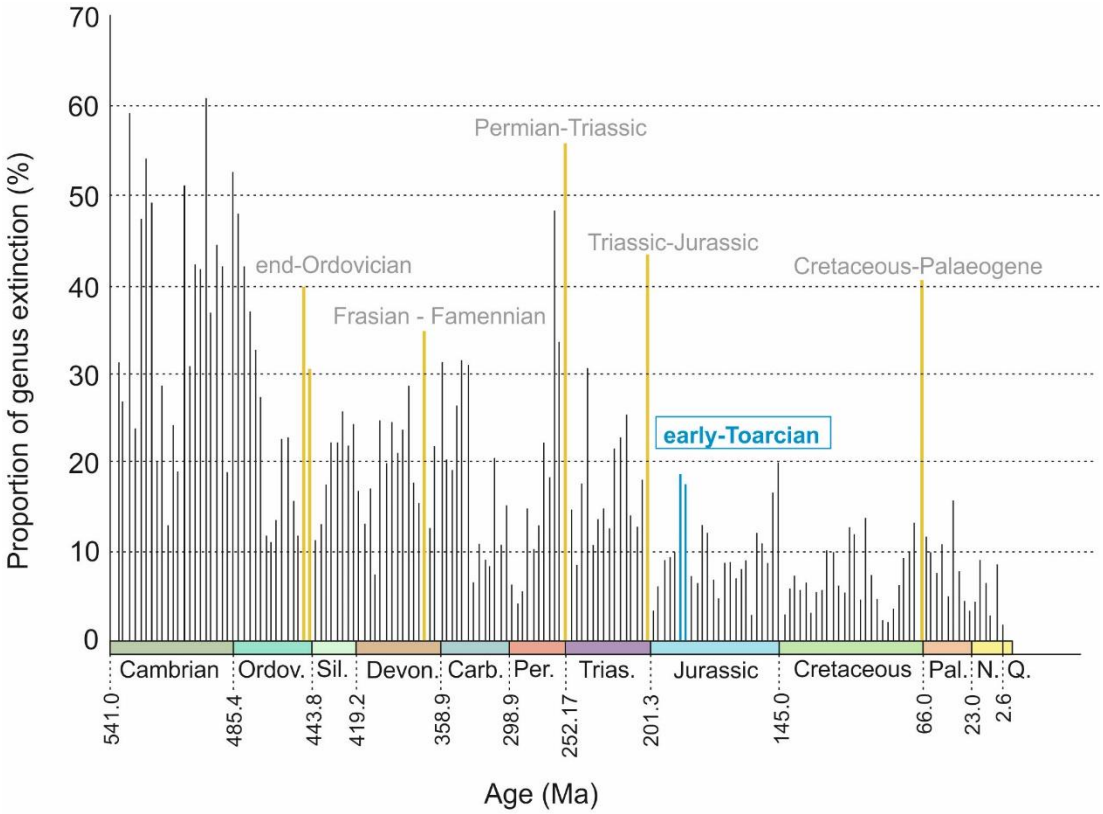

Figure 1.5 Taxonomic severity of the major Phanerozoic mass extinction events (based on Sepkoski, 1996, 2002; Bambach, 2004, 2006). The ‘big five’ mass extinction events are highlighted in yellow and the second-order early Toarcian event highlighted in blue with the blue box. Taxonomic severity is expressed as proportion of genus extinction at the substage level (%).

Numerous faunal groups were a part of the early Toarcian biotic crisis, with extinctions recorded in bivalves (Little and Benton, 1995; Aberhan and Fürsich, 1996; Aberhan and Fürsich, 2000; Aberhan and Baumiller, 2003; Caswell et al., 2009), ammonites (Macchioni and Cecca, 2002; Dera et al., 2010; Guex et al., 2012; Caruthers et al., 2014), belemnites (Little and Benton, 1995), brachiopods (Vörös, 1993; Vörös, 2002; Vörös et al., 2016), foraminifers (Zakharov et al., 2006; Wignall et al., 2006), ostracods (Arias, 2009), dinoflagellates (Palliani and

Riding, 1999; Bucefalo Palliani et al., 2002; Correia et al., 2017) and nannofossils (Mattioli et al., 2009). The ETME was first recognised by Hallam (1961,1967) and was originally thought to be a regional event within the European epicontinental basins (Hallam, 1986) but the extinction has now been recorded globally.

Although some studies have suggested a single extinction crisis (Beerling et al., 2002; Kemp et al., 2005), the early Toarcian appears to record multiple extinction horizons (Harries and Little, 1999; Caswell et al., 2009; Caruthers et al., 2014). An end-Pliensbachian age for the ETME was first attributed by Hallam (1986), Raup and Sepkoski (1988) and Sepkoski (1989, 1996, 1992), but subsequent records show a more gradual loss during the late Pliensbachian and the early Toarcian over a period of 0.6 Myr rather than a single catastrophic event (Harries and Little, 1999). This extinction interval was later dated as early Toarcian in age (Hallam, 1987; Arias et al., 1992; Little and Benton, 1995) with multiple extinction horizons. The most recognised extinctions in the early Toarcian interval occur at around the Pl-To boundary, near the top of the *tenuicostatum* Zone and around the *tenuicostatum/falciferum* Zone boundary, or their equivalents in other ammonite bioprovinces (Almeras and Fauré, 1990; Bassoullet et al., 1991; Arias et al., 1992; Bassoullet and Baudin, 1994).

Bivalves were one of the first faunal groups to be studied during the ETME and provide one of the best records of the event. Bivalve records from the Yorkshire Coast clearly show that infaunal bivalves were most prominently affected with up to 100% species loss, but also includes loss of epifaunal bivalves with up to 78% species loss (Little and Benton, 1995; Harries and Little, 1999). A drop in the diversity of bivalves has been globally recorded with key studies documented in Argentina (Aberhan and Fürsich 2000; Aberhan and Baumiller, 2003), Canada (Martindale et al., 2017) and Siberia (Zakharov et al., 2006). In Europe, bivalve records are more common in northern Europe (Boreal realm) and brachiopod studies more common in southern and eastern Europe (the Tethyan realm) (Joral and Goy, 2000, 2009; Joral et al., 2011; Comas-Rengifo et al., 2013, 2015; Baeza-Carratalá et al., 2016, 2017).

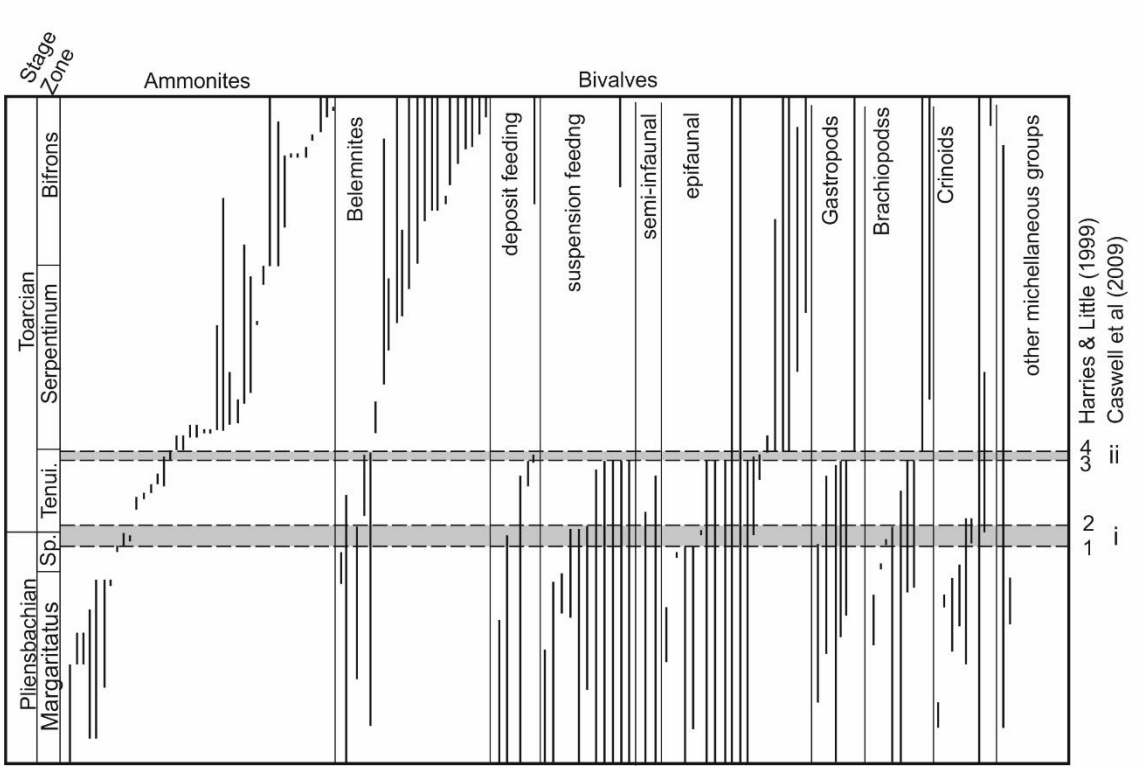

Figure 1.6 A summary of composite taxonomic ranges of the late Pliensbachian to middle Toarcian marine species in four localities of northwest Europe (modified after Harries and Little, 1999). Ranges show heightened extinction among marine groups at two main intervals (shaded grey boxes). Intervals of heightened extinction denoted by Harries and Little (1999) with steps 1-4 and by Caswell et al. (2009), with extinction horizons i and ii. Tenui. = *tenuicostatum Zone*, Sp. = s*pintaum Zone*. Specific identification of marine taxa in Harries and Little (1999). Ammonite Zonal scheme after Page (2003).

The faunal recovery from the ETME has not been well documented, with research predominately focussing on the extinction event itself, rather than subsequent recovery (Hallam, 1996; Aberhan and Fürsich, 2000; Ruban, 2004; Joral et al., 2011). Current studies that extend past the main extinction intervals suggest diversity did not begin to increase until later in the middle Toarcian (during the b*ifrons* Zone), at the same time infaunal organisms began to reappear in northwest Europe (Little, 1995; Fürsich et al., 2001; Röhl et al., 2001).

For calcareous nannoplankton, the Early Jurassic on the whole records a significant diversification that started in the late Pliensbachian (Jenkyns, 1988; Mattioli et al., 2004). This diversification was interrupted during the early Toarcian, during the so called “calcareous nannofossil or biocalcification crisis” (Mattioli et al., 2004; Tremolada et al., 2005; Mattioli et al., 2009). Calcareous nannofossils are also useful biostratigraphical markers in the Lower Jurassic,

particularly for more carbonate-rich sections in the south and south-east EES, where there is often a more noticeable lack of ammonites in some sections (Mattioli et al., 2004).

1.4.4.7 Proposed kill mechanisms for the ETME

The Karoo-Ferrar LIP volcanism is considered an initial driver for the ETME. The notion that volcanism might drive mass extinctions is nearly fifty years old (Kennet and Watkins, 1970; Vogt, 1972) and the general link between LIP eruptions and mass extinctions is now well-established (Wignall, 2001; Courtillot and Renne, 2003; Wignall, 2007; Bond and Wignall, 2014). However, the link between the two phenomena is still not fully understood.

Given the well-evidenced changes of global chemical cycles during the Jurassic, particularly from western Europe, the ETME is relatively poorly documented in comparison. As such, there is not a general agreement on the causes of the extinction, with the debate mainly centred around two different hypothesised kill mechanisms: global warming and anoxia. Exploring the dynamics and global nature of the ETME in relation to these environmental perturbations is essential to understanding the role of different kill mechanisms, including their relative temporal and spatial differences.

Warming as a kill mechanism for the ETME

Warming is hypothesised as one of the main kill mechanisms for the ETME (e.g. Gómez and Goy, 2011). Clear temporal links between warming and the extinction are recorded with Jurassic seawater oxygen isotope curve indicating a short warming event in the *tenuicostatum* Zone, coincident with the first extinction pulse. The short lived nature of this initial warming may record part of a long term trend that initially global feedback mechanisms could compensate and account for. By the end of the *tenuicostatum* Zone a more permanent shift to hotter temperatures was established, coincident with the second pulse of extinction (Gómez et al., 2008; Gómez and Arias, 2010; García Joral et al., 2011). High sea surface temperatures during the early Toarcian likely induced severe thermal stress in marine shelf environments. Thermal shock and protein degradation has been demonstrated for marine invertebrates in temperatures exceeding 45^{o}C, but severe metabolic restriction can occur at temperatures of just 35^{o}C (Somero, 1995). However, warming as a prominent kill mechanism has been questioned by some authors (e.g. Wignall et al., 2005). Although there

is evidence of global warming, sea-level transgression and the development of anoxia in parts of the EES during the early Toarcian, Wignall (2005) argues that only anoxia is synchronous with the ETME. Evidence against warming a prominent kill mechanism for the extinction is linked to the postulated release of methane from gas hydrates, that would cause severe global warming, occurring after the main stages of extinction (Wignall et al., 2005).

Anoxia as a kill mechanism for the ETME

Many authors have argued that the mass extinction is caused by the widespread development of dysoxic to anoxic waters, as a result of a supposed major and global OAE (Jenkyns, 1988; Bassoulet et al., 1991; Little and Benton, 1995; Hallam and Wignall, 1997; Palliani and Riding, 1999; Harries and Little, 1999; Hylton, 2000; Vörös, 2002; Aberhan and Baumiller, 2003; Mattioli et al., 2004; Tremolada et al., 2005; Zakharov et al., 2006; Wignall et al., 2006; Mailliot et al., 2006; Mattioli et al., 2009; Caswell et al., 2009; Danise et al., 2013; Martindale and Aberhan, 2017).

For the ETME it is argued that anoxia itself is the only kill mechanism coincident with the extinction, and although developed diachronously, anoxia was simultaneously developed throughout Europe for a brief interval in the *tenuicostatum* Zone (mid-s*emicelatum* Subzone) (Wignall et al., 2005). However, this is argued against by Gomez and Goy (2008), who propose lack of direct relationship in time and space between mass extinction and anoxic environments.

Anoxia as the prominent cause for the extinction has been questioned due to the exact timing of extinction at the subzonal level with respect to black shale deposition within northwest Europe (Gómez et al., 2008; McArthur et al., 2008; Joral et al., 2011). It is argued that anoxia could have been an important factor for regional extinction in some areas, but not necessarily all. That the deposition of anoxic laminated black shales, particularly co-incident with the acme of the T-OAE and coincident negative CIE, faunas have already become extinct (Gomez and Goy, 2011).

It is important to note that although the presence of anoxia can be explained by a global temperature rise, a temperature rise does not always result in prevalent anoxia throughout every basin system globally. In the Spanish early Toarcian platform system, as well as in many other sections of Europe and northern Africa, mass extinction has also been demonstrated, but no clear evidence for anoxia has been found. The deposition of organic-rich facies outside the

European platform is diachronous and generally does not coincide with extinction (e.g. Caruthers et al., 2013). These lines of evidence discard anoxia as the origin of the global ETME. However, an ongoing debate concerning the intensity of marine anoxia, the geographic extent of the T-OAE and its link with the ETME.

Other potential kill mechanisms and causes of the ETME

Ocean acidification may have also played a role during the extinction event, but the importance of acidification during the early Toarcian is less clear than during the Triassic-Jurassic extinction event (Martindale, 2012; Greene et al., 2012). Arguments for Toarcian acidification comes predominately from shallow marine carbonate platform sections in Italy (Hermoso et al., 2012; Trecalli et al., 2012). Other authors however, clearly note a biocalcification crisis' but are careful not to necessarily link this to widespread oceanic acidification, linking it only as a consequence to rapid and pervasive seawater warming (Suan et al., 2008; Clémence et al., 2015; Han et al., 2018).

Sea-level changes are often associated with mass extinction events, a link first proposed by Newell (1967). Although it is accepted sea-level change is not the clear kill mechanism for the ETME and the causative mechanisms are likely part of a more complex cause-and-effect scenario, the effects of sea-level should not be disregarded as a potential intrinsic factor for the ETME. Rapid transgression in the early Toarcian is a worldwide phenomenon (Jenkyns 1988) that, particularly across the Boreal realm of northern Europe, is coeval with the onset of anoxic/dysoxic black shale facies, which can be linked to a mass extinction horizon.

1.4.4.8 Importance of defining the T-OAE

The early Toarcian Oceanic Anoxic Event (T-OAE), was defined by Jenkyns (1988) as a period of time characterized by abnormally high depositional and preservational rates of organic carbon in favourable marine environments, due to widespread anoxia, that gave rise to the synchronous deposition of black shale facies in many parts of the globe (Jenkyns 1988; Jenkyns et al., 2002). According to this definition, the anoxic environments linked to the T-OAE are marked in the stratigraphical record by the presence of synchronous black shale deposits. According to Bates and Jackson (1987), Kearey (2001) and McArthur et al. (2008), black shale facies should only be considered those shales where

total organic carbon (TOC) content is above 5 wt.%. Based on this definition, compilation of data from the European sections indicate that real black shale facies having more than 5 wt.% TOC are constrained to a sub area of the European Epicontinental Sea, on which euxinic facies were developed during the early–middle Toarcian.

No strict definitions for the T-OAE and P-To event have yet been proposed and officially ratified, with the general use of the term 'T-OAE' changing between authors. Often the term 'T-OAE' is used to represent the interval in time that encompasses a whole suite of records of environmental change during this time, rather than evidence only for anoxic conditions.

The broad suite of changes commonly attributed to the T-OAE include: the development of organic rich shales, an increased hydrological cycle and weathering, rapid rise in global temperature and significant perturbations of the carbon cycle, particularly the negative carbon isotope excursion. Many authors are more selective and use the presence of a negative CIE in marine sediments, recorded from the upper *Tenuicostatum* to lower f*alciferum/serpentinum* Zones in both organic and carbonate carbon, as the geochemical expression that defines the classic T-OAE interval (Hesselbo et al., 2007; Kafousia et al., 2014; Reolid, 2014; Suan et al., 2015; Bodin et al., 2016). (Figure 1.7). Some authors even go as far as to call the negative CIE the 'T-OAE CIE' (Them et al., 2017; Martindale et al., 2017). Others include the negative CIE and the subsequent positive CIE in the middle/upper part of the *falciferum* Zone, (Hesselbo et al., 2000; Jenkyns et al., 2002) which will be the chemostratigraphic approach used to define the 'T-OAE' interval for this study (Figure 1.7).

It is likely that the variability of the term 'T-OAE' and exactly what that encompasses originates from where the event was first documented. Early research from section on the Yorkshire Coast (UK), recognised the development of organic-rich laminated black shales (known as the Jet Rock) that recorded bottom water anoxia (Jenkyns, 1985, 1988). Over the following decades a multitude of geochemical records were produced for the Yorkshire Coast sections, including the recognition of the overarching positive CIE with abrupt negative CIE (e.g. Kemp et al., 2005), clear inflections of the strontium seawater curve (McArthur et al., 2000) and evidence for an enhanced hydrological cycle that led to increased run-off (Cohen et al., 2004; Percival et al., 2016), nutrient input and subsequent deposition of the organic-rich shales (Jenkyns et al., 2010).

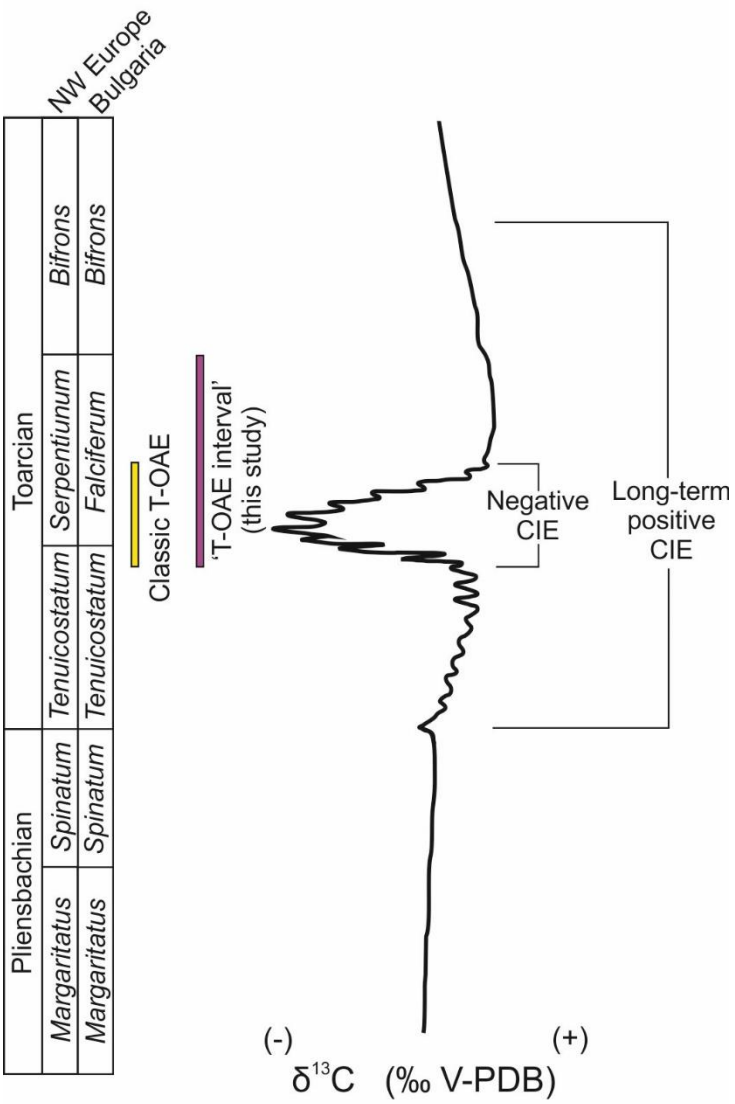

Figure 1.7 Idealised Pliensbachian and Toarcian carbon isotope stratigraphy modified after Them *et al.,* 2017. Ammonite biostratigraphic Zones from NW Europe (Page, 2003) and equivalent Zones in Bulgaria (Metodiev *et al.,* 2008).

As studies continued, recognition of the event both from additional sites in Europe and outside Europe, the term T-OAE remained, although evidence for organic-rich laminated shales and recognition of oceanic anoxia were not always present. The term T-OAE continues to be used, although it is now clearly acknowledged that the development of oceanic anoxia during this time did not expand to cover the whole EES, and rather is limited to areas such as the northern EES, where the event was initially recognised. Although the development of anoxic conditions was not spatially continuous, it has been documented from numerous global sections and studies have shown that the global areal extent of marine anoxia periodically increased at this time (Pearce

et al., 2008). It has recently been suggested that for areas where low oxygen conditions are present, and may be accompanied by the deposition of organic rich shales, a feature typically indicating the presence of an OAE, the definition of a temporal OAE should be reconsidered to also include other geochemical proxies that reconstruct redox states if the ocean (Them et al., 2017).

Discrepancies in the use of the T-OAE has several implications. The first example is changes in the definition of the negative CIE itself, often considered as representative of the T-OAE, this can lead to differences in the stated duration of the T-OAE (e.g. Huang and Hesselbo, 2014; Ruebsam et al., 2014). A second example is the definition of the T-OAE and links to the ETME. Whereby, if evidence for the T-OAE is presented alongside evidence for the ETME, the definition of the T-OAE (whether recording direct evidence for anoxia or just a record of environmental change such as the negative CIE or warming) has critical implications for the driving mechanisms behind the extinction event (e.g. Martindale and Aberhan, 2017). A third and final example is the mis-representation of the extent of anoxic bottom waters across the world's oceans, when the T-OAE is recorded, without evidence for anoxia. For example, the identification of the T-OAE from the open ocean carbonate platform recorded in the southern Hemisphere (southern Tibet) with negligible evidence of dysoxia (Han et al., 2018).

It should be noted that in this study, the use of the term 'T-OAE interval' in the Moesian Basin, refers to the time interval (upper *Tenuicostatum* to the mid/upper f*alciferum* Zone), rather than a recognition of anoxic waters in the basin itself.

1.5 Bulgaria review

1.5.1 Palaeogeography and geological history

In the Early Jurassic present day Bulgaria was a part of the wide epicontinental sea, the so-called European Epicontinental Seaway (EES), that covered most of present day Europe and was part of the northwest Tethys Ocean. This epicontinental seaway opened in the northwest Tethys Ocean concomitant with the break-up of Pangea. Bulgaria was situated on the eastern margin of this epicontinental platform, close to the open ocean and at a palaeolatitude between 33°N and 38°N (Dera et al., 2009).

Throughout the Early-Middle Jurassic, sediments accumulated in a tectonically active basin (Zagorchev et al., 2009). The basin formed as a result of extensional tectonics along the northern Tethyan margin, where extension was driven by the opening of western Tethys Ocean (Bassoulet et al., 1993; Fourcade et al., 1995). Extensional faulting and associated differential subsidence rates led to the formation of a highly fragmented basin that comprised a series of horst-and-graben structures (e.g. Sapunov, 1971; Tchoumatchenco and Sapunov, 1994; Sapunov and Tchoumatchenco, 1998). The basin was situated on the southern edge of the landmass named Moesia (Bassoulet et al., 1993; Fourcade et al., 1995).

In the literature the term ‘Moesian Platform’ has been used to describe both the landmass Moesia and the surrounding basins through the Mesozoic-Cenozoic. However, and somewhat confusingly, the definition of what comprises the Moesian Platform is not consistent between authors. For the purposes of this study the term ‘Moesian Basin’ will also be used to define the basin in which Jurassic sediments accumulated at the southern edge of the Moesian landmass.

In the early Hettangian, the area was a continental landmass, but was subsequently covered by a marine transgression that initiated marine carbonate deposition heterogeneously across the basin (Sapunov and Tchoumatchenco, 1998). This transgressive surface is sometimes recognised in stratigraphy as the Lower Jurassic sediments unconformably overlying over Middle Triassic and Palaeozoic rock units (Sapunov and Tchoumatchenco, 1998). Lower-Middle Jurassic sedimentary successions in the NW and Central Balkan region display an evolution from an initially isolated lacustrine setting (early Hettangian) to a rapidly expanding shallow marine sandy and carbonate depositional setting (late Hettangian-early Bajocian) (Sapunov and Metodiev, 2007). A diachronous

pattern of carbonate deposition linked to sea-level changes, subsidence and fault block movement continued throughout the Early and Middle Jurassic (Sapunov and Tchoumatchenco, 1987b; Tchoumatchenco, 1988; Tchoumatchenco and Sapunov, 1994; Sapunov, 1999; Sapunov and Metodiev, 2007). By the Late Jurassic and Cretaceous the basin had stabilised tectonically and laterally extensive and thick carbonate platform formed on the passive margin of the northern Tethys Ocean.

Following the Jurassic, the Alpine Orogeny saw the collision of the African and Eurasian plates, this resulted in the closure of the Tethys Ocean with oceanic lithosphere being subducted northwards beneath the Eurasian plate (Stampfli and Borel, 2002; Golonka, 2004; Stampfli et al., 2013). This led to the development of the Alpine-Himalayan Belt, which is an extensive chain of mountain ranges extending across present-day Europe and Asia, including the Balkan Mountains in Bulgaria (Dabovski et al., 2002; Dabovski and Zagorchev, 2009; Şengör, 2011).

Bulgaria comprises three distinct major tectonic units: the Moesian Platform, the Alpine Orogenic Belt and the Rhodope Massif (Figure 1.8). Each of these three units have been subdivided into smaller tectonic units, delineated by major thrust faults linked to the Alpine Orogeny (Figure 1.8). The tectonic units of Bulgaria were originally defined by (Bončev, 1971; Bončev, 1986). Since this work, numerous controversial and contradicting tectonic models for the structure and geological evolution of Bulgaria have since been proposed (Boyanov and Ruseva, 1989; Dabovski et al., 1989; Dončeva and Ovčarova, 1989; Dabovski et al., 2002; Zagorchev et al., 2009). The key characteristics of the three main tectonic units in Bulgaria are briefly summarised below. For further details on geological evolution of Bulgaria see Dabovski et al. (2002) and Zagorchev et al. (2009).

The first major tectonic unit, the Moesian Platform, is the foreland of the Alpine Orogeny. It extends across most of north Bulgaria and consists of gently folded Mesozoic and Cenozoic sediments (Dabovski and Zagorchev, 2009). The Moesian platform has an Archaean-Palaeoproterozoic basement that acted as a relatively stable tectonic fragment throughout the Phanerozoic (Golonka, 2004; Zagorchev et al., 2009). The second major tectonic unit, the Alpine Orogenic Belt, developed between the Eurasian and African plates after multiple collisional and extensional tectonic events from the Late Palaeozoic to Middle Eocene. It now flanks the southern edge of the Moesian Platform (Zagorchev et al., 2009). The belt is divided into the South Carpathian System and the Balkan Orogenic System, and links the South Carpathians to the north of Bulgaria

(Figure 1.8). Lower Jurassic outcrops are part of the Balkan Orogenic System and often exhibit a WNW-ESE outcrop pattern, reflecting their position at the northern part of the Alpine Orogeny. The Balkan Orogenic System is further subdivided into two zones, the Balkan and Srednogorie Zones (each divided into further units (Figure 1.8). These zones and units are also delineated by Alpine faults. The third major tectonic unit, the Rhodope part of the Alpine-Himalayan mountain belt, called the Rhodope Massif, is more enigmatic (Dabovski and Zagorchev, 2009). It was originally thought that this tectonic unit originated in the Precambrian and was subsequently affected by Hercynian and Alpine tectono-metamorphic event (Kronberg et al., 1970; Jones et al., 1992; Kozhoukharova, 1996). It has since been proposed the Rhodope Massif is an Alpine metamorphic complex formed by Cenozoic accretion processes (Barr et al., 1999; Himmerkus et al., 2006). The uncertainty surrounding the formation and development of the Rhodope Massif has meant the palaeogeographic location of the Rhodope massif is uncertain. In the available reconstructions for the Lower Jurassic some show the massif being located south of Moesia (Blakely, 2010), others do not show this additional landmass (Bassoulet et al., 1993; Fourcade et al., 1995). Due to this uncertainty, the Rhodope Massif is not shown on palaeogeographic maps in this study.

The Early Jurassic tectonic evolution of the Moesian Basin is poorly understood. This has led to considerable challenges in understanding the Early Jurassic palaeoenvironments. Previous work in Bulgaria has attempted to define specific horst and graben structures, often referred to as ‘steps’, that were regionally connected (Tchoumatchenco and Sapunov, 1994). However, these studies do not use palinspastic reconstructions (which account for the original positions of landmasses prior to crustal deformation) and fault block movements are not considered. As such, the regional palaeogeographic maps constructed for the basin and interpreted transgressive-regressive patterns (Tchoumatchenco and Sapunov, 1994; Zagorchev et al., 2009) should be treated with caution.

A further challenge to understanding the stratigraphy and palaeoenvironments of the Moesian Basin is the extensive Alpine faulting within the Lower Jurassic sediments. In regional palaeoenvironmental reconstructions the thrust faults between units are often not taken into account. This somewhat diminishes the reliability of previous studies as it is not clear how far apart depositional units were in the Lower Jurassic, prior to being thrusted. Although geographically close in the present day, thrust faults present between the Lower Jurassic sedimentary sequences means that the lateral variability between units cannot be assessed in detail. Despite this limitation for sequence stratigraphic

interpretation, all Lower Jurassic units across northwest and central Bulgaria are part of the same lithological framework and likely represent deposition into the same basin. This allows recognition of past deepening and shallowing events within the basin, as well as the depositional environments of sediments that lie within tectonic units.

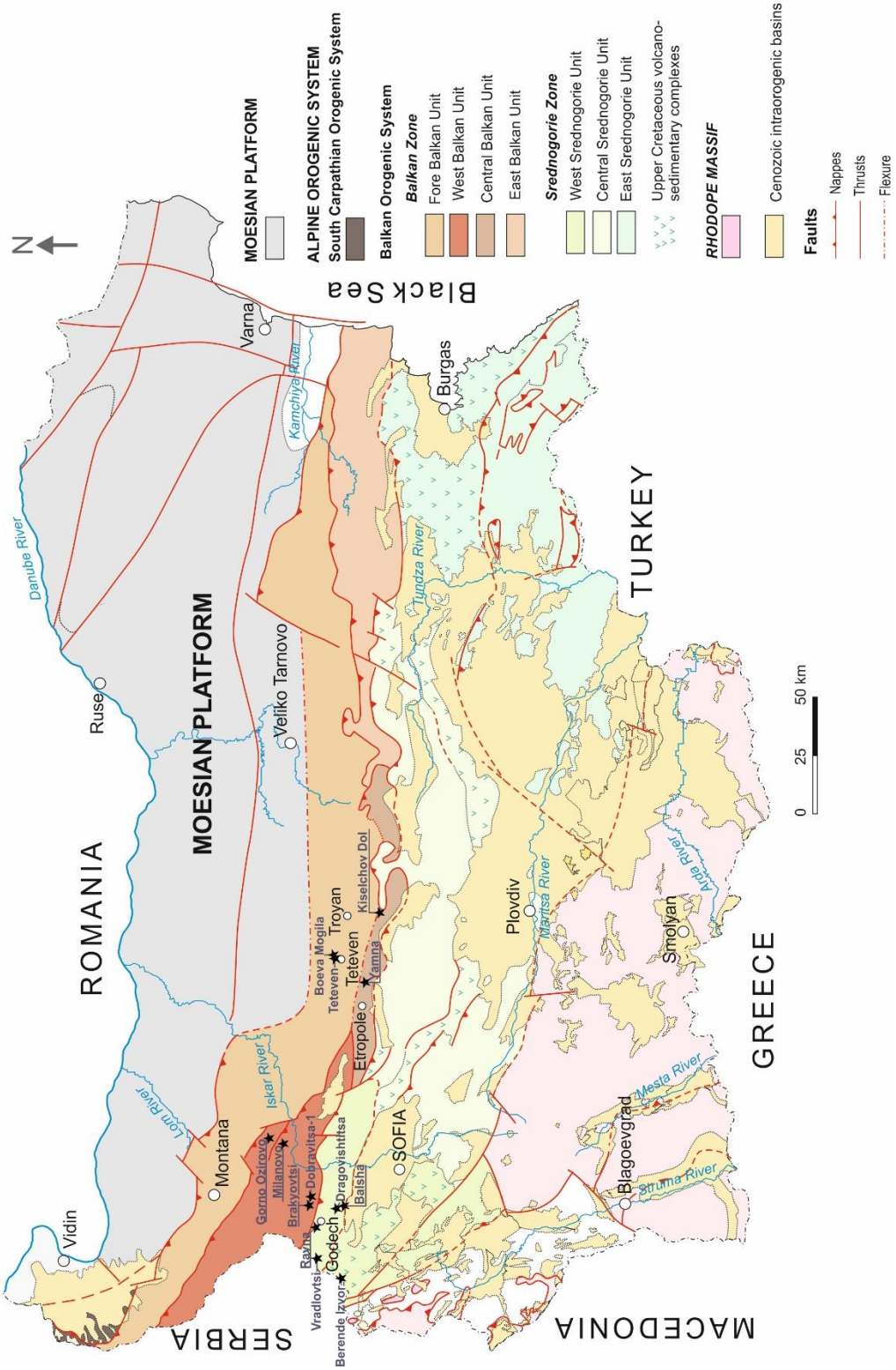

Figure 1.8 Geological map of Bulgaria with defined tectonic units modified from Dobovski et al. (2002) and Zagorchev et al. (2009). Study sections are indicated by black stars.

1.5.2 The distribution of the Lower Jurassic in Bulgaria and surrounding countries

In Bulgaria, Lower Jurassic outcrops in the present day are distributed in three main regions: the North-West and Central Balkan region; the East Kotel region; and the South-East Strandzha region (Figure 1.9). These regions are separated by their Jurassic depositional history, their post-Jurassic tectonic activity (Alpine Orogeny) and their present day geographic setting. The North-West and Central Balkan region and the East Kotel region lie within the Balkan Mountain range (Figure 1.9). Lower Jurassic outcrops in Bulgaria are exposed as long narrow strips that trend NNW-SSE within thrusts systems during Alpine inversion (Dabovski et al., 2002).

A significant proportion of Lower Jurassic rocks that comprise the North-West and Central Balkan region also extend northwards into the Moesian Platform (Sapunov et al., 1986a,b)(Figure 1.8). They are relatively extensive and tectonically undisturbed, but sit at depths of 4-5 km due to subsidence at the forefront of the Alpine Orogeny. Unfortunately, Lower Jurassic cores from boreholes have been destroyed or are no longer accessible.

Figure 1.9 The distribution of Lower Jurassic exposures in Bulgaria Modified from Zagorchev et al. (2009).

The East Kotel region comprises several exposures of allochthonous Lower-Upper Jurassic flysch deposits in eastern Bulgaria (Sapunov and Tchoumatchenco, 1987a; Tchoumatchenco, 1988; Tchoumatchenco and Černjavska, 1989; Tchoumatchenco and Černjavska, 1990; Sapunov et al., 1990)(Figure 1.9). Although there is no lithological or palaeogeographical link between the East Kotel region flysch deposits and the other Lower Jurassic deposits in Bulgaria, the deposits can be correlated with similar successions in the Tulcea zone (north Dobrogea, Romania; Figure 1.10) and the Tauric series of South Crimea (Ukraine) (Tchoumatchenco, Zagorchev, et al., 2006). The flysch-type units in Romania and the Ukraine are part of a system linked to the formation of the Küre Basin, as part of the evolution of Early Mesozoic back-arc basins in the Black Sea-Caucasus segment of the active Tethyan margin (Kazmin and Tikhonova, 2006).

The North-West and Central Balkan region comprises the main area of distribution the Lower Jurassic sediments in Bulgaria. All sections for this study are located in this region. The Jurassic rocks of this region continue across the border into east Serbia and have been lithostratigraphically correlated (Tchoumatchenco et al., 2006; Tchoumatchenco et al., 2008; Tchoumatchenco et al., 2011; Petrova et al., 2012).

The South-East Strandzha region is located in southeast Bulgaria (Figure 1.10))**. T**he Lower Jurassic rocks in this region were relatively similar lithologically to those exposed in the North-West and Central Balkan region, although they have been affected by low grade metamorphism (Sapunov, 1999). Whilst the Lower Jurassic lithostratigraphic formations are very similar to the those classified in the North-West and Central Balkan region, some formations are given new names due to geographical separation in the present day (Tchoumatchenco et al., 2008). The Jurassic rocks of the Strandzha region extend through northwest Turkey (Figure 1.10). The South East Strandzha region outcrops have been correlated to the formal Turkish lithostratigraphical scheme (Bedi et al., 2013).

In this study, only the Lower Jurassic sediments exposed in the North-West and Central Balkan region are discussed in further detail.

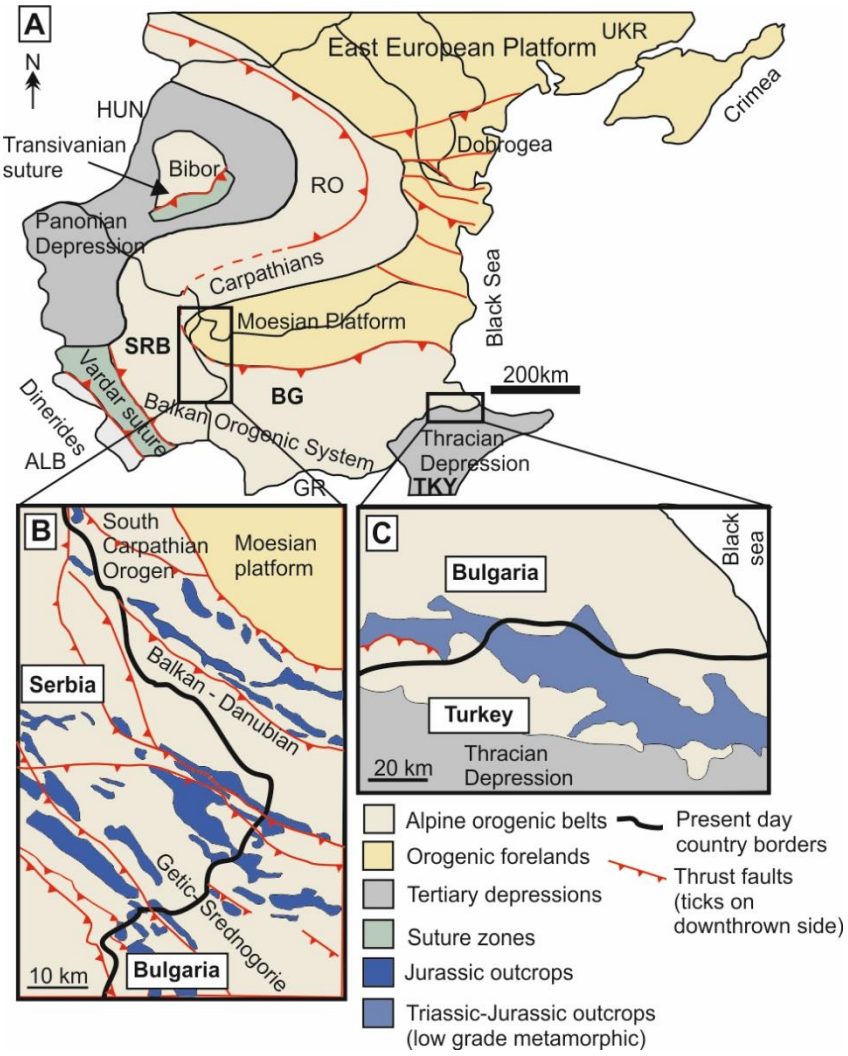

Figure 1.10 A) Simplified tectonic map of the orogenic belts, suture zones and forelands involved in the Alpine Orogeny on the Balkan Peninsula (Modified from Zagorchev et al., 2009). ALB= Albania, RO= Romania, SRB = Serbia, BG= Bulgaria, MK= Macedonia, GR= Greece, UKR = Ukraine, TKY= Turkey. B) Sketch map of the Jurassic outcrops across the Bulgarian-Serbian border (modified after Tchoumatchenco, 2006). C) Sketch map of the Triassic-Jurassic outcrops across the Bulgarian-Turkish border (modified after Bedi et al., 2013).

1.5.3 Lithostratigraphy of the Lower Jurassic in NW and central Bulgaria

The formal lithostratigraphic framework constructed for Bulgaria is relatively recent (Nikolov and Sapunov, 2002) and builds on previous Lower Jurassic stratigraphic studies (Kojumdgieva et al., 1982; Sapunov, 1983; Sapunov and Tchoumatchenco, 1986; Sapunov and Tchoumatchenco, 1987b; Sapunov and Metodiev, 2007) (Figure 1.11).

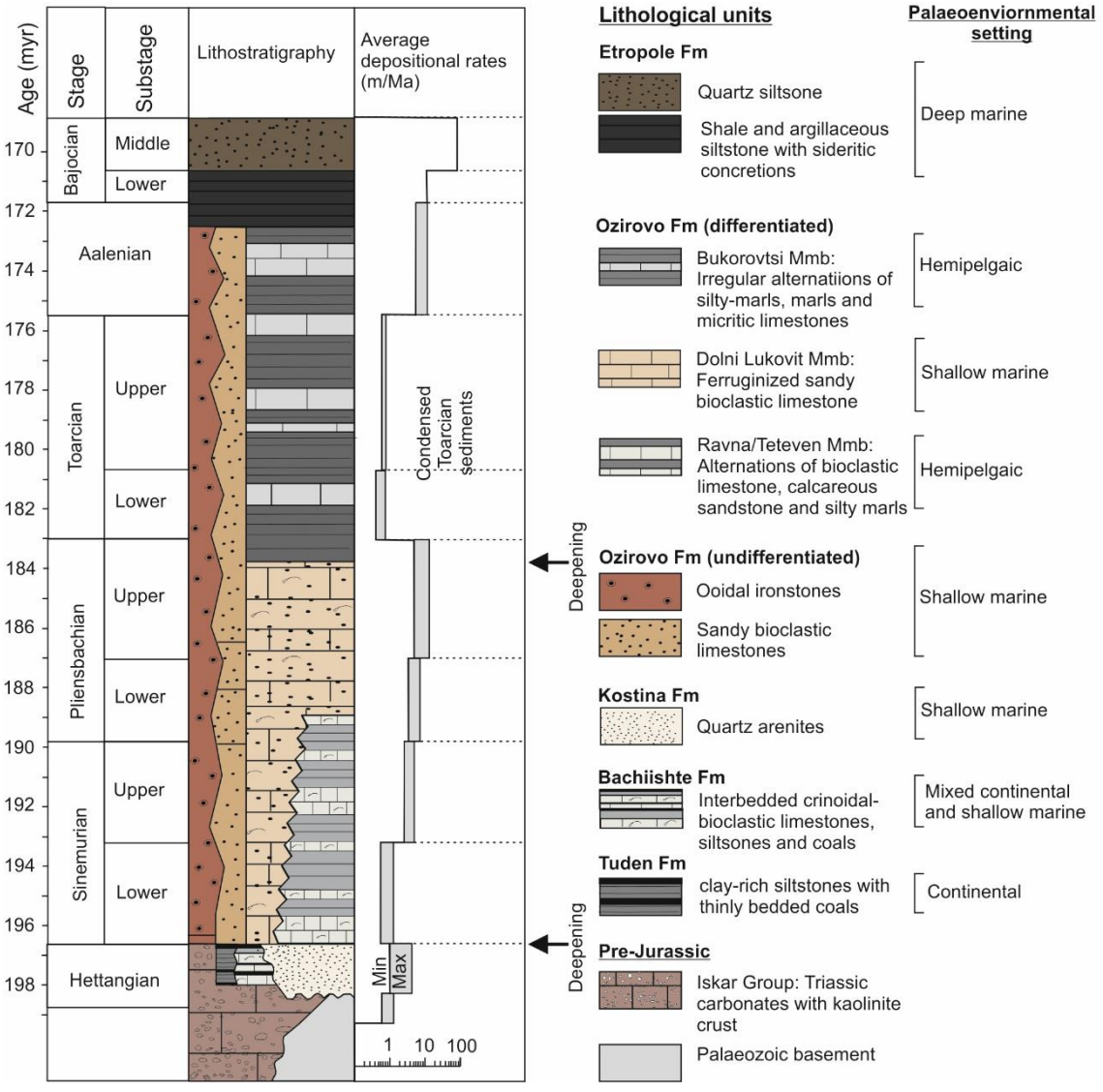

Figure 1.11 The generalised lithostratigraphic scheme of the Lower-Middle Jurassic deposits in Bulgaria and corresponding depositional environments. The average depositional rates of the Early-Middle Jurassic sediments are shown. Modified after (Metodiev et al., 2014). Ages after Gradstein et al., (2012).

Most stratigraphic units are diachronous in age and show large thickness variations due to differences in sedimentation rate, most strongly linked to differential subsidence in the Moesian Basin. The highest depositional rates occurred during the Sinemurian-Pliensbachian and lowest during the Toarcian (Sapunov and Tchoumatchenco, 1986; Sapunov and Tchoumatchenco, 1991; Sapunov et al., 1991; Sapunov and Metodiev, 2007) (Figure 1.11).

The base of the Lower Jurassic in Bulgaria is characterised by continental and paralic (mixed continental and marine) successions that unconformably and diachronously overlie either Lower–Middle Triassic or Palaeozoic rocks (Figure 1.11). A conformable Triassic-Jurassic boundary is not recorded in Bulgaria. In central Bulgaria the paralic deposits have been dated as Hettangian-Lower Sinemurian (Černjavska, 1986) but have not been biostratigraphically dated. The continental deposits are part of the Tuden Formation in northwest Bulgaria and are dated as Hettangian. The Tuden Formation comprises ferruginised terrigenous clastic rocks and clay-rich sediments, with horizons rich in carbonatised wood detritus and locally developed thin coal beds. The paralic deposits comprise the Bachiishte Formation which consists of mixed continental beds (lithologically similar to the continental deposits) with thin interbeds of marine sandy crinoidal-bioclastic limestones. These continental and paralic successions gradually grade into marine sediments and record a major transgressive event (Sapunov and Metodiev, 2007).

The Kostina Formation, Hettangian to Sinemurian in age, either diachronously overlies continental/paralic deposits, or it unconformably overlies Middle Triassic or Palaeozoic rocks (Figure 1.11). It is composed almost exclusively of quartz arenites that quickly grade into the overlying Ozirovo Formation.

The deposition of the Ozirovo Formation is diachronous in nature across the Moesian Basin and is recorded as either ‘undifferentiated’ Ozirovo Formation or ‘differentiated’ Ozirovo Formation (Figure 1.11). The differentiated Ozirovo Formation is subdivided into three members: the Ravna/Teteven Member, the Dolni Lukovit Member and the Bukorovtsi Member. The differentiated Ozirovo Formation records extreme lateral variations in thickness (Sapunov, 1971). For example, in the Teteven area the Ozirovo Formation reaches a maximum thickness of more than 180 m, yet only 7 km to the northwest, the thickness decreases to less than 1 m (Sapunov et al., 1971).

The Teteven/Ravna Member is developed in two areas in Bulgaria, one area in west Bulgaria around the town of Ravna, and one area in central Bulgaria near

the town of Teteven. Lithologically the members are the same with differences only being attributed to their geographical locations. The Teteven/Ravna Member records a regionally extensive shallow marine sequence from an early Sinemurian to early Pliensbachian age. It consists of a 10-30 m thick succession of alternating sandy bioclastic limestones, calcareous sandstones and silty marls. The Dolni Lukovit Member is a 30-80 m thick succession of ferruginised sandy bioclastic limestones, of early Sinemurian to late Pliensbachian age (Figure 1.11). Above this the Bukorovtsi Member is a 20-40 m thick hemipelagic, irregular shale–marl– limestone alternation of late Pliensbachian to late Aalenian age (Figure 1.11). Previous work in Bulgaria has stated that organic–rich laminated shales are present from the f*alciferum* Zone although no evidence of this lithology, such as photomicrographs, are given (Metodiev et al., 2014). The undifferentiated Ozirovo Formation shows no major facies changes and is not subdivided into members. This formation typically comprises sandy bioclastic limestones or ooidal ironstones (Metodiev and Koleva-Rekalova, 2008).

The Ozirovo Formation is sharply overlain by poorly fossiliferous, deeper-water shales and siltstones of the Etropole Formation. This formation spans the late Aalenian to the middle Bajocian and here is up to 150 m thick (Tchoumatchenco et al., 1989).

1.5.4 Biostratigraphy of the Lower Jurassic in Bulgaria

1.5.5 Ammonite biostratigraphy

The biostratigraphic classification of the Lower Jurassic system is based predominately on ammonites in Bulgaria, first identified by Zlatarski (1908) and later built upon (Sapunov, 1961; Sapunov, 1963; Sapunov, 1964; Sapunov and Stephanov, 1964; Sapunov, 1968; Sapunov, 1979; Metodiev, 1997; Metodiev and Sapunov, 1999; Metodiev, 2000; Metodiev, 2002; Metodiev, 2003; Metodiev, 2003; Metodiev et al., 2005; Metodiev, 2006).

A synthesis of ammonite biostratigraphy for the Hettangian, Sinemurian and Pliensbachian stages is presented by Sapunov and Metodiev (2007), and for the Toarcian stage by Metodiev (2008) (Figure 1.12).

Five Hettangian and Sinemurian zones are recorded (Sapunov and Metodiev, 2007): *Alsatitinae* gen. and sp. indet. Zone, *Ectocentrites (Fucinites) gemmelaroi* Zone, *Coroniceras (Arietites) bucklandi* Zone, *Xipheroceras* Zone and *Radstockiceras* Zone. Six ammonite zones are described for the Lower

Pliensbachian: *Uptonia jamesoni* Zone (with two subzones: *Platypleuroceras aurenum* Subzone and *Uptonia jamesoni* Subzone), *Acanthopleuroceras valdani* Zone, *Beaniceras luridum* Zone, *Aegoceras maculatum* Zone, *Aegoceras Capricornus* Zone and *Oistoceras figulinum* Zone. Three ammonite zones are described for the upper Pliensbachian: *Amaltheus stokesi* Zone, *Amaltheus margaritatus* Zone and *Pleuroceras spinatum* Zone (with two Subzones: *Pleuroceras apyrenum* Subzone and *Pleuroceras hawskerense* Subzone).

A scheme of nine ammonite zones and 16 subzones for the Toarcian in Bulgaria is given in Metodiev (2008) (Figure 1.12). The lower Toarcian is divided into: *Dactylioceras (Orthodactylites) tenuicostatum* Zone (divided into *Dactylioceras (Orthodactylites) semicelatum* and *Dactylioceras (Orthodactylites) crosbeyi* Subzones); *Harpoceras falciferum* Zone (divided into *Harpoceras falciferum* and *Harpoceras serpentinum* Subzones), and *Hildoceras bifrons* Zone (divided into *Hildoceras semipolitum*, *Hildoceras bifrons* and *Hildoceras lusitanicum* Subzones).

The upper Toarcian is divided into: *Haugia variabilis* Zone (divided into *Denckmannia* spp. and *Collina* spp. Subzones); *Grammoceras thouarsense* Zone (divided into *Esericeras fascigerum*, *Grammoceras thouarsense* and *Pseudogrammoceras bingmanni* Subzones); *Pseudogrammoceras fallaciosum* Zone; *Phlyseogrammoceras dispansum* Zone; *Dumortieria pseudoradiosa* Zone (divided into *Dumortieria pseudoradiosa* and *Dumortieria levesquei* Subzones) and *Pleydellia aalensis* Zone (divided into *Pleydellia aalensis* and *Pleydellia mactra* Subzones).

There are a few exceptions and differences between the ammonite biostratigraphy defined in Bulgaria compared to northwest Europe. For the Toarcian, the ‘f*alciferum* Zone’ under the Bulgarian biostratigraphic framework is the equivalent of the NW European ‘s*erpentinum* Zone’ (Page, 2003).

Ammonite assemblages recorded in the upper Pliensbachian to upper Toarcian of the Moesian Basin show strong affinities to ammonite assemblages from the northwest European Boreal realm (Metodiev, 2008). The ammonite zones defined in Bulgaria are directly comparable to northwest Europe (Sapunov and Metodiev, 2007; Metodiev, 2008) (Figure 1.12).

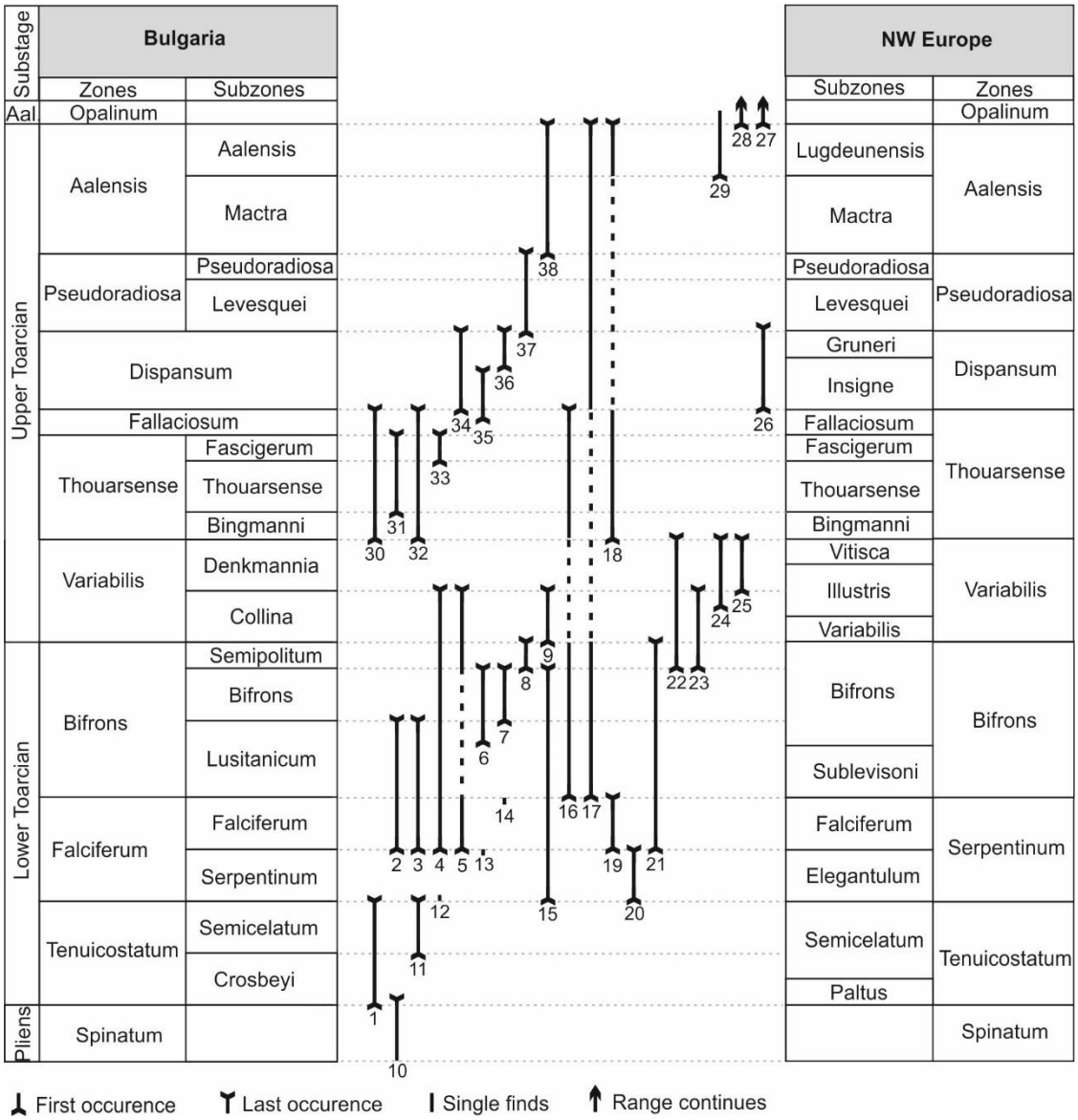

Figure 1.12 The ammonite zones and subzones of the upper Pliensbachian and Toarcian from Bulgaria (left) (from Metodiev et al., 2008; Metodiev et al., 2014) represented against the ammonite zonal standard of north-western Europe (right) (after Elmi et al., 1997). Range chart occurrences of ammonite genera from Bulgaria are plotted for each zone and subzone. Dactylioceratidae: 1. *Dactylioceratidae (Orthodactylites*), 2. *Dactylioceras (Dactylioceras (Dactylioceras)*, 3. *Nodicoeloceras*, 4. *Catacoeloceras,* 5. *Murcodactylites*, 6. *Zugodactylites,* 7. *Peronoceras,* 8. *Porpoceras*, 9. *Collina.* Hildoceratidae: *Harpoceratinae* - 10. *Protogrammoceras*, 11. *Tiltoniceras*, 12. *Eleganticera*s, 13*. Cleviceras,* 14. *Ovaticeras*, 15. *Harpoceras*, 16. *Polyplectus*, 17. *Pseudolioceras*, 18. *Osperleioceras*. Hildoceratinae: 19. *Orthildaites*, 20. *Hildates*, 21. *Hildoceras*. Grammoceratinae: 30. *Pseudogrammoceras*, 31. *Grammoceras*, 32. *Podagrosites*, 33. *Esericeras,* 34. *Phlyseogrammoceras*, 35. *Pseudolilia*, 36. *Hudlestonia*, 37. *Dumortieria,*

38, *Pleydellia*. Atoceratidae: 22. *Haugia*, 23. *Phymatoceras*, 24. "Chartonia", 25. *Denckmannia*. Hammatoceratidae: 26, *Hammatoceras,* 27. *Bredyia*, 28. *Czernyeiceras*, 29. *Pseudammatoceras*.

1.5.5.1 Additional biostratigraphic work

Parallel biozones based on the occurrence of ammonites, belemnites, bivalves and brachiopods from a single Lower Jurassic section in west Bulgaria was proposed by Sapunov et al. (1967) to date all Lower Jurassic sediments in Bulgaria. This parallel biozone framework was later modified by Shopov (1970), Stoyanova-Vergilova (1979), Sapunov and Tchoumatchenco (1988). Such parallel biozonations are not considered suitable for this study, particularly with consideration for bivalve biozones. For example, the lower limit of the Pliensbachian stage was drawn at the base of the bivalve *Entolium hehlii* Zone (Shopov, 1970). However, *Entolium hehli* has since been synonomised in bivalve taxonomy (Johnson, 1984) and is now considered to be *Entolium lunare*. This species has also been recorded in the late Sinemurian in South America (Damborenea, 2002a) and thus is not a reliable indicator for the base of the Pliensbachian.

Limited studies have recorded palynomorphs from the Lower Jurassic of Bulgaria (Čatalov and Černjavska, 1982; Černjavska, 1986) and calcareous nannofossils are undocumented for the Lower Jurassic.

Chapter 2 Methodology

The data used for this study were collected during four field seasons in north-west and central Bulgaria. Field seasons took place in April 2015, July 2015, August 2016 and November 2017. In total 13 sections were used for this study, with specific methods applied to individually selected sections. Details of the sample collection for each section are shown in Figure 2.1.

Material has been analysed at the University of Leeds (Univ. of Leeds), University of Copenhagen, University of Lyon, University of Lusanne and at the British Geological Survey (BGS), Nottingham, UK. The order of analysis carried out on material collected following fieldwork is shown in Figure 2.2.

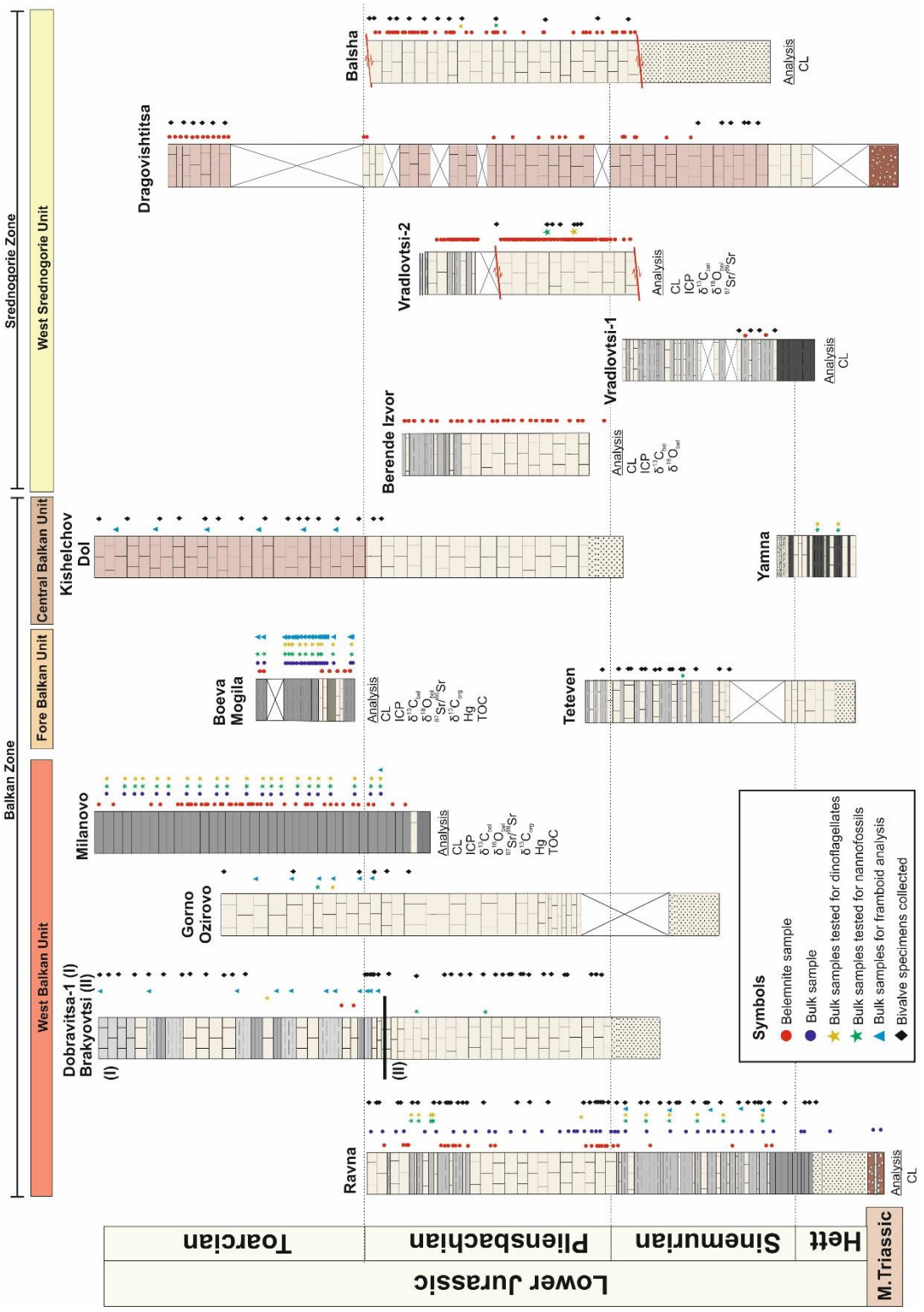

Figure 2.1 Schematic sedimentary logs of study sites. Drawn approximate to the Lower Jurassic with approximate sample horizons for geochemical analysis and macrofauna collections represented by coloured symbols. M.Triassic = Middle Triassic, Hett = Hettangian.

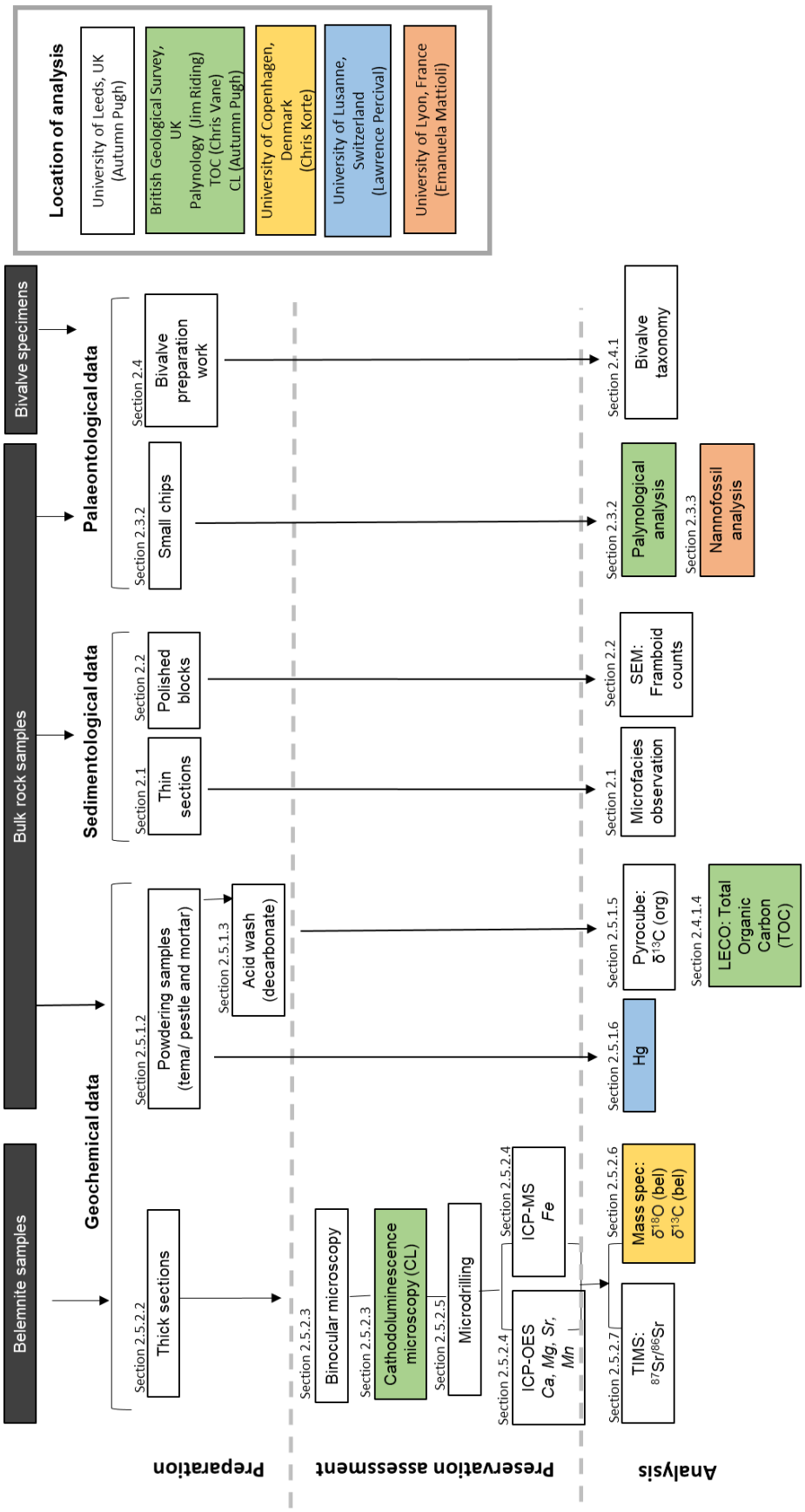

Figure 2.2 Flow chart to show the order of methods. Coloured boxes correspond to external collaborators.

2.1 Sedimentological analysis

Sedimentary successions selected for this thesis were logged using the formation and member definitions defined for the Jurassic formal lithostratigraphic scheme in Bulgaria (National commission on stratigraphy of Bulgaria, 2002). Initial reconnaissance fieldwork surveyed the Lower Jurassic exposures across NW Bulgaria and provided an overview of the regional tectonic setting. The type localities for all lithostratigraphic groups and members through the Pliensbachian and Toarcian were observed to aid with lithostratigraphic correlations for sections studied during the following field seasons.

Field data for 12 sections were recorded using graphic logs (Chapter 3). The Berende Izvor section could not be logged due to a lack of exposure and a previously published sedimentary log of Metodiev et al. (2012) is used for further analysis. A bed-by-bed graphic log was constructed for each of the 12 exposed sections, logged from the base of the succession upwards. Where the outcrop was good but not continuous, logs were created following beds laterally along section to find outcrops of succeeding beds. For the parts of the succession with no visible outcrop, rocks such as siltstones were excavated where possible, or recorded as ‘no exposure’ on the log. Beds and units for each section were given numbers to facilitate later reference to the collection of samples for thin sections, palaeontological data and bulk samples for geochemical work.

Key features recorded during logging included lithology, sedimentary structures, colour, fossil distribution and the lateral and vertical changes in thickness and composition of each bed. Other features noted included presence of hardgrounds, discontinuity surfaces and bioturbation. Additionally, when logging carbonate rocks, the presence of specific skeletal grains (e.g. crinoids, echinoids, bryozoan, bivalves, brachiopods) and non-skeletal grains (e.g. ooids, peloids and carbonate lithoclasts) were recorded, when identifiable in the field.

Analysis of sediment fabric (i.e. presence of lamination) provides a simple indication of depositional oxygen levels. During sedimentary logging, the presence (or absence) or fine lamination was recorded. Field determinations were supplemented by petrographic observation of thin sections.

Further work on facies identification was carried out using petrographic examination of thin sections. A total of 156 bulk rock hand samples (~10 cm^3) were collected for thin section work. Sample orientation was labelled in the field, allowing depositional and structural top and bottom to be recognised. To make

thin sections, hand samples were mounted on 4.5 cm x 3 cm slides and cut to 30 μm. All sections are now housed in the SOEE (Univ. of Leeds, UK).

The Lower Jurassic successions studied are predominantly carbonate rocks and were described and characterised (from thin sections and hand samples), using the limestone classification of Dunham (1962). Lithological characters from field observations were integrated with thin section evaluation to provide any additional information useful for palaeoenvironmental interpretation.

2.2 Pyrite framboid petrography

A total of 66 bulk samples were collected for framboid analysis. Samples were selected for each section through the upper Pliensbachian-Toarcian interval (Milanovo, Kiselchov Dol, Gorno Ozirovo, Boeva Mogila and Dobravista-1 sections) and additionally from one other section comprising marl, siltstone or mud-rich lithologies (Ravna section). For location and stratigraphic height of samples selected for framboid analysis see Appendix C.1.

Bulk samples were cut perpendicular to bedding into approximately 2 cm x 2 cm x 1.5 cm blocks using a water lubricated saw. Each block was mounted in epothin resin and left to set overnight at room temperature. One face of the cut block was ground down to ensure a flat, level surface for analysis, and subsequently polished to ¼ μm. Bulk samples in mounted blocks were carbon coated and viewed under a Scanning Electron Microscope (SEM; FEI Quanta 650 FEGESEM) at the Lemas facility (Univ. of Leeds, UK). Pyrite framboid size distribution for each sample was carried out using backscatter mode following the procedure of Bond and Wignall (2010). Pyrite framboid sizes were measured on-screen using built-in measurement software, and their size distribution counted (details of procedure given in Bond and Wignall, 2010). The framboids were measured on their longest diameter with an uncertainty of about 0.12 μm. Because the polished surfaces represent a random cut and thus do not necessarily represent the maximum sections of the framboids, the employed methodology underestimates the true maximum diameter of the pyrite framboids. Nevertheless, this offset does not exceed 10% of the measured diameter compared with other methods (Wilkin et al., 1996).

SEM analysis (backscattered imaging and EDX elemental mapping) and use of Aztec software was undertaken to examine more detailed petrographic features including the nature of the pyrite content. EDX elemental mapping allowed for quantitative information about the concentration of each element for any selected grain, allowing minerals to be identified. Data collected using EDX

elemental mapping included evaluating if the sample had been oxidised, the presence of diagenetic pyrite, matrix composition, key allochems and presence of accessory minerals.

Framboid counts and size measurements were carried out only on densely packed spherical or oovoid aggregates of equal sized microcrysts or loosely packed aggregates (categorised as type 1 and type 2 framboids by Wignall and Newton, 1998). Pyrite microcrystals, pyrite lumps and polyframboids (spherical aggregates of several framboids) were noted but not used for size measurements. The presence of framboids was categorised semi-quantitatively into absent, rare (<50 framboids could be counted), low abundance (> 50 but <100 framboids could be counted) and common (>100 framboids could be counted for each sample) (Appendix C.1). Where <50 samples could be counted in an individual sample, the presence of framboids was noted as 'rare', and not included in the cross-plot of standard deviation versus framboid mean.

When present, framboid size data (including distribution histograms, the size range, and average sizes) from each sample has been used to infer redox conditions. Mean versus standard deviation plots were used to differentiate euxinic/anoxic and dysoxic-oxic depositional environments following Wilkin et al. (1996) for each section analysed. The euxinic/anoxic field is not split as framboid size and distribution cannot differentiate between these conditions. The dysoxic/oxic field is not separated as no calibration line has been established for the dysoxic/oxic boundary, only the boundary between dysoxic and euxinic/anoxic.

2.3 Biostratigraphic framework

To build on the current biostratigraphic framework for the Lower Jurassic sections in Bulgaria, ammonites specimens and bulk material (to process for the abundance and occurrence of nannofossils and dinoflagellates) were collected.

2.3.1 Ammonite collections

Age determinations were carried out using ammonite biostratigraphy by Dr. Lubomir Metodiev, following the published ammonite zonal scheme for Bulgaria of Metodiev (2008). Age assignments based on ammonite biostratigraphy were made using both previously published work (Sapunov and Metodiev, 2007b; Metodiev, 2008) and additional sampling and identifications made in the field. Where specific ammonite species occurrences were already documented, only

representative samples were collected. For sections that were previously unstudied with no recorded ammonites, all ammonites were recorded and collected. Ammonite occurrences are given for all sections studied, where ammonites are present.

2.3.2 Palynological preparation and processing techniques

Bulk samples for palynological studies were prepared and processed at the BGS (Nottingham, UK). An initial five test samples were processed for palynomorphs from several lithologies to indicate the degree of preservation and/or abundance throughout the Lower Jurassic sections. Bulk samples were processed from Dobravitsa-1, Balsha, Beledie Han, Vradlovtsi-2 and Ravna. However, these samples were mainly sandy limestones with low amounts of organic matter and yielded no palynomorphs. A further 27 samples were processed from Milanovo, Boeva Mogila, Yamna and Ravna sections. These sections had higher TOC values and were silty marls or shales considered more likely to contain palynomorphs.

For samples with high carbonate content, and where enough material was collected, ~100 g of each sample was processed. The cleaned and weighed samples were crushed into pea-sized fragments and a *Lycopodium* tablet (batch number 3862) was added. Once prepared, each sample was processed using the standard palynological technique described by Wood (1996). The only modification from this method was that the organic residues were not oxidised, as the samples lacked finely disseminated or amorphous organic matter. All slides are now housed at the BGS (Nottingham, UK).

2.3.3 Nannofossil preparation and processing techniques

An initial batch of 26 test samples, comprising about 10 g of small bulk sample chips, were processed for nannofossil analysis at the University of Lyon (France). Samples were selected from eight sections: Milanovo (8), Boeva Mogila (1), Yamna (2), Balsha (1), Teteven (1), Brakyovtsi (2), Vradlovtsi-2 (1), Ravna (10). These samples were selected in order to evaluate lithologies most suitable for nannofossil work from Bulgaria, and included sandy limestones, bioclastic limestones, marls and clay rich siltstones. Processing a range of samples from multiple field sections also provided an indication of the degree of preservation and/or abundance of nannofossils through the Lower Jurassic sections in northwest Bulgaria.

Only Boeva Mogila and Milanovo sections yielded abundant nannofossil assemblages, with all remaining samples from other sections being very sparse or barren of nannofossils. A further 41 samples were then processed from Milanovo (12) and Boeva Mogila (29) sections.

The absolute abundance of calcareous nannofossils was estimated in 41 samples using smear slide preparation techniques described by Bown (1998). In summary, a homogeneous suspension of ~300 mg of dried rock-powder and water (oversaturated with respect to $CaCO_3$ and with a basic pH) was allowed to settle for 24 h on a cover slide put in a settling device. The cover slide is eventually recovered, dried and attached to a microscope slide. All slides are currently housed at the University of Lyon (Lyon, France) with Prof. Emanuela Mattioli.

2.4 Macrobenthic collections for extinction study

Following the construction of detailed sedimentary logs for all 13 fieldwork sections, the presence or absence of bivalves in each section was noted and evaluated. Eleven sections contained samples suitable for collection of macrofauna, based on preservation, abundance and ability to extract fossils. These sections were: Balsha, Teteven, Dragovishtitsa, Vradlovtsi-1, Vradlovtsi-2, Ravna, Dobravitsa-1, Brakyovsti, Gorno Ozirovo, Kiselchov Dol and Boeva Mogila.

Bed-by-bed sampling, with typical sample spacing between 10-50 cm, was carried out for collections of macrofauna, with a predominant focus on the collection of bivalves. Other sampled fossils included brachiopods, ammonites and belemnites. For each sampled bed rock was mechanically broken up, using geological hammers, and all macrofauna were counted and collected. Due to exposure restrictions, some outcrops did not allow for bed by bed sampling.

All specimens collected were brought back to the Geological Institute of the Bulgarian Academy of Sciences in Sofia and specimens selected for taxonomic work were sent on to the SOEE (Univ. of Leeds, UK). Selection criteria included overall preservation and the presence of particular taxonomic features for genus and species identification.

To prepare specimens, they were initially washed using DI water, and a soft toothbrush was used to remove excess dirt and vegetation. Following this, a compressed air drill was used to remove attached rock from specimens to expose features key to taxonomic identifications.

2.4.1 Bivalve taxonomic identifications

Preliminary identification of fossils was carried out in the field, with each specimen recorded and most specimens photographed, in case of damage during transport. Further taxonomic work of selected faunas (see above) was carried out at the SOEE (Univ. of Leeds, UK). All bivalves have been identified to the lowest taxonomic level to which they could be confidently assigned.

2.4.1.1 Reference texts and collections

A range of reference material was used to aid taxonomic identifications. As it was not an aim to revise Lower Jurassic bivalve taxonomy, both published literature and collections were used as a source of reference.

Many species could be identified on the basis of current published literature for Lower Jurassic bivalves (Shopov, 1968b; Cox et al., 1969; Johnson, 1984; Damborenea, 1987; Hodges, 1987; Damborenea, 1993; Aberhan, 1994; Cox, 1994; Johnson, 1994; Damborenea and Gonzalez-Leon, 1998; Hodges, 2000; Ibarrola, 2002; Damborenea, 2002a; Valls et al., 2004; Aberhan, 2004; Aberhan et al., 2011; Radulović, 2013; Paredes, 2014; Paredes et al., 2015).

The UK Natural History Museum (NHM) Toarcian bivalve collections from the Yorkshire Coast (UK), collected and prepared by Silvia Danise, were viewed in March 2015. Corresponding publications from these collections include Danise et al. (2013) and Danise et al. (2015).

The Whitby Museum Lower Jurassic bivalve collections from the Yorkshire Coast (UK) were also viewed in March 2015.

The BGS (Nottingham, UK) Lower Jurassic bivalve collections from across the UK were viewed in May 2015. Further details on materials housed in the BGS collections, in particular type specimens, can be found online at http://www.3d-fossils.ac.uk.

The Lower Jurassic bivalve collection from the Yorkshire Coast, collected and prepared by Dr Crispin Little, are permanently housed in the Palaeontology Laboratory in the SOEE (Univ. of Leeds, UK) and were continuously used as reference material. Publications utilising these collections are Little (1995), Little and Benton (1996) and Harries and Little (1999).

The Jurassic bivalve collections from NW Bulgaria are housed between the Bulgarian Academy of Sciences, the University of Sofia and the Bulgarian

Natural History Museum. These collections were viewed in September 2014, April 2015, July 2016 and July 2018.

2.4.1.2 Synonymised taxa

Updated taxonomic identification studies in recent years have re-assigned certain bivalve species to different species or genera. These studies were used to update taxonomic identifications of bivalves previously recorded in Bulgaria. Appendix D summarises, the taxa recorded in Bulgarian literature from the Lower Jurassic, alongside the new synonymised taxa names and associated reference text. The bivalve taxa previously identified in Bulgaria are evaluated in addition to collections from fieldwork during this PhD.

2.4.1.3 Nomenclature

Open nomenclature taxa (Bengston, 1988) are included, herein, in the stratigraphic range charts of this study. The term “cf.”, short for “Confer”, is used to denote a tentative or provisional level of identification, mostly used when preservation is poor. The terms “*species indet*.” Or “sp.” refers to an indeterminate species of a particular genus and a question mark is used to denote uncertainty, mostly at the genus level.

2.4.1.4 Plates

At least one representative individual of each species identified has been photographed. Photographs were taken of specific and distinguishing features that enabled taxonomic identification. All photographed specimens were coated with ammonium chloride powder, unless otherwise stated. All plates of photographed bivalves can be found in Chapter 6.

2.4.2 Trace fossils and bioturbation

The degree of bioturbation was evaluated systematically for two sections (Milanovo and Boeva Mogila), with a focus on recording bioturbation through the Toarcian. These sections were selected because the lithologies, comprising siltstones and marls, allowed bioturbation to be assessed continuously through the Toarcian. Many other sections were often represented by carbonate rocks that had complex diagenetic histories, such as dolomitisation, so trace fossils

were only intermittently observed and recorded and could not be assessed continuously. In circumstances where individual trace fossils could be observed, they were recorded and classified following (Seilacher, 1964; Droser and Bottjer, 1993).

For the Boeva Mogila and Milanovo sections, semi-quantitative estimates of bioturbation proportions from thin sections and hand samples was used to categorise the degree of bioturbation, following the classification of IODP: Absent or non-visible (0%), Slight (0%–30%), Moderate (>30%-60%) or Strong (>60%-100%). A more detailed ichnofacies scheme or index, such as Droser and Bottjer (1986) could not be used due to the poor exposure of outcrops, fissile and weathered nature of exposures and lack of bedding planes, which restricted more detailed identification of individual traces.

2.5 Geochemical analyses

2.5.1 Bulk samples for geochemical analyses

2.5.1.1 Field sampling

A total of 97 bulk samples were collected from the Milanovo (17), Ravna (51) and Boeva Moglia (29) sections. Lithological information and section heights for bulk samples are given in Appendix B. Around 100 g of bulk rock was collected for each sample and sampling avoided areas with evidence of weathering, close proximity to post-depositional mineral (hydrothermal) veins, fractures, faults or observable areas of alteration, such as colour change.

2.5.1.2 Preparation

Weathered surfaces of bulk rocks were initially removed. Bulk samples were broken down with a hammer to small chips and any weathered surfaces or rinds were chipped off or ground off using a water-cooled, diamond tipped bench circular saw.

Rock chips were then powdered and homogenised to a fine powder <150 μm, giving a flour-like consistency. Samples were ground down mechanically using an agate mill (TEMA) or by hand using an agate pestle and mortar. In between samples, the TEMA or agate pestle and mortar were cleaned using pure quartz sand and wiped clean using acetone to avoid cross contamination of samples. All crushed powders were divided into two aliquots, with ~10 g taken to be treated (de-carbonated) and the remaining powder left untreated.

To remove the water content from samples prior to analyses, ~5 g of powdered sample was placed in a crucible and left in an oven at 60°C overnight. Samples were subsequently dried and stored in a sealed container.

2.5.1.3 De-carbonation

Sediments that contained inorganic carbon were treated with acid to remove the inorganic carbon, prior to being analysed for TOC and C_{org}. Due to the presence of a dolomitic matrix in some sections, sediments were acid washed twice to ensure all of the carbonate fraction was removed.

To treat samples, 40 ml 10% HCl was added to ~2 g of sample powder in a non-skirted 50 ml plastic vial. The vial was subsequently shaken to ensure all dry material was in contact with solution. The solute was left for 24 hours at room temperature then decanted. The sediment was washed in de-ionised (DI) water at least three times or until neutrality was reached (pH ~6). Samples were oven dried at 60° C, cooled and weighed. The sample was then crushed to homogenise the rock, using an agate pestle and mortar and cleaned in-between samples with quartz sand and acetone.

During the process of acid washing, the weights of the following were recorded for each sample: the centrifuge tube (m_{tube}), the sample and tube ($m_{initial}$) and the sample and tube following acid washing (m_{final}). This allowed a mass change to be calculated using the equation:

$$m_{lost}=(m_{initial}-m_{tube})-(m_{final}-m_{tube}),$$

where m_{lost} includes carbonate and other soluble elements.

Decalcified bulk samples were then split. Around ~ 50 mg was kept and subsequently weighed into a tin capsule (8 x 5 mm) and sealed ready for C_{org} analysis at the SOEE (Univ. of Leeds, UK), and between 0.5 g and 1 g weighed out and sent to the BGS (Nottingham, UK) for TOC analysis.

2.5.1.4 Total Organic Carbon (TOC) determination

A total of 46 samples from Milanovo and Boeva Moglia sections were analysed for TOC concentrations. The bulk samples from the Ravna member were too poor in organic carbon to yield a reliable value.

Approximately 1 g of acid treated sediment was dried at 100°C for 1.5 h and a 300 mg sub-sample transferred into a pre-weighed ceramic crucible. Total organic carbon was measured using a Elementar Vario Max C/N analyser

configured with vertical tubular quartz combustion furnace (1050°C) using helium as a carrier gas. Carbon content was determined by measuring the amount of CO_2 generated as a function of time during combustion in a stream of oxygen in the presence of cerium dioxide catalyst. The limits of quantification for a typical 300 mg sample were 0.18%. Details of this method have been described previously (Vane et al., 2007; Vane et al., 2014). TOC analysis was carried out at the BGS (Nottingham, UK) by Chris Vane. The results of TOC are expressed as a percentage (%) of the original sample mass. Reproducibility and quality of the measurements were checked by a standard every 10 samples. Replicate analysis (n=10) of the standard NIST-1941b with a certified value of 2.99 ± 0.24 gave a 0.035 standard deviation, a 7% bias, 1% relative standard deviation (r.s.d) for TOC %.

The value given from the TOC analyser is Percentage of Carbon (POC), not the TOC. To calculate the TOC and TIC (Total inorganic Carbon) accurately the following calculations were used:

$TOC = POC * ((m_{final}-m_{tube})/ m_{initial}-m_{tube}))$

$TIC = TC – TOC$

An estimate of the calcite content for each sample was made by assuming that all TIC is hosted by calcite (wt% calcite = TIC x 8.333).

2.5.1.5 Organic carbon isotopes (bulk rock)

The organic carbon isotope content of decalcified bulk samples was performed on an Isoprime continuous flow mass spectrometer coupled to an Elementar Pyrocube elemental analyser, in the SOEE (Univ. of Leeds, UK). Samples were weighed into tin cups in sufficient quantity to produce peaks of between 1 and 10nA. The encapsulated samples were converted to CO_2 by combustion at 1150°C in the presence of pure oxygen (N5.0) injected into a stream of helium (CP grade). Quantitative conversion to CO_2 was achieved by passing the gases through tungstic oxide also at 1150°C. Excess oxygen was removed by reaction with hot copper wires at 850°C, and water was removed in a Sicapent trap. All solid reagents were sourced from Elemental Microanalysis, UK, and all gases were sourced from BOC, UK. N_2 continued through the system unchecked, whilst CO_2 and SO_2 were removed from, and re-injected into, the gas stream using temperature controlled adsorption/desorption columns.

The $\delta^{13}C$ of the sample is derived from the integrated mass 44, 45 and 46 signals from the pulse of sample CO_2, compared to those in an independently

introduced pulse of CO_2 reference gas (CP grade). Carbon isotope analyses were calibrated with in-house C4-sucrose and urea standards assigned values of -11.93 ‰ and -46.83 ‰ respectively via calibration with the international standards (assigned values in brackets), LSVEC (-46.479 ‰), CH7 (-31.83 ‰), CH6 (-10.45 ‰), and CO-1 (+2.48 ‰).

2.5.1.6 Sedimentary mercury concentrations

A total of 52 samples from Milanovo (21) and Boeva Moglia (31) sections were analysed for mercury (Hg) concentrations. The shallow water Toarcian sections comprising ironstone and sandy bioclastic limestones are likely to have too little Hg present, due to low organic carbon content (e.g. Sanei et al., 2012; Percival et al., 2017), so were not selected for Hg analysis.

Hg concentrations were determined on a mercury Analyzer RA 915 F coupled to a PYRO-915+ Pyrolyzer (Lumex) at the University of Lausanne (Switzerland), broadly following the method outlined in Percival et al. (2017). 100±2 mg of powdered untreated bulk sample was weighed out into a quartz boat and its precise mass measured. The quartz boat (with powder) was placed into the pyrolyser unit, set to Mode 1 (700˚C), which volatilised the mercury. The resultant gas passed into the analyser unit, where it was detected by Zeeman atomic absorption spectroscopy (see Sholupov and Ganeyev, 1995). The detected quantity was registered on the Lumex software on a computer coupled to the analyser unit, and the mercury concentration calculated following input of the measured sample mass. Each sample was measured twice to check measurement repeatability, which was typically within 10% of the measured concentration. The measurements were calibrated using the Certified Reference Material NCS DC73309 (stream sediment) as a standard, which has a concentration of 72±9 ppb. Four standards were measured at the start of an analytical run, with a further standard measured after each subsequent set of ten unknown measurements to check for machine drift. Hg measurements have up to ±10% uncertainty.

2.5.2 Belemnite samples for geochemical analyses

Belemnite calcite was used for stable isotopic analysis of $\delta^{13}C_{bel}$ and $\delta^{18}O_{bel}$ (167) and radiogenic isotopic analysis of $^{87}Sr/^{86}Sr$ (36).

2.5.2.1 Field sampling

A total of 328 belemnites were collected from the Ravna (82), Balsha (82), Dragovishtitsa (24), Vradlovtsi-1 (2), Vradlovtsi-2 (74), Teteven (3), Brakyovtsi (1), Milanovo (45), Dobravitsa-1 (2) and Boeva Mogila (13) sections. Although belemnites were present in the Gorno Ozirovo and Kiselchov Dol sections, all of the belemnites from these sections were visibly heavily weathered, indicative of alteration and not collected for isotopic analysis.

An additional set of 45 belemnites were used from a previously sampled section, called Berende Izvor (Metodiev et al., 2012). Each belemnite collected by Metodiev et al. (2012) was re-drilled for trace element analysis and stable isotope analysis (carbon and oxygen).

2.5.2.2 Preparation

A total of 115 individual belemnites were screened to give an overall indication of belemnite preservation for each study section and, for individual belemnites, to ensure least altered calcite was drilled for isotope analysis. Each belemnite was cut dorsoventrally perpendicular to its length into two counterpart segments. One piece was turned into a thick section (~100 μm) and used for cathodoluminescence (CL) analysis, and the corresponding surface of the second piece was kept for microdrilling powders used for isotopic analysis for $\delta^{13}C$, $\delta^{18}O$, $^{87}Sr/^{86}Sr$. A total of 115 thick sections were made at the Bulgarian Academy of Sciences, Sofia (Bulgaria) and 12 in the SOEE (Univ. of Leeds, UK). Further preservation assessment, using trace element concentrations, were determined for each sample drilled.

2.5.2.3 Belemnite preservation/diagenetic screening

Belemnites were examined and optically screened using transmitted light and CL as a primary test for evidence of fossil calcite degradation or recrystallisation during diagenesis. These initial diagenetic screening techniques directed which parts of each belemnite to drill, for most unaltered calcite. Following microdrilling, trace element analysis provided a further indication of diagenetic alteration to individual subsamples.

Binocular microscope evaluation

Evidence of fossil preservation was evaluated for all belemnites drilled for isotope analysis through a binocular microscope. Evidence of recrystallisation

and cementation was associated with a loss of transparency and the development of grainy textures of belemnite calcite. In addition, areas of clear alteration and secondary precipitates concentrated along fracture surfaces in rostra allowed further alteration to be recognised. Areas of likely alteration identified through binocular microscope evaluation were mapped out and avoided during microdrilling.

Physical abrasion and belemnite powder colour

During microdrilling, the hardness of belemnite calcite was noted. If the calcite broke easily, this indicated biogenically precipitated calcite. Whereas if the belemnite calcite was noticeably hard, this may be a result of the calcite being recrystallised or silicified. In addition, the colour of belemnite powder for each subsample was recorded, as colour can be indicative of well-preserved calcite (white powder) or diagenetically altered calcite due to the presence of impurities such as silica, oxides and hydroxides (brownish powder) (Ullmann and Korte, 2015).

Cathodoluminescence

Cathodoluminescence (CL) microscopy was carried out on belemnite thick sections at the BGS (Nottingham, UK), using a Technosyn Cold Cathode Model 8200MK11 with an electron gun current of 15 ± 1 keV 0.7 ± 0.1 ma.

A total of 115 belemnites were screened using CL. All belemnites from sections through the Toarcian were selected for CL, which comprised the Boeva Mogila and Milanovo sections. For all other sections (Balsha, Vradlovtsi-1, Vradlovtsi-2, Ravna and Brakyovtsi), ~25% of all collected belemnites were selected for CL. Samples were chosen from each section at relatively evenly spaced intervals and/or where there was observable lithological change. These samples were chosen to be representative and indicative of overall belemnite preservation for each section.

All belemnite rostra examined as thick sections were mapped out using CL microscopy, carefully detailing the areas of luminescence of each belemnite. Each ‘mapped’ belemnite was then classified using the styles of alteration scheme, designed to semi-quantitatively assign a degree of potential alteration to each belemnite, based on recognisable alteration of CL characteristics. Six key styles with increasingly altered belemnite rostra, from non-luminescence to luminescent depending on characteristic CL behaviours are explained in Figure 2.3. Examples of the six alteration styles were photographed in transmitted light (TL) and CL using a Zeiss Axiocam MRC5, at a magnification x5 and 60 second

exposure time. The Milanovo and Boeva Mogila images were taken using a 12-megapixel camera directly through the microscope lens.

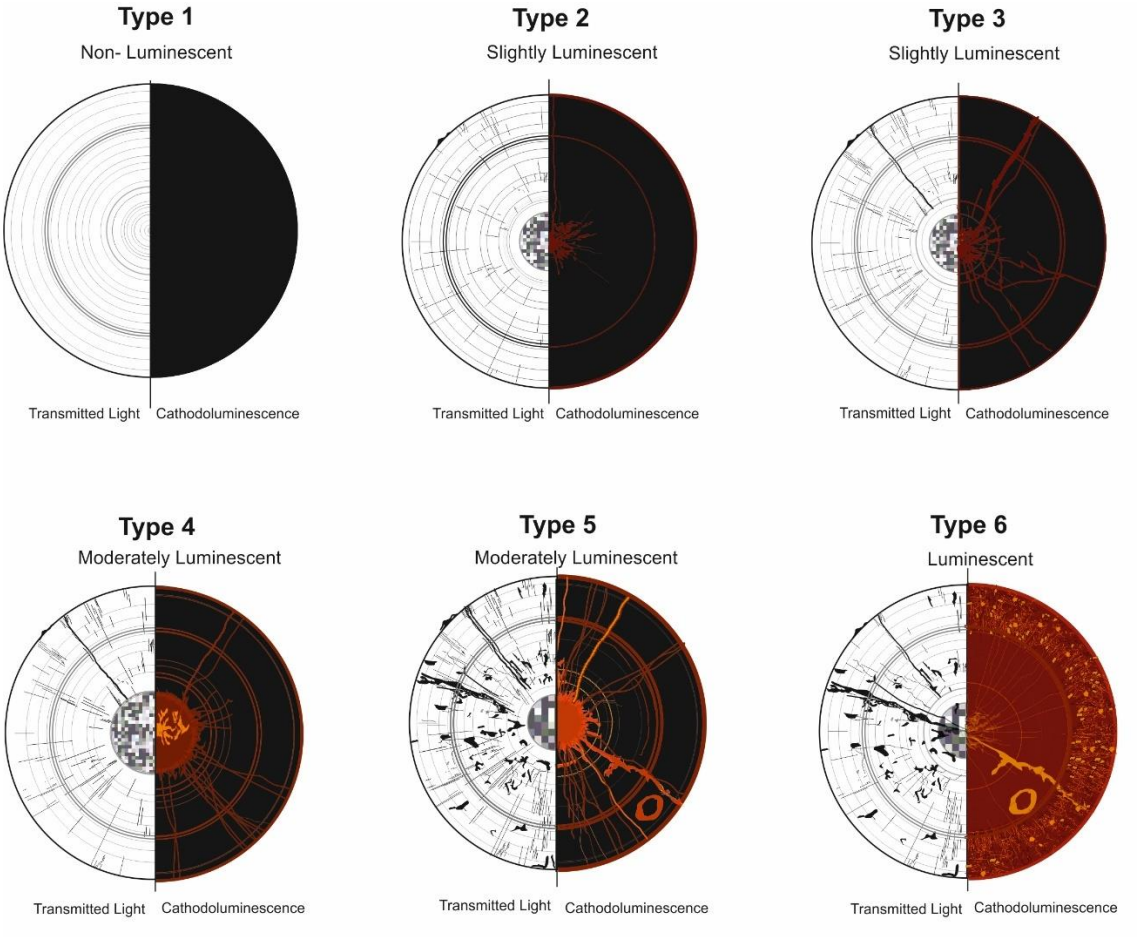

Figure 2.3 Schematic to show the six characteristic styles of alteration observed in belemnites in Bulgaria. Details of each alteration style classification and indication of where belemnite was microdrilled are found below.

Type 1: ‘Non Luminescent’ alteration style, with nearly all primary calcite with no, or very minute amounts, luminescence. Drilled: anywhere in belemnite.

Type 2: ‘Slightly Luminescent’ alteration style, with overall <10% luminescence. Dull luminescence occurs along the rostrum’s outer margin, in a constrained area around the apical line, prominent concentric growth lines and/or in small radial fractures. Drilled: anywhere in between outer rim and apical line.

Type 3: ‘Slightly Luminescent’ alteration style, with overall 10-20% luminescence. Dull and bright luminescence can be observed along the rostrums outer margin, around the apical line, with some radiating fractures around the apical line areas and prominent concentric growth lines. Drilled: in between outer rim and apical line, avoiding prominent fractures.

Type 4: ‘Moderately Luminescent’ alteration style with 20-50% luminescence. Bright luminescence is observed along the rostrums outer margin and a relatively constrained area around the apical line. Both prominent and minor growth lines show luminescence as well as microfractures or pressure solution seams. Drilled: in between outer rim and apical line, avoiding prominent fractures and main growth rings.

Type 5: ‘Moderately Luminescent’ alteration style with 50-90% luminescence. Often very bright luminescence is observed within a wide zone along the rostrums outer margin and a large area around the apical line. Both prominent and minor growth lines show luminescence as well as a high density of microfractures or pressure solution seams. Significant fractures or borings with bright luminescence often occur. Drilled: carefully select specific areas in between outer rim and apical line, avoiding prominent fractures and main growth rings or radial fractures.

Type 6: ‘Luminescent alteration’ style with >90% luminescence. Defined by very bright luminescence colours of yellow and orange throughout the calcite, with very few areas showing no luminescence as almost all secondary calcite preserved. The amount of primary calcite preserved is not large enough from which to obtain material. Drilled: a belemnite that is considered ‘luminescent’ will not be drilled as it is considered too altered.

2.5.2.4 Elemental analysis

For elemental analysis, a 2 mg subsample was weighed and transferred into a 15 ml Sarstedt tubes and dissolved in 5 ml 0.1M hydrochloric acid. Five duplicates and blank samples were run for belemnites from each section. Element ratios of samples were measured using a Thermo Fisher iCAP 7400 Radial Inductively Coupled Plasma Optical Emission Spectrometer (ICP-OES) and Thermo Fisher iCAPQc 7400 Inductively Coupled Plasma Mass Spectrometer (ICP-MS). The ICP-OES determined concentrations of Ca, Mg, Sr and Mn and solutions were ran with a 1 p.p.b. Y internal standard. The limit of detection (LOD), limit of quantification (LOQ), and percentage of uncertainty on each measurement (ICP-OES) is shown in Table 2.1. The ICP-MS determined concentrations of Fe and solutions were ran with a 1 p.p.b. Rh internal standard (ICP-MS).The limit of detection (LOD), limit of quantification (LOQ), and percentage of uncertainty on each measurement (ICP-OES) is shown in Table 2.1.

Table 2.1 LOD, LOQ, and recovery percentages uncertainty for element analyses on the ICP-OES (Ca, Mg, Sr, Mn) and ICP-MS (Fe).

	Ca ppm	Mg ppm	Sr ppm	Ba ppm	Mn ppm	Fe ppb
LOD	0.235	0.023	0.002	0.002	0.002	0.370
LOQ	0.783	0.077	0.008	0.007	0.008	1.23
% uncertainty	2.36	2.83	1.22	1.94	1.39	3.49

The concentration (ppm) of the total elements in each sample was calculated as:

Concentration of sample (ppm) = (ICP Concentration (ppm)/ sample weight (g)) x volume (ml)

The ICP concentration is the number taken from ICP analysis. The volume is the total volume of digest solution (5 ml). The final wt% of the sample was then determined as:

Total (wt%) = (ICP concentration (ppm) x 10-6 x volume (ml)/ sample weight (g)) x 100

2.5.2.5 Microdrilling

Belemnite calcite was drilled in the SOEE (Univ. of Leeds, UK) using a hand held dental core drill MF-PERFECTA with diamond tipped stainless steel drill bits, with a drill tip diameter of 0.3 mm and drill speed of 0 – 35 n x 1000.

Each belemnite was drilled to provide between one and three subsamples depending on preservation determined in pre-screening methods. Each subsample was drilled according to: a) where CL mapping has indicated least altered calcite (e.g. least luminescent areas), b) were light petrography showed least alteration or silicification (e.g. no discoloured calcite) and c) away from all outer edge, apical line and clear cracks in all belemnites, as these areas are frequently diagenetically altered (Podlaha et al., 1998; McArthur et al., 2000; McArthur et al., 2007; Ullmann, et al., 2013; Ullmann et al., 2015b). Additionally, microdrilling was avoided around the central part of the rostrum, as recent work has suggested strong crystal bending in these areas is likely to result in element enrichment (Ullmann and Korte, 2015). Prior to drilling each sample the very top layer (< 1 mm thickness) of surface calcite was removed and discarded, to expose a clean surface and coat the drill tip in the subsample powder to avoid contamination from previous samples. The drill bit was cleaned carefully with a wire brush between each belemnite and a new drill bit used every ~15 belemnites and for belemnites from new sections. An additional 20 belemnite powders were drilled from visibly altered areas of belemnite including the apical line, outer edges and borings to provide an indication if any diagenetic pull from stable isotope and trace element analysis.

For each belemnite subsample, 6 mg of powder was drilled and divided into three parts: 2 mg for element ratio determinations, 2 mg for carbon and oxygen stable isotopic analysis and 2 mg for strontium isotope analysis. Each 6 mg subsample powder was drilled onto clean weighing paper, transferred into a 1 ml capped vial and shaken to homogenise.

An additional acid treatment of the surface was avoided because acid leaching has been found to preferentially attack well-preserved parts of the rostra (Podlaha et al., 1998). The results are reported in per mil (‰) relative to the LEO = Carrara Marble or the V-PDB, respectively.

2.5.2.6 Carbon and oxygen isotope analysis

The calcite carbon ($^{13}C/^{12}C$) and oxygen ($^{18}O/^{16}O$) isotope values from belemnite calcite were measured at the Department of Geosciences and Natural Resource Management, University of Copenhagen (371 subsamples).

The stable isotope work processed at the University of Copenhagen followed Ullmann (2013). Sample powders (500 to 700 µg) of belemnite rostra were reacted at 70°C in sealed glass vials with ~50 µl manually added anhydrous phosphoric acid after the removal of atmospheric gases with helium. Liberated CO_2 was subsequently analysed for oxygen and carbon isotope ratios using an IsoPrime triple collector Isotope Ratio Mass Spectrometer. Sample-weight-dependent isotope fractionation was corrected by using calibration curves constructed from repeated measurements of the in-house standard (LEO = Carrara Marble: $\delta^{13}C$ = +1.96 ‰ V-PDB; $\delta^{18}O$ = -1.93 ‰ V-PDB) covering the utilised sample weight ranges (see also Ullmann et al., 2013). The analytical precision (2sd) of the analyses calculated from repeated measurements of the LEO standard was better than 0.2 ‰ for $\delta^{18}O$ and better than 0.1 ‰ for $\delta^{13}C$.

The stable isotope values are reported as the per mil difference between sample and the VPDB standard in delta notation where $\delta^{18}O$ or $\delta^{13}C$ = (Rsample / Rstandard − 1) x 1000, and R is the ratio of the minor to the major isotope.

Using $\delta^{18}O$ as a proxy for palaeotemperature

The $\delta^{18}O$ of belemnite calcite is thought to reflect isotopic composition of the Jurassic seawater in which the belemnites lived (Urey et al., 1951; Saelen et al., 1996; Podlaha et al., 1998; Bailey et al., 2003). It is difficult to directly understand vital effects (biological fractionation) and species-specific effects as belemnites are now extinct. However, belemnites are considered to have precipitated shell carbonate in near oxygen-isotope equilibrium with ambient sea water, based on their similarities to modern analogue cuttlefish (Rexfort and Mutterlose, 2006; Wierzbowski and Joachimski, 2007).

For $\delta^{18}O_{bel}$ to be utilised as a proxy for palaeotemperature, assumptions are made that belemnite calcite is well-preserved and precipitated in equilibrium with ambient seawater with no major changes in salinity. The $\delta^{18}O_{bel}$ value of Early Jurassic seawater is assumed to have been -1 ‰ Standard Mean Ocean Water (SMOW), for an ice-free world (Shackleton and Kennett, 1975).

To calculate temperatures from the belemnite rostra the equation of Anderson and Arthur (1983) is used, which represents a modified equation of that of Craig (1965):

$T\ (^{\circ}C) = 16.0 - 4.14\ (\delta_c - \delta_w) + 0.13\ (\delta_c - \delta w)^2$

where δ_c = is $\delta^{18}O_{bel}$ (‰ VPDB) of the sample and δ_w = $\delta^{18}O$ SMOW, the composition of ambient seawater.

2.5.2.7 Strontium isotope analysis

Drilled belemnite powders were used for analysis of $^{87}Sr/^{86}Sr$. A total of 32 belemnite powders in total have been analysed. Pre-screened belemnite calcite powders were analysed for $^{87}Sr/^{86}Sr$. The $^{87}Sr/^{86}Sr$ ratios were measured on a Thermo-Finnigan Triton series thermal ionisation mass spectrometer (TIMS) in the SOEE (Univ. of Leeds, UK). Analysis of $^{87}Sr/^{86}Sr$ followed stages of leaching, digests, microcolumn separations (Sr purification) and loading.

2.5.2.7.1 Leaching

An initial step that involves the chemical corrosion of calcite shells or fragments through the use of weak acids such as HCl, is sometimes referred to as leaching. The approach is thought to chemically remove traces of diagenetic carbonate and clean the surface of calcite before processing.

Different leaching approaches have been adopted for belemnite calcite (for examples see Jones et al., 1994; McArthur et al., 2000; McArthur et al., 2007; Ullmann, 2013). The approaches differ in their preferred use of amount and strength of leaching acids, quantity of belemnite calcite and leaching the calcite as a powder or in the form of small cleaned chips. However, it has been suggested that leaching has little or, in fact, a negative effect on calcite or carbonate when processing for $^{87}Sr/^{86}Sr$. It has been found that the acid can preferentially attack well-preserved fossil material, leaving behind a residuum with increased altered calcite fraction (Podlaha et al., 1998). In addition, Ullmann (2013) found that there was little effect of acid leaching on marly sediments when using different acids, with no effect of the acid type and concentration observed. Following the methods of Ullmann (2013), leaching was not carried out on belemnites in this study.

2.5.2.7.2 Digestions

The method of Ullmann (2013) was followed with 2 mg of belemnite calcite digested in 3 M HNO_3, with the modification that digested solution was loaded

directly into the column and not left to dry on a hot plate, in order to mitigate the risk of contamination between pots.

2.5.2.7.3 Column work

Digested samples were processed through microcolumns, made using 1 ml pipette tips that had been cut obliquely at the base with a steel blade and a frit (porous plastic no 3515) fitted in the conical part of pipette tips. Sr spec resin was added to each microcolumn, ensuring resin just filled above the conical base of the pipette tip.

For column work, the resin was initially cleaned. Following this, digested biogenic calcite samples were passed twice through columns to ensure full Sr purification. Standard procedure for column work is as follows:

Resin cleaning

- 500 µl ultra high quality water (UHQ)
- 500 µl 0.1 M H_2SO_4
- 500 µl 0.1 M H_2SO_4
- 500 µl UHQ
- 500 µl 0.05 M HNO_3
- 500 µl 0.05 M HNO_3
- 500 µl UHQ

Column separation

Pass 1

- 100 µl of 3 M HNO_3 (precondition column)
- Load sample in 300 µl of 3 M HNO3
- 50 µl of 3 M HNO_3 (Rinse 1)
- 50 µl of 3 M HNO_3 (Rinse 2)
- Elution of 300 µl of 3 M HNO_3 (Rb fraction-not used in this study)
- Elution 750 µl of 0.05 M HNO_3 (Sr fraction)
- Eluted Sr fraction in solution in a 30 ml Teflon beaker overnight on a hotplate at 125°C, ensuring Teflon beakers are placed as far apart as possible on hotplate

Pass 2

- 100 µl of 3 M HNO_3 (precondition column)
- Load sample in 100 µl of 3 M HNO3
- 50 µl of 3 M HNO_3 (Rinse 1)
- 50 µl of 3 M HNO_3 (Rinse 2)

- Elution of 300 µl of 3 M HNO_3 (Rb fraction-not used in this study)
- Elution 750 µl of 0.05 M HNO3 (Sr fraction)
- 25 µl 0.1 M H_3PO_4* added to eluted solution
- Eluted Sr fraction in solution in a 30 ml Teflon beaker overnight on a hotplate at 125°C, ensuring Teflon beakers are placed as far apart as possible on hotplate

Phosphoric acid was also added to the eluted solution directly after the elution process rather than during preparation of filaments. The low vapour pressure and high viscosity of H_3PO_4 acted to concentrate Sr in a single drop in the centre of the beaker, to ensure the sample was not missed during loading. It also ensured no Sr nitrates would be lost in the air stream of the flow hood through flaking.

2.5.2.7.4 Sample loading

Samples processed through columns were loaded onto single tungsten wire filaments, previously outgassed to ensure no contamination from previous samples or surroundings.

To ensure minimal contamination during the loading process, a new pipette tip for each sample was cleaned by picking up and discarding 3 drops each of 10% HNO_3, 18 MilliQ water and 2 M HCl, consecutively.

Each sample was then taken up in 2 µl of 5% TaClS loading solution and dropped onto a tungsten filament. Sample was added in as small an increment as possible, with each increment allowed to dry prior to the next increment being loaded. The solution was subsequently evaporated by applying a 1 Amp to the filament.

In addition to loading samples through columns, a NBS-987 sample was added for each set of analysis. When loading these NBS-987 2 µl of 2.5% TaClS was added to the filament and evaporated first and then 2 µl of NBS-987 solution was added to the filament and evaporated. The NBS-987 solution was dropped onto parafilm three times, and only the third drop used for loading to prevent contamination.

After the entire solution was loaded onto the filament, the current was increased slowly until the filament began to go blue towards the edge, at which point a sharp increase of current between 4-5 Amps was pushed through the filament until it glowed red for two seconds. The current was then quickly stopped and filament allowed to cool.

The prepared filaments were then placed in a magazine and shielded with a slit plate. Commonly 12 samples, one reference (YCB), two standards (B-7, JLS-1), one blank and one NBS-987 were placed on each magazine. The magazine was then placed into the TIMS and the sample chamber left for a minimum of six hours prior to running.

2.5.2.7.5 TIMS sample runs

All samples were run manually via *Thermo Scientific* Thermal Ionisation Mass Spectrometer (TIMS), in the SOEE (Leeds, UK). To achieve maximum precision and accuracy (see McArthur et al., 2000), the ^{88}Sr signal was bracketed between 5 and 10 V and a minimum of 200 isotope ratios were collected. The internal precision was maintained between 1.3×10−6 and 7.1×10−6. The accuracy and reproducibility of Sr isotope data were monitored using the external standard NIST SRM987. The $^{87}Sr/^{86}Sr$ ratios of SRM987 yielded a mean of 0.710246 ± 0.000008 (2sd, n=10) during the analysis. Data mentioned in the text have been normalised to the SRM987 standard value of 0.710248 (McArthur et al., 2000). Concentrations of Rb were too low to require correction for radiogenic ^{87}Sr.

Blank samples were run alongside standards and reference materials. Blanks were spiked with a Blue 2 ^{84}Sr spike containing 0.1796 nM/g strontium. A threshold for the absolute amount of Sr was set at <2 ng, as 1-2 ng contamination can be expected from using SpA reagents in a standard laboratory setting and therefore a value <2 ng is considered to be of acceptably low contamination value given the geochemical methods of sample extraction.

2.5.2.7.6 Standards and reference material

A range of standards and reference materials were used during $^{87}Sr/^{86}Sr$ analysis (Table 2.2), as there is currently no Certified Reference Material (CRM) for $^{87}Sr/^{86}Sr$ that is directly comparable to belemnite calcite. Each suite of samples were run alongside a JLS-1, B-7 and YCB sample, following the same methods as for all other samples.

JLS-1 (Japanese Triassic Limestone, Geological Survey of Japan) is used as one of the most widespread standards for belemnites as it has a suitable matrix to compare fossil measurements. Although there is no certified $^{87}Sr/^{86}Sr$ ratio for JLS-1, it can be compared to published values from peer reviewed literature (e.g. Ohno and Hirata, 2007).

Table 2.2 Replicate $^{87}Sr/^{86}Sr$ analysis by TIMS on reference and standard material and comparison to published values (given below in text for each reference/standard).

Reference/standard	Measured	Number of analyses (n)	Standard deviation	Published value
YCB	0.70709908	n=8	0.000013	0.70708
B-7	0.70832624	n=5	0.000022	0.708377
JLS-1	0.70786337	n=3	0.000035	0.70785
Do-1	0.707135	n=1	-	0.707134
Do-6	0.707131	n=1	-	0.70712

B-7 Miocene Limestone is a Miocene marine limestone powder from Abruzzo, Italy. This is not a certified standard, but has been run by the IGG Lab-CNR-Pisa and is an internal standard used by the TIMS lab (Univ. of Leeds).

A belemnite from the Lower Jurassic Yorkshire Coast, termed 'Yorkshire Coast Belemnite' (YCB) was crushed, homogenised and used as a reference material. As the exact lithostratigraphic location of the belemnite is known, the $^{87}Sr/^{86}Sr$ ratio of the material is taken from the LOWESS curve (McArthur et al., 2000). This was selected as it is a Lower Jurassic calcite material directly comparable to Lower Jurassic calcite from the Bulgarian belemnites. The YCB was collected from Normamby Style Batts, 6 cm below the base of the middle sulphur band, Yorkshire Coast, UK (McArthur et al., 2000).

To ensure reproducibility duplicate samples were run on belemnites collected from Lower Jurassic sections in NW Bulgaria (Dobravitsa-1, samples Do-1 and Do-6), with previously published $^{87}Sr/^{86}Sr$ ratios (Metodiev and Koleva-Rekalova, 2008). These duplicated samples provided values within ± 0.000011 variability of published values.

Chapter 3 Sedimentology, biostratigraphy and chemostratigraphy of the Lower Jurassic study sites

3.1 Introduction

This chapter introduces the study sites selected for this thesis and how they fit into the established lithostratigraphic and biostratigraphic framework for the Lower Jurassic of northwest and central Bulgaria (Nikolov and Sapunov, 2002). Additional sedimentological observations are used to improve current understanding of palaeoenvironmental settings within the Moesian Basin. Ammonite and dinoflagellate occurrences are used to improve established biostratigraphy and calcareous nannofossil occurrences and provide the first nannofossil biostratigraphic record in Bulgaria. Strontium isotope records from belemnites are also be used to improve chemostratigraphic control for sections.

3.2 Methods

Methods applied in this section are cross-referenced to detailed methods in Chapter 3 (see Table 3.1).

Table 3.1 List and location of methods employed for analysis in Chapter 3

Method	Heading # (Page #)	Sections	Sample material
Sedimentological logs	2.1 Page 66	All sections	Bulk rock
Ammonite biostratigraphy	2.3.1 Page 68	Teteven Vradlovtsi-2 Dragovishtitsa	Bulk rock
Palynomorph biostratigraphy	2.3.2 Page 69	Yamna Ravna Milanovo	Bulk rock
Calcareous nannofossil analysis	2.3.3 Page 69	Milanovo Boeva Mogila	Bulk rock

Strontium isotopes ($^{87}Sr/^{86}Sr$)	2.5.2.7 Page 184	Vradlovtsi-2 Milanovo	Belemnites

3.3 Overview of sections from northwest and central Bulgaria

This introduces all of the sections used throughout the rest of the thesis (Figure 3.1). Different sections are selected for analysis and the rationale for site selection is given in each of the following data chapters. All sections have been previously dated and follow (Sapunov and Metodiev, 2007b; Metodiev, 2008). The sections are described by tectonic unit, in an order that follows sections in Figure 2.1.

Figure 3.1 Map of Bulgaria with study sites. A) Outline of Bulgaria with the study area highlighted by grey box. B) Detailed map of west and central Bulgaria with sections used in this study shown by black dots. Jurassic outcrops are shown in grey and key faults shown in red. For detailed map of faults in study area see Chapter 1 (geological map).

3.3.1 Ravna section

The Ravna section is located 2.5 km north east of Ravna Village in the Vildich Mountains in the Western Balkan Mountains (23° 01' 58.2600" E, 43° 03' 5.3316" N). The section comprises the Kostina Formation and the Ozirovo Formation (Teteven Member, Dolni Lukovit Member and Bukorovtsi Member) (Figure 3.2). This is the type section for the Ravna Member of the Ozirovo Formation (Sapunov and Metodiev, 2007a).

3.3.2 Dobravitsa-1 section

The Dobravitsa-1 section is located 2.5 km north east of Breze Village in the Ponor Planina Mountains in the West Balkan Mountains (23° 13' 53.1372" E, 43° 01' 37.9200" N). The section comprises a 7 m thick Bukorovtsi Member of the Ozirovo Formation, overlain by the Etropole Formation (Figure 3.3). The section has previously been recorded by Metodiev and Koleva-Rekalova (2008).

3.3.3 Brakyovtsi section

The Brakyovtsi section is located 1.5 km north west of the Brakyovtsi Village, in the Ponor Planina Mountains of the west Balkan Mountains (23° 08' 27.3120" E, 43° 03' 48.7332" N). The Brakyovtsi section comprises the Bukorovtsi Member of the Ozirovo Formation (Figure 3.4). The top of the Brakyovtsi section can be laterally traced to the base of the nearby Dobravitsa-1 section (Sapunov and Metodiev, 2007).

3.3.4 Gorno Ozirovo section

The Gorno Ozirovo section is located 6.5 km north west of Gorno Ozirovo Village, in the Vratsa Mountains in the West Balkan Mountains (23° 24' 30.3336" E, 43° 15' 10.8432" N). This section comprises the Kostina Formation and the undifferentiated Ozirovo Formation (Figure 3.5). This is the type section for the Ozirovo Formation (Sapunov and Metodiev, 2007a).

3.3.5 Milanovo section

The Milanovo section is located 7.5 km north east of Milanovo Village in the Vratsa Mountains, in the West Balkan Mountains (23° 26' 0.1392" E, 43° 06' 46.9944" N). The section comprises 4.3 m of black, thinly-bedded marls as part of the Bukorovtsi Member (Ozirovo Formation) (Figure 3.6).

The Milanovo sections dating from the upper Pliensbachian (*spintaum* Zone) to upper Toarcian (*aalensis* Zone), with a likely hiatus around the Pliensbachian-Toarcian boundary, indicated by ammonite and nannofossil biostratigraphy, and strontium isotope stratigraphy (see Sections 3.7.1, 3.7.3 and 3.8.1.1). The Milanovo section comprises dark grey marls, deposited in relatively deeper water conditions of the Moesian Basin (Metodiev et al., 2014).

3.3.6 Boeva Mogila section

The Boeva Mogila section is located 1 km north of the town of Teteven, in the Central Balkan Mountains (24° 16' 15.4362" E, 42° 55' 10.8132" N). The Boeva Mogila section comprises grey limestones in the upper Pliensbachian, that transition into silty marls at the *tenuicostatum/falciferum* boundary as part of the Bukorovtsi Member (Figure 3.7). The Boeva Mogila section records the thickest early Toarcian (*tenuicostatum* Zone – *bifrons* Zone) section in Bulgaria, although sediments are still condensed relative to many other equivalent European records of this time. A nearby section (Varbanchovets section) has previously been recorded by Metodiev et al. (2014).

3.3.7 Teteven section

The Teteven section is located in the town of Teteven in the Beli Vit River Valley in the Central Balkan Mountains (24° 16' 42.6648" E, 42° 54' 54.0180" N). The section comprises the Kostina Formation and the Ozirovo Formation (Teteven Member and the Dolni Lukovit Member) (Figure 3.8) and has been previously recorded by Sapunov (1959) and Sapunov et al. (1971). This is the type section for the Teteven Member of the Ozirovo Formation (Sapunov et al., 1971). The occurrence of *Uptonia* sp. and *Uptonia jamesoni* (Figure 3.15) are previously undocumented ammonites from this section and indicate the lower Pliensbachian *jamesoni* Zone (see Section 3.7.1).

3.3.8 Kiselchov Dol section

The Kishelchov Dol section is located 15 km east of the Troyan Pass, in the Troyan National Park (Cherni Osam River Valley) in the Central Balkan Mountains (24° 42' 51.2460" E, 42° 45' 57.7800" N). The Kiselchov Dol section required a permit for sampling. The permit was issued by the Bulgarian Ministry of Environment and Water (Nr. NSZP-158/30.05.2016).

Lower Jurassic ironstones are common in the Troyan region of central Bulgaria, and include the Kiselchov Dol section (Nachev, 1960; Nachev, 1968; Nachev, 1973; Nachev, 1974; Sapunov et al., 1991; Sapunov et al., 1996). The Kiselchov Dol section comprises sandy bioclastic limestones through the upper Pliensbachian (*spintaum* Zone), with a transition into red ooidal ironstones at the Pl-To boundary that continue through the Toarcian (Figure 3.9). This section records undifferentiated Ozirovo Formation.

3.3.9 Yamna section

The Yamna section is located 3 km south-southeast of Yamna Village in the Teteven Region of the central Balkan Mountains (24° 07' 38.1288" E, 42° 49' 6.6036" N). The section comprises alternating silty marls, clay-rich siltstones, a thin coal horizon and sandy crinoidal bioclastic limestones as part of the Bachiishte Formation (Figure 3.10). The depositional setting has previously been interpreted as a transitional marginal marine environment, that fluctuated between terrestrial swamp, coastal sub-littoral and littoral (Shopov, 1975; Sapunov and Metodiev, 2007a). This fluctuating depositional environment is supported in this study by the presence of both marine and terrestrial palynomorphs (see Section 3.7.2).

The Bachiishte Formation is estimated to be Hettangian in age (Shopov, 1975; Černjavska, 1986), although no previous biostratigraphic work has been able to confirm this. Palynological work in this study indicates the age of this formation as Hettangian in age is plausible (see Section 3.7.2). The boundary between the Hettangian and Sinemurian in this section is based on lithostraigraphic correlation only and is therefore subject to change.

3.3.10 Berende Izvor section

The Berende Izvor section is located in the west Balkan Mountains (22° 53' 5.0013" E, 43° 011' 04.0139" N). The section has been previously logged and dated (using ammonite biostratigraphy) by Metodiev et al. (2012). This section was not re-logged during fieldwork for this study due to limited outcrop exposure. The section is included in this study as previously collected belemnites are used to construct stable isotope curves (Chapter 4).

3.3.11 Vradlovtsi-1 section

The Vradlovtsi-1 section is located 2 km east of Vradlovtsi Village in the Godech Basin (Zabarde Area) of the West Balkan Mountains (22° 55' 59.5956" E, 43° 02' 21.2352" N). The section comprises the Tuden Formation and the base of the Ozirovo Formation (Ravna Member) (Figure 3.11).

3.3.12 Vradlovtsi-2 section

The Vradlovtsi-2 section is located 3 km east of Vradlovtsi Village in the Godech Basin (Zabarde Area) of the West Balkan Mountains (22° 56' 27.7836" E, 43° 01' 56.1576" N). The section comprises the Tuden Formation and the Ozirovo Formation (Teteven Member, Dolni Lukovit Member and Bukorovtsi Member) (Figure 3.12). This area has previously been recorded by Benatov (1994). The occurrence of *Uptonia jamesoni* (bed 3*,* Figure 3.12*,* Figure 3.15) is previously undocumented from this section and indicates the lower Pliensbachian *jamesoni* Zone (see Section 3.7.1). The $^{87}Sr/^{86}Sr$ ratios from belemnites were analysed and strontium curve shown against log (Figure 3.12).

3.3.13 Dragovishtitsa section

The Dragovishtitsa section is located 4.5 km north east of Dragovishtitsa Village, Sofiyska Planina Mountains, in the West Balkan Mountains (23° 13' 34.7520" E, 42° 52' 45.1812" N). The section is part of the long exposure of Lower Jurassic called the Ponor Kremikovtsi strip in west Bulgaria, which includes the Dragovishtitsa, Balsha and Beledie Han sections (Koleva-Rekalova et al., 2006; Metodiev and Koleva-Rekalova, 2008). Beledie Han is not used as a study site but published data (carbon and oxygen isotopes) from this section (Metodiev and Koleva-Rekalova, 2008) are utilised in Chapter 4. Lithologically, this section is very similar to the Kiselchov Dol section and comprises oolitic ironstones, as part of the Undifferentiated Ozirovo Formation (Figure 3.13).

The ammonite *Fuciniceras* (see Figure 3.15) is recorded in bed 4 of the Dragovishtitsa section (Figure 3.13), was found during this study and provides the first record of the *ibex* Zone in Bulgaria (see 3.7.1).

3.3.14 Balsha section

The Balsha section is located 3.5 km north west of Balsha Village, in the Sofiyska Planina Mountains in the West Balkan Mountains (23° 14' 52.5300" E, 42° 51' 30.7368" N). This section comprises Kostina Formation, overlain by undifferentiated Ozirovo Formation and is faulted at the top, with Middle Jurassic sandstones above the fault (Figure 3.14). This area has previously been recorded by (Sapunov, 1969; Nachev, 1975a, b). The occurrence of the ammonite *Pleuroceras* was found in this study and indicates an upper Pliensbachian age of bed 20a (Figure 3.15).

3.4 Sedimentary logs

The following sedimentary logs correspond to section overviews (section 3.3). Strontium data is shown against logs for Milanovo section (Figure 3.6) and Vradlovtsi Section (Figure 3.12) and discussed later in this chapter (section 3.8.1). The sedimentary logs for this chapter are dated using biostratigraphy, and lithostratigraphy, where possible. The biostratigraphic framework predominantly comes from ammonite occurrences, which are documented in the doctoral thesis of Dr Lubomir Metodiev, held at the University of Sofia. This work informed previous work of Dr I.G. Sapunov, and was used to develop the ammonite biostratigraphic framework for the Jurassic in Bulgaria (see Chapter 1, Section 1.5.5 for further details). This framework has been used, where possible, to date the sections in northwest and central Bulgaria, used for this study. Detailed range charts for the Milanovo (Figure 3.6) and Boeva Mogila (Figure 3.7) sections are shown in Chapter 5 (Figure 5.11 and Figure 5.12). The lithostratigraphic framework for the Lower Jurassic (see Chapter 1, Section 1.5.3 for further details) to provide an indication of age for sections, but it is important to be aware these ages provide only an indication.

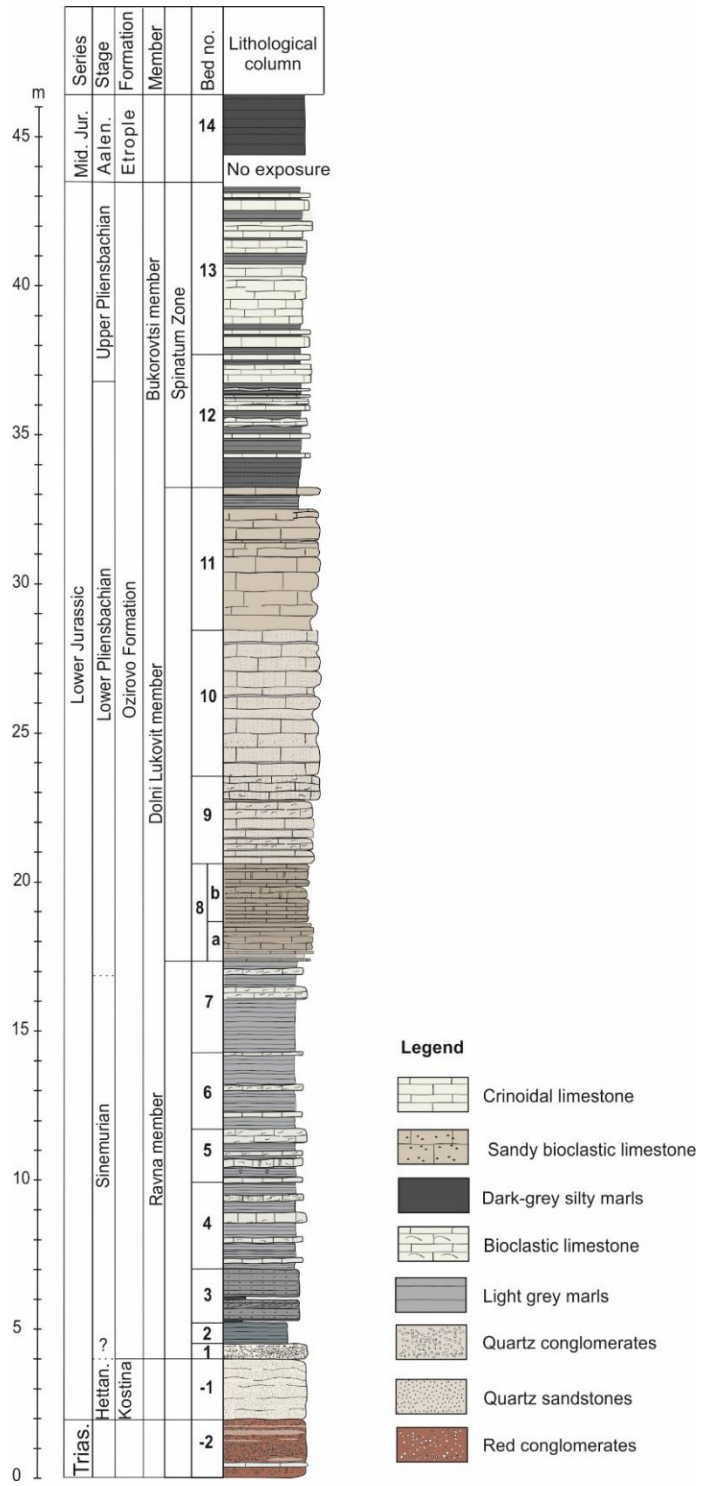

Figure 3.2 Sedimentary log of the Ravna section. Trias.=Triassic. Hettan.=Hettangian

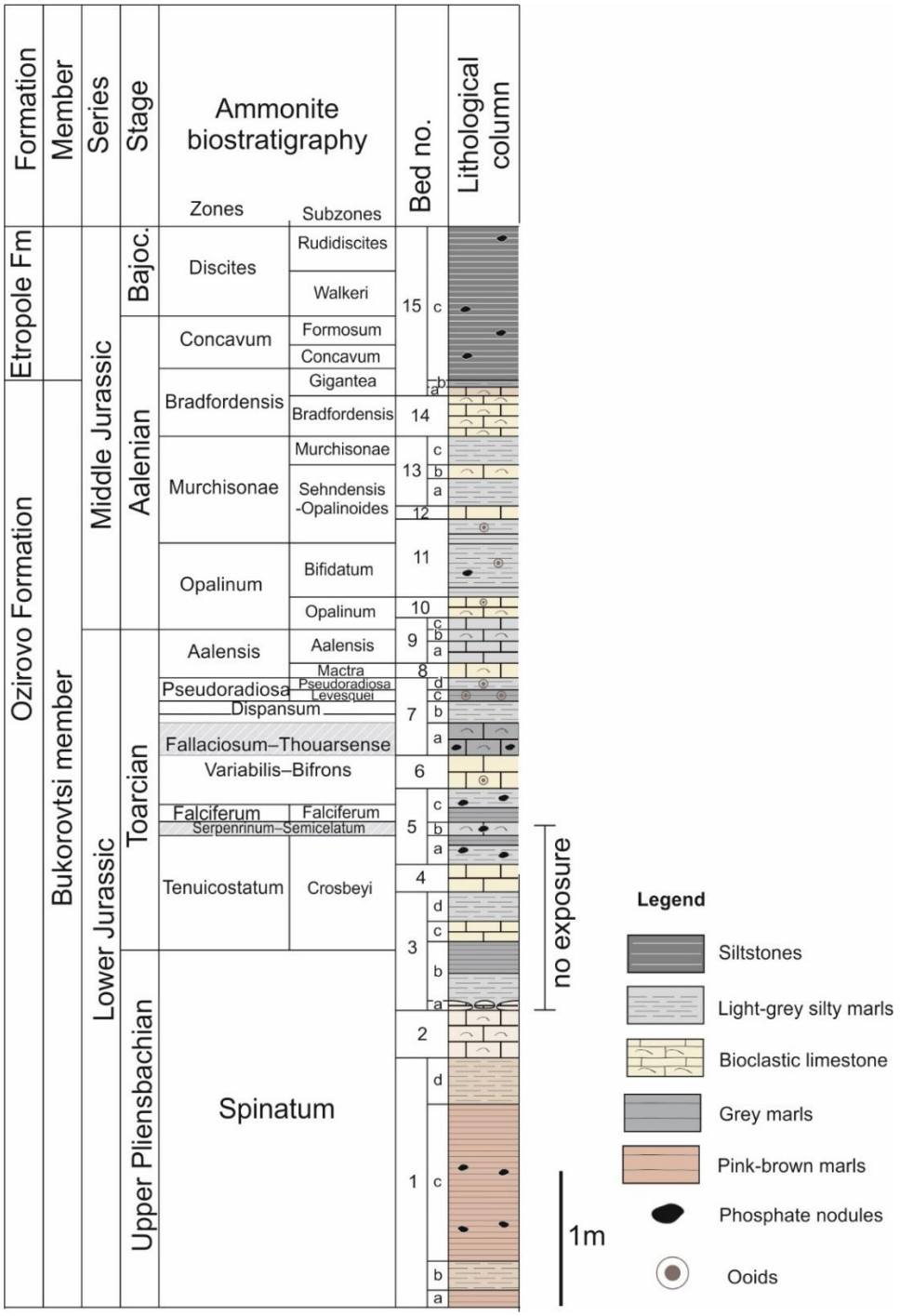

Figure 3.3 Sedimentary log of the Dobravitsa-1 section. Bajoc.=Bajocian.

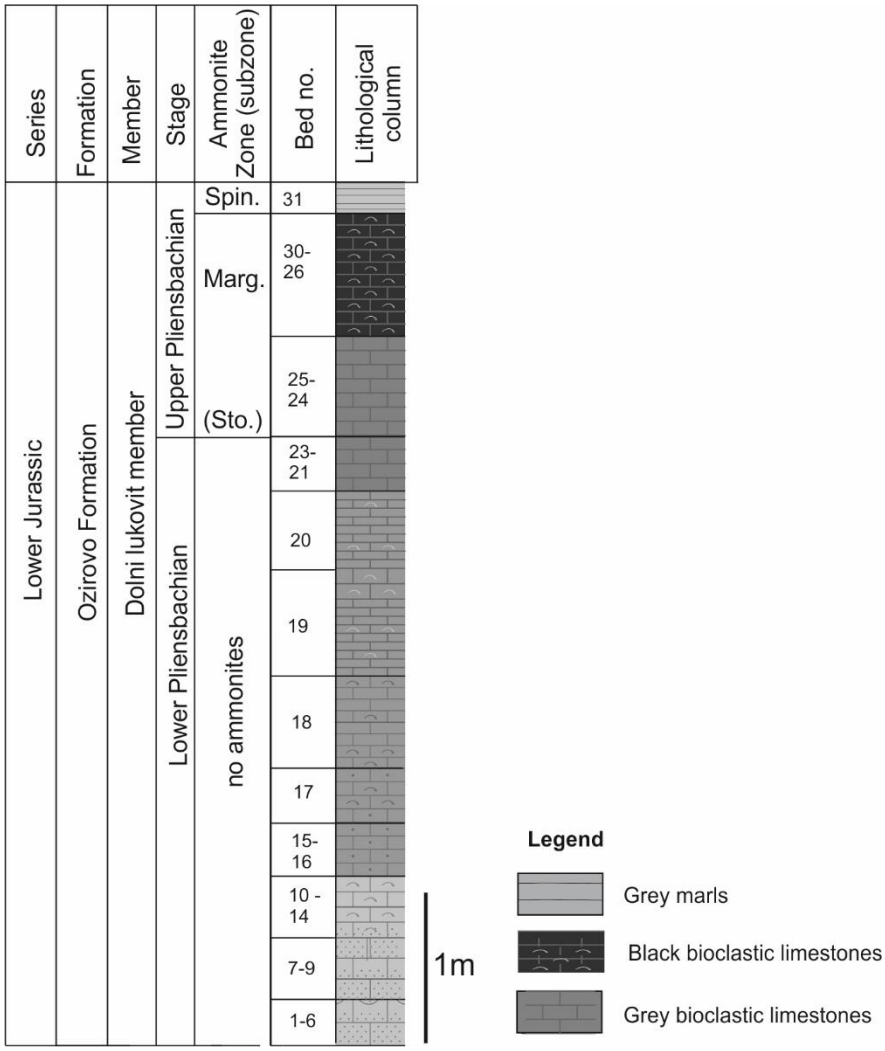

Figure 3.4 Sedimentary log of the Brakyovtsi section.

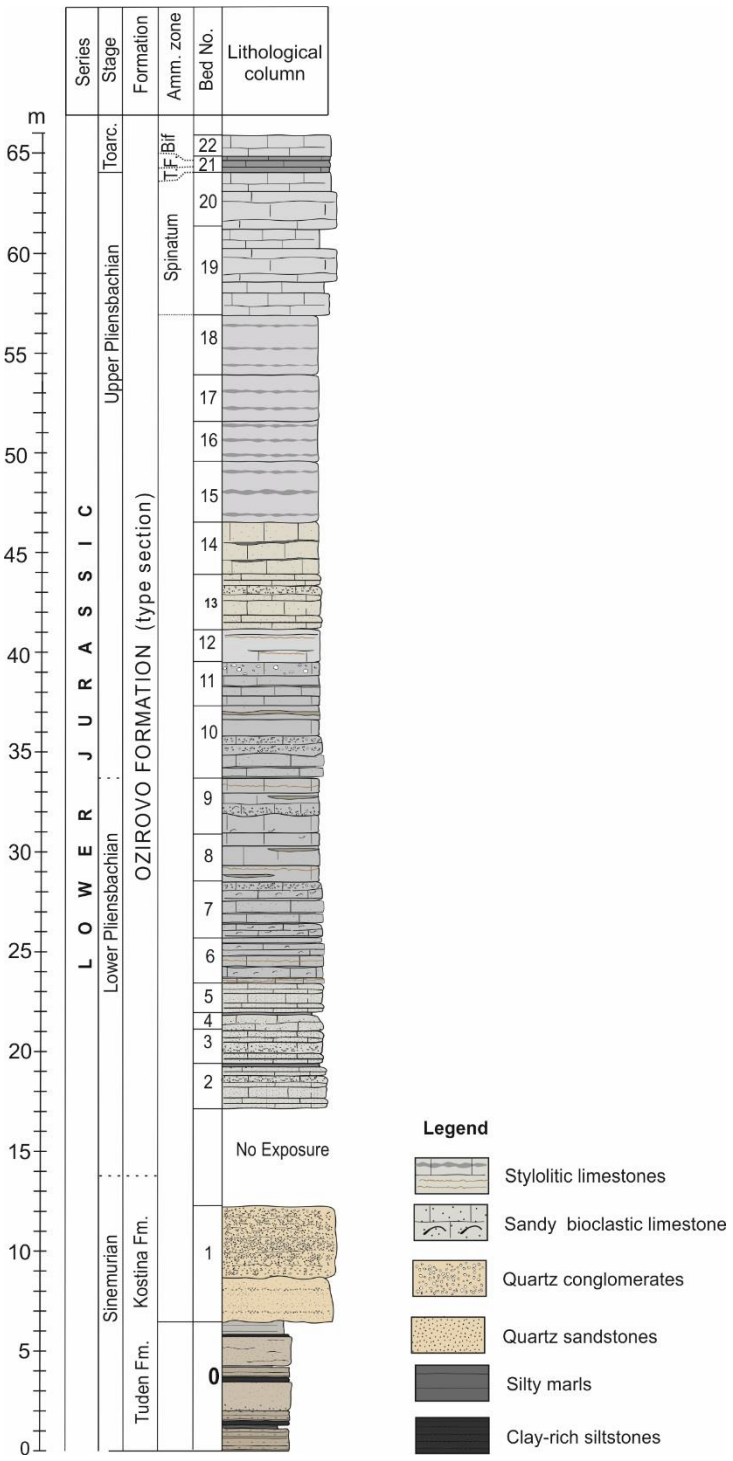

Figure 3.5 Sedimentary log of the Gorno Ozirovo section.

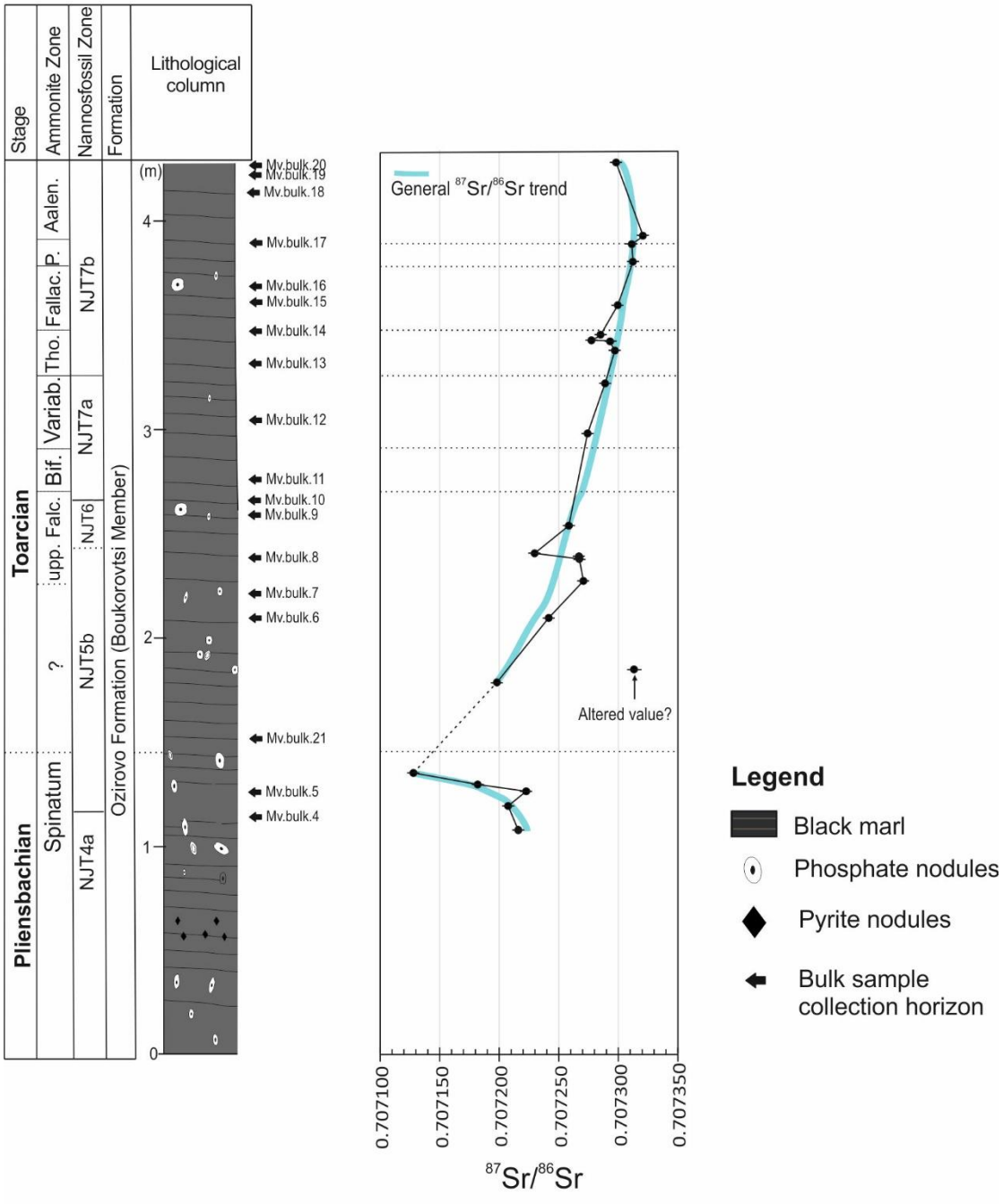

Figure 3.6 Sedimentary log of the Milanovo section. $^{87}Sr/^{86}Sr$ values from belemnites are displayed next to the section, with analytical uncertainty shown by black bar for individual values. Upp Falcif. = upper Falciferum, Bif= Bifrons, Thou.= Thouarsense, Fallac.=Fallaciosum, Ps= Pseuoradiosa, Aalen= Aalensis. Ammonite ranges for section shown in (Figure 5.12).

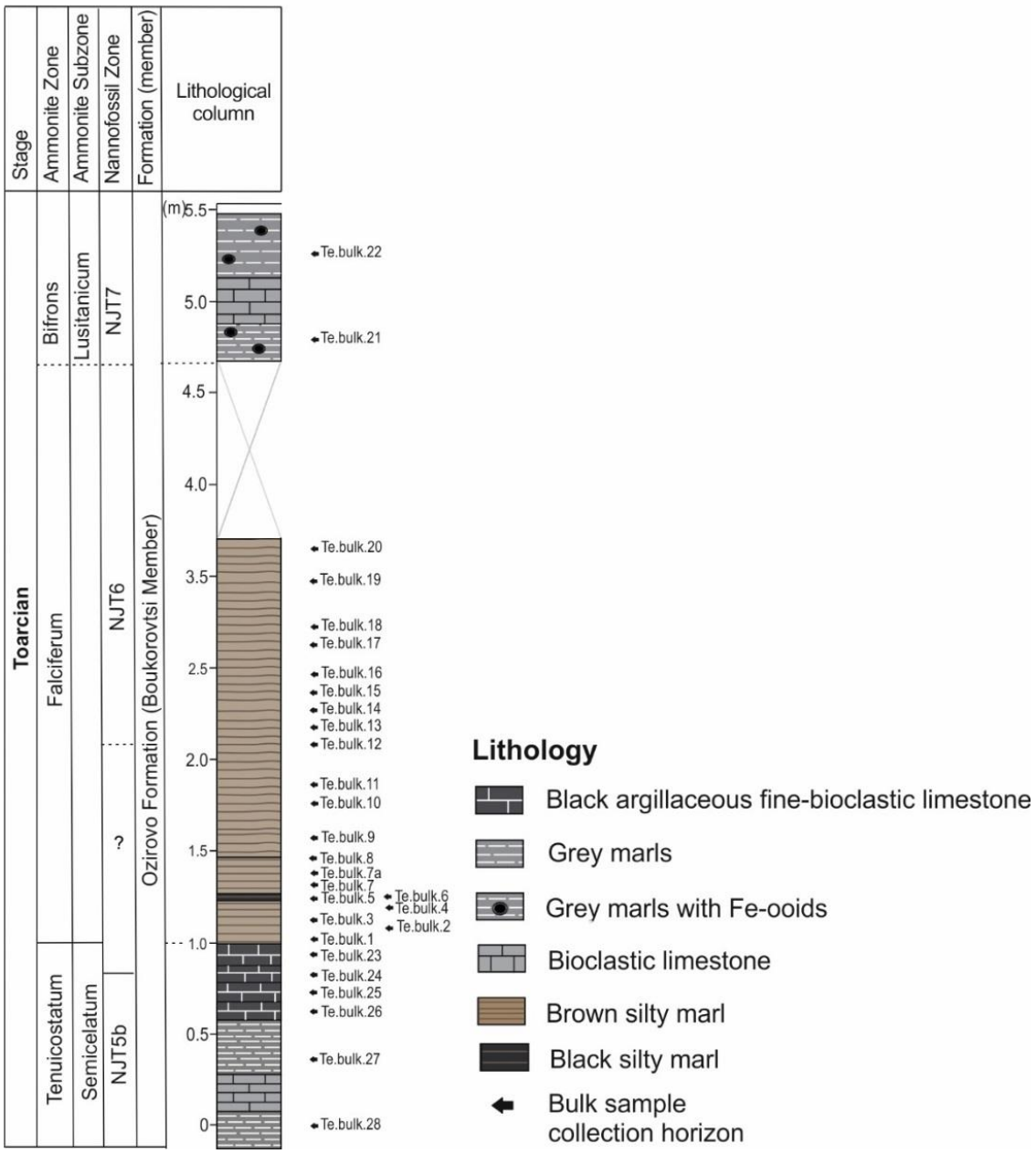

Figure 3.7 Sedimentary log of Boeva Mogila section. Ammonite ranges for section shown in (Figure 5.11).

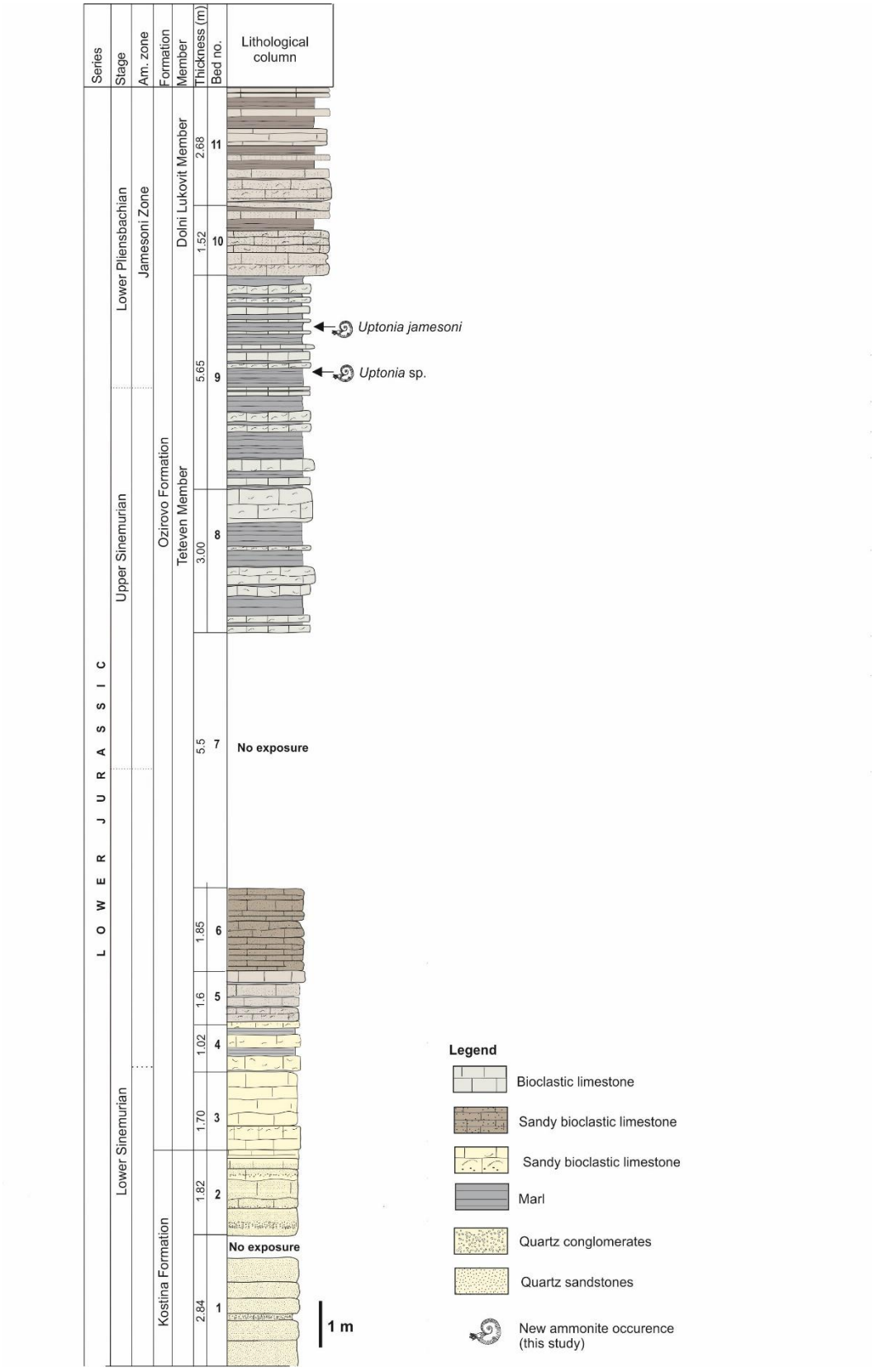

Figure 3.8 Sedimentary log of Teteven section.

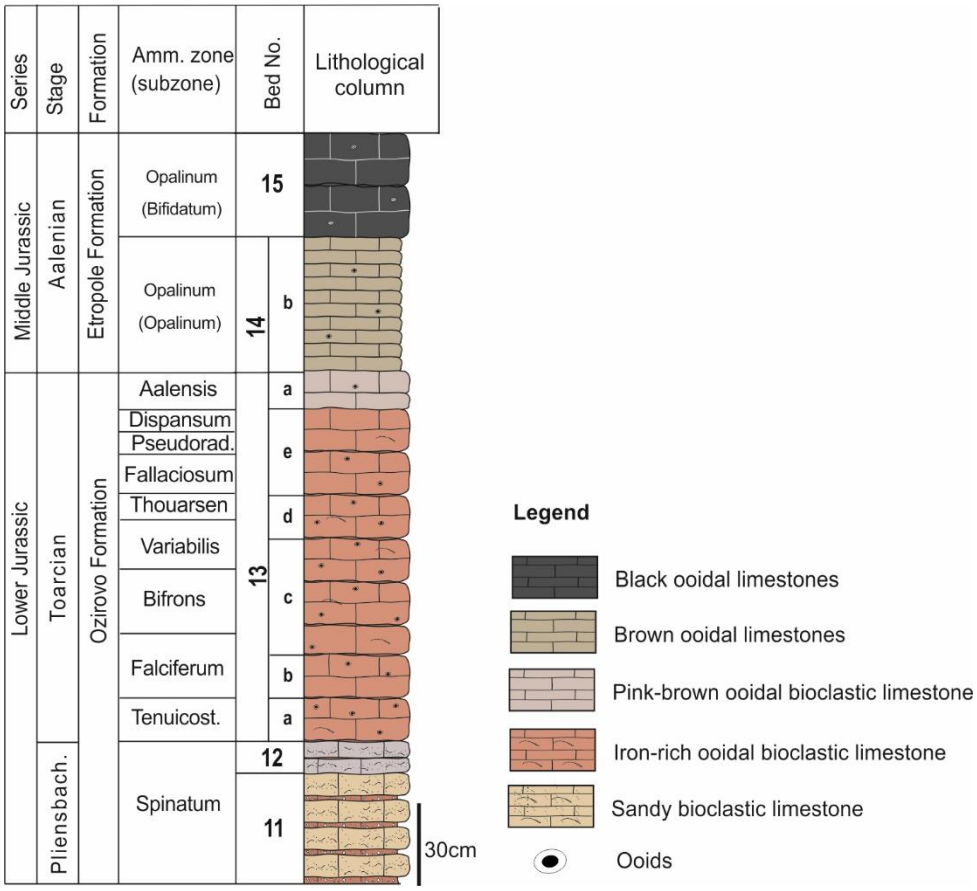

Figure 3.9 Sedimentary log of the Kiselchov Dol section.

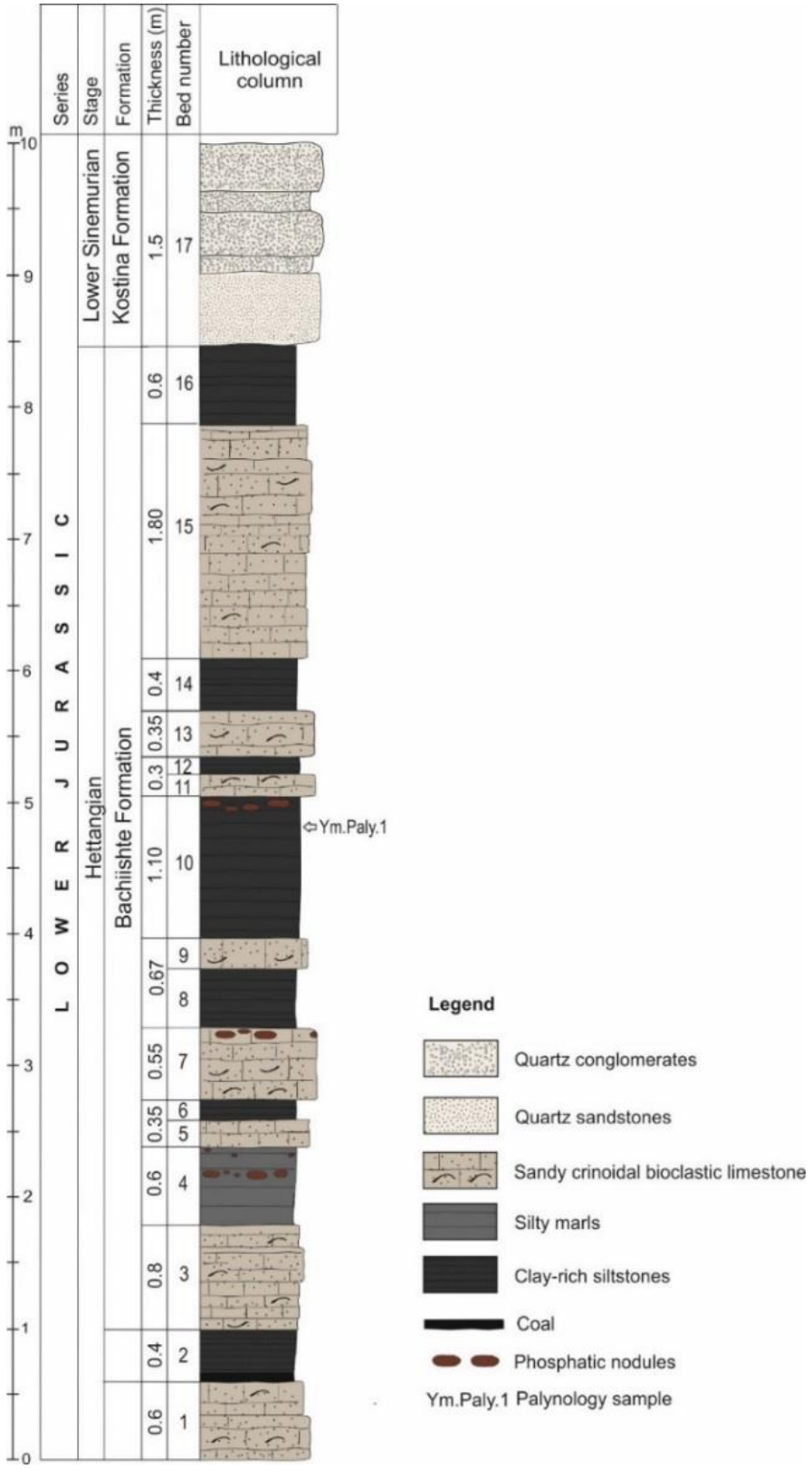

Figure 3.10 Sedimentary log of Yamna section.

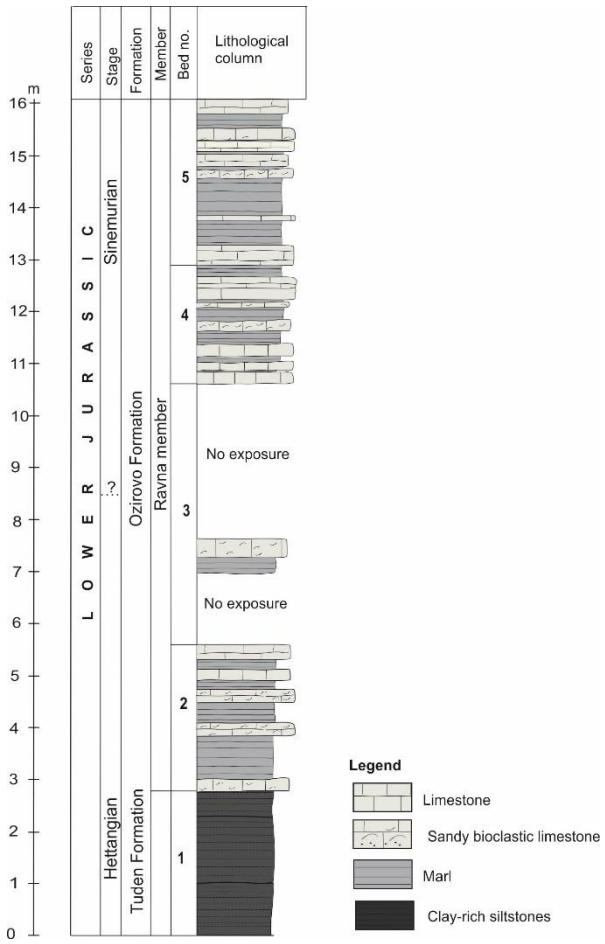

Figure 3.11 Sedimentary log of the Vradlovtsi-1 section.

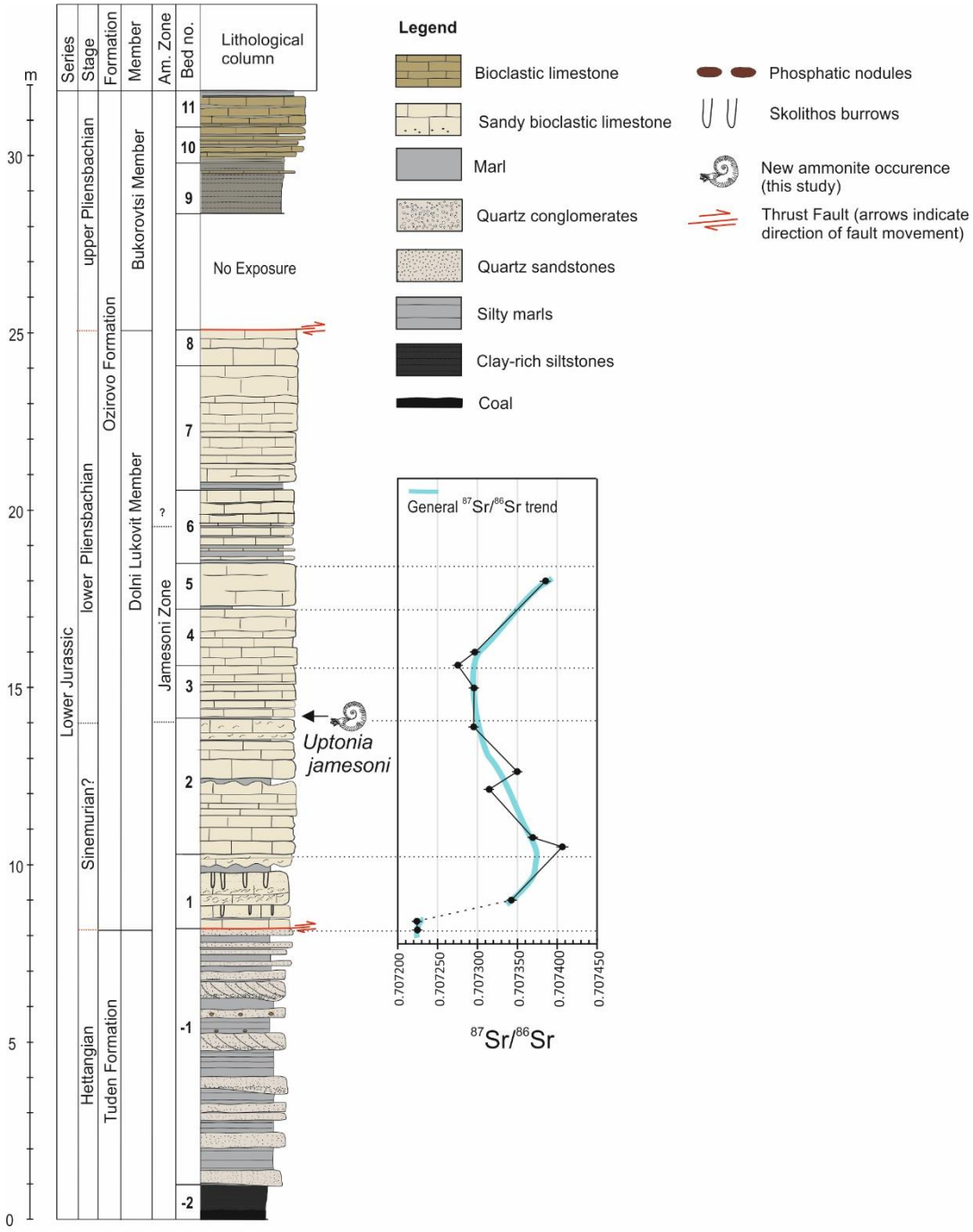

Figure 3.12 Sedimentary log of the Vradlovtsi-2 section. $^{87}Sr/^{86}Sr$ values from belemnites are displayed next to the section, with analytical uncertainty shown by black bar for individual values.

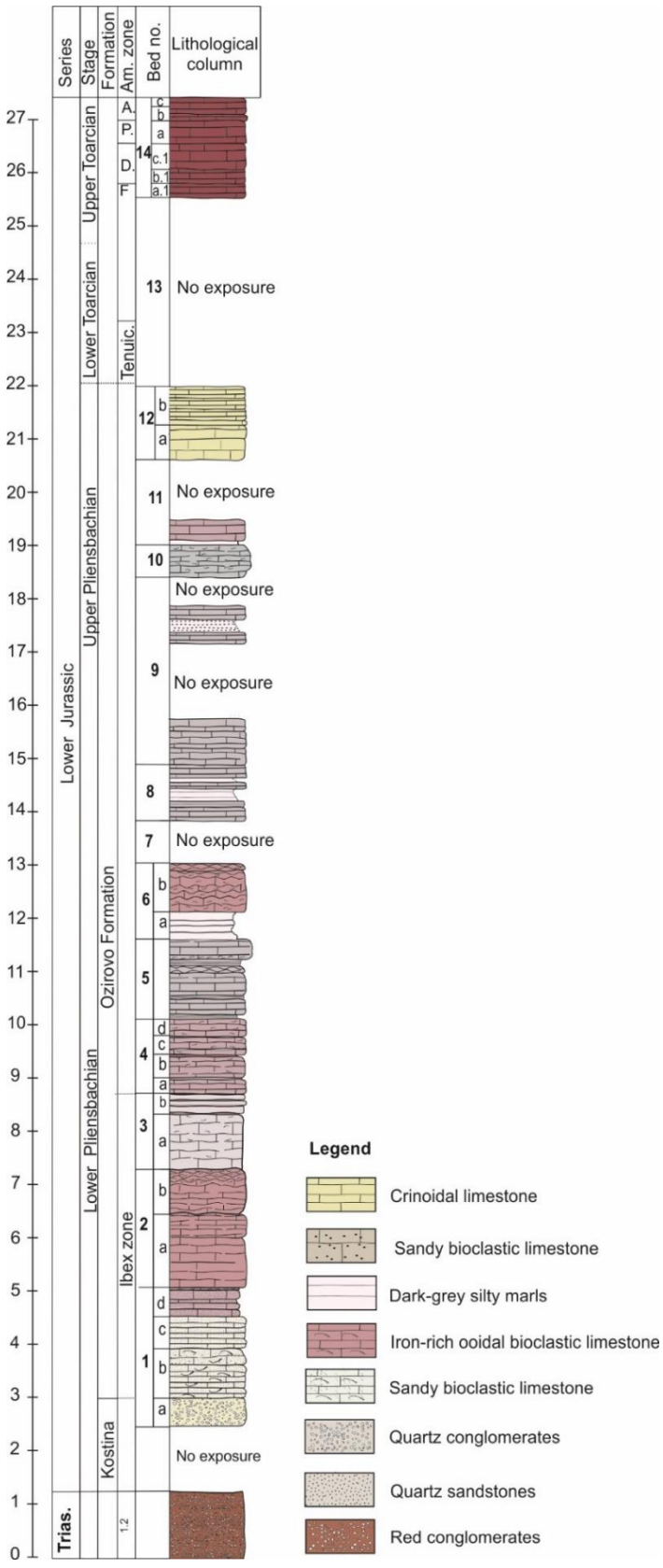

Figure 3.13 Sedimentary log of the Dragovishtitsa section. Trias=Triassic, Tenuic.= Tenuicostatum, F=Fallaciosum, D=Dispansum, P=Pseudoradiosa, A=Aalensis.

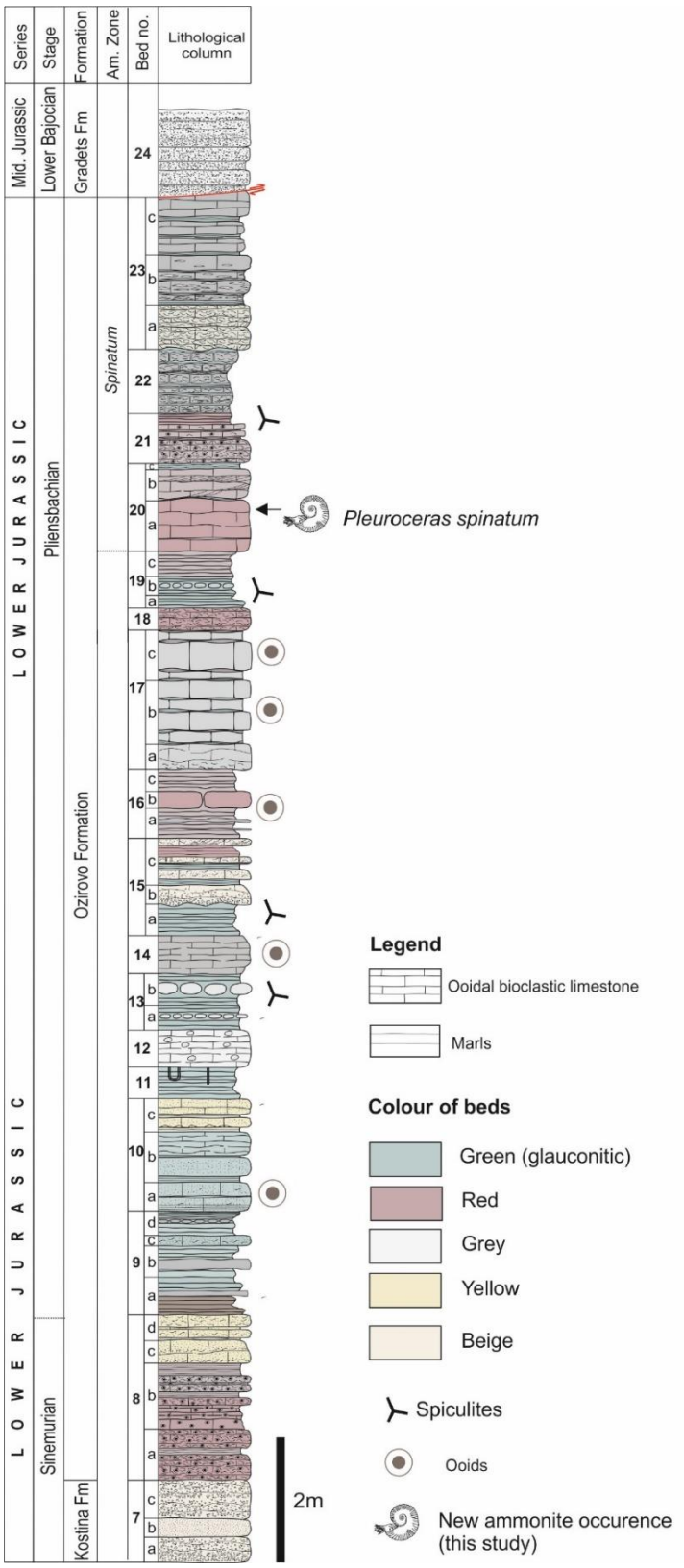

Figure 3.14 Sedimentary log of the Balsha section.

3.5 Facies variability through the Pliensbachian-Toarcian in Bulgaria

The Lower Jurassic of Bulgaria records a broad range of carbonate sedimentation styles in an extensional basin related to the opening of the Tethys. These include high energy proximal facies on the inner shelf to more distal, lower energy facies deposited in deeper parts of the basin.

There are two major deepening events recorded in the Sinemurian and the Pliensbachian, although understanding the exact timing is hindered by low biostratigraphic resolution and an inability to trace lateral variations in facies due to alpine tectonics. There are no clear facies changes that might indicate deepening across the Pl-To boundary or in the early Toarcian, despite the known major transgression in global sea-level during this time. Facies types across the Pl-To boundary transition include ooidal ironstones, sandy bioclastic limestones and silty marls. Throughout the Lower Jurassic, active tectonics and associated subsidence within the basin likely 'overprinted' regional or global sea-level changes.

3.6 The distribution of ammonites and belemnites in the Moesian Basin

Ammonites and belemnites are not abundant in all Lower Jurassic sections in Bulgaria. Sections dated Hettangian and Sinemurian in age have the overall lowest abundance of both ammonites and belemnites, with increasing abundance noted through the Pliensbachian. Both belemnites and ammonites become most abundant through the latest Pliensbachian-Toarcian interval.

This common distribution through the Lower Jurassic of the Moesian Basin could be explained in several ways. The first, an increase in belemnite populations in the Moesian Basin during this time. Secondly, the connectivity of the Moesian Basin with the EES and open Tethyan Ocean. This could be a result of the long-term transgressive episode that occurs throughout the Lower Jurassic in Bulgaria, which might allow additional connectivity of the basin to the epicontinental seawater masses. Thirdly, the relative abundance may be affected by diagenetic controls. Finally, the relative abundance increase particularly in the early Toarcian may also be accentuated by the condensed nature of the Toarcian sediments.

3.7 Biostratigraphic records

3.7.1 Ammonite biostratigraphy

The ammonite *Fuciniceras* (Figure 3.15) is reported from the Dragovishtitsa section (Figure 3.13). This ammonite is identified by Dr Lubomir Metodiev (Bulgarian Academy of Science, Sofia) as *Fuciniceras* gr. *costicillatum* (Fucini) – *detractum* (Fucini) (Figure 3.15). The ammonite is evolute and compressed, with flat whorl sides and flat venter, and there are ventro-lateral shoulder that border the keel. The ribs are fine and dense falcoid and strongly projected forwards on approaching the venter. The diameter of the specimen identified is 3.25 cm. The identified taxa corresponds to a taxon complex, which includes coeval and similar lower Pliensbachian faunas that are still not specifically defined and separated, and as a result have left in open nomenclature (Meister et al., 2011). This ammonite is an indication of the lower Pliensbachian *Tragophylloceras ibex/Prodactylioceras davoei* Zone boundary (Dommergues et al., 1997). This provides the first record of the *Ibex* Zone in Bulgaria.

The ammonite *Uptonia bronni* (Figure 3.15), identified by Dr Lubomir Metodiev (Bulgarian Academy of Science, Sofia) is recorded from the Teteven section (Figure 3.8). Two incomplete specimens, with diameters of 3.95 cm and of 2.8 cm, show only the inner whorls of the phragmocone (Figure 3.15). These ammonites are evolute and compressed, with subquadrate whorl sections and a thin keel, bearing strong and rounded simple ribs that are moderately closely spaced. The ribs are slightly prorsiradiate and project forward on the ventro-lateral margin, bearing small tubercles and forming strong chevrons on the venter. *Uptonia bronni* is a microconch of *Uptonia jamesoni* (J. de C. Sowerby) that has a narrow stratigraphical distribution confined to the very top of the lower Pliensbachian *Uptonia jamesoni* Zone (Fauré, 1993; Dommergues et al., 1987; Meister and Böhm, 1993; Dommergues et al., 1997; Dommergues et al., 2008). Ammonites recording this ammonite zone are particularly rare in Bulgaria and this provides an additional record from the Teteven area.

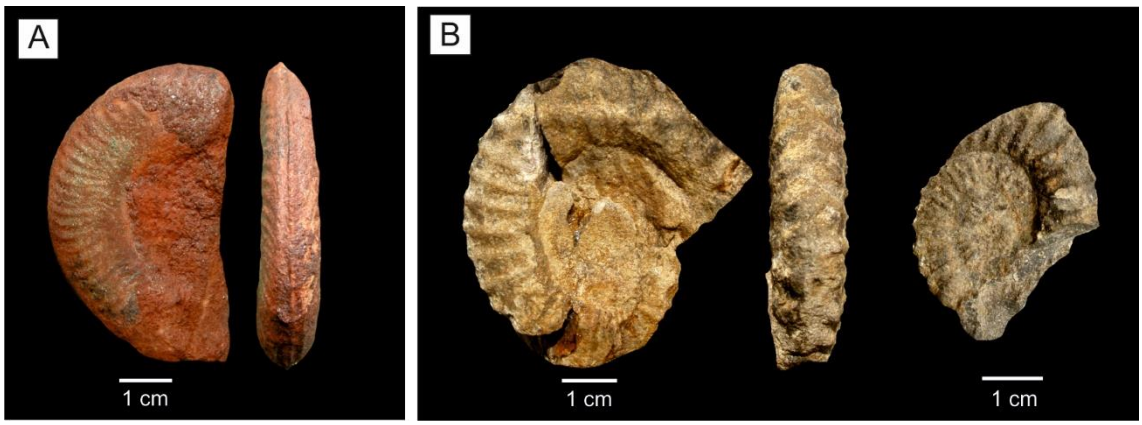

Figure 3.15 New ammonite occurences of A) *Fuciniceras* from the Dragovishtitsa section and B) *Uptonia bronni* (2 specimens) from the Teteven section.

3.7.2 Palynomorph biostratigraphy

Most samples from Lower Jurassic sections yielded no palynomorphs. One palynomorph assemblage from the Yamna section (Figure 3.10) provides biostratigraphic information (Table 3.2). Seven samples yielded limited palynomorphs and organic material information from the Milanovo (Figure 3.6) and Ravna (Figure 3.2) sections, but provided no biostratigraphic information (Table 3.2).

All palynomorph assemblages are thermally overmature, indicated by a high thermal alteration index (TAI) and distinct black colour (Figure 3.16). The darkness (‘blackness’) of the phytoclasts arose partly from geological age, but predominately from geothermal heat. A minimum temperature ca. 160°C is indicated from the high TAI, but less than 200 °C for organic matter to be present (Gaupp and Batten, 1985; Batten, 1996). This is equivalent to semi-anthracite and anthracite on the coal classification scale (Batten, 1996). The thermal alteration may account for the paucity in palynomorphs from the Lower Jurassic of Bulgaria. The geothermal heat source is potentially linked to nearly located granite plutons, intruded throughout northwest and central Bulgaria in the Cretaceous (Kamenov et al., 2002).

Palynomorphs are very sparse with *Micrhystridium* present in the Milanovo section and tentatively identified ?*Micrhystridium* in the Ravna section (Table 3.2). The presence of *Micrhystridium* indicates deposition in a marine environment, but provides no biostratigraphic information. Relative percentages of organic matter indicate high percentages of wood (72-75%) recorded in two horizons of the Milanovo section. Additionally, low percentages (2-10%) of plant

fragments in most samples and the highest percentages of amorphous organic matter (AOM) recorded in the Ravna samples (67-76%) (Table 3.2).

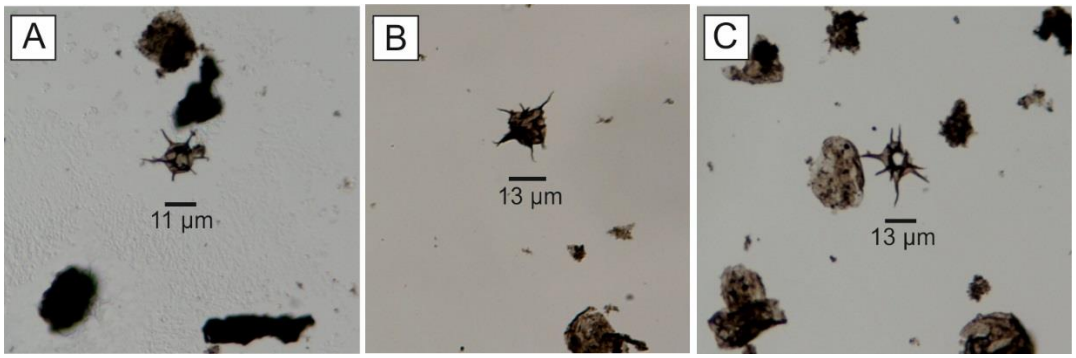

Figure 3.16 Spinose acritarchs of the genus *Micrhystridium* from the Yamna section.

An assemblage of both terrestrial and marine palynomorphs is recorded in the Yamna section (Table 3.2). Terrestrial palynomorphs include: *Baculatisporites* sp. (spore); Bisaccate pollen (undifferentiated) (pollen); *Chasmatosporites* sp. (pollen); *Classopollis classoides* (pollen); *Cyathidites* spp. (spore); *Perinopollenites elatoides* (pollen); *Retitriletes* sp. (spore); Spores indeterminate (spores) and *Vitreisporites pallidus* (pollen). Marine palynomorphs include: dinoflagellate cysts – indeterminate; *Micrhystridium* spp. (acritarchs) and foraminiferal test linings. The sample was deposited in marine conditions, indicated by the presence of *Micrhystridium,* but spores/pollen dominates over the marine elements.

The lack of *Cerebropollenites macroverrucosus* and other post Hettangian pollen and spores, together with the absence of Triassic marker taxa, is consistent with a Hettangian age, but does not provide certainty of a Hettangian age. The range base of *Cerebropollenites macroverrucosus* is early Sinemurian (Morbey, 1978). This assemblage marks the first record of palynomorphs from the Bachiishte Formation in Bulgaria.

Table 3.2 Palynofacies recorded from the Lower Jurassic in Bulgaria. Relative proportions of organic matter are given for each sample in percentage. Corresponding sample horizons are recorded sedimentary logs. BGS ref. no.(MPA) = British Geological Survey reference number, TAI = thermal alteration index, T = terrestrial, M = marine, Plant frags = Plant fragments, Palys = palynomorphs, AOM = amorphous organic matter, n/a= data not available.

Section	Sample horizon	BGS ref. no. (MPA)	TAI	Palynomorph abundance	Recorded occurrences	Wood (%)	Plant frags (%)	Palys (%)	AOM (%)
Milanovo	MV.12	69150	High	Barren	-	75	10	0	15
Milanovo	Mv.15	69151	High	Barren	-	72	8	0	20
Milanovo	MV.18	69156	High	Very sparse	*Micrhystridium* (acritarch) (M)	12	10	-	78
Ravna	RV.16.60	69152	High	Very sparse	?*Micrhystridium* (acritarch) (M)	30	3	-	67
Ravna	RV.16.90	69153	High	Very sparse	-	22	2	-	76
Ravna	RV.16.250	69154	High	Barren	-	23	3	0	74
Ravna	RV.17.20	69155	High	Barren	-	30	-	-	70
Yamna	YM.10	69149	High	n/a	*Baculatisporites* sp. (spore) (T) Bisaccate pollen (pollen) (T) *Chasmatosporites* sp. (pollen) (T) *Classopollis classoides (pollen) (T)* *Cyathidites* spp. (spore) (T) *Perinopollenites elatoides (pollen)(T)* *Retitriletes* sp.(spore) (T) *Vitreisporites pallidus (pollen) (T)* Dinoflagellate cysts (M) *Micrhystridium* spp. (acritarch) (M))	n/a	n/a	n/a	n/a

3.7.3 Calcareous Nannofossil biostratigraphy

Nannofossil zones for two Toarcian sections follow the scheme of Mattioli and Erba, (1999), based on bed-by-bed occurrence and preservation data for the Milanovo section (Figure 3.6 and Figure 3.18) and the Boeva Mogila section (Figure 3.7 and Figure 3.17). Due to the scarcity of Tethyan taxa (such as *Schizosphaerella* spp., and *Mitrolithus jansae* (Bown, 1987; Mattioli et al., 2008) the nannofossil assemblage of Milanovo and Boeva Mogila sections have an affinity for the NW European Boreal Realm. Nannofossil identifications have been undertaken by Emmanuela Mattioli (University of Lyon, France).

3.7.3.1 Boeva Mogila section

Calcareous nannofossils from the Boeva Mogila section (Figure 3.7) are moderately to very poorly preserved and where nannofossils are present, have abundances ranging from rare to common (Figure 3.17). The base of the section is assigned to NJT5b nannofossil zone up to 0.8 m, followed by a nannofossil decline over 30 cm interval and a subsequent nannofossil blackout recorded over a 70 cm interval, in which nannofossils become extremely rare (Figure 3.17). Nannofossil zone NJT6 records a nannofossil recovery over a 1.5 m interval and after a no-exposure gap, nannofossil zone NJT7 is assigned to the top of the section (Figure 3.17). The implications of the nannofossil decline, blackout and recovery are discussed further in Chapter 6. Overall, the calcareous nannofossil biostratigraphy is in agreement with the ammonite biostratigraphy for the Boeva Mogila section (Figure 3.7 and Figure 3.17). However, for this section, ammonite biostratigraphy provides the highest resolution biostratigraphic control. Further sampling from both this section at a higher resolution and from more sections across northwest Bulgaria would be needed in able to construct a calibrated timescale between the ammonite and calcareous nannofossil frameworks.

3.7.3.2 Milanovo section

Calcareous nannofossils from the Milanovo section (Figure 3.6) are, overall, better preserved and more abundant than the Boeva Mogila section. Nannofossils from Milanovo have good to very poor preservation, and where present, abundances ranging from rare to very abundant (Figure 3.18).

The main nannofossil zones and subzones of upper Pliensbachian and Toarcian are recognized (Figure 3.18). Because of the presence of markers of

the NW European and Tethyan provinces, both the zonations of Bown (1987) and Mattioli and Erba, (1999) can be used. Several first occurrences (FO) are observed during the upper Pliensbachian and lower Toarcian interval, such as *Lotharingius velatus*, *Biscutum dubium*, *Zeugrhabdotus erectus*, *Diductius constans* and *Discorhabdus ignotus* (Figure 3.19).

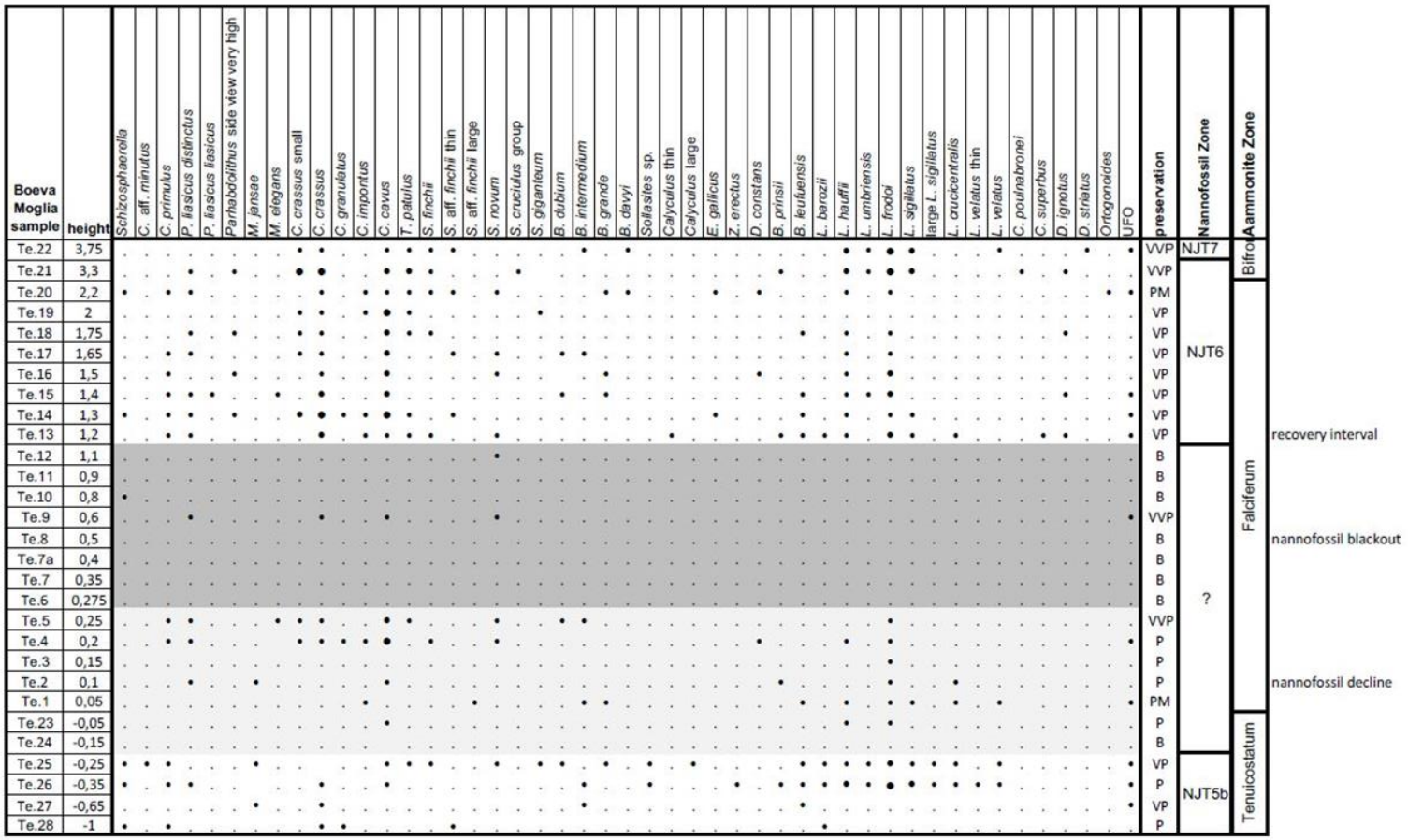

(PTO for caption)

Figure 3.17 (previous page) Nannofossil distribution chart for Boeva Mogila section. Sample numbers correspond to numbers given in sedimentary log (Figure 3.7).

Assemblages are largely dominated by imbricated coccoliths (Figure 3.18), mainly belonging to the *Lotharingius* genus in the upper part of Pliensbachian and lower Toarcian. In the middle Toarcian, a peak of loxolith-coccoliths occurs, mainly *Crepidolithus crassus* and *Tubirhabdus patulus* (Figure 3.18). These are characterized by a vertical distal rim with oblique elements. Of the imbricated placolith-coccoliths (formed by two superposed shields with imbricated elements) the small *Lotharingius*, mainly *L. hauffii* and *L. frodoi* are very abundant in the upper part of Pliensbachian and lower Toarcian (Figure 3.18). From the middle Toarcian, these are replaced by large specimens of *Lotharingius barozii* and large-sized forms like *Lotharingius velatus*. A similar trend has already been observed in Portugal and southern France (Ferreira et al., 2017).

The calcareous nannofossil biostratigraphy, is in general agreement with the ammonite biostratigraphy for the Milanovo section. Biostratigraphy using ammonite records from the Milanovo section only indicates the early Toarcian (*tenuicostatum*-middle *falciferum* Zone), and cannot be further subdivided due to a lack of ammonite records in the section. Similarly, concerning nannofossil assemblage and biostratigraphy, higher-resolution sampling would be needed to provide a more precise biostratigraphic frame. A hiatus at the Pl-To boundary is possible, but it is not detected by means of nannofossils.

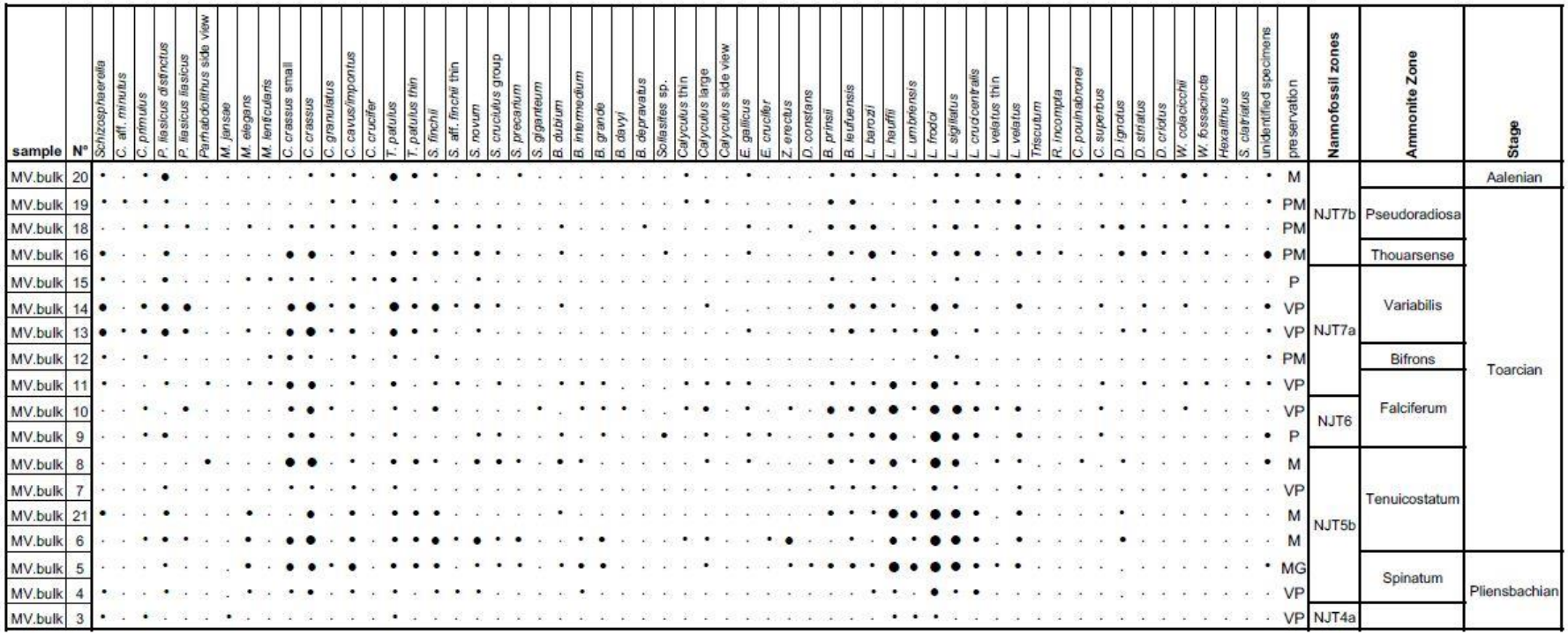

Figure 3.18 Nannofossil distribution chart for the Milanovo section. Sample numbers correspond to numbers given in sedimentary log (Figure 3.6).

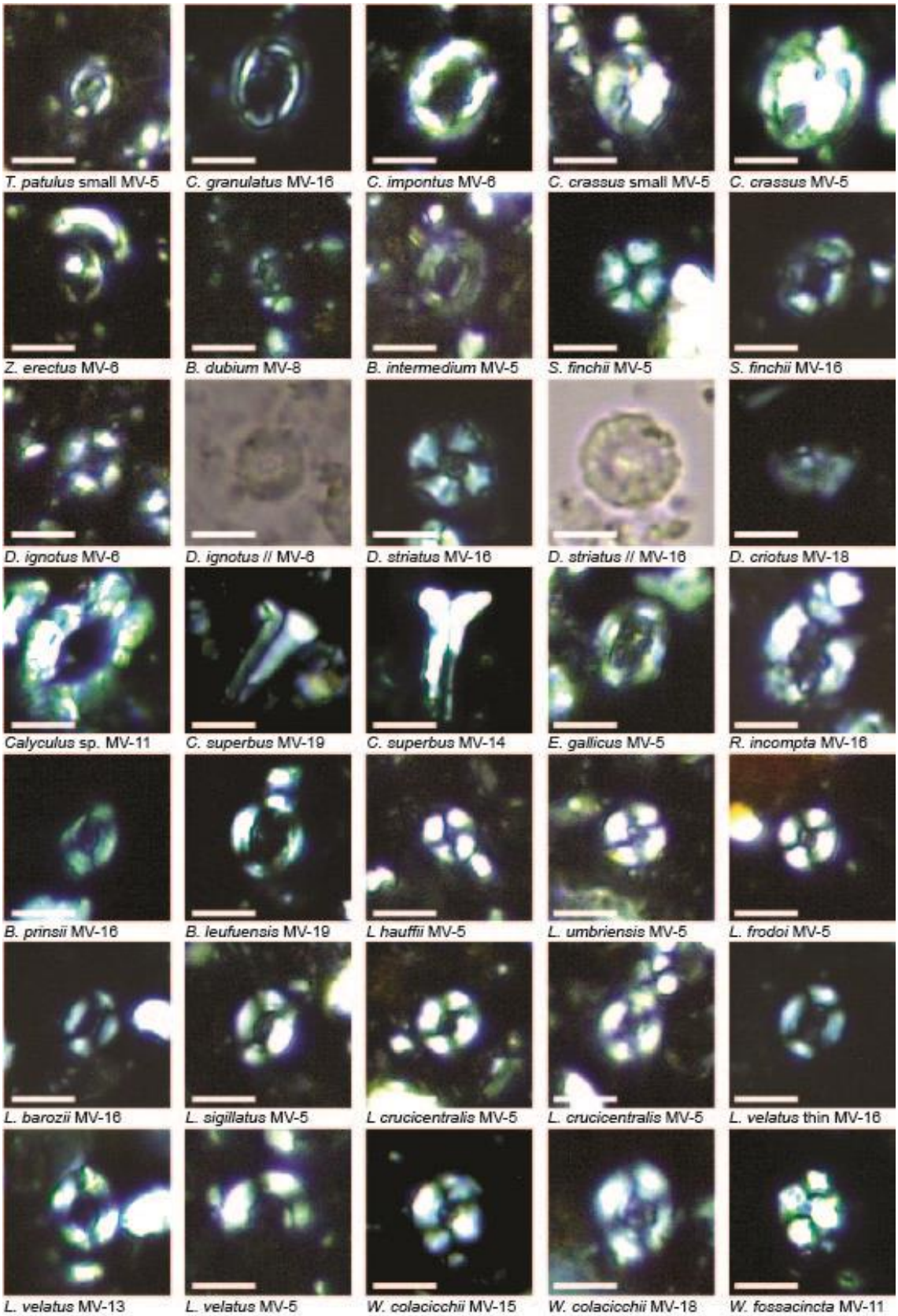

Figure 3.19 Photomicrographs of calcareous nannofossils from the upper Pliensbachian and Toarcian in northwest Bulgaria. Photographs provided by Emanuela Mattioli (University of Lyon, France).

3.8 Chemostratigraphic records

3.8.1 $^{87}Sr/^{86}Sr$ isotopic trends

$^{87}Sr/^{86}Sr$ ratios were obtained from the Milanovo and Vradlovtsi-2 sections in order to use strontium isotope stratigraphy to provide chemostratigraphic age constraint and to compare to biostratigraphic information.

All strontium ratios obtained from belemnites have undergone diagenetic pre-screening (Chapter 4). All $^{87}Sr/^{86}Sr$ ratios and associated analytical error for each subsample is graphically represented in Figure 3.6 and Figure 3.12 and provided numerically in Appendix A. Analytical uncertainty for all data points was relatively low, with precision of analysis to the sixth decimal place for all values (Appendix A).

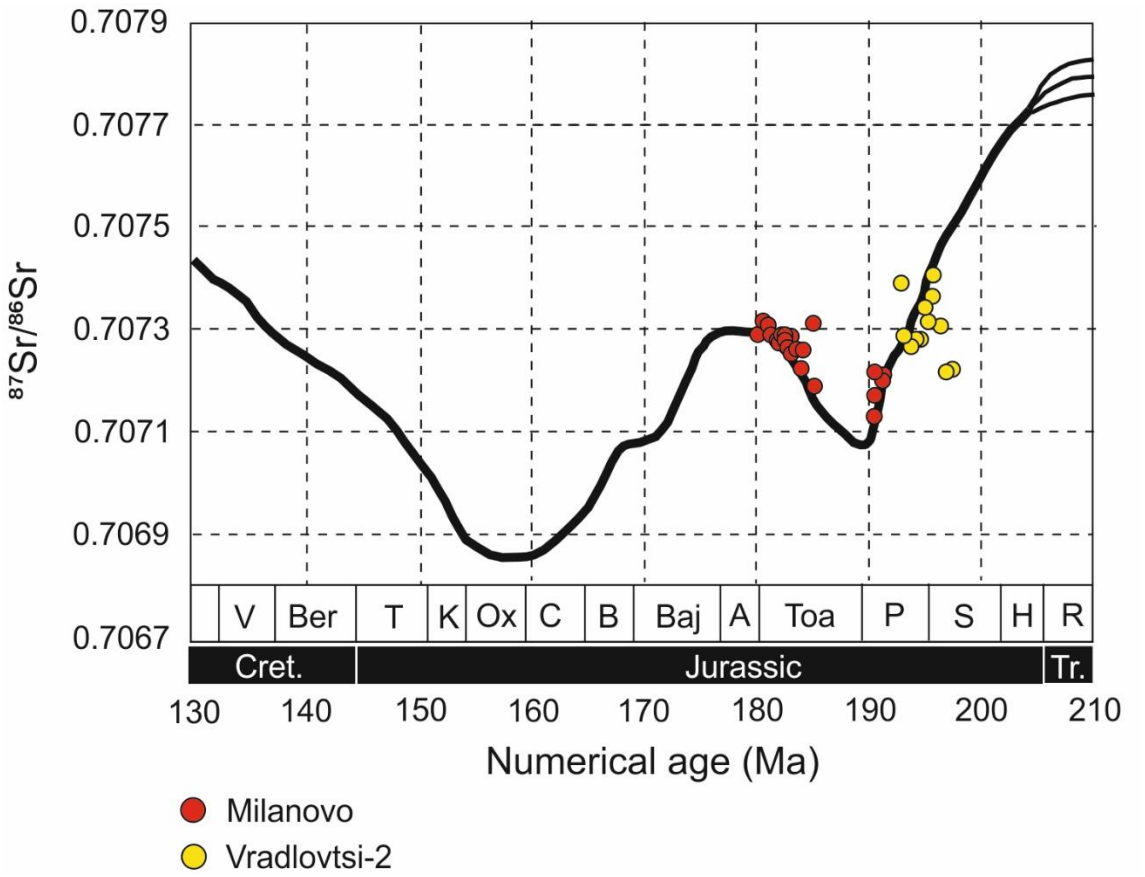

Figure 3.20 $^{87}Sr/^{86}Sr$ values of belemnites from the Milanovo section (red circles) and Vradlovtsi-2 section (yellow circles), plotted onto the LOWESS $^{87}Sr/^{86}Sr$ reference curve, modified after McArthur et al. (2001). R=Rheatian, H=Hettangian, S=Sinemurian, P=Pliensbachian, Toa=Toarcian, A=Aalenian, Baj=Bajocian, B=Bathonian, C=Callovian, Ox=Oxfordian, K=Kimmeridgian, T=Tithonian, Ber=Berriasian, V=Valanginian.

3.8.1.1 Milanovo section

The $^{87}Sr/^{86}Sr$ curve, measured on belemnites from the Milanovo section, is composed of two distinct segments. The first segment records a rapid decrease in $^{87}Sr/^{86}Sr$, towards less radiogenic values at the base of the section in the late Pliensbachian (*spinatum* Zone) (Figure 3.6). The second segment records a general increase of $^{87}Sr/^{86}Sr$, towards more radiogenic values, through the Toarcian (1.51-4.33 m) (Figure 3.6). The two segments are separated by a section lacking in belemnites (1.1-1.3 m) (Figure 3.6).

In the lower part of the strontium curve, the rapid decrease records values from 0.7072159 to 0.7071279. Through the Toarcian, the measured $^{87}Sr/^{86}Sr$ ratios range between 0.7071982 to 0.7072981, with slightly more radiogenic values of 0.7073123 and 0.7073208, measured in at the top of the late Toarcian *pseudoradisoa* Zone (Figure 3.6). There is an exceptionally radiogenic $^{87}Sr/^{86}Sr$ ratio with respect to underlying values, of 0.7073131 (1.58 m) in the early Toarcian (Figure 3.6).

In the Milanovo section, there is general agreement between the ammonite biostratigraphic age assignments and indicated ages from comparison with the LOWESS curve (Figure 3.20). Sr isotope curve from the Bulgarian sections confirms that produced from other European records. The key results from the $^{87}Sr/^{86}Sr$ curve recorded from the Milanovo section are as follows:

1) A decrease in $^{87}Sr/^{86}Sr$ ratios are recorded through the Late Pliensbachian *spinatum* Zone in the Milanovo section suggests the sequence might be highly condensed in this zone.

2) The rapid rise of $^{87}Sr/^{86}Sr$ that coincided with the onset of the T-OAE is not recorded from the Toarcian Milanovo section due to the indicated hiatus across the Pl-To boundary that continues through the *tenuicostatum* Zone. This is comparable to a hiatus from the Late Pliensbachian (*spintaum* Zone) to the early Toarcian *bifrons* Zone that has also been recorded in central Bulgaria, in the Teteven region (Metodiev et al., 2014).

3) The continued rise of $^{87}Sr/^{86}Sr$ through the late Toarcian interval is comparable to the long- term increase in $^{87}Sr/^{86}Sr$ overserved in Western Europe (McArthur and Wignall, 2007), the Mediterranean realm (Woodfine et al., 2008) and the Panthalassa Ocean (Gröcke et al., 2007).

3.8.1.2 Vradlovtsi-2 section

The $^{87}Sr/^{86}Sr$ curve, measured on belemnites from the Vradlovtsi-2 section show a more fluctuating trend than the strontium isotope curve recorded in the Milanovo section.

At the base of the Dolni Lukovit Member, $^{87}Sr/^{86}Sr$ ratios are 0.7072247 (0.0 m) and 0.7072239 (0.15 m) (Figure 3.12). Following this is a shift to more radiogenic $^{87}Sr/^{86}Sr$ ratios of 0.7074064 (0.9 m) and 0.7073693 (1.1 m) (Figure 3.12). The sudden shift to more radiogenic values at the base of the strontium curve, may indicate a hiatus or condensed sediments. The overall trend then decreases towards less radiogenic values between 0.7073693 (2.7 m) and 0.7072754 (7.53 m). The final segment of the strontium curve from the Vradlovtsi-2 section shows an increase to more radiogenic values reaching a highest radiogenic value of 0.7073855 (9.95 m) (Figure 3.12).

In the Vradlovtsi section, there is very little biostratigraphic age constraint and so the $^{87}Sr/^{86}Sr$ ratios are plotted against the LOWESS curve to provide a chemostratigraphic indication of the age of the Dolni Lukovit Member (Figure 3.20). The $^{87}Sr/^{86}Sr$ ratios indicate the base of the section is upper Sinemurian to lower Pliensbachian in age. Overall, some of the $^{87}Sr/^{86}Sr$ ratios for this section are lower than would be expected (Figure 3.20), which could indicate diagenetic alteration of belemnite calcite. However, there is no evidence of these specific samples being more affected by diagenetic alteration (see Chapter 4).

3.9 Conclusions

Sediments deposited in the Moesian Basin record a predominantly carbonate system, often with continued siliciclastic input. The Toarcian sedimentary successions in the Moesian Basin record high levels of condensation and occasional hiatuses. New data from Bulgaria improved parts of the Lower Jurassic biostratigraphic framework. Firstly, Palynomorphs indicated the date of the Bachiishte Formation could be Hettangian. Secondly, the *ibex* Zone of the early Pliensbachian was identified for the first time in Bulgaria. Thirdly, the first record of Toarcian calcareous nannofossils was recorded for Bulgaria, belonging to the NJT4a, NJT5b, NJT6, NJT7a and NJT7b Zones. New chemostratigraphic records are provided for the Pliensbachian and Toarcian. Strontium isotope stratigraphy for the Milanovo and Vradlovtsi $^{87}Sr/^{86}Sr$ curves generally matched the Lower Jurassic LOWESS curve.

Chapter 4 : Long-term stable isotope trends (carbon and oxygen) through the Lower Jurassic

4.1 Introduction

This chapter presents new geochemical data from well-preserved, calcitic belemnites screened for diagenetic overprint from three Lower Jurassic (Sinemurian-Toarcian) sections from northwest Bulgaria. The carbon and oxygen isotope ratios from these belemnites are used to provide insight into long term palaeoenvironmental changes. Specifically, they are used to investigate carbon cycle and palaeoclimatic changes in seawater temperatures of the basin.

This chapter presents data from 369 new analyses, together with 174 analyses from published datasets from the same time interval in Bulgaria (Metodiev and Koleva-Rekalova, 2008; Metodiev et al., 2014). Although, this previously published work gives an initial understanding of carbon and oxygen isotope trends through the Lower-Middle Jurassic (latest Pliensbachian-Early Bajocian), the existing records are at a low resolution, particularly for the early Toarcian. interval. Given the natural scatter of $\delta^{13}C_{bel}$ and $\delta^{18}O_{bel}$ data, it is important to assess if these previous records represent actual shifts in the isotopic composition of seawater in the Moesian Basin. This chapter expands on previous work from the early Toarcian and provides the first $\delta^{13}C_{bel}$ and $\delta^{18}O_{bel}$ records through the late Pliensbachian interval (*davoei-spinatum* Zone) and part of the Sinemurian. This provides a significantly more robust record of palaeoenvironmental and climatic change from the eastern part of the EES.

4.2 Methods

Methods applied in this chapter are for belemnite rostra material and are cross-referenced to detailed methods in Chapter 2 (see Table 4.1).

Table 4.1. List of methods employed for analysis in chapter 4

Method	Heading # (page #)	Sections
Belemnite preparation	2.5.2.2 (page 77)	Milanovo Boeva Mogila

		Vradlovtsi Balsha Brakyovtsi Vradlovtsi-1 Ravna Dragovishtitsa Brakyovtsi
Microscopy: Cathodoluminescence (CL) and Transmitted Light (TL)	2.5.2.3 (page 27)	Milanovo Boeva Mogila Vradlovtsi-2 Berende Izvor Balsha Brakyovtsi Vradlovtsi-1 Ravna Dragovishtitsa Brakyovtsi Dobtavitsa-1 Beledie Han
Element analysis	2.5.2.4 (page 81)	Milanovo Vradlovtsi-2 Berende Izvor
Carbon and oxygen isotopes ($\delta^{13}C_{bel}$ and $\delta^{18}O_{bel}$)	2.5.2.6 (page 83)	Milanovo Vradlovtsi-2 Berende Izvor

4.2.1 Selected study sites and material

Figure 4.1 A) Detailed outcrop map of west and central area in Bulgaria. Sections with new belemnite geochemical data shown in red and published data (from Metodiev and Koleva-Rekalova, 2008; Metodiev *et al.*, 2014) shown in blue. Other studied sections shown in black for reference. B) Outline map of Bulgaria, with the study area highlighted by black box.

Belemnites were selected as the most suitable material to construct $\delta^{13}C$ and $\delta^{18}O$ curves, as their low-Mg calcite composition makes them relatively stable and resistant to diagenetic alteration (Veizer and Compston, 1974; Saelen, 1989; Podlaha et al., 1998; Rosales et al., 2001). In addition, the relatively large number of belemnites through the Lower Jurassic sections allow high resolution sampling, enabling long-term trends in past seawater to be established. Although brachiopods and bivalves are present in some of the sections, they are not as abundant and time constraints did not allow for multiple sources of biogenic carbonate to be screened and analysed.

A four-step selection criterion for belemnites was designed to ensure a stratigraphically continuous $\delta^{13}C_{bel}$ and $\delta^{18}O_{bel}$ record from well-preserved belemnites, at the highest resolution possible (Table 4.2). These criteria were applied to all the 14 studied sections (Table 4.2).

Step one assessed the abundance of belemnites within each section, ranging from rare (present in 5-30% of beds), common (present in >30–70% of beds) to abundant (present in >70% of beds). Where belemnites were ‘absent’ or ‘rare’ the sections were not considered suitable for this study. Step two assessed overall belemnite preservation in the field, classifying preservation as good (no clear signs of weathering or alteration) or poor (heavily altered, clearly weathered calcite). Belemnites with evidently poor preservation were not collected. Step three used microscopy (under TL and CL) on a representative number of belemnite thick sections (25% of belemnites evenly distributed through the section) to evaluate the preservation state. Each belemnite was given a luminesce type between 1 and 6, with ‘type 1’ representing non-

luminescent calcite (indicative of less-altered calcite) and ‘type 6’ representing pervasive highly luminescent calcite (indicative of heavily altered calcite). Average CL types are given for each section (individual CL types for all belemnites are shown in Appendix B). Belemnites with CL types between 1 and 4 were considered for further analysis. Where CL types were predominately 5-6, belemnites from the section were not used for further analysis. Step four noted the biostratigraphic constraint for each section and these were classified as ‘well-established’, where the section has been biostratigraphically dated, or ‘limited’ where a rare occurrences or single occurrences of ammonites gave an indication of age, but at a very low resolution.

Well-preserved belemnites from sections with abundant belemnites, with good biostratigraphic control were selected for carbon and oxygen isotope analysis. These sections were Milanovo and Berende Izvor. Vradlovtsi-2 was also chosen because it provides the first Sinemurian carbon and oxygen isotope record from Bulgaria, although its biostratigraphy is less well known. As $\delta^{13}C_{bel}$ and $\delta^{18}O_{bel}$ values have already been recorded for Dobravitsa-1 and Beledie Han sections (Metodiev and Koleva-Rekalova, 2008) belemnites were not re-collected.

Table 4.2 Selection criteria for sections suitable to generate $\delta^{18}O_{bel}$ and $\delta^{13}C_{bel}$ curves. Biostrat. = biostratigraphic, n/a = not/applicable. Sections selected are highlighted dark grey and sections with published data are highlighted light grey.

All sections	**Step 1** Belemnite abundance	**Step 2** Initial textural preservation assessment	**Step 3** Average CL ‘type’	**Step 4** Biostrat. constraint
Milanovo	Abundant	Good	2-4	Well-established
Vradlovtsi-2	Abundant	Good	2-5	Limited
Berende Izvor	Abundant	Good	n/a	Well-established
Boeva Mogila	Abundant	Good	2-4	Well-established
Balsha	Abundant	Good	4-6	Limited
Kiselchov Dol	Abundant	Poor	n/a	Well-established

Gorno Ozirovo	Abundant	Poor	n/a	Well-established
Dragovishtitsa	Common	Good	4-5	Limited
Vradlovtsi-1	Rare	Good	3	Limited
Ravna	Rare	Good	4-6	Limited
Teteven	Rare	Good	5	Limited
Brakyovtsi	Rare	Good	5	Limited
Yamna	Absent	Good	n/a	Limited
Dobravista-1	Abundant	Good	2-5	Well-established
Beledie Han	Abundant	Good	2-3	Well-established

4.3 Results

4.3.1 Diagenetic evaluation

The degree of preservation of belemnite calcite was evaluated through belemnite microscopy and trace element analyses. Taking into account that none of these screening techniques are without limitations, a combination of approaches was utilised. Diagenetic effects on belemnite calcite must be evaluated through belemnite microscopy and elemental data before environmental implications of the carbon and oxygen isotope data can be utilised.

4.3.1.1 Belemnite microscopy

Examination of belemnite calcite using optical microscopy and cathodoluminescence revealed variable degrees of preservation. All belemnites from the Vradlovtsi-2, Berende Izvor and Milanovo sections show prominent fractures, likely to be associated with burial and tectonic events. Belemnite calcite away from fractures showed no clear indications of the alteration of calcite when viewed under an optical microscope. All belemnites from these sections recorded predominantly transparent calcite, with no evidence of recrystallisation (e.g. cloudy calcite).

A qualitative record of ‘cathodoluminescence types’ has been applied to all belemnites. Common alteration features were observed in all belemnites investigated under cathodoluminescence. These features include bright luminescence in the apical zone, the first bands around the apical zone, the outermost edge of the rostrum and along prominent fractures. Alteration is also commonly recorded in the same areas of belemnite rostra from other studies suggesting that the observations are representative of belemnite rostra in general (Podlaha et al., 1998; McArthur et al., 2000; McArthur et al., 2007; Ullmann, 2013). The presence of small microstylolite fractures with dull luminescence was observed in most belemnites. These are a compaction feature associated with the strong tectonic compression of the Lower Jurassic sections during the Alpine Orogeny. As the Lower Jurassic sedimentary rocks were involved in this compressional system, microstylolites will have developed in softer calcite macrofossils, such as belemnites, allowing greater access to biogenic calcite by post-depositional fluids. These microstylolites are not a common feature in Lower Jurassic belemnites from other European sections, but have been noted as a late diagenetic feature from Lower Jurassic belemnites in Spain, from the Basque–Cantabrian Basin (Rosales et al., 2001; Rosales et al., 2004a,b) and the Austrian Basin (Armendáriz et al., 2012; Gómez et al., 2016).

Belemnites selected for this study from sections Vradlovtsi-2 and Milanovo indicate well-preserved belemnite calcite under both optical microscopy and cathodoluminescence. Although many belemnites indicated some diagenetic alteration and secondary calcite, careful microdrilling allowed areas of more pristine calcite from each belemnite to be selected. The belemnites from the Vradlovtsi-2 section are the best preserved, with most rostra categorised under CL as types 3, with a low amount categorised as CL types 4-5. Belemnites from the Milanovo section are relatively well-preserved. Although CL types between 2 and 5 were recorded from the Milanovo section, most were below CL type 4. Belemnites from the Boeva Mogila section are moderately well-preserved, with most belemnites categorised as CL types between 2 and 4. Unfortunately, belemnites from the Berende Izvor section could not be analysed using CL as they were too fragmentary to enable thick sections to be made.

Belemnites removed from further analysis recorded high levels of luminescence indicative of post-depositional diagenetic alteration, (categorised with CL types predominately between 5 and 6). Such belemnites were recorded from Balsha and Ravna sections. Belemnites from Dragovishtitsa, Vradlovtsi-1, Teteven and Brakyovtsi sections showed variable degrees of preservation (CL

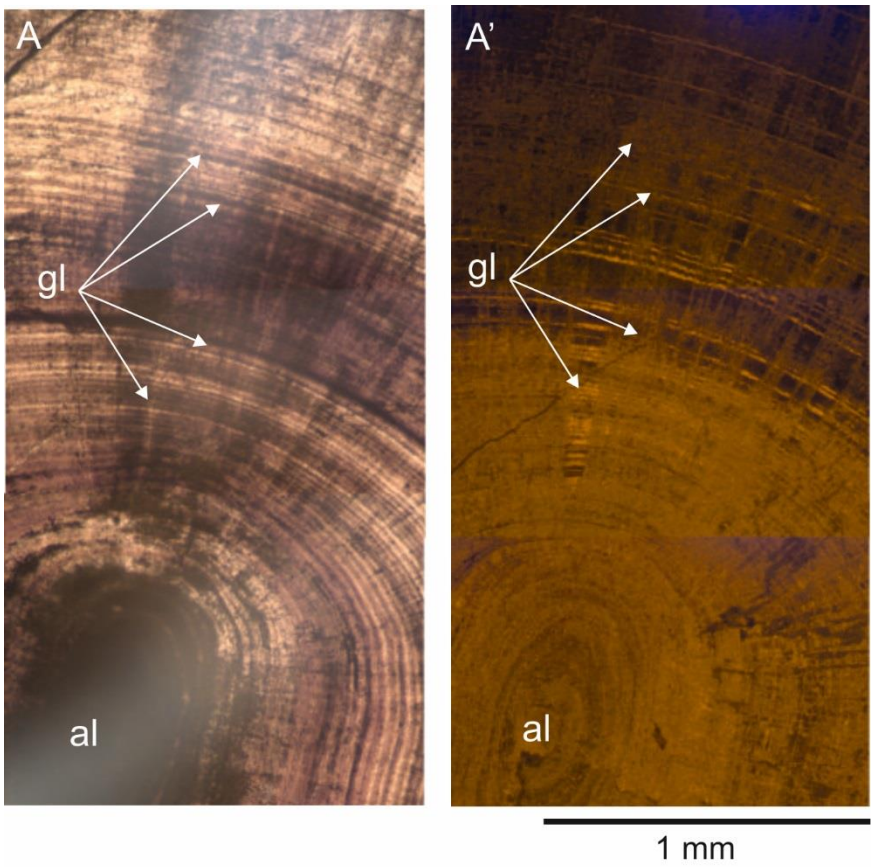

Figure 4.2. Thick-section photomicrographs of belemnite (Ba.9.10) from Balsha section in transmitted light (A) and cathodoluminescence (A'). Photomicrographs show highly altered belemnite calcite, with apical line (al) and all growth lines (gl) orange luminescence. This belemnite is categorised as cathodoluminescence type 6, as very limited non-luminescent calcite remains.

types between 3 and 5). However, the limited number of belemnites present in each section, along with limited biostratigraphic constraint, would only generate low resolution data of an uncertain age and so belemnites from these sections are not analysed any further.

Previous CL work on belemnite samples from Dobravitsa-1 (Metodiev and Koleva-Rekalova, 2003) and Beledie Han (Metodiev and Koleva-Rekalova, 2005) sections enabled a 'CL type' to be assigned to all individual belemnites . This allowed all belemnites to be assessed and evaluated under the same classification scheme. Belemnites from Dobravista-1 showed CL types between 2 and 5 and from Beledie Han were between CL types 2 and 3.

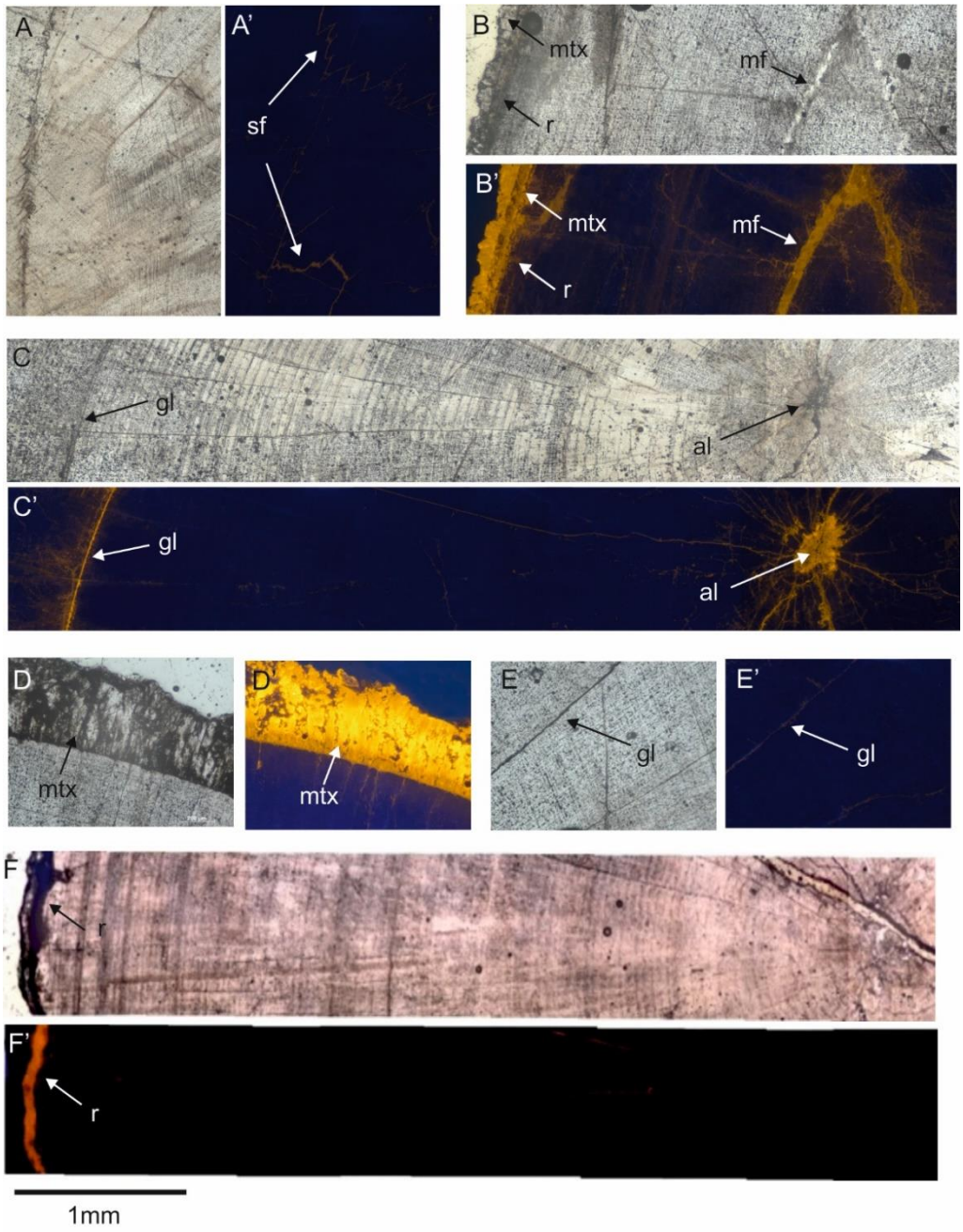

Figure 4.3 Thick-section photomicrographs of belemnites from Milanovo (Mv) and Vradlovtsi (Vd) sections. A-F are under transmitted light and A'-F' the same views under cathodoluminescence. (A-A') MVv.18.3, CL type 4. Well-preserved non-luminescent belemnite calcite with stylolitic microfractures (sf). (B-B') Mv.3.5, CL type 4. Moderately well-preserved luminescent outer rim (r) in contact with luminescent matrix (mtx), dull luminescent growth lines (gl) and luminescent microfractures (mf). (C-C') MVv.2.40.2, CL type 3. Well-preserved non-luminescent belemnite rostrum, with luminescence at the apical line (al) and growth line (r). (D-D') Mv.5.43, CL type 4. Luminescent matrix (mtx), with limited alteration to belemnite calcite. (E-E') Mv.5.43, CL type 4. Well-preserved non-luminescent belemnite calcite, with dull luminescent growth lines (gl). (F-F') Mv.5.25, CL type 2. Well-preserved non-luminescent belemnite rostrum, with orange luminescence only at the outer rim (r) and very faintly luminescent microfractures.

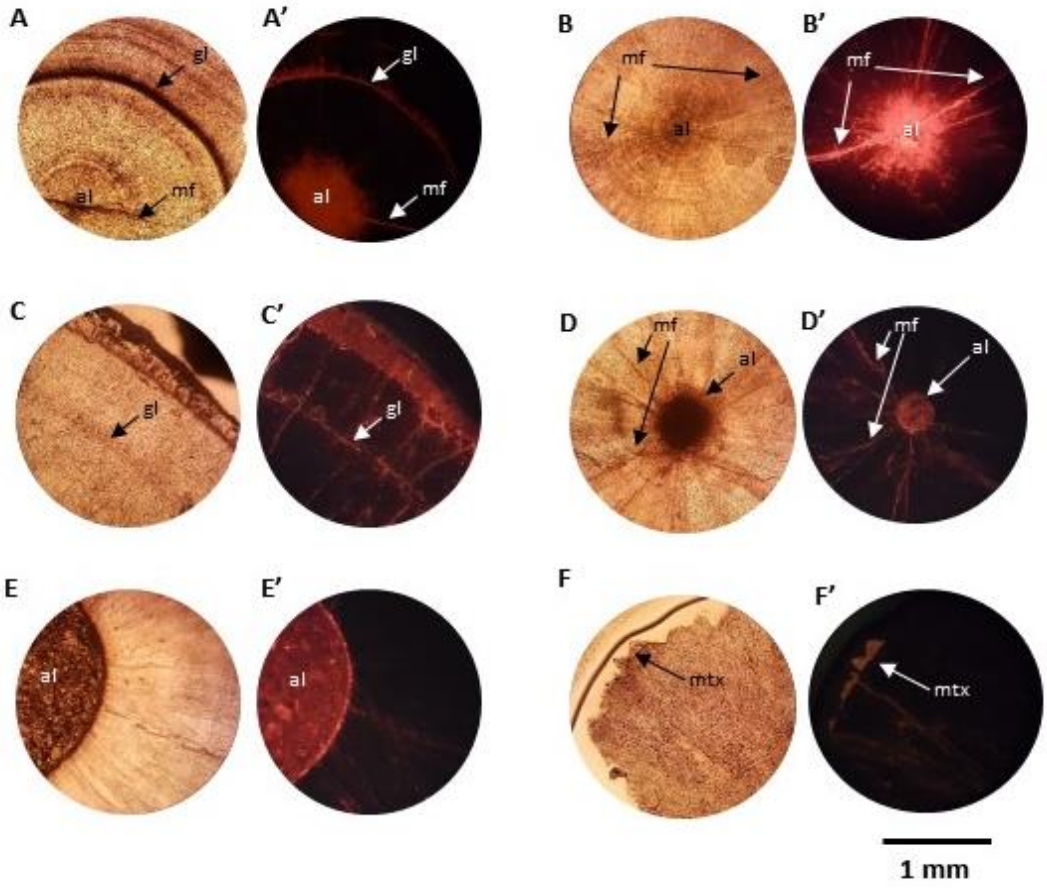

Figure 4.4. Thick-section photomicrographs of belemnites from the Boeva Mogila section. A – F are under transmitted light (TL) and A'-F' the same views under cathodoluminescence (CL). (A-A') Te-21, CL type 3. Well-preserved non-luminescent belemnite calcite with apical line (al), growth lines (gl) and microfractures (mf) showing orange luminescence. (B-B') Te-22a.1, CL type 4. Apical line (al) displays bright orange luminescence with some radial microfractures (mf). Luminescence around apical line is well-constrained to centre of belemnite rostrum. (C-C') Te-23, CL type 3. Moderately preserved belemnite calcite, with prominent orange luminescent growth lines (gl), outer rim and pervasive microfractures. (D-D') Te-24, CL type 3. Moderately preserved belemnite calcite, with prominent orange luminescent apical line (al) and radial microfractures (mf). (E-E') Te-28, CL type 2. Well-preserved non-luminescent belemnite calcite with bright orange luminescent infill that is well-constrained. (F-F') Te-3, CL type 3. Dull orange luminescence at edge of belemnite where matrix is attached.

4.3.1.2 Trace element concentrations

All elemental concentrations are displayed in Appendix B. Elemental concentrations of Manganese (Mn), Strontium (Sr), and Iron (Fe) from belemnite calcite are utilised as indicators of post-depositional diagenetic

alteration. Upper operational limits (UOL) for Mn/Ca and Fe/Ca ratios, and lower operational limits (LOL) for Sr/Ca ratios in belemnites are used to indicate diagenetically altered samples. There are currently no universally adopted limits to indicate alteration of biogenic calcite for each element. Limits adopted may differ depending on fossil type, diagenetic and depositional setting, and even vary by author (Ullmann and Korte, 2015). The limits adopted for this study have been selected based on commonly adopted limits for belemnite calcite from Lower Jurassic calcite seas (Ullmann and Korte, 2015).

Mn and Mn/Ca

Mn is the most widely employed monitor of alteration as Mn levels in primary shell material are usually very low, but become enriched during diagenesis due to post-depositional dissolution and recrystallisation of calcite (Veizer, 1974; Veizer et al., 1986; Denison et al., 1994).

An upper limit for Mn concentrations of 100 ppm is adopted after (McArthur et al., (2004) and ; Nunn and Price, (2010) (Figure 4.5, UOL.1). A higher blanket upper limit of 250 ppm is often used for biogenic carbonate (e.g. Korte and Hesselbo, 2011) (Figure 4.5, UOL .2). This, however, is used for multiple fossil shell types, including bivalves, brachiopods and belemnites, whereas only belemnites were evaluated in this study. Mn values <100 ppm were recorded in most samples from the Milanovo and Vradlovtsi-2 sections (Figure 4.5). Only two Mn concentrations were obtained from Berende Izvor section, with values of 24 ppm and 20 ppm (samples BI.1b.2 and BI.3.2, respectively), as all other samples had values lower than the detection limit of analysis. These very low and, in some cases, undetectable Mn concentrations verify good chemical preservation of belemnites in this study. Belemnite calcite samples with higher Mn concentrations over 100 ppm were recorded from five samples in the Boeva Mogila section (samples Te.21, Te.22a, Te.22c and Te.24), with Mn concentrations between 101 and 294 ppm. One anomalously high Mn concentration of 447 ppm was recorded from the Vradlovtsi-2 section (sample Vd.10.40.2).

For Mn/Ca ratios, a limit of <0.06 mmol/mol is adopted after (Jones et al., (1994) and van de Schootbrugge et al. (2005) is adopted (Figure 4.5, UOL.1). Some authors use higher Mn/Ca limits of <0.10 mmol/mol (e.g. Ullmann et al., 2015) for belemnites (Figure 4.5, UOL.2), but a limit at the lower end of applied limits is adopted here, to provide the most critical view of potential diagenetic alteration. The Mn/Ca ratios yielded from belemnite calcite are relatively low,

with most samples recording Mn/Ca ratios < 0.06 mmol/mol. The few samples over this operational limit (UOL.1, Figure 4.5) record Mn/Ca values between 0.07-0.08 mmol/mol. Interestingly, if the UOL for Mn/Ca >0.1 mmol/mol used by Ullmann et al., 2014 were to be adopted (UOL.2, Figure 4.5), all samples would be considered unaltered. There is no strong evidence of consistently elevated Mn/Ca ratios from belemnites corresponding to particular sections or ammonite zones. Elevated Mn/Ca ratios recorded in the early Toarcian in the Milanovo section, are likely to correspond to diagenetically altered calcite, with lighter $\delta^{18}O$ (below -4 ‰) and luminescent calcite (CL type 4-5).

Sr and Sr/Ca

Strontium, modulated by its variable initial concentration in primary carbonate phases (Korte and Hesselbo, 2011; Ullmann, et al., 2013), is lost due to dissolution and recrystallisation of diagenetic calcite phases (Brand and Veizer, 1980), resulting in a depletion of Sr in diagenetically altered samples. A lower limit for Sr concentrations of 400 ppm is adopted from (Nunn and Price, (2010). No samples in this study had values where Sr concentration <400 ppm. The most depleted values recoded Sr concentrations of ~800 ppm (Figure 4.5).

A lower limit for Sr/Ca is 1.2 mmol/mol for Sr/Ca was adopted from Ullmann et al. (20014) (Figure 4.5, LOL 1). The Sr/Ca ratios recorded from biogenic calcite from all sections studied were between 0.91 and 1.91 mmol/mol. The majority of belemnite samples have Sr/Ca ratios above the adopted lower operational limit > 1.2 mmol/mol (LOL.1). Lower limits of 0.46 mmol/mol have been adopted by previous authors (Figure 4.5, LOL 2). If this limit is applied to samples in this study, no Sr/Ca values indicate diagenetic alteration. Samples with slightly depleted Sr/Ca values do not correspond to particular sections, facies or ammonite zones.

Fe/Ca

High Fe/Ca ratios can be indicative of diagenetic alteration. Where Fe is present as soluble Fe(II) (Glasby and Schulz, 1999) under reducing conditions and at a reduced pH, it can be incorporated into biogenic calcite (e.g. (Brand and Veizer, 1980). An upper limit for Fe/Ca of 0.27 mmol/mol is adopted for this study (Figure 4.5, UOL.1) from McArthur et al. (2004); Jones et al. (1994) and Nunn and Price, (2010). A higher upper limit of 0.45 mmol/mol is has been adopted by some authors (Price and Sellwood, 1997; Rosales et al., 2004; Benito and Reolid, 2012) (Figure 4.5, UOL.2).

Overall, the Fe/Ca ratios of belemnite calcite in Bulgaria provide highly heterogeneous results. Fe/Ca ratios from the relatively deeper water Milanovo section range from 0.03-1.04 mmol/mol, with over 75% of samples below the 0.27 mmol/mol upper limit (Figure 4.5). High Fe/Ca ratios from these belemnites corresponded to simultaneously enriched Mn/Ca ratios (samples Mv.20.40.2, Mv.6 and Mv.7.10.2). Elevated Fe/Ca ratios are more common from the shallower marine Vradlovtsi-2 section, with most values ranging from 0.05 – 0.80 mol/mol (Figure 4.5). Higher peaks around 1.37, 1.98 and 3.85 mmol/mol were also recorded (Figure 4.5). The highest Fe/Ca ratios are recorded from the shallow water Berende Izvor section, which show consistently elevated values between 0.17-2.65 mmol/mol, with 96% of all samples over the upper limit of 0.27 mmol/mol . If the Fe/Ca limit is increased to 0.46 mmol/mol (Figure 4.5), almost 80% of samples are above this limit . In previously published datasets for Lower Jurassic belemnites in Bulgaria, high Fe/Ca ratios are also observed (Metodiev and Koleva-Rekalova, 2008), particularly in shallow marine oolitic ironstones of the Beledie Han section (Figure 4.5). Interestingly, the unusually high Fe/Ca ratios are not noted in the study. When belemnites from numerous sections in the Moesian Basin are analysed, there is clear difference between low Fe/Ca in relatively deeper sections and very high Fe/Ca from shallow marine sections.

The high Fe/Ca ratios observed in belemnites from Berende Izvor, Beledie Han and Vradlovtsi-2 may point to diagenetically altered calcite. The lack of luminescence in belemnite calcite with high Fe/Ca ratios may be induced by diagenetically incorporated Fe, supressing the emission of the characteristic-orange light from Mn-enriched material (Frank et al, 1982; Barbin, 2000). However, there is no clear correlation between elevated Fe/Ca ratios with elevated Mn/Ca or depleted Sr/Ca ratios, and thus does not support strongly altered belemnite calcite.

Elevated Fe/Ca ratios has previously been linked to contamination from the steel device used for drilling (Ullmann and Korte, 2015). This is unlikely as the same type drill bits were used for all belemnites in this study and Fe/Ca ratios are not consistently high.

Elevated Fe/Ca ratios are recorded from belemnites from the more proximal shallower marine sections of Vradlovtsi-2 and particularly from the Pliensbachian ironstones in Berende Izvor section (this study) and Toarcian ironstones in the Beledie Han section (Metodiev and Koleva-Rekalova, 2008). It is likely that high Fe/Ca values are a result of post-depositional iron-rich sediment pore waters in these sections.

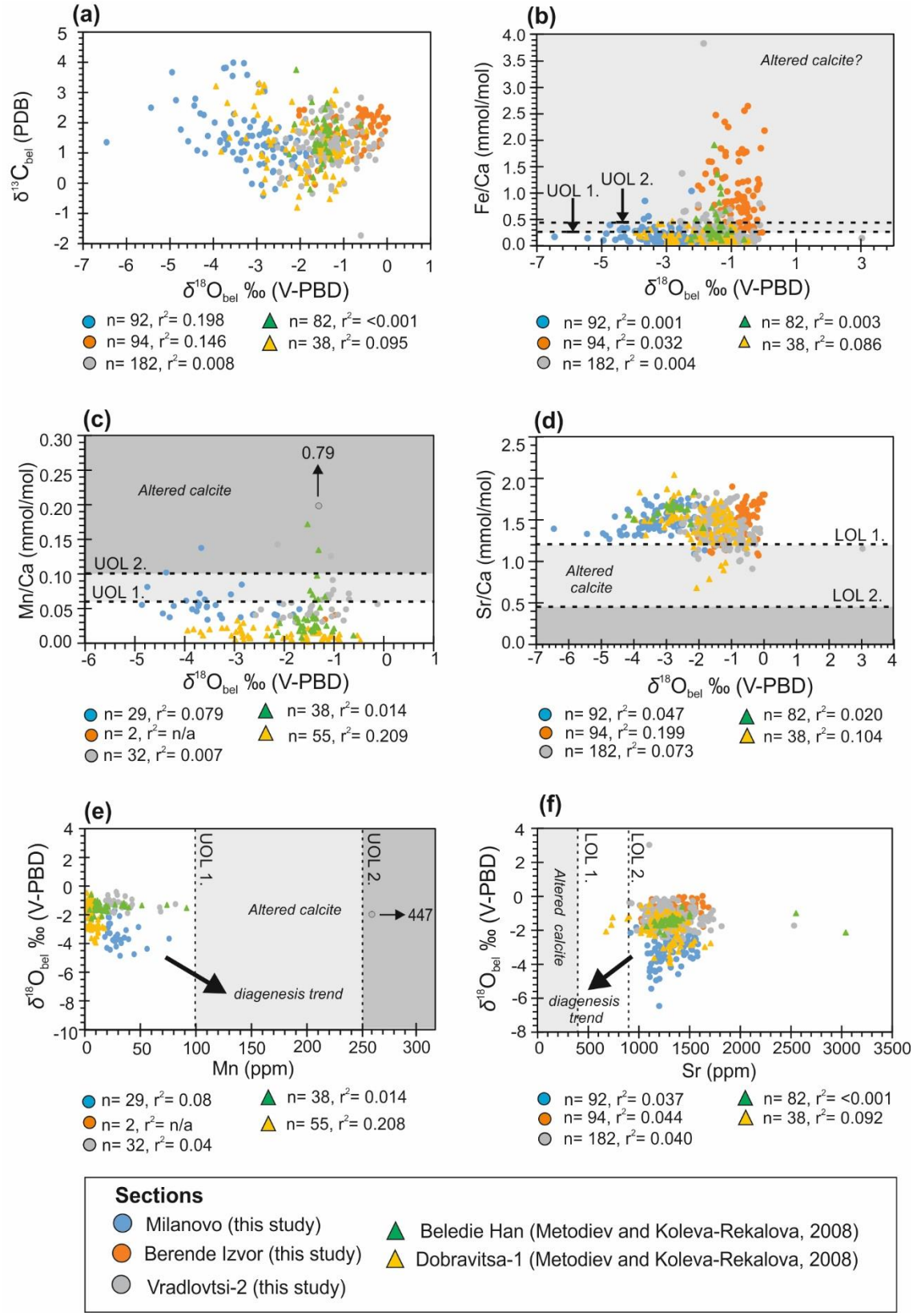

Figure 4.5 Cross-plots of (a) $\delta^{13}C$-$\delta^{18}O$; (b) Fe/Ca-$\delta^{18}O$; (c) Mn/Ca-$\delta^{18}O$; (d) Sr/Ca-$\delta^{18}O$; (e) $\delta^{18}O$-Mn and (f) $\delta^{18}O$-Sr. Results are separated into sections with key given in figure. Dashed lines show different upper operational limits (UOL) and lower operational limits (LOL) used by various authors (values given in text).

4.3.1.3 Co-variation between $\delta^{13}C_{bel}$ and $\delta^{18}O_{bel}$

Diagenetic alteration of marine carbonate has been shown to result in covariation of carbon and oxygen isotope ratios (e.g. Brand and Veizer, 1981). The correlation between $\delta^{13}C_{bel}$ values and $\delta^{18}O_{bel}$ is quantified using Pearson's r correlation co-efficient (e.g. Heydari et al., 2001).

All sections (except Milanovo) show no significant correlation between $\delta^{18}O_{bel}$ and $\delta^{13}C_{bel}$, with low co-variance (between R^2= <0.001 and R^2 = 0.146) and cluster-type distributions, indicating a lack of post-depositional diagenesis. A weak negative correlation (R^2 = 0.194), is observed in belemnites from the Milanovo section. The weak correlation is unlikely to be a result of diagenetic alteration, as a positive, rather than negative correlation, is usually observed in diagenetically altered belemnite calcite or cement (e.g. Ullmann and Korte, 2015).

For time periods where severe and concurrent palaeoenvironmental perturbations in the carbon cycle are associated with a change in temperature, the result may be a unidirectional. This will result in an environmentally controlled signal on both isotope systems that might record correlation between $\delta^{18}O_{bel}$ and $\delta^{13}C_{bel}$ that is not related to diagenesis. Similar weak negative correlations in $\delta^{18}O_{bel}$ and $\delta^{13}C_{bel}$ have also been recorded from Toarcian belemnites from the Yorkshire Coast, UK (Saelen et al., 1996; Li et al., 2012), from bulk-carbonate at the end-Permian (Schobben et al., 2016) and the end-Triassic (Todaro et al., 2018). In the case of the Toarcian belemnites from the Milanovo section, a warming event (evidenced by decreasing $\delta^{18}O_{bel}$ values) co-occurring with a positive CIE (shown by increasing $\delta^{13}C_{bel}$), would show a negative correlation linked to environmental change, that could be mis-interpreted as a correlation due to diagenesis. For this reason, correlation between $\delta^{13}C_{bel}$ and $\delta^{18}O_{bel}$ in the early Toarcian is not taken to be a reliable indicator of diagenesis as it may reflect a primary signal.

4.3.1.4 Overall assessment of belemnite preservation

Well-preserved belemnite calcite is defined in this study firstly by belemnites that showed transparent calcite when viewed under optical microscopy. This included mappable areas within belemnites from sections Vradlovtsi-2, Milanovo and Berende Izvor, in which transparent calcite could be micro-drilled. Secondly, belemnites calcite that showed high amounts of luminescence (e.g. belemnites with CL type 6) were not further used in this study (See Appendix B for individual CL styles).

Finally, trace element concentrations (in belemnites that recorded CL styles 1-5) were used as a final indicator of diagenetic alteration. Mn/Ca and Sr/Ca ratios from belemnite calcite from Vradlovtsi-2, Milanovo and Berende Izvor, generally indicated well-preserved calcite when Mn and Sr were used as the most robust indicators of diagenesis. Samples that record Sr/Ca ratios <1.2 mmol/mol, Mn >100 ppm and/or Mn/Ca ratios >0.06 mmol/mol may represent altered samples, but are not removed from the data, as these values often fall close to the adopted limits of diagenetic alteration (Figure 4.5). These samples are presented with a different colour coding in the stable isotope curves (Figure 4.7, Figure 4.8, Figure 4.9). Published Sr, Mn and Ca values from the sections Dobravitsa-1 and Beledie Han sections fall within similar limits of belemnites from other sections in this study and are therefore indicate well-preserved calcite under the limits set in this study (Figure 4.5). Fe/Ca ratios are not used as a diagenetic indicator in this study, due to their heterogeneous nature and lack of agreement with other indicators.

4.3.2 Mg/Ca and Sr/Ca as palaeotemperature proxies

There is an extensive discussion in the literature about the Element/Ca composition of belemnites and if it retains a temperature-dependant signal, with high Mg/Ca and Sr/Ca ratios being associated with higher temperatures (e.g. Rosales et al., 2004; McArthur et al., 2007; Dutton et al., 2007; Nunn and Price, 2010; Armendáriz et al., 2012; Li et al., 2012; Armendáriz et al., 2013; Ullmann and Korte, 2015; Price et al., 2016; Rosales et al., 2018).

In this study, the temperature dependence of Mg/Ca and Sr/Ca ratios in Early Jurassic belemnites was assessed by plotting ratios against $\delta^{18}O_{bel}$. Sr/Ca values from belemnites cross plotted against $\delta^{18}O_{bel}$, evaluated for each section, record no statistically significant correlations, except for belemnites from the Berende Izvor section show a very weak statistically significant correlation (R^2 = 0.1986, P= 1.5E-05) (Figure 4.6). For Mg/Ca values, belemnites from most sections show no strong significant correlations between Mg/Ca and $\delta^{18}O_{bel}$ (Figure 4.6), with the exception of belemnites from Milanovo, which show a weak, statistically significant negative correlation (R^2 = 0.252, P= 3.4931E-07; Figure 4.6).

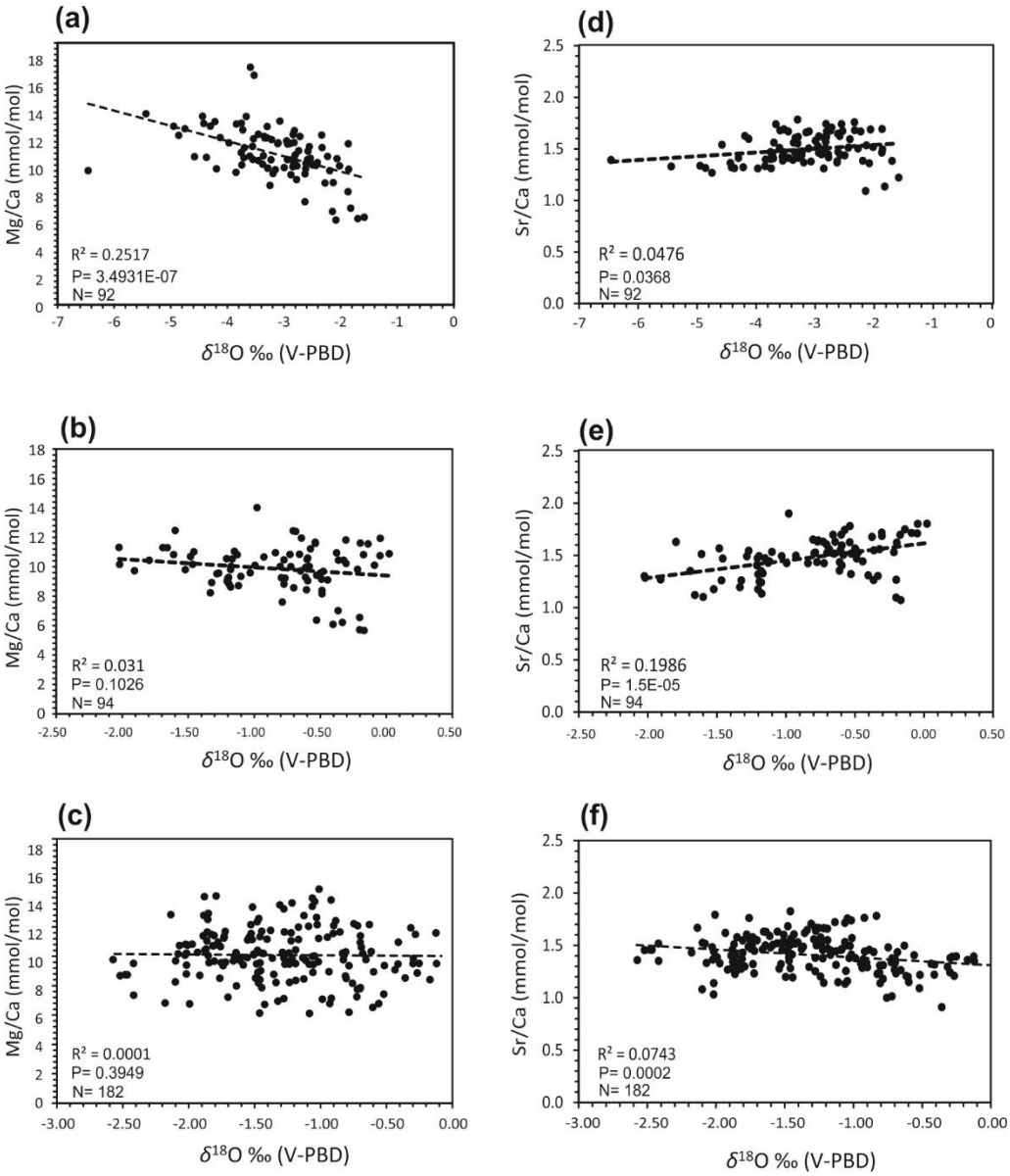

Figure 4.6 Cross-plots of Mg/Ca - $\delta^{18}O_{bel}$ for sections (a) Milanovo; (b) Berende Izvor; (c) Vradlovtsi-2. Cross-plots of Sr/Ca - $\delta^{18}O_{bel}$ for sections (d) Milanovo; (e) Berende Izvor; (f) Vradlovtsi-2. R^2 is the coefficient of determination, P is the F-test of overall significance and N is the number of samples in analysis.

4.3.3 Stable isotope results (carbon and oxygen)

The carbon and oxygen isotope results from belemnites are shown for the Vadlovtsi-2 (Figure 4.7), Berende Izvor (Figure 4.8) and Milanovo (Figure 4.9) sections, with individual values listed in Appendix B. The carbon and oxygen isotope values for well-preserved (>0.06 Mn/Ca, <0.01 Sr/Ca) and potentially

less well-preserved (>0.06 Mn/Ca, <0.01 Sr/Ca) belemnites all follow similar temporal trends.

A ‘running average’ through the carbon and oxygen data is not displayed. Any diagenetic influence, which may not have been recognised using screening techniques, will act to shift carbon and oxygen to lighter values (e.g. Marshall, 1992) and so a running average may reflect an isotopically lighter trend than is realistic. It is recommended by Craig (1966) and Korte et al. (2008) and Craig (1966) to focus mainly of the upper (heavier) envelopes of the isotope curves from marine calcite to reveal the most likely isotope trends. A running average would also smooth out isotopic trends, which may result in either small scale fluctuations being overlooked or the full extent of isotopic excursions appearing to be less extreme.

4.3.3.1 Carbon isotopes

Vradlovtsi-2 section

$\delta^{13}C$ values are variable throughout the section, ranging from -0.40 to +2.83 ‰. Outside this range unusually lighter $\delta^{13}C$ values of -1.73 ‰ and -1.39 ‰ are recorded from two sub-samples in one belemnite (samples Vd.4.7.1 and Vd.4.7.2). There are coincident with depleted Sr/Ca value of <1.2 mmol/mol and indicate diagenetic overprint (Figure 4.7). Throughout the section fluctuations in $\delta^{13}C$ up to ~3 ‰ are recorded (Figure 4.7), although no long-term shifts or clear CIEs are observed there is a general trend upwards to heavier values (~ 1 ‰).

Berende Izvor section

The $\delta^{13}C$ values are relatively stable throughout the section, ranging from -0.23 to +2.52 ‰ (Figure 4.8). This excludes samples indicated to be diagenetically altered with depleted Sr/Ca ratios of <1.2 mmol/mol. Through the base of the section in the upper part of the early Pliensbachian (d*avoei* Zone) $\delta^{13}C$ values record minor fluctuations, with an overall increasing trend of ~1.7 ‰ up to the *davoei/margaritatus* Zone boundary (Figure 4.8). Through the late Pliensbachian *margaritatus* Zone $\delta^{13}C$ values remain relatively constant ~2.3 ‰, throughout the *stoksei* Subzone and into the *subnodosus* Subzone (10 and 17. 5 m) (Figure 4.8). Small fluctuations are recorded through the rest of the *Margaritatus* Zone and values remain ~2 ‰ (Figure 4.8).

Milanovo section

$\delta^{13}C$ values at the base of the section in the late Pliensbachian (*spinatum* Zone) are between -0.02 and +0.18 ‰. The general trend in $\delta^{13}C$ values through the section is marked by a prominent positive excursion in the early Toarcian from values ~1.5 ‰% and increasing to ~4 ‰% in the mid-upper *Falciferum* Zone, marking a positive shift of ~ 2.5 ‰ (Figure 4.9). This is followed by a ~3.5 ‰ decrease to ~ 0.79 ‰ around the *falciferum/bifrons* Zone boundary. $\delta^{13}C$ values become progressively lighter through the rest of the Toarcian interval (late *falciferum* Zone – *aalensis* Zone), with the isotopically lightest $\delta^{13}C$ values recorded in the late Toarcian *fallaciosum* zone (-0.41 ‰, 3.74 m) and *pseudoradiosa* Zone (~ 0.3 ‰, 3.88 m) (Figure 4.9). The isotopically lighter $\delta^{13}C$ values recorded in the *fallaciosum* Zone coincide with belemnite subsamples depleted in Sr/Ca values (< 1.2 mmol/mol) and may be diagenetically overprinted. At the top of the Toarcian in the *aalensis* Zone, $\delta^{13}C$ values increase slightly to 1.24 ‰ (4.3 m) (Figure 4.9).

4.3.3.2 Oxygen isotopes

Vradlovtsi-2 section

The $\delta^{18}O$ values show less scatter when compared to the $\delta^{13}C$ record from the section (Figure 4.7). $\delta^{18}O$ values range from -2.57 to -0.12 ‰ (Figure 4.7). Outside this range, an anomalously high $\delta^{18}O$ value of 3.1 ‰ is recorded in sample Vd.10.10.1, but a depleted Sr/Ca value (<1.2 mmol/mol) for this sample indicates diagenetic overprint. Most $\delta^{18}O$ values fall between -1 and -2 ‰ in the Sinemurian (8-25 m) and slightly heavier $\delta^{18}O$ values between -2 and 0 ‰ are recorded at the top of the section in the Pliensbachian (28-30 m). Minor fluctuations up to 1.5 ‰ are observed throughout the section (Figure 4.7).

Berende Izvor section

The $\delta^{18}O$ values are also relatively stable throughout the section, ranging from -2.02 to +0.02 ‰ (Figure 4.8). The most negative $\delta^{18}O$ value is recorded at the *davoei/margaritatus* Zone boundary (10 m), following a small negative trend through the *maculatum* Subzone and positive trend through the *capricornus* and *figulinum* Subzones (Figure 4.8). A small positive shift of ~2 ‰ is recorded through the base of the *margaritatus* Zone, through the *stokesi* Subzone and into the *subnodosus* Subzone (10-17.5 m) (Figure 4.8). Like the $\delta^{13}C$ isotopes,

the $\delta^{18}O$ values remain relatively constant through the *margaritatus* Zone, with values ranging from -1 to -2 ‰ (Figure 4.8).

Milanovo section

At the base of the section, in the late Pliensbachian *spintaum* Zone, $\delta^{18}O$ values are between -3.76 and -1.58 ‰ (Figure 4.9). Following the hiatus across the Pl-To boundary, $\delta^{18}O$ values shift towards isotopically lighter values of between -2.82 and 5.4 ‰ (1.51-2.36 m) through the *tenuicostatum*- mid *falciferum* Zones. Four of the isotopically lighter belemnite calcite $\delta^{18}O$ values in this interval also have an enrichment in Mn/Ca values (>0.06 mmol/mol), which could indicate diagenetic overprint. If the potentially altered belemnite calcite values are removed, a negative trend to isotopically lighter $\delta^{18}O$ values is also observed. The $\delta^{18}O$ values become progressively heavier through the rest of the Toarcian interval (late *falciferum* Zone-*aalensis* Zone), with the isotopically heaviest $\delta^{18}O$ values of 1.70 ‰ (3.88 m) recorded in the late Toarcian *pseuoradiosa* Zone (Figure 4.9). At the top of the Toarcian in the *aalensis* Zone, $\delta^{18}O$ values fall slightly to -2.5 ‰ (4.3 m) (Figure 4.9).

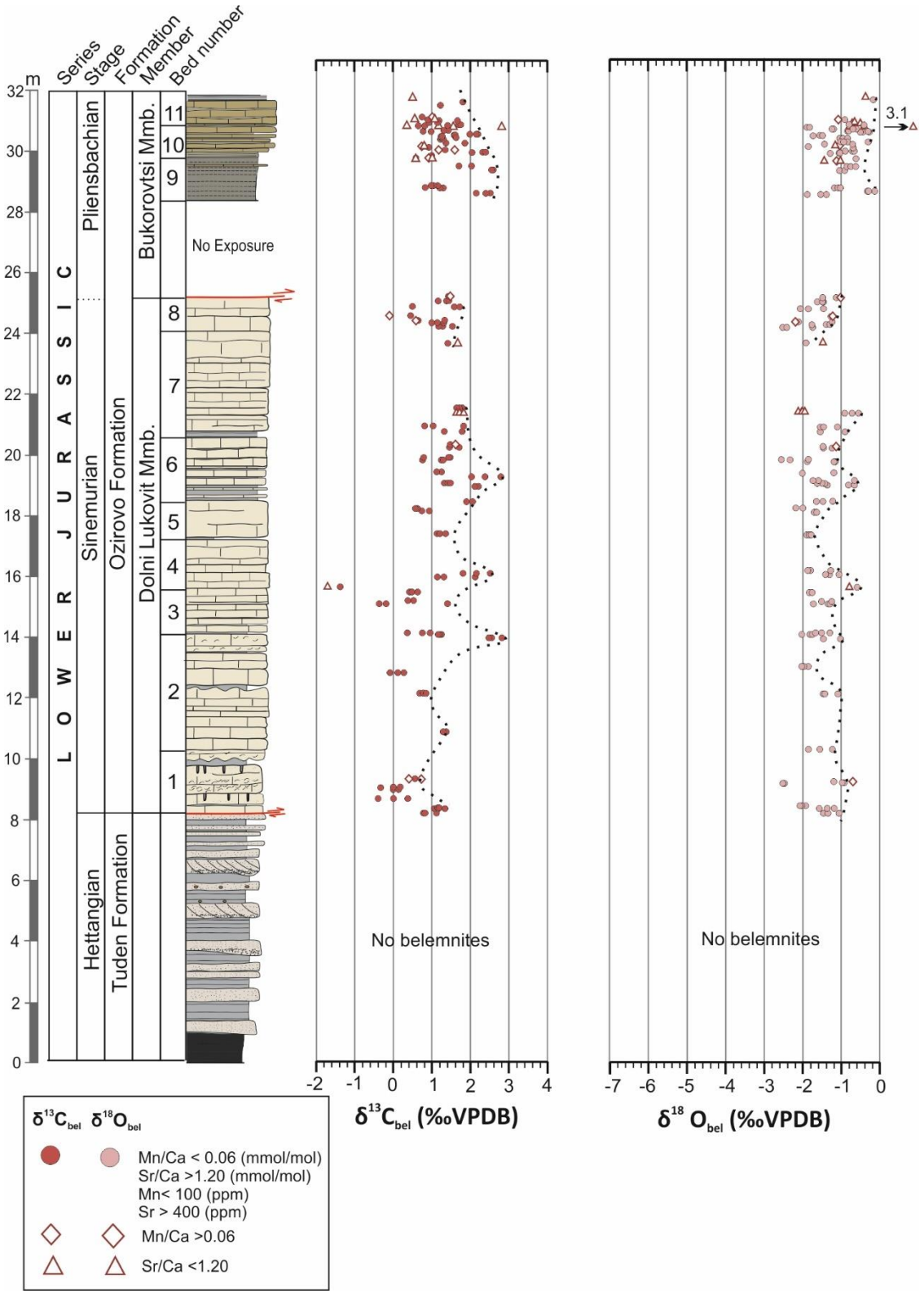

Figure 4.7 Carbon and oxygen isotope record of the Vradlovtsi-2 section. Well-preserved samples are denoted with closed symbols, where Mn <100 ppm and Sr >400 ppm Potentially altered samples with Mn/Ca > 0.06 mmol/mol and Sr/Ca <1.2 mmol/mol are denoted with open symbols. No samples with >100 ppm Mn and/or <400 ppm Sr are recorded. Note ammonite zonation is not known for this section.

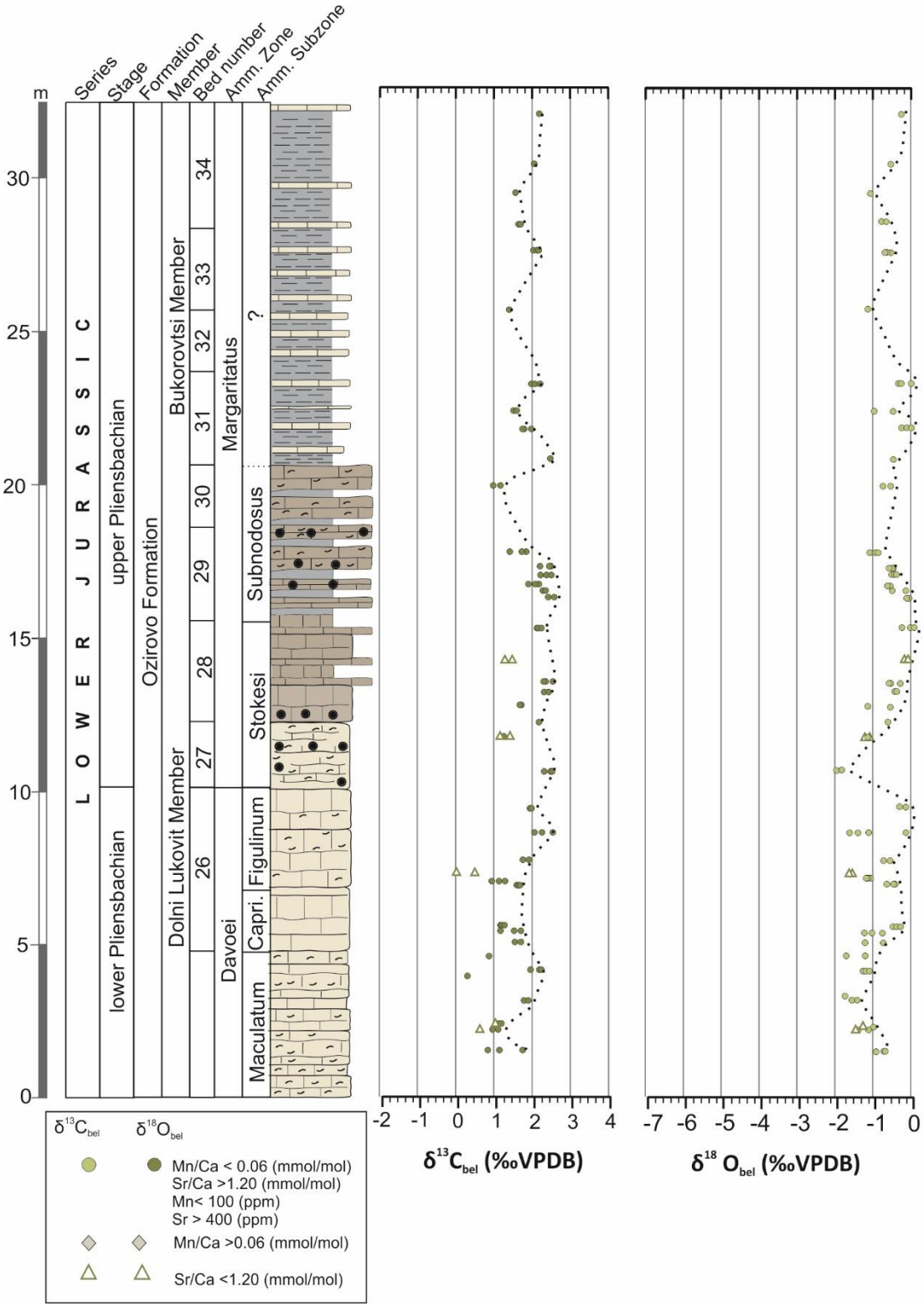

Figure 4.8 Carbon and oxygen isotope record of the Berende Izvor section. Well-preserved samples are denoted with closed symbols, where Mn <100 ppm and Sr >400 ppm. Potentially altered samples with Mn/Ca >0.06 mmol/mol and Sr/Ca <1.2 mmol/mol are denoted with open symbols. No samples with >100 ppm Mn and/or <400 ppm Sr are recorded. Capri. = capricornum.

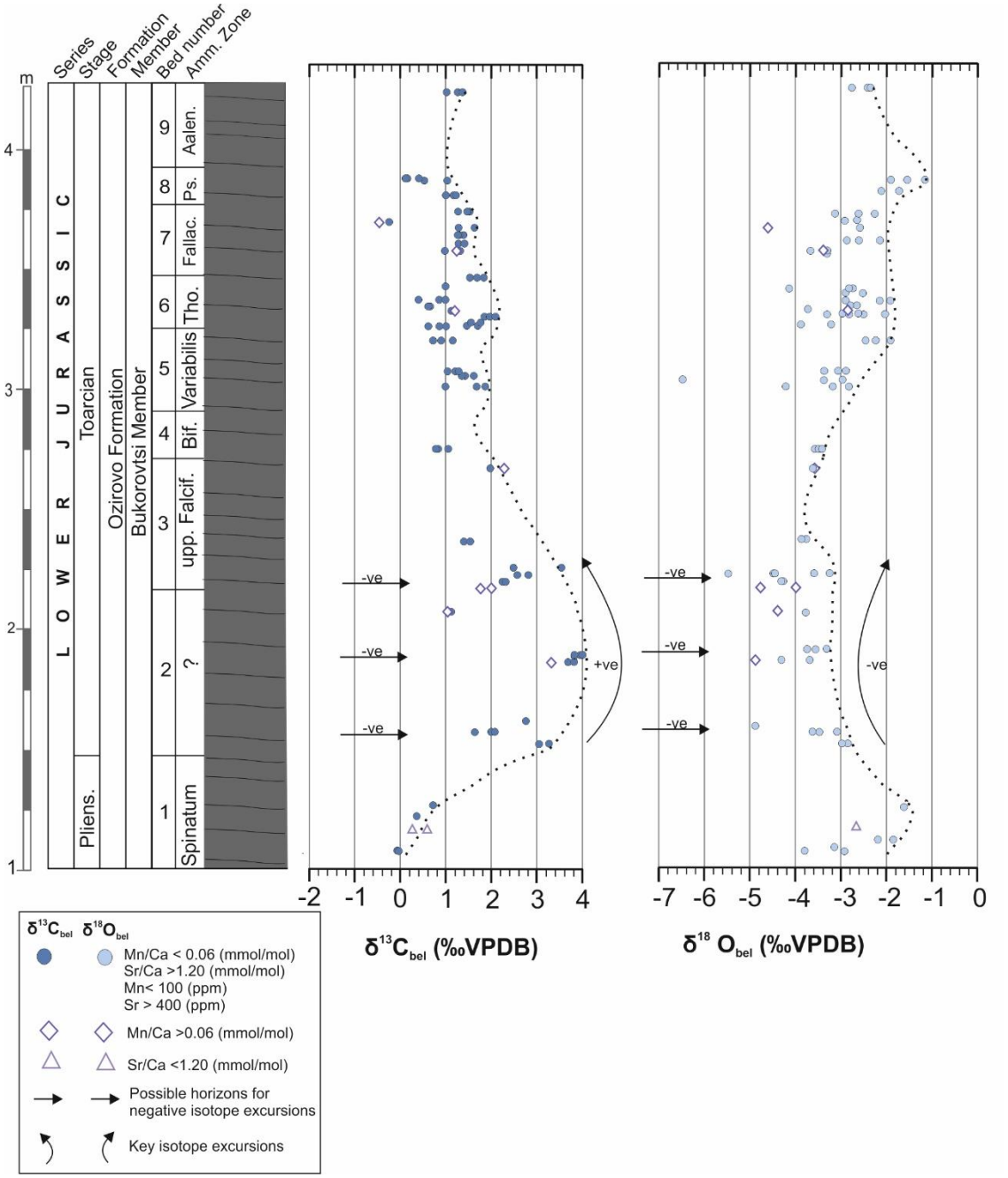

Figure 4.9 Carbon and oxygen isotope record of the Milanovo section. Well-preserved samples are denoted with closed symbols, where Mn <100 ppm and Sr >400 ppm. Potentially altered samples with Mn/Ca >0.06 mmol/mol and Sr/Ca <1.2 mmol/mol are denoted with open symbols. No samples with >100 ppm Mn and/or <400 ppm Sr are recorded. Upp Falcif. = upper Falciferum, Bif= Bifrons, Thou.= Thouarsense, Fallac.=Fallaciosum, Ps= Pseuoradiosa, Aalen= Aalensis.

4.4 Discussion

4.4.1 $\delta^{13}C$ and $\delta^{18}O$ scatter from coeval belemnites

The $\delta^{13}C$ and $\delta^{18}O$ values have a spread of more than 2 ‰, for example in the *falciferum* and *thouarsense* Zones (Figure 4.7, Figure 4.8, Figure 4.9). To some extent, this scatter is due to the small scale internal variability of $\delta^{18}O$ and $\delta^{13}C$ recorded in well-preserved belemnite calcite (Podlaha et al., 1998; Dera et al., 2011; Ullmann and Korte, 2015). Scatter may also be exaggerated due to the condensed nature of the Toarcian in Bulgaria. A high degree of spread of data from belemnite calcite however, is often found through the Jurassic, which can make it problematic to interpret (e.g. Korte and Hesselbo, 2011).

The variability of all geochemical proxies in belemnite rostra, which is noted in many studies, has led to considerable data spread within chemostratigraphic records derived from belemnites (McArthur et al., 2000; Bailey et al., 2003; Dera et al., 2011; Ullmann, 2013; Ullmann et al., 2014). The reasons for this heterogeneity are not very well constrained, but are important for our understanding of past environments. For oxygen isotopes, the most frequent cause is the variability in ambient seawater temperature, due to bathymetric differences or seasonal upwelling (James et al., 1997). Carbon isotopic variability between belemnite calcite rostra may be caused by multiple controls, including metabolic and taxon-specific effects, calcite precipitation rate and position of the animal within water column (Rosales et al., 2004; Rexfort and Mutterlose, 2006; McArthur et al., 2007; Dutton et al., 2007; Wierzbowski and Joachimski, 2009; Li et al., 2012; Li et al., 2013). However, Ullmann et al. (2017) demonstrated that $\delta^{13}C$ and $\delta^{18}O$ values of an Early Jurassic belemnite rostrum (*Passaloteuthis bisulcata*) gave consistent results, regardless of the sampling areas within the rostrum. This study also showed that growth rate effects on element incorporation are minor with respect to the control exerted by secular changes in seawater composition through time. This built on earlier work of Ullmann et al. (2015b) that provided evidence that $\delta^{13}C$ and $\delta^{18}O$ analyses of belemnite rostra produce consistent results regardless of the sampling area within the rostrum. Thus, demonstrates that variability within belemnite rostra is unlikely to be the main contributing factor in $\delta^{13}C$ or $\delta^{18}O$ variability and long-term palaeoenvironmental trends in this study.

4.4.2 Compiling carbon and oxygen isotope curves

A composite curve recording long term $\delta^{13}C_{bel}$ and $\delta^{18}O_{bel}$ through the late Pliensbachian–Toarcian is presented to give a full view of all stable isotope data currently recorded from Bulgaria during the Lower Jurassic (Figure 4.10).

Stratigraphic assessment for all sections uses the ammonite biostratigraphic framework given by Metodiev (2008) (Chapter 1). This framework is directly comparable to ammonite biostratigraphy from the NW European ammonite biostratigraphy. This allows for construction of a scale of reference that facilitates comparison of palaeoenvironmental changes within the EES. Additional stratigraphic assessment is given in Metodiev et al. (2005) (Beledie Han sections), Metodiev and Koleva-Rekalova (2008) (Dobravista-1 and Beledie Han sections) and Metodiev et al. (2014) (Varbanchovets and Babintsi sections). The $\delta^{13}C_{bel}$ and $\delta^{18}O_{bel}$ values from the Vradlovtsi-2 section (this study) or from the Pliensbachian of the Babintsi section (Metodiev et al., 2014) are not incorporated into the composite curves due poor biostratigraphic constraint. In the following discussion, stratigraphic nomenclature is used rather than the numeric ages.

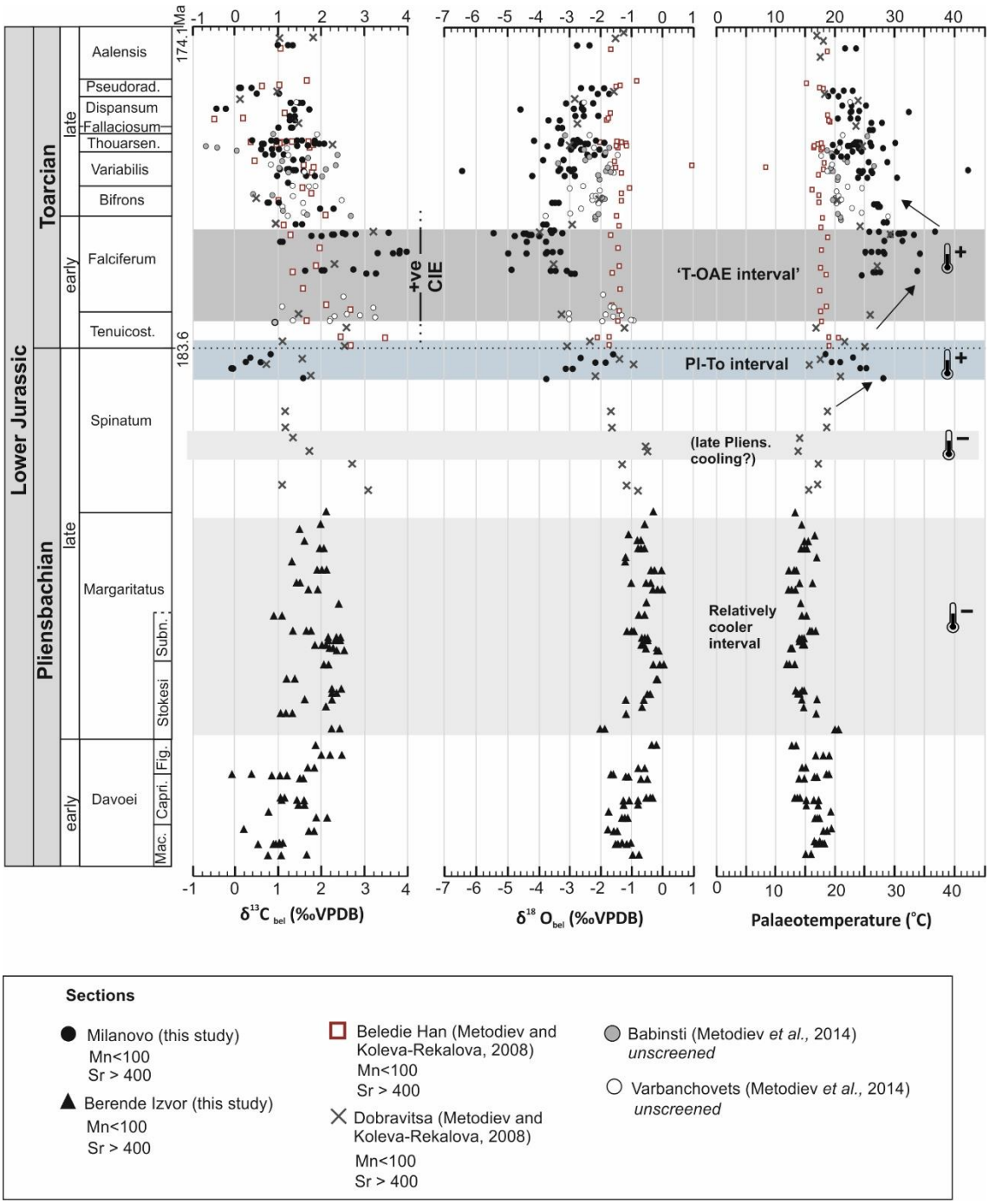

Figure 4.10 Composite carbon and oxygen isotope record of Lower Jurassic (Pliensbachian-Toarcian) seawater in the Moesian Basin. $\delta^{13}C$ and $\delta^{18}O$ values from this study are shown by black symbols and published values (Metodiev and Koleva-Rekalova, 2008; Metodiev et al., 2014) are shown by red and grey symbols. Only belemnite samples with Mn<100 ppm and Sr>400 ppm are shown, indicative of well-preserved calcite. Temperature estimates are based on $\delta^{18}O$ using the equation of Anderson and Arthur (1983) and assuming an original $\delta^{18}O$ of non-glacial seawater of -1 ‰ SMOW. Mac. = Maculatum, Capri. = Capricornus, Fig. = Figulinum, Subno. = Subnodosus, Thouarsen. = Thouarsense, Pseudorad.= Pseudoradiosa, Pliens = Pliensbachian. Numerical ages from Gradstein et al. (2012).

4.4.3 Long term carbon cycle changes

4.4.3.1 Sinemurian

$\delta^{13}C_{bel}$ from the Vradlovtsi-2 section comprises the first carbon record from part of the Sinemurian in the Moesian Basin, and extend into the Pliensbachian. The small scale fluctuations observed indicate no major change in the global carbon cycle during the this time. Unfortunately, this record cannot be incorporated with the Lower Jurassic composite curve for the Moesian Basin due to poor biostratigraphic control. Because of the poor biostratigraphic control the Sinemurian – Pliensbachian boundary in the section cannot be clearly recognised. There are no clear isotopic excursions in this part of Sinemurian (Figure 4.7) and further work is needed to establish if the Sinemurian-Pliensbachian boundary event (SPBE), which is recognised in the northern EES (e.g. Korte and Hesselbo, 2011), is also recorded in the Moesian Basin.

4.4.3.2 Pliensbachian

Belemnite $\delta^{13}C$ values through the early-late Pliensbachian interval (*davoei* – *margaritatus* Zone), records small- scale temporal variations of an amplitude on the scale of 1-2 ‰ (Figure 4.10). Small scale fluctuations in the carbon isotope record through this interval are commonly associated with short-term warming events (van de Schootbrugge et al., 2005; Suan et al., 2010) and palaeoceanographic changes across the EES, including the deposition of organic-rich intervals (Silva et al., 2011; Silva and Duarte, 2015). However, it is difficult to determine any small scale variability in the sections as a record of small perturbations in the carbon cycle versus the natural variability and scatter $\delta^{13}C$ values from the biogenic carbonate.

4.4.3.3 Pliensbachian-Toarcian (Pl-To) boundary

A small negative shift of nearly 2 ‰ is recorded near top of the upper Pliensbachian, in the late *spinatum* Zone, close to the Pl-To boundary (Figure 4.10).

The small negative CIE recorded near the Pl-To boundary in Bulgaria, is recorded in belemnite calcite. This is unusual, as the negative CIE recorded ~1 Myr later in the early Toarcian, most clearly expressed in organic carbon, is notably absent or diminished in the global belemnite record (van de Schootbrugge et al., 2005). For the Pl-To event, it remains unclear if the

negative CIE is recorded in biogenic calcite, with fluctuating values recorded in brachiopods from Spain (Suan et al., 2010) and belemnite-derived data from Yorkshire, UK (Korte and Hesselbo, 2011). More recent studies present contrasting records from belemnites across the Pl-To boundary, with no change to lighter $\delta^{13}C$ values recorded in Morocco (Ait-Itto et al., 2017), but a small ~1.5 ‰ shift recorded in Mallorca (Rosales et al., 2018). The latter has been reported to provide the first record of a negative shift from belemnite calcite (Rosales et al., 2018). In the case of belemnites from the Moesian Basin, given that there is no clear diagenetic alteration to belemnite samples, two scenarios are postulated to explain the small negative CIE recorded.

Either the values reflect the natural scatter of belemnites that may be expected for condensed sections with measurements from different belemnites species or, the small shift to negative $\delta^{13}C_{bel}$ values could be a true short-term shift in the carbon isotope record. The magnitude of the shift is similar ~ 2 ‰ negative CIE recorded in co-eval sections in Yorkshire, UK (Littler et al., 2010), the Mochras Borehole, UK (Jenkyns and Clayton, 1997; Xu et al., 2018a) and at Peniche, Portugal (Hesselbo et al., 2007). However, the exact timing of this excursion and correlation to regional and global sections is an issue. The negative CIE in the Bulgarian sections occurs at the top of the *spinatum* Zone, rather than at the Pl-To boundary as seen in other studies (e.g. Hesselbo et al., 2007; Bodin et al., 2016). The negative CIE in Bulgaria either reflects part of the same perturbation, and records a longer duration event, or the same event occurring diachronously.

With respect to the apparently earlier timing this negative shift in Bulgaria, it has been suggested that if this carbon cycle perturbation is global in nature it might actually also correspond to negative CIEs also recorded in the late Pliensbachian *spinatum* Zone. Records of negative $\delta^{13}C$ peaks have been reported from this interval in the French Grand Causses Basin (Harazim et al., 2013), the Basque-Cantabrian Basin (Quesada et al., 2005), and the Austrian Basin (Gómez et al., 2016). In which case the negative CIE at the top of the *Spinatum* Zone would support a more widespread and longer negative CIE interval of at least supra-regional extent, with the Bulgaria record documenting the most easterly occurrence of this perturbation in the EES. Such a perturbation has been linked, in part, to a release of isotopically light carbon, such as mantle source CO_2 (Littler et al., 2010). This would likely be a result of an early pulse of the Karoo-Ferrar LIP, supported by Xu et al. (2018b) who show an eruptive phase around Pl-To boundary, through palaeomagnetic correlation.

4.4.3.4 Early Toarcian

A clear positive CIE, with a shift of 3 ‰, is recorded in well-preserved belemnites through the early Toarcian interval in the Bulgaria, reaching a maximum in the *falciferum* Zone (Figure 4.10). An overarching, broad positive CIE is a commonly recognised feature in of the early Toarcian, and is regarded as a global perturbation in the exogenic carbon cycle (Jenkyns, 1988; Jenkyns and Clayton, 1997). The open marine character of the investigated sediments and the coherence of overlapping sections, indicates the long-term $\delta^{13}C$ fluctuations reflect real secular variations of global, or at least regional, significance.

The condensed nature of the Toarcian does not permit high resolution sampling within each ammonite Zone or Subzone, limiting the record of short-term variations in the isotope signal. A potential problem also caused by the condensed nature of the Toarcian is the full extent of any isotope excursions may not be represented. This is due to a relatively lower-resolution stable isotope curve generated, compared to expanded sections, such as the Mochras Borehole, UK (Xu *et al.,* 2018a). However, the clear positive CIE (3 ‰) recorded in the Moesian Basin is comparable with the magnitude recorded in marine carbonate (3‰) globally with a similar duration (estimated ~3.5 Myr) from the latest Pliensbachian (*spinatum* Zone) until midway through the Toarcian (*bifrons* Zone) (Jenkyns et al., 2002; Gradstein et al., 2012; Xu et al., 2018a). This broad positive CIE could reflect the globally significant burial of photosynthetically derived (C_{12}-rich) organic matter during the early Toarcian (e.g. Jenkyns and Clayton, 1997; Schouten, 2000). The $\delta^{13}C_{bel}$ record in Bulgaria shows the carbon cycle was perturbed, causing a positive CIE, at least on a regional scale, across the entire EES from the most western epicontinental basins to the most easterly edge of the EES in the Moesian Basin.

There is no evidence for the negative CIE in the early Toarcian from biogenic carbonate in Bulgaria. A poorly expressed negative CIE recorded from belemnites during the T-OAE interval is common from many sections across the EES (e.g. van de Schootbrugge et al., 2005). The lack of this CIE in Bulgaria could be a result of sample gaps and a bulk $\delta^{13}C_{org}$ curve would potentially help clarify this.

4.4.3.5 Late Toarcian

In the Moesian Basin there is a generally stable carbon isotope record through the Toarcian following the early –Toarcian positive CIE, with a trend back to

isotopically light carbon values, which is comparable to other records across the EES (Jenkyns, 1988; Jones et al., 1994; Jenkyns et al., 2002). However, few studies focus on the remaining carbon isotope record through the late Toarcian compared to the early Toarcian. Previous research from Bulgaria suggested a possible negative CIE in the *thouarsense* Zone (Metodiev et al., 2014). This, however, may be a reflection of diagenetically altered calcite, as no clear trend is observed during this time from other sections.

4.4.3.6 No clear facies control on $\delta^{13}C_{bel}$ values

In sections with changing facies, such as Vradlovtsi-2 and Berende Izvor, there is no clear link between facies type and $\delta^{13}C_{bel}$. This contrasts to biogenic calcite (from belemnites, brachiopods and oysters) from the Cleveland Basin, whereby a link between lighter carbon isotopes in shallow water facies and heavier isotopes in deeper water facies is attributed to climatic change and the presence of continental ice in the Pliensbachian *margaritatus* Zone (Korte and Hesselbo, 2011). Although similar ironstone-mudstone cycles are observed in the Moesian Basin during the late Pliensbachian in the Berende Izvor section, a similar correlation is not observed. Therefore, long term trends and strong shifts in the Early Jurassic seawater $\delta^{13}C$ for diagenetically screened belemnites, likely reflects global instability of the carbon cycle, rather than any facies-specific effects. Additionally, in the Milanovo section, which records little lithological change, long-term trends observed in carbon and oxygen isotopes will likely reflect changes in seawater signal, as fluctuations cannot be attributed to changes in lithology.

4.4.4 Long term oxygen isotope changes

For $\delta^{18}O_{bel}$ to be used as a proxy for palaeotemperature, assumptions are made that belemnite calcite is well-preserved and precipitated in equilibrium with ambient seawater with no major changes in salinity. To calculate temperatures from the belemnite rostra the equation of Anderson and Arthur (1983) is used (see Chapter 2, Section 1.5.2.6 for equation and assumptions).

It should be noted that the exact calibration of $\delta^{18}O$-temperature dependence is still not fully understood, and therefore, the actual values for temperature calculated from $\delta^{18}O$ should be treated with caution (McArthur et al., 2000; Gutowska et al., 2010; Richter et al., 2011). Additionally, it is difficult to obtain a ‘mean’ temperature values from the oxygen isotope values as the lowest

seawater temperatures might not be recorded in the belemnite calcite. Previous research on modern-day Pacific oysters has shown the lowest temperature seawater values, recorded in $\delta^{18}O$, might not be represented in the shell (Ullmann et al., 2010). This means that higher seawater temperatures could be potentially over-represented in the past $\delta^{18}O$ record of biogenic calcite, leading to a bias of mean seawater variations towards higher temperatures (Ullmann et al., 2010).

The oxygen isotope composition of calcite ppm from seawater can be affected by changes in temperature and salinity (Spaeth et al., 1971; Stevens and Clayton, 1971; Saelen et al., 1996; Podlaha et al., 1998; Rosales et al., 2004a,b).

4.4.4.1 Sinemurian

No significant temporal variations in the $\delta^{18}O_{bel}$ record are observed in the Moesian Basin during the Sinemurian (Figure 4.7). Unfortunately, values cannot be correlated at any higher resolution to other sections outside the Moesian Basin due to poor biostratigraphic control at this level.

4.4.4.2 Pliensbachian

Seawater temperatures through the early-late Pliensbachian interval *Davoei-Margaritatus* Zone are calculated to have been between 11 and 19°C (Figure 4.10). Small fluctuations trending towards lighter $\delta^{18}O_{bel}$ values are recorded in the *davoei* Zone (*maculatum* Subzone and at the c*apricornus/Figulinum* Subzone boundary) and in the middle of the *margaritatus* Zone. These fluctuations, recorded from the Lusitanian Basin in Portugal, may reflect short-term warming events previously recorded through the d*avoei-margaritatus* Zone interval (Silva and Duarte, 2015). In contrast, the heaviest oxygen isotope values in this interval (0-0.5 ‰), which could reflect the coolest seawater temperatures, are recorded in the *margaritatus* Zone (*stokesi/subnodosus* Subzone boundary) and *spinatum* Zone (Figure 4.10). In general the *Margaritatus* Zone reflects relatively cooler seawater temperatures (Figure 4.10). At the top of the Pliensbachian, in the *spinatum* Zone, a temporary shift to heavier $\delta^{18}O_{bel}$ values may also represent a short-lived cooling episode in the Moesian Basin (Figure 4.10). Evidence of a cooling phase, is recorded by a synchronous shift to more positive $\delta^{18}O_{bel}$ values, across the EES in the *spinatum* Zone (Price, 1999; Rosales et al., 2001; Bailey et al., 2003; Rosales

et al., 2004a,; Rosales et al., 2004; Gómez et al., 2008; Suan et al., 2010; Korte and Hesselbo, 2011; Dera et al., 2011; Korte et al., 2015; Gómez et al., 2016). More $\delta^{18}O$ data would be needed to determine definitively the presence of a cooling episodes in the Moesian Basin.

A negative shift of ~2.5 ‰ is recorded in $\delta^{18}O_{bel}$ in the late Pliensbachian (latest *spinatum* Zone), close to the Pl-To boundary (Figure 4.10), which may represent the trend towards high seawater temperatures, which continues into the early Toarcian.

4.4.4.3 Early Toarcian

The -2.82 and -5.4 ‰ $\delta^{18}O_{bel}$ range translates into temperatures of ~24 to 37°C (Figure 4.10). Although these seawater temperatures are below the 38°C tolerance limit for higher organisms (Brock, 1985; Rothschild, 2001), the maximum temperature range is unrealistically high for seawater temperatures during the Early Jurassic (cf. Ruebsam et al., 2019).

This discrepancy of very negative $\delta^{18}O_{bel}$ record in the early Toarcian of the Moesian Basin can be resolved in two ways. The first resolution is that the lightest oxygen isotope values, although characterised as well-preserved, may still be diagenetically altered. It can be assumed that some altered samples may not have been identified by the trace element screening and the isotopically lighter $\delta^{18}O_{bel}$ data could represent values from non-pristine belemnite material. Some of the isotopically light $\delta^{18}O_{bel}$ values show slight enrichments in Mn/Ca ratios, which suggest they are diagenetically altered, although most samples fall within normal limits. Some authors argue a lower limit for $\delta^{18}O$ of <-4 ‰ for biogenic carbonate (e.g. Rosales et al., 2004). If all samples with $\delta^{18}O$ values <-4 ‰ are removed, the calculated palaeotemperatures range from ~24 to 30°C. Although this is a more reasonable value, it suggests high seawater temperatures. However, this assumes that the most negative oxygen-isotope values are caused only by variations in temperature.

A second resolution for the very negative $\delta^{18}O_{bel}$ early Toarcian values is that the seawater in this part of the Moesian Basin was influenced by salinity changes, likely through an influx of meteoric water, which would have further lowered the $\delta^{18}O_{bel}$ values. Salinity changes have been documented across the EES, associated with the estimated temperature rise of 4-7°C in global seawater temperatures, that resulted in increased run-off of freshwater run-off into the epicontinental Tethys (Bailey et al., 2003; Rosales et al., 2004a; Dera et al., 2011; Joral et al., 2011; Korte et al., 2015; Gómez et al., 2016). The additional

effect of meteoric water input into some areas of the Tethys is supported by the N-S gradient in O-isotope values for the Toarcian OAE across the EES (Rosales 2004a,b; Dera et al., 2009) with the most positive oxygen isotope values at the lowest latitude site (Morocco) and most negative values at the highest latitude site (Raasay, Scotland). Given that the opposite trend would be expected from a normal temperature profile (i.e. warm subtropics and cooler temperate regions), this suggests that salinity is also a key control on belemnite oxygen isotope values. As the Moesian Basin was situated at palaeo mid-latitudes, similar to other basins in the northern EES, the explanation of the $\delta^{18}O_{bel}$ trends in terms of temperature and salinity changes represents the simplest interpretation of the data.

4.4.4.4 Mid-late Toarcian

In the early Toarcian of the Moesian Basin, $\delta^{18}O_{bel}$ values sharply declined from the middle-f*alciferum* Zone to the end of the *bifrons* Zone, similar to records from the Yorkshire Coast in the northern EES. The $\delta^{18}O_{bel}$ values continue to gradually decline through the rest of the Toarcian (Figure 4.5). In the late Toarcian, there is a relatively large scatter of $\delta^{18}O_{bel}$, with no clear return back to values seen in the Pliensbachian. The late Toarcian witnessed the appearance radiation of several new belemnite lineages genera (Little and Benton, 1995; Schlegelmilch, 1998). The scatter in $\delta^{18}O_{bel}$ records through this interval may reflect average sea water temperatures captured from coevally occurring belemnite genera, living in separate water depths, rather than short-term fluctuations in sea water temperature.

In addition to faunal changes, the overall lighter $\delta^{18}O$ values through the late Toarcian may be linked to a continuation of relatively warmer temperatures and/or continued meteoric water input into the Basin. However, a globally reduced hydrological cycle and associated continental weathering has been recorded following the T-OAE interval as low kaolinite/illite ratios (Xu et al., 2018a) and lower osmium isotope values (Cohen et al., 2004a; Percival et al., 2016; Them et al., 2017).

Some minor fluctuations are observed with a spread of data recording lower $\delta^{18}O_{bel}$ values through the *variabilis, thouarsense* and f*allaciosum* Zones. This may reflect, in part, of minor, short-term $\delta^{18}O_{bel}$ oscillations on a regional scale, documented specifically from the *variabilis* Zone in across the EES in Wales, (Jenkyns and Clayton, 1997), Spain (Gómez et al., 2008), Morocco (Bodin et al., 2010) and also in previous studies from Bulgaria (Metodiev and Koleva-

Rekalova, 2008). However, it is unknown if these events record further palaeoenvironmental changes and faunal turnover after the T-OAE or if they are discrete events or a consequence of the post-T-OAE stabilisation (Gómez et al., 2008). Because of the pulsed nature of the Karoo-Ferrar LIP activity during Toarcian (Jourdan et al., 2008), it is thought that this long-lasting volcanic episode is ultimately responsible for pacing these environmental perturbations (Dera et al., 2011; Caruthers et al., 2013).

4.4.4.5 $\delta^{18}O$ record from the Beledie Han section: Local or diagenetic signal?

The oxygen isotope record for the Beledie Han belemnites (Metodiev and Koleva-Rekalova (2008) is inconsistent with the isotopic changes recorded on the long-term composite curve generated for the Moesian Basin (Figure 4.10). In comparison to the composite curve, the Beledie Han $\delta^{18}O_{bel}$ values are consistently heavier and do not fluctuate, with an average -1.48 ‰, ± 0.87 ‰ (Figure 4.10). It is important to consider if the different Beledie Han $\delta^{18}O$ values reflect either a true variation in the isotopic values of seawater in the basin or is a diagenetically altered signal, particularly evaluating the broader, regional palaeoenvironmental and climatic trends from the Moesian Basin.

The first possibility is that the heavier Beledie Han $\delta^{18}O$ values record a true signal of oxygen isotope values of seawater throughout the Toarcian interval. This could have been a result of a localised change in salinity, with the development of hypersaline waters compared to normal marine conditions recorded in the other sections. In an isotopic study of Middle Jurassic oysters from England, Hendry and Kalin (1997) explained heavy oxygen isotopes in shells from nearshore settings as a result of evaporative concentration within low-salinity waters of hydrodynamically closed lagoons. However, sedimentological aspects of the Beledie Han section do not support a lagoonal setting, due to the presence of the oolites. Faunal evidence, including echinoderms, brachiopods, gastropods and scarce foraminifera in the Beledie Han section favour a normal marine environment interpretation (Metodiev et al., 2005). The absence of taxa such as infaunal bivalves may be due to unsuitable substrate, high energy conditions or the severe ecological disturbance that occurred during the early Toarcian, or unsuitable substrate in a high energy environment, rather than simply a salinity control.

The second possibility, of diagenetic effects, is the most likely explanation for the $\delta^{18}O_{bel}$ values from Beledie Han. Particularly as the $\delta^{18}O_{bel}$ remains almost

unchanged throughout the Toarcian interval (~8 Myr), and does not record the expected climatic changes.

If a diagenetic control is considered for the oxygen isotope values from belemnites from the Beledie Han section, post-depositional influence of hypersaline or hydrothermal fluid compositions can explain the heavier $\delta^{18}O$ calcite values (O'Neil et al., 1969). This has been suggested for the previously isotopically lighter $\delta^{18}O$ signal recorded from bulk samples in the Beledie Han section (Koleva-Rekalova and Metodiev, 2007). Oxygen isotopes are more susceptible to diagenetic alteration than carbon isotopes (Brand and Veizer, 1981; Lohmann, 1988; Marshall, 1992). This may explain why the Beledie Han $\delta^{13}C$ values are consistent with the overall regional composite carbon isotope curve.

4.4.4.6 Significance of oxygen isotope record from Bulgaria

The long-term oxygen isotope record from Bulgaria is important for understanding the global palaeoclimatic changes through the Early Jurassic, and specifically for the early Toarcian. As the Moesian Basin was situated on the very eastern edge of the EES, the main water mass influences would have been a combination of seawater transported eastwards, from the northern EES towards the open Tethys ocean (Röhl et al., 2001; Krencker et al., 2015; Baroni et al., 2018). The palaeogeographic position of the Moesian Basin provides a new insight into oxygen isotope records from the EES. This is because the oxygen isotope composition of the Moesian Basin seawater was not directly influenced by cool nutrient-rich water from the Laurasian Seaway to the north or warmer saline water from the southwest. Therefore, the recorded temperature rise recorded in seawater from the Moesian Basin is considered to represent long-term changes more representative of the global record. The oxygen isotope record and associated warming from the Moesian Basin is actually very similar to other records across EES, which shows overall trends from oxygen isotopes (and inferred global warming during the early Toarcian) are not as affected by the oceanographic heterogeneity of the EES as other isotopic records, such as sulphur (e.g. Newton et al., 2011). Oxygen isotope values in the Moesian Basin are also likely to be less susceptible to short term influences of the Laurasian Seaway, such as colder water currents.

The $\delta^{13}C_{bel}$ and $\delta^{18}O_{bel}$ dataset from Bulgaria can be correlated with the records obtained in different sections of Europe and it is clear that evidence of rapid warming in the Moesian Basin during the early Toarcian correlates with rapid

global warming across the EES, postulated to be driven by the eruption of the Karoo-Ferrar LIP (Gómez et al., 2008; Jourdan et al., 2008). However, the local influx of freshwater into the basin, during the early Toarcian, linked to the well-documented increase in the hydrological cycle during this time (e.g. Percival et al., 2016; Xu et al., 2018a; Ruesbsam et al., 2019), makes the actual magnitude of the temperature shift appear more extreme than is realistic. This decline in oxygen isotopes is recorded across Europe, linked to a rise in sea surface temperatures, but might also reflect changes in continental and sea ice volume as well as changes in salinity and oxygen isotope values from Bulgaria show similar trends (Figure 4.11).

It is also worth noting that although there is increasing evidence suggesting that belemnite rostra are problematic palaeoenvironmental archives (see Hoffmann et al., 2016 and Immenhauser et al., 2016 for detailed discussions). However, synchronous global records of an early Toarcian negative oxygen isotope excursion and positive carbon isotope excursion, now also documented from the Moesian Basin, are likely to reflect true long-term perturbations in global temperature and the both carbon and oxygen cycles. It is therefore argued that even if belemnites are prone to early diagenetic effects, they still reflect secular global changes of seawater composition and can continue to be a useful palaeoenvironmental and palaeoclimatic indicator.

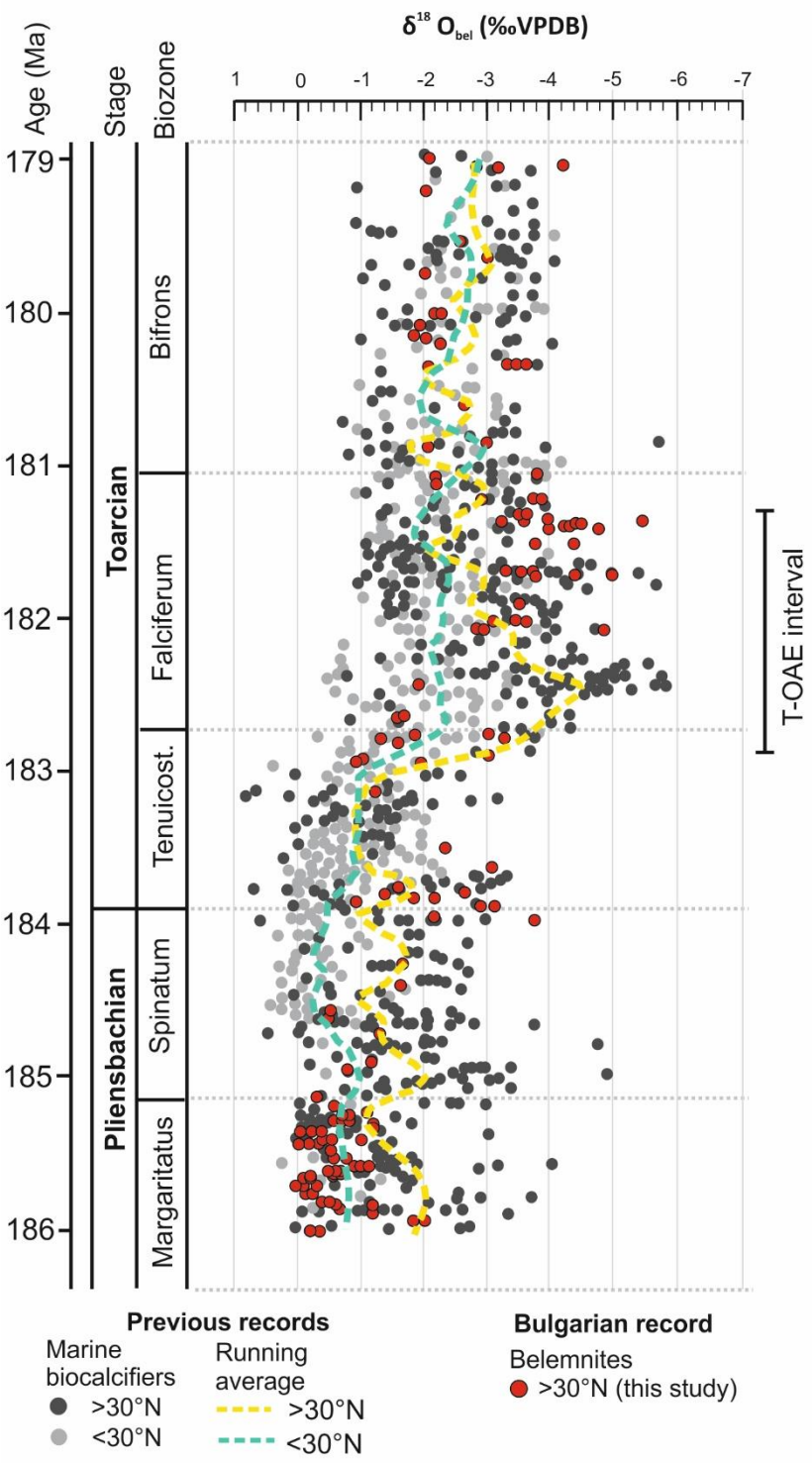

Figure 4.11 Composite oxygen isotope record of the late Pliensbachian-early Toarcian interval. $\delta^{18}O$ values from this study (belemnites) are shown by red circles. All $\delta^{18}O$ values from this study are displayed, except values from Beledie Han section, as samples are diagenetically altered. Published $\delta^{18}O$ values (marine calcifiers, including belemnites) from locations in Europe and Africa are shown by light (>30°N) and dark grey (>30°N) circles, modified after (Ruebsam et al., 2019).

4.4.5 Evaluating Mg/Ca and Sr/Ca ratios as a palaeotemperature proxy from belemnites in the Moesian Basin

There is extensive discussion about whether the El/Ca composition of belemnites retains a temperature-dependant signal. Some studies from belemnites in the northern EES have found high Mg/Ca and Sr/Ca ratios being associated to higher temperatures (Bailey et al., 2003; Rosales et al., 2004; McArthur et al., 2007; Armendáriz et al., 2013; Price et al., 2016), whereas other studies have found no clear link between Mg/Ca or Sr/Ca with $\delta^{18}O$ (e.g. Wierzbowski and Rogov, 2011; Korte and Hesselbo, 2011; Ullmann et al., 2015).

Data in this study show no, or very weak, correlations between Sr/Ca ratios and Mg/Ca ratios and $\delta^{18}O$ values (Figure 4.6). This differs from previous studies in Lower Jurassic belemnites from Bulgaria (Metodiev and Koleva-Rekalova, 2008) that claim to record a strong link between Mg/Ca and a weak correlation between $\delta^{18}O$ and Sr/Ca. The apparent link between Mg/Ca and $\delta^{18}O$ reported by Metodiev and Koleva-Rekalova, (2008), is used to provide support for the Mg/Ca ratio as a suitable tool for reconstruction of palaeotemperature. However, an oversight in the data from Metodiev and Koleva-Rekalova, (2008), is apparent if Mg/Ca and $\delta^{18}O$ values from the study are plotted and correlation assessed by linear regression. These linear regression plots show belemnites from only one of three sections shows a significant positive correlation between Mg/Ca and $\delta^{18}O$ ($R^2 = 0.495$), with other sections showing no correlation ($R^2 = 0.0697$, $R^2 = 0.0912$). Therefore the claims for the use of Mg/Ca as a suitable palaeotemperature proxy, based on correlations between Mg/Ca and $\delta^{18}O$ from their study are not well-supported.

A lack of correlation between Mg/Ca and $\delta^{18}O_{bel}$ in this study may be hampered by the assessment of multiple belemnite species, rather than species-specific assessment (Li et al., 2012). Although species specific fractionation on belemnite El/Ca ratios has been suggested (e.g. Li et al., 2013), it has not yet been quantified. Additionally, some uncertainty may be introduced due to salinity changes, which may introduce further scatter into the correlation. In the case of this study, this might be the case where salinity changes are likely to have a combined effect with temperature on the Moesian Basin $\delta^{18}O$ record (particularly during the early Toarcian).This is less likely to be the case at times of limited freshwater run-off (e.g. in the late Pliensbachian). As a weak correlation between Mg/Ca and $\delta^{18}O_{bel}$ is observed in the Milanovo Toarcian section and not in the Berende Izvor Pliensbachian section, it is unlikely salinity

would have added a significant amount of scatter to the records, as $\delta^{18}O_{bel}$ values from belemnites in the Milanovo section indicate a local influx of meteoric water in the early Toarcian. In this study, changes in Mg/Ca and Sr/Ca throughout the belemnite rostrum, which are not linked to diagenesis, do not represent changes in the temperature of the seawater. This provides further evidence against the use of Mg/Ca and Sr/Ca from belemnites as valid palaeoproxies for reconstructing past seawater temperatures (cf. Wierzbowski and Rogov, 2011; Korte and Hesselbo, 2011; Ullmann 2015; Rosales et al., 2018).

If temperature is not the only control on Mg/Ca and Sr/Ca values of belemnites in the Moesian Basin, other controlling factors could include: the composition of the Moesian Basin seawater in which they were precipitated, particularly for Sr/Ca ratios (see Ullmann et al., 2013); ontogeny-related biofractionation during biomineralisation (Li et al., 2012) and metabolically controlled changes in the calcifying medium (Ullmann et al., 2015).

4.5 Conclusions

Major carbon and oxygen isotope fluctuations are preserved within low-Mg calcite from belemnites collected through parts of the Lower Jurassic interval in NW Bulgaria. The good textural preservation of the belemnite samples argues for retention of the near-primary carbon and oxygen isotope record of ancient seawater. Carbon and oxygen isotopes are relatively stable through the Pliensbachian, with minor perturbations just before the Pl-To boundary.

During the upper Pliensbachian, relatively heavier $\delta^{18}O_{bel}$ values suggest intervals of colder seawater temperatures during the *Margaritatus* and *Spinatum* Zones. The negative shift in $\delta^{18}O_{bel}$ during the early Toarcian provides evidence of In the early Toarcian interval there is evidence of rapid global warming an increased freshwater run-off into the basin.

Recognition of a broad positive carbon isotope excursion (recorded from a positive shift in $\delta^{13}C$ of ~3 ‰), commonly recognised during the T-OAE interval is recorded from belemnite calcite, but not the negative CIE.

These fluctuations in both carbon and oxygen isotopes follow trends previously established from biogenic carbonate samples from time-equivalent sections across Europe, and thus confirm the pan European global nature of observed isotopic signals from belemnites within the Moesian Basin.

Chapter 5 Characterisation of the T-OAE in the Moesian Basin

5.1 Introduction

This chapter examines sections spanning the late Pliensbachian-late Toarcian interval from Bulgaria, documenting environmental change and its potential drivers in the Moesian Basin. The chapter firstly evaluates if reduced oxygen conditions are developed in the early Toarcian using pyrite petrography and reviewing sedimentological indicators of redox conditions. Secondly, it assesses if other globally recognised environmental perturbations including significant carbon isotope excursions, global warming, and Hg concentrations (a recently developed proxy to indicate volcanic activity during this time), are documented in the Moesian Basin. Documenting these changes will provide previously unknown records of environmental change from the eastern EES during the early Toarcian, improving our spatial understanding of the development of anoxia and links between carbon cycle perturbations and possible volcanic activity during the 'TOAE interval'.

5.2 Selected study sites

Figure 5.1. A) Detailed outcrop map of the west and central area in Bulgaria with study sections shown in red. Lower Jurassic outcrops are shown in grey. B) Outline map of Bulgaria, with the study area highlighted by black box.

The Lower Jurassic successions of the Moesian Basin constitute the primary field locations of this study. Out of the thirteen sections studied, six sites were selected (Figure 5.1) to address the research questions set out for this chapter.

A total of six sections, that represent different depositional environments of the Moesian Basin, were selected for framboid analysis. All sections for framboid

analysis cover sediments deposited prior, during and after the T-OAE. The Ravna section, which is Sinemurian in age, was also analysed for framboids, to give an indication of redox conditions earlier in the Jurassic compared to the rest of the sections, which are all Toarcian.

Two sections (Boeva Mogila and Milanovo) were selected for the analysis of carbon isotopes, TOC and mercury (Hg) concentrations through the selected Toarcian interval. The fine-grained, dark coloured nature of the sections indicated suitable lithologies to analyse organic carbon isotopes, TOC and Hg concentrations. The Toarcian shallow marine ooidal sediments from the Gorno Ozirovo and Kiselchov Dol sections were unsuitable for these geochemical analysis, due to extreme condensation, likely re-working and diagenetically altered sediment.

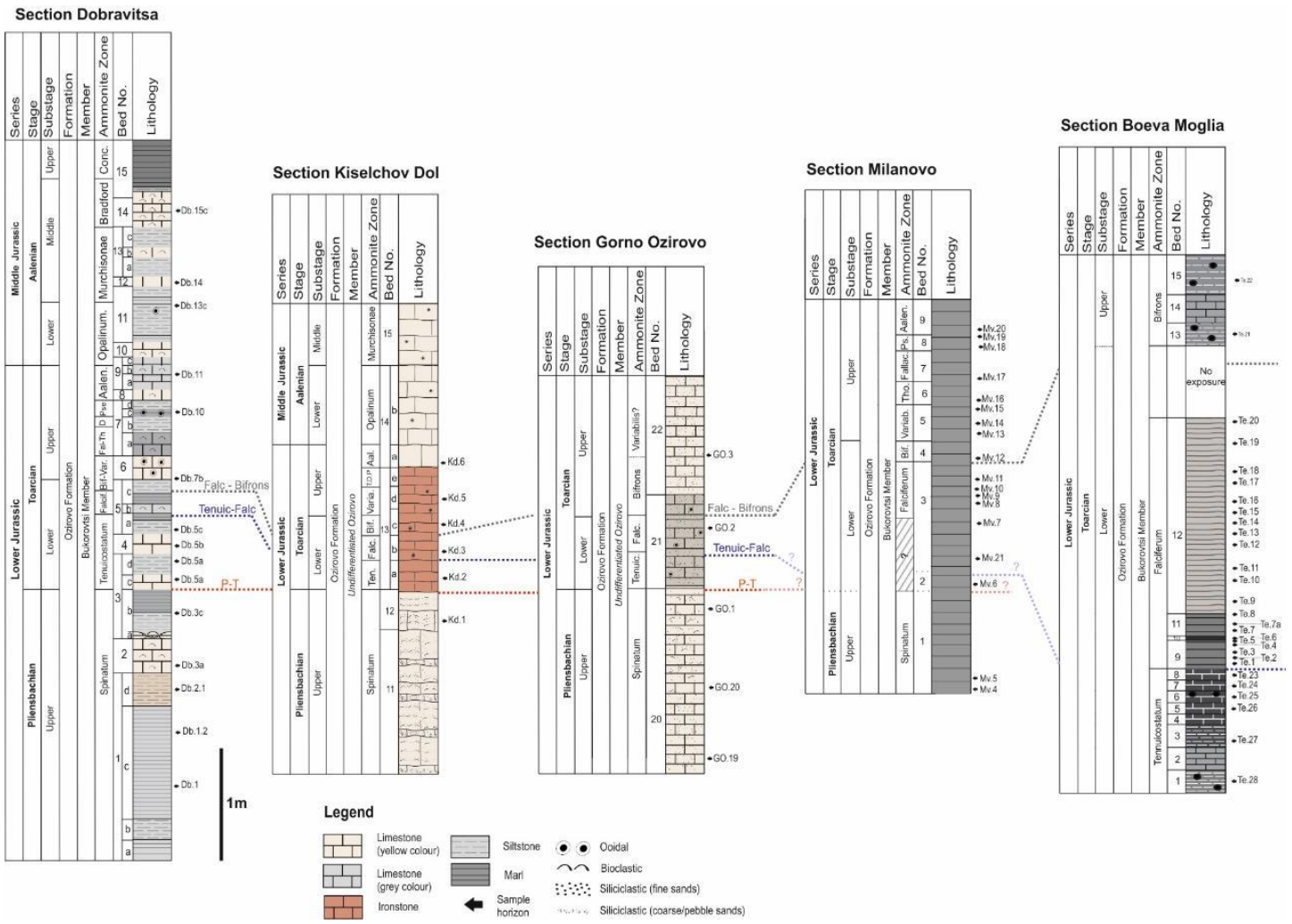

Figure 5.2. Composite figure of Toarcian study sites in Bulgaria.

5.3 Methods

Methods applied in this section are cross-referenced to detailed methods in Chapter 5 (see Table 5.1.).

Table 5.1 List and location of methods employed for analysis in Chapter 5

Method	Heading # (page #)	Sections	Sample material
Bulk preparation (sedimentary geochemistry)	2.5.1.2 (page 73)	Milanovo, Boeva Mogila	Bulk rock
Bulk preparation (framboid analysis)	2.2 (page 67)	Milanovo, Boeva Mogila, Dobravitsa-1, Gorno Ozirovo, Kiselchov Dol	Bulk rock
$\delta^{13}C_{org}$	2.5.1.5 (page 75)	Milanovo, Boeva Mogila	Bulk rock
Total Organic Carbon (TOC)	2.5.1.4 (page 74)	Milanovo, Boeva Mogila	Bulk rock
Mercury (Hg) concentrations	2.5.1.6 (page 76)	Milanovo, Boeva Mogila	Bulk rock
Framboid analysis	2.2 (page 67)	Milanovo, Boeva Mogila, Dobravitsa-1, Gorno Ozirovo, Kiselchov Dol, Ravna	Bulk rock

5.4 Results

5.4.1 Framboid petrography

Pyrite petrography revealed highly variable pyrite abundances. Sediments from the Kiselchov Dol, Gorno Ozirovo and Milanovo (upper Pliensbachian, *spinatum* Zone) sections contain no framboids. Framboids are relatively common in the

Milanovo and Dobravitsa-1 sections and are abundant in the Boeva Mogila section. Raw data from framboid petrography are shown in Appendix C.1.

Framboids are typically preserved as iron oxyhydroxides due to weathering, with either minor or no original pyrite preserved in their core (Figure 5.3, Figure 5.9 and Figure 5.10). When pyrite framboids are fully oxidised, no sulphur is present as evidenced by their EDS spectra (Figure 5.3). Weathering is likely a result of the soft nature of the marls and silts comprising the sections where framboids are present. Only five samples from Dobravista-1 (Db.5b, Db.10, Db.13c, Db.14, Db.15c) and five samples from Boeva Mogila (sample Te.5, Te.24, Te.26, Te.27, Te.28) contained unweathered pyrite, present as FeS (Figure 5.3).

Where framboid populations for the Moesian Basin are present, deposition in predominately dysoxic/oxic conditions with occasional fluctuations into anoxic/euxinic conditions are recorded, with redox conditions interpreted using euxinic/anoxic versus oxic/dysoxic fields set by Wilkin et al. (1996) from modern environments. These potential fluctuations into more anoxic/euxinic conditions do not correlate across sections to a particular time interval or change in facies.

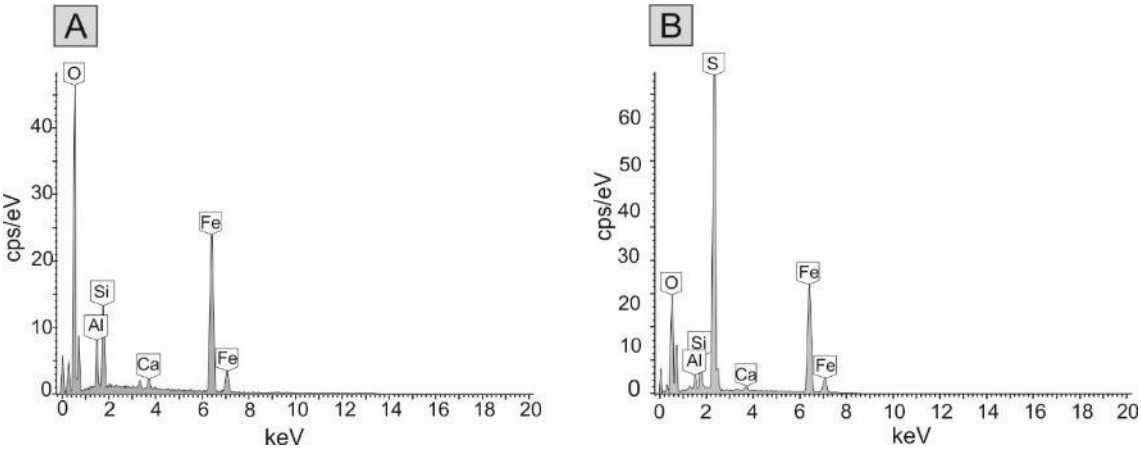

Figure 5.3 Representative EDS spectra taken from A) oxidised framboids (no S present) (bulk sample Te.5) and B) framboids that retained original pyrite (FeS_2) composition (bulk sample Te.7a).

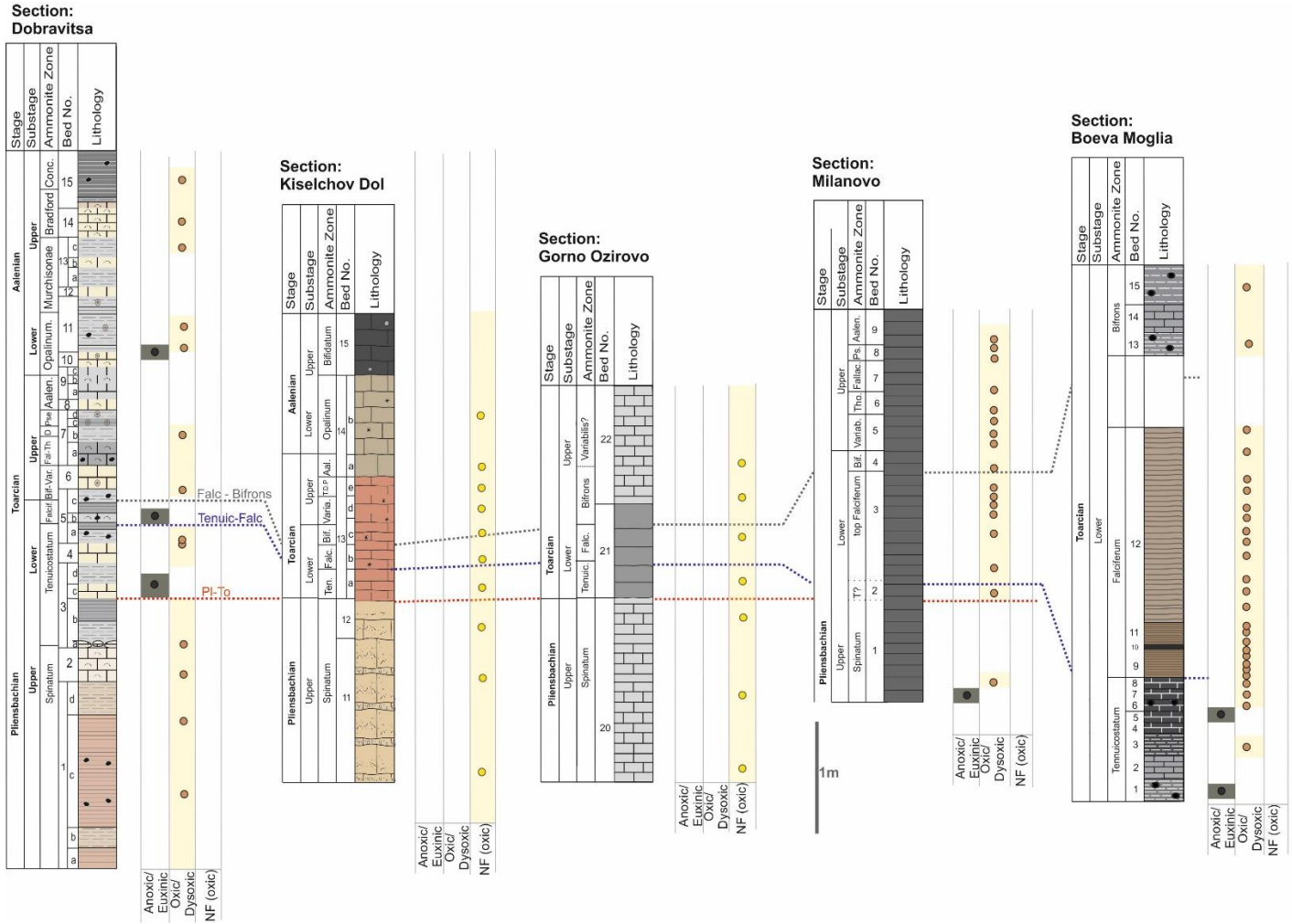

Figure 5.4 Framboids plotted stratigraphically for Toarcian sections. NF=No framboids.

Boeva Mogila section

The Boeva Mogila section record abundant framboids present in each bed, with the exception of sample Te-3 (bed 3) near the base of the *falciferum* Zone, where only four framboids were counted, with a mean diameter of 7 µm (Figure 5.5). Throughout the section mean framboid diameters vary between 5.8 and 10.2 µm. In the *tenuicostatum* Zone, framboid mean diameters between 7.2 and 7.4 µm are recorded from the bottom of section, typical of upper dysoxic conditions (Wignall and Newton, 1998). A small drop at the top of the *tenuicostatum* Zone to smaller mean framboid diameters (between 6.3 and 6.9 µm) and a smaller standard deviation (1.7-2.2), is more typical of lower dysoxic conditions (Wignall and Newton, 1998). Throughout the *falciferum* Zone and into the *bifrons* Zone, framboid distributions suggest deposition under predominately dysoxic/oxic conditions (Figure 5.5). The most framboid-rich level is from the thinly developed darker, more organic-rich bed (bed 6) near the base of the *falciferum* Zone. This sample records the smallest mean framboid diameter (5.79 µm) in the section (Figure 5.5). Samples Te.28 (top *tenuicostatum* Zone) and Te.8 (*falciferum* Zone) are samples that suggest deposition in a euxinic/anoxic water column (Figure 5.5).

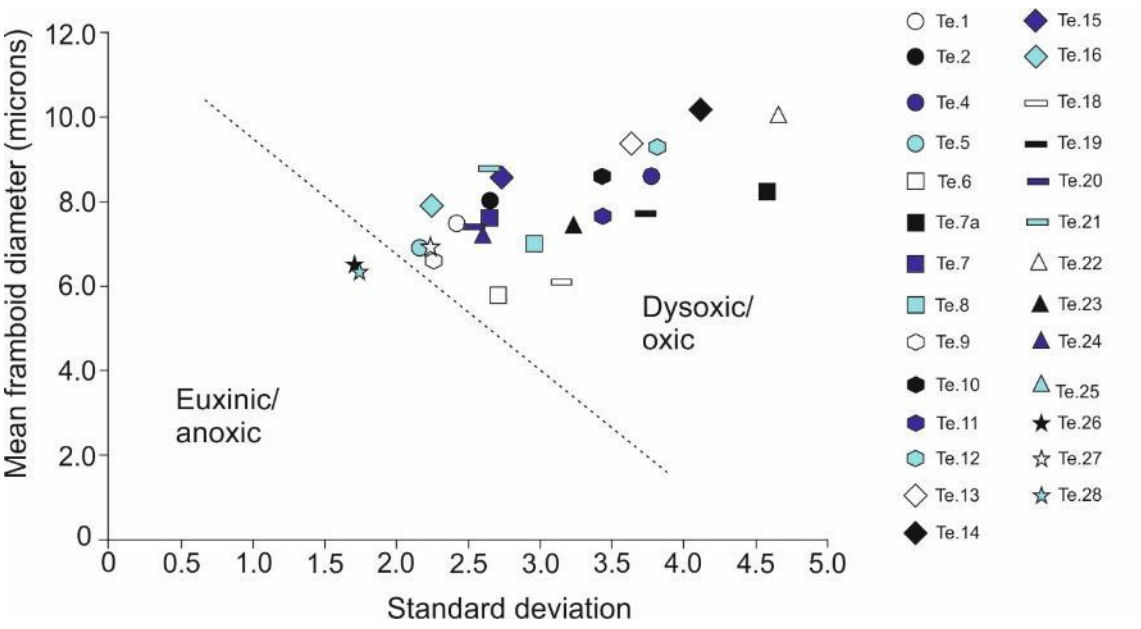

Figure 5.5 Mean framboid diameter (microns) vs. standard deviation for pyrite framboids from the Boeva Mogila section. Anoxic/euxinic and dysoxic/oxic fields, based on Wilkin et al. (1996), are shown by black dashed line.

Milanovo section

In the Milanovo section, framboids are present all beds, although not as abundant as in the early Toarcian (*tenuicostatum-falciferum* Zones) of the Boeva Mogila section. Two samples (Mv.9 and Mv.21) are classed as having rare framboids (<50 counted) and three samples (Mv.10, Mv.11 and Mv.15) record low framboid abundances (>50 but <100 counted) (Appendix C.1). Samples with rare or low framboid abundances correspond to the framboid populations with the largest mean diameters (~10 µm) (Figure 5.6).

Throughout the section, mean framboid diameters vary between 5.85 and 10.3 µm, similar to the Boeva Mogila section. Overall framboid populations suggest deposition in dysoxic to oxic conditions. Sample Mv.4 (*spinatum* Zone, latest Pliensbachian) is the only sample that suggests, based on framboid size analysis, deposition in a euxinic/anoxic water column (Figure 5.6).

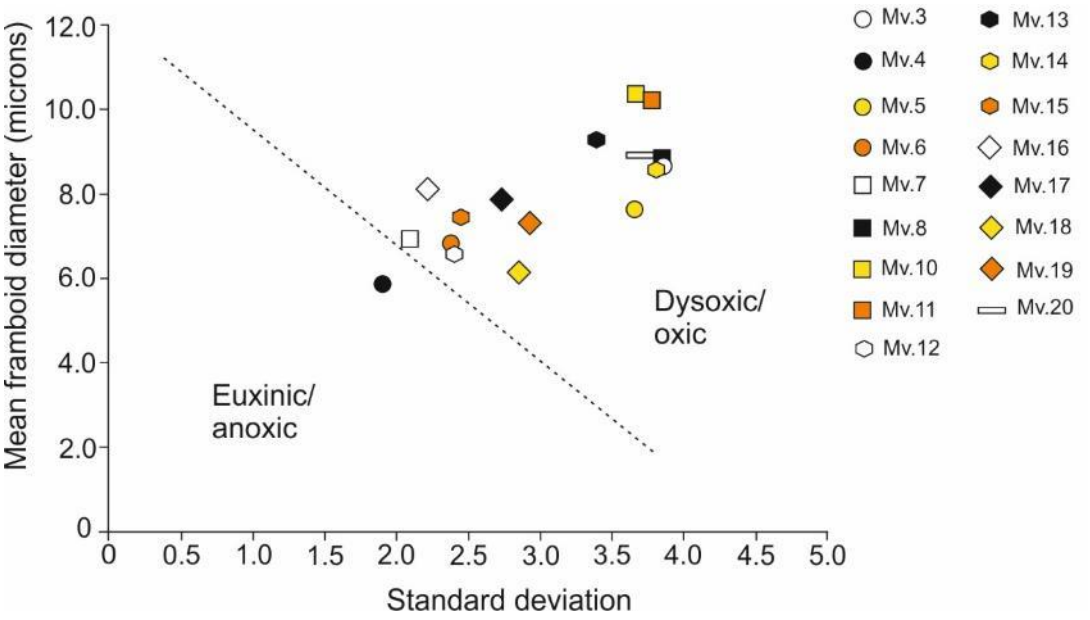

Figure 5.6 Mean framboid diameter (microns) vs. standard deviation for pyrite framboids from the Milanovo section. Anoxic/euxinic and dysoxic/oxic fields, based on Wilkin et al. (1996), are shown by black dashed line.

Dobravista-1 section

Framboid counts of samples from Dobravitsa-1 show framboids present in all samples. Two samples (Db.5a.2 and Db.7b.2) are classed as having rare framboids (<50 counted) and one sample (Db.1.2) records low framboid abundances (>50 but <100 counted). Similarly to Milanovo, samples with rare or low framboid abundances correspond to the framboid populations with the

largest mean diameters (between 10.7 – 11.4 µm). Toarcian sample Db.5b (*tenuicostatum* Zone, *semicelatum* Subzone), along with Aalenian samples Db.10 (o*planiunum* Zone, *opalinum* Subzone) and Db.13c (*murchisonae* Zone, *murchisonae* Subzone) suggest deposition in a euxinic/anoxic water column (Figure 5.7).

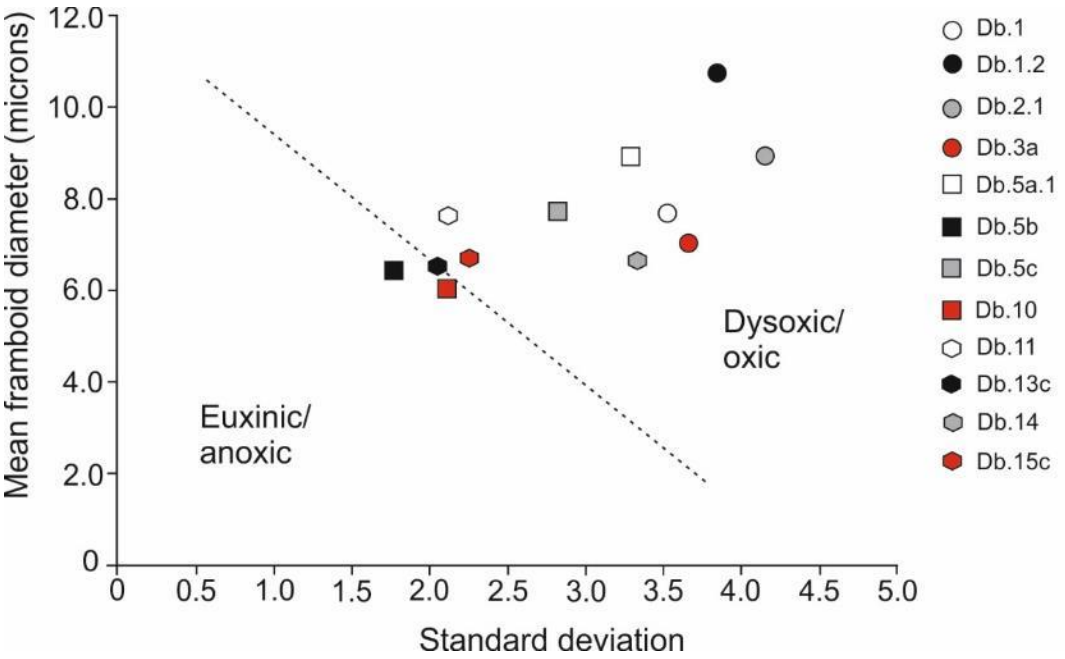

Figure 5.7 Mean framboid diameter (microns) vs. standard deviation for pyrite framboids from the Dobravitsa-1 section. Anoxic/euxinic and dysoxic/oxic fields, based on Wilkin et al. (1996), are shown by black dashed line.

Ravna section

Framboid populations from the Ravna sections indicate that during the late Sinemurian, seawater conditions may also have fluctuated between oxic/dysoxic conditions in the Moesian Basin (Figure 5.8).

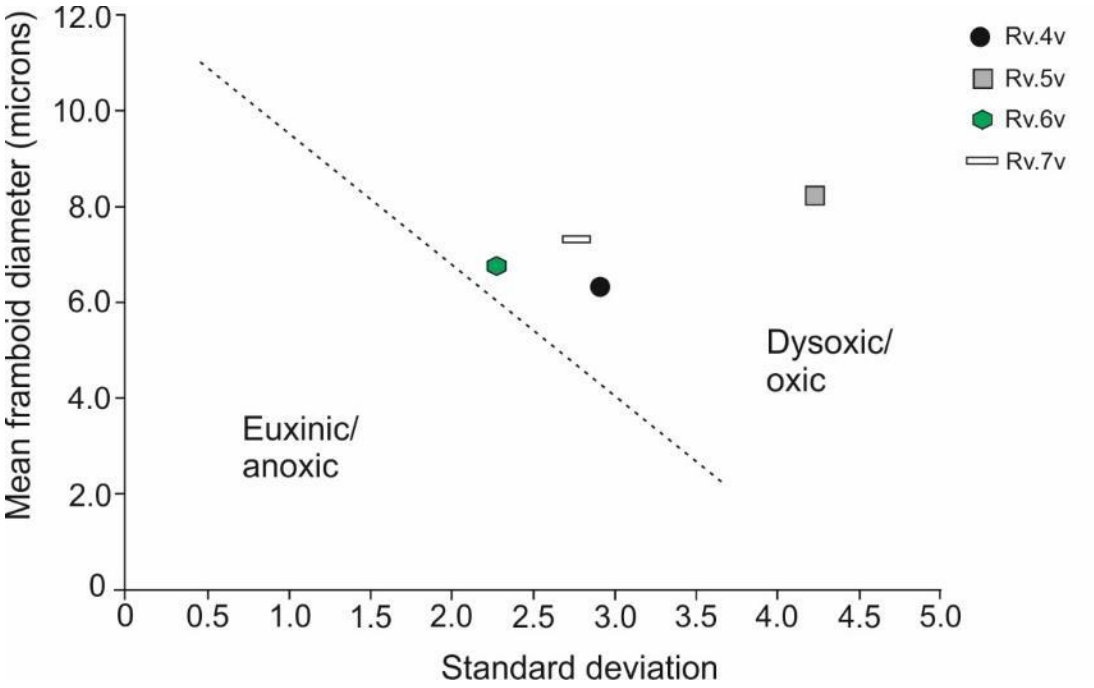

Figure 5.8 Mean framboid diameter (microns) vs. standard deviation plot for pyrite framboids for the Ravna section. Anoxic/euxinic and dysoxic/oxic fields are shown, based on Wilkin et al., 1996 (black dashed line).

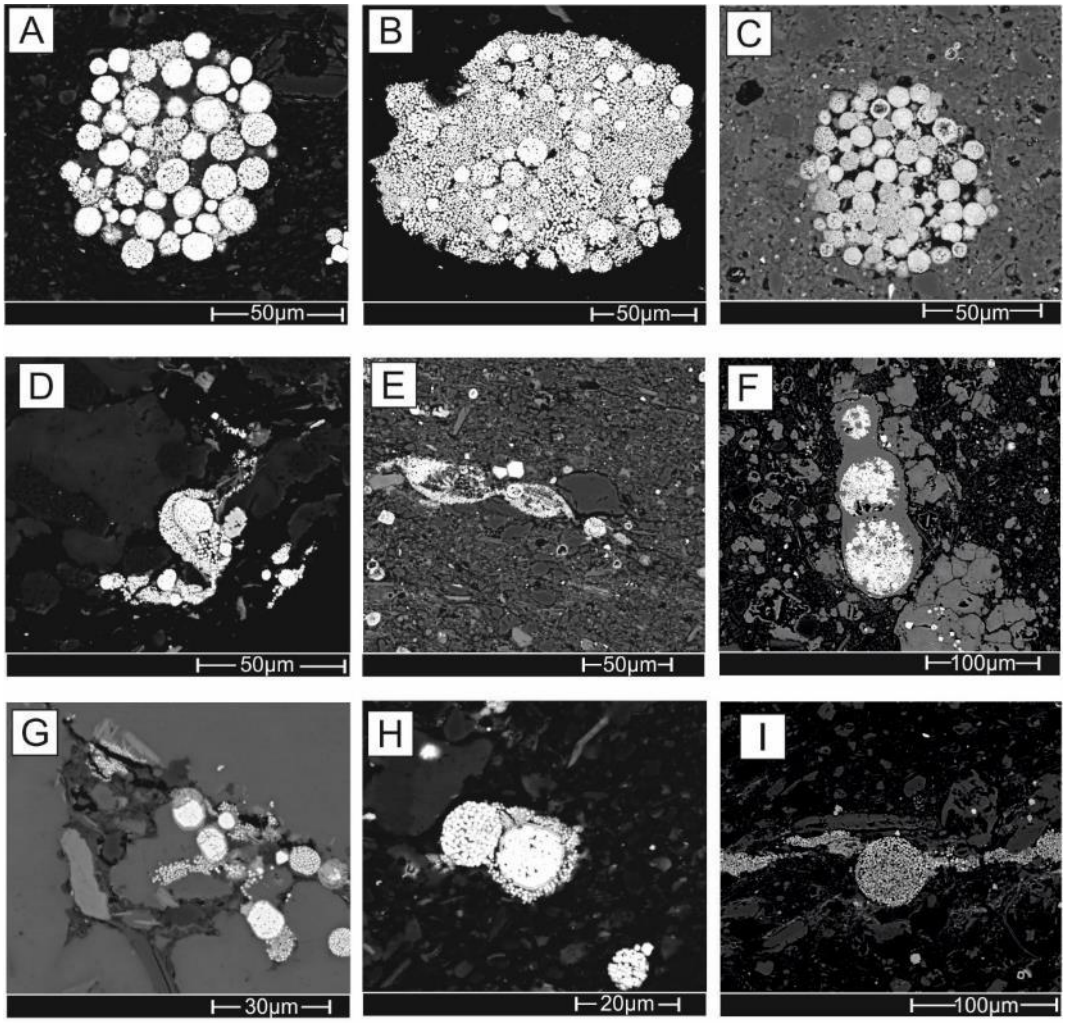

Figure 5.9 Representative backscatter images of framboids. A) typical framboids from sample Te.6, bed 6, Boeva Mogila section (oxic/dysoxic field), B) relatively large framboids from sample Te.6, bed 6, Boeva Mogila section (oxic/dysoxic field), C) high abundance of framboids from sample Te.6, bed 6, Boeva Mogila section (oxic/dysoxic field), D) framboid distribution from sample Mv.14, bed 14, Milanovo section (oxic/dysoxic field), E) typical framboids from sample Mv.14, bed 14, Milanovo section (oxic/dysoxic field), F) framboids and euhedral pyrite from sample Te.7, bed 7, Boeva Mogila section (oxic/dysoxic field), G) oxidised and weathered framboids from sample Te-11, bed 11, Boeva Mogila section (oxic/dysoxic field), H) framboid infill from sample Te.12, bed 12, Boeva Mogila section (oxic/dysoxic field) and I) typical framboids from sample Mv.5, bed 5, Milanovo section (oxic/dysoxic field).

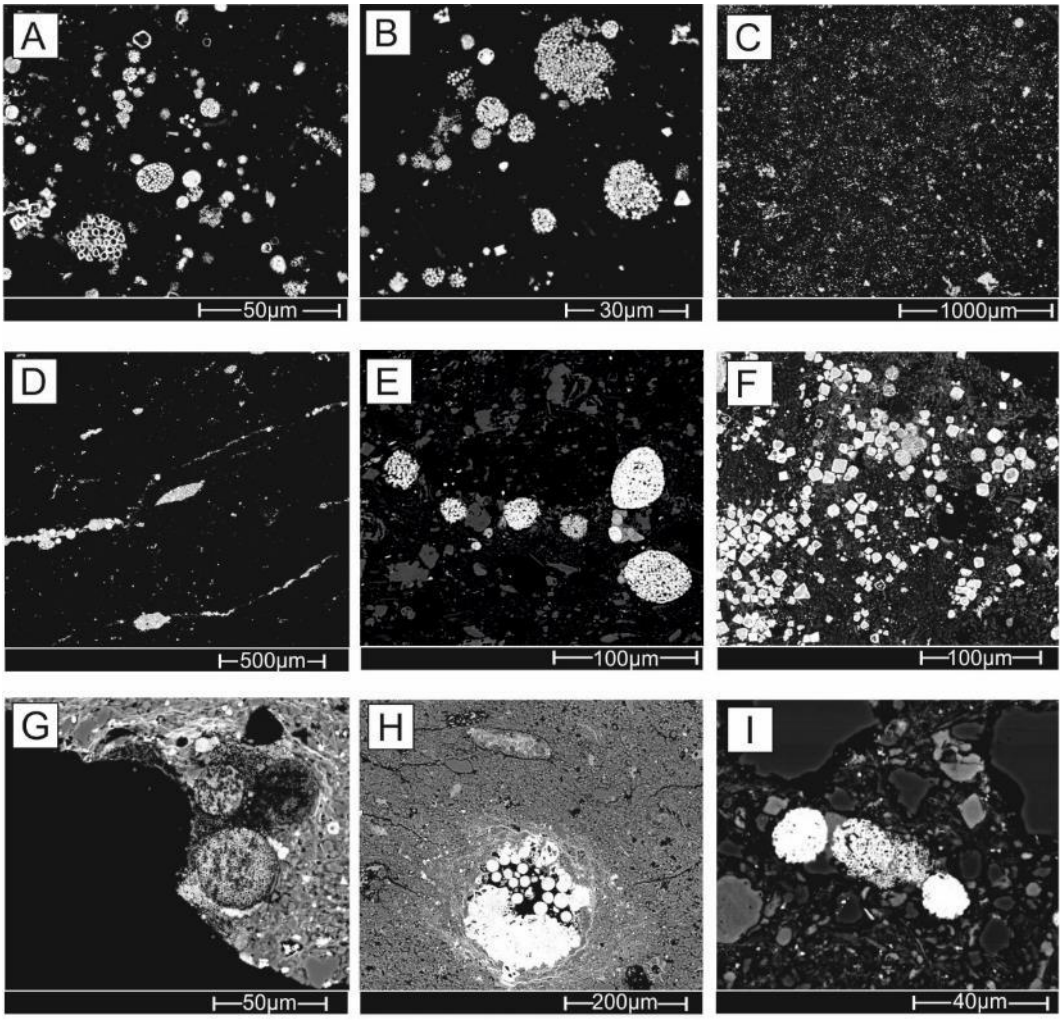

Figure 5.10 Representative backscatter images of framboids. A) polyframboid from sample Db.5a, bed 5, Dobravitsa-1 section (oxic/dysoxic field), B) polyframboid from sample Db.5b, bed 5, Dobravistsa-1 section (euxinic/anoxic field), C) polyframboid from sample Te.8, bed 8, Boeva Mogila section (oxic/dysoxic field), D) typical framboids from sample Te.27, bed 27, Boeva Mogila section (oxic/dysoxic field), E) framboids infilling ostracods from sample Te.20, bed 20, Boeva Mogila section (oxic/dysoxic field), F) framboids infilling gastropod from sample Mv.10, bed 10, Milanovo section (oxic/dysoxic field), G) framboids with oxidised rim from sample Te.26, bed 26, Boeva Mogila section (euxinic/anoxic field), H) framboids with oxidised rim from sample Db.5a, bed 5a, Dobravitsa-1 section, I) oxidised framboid with low brightness and grey colour from sample Mv.13, bed 13, Milanovo section (euxinic/anoxic field).

5.4.2 TOC concentrations

For both Boeva Mogila and Milanovo sections, the TOC content is very low, with overall lower values recorded from the Milanovo section (Figure 5.11, Figure 5.12).

Boeva Mogila section

TOC values through early Toarcian in the Boeva Mogila section range from 0.23 – 0.98 wt% TOC, with an average of 0.41 wt% TOC. The *tenuicostatum* Zone (*Semicelatum* Subzone) and early *falciferum* Zone (0.05-0.90 m) records relatively low TOC values fluctuating between 0.31 and 0.45 wt% (Figure 5.11). A clear peak in TOC values of 0.98 wt% (1.3 m) and continued slightly elevated TOC values around 0.5 wt% are recorded in the *falciferum* Zone (1.35-1.90 m), coincident with the negative CIE (Figure 5.11). Values decrease slightly, coincident with the end of the CIE to around 0.25 wt% (2.1 m) and then continue to record small fluctuations between 0.26 and 0.52 wt% (2.2-4.8 m) (Figure 5.11).

Milanovo section

TOC values through the late Pliensbachian (*spinatum* Zone) and Toarcian in the Milanovo section are slightly lower than those in the Boeva Mogila section with an average of 0.25 wt% TOC. The maximum TOC value of 0.32 wt% (1.9 m) is recorded in the early Toarcian following the hiatus, likely to represent the *falciferum* Zone and the lowest TOC values of 0.14 wt% (3.93 m) are recorded in the latest Toarcian, in the a*alensis* Zone (Figure 5.12). TOC values remain relatively constant throughout the section with only minor fluctuations (Figure 5.12).

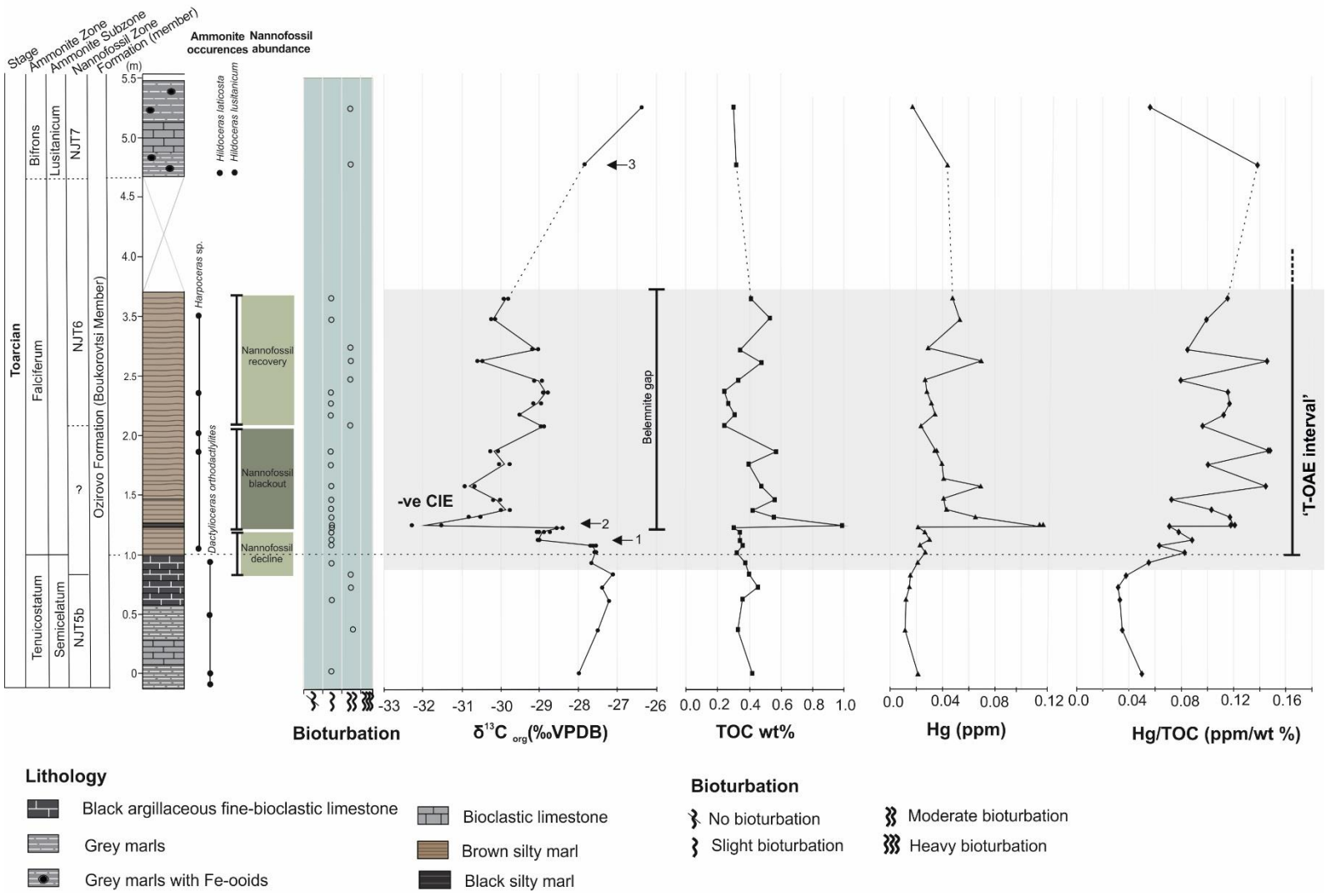

(PTO for caption)

Figure 5.11 (previous page) Geochemical data from the Boeva Mogila: $\delta^{13}C_{org}$ (permil), TOC wt %, Hg (ppm) and Hg/TOC (ppm/ wt % C). Ammonite occurrences for biostratigraphy and a semi-quantitative bioturbation record from specific horizons are noted next to the sedimentary log. 'T-OAE interval' is shown as grey shaded area.

5.4.3 Carbon isotope record

The inorganic and organic $\delta^{13}C$ record shows two excursions recorded in the early Toarcian. The first, a negative CIE is recorded in organic carbon from bulk rock in the Boeva Mogila section and the second, a subsequent positive CIE, recorded most clearly in belemnite calcite.

5.4.3.1 Organic carbon isotope record

Boeva Mogila section

The Boeva Mogila section records a continuous organic carbon isotope record through the *tenuicostatum* and *falciferum* Zones in the Lower Jurassic (0.05m – 3.2 m, Figure 5.11). At the base of the section, in the *tenuicostatum* Zone, organic carbon values are relatively stable between -27 and -28 ‰ (Figure 5.11). A clear negative carbon isotope excursion, with a ~ 5 ‰ shift, is recorded beginning around the *tenuicostatum/falciferum* Zone boundary and continues into the *falciferum* Zone. The magnitude of the negative CIE excursion is described by the difference between the last value representative of background values in *tenuicostatum* Zone and the most negative value reached during the negative CIE. The excursion is 'stepped' on the negative limb, with an initial shift to -29.04 ‰ (1.15 m) (Figure 5.11, step 1) and then a second negative shift approaching a minimum of -32.28 ‰ (1.3 m) (Figure 5.11, step 2). Minimum values correspond to a thinly-developed interval with increased TOC content. Following this maximum, a gradual return towards isotopically lighter $\delta^{13}C_{org}$ values is recorded through the remaining *falciferum* Zone. Due to a lack of exposure through the uppermost *falciferum* Zone, a return to pre-excursion values is not recorded. In the *bifrons* Zone, where outcrop continues again, values have returned to values of -27.7 to -26.2 ‰ (4.4 to 4.8 m), similar to those recorded prior to the negative carbon isotope excursion in the *tenuicostatum* Zone (Figure 5.12, step 3).

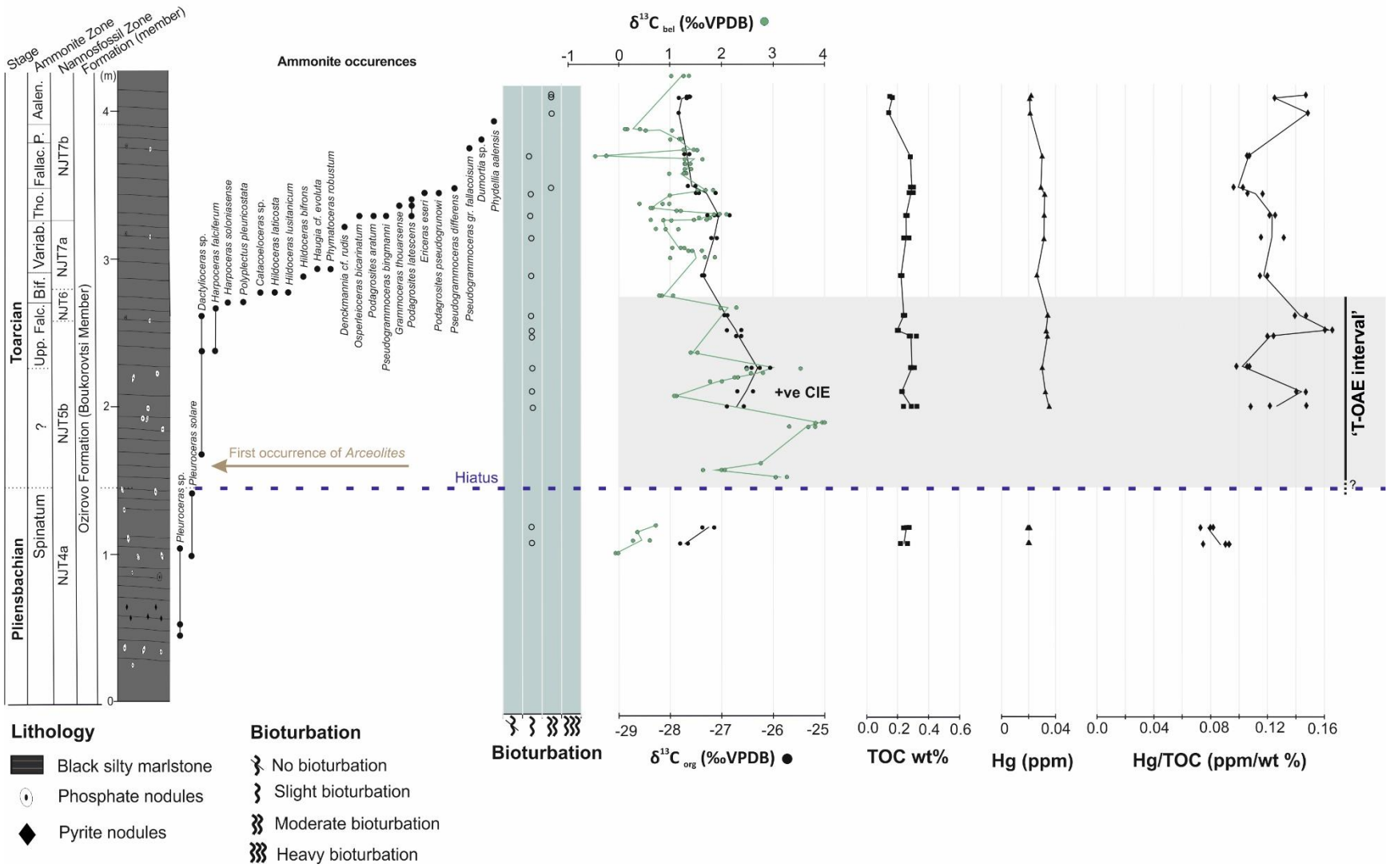

(PTO for caption)

Figure 5.12 (previous page) Geochemical data from the Milanovo section: $\delta^{13}C_{org}$ (permil), TOC wt %, Hg (ppm) and Hg/TOC (ppm/ wt % C). Ammonite occurrences for biostratigraphy, a semi-quantitative bioturbation record, and the first occurrence of the post T-OAE belemnite *Arceolites* are noted from specific horizons noted next to the sedimentary log. 'TOAE interval' is shown as grey shaded area.

Milanovo section

In the Milanovo section, the negative CIE recorded organic carbon from the Boeva Mogila section is not present, due to the hiatus between the late Pliensbachian (*spinatum* Zone) and early Toarcian (*falciferum* Zone). Prior to the hiatus, the late Pliensbachian (*spinatum* Zone), records $\delta^{13}C_{org}$ values between -26.9 and -27.4 ‰. Following the hiatus, a continuous organic carbon curve is recorded from the late *falciferum* Zone to the top of the Toarcian (a*alensis* Zone), albeit at a relatively low resolution due to the condensed nature of the section. A difference of ~1.2 ‰ is recorded between the Pliensbachian values and the first Toarcian values. This small positive shift reaches the heaviest $\delta^{13}C_{org}$ values in the section in the *falciferum* Zone (placement within ammonite zone is unclear due to hiatus and lack of ammonites). Throughout the Toarcian interval $\delta^{13}C_{org}$ values fluctuate slightly, with a maximum variability of ~1 ‰, but an overall trend to slightly more negative values through the Toarcian, reaching 27.4 ‰, in the latest Toarcian (a*alensis* Zone).

5.4.3.2 Inorganic carbon isotope record

Milanovo section

The $\delta^{13}C_{org}$ isotope values range from -25 to -29 ‰ (Figure 5.12). In the latest Pliensbachian (*spinatum* Zone) values of -0.06 ‰ and 0.74 are recorded. The first belemnite calcite value recorded, following the inferred hiatus around the Pliensbachian/Toarcian boundary, is 0.35 ‰ (1.51 m) (Figure 5.12). Following this $\delta^{13}C_{bel}$ values show a positive excursion reaching a maximum of 3.97 ‰ in the late *falciferum* Zone (1.89 m) (Figure 5.12). Following the positive CIE, values show an overall decreasing trend through the Toarcian, reaching values between 0-1 ‰ in the *aalensis* Zone (3.93 to 4.33 m) (Figure 5.12).

5.4.4 Hg and Hg/TOC

The Milanovo and Boeva Mogila sections both show enrichments in Hg concentrations (ppm) and excursions in Hg/TOC (ppm/wt% TOC) ratios.

Boeva Mogila section

Background Hg values closely track the TOC record through the section. Hg values around 0.01 (ppm) are record through the *tenuicostatum* Zone with a small increase to around 0.020 – 0.035 (ppm) across the *tenuicostatum/falciferum* Zone boundary, coincident with the beginning of the negative CIE (Figure 5.11). A rapid increase to 0.12 (ppm) in the early *falciferum* Zone (1.3 m) is synchronous with the minima of the negative CIE (Figure 5.11). Hg values remain slightly elevated (between 0.039-0.550 ppm) relative to the background values from the *falciferum* Zone. Background values (around 0.020 ppm) are recorded again by the mid *falciferum* Zone and continue into the *bifrons* Zone (*lusitanicum* Subzone), with only minor fluctuations (Figure 5.11).

Hg/TOC ratios record the same general trend of Hg (ppm), with lower values recorded through the *tenuicostatum* Zone (0.03-0.05 ppm/wt %), increasing towards and across the *tenuicostatum/falciferum* Zone boundary and the beginning of the *falciferum* Zone (0.05 – 0.09 ppm/wt %). The Hg/TOC record however continue to show elevated values, with minor fluctuations (between 0.06 – 0.15) throughout the *falciferum* Zone, coincident with the negative CIE (Figure 5.11). The peak Hg/TOC value of 0.015 ppm/wt % (1.9 m) is recorded after the negative CIE minimum (1.3 m). A background value of 0.05 ppm/wt % (4.8 m) is only recorded again in the *bifrons* Zone (*lusitanicum* Subzone) (Figure 5.11).

Milanovo section

Low Hg values of around 0.02 ppm in the late Pliensbachian *spinatum* Zone are comparable to the lower values in the Boeva Mogila section, present in the *tenuicostatum* Zone. Hg concentrations remain low through the Milanovo section between 0.02 – 0.034 ppm (Figure 5.12).

Hg/TOC ratios through are elevated compared to the Boeva Mogila section. The lowest values are recorded in the Pliensbachian (*spinatum* Zone) around 0.07 ppm/wt %, with a subsequent positive shift in values to between 0.1-0.17 ppm/wt % (1.9 – 2.5 m), coincident with the positive CIE recorded in inorganic carbon (Figure 5.12). Due to a hiatus around the late Pliensbachian and

tenuicostatum Zone in the Milanovo section, the shift cannot be pinpointed. The higher Hg/TOC values recorded in Milanovo correspond to similar values, in the Boeva Mogila section, also recorded during the mid-late falciferum. After the *falciferum* Zone, values show an overall decrease through the Toarcian to 0.1 ppm/wt % in the *fallaciosum* Zone (3.31 m), with a subsequent small increase through the latest Toarcian to around 0.15 ppm/wt % (3.94 m) (Figure 5.12).

5.5 Discussion

5.5.1 Carbon isotope excursions

Chemostratigraphic correlations, constrained by biostratigraphic data between the Bulgarian and published European and other global sections, confirm the ubiquitous presence of a characteristic overarching positive CIE, interrupted by a negative CIE in the early Toarcian during the 'T-OAE interval', commonly recognised across the EES and globally during this time (Jenkyns and Clayton, 1997; Jones and Jenkyns, 2001; Jenkyns et al., 2002; Jenkyns, 2003; Katz et al., 2005; van de Schootbrugge et al., 2005; Kemp et al., 2005; Al-Suwaidi et al., 2010; Izumi et al., 2012; Bodin et al., 2016; Al-Suwaidi et al., 2016; Them et al., 2017; Xu et al., 2018a; Suan et al., 2018 and references therein). This study documents the most easterly record of these major early Toarcian carbon cycle perturbations, recorded from two carbon reservoirs ($\delta^{13}C_{bel}$ and $\delta^{13}C_{org}$) in the epicontinental Tethys.

The positive CIE recorded from $\delta^{13}C_{bel}$ is interrupted by a negative CIE ~5 ‰ (-27.0 to -32.5 ‰) recorded in $\delta^{13}C_{org}$, comparable to other global records of the early Toarcian negative CIE which document a negative shift between 3-8 ‰. In the Moesian Basin the negative CIE is marked by a step-wise onset at the *tenuicostatum-falciferum* transition. Decimetre scale ~1 ‰ $\delta^{13}C_{org}$ fluctuations are broadly recorded (albeit at a low resolution) and superimposed onto the long-term trend during the negative CIE (Figure 5.11, steps 1 and 2). The discrete negative steps in $\delta^{13}C_{org}$ at the onset of the T-OAE negative CIE have previously been observed in both organic and inorganic matter globally during this time (e.g. Jenkyns et al., 2001; Jenkyns et al., 2002; Kemp et al., 2005; Hermoso et al., 2012; Them et al., 2017) These small-scale CIEs, here recorded in the Moesian Basin, have been interpreted to represent discrete methane clathrate destabilisation events tied to astronomically forced changes to the global climate (Kemp et al., 2005; Hesselbo and Pienkowski, 2011; Hermoso et al., 2012). Recognition of the negative CIE, including the smaller

CIE fluctuations on the falling limb, help provide further evidence for multiple global carbon cycle perturbations across the T-OAE interval, with the stepped negative CIE recently recorded in Canada (Them et al., 2017). It is likely morphological changes in the shape of the negative CIE, including the morphological shape recorded from the negative CIE in Bulgaria, is influenced by sedimentary processes, accumulation rates and changes in sea-level, as is the case with other European $\delta^{13}C$ records across the EES (e.g. Hesselbo and Pienkowski, 2011; Hermoso et al., 2012; Pittet et al., 2014). Although the carbon isotope record from Bulgarian sections is more condensed than North American (Caruthers et al., 2011; Them et al., 2017) and other European records (e.g. Kemp et al., 2005; Hesselbo et al., 2007; Xu et al., 2018a), it has clear similarities recorded in the timing and morphology of the negative CIE. This provides evidence that despite a comparatively lower-resolution carbon-isotope record, the Moesian Basin responded and recorded the same effects of palaeoenvironmental perturbations recorded from coeval sections globally.

The magnitude of the negative CIE recorded in Bulgaria is lower than that of coeval sections in the northern EES, that document a ~7 to 8 ‰ negative shift in organic carbon, with actual $\delta^{13}C_{org}$ values ranging from −24 to −31 ‰ in the Mochras core (UK) (Xu et al., 2018a) (Figure 5.13) and −25 to −33 ‰ from the Yorkshire Coast (Kemp et al., 2005). The Boeva Mogila section in Bulgaria records slightly higher $\delta^{13}C_{org}$ values through the *tenuicostatum* Zone between -27 to -28 ‰ compared to northern EES sections were values are around -24 to -25 ‰ (Kemp et al., 2005; Xu et al., 2018a). The negative CIE from the Boeva Mogila section in Bulgaria reaches a similar minimum of ~33 ‰ as recorded from Yorkshire Coast, which are lighter than the minimum ~31 ‰ recorded from Mochras (Figure 5.13). Differences in the compositions of the bulk organic matter may account for the differences in absolute values of the CIE minimum (Xu et al., 2018a). It has been noted that terrestrial matter accounts for a higher proportion of the total organic matter in the Mochras Core (indicated by abundant fossil wood and lower HI values of 339 mg HC/g TOC) and a higher-proportion of algal sourced organic matter for the Yorkshire Coast sections (indicated by higher HI values, up to 734 mg/ HC/g) (Sælen et al., 2000; French et al., 2014; Xu et al., 2018a). Given the differences recorded in the UK, a lack of fossil wood in the Bulgarian sections, and previous research that suggests during the Early Jurassic marine algae generally also took up a higher proportion of the light (^{12}C) carbon compared to terrestrial higher plants (Van Bergen and Poole, 2002), it could be argued that the slightly lighter absolute values recorded for the negative CIE in Bulgaria is due to a higher percentage

of marine organic matter. This however, is speculative, and particular sources of organic carbon would need to be quantified and evidenced.

The $\delta^{13}C_{org}$ values in the top of the *tenuicostatum* Zone (*Semicelatum* Subzone) in Bulgaria are around 27 ‰ (Figure 5.11). Due to a lack of exposure, values lower in the *tenuicostatum* Zone are not recorded in the Boeva Mogila section. In coeval sections across the EES, the lower-mid *tenuicostatum* Zone characterise pre-CIE background values with isotopically lighter $\delta^{13}C_{org}$ around 23-26 ‰ and begin decreasing with the onset of the CIE to ~27 ‰ in the *Semicelatum* Subzone (Cohen et al., 2004; Kemp et al., 2005). In the case of Bulgaria, the start of the record in the *Semicelatum* Subzone may not represent the lightest pre-CIE $\delta^{13}C_{org}$ values recorded earlier in the tenuicostatum. The implication of this is that the maximum negative CIE shift in $\delta^{13}C_{org}$, may not represent the full magnitude of the excursion as lower *tenuicostatum* Zone background values are unknown. The 5 ‰ shift in $\delta^{13}C_{org}$ recorded during the early Toarcian in Bulgaria is therefore only a minimum value and the true shift may have been of a higher magnitude.

Some records of the early Toarcian negative CIE on the most southerly edge of the EES and outside the EES have a notably smaller magnitude CIE, with minima reaching -27 ‰ in Morocco (Krencker et al., 2014), -30.7 ‰ in British Columbia and Alberta (Them et al., 2017), -29 ‰ in Japan (Kemp and Izumi, 2014), -27 ‰ in southern Tibet (Han et al., 2018) (Figure 5.13). Although this is not the case for all southern EES negative CIE records, with the Moesian Basin recording a similar negative CIE excursion (from organic carbon) in magnitude to sections in Greece (Kafousia et al., 2014) and Morocco (Bodin et al., 2016).

As both the organic carbon and inorganic carbon isotope data from Bulgaria show a high degree of similarity in stratigraphic position and magnitude, it provides evidence that the carbon isotope signatures are not simply a response to local basin conditions and emphasise the global nature of carbon cycle changes at this time. The Moesian Basin therefore provides an additional record of the CIEs, in particular the early Toarcian negative CIE, from a relatively undocumented area of the EES, close to the open ocean. Given the similarity in the nature of the CIE to other global sections, this record is consistent with the suggestion that the CIE reflects a global perturbations to the carbon cycle associated with the increased CO_2 release from the emplacement of the Karoo–Ferrar LIP and possibly thermogenic methane (CH_4) from sill intrusions into organic rich rocks or the dissociation of methane clathrates (Duncan et al., 1997; Hesselbo et al., 2000; McElwain et al., 2005; Kemp et al., 2005; Svensen et al., 2007; Svensen et al., 2012; Percival et al., 2015).

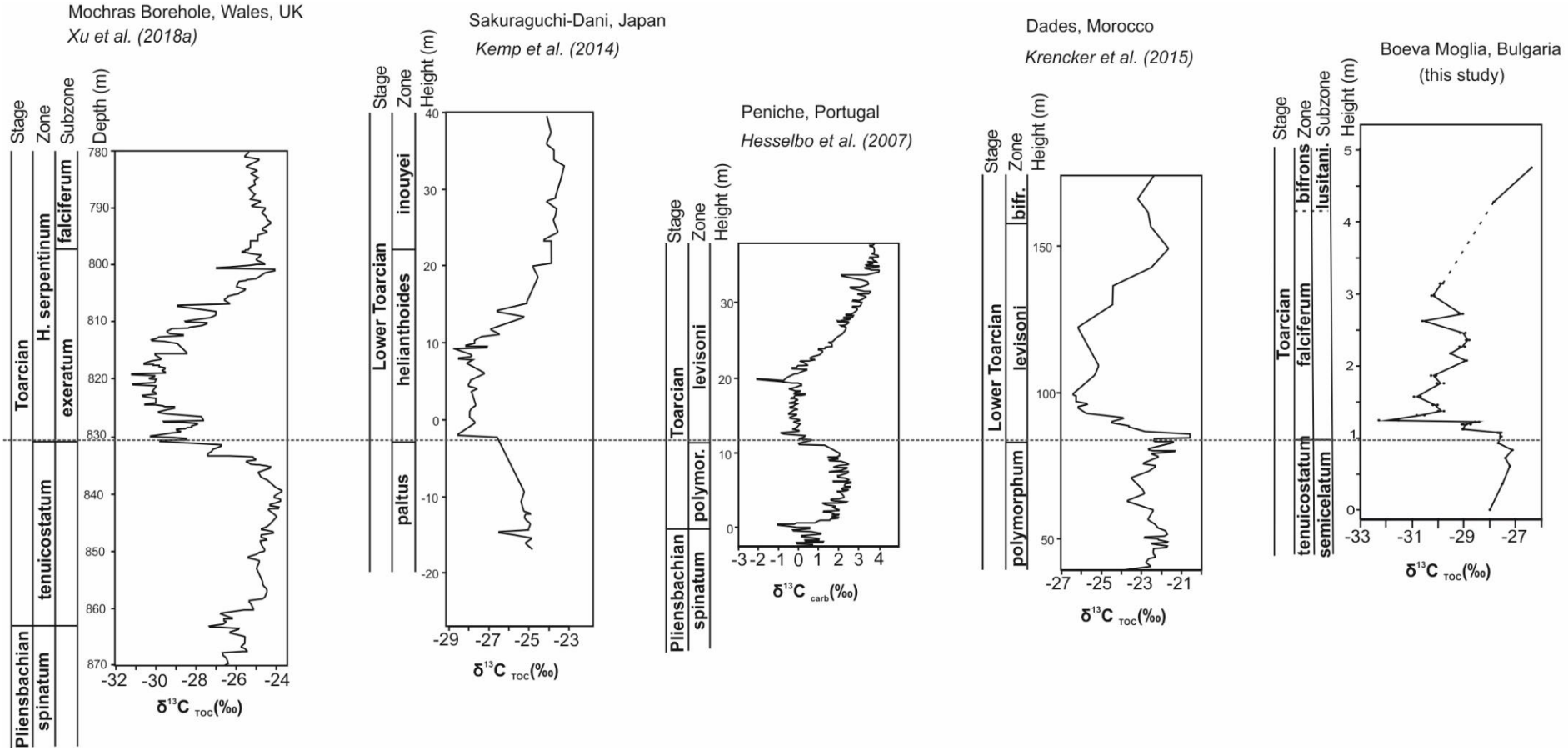

Figure 5.13 Correlation of the $\delta^{13}C_{org}$ data from the Boeva Mogila section, Bulgaria (this study) to Mochras borehole, UK (Xu et al., 2018a), Sakuraguchi-Dani, Japan (Kemp et al., 2014), Peniche, Portugal, Lusitanian Basin (Hesselbo et al., 2007), Dades, Morocco (Krencher et al., 2015). Correlation between the carbon isotope data and the biostratigraphy are based upon those presented by the authors cited above for each dataset.

5.5.2 Chemostratigraphic constraint provided by carbon isotope record

5.5.2.1 Boeva Mogila section

Ammonite biostratigraphy indicates the Boeva Mogila section is condensed, but with no biostratigraphic or sedimentological evidence of a hiatus through the *tenuicostatum* Zone (*semicelatum* Subzone) and *falciferum* Zone. The onset of the negative CIE is used as chemostratigraphic marker to strengthen the age model for this section, with the onset of the negative CIE around the *tenuicostatum/falciferum* Zone boundary. The negative CIE, is one of the key characteristics of the 'T-OAE interval', as it has been documented from multiple oceanic basins spanning the globe, corresponding with the base of the *falciferum* Ammonite Zone (equivalent to the *exaratum* Subzone in northern Boreal EES; (Jenkyns and Clayton, 1997; Hesselbo et al., 2000; Bailey et al., 2003) and to the *C. superbus* nannofossil Zone (Mattioli et al., 2004; Mailliot et al., 2006). The record of the early Toarcian negative CIE in the Moesian Basin further confirms the utility of the overall T-OAE negative CIE as a global chemostratigraphic marker.

5.5.2.2 Milanovo section

There is no sedimentological evidence for a fault or break in sedimentation through the Milanovo section. Ammonite biostratigraphy assigns the base of the section to the late Pliensbachian (*spinatum* Zone), but due to the scarcity of ammonites, cannot provide zonal classification for the overlying sediment, indicating only an early Toarcian age. The first early Toarcian ammonite zone is recorded by ammonites with assemblages typical of the late *falciferum* Zone. Carbon isotope stratigraphy indicates a likely hiatus around the Pl-To boundary as a clear lack of the negative CIE in organic carbon, with a subsequent $\delta^{13}C_{bel}$ positive isotope excursion up to ~4 ‰. The positive CIE is characteristic of carbon isotope values in the post 'T-OAE interval' (Hesselbo et al., 2007), supporting a possible hiatus. Most important, in supporting a possible hiatus, is the occurrence of the Toarcian belemnite *Arceolites* sp., immediately following the last Pliensbachian ammonites (Figure 5.12). *Arceolites* sp., are typically a genus occurring after the negative CIE, as part of the positive CIE at the end of the 'T-OAE interval' (Ullmann et al., 2015).

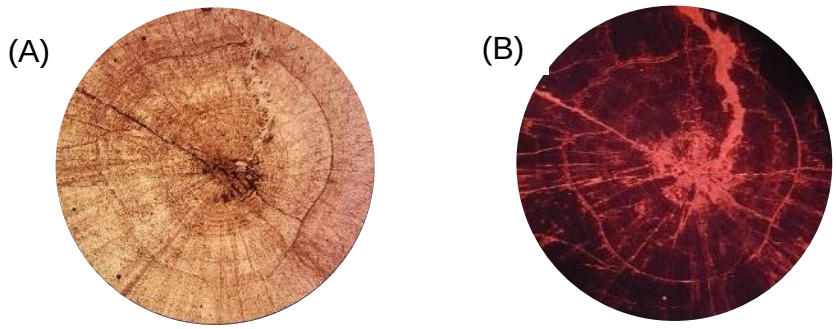

Figure 5.14 Belemnite genus *Arceolites* sp from Milanovo section (1.6 m). Identified by characteristic '3-groove' profile in (A) transmitted light and (B) under cathodoluminescence, recorded in the early Toarcian of the Milanovo section. Scale x5. *Arceolites* is typically a post T-OAE belemnite (Ullmann et al., 2014).

5.5.3 Links between carbon isotope record, Hg and Hg/TOC

In modern marine settings, there is a strong linear relationship between mercury and organic matter (e.g. Fitzgerald et al., 2007). This relationship has been used in ancient sediments as a proxy for volcanism (Sial et al., 2013; Percival et al., 2015; Font et al., 2016; Jones et al., 2017; Scaife et al., 2017). The relationship between volcanism, Hg and TOC is as follows; during volcanism gaseous Hg^0 is emitted as a volcanic gas that can reside in the atmosphere for 0.5-2 years (Pyle and Mather, 2003; Blum et al., 2014). In the atmosphere, Hg^0 is oxidised, most effectively by bromine, and forms reactive Hg^{2+}. Oxidation is most commonly linked with organobromines in particular, a product of phytoplankton photosynthesis (Horowitz et al., 2017). In the marine realm Hg^{2+} forms complexes with clay minerals (Kongchum et al., 2011), or is adsorbed onto organic matter (Benoit et al., 2001). This process leads to a strong relationship between organic matter and Hg in sediments as the complexing of Hg by organics and sulphides in the marine realm establishes marine sediments as an efficient sink of atmospheric Hg (Benoit et al., 1999; Emili et al., 2011; Horowitz et al., 2017). Therefore, marine siliciclastic and carbonate rocks can record increased Hg during times of heightened environmental loading (Percival et al., 2015; Grasby et al., 2016). The strong affinity of Hg with organic matter makes it necessary to report Hg/TOC values when identifying Hg anomalies, a standard practice when documenting anthropogenic enrichments in modern sediments (e.g. Fitzgerald et al., 2007). However, in ancient sediments deposited during times such as the early Toarcian, the relationship between Hg and TOC appears to be more complicated as the Hg/TOC record is affected by the high TOC contents of organic-rich rocks (Percival et al., 2015).

In the Moesian Basin, the close temporal relationship between Hg and TOC is shown by a small, but contemporaneous, increase in carbon, TOC and Hg records in the early Toarcian (Figure 5.11, Figure 5.12). Overall Hg and Hg/TOC values are relatively low and record a less significant shift during the early Toarcian compared to sections with organic-rich sediments, such as the Yorkshire Coast (UK) and Sancerre (France) (Percival et al., 2015). When compared to coeval sections such as Peniche (Portugal) and Arroyo Lappa (Argentina) (Percival et al., 2015). Where black shales are absent or thinly developed and have similar lithological characteristics to the Moesian Basin, Hg and Hg/TOC are more directly comparable (Figure 5.15).

The low absolute Hg and Hg/TOC ratios recorded from the Moesian Basin are likely a result of the higher $CaCO_3$ content of sediments deposited during this time, as pure carbonates will unlikely fix Hg, due to low amounts of organic-matter burial (the mechanism responsible for draw down of Hg into sediments), as is seen in carbonate rich early Toarcian successions such as Velebit in Croatia (Percival et al., 2015).

Overall, the Hg concentrations in the Milanovo section are slightly higher than the background concentrations throughout the Boeva Mogila section, although TOC values are relatively higher in the Boeva Mogila section, when compared with the Milanovo section. This shows total organic content of sediments cannot be the only controlling factor on Hg sequestration. The elevated values in Hg and Hg/TOC documented at the end of the TOAE interval and through the Toarcian may be controlled by other environmental or diagenetic factors acting on a local scale in the Moesian Basin at this time. Although both sections record relatively deeper deposition in the Moesian Basin, the distance between deposition of each section is unknown, due to later Alpine thrust tectonics, and thus each section may have been subject to different diagenetic conditions, which may also have affected the Hg values recorded from each section.

For the Boeva Mogila section, the shift in Hg/TOC values coeval with the negative carbon-isotope excursion provides an additional record for the globally recorded positive excursions observed in early Toarcian sediments and provide further evidence for enhanced atmospheric Hg concentrations, possibly derived from volcanic Hg from the Karoo-Ferrar LIP (Percival et al., 2015).

A recent study by Them et al. (2018) suggests that increased Hg/TOC ratios are most notable from shallow marine environments, with no or little increase in Hg/TOC ratios from deeper water sections during the early Toarcian. Although it is difficult to know the exact water depth for the Boeva Mogila section in the Moesian Basin, it is thought to reflect a more distal setting relative to many

others recorded in the EES in which wood fragments are very common. In the Boeva Mogila section, no wood fragments are found and sediments do not record evidence of storms. Although the relationship between volcanism and increased Hg/TOC ratios is still not fully understood, the Bulgarian record does still record a slight increase in Hg/TOC values in a relatively deeper setting than those from the Yorkshire Coast or Mochras.

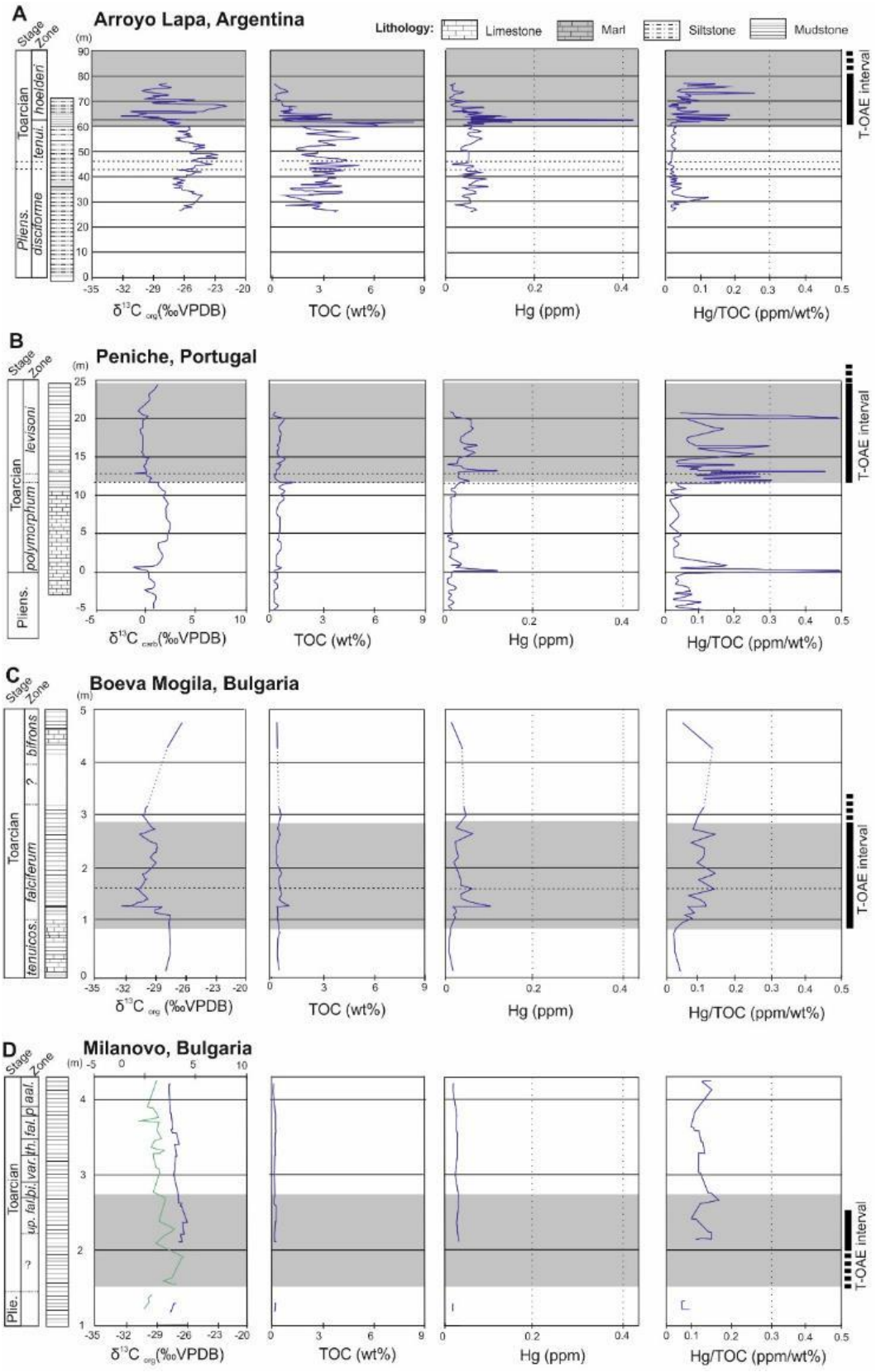

Figure 5.15 $\delta^{13}C_{org}$, Total Organic Carbon (TOC), Hg and Hg/TOC from published data for (A) Arroyo Lapa, Argentina and (B) Peniche, Portugal (published data from Percival et al., 2015), and new data (this study) from (C) Boeva Mogila and (D) Milanovo sections in Bulgaria.

5.5.4 Evaluating the paleo-redox state of the Moesian Basin

5.5.4.1 Carbon cycle perturbations

The T-OAE was defined by Jenkyns (1988) as ‘a period of time characterised by abnormally high depositional and preservational rates of organic carbon in favourable marine environments, due to widespread anoxia, that gave rise to the synchronous deposition of black shale facies in many parts of the globe’. In the early Toarcian the positive CIE is interpreted as a reflection of the global burial of carbon through the deposition of organic rich mudrocks under anoxic conditions (Jenkyns et al., 2002; Jenkyns, 2010).

However, a positive CIE can also be affected by other environmental factors, with a complex relationship between redox conditions and organic matter preservation that means a positive CIE does not necessarily require global deoxygenation or global organic carbon burial (Middelburg et al., 1993; Canfield, 1994; Hartnett et al., 1998; Kump and Arthur, 1999; Tyson, 2005; Burdige, 2007). In addition, comparison of CIEs in the Lusitanian Basin (Portugal) and Paris Basin (France) showed the negative CIE can be decoupled from black shale deposition (Hermoso et al., 2009). This shows organic carbon concentration and presence of a negative CIE, although often used to describe the T-OAE, cannot be used to independently characterise anoxia (Hermoso et al., 2009; Caruthers et al., 2011). In the Moesian Basin the presence of CIEs and a small concomitant increase in TOC (to <1 wt%) does not itself rule out the expansion of anoxia elsewhere, but it cannot support its formation in the Moesian Basin. It is important to look at other proxies that assess redox conditions of the basin, such as sedimentological evidence and framboid analysis.

5.5.4.2 Pyrite framboids as a proxy for redox conditions

Pyrite framboid analysis suggests fluctuating oxic to dysoxic conditions prevailed in the Toarcian, with the most oxygen deficient conditions developing in the relatively deeper hemipelagic part of the Moesian Basin (represented by Milanovo, Boeva Mogila and Dobravitsa-1 sections) and no evidence for oxygen restriction (i.e. no framboids) in the shallower parts of the basin (represented by Gorno Ozirovo and Kiselchov Dol sections). Where framboids are present, there is no significant change across the ‘T-OAE interval’ (Figure 5.4).

It is important to note that each sample used for framboid analysis typically recorded ~1 cm of sediment. In the condensed sediments from Bulgaria 1 cm of sediment could represent tens of thousands of years, and therefore results over

this time will be time-averaged. Framboid populations that were deposited under quickly fluctuating euxinic and dysoxic conditions cannot be differentiated at this scale and more likely show dysoxic framboid population characteristics throughout. Such time-averaged intervals are inevitable in ancient studies (e.g. Wignall and Newton, 1998; Bond et al., 2004; Wignall et al., 2005; Bond and Wignall, 2010). In the Moesian Basin, very limited framboid populations were indicative of anoxic/euxinic redox conditions of the Moesian Basin, with no samples containing all framboids <5-6 μm in mean diameter, arguing against their formation in a euxinic/anoxic water column. Samples that may indicate the most oxygen-deficient conditions (that plot in the anoxic/euxinic field on the Wilkin et al., 1996 plot) are limited in number and do not consistently coincide with the T-OAE interval. The occasional sample that plots in the anoxic/euxinic represent localised, occasional, and relatively short-lived development of euxinia, unrelated to more widespread change elsewhere. Although there is no direct evidence of more pervasive and continued levels of anoxia in the Moesian Basin, short-term anoxia cannot be cannot be completely excluded, due to the condensed nature of the Toarcian records from the Moesian Basin.

The lack of framboids from Gorno Ozirovo and Kiselchov Dol suggests that fully oxygenated conditions on the shallow marine seafloor of the Moesian Basin prevailed throughout the Toarcian (Figure 5.4). Arguably, these conditions are expected for shallow marine conditions, although it has been known for OMZs to expand to shallow marine oolitic facies during widespread anoxia during the time of the Permian-Triassic mass extinction (Bond and Wignall, 2010). In more carbonate-rich sections, where iron content is low, to restrict the growth of framboids, even if low oxygen conditions are present (e.g. Bond and Wignall, 2010).

It is important to also assess the limitations of pyrite framboids as a proxy for redox conditions. Unlike other geochemical proxies, pyrite framboid analysis is not influenced by diagenetic alterations and most importantly, is relatively robust to weathering. This is particularly important for sections addressed in Bulgaria as most sections outcrop as paths or hill-slopes, which are particularly prone to weathering.

A drawback of the pyrite framboid proxy is the problem with distinguishing between a euxinic (O_2 free, H_2S excess) or ferruginous (O_2 free, Fe^{2+} excess) water column. The factor controlling pyrite formation and size growth is its ambient buoyancy in the water column during formation, which is crossed once it reaches a diameter of ~5-6 μm (Wilkin et al., 1996) therefore euxinic size distributions could potentially accumulate under a ferruginous water column

(e.g. Hammarlund et al., 2012). Despite this, the proxy still differentiates between euxinic size distributions and dysoxic populations.

As predominantly oxic or fluctuating conditions between oxic and dysoxic prevail through the Toarcian of the Moesian Basin, other proxy methods that might be employed in addition to framboid analysis, are not particularly useful. For example, iron speciation, which uses geochemical techniques to indicate if firstly a water column is oxic or anoxic and secondly to discriminate if anoxic conditions are ferruginous or euxinic (Poulton and Canfield, 2005), would add limited new data to the Moesian Basins redox conditions, as most samples would likely plot in the oxic zone, which is also established by framboid petrography. Additionally, techniques such as iron speciation would be unsuitable for sediments from the Moesian Basin due to their oxidised nature (Figure 5.3) and significant amounts of diagenetic euhedral pyrite.

5.5.4.3 Sedimentological evidence for oxic, dysoxic or anoxic conditions

The main facies indicators of anoxic conditions include the absence of bioturbation and presence of fine-laminations (Savrda and Bottjer, 1987). In anoxic settings laminated sediment will form as a consequence of no bioturbation in often muddy or silty sediments on the seafloor. Field observations from the Toarcian sections in Bulgaria show no evidence of laminated sediments deposited in the Moesian Basin, with some level of bioturbation documented throughout the early Toarcian interval (Figure 5.11, Figure 5.12).

As sections are very condensed, it could be argued that the sediments may have been deposited as laminated sediments and later bioturbated from overlying sediments. If bioturbation was intense enough to allow sufficient mixing of the sediment, the result would be the clear steps recorded on the negative limb of the organic carbon isotope curve would have been ‘smoothed out’. if there was later bioturbation, due to mixing of the sediments. Although there is no evidence for this heavy bioturbation, further work would be required to quantify the relationship between sample resolution versus burrowing depth to further use burrowing as an indication of water depth and further determination between oxic/anoxic sediments. .

5.5.4.4 Previous recognition of the ‘T-OAE’ in the Moesian Basin

The lack of anoxic black shales in the early Toarcian of Bulgaria disagrees with previously published studies that claim to record finely laminated shales from in

the *falciferum* Zone of the Bukorovtsi Member in the Teteven area (Metodiev et al., 2014). This facies is reported to be 'a clear a manifestation of the T-OAE' in Bulgaria (Metodiev et al., 2014). However, the same facies are observed in this study in the nearly located Boeva Mogila section and although sediments are thinly-bedded, they are not laminated and do show bioturbation. No evidence is provided in previous studies and it is suggested here that they have been mis-identified as laminated shales on the basis of this being a typically recognised lithology to develop in early Toarcian sections in parts of Europe, characterising the T-OAE at this time (Jenkyns, 1988 and references therein).

5.5.4.5 The 'Belemnite gap'

The 'belemnite gap' present in the Boeva Mogila section does not allow for $\delta^{13}C_{bel}$ to be recorded through the 'T-OAE interval'. The belemnite gap is recorded as a notable lack of belemnites or severely diminished presence in the early Toarcian (often between the *tenuicostatum* and early-late *falciferum* Zone). The gap is common across many regions of the EES in both the northern EES, recorded from the Cleveland Basin (Cohen et al., 2004a; Kemp et al., 2005; Littler et al., 2010) and Cardigan Bay (Xu et al., 2018a) and the southern EES, recorded from the Lusitanian Basin (Hesselbo et al., 2007) and Balearic Basin (Rosales et al., 2018). This temporary disappearance of belemnites has been interpreted as a response to regionally extensive anoxic to euxinic bottom waters (Ullmann, et al., 2014). However, as there is no clear evidence of extensive anoxia or euxinia in the Moesian Basin, it suggests this is not the only controlling factor on the low abundance of belemnites across the EES during this time. Whilst deoxygenation is considered the most important factor in the decrease in belemnite abundance in the northern EES (Ullmann et al., 2014; Danise et al., 2015), other factors such as preservation and/or other physico-chemical conditions (e.g. temperature and pH) may have played a more important role in the Moesian Basin. Low oxygen conditions are still however recorded in the deeper parts of the Moesian Basin, albeit fluctuating and not developing into long-term anoxia. The lack of belemnites in the 'T-OAE' interval from the Boeva Mogila section may be a response to these fluctuating conditions that still produce bottom-water conditions that are unfavourable for belemnites. If this were the case, it might be expected that belemnites were also absent from relatively deeper water sections in the basin that record similar redox conditions in the middle and late Toarcian, but this is not seen, favouring the option that other controlling factors may be at play in the Moesian Basin to create the belemnite gap.

5.5.4.6 A lack of oceanic anoxia

A recent study on the development of anoxia across the EES using ocean-atmosphere models, argues the southern Tethyan realm did not become anoxic during the early Toarcian due to the presence of a strong clockwise gyre over the EES, which brought oxygenated equatorial waters from the Tethys Ocean to the southern shelf (Dera and Donnadieu, 2012; Baroni et al., 2018). The Moesian Basin sat at a latitude between 33°N and 38°N (Dera et al., 2009; Metodiev et al., 2014), similar to that of basins in the more temperate latitudes of the northern EES. At this latitude, riverine input into the Moesian Basin was from the north as part of the Laurasian landmass, where wet conditions prevailed and provided a high nutrient supply (Valdes et al., 1995; Cohen et al., 2004a; Hesselbo et al., 2007; Dera and Donnadieu, 2012). The high nutrient supply likely contributed to elevated productivity which, alongside basin bathymetry and a slightly restricted nature, promoted the development of anoxia in the northern EES basins (Cohen et al., 2004a; Montero-Serrano et al., 2015; Fantasia et al., 2018). This is somewhat similar to modern euxinic settings, whereby sluggish circulation and nutrient trapping promotes euxinia (Lyons and Severmann, 2006; Meyer and Kump, 2008; Scholz et al., 2013). In the case of the Moesian Basin, it is possible that a less restricted nature of the basin with its location near the open ocean inhibited the formation of prevalent anoxic conditions within the basin through the early Toarcian.

5.6 Conclusions

These sections are constrained within a biostratigraphic and chemostratigraphic framework for the late Pliensbachian-late Toarcian interval. At this time, the characteristic negative CIE (~3.5 ‰) is recorded. The negative CIE is of a similar magnitude to coeval global records, in which methane hydrate disassociation or carbon released thermogenically from organic matter sources are suggested causes, ultimately triggered by Karoo-Ferrar LIP. In the Moesian Basin, the negative CIE is co-incident with a positive shift in Hg values and Hg/TOC values with maximum enrichments near the base of the *falciferum* Zone. These enrichments are interpreted as a possible indication of increased LIP volcanism.

Chapter 6 Bivalve record through the Lower Jurassic of the Moesian Basin

6.1 Introduction

This chapter provides an overview of bivalve occurrences through the Lower Jurassic of the Moesian Basin. Specifically, it aims to determine whether there was an extinction amongst bivalves during the late Pliensbachian-early Toarcian interval. This study builds on current bivalve records from the Sinemurian-Pliensbachian in Bulgaria and provides the first detailed bivalve record from the Toarcian. xxx

6.2 Methods and study sites

This chapter presents data from thirteen sections in northwest and central Bulgaria (Figure 6.1), spanning from the upper Sinemurian (Lower Jurassic) to the Aalenian (Middle Jurassic), from which bivalve specimens were collected and identified to the lowest possible taxonomic level.

Figure 6.1 A) Detailed outcrop map of the west and central area in Bulgaria. Study sections are shown in red, sections not used in this chapter shown in black and Lower Jurassic outcrops are shown in grey. B) Outline map of Bulgaria, with the study area highlighted by black box.

6.2.1 Integrated Bulgarian bivalve occurrences

Previous studies have shown that Lower Jurassic bivalve faunas from Bulgaria are rich and diverse (Sapunov, 1959; Sapunov, 1961; Sapunov, 1971; Sapunov, 1983; Tchoumatchenco and Sapunov, 1994; Sapunov et al., 1996).

However, due to limited specimens remaining in the collections from these studies, no taxonomic descriptions, and lack of a photographic record, the validity of all the species within Sapunov's literature are difficult to authenticate. For this reason, Sapunov's works are not integrated into this study.

The bivalve collections from Shopov (1968) have been photographed and some of the collection is accessible in the Palaeontology Museum at Sofia University (Bulgaria). This allows the bivalve taxa from the doctoral thesis of Shopov (1968) to be compared to those collected during this study. Numerous studies based on Shopov (1968) have now been published (Shopov., 1966; Shopov, 1968a; Shopov, 1969; Shopov, 1970; Shopov, 1974a,b). Where there is taxonomic agreement between the bivalve specimens from Shopov (1968) and those in this study, the bivalve taxonomic ranges have been combined. Since 1968 there has been a considerable amount of work on the taxonomy of Early Jurassic bivalves, which has resulted in the synonymy of many bivalve taxa (see Chapter 2 for literature used in this study for synonymising bivalve taxa). For this reason individual taxa in Shopov (1968) have been reviewed and synonymised before species ranges could be integrated into this work. A list of bivalve species, reference to imaged plates in Shopov's work, and synonymised taxa, are given in Appendix D.1. The occurrence data from Shopov (1968) are only used to extend the ranges of taxa that have already been identified in this study.

Some bivalve species recorded by Shopov (1968) are not integrated into this study. These are species that are not found during this study, and species in which there is insufficient material or photographic evidence to confirm a species assignment. Including these taxa would require taxonomic revision that is beyond the scope of this thesis. Bivalve species noted in Shopov (1968) that are not included in this thesis are also shown in Appendix D.1 for completeness.

Following taxonomic identification, individual range charts were constructed for each section, and then combined with additional ranges from Shopov (1968). All bivalve ranges were then amalgamated into a single range chart through the upper Sinemurian-Aalenian.

6.3 Results

The data for this study comprises 1500 bivalve specimens, belonging to 29 species in 27 genera. No new species have been recorded, with all species referred to previously described taxa. All individual bivalve occurrences are given in Appendix D.2 and representative photographs of all named genera and

species are provided in Figure 6.2, Figure 6.3, Figure 6.4, Figure 6.5, Figure 6.6 and Figure 6.7.

In terms of taxonomic composition, the fauna is dominated by individuals belonging to the members of the families Pectinidae, Entolidae, Pinnidae, Gryphaeidae, Propeamussidae, Plicatulidae, Astartidae, Limidae, Oxytomidae, and Pleuromyidae. Rarer examples of taxa belonging to the Grammatodontinae, Mytilidae, Mactromyidae, Anomiidae, and ?Modiomorhphidae and ?Archomyidae are also present.

A composite range chart through the late Sinemurian-Aalenian comprising all bivalve occurrences presents they key findings of this study. The same composite range chart is presented in two ways: first by highlighting bivalve ranges from individual sections with indication of biostratigraphic control, (Figure 6.18) and secondly, with all sections combined, recording possible extinction intervals (Figure 6.19).

6.3.1 Preservation of Lower Jurassic bivalves in Bulgaria

Different lithologies within the large spatial and temporal framework of the Lower Jurassic sediments from Bulgaria produce different preservation potentials for the fossils within the studied record. For bivalves, the taxonomically relevant features, such as dentition, are more commonly observed in bivalves from the coarser grained bioclastic limestones and ironstone lithologies. Although in the more siliciclastic-rich bioclastic ooidal or crinoidal limestones, often represented by the undifferentiated Ozirovo Formation, many bivalves are disarticulated, sometimes broken and often the full shell and shape of the bivalve (including auricles) is less frequently preserved. This is particularly common for thin-shelled epifaunal pectinids, including the genera *Entolium*, *Chlamys*, *Propeamussium* and *Pseudopecten*. In finer grained lithologies, often represented by the Bukorovtsi Member of the Ozirovo Formation, external features on bivalve shells, such as ornamentation on ribbing, is commonly well-preserved, but other relevant features such as dentition and musculature is very difficult to observe.

Calcitic shell replacement is common in the Lower Jurassic bivalve fauna. In sections where ironstones are recorded as part of the Ozirovo Formation, bivalves can be haematised. This preservation type is recorded within the lower Pliensbachian *ibex* Zone of the Dragovishtitsa section and the lower Toarcian *tenuicostatum* Zone of the Kiselchov Dol section. One horizon in the upper Pliensbachian *spinatum* Zone of the Ozirovo Formation (Bukorovtsi Member) in

the Dobravitsa-1 section, has de-calcification of sediment, only mouldic preservation of the bivalve shells. Many specimens in Bulgaria, particularly those from sandy bioclastic limestones, show relatively poor preservation. The poor preservation of some specimens led to them to only being identified at genus level (represented by genus name followed by sp. in the data). These taxa may represent more than one species, which has implications for the recognition of species-level extinctions. Poor preservation of such specimens is particularly common in those preserved in sandy bioclastic limestones.

6.3.2 Characteristic bivalve assemblages of the Lower Jurassic Ozirovo Formation

Bivalve occurrences from the Lower Jurassic sections in this study are all recorded from the Ozirovo Formation. The underlying Kostina Formation, is poorly fossiliferous and records no identifiable bivalve taxa, with only small crushed shell fragments observed. Bivalve assemblages from the Ozirovo Formation are described below in a lithological order, which roughly follows chronostratigraphic stages from the Sinemurian to the Aalenian.

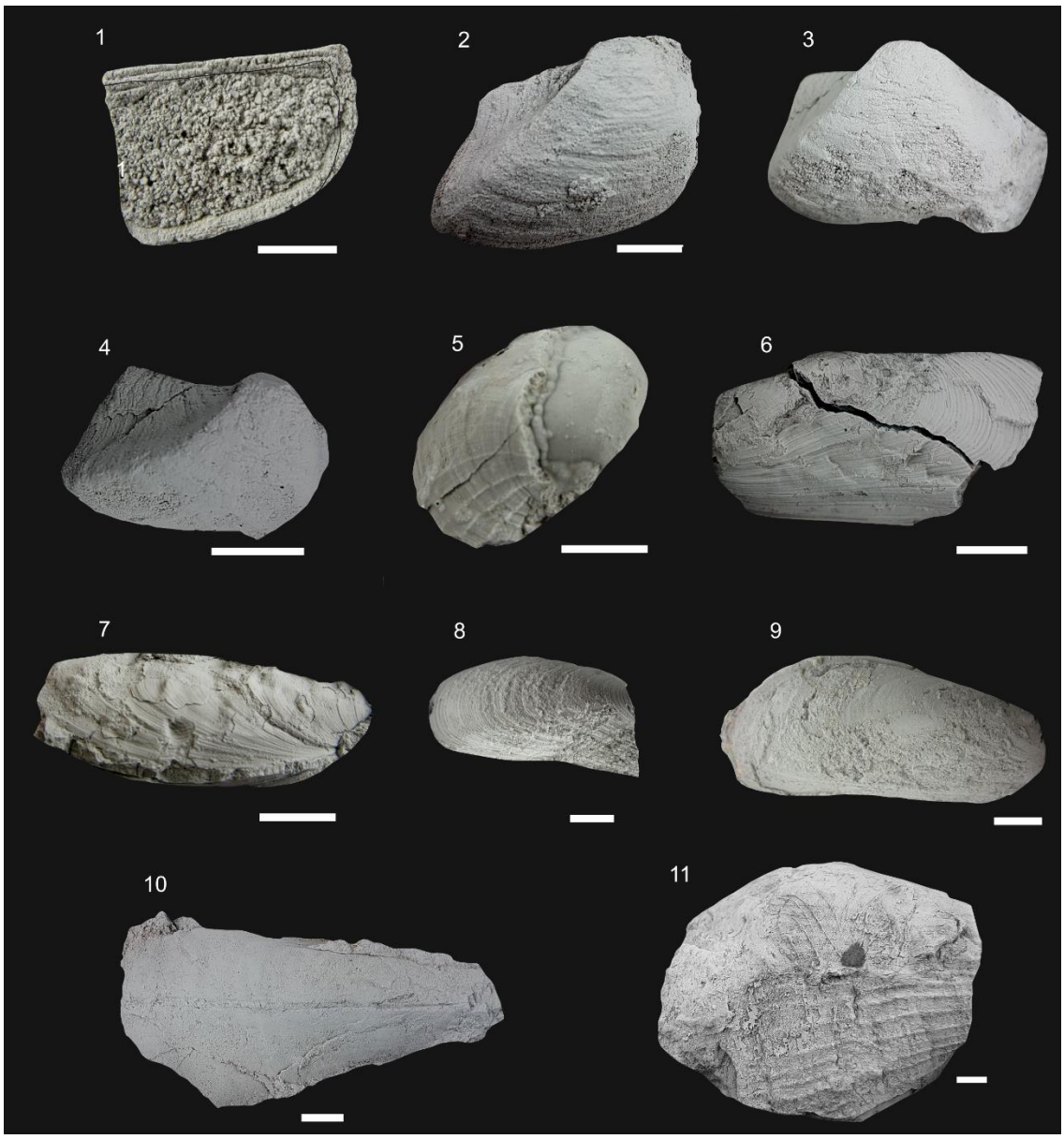

Figure 6.2. Plate 1. 1. *Grammatodon insons* (Melville, 1956), Gorno Ozirovo section, bed 21, *falciferum* Zone, early Toarcian. 2. *Grammatodon insons* (Melville, 1956), Gorno Ozirovo section, Bed 21, *falciferum* Zone, early Toarcian. 3. *Grammatodon insons* (Melville, 1956), Gorno Ozirovo section, bed 21, *bifrons* Zone, late Toarcian. 4. *Grammatodon insons* (Melville, 1956), Gorno Ozirovo section, bed 21, *bifrons* Zone, late Toarcian. 5. *Grammatodon* sp. (Melville, 1956), Kiselchov Dol section, bed 13e, *fallaciosum* Zone, late Toarcian. 6. *Modiolus* sp., Teteven section, bed 10, *jamesoni* Zone, early Pliensbachian. 7. *Modiolus* sp., Teteven section, bed 6. Sinemurian. 8. *Modiolus ventricosa* (Roemer, 1836), Ravna section, bed 7, late Pliensbachian. 9. Modiolus sp., Dragovishtitsa section, bed 14a, *aalensis* Zone, late Toarcian. 10. *Pinna folium* (Young and Bird, 1822), Vradlovtsi-2 section, bed 3, *jamesoni* Zone, late Pliensbachian. 11. *Pinna radiata* (Münster, 1837), Ravna section, bed 8i, late Pliensbachian. All specimens coated in ammonium chloride. White scale bar =1 cm.

Figure 6.3. Plate 2. 1.*Gryphaea gigantea* (Sowerby, 1823), Teteven section, bed 8, late Sinemurian/ early Pliensbachian. 2. *Gryphaea muccollochii* (Sowerby, 1826), Ravna section, bed 6(ii), Sinemurian. 3. *Gryphaea gigantea* (Sowerby, 1823), Ravna section, bed 10, late Pliensbachian. 4. *Gryphaea* sp., Teteven section, bed 6, late Sinemurian. 5. *Gryphaea* sp., Vradlovtsi-2 section, bed 3, *jamesoni* Zone, late Pliensbachian. 6. *Gryphaea* sp., Ravna section, bed 9, late Pliensbachian. 7. *Liostrea* sp., Kiselchov Dol section, bed 13e, *fallaciosum* Zone, Late Toarcian. 8. *Liostrea* sp., Teteven section, bed 9, *jamesoni* Zone, late Pliensbachian. 9. *Bositra* sp., Stara Reka River section, Central Balkan Mountains (42º50'38.15''N; 24º5.0'20.50''), section not included in this thesis, Aalenian, Middle Jurassic. All specimens coated in ammonium chloride. White scale bar =1 cm.

Figure 6.4. Plate 3. 1. *Entolium (Entolium) lunare* (Rofmer, 1839), Ravna section, bed 8, upper Sinemurian. 2. *Entolium (Entolium) lunare* (Rofmer, 1839), Gorno Ozirovo section, bed 21, *falciferum* Zone, early Toarcian. 3. *Camptonectes (Camptonectes) auritus* (Scholtheim, 1813), Kiselchov Dol section, bed 13b, *falciferum* Zone, late Toarcian. 4. *Chlamys textoria* (Scholtheim, 1820), Dobravitsa-1, bed 1, *spinatum* Zone, late Pliensbachian. 5. *Chlamys* sp., Dragovishtitsa section, bed 14a, *pseudoradiosa* Zone, late Toarcian. 6. *Propeamussium (Propeamussium) pumilum* (Lamarck, 1819), Kiselchov Dol section, bed 13e, *fallaciosum* Zone, late Toarcian. 7. *Placunopsis radiata* (Phillips, 1929), Gorno Ozirovo section, bed 21, late *falciferum* Zone, early Toarcian. 8. *Pseudopecten (Pseudopecten) equivalvis* (J. Sowerby, 1816), Balsha section, bed 22a, *spinatum* Zone, late Pliensbachian. 9. *Pseudopecten (Pseudopecten) equivalvis* (J. Sowerby, 1816), Ravna section, bed 8(vi), upper Sinemurian. 10. *Weyla* sp., Dragovishtitsa section, bed 14a, *pseudoradiosa* Zone, late Toarcian. 11. *Weyla* sp., Dragovishtitsa section, bed 14a. *pseudoradiosa* Zone, late Toarcian. 12. *Weyla* sp., Dragovishtitsa section, bed 14a, *pseudoradiosa* Zone, late Toarcian. All specimens coated in ammonium chloride. White scale bar =1 cm.

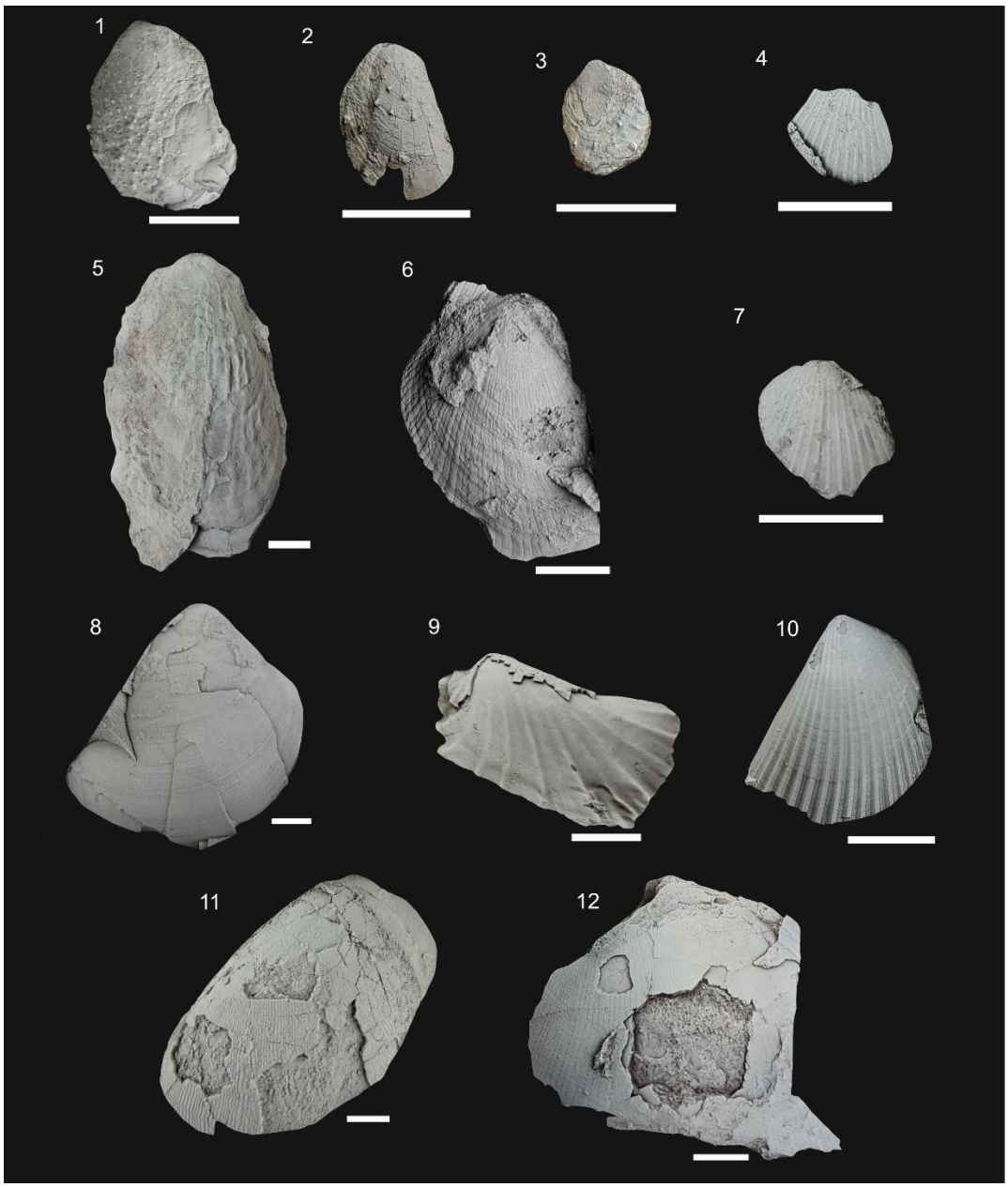

Figure 6.5. Plate 4. 1. *Harpax spinosa* (J.Sowerby, 1819), Teteven section, bed 9, late Sinemurian. 2. *Harpax spinosa* (J.Sowerby, 1819), Ravna section, bed 7, late Sinemurian. 3. *Harpax spinosa* (J.Sowerby, 1819), Teteven section, bed 9, late Sinemurian 4. *Pseudolimea pectinoides* (J.Sowerby, 1815), Ravna section, bed 7, late Sinemurian. 5. *Antiqulima succincta* (Scholtheim, 1813), Vradlovtsi-2 section, bed 8, Pliensbachian. 6. *Antiquilima hermanni* (Voltz, 1856), Teteven section, bed 9, late Sinemurian. 7. *Pseudolimea acuiticostata* (Münster, 1836), Boeva Mogila section, *tenuicostatum* Zone, early Toarcian. 8. *Plagiostoma punctatum* (J.Sowerby, 1815), Ravna section, bed 12, *spinatum* Zone, late Pliensbachian. 9. *Oxytoma inequivalvis* (J.Sowerby, 1819), Ravna section, bed 7 (ii), late Sinemurian. 10. *Pseudolimea acuiticostata* (Münster, 1836), Boeva Mogila section, *tenuicostatum* Zone, early Toarcian. 11. *Plagiostoma* sp., Ravna section, bed 9, Pliensbachian. 12. *Plagiostoma* sp., Kiselchov Dol section, bed 13e, *fallaciosum* Zone, late Toarcian. All specimens coated in ammonium chloride. White scale bar =1 cm.

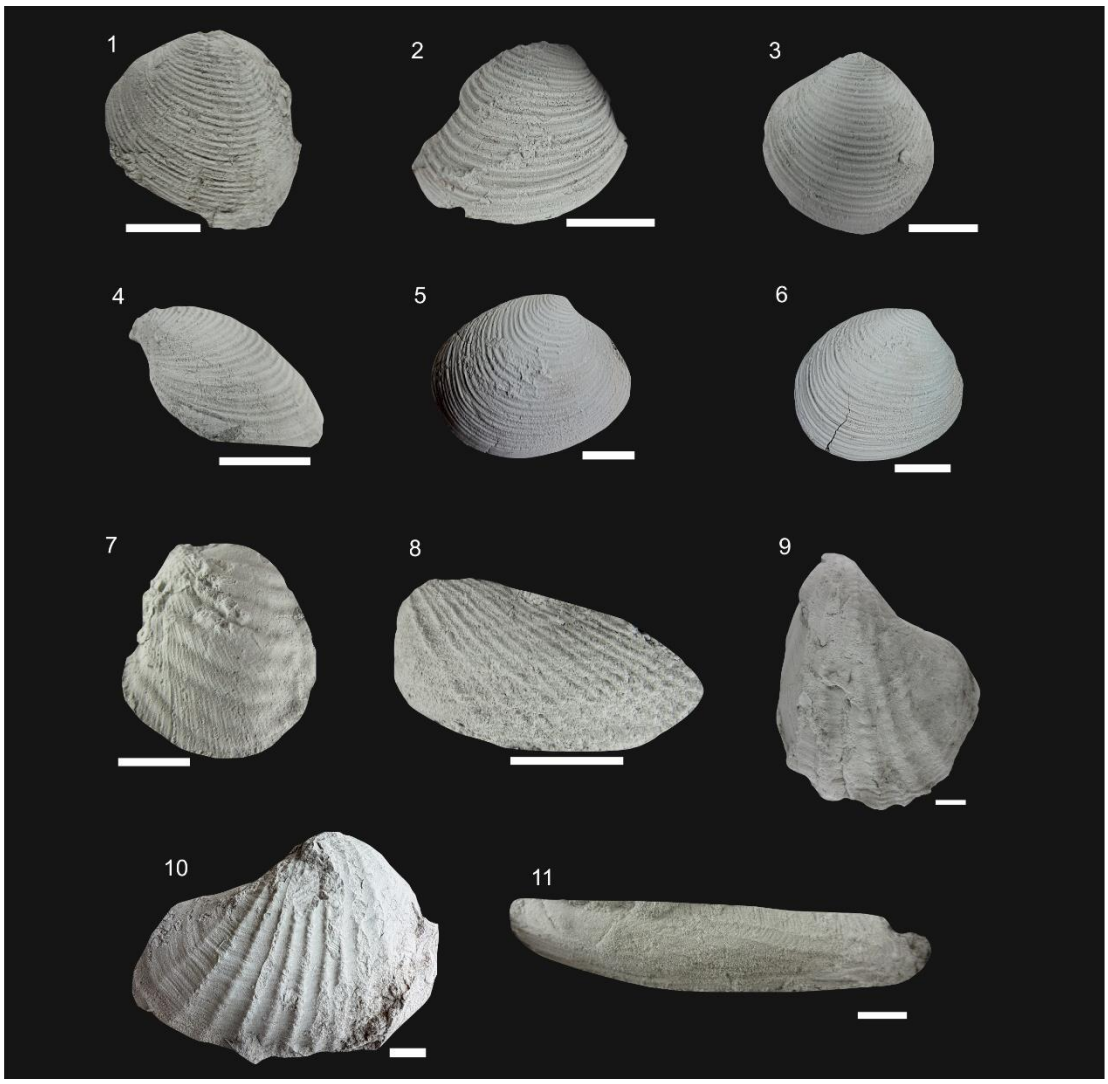

Figure 6.6. Plate 5. 1. Coelastarte, Kiselchov Dol section, bed 13c. *bifrons* Zone. late Toarcian. 2. Coeslasterte, Kiselchov Dol section, bed 13e, *thouarsense* Zone, late Toarcian. 3. Coelastarte, Gorno Ozirovo section, bed 21, *bifrons* Zone, late Toarcian. 4. Coelastarte, Gorno Ozirovo , section, bed 21, *bifrons* Zone, late Toarcian. 5. Coelastarte, Gorno Ozirovo section, bed 21, *bifrons* Zone, late Toarcian. 6. Coelastarte, Gorno Ozirovo section, bed 21, late *falciferum* Zone, early Toarcian. 7. *Trigonia* sp., Dobravista-1 section, bed 7b, *dispansum* Zone, late Toarcian. 8. *Pholadomya fidicula* (J. Sowerby, 1826), Dragovishtitsa section, bed 14c, *aalensis* Zone, late Toarcian. 9. *Pholadomya decorata (Hartmann, 1830),* Ravna section, bed 6 (IV), late Sinemurian. 10. *Pholadomya ambigua* (J.Sowerby, 1819), Teteven section, bed 5, late Sinemurian. 11. *Myoconcha decorata* (Münster, 1837), Teteven section, bed 5, late Sinemurian. All specimens coated in ammonium chloride. White scale bar =1 cm.

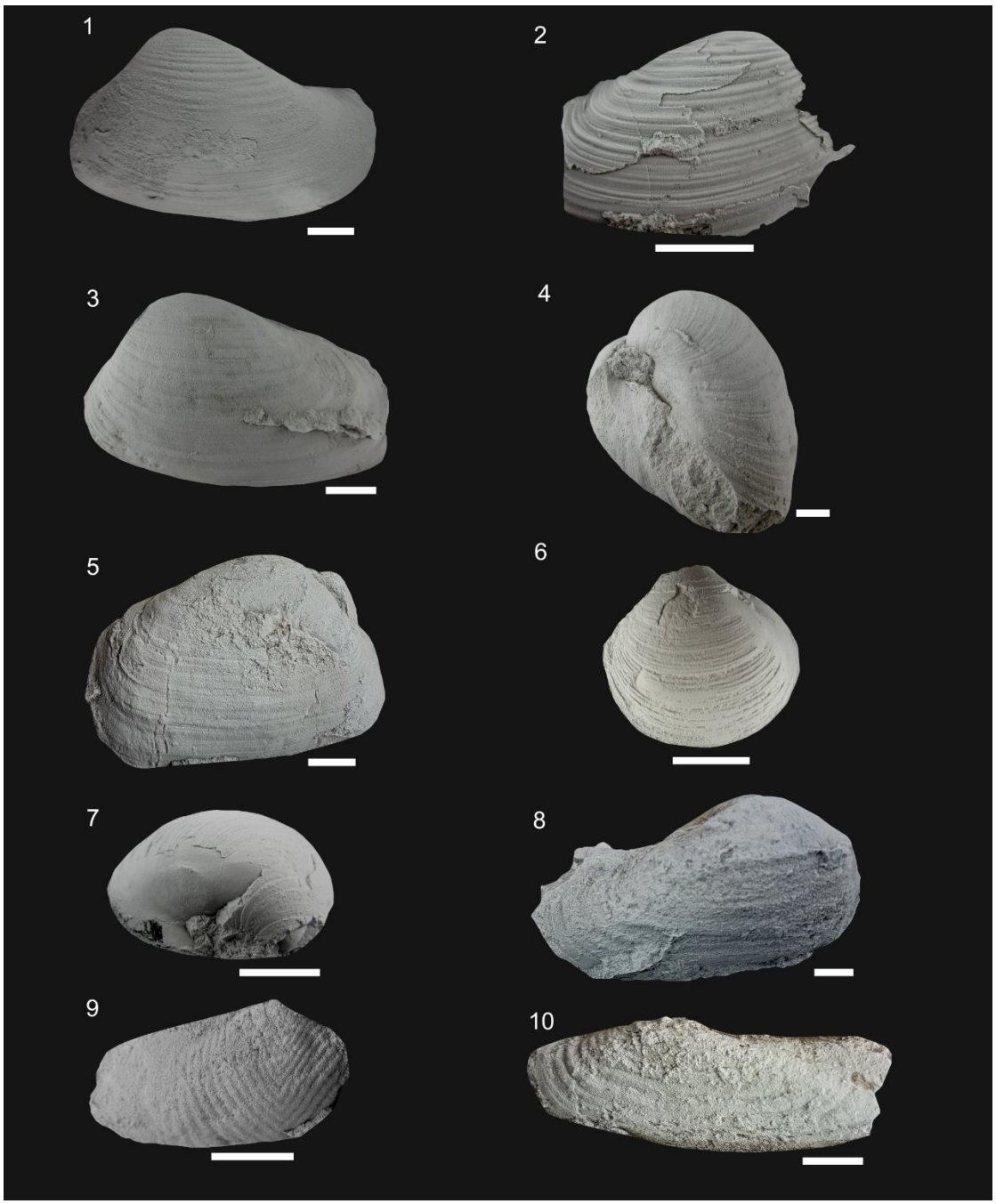

Figure 6.7. Plate 6. 1. *Pleuromya costata* (Young and Bird, 1828), Teteven section, bed 9, *jamesoni* Zone, early Pliensbachian. 2. *Pleuromya costata* (Young and Bird, 1828), Kiselchov Dol section, bed 13c, *bifrons* Zone, early Toarcian. 3. *Pleuromya costata* (Young and Bird, 1828), Teteven section, bed 8, late Sinemurian 4. *Pleuromya costata* (Young and Bird, 1828), Teteven section, bed 8, late Sinemurian. 5. *Gresslya* sp., Teteven section, bed 8, late Sinemurian. 6. Mactromya sp., Gorno Ozirovo section, bed 21, late *falciferum* Zone, early Toarcian. 7. *Mactoryma* sp., Gorno Ozirovo section, bed 21, *falciferum* Zone, early Toarcian. 8. ?*Pachymya (Arcomya) elongata* (Agassiz, 1843), Teteven section, bed 8, late Sinemurian. 9. *Goniomya hybrida* (Münster, 1841), Kiselchov Dol section. bed 13a, *tenuicostatum* Zone, early Toarcian. 10. *Pachymya (Arcomya) elongata* (Agassiz, 1843), Teteven section, bed 8, late Sinemurian. All specimens coated in ammonium chloride. White scale bar =1 cm.

6.3.2.1 Differentiated Ozirovo Formation

Ravna/Teteven Member

This basal member of the Ozirovo Formation has the first Lower Jurassic bivalves, from the upper Sinemurian and extends into the lower Pliensbachian. It is worth noting that the first occurrences of these taxa may occur earlier, but the lower Sinemurian is not recorded in the sections. Bivalves from this member are recorded from the Teteven, Ravna and Vradlovtsi-1 sections.

This member includes rich and diverse bivalve assemblages, that are often well-preserved. Bivalve taxa found in the Ravna and Teteven Member commonly include *Modiolus ventricosa*, *Gryphaea mcullochii*, *Oxytoma inequivalvis, Antiquilima succincta, Pseudopecten equivalvis and Pseudolimea pectinoides* (Figure 6.8, Figure 6.9, Figure 6.10, Figure 6.11).

The deep-infaunal bivalve species *Pholadomya ambigua* and *Pleuromya costata* are also common and are invariably orientated in their growth position (i.e. anterior obliquely downwards). Individual beds in the Teteven section record particularly high abundances of *Pleuromya costata* and *Pholadomta ambigua* (beds 8 and 9, Figure 6.11). The Ravna section includes another species of *Pholadomya*, identified as *Pholadomya decorata*, found towards the top of the member (beds 6 and 7; Figure 6.10). Occasional limestone beds in this member contain oysters and small accumulations of abundant *Harpax spinosa* specimens.

Dolni Lukovit Member

The Dolni Lukovit Member of the Ozirovo Formation is heterogeneous and spans the upper Sinemurian-upper Pliensbachian, although rarely includes the *spinatum* Zone. This member occurs in the Teteven, Ravna, Vradlovtsi-2 and Brakyovtsi sections.

Many of the bivalves found in the base of the Dolni Lukovit Member range up from the underlying Ravna/Teteven Member, particularly in the siliciclastic rich limestones, and include *Pseudopecten equivalvis, Antiquilima succincta, Gryphaea* sp., *Pleuromya costata, Pholadomya ambigua, Pholadomya decorata, Entolium lunare*, *Pinna folium, Pinna radiata and Plagiostoma punctata* (Figure 6.9*,* Figure 6.10*,* Figure 6.11)*.* In the Ravna section many of these taxa do not continue through the Dolni Lukovit Member and stop around bed 8 or 9 (Figure 6.10), and a similar decrease in abundance and diversity is observed in the Teteven section. This decrease in bivalve occurrences

coincides with a change in facies towards more crinoidal, bioclastic limestones. Bivalve assemblages comprise *Entolium lunare*, *Chlamys textoria*, with less common *Pleuromya costata* and *Pholadomya ambigua* (Figure 6.11). In the Brakyovtsi section beds containing particularly abundant and well-preserved *Entolium lunare* are recorded in the *margaritatus* Zone (*stokesi* Subzone).

Bukorovtsi Member

The youngest member of the Ozirovo Formation, the Bukorovtsi Member, is also heterogeneous and spans the upper Pliensbachian-Bajocian. Bivalves in the Bukorovtsi Member are not as diverse as the lower members of the Ozirovo Formation.

Bivalve taxa from the upper Pliensbachian *spinatum* Zone in the Ravna and Dobravista-1 sections, typically include *Chlamys textoria, Pseudopecten equivalvis, Plagiostoma punctata, Gryphaea gigantea* and less common occurrences of *Antiquilima* (Figure 6.10, Figure 6.13). The Vradlovtsi-2 section includes this member as part of the upper Pliensbachian, but no bivalves were recovered (Figure 6.9).

Toarcian records of the Bukorovtsi Member are found in the Dobravitsa-1 section, although the Lower Toarcian strata are not exposed. Upper Toarcian bivalve taxa from the Bukorovtsi Member include *Plagiostoma* sp., *Pseudolimea* cf*. pectinoides* and a single occurrence of *Trigonia* sp (Figure 6.13). Additional upper Toarcian bivalves, that continue into the Aalenian, include *Coelastarte* sp., *Antiquilima* sp., *Chlamys* sp. and abundant *Entolium corneolum*. No infaunal bivalves are recorded from the Dobravitsa-1 section (Figure 6.13).

Other Toarcian records of the Bukorovtsi Member include the Milanovo and the Boeva Mogila sections. Bivalves in these sections are very rare. The only bivalves found in the Boeva Mogila section, were two specimens of *Pseudolimea* cf. *acuticostata* in the *tenuicostatum* Zone. No bivalves were recorded in the Milanovo section. Despite a lack of bivalves in these sections, ammonites are common and abundant throughout. Belemnites are also common through the Milanovo section and the Boeva Mogila section (excluding the belemnite gap recorded in the *falciferum* Zone in the latter section). As very limited fauna is found in these sections, individual range charts are not shown, but occurrences are included in the composite range chart.

6.3.2.2 Undifferentiated Ozirovo Formation

During the Pliensbachian, faunal assemblages are dominated by large *Gryphaea gigantea* and *Pseudopecten equivalvis*. These common upper Pliensbachian species from the Balsha (Figure 6.14) and Gorno Ozirovo section (Figure 6.16*)* and are often associated with *Chlamys textoria* and *Entolium lunare* . In the lower Pliensbachian (*ibex* Zone) in Dragovishtitsa, there is an abundance of *Pseudopecten equivalvis*, with a distinctive 'pecten bed' at the top of bed 2 (Figure 6.15). Through the rest of the Pliensbachian in the Dragovishtitsa section there are very few identifiable bivalve taxa (Figure 6.15).

The Toarcian bivalve faunas in of the Gorno Ozirovo section show differences in bivalve assemblages through the early Toarcian interval, despite its condensed nature. Bivalve faunas in the *tenuicostatum* Zone include *Pleuromya costata*, *Propeamuseum* sp., *Placunopsis radiata*, *Entolium* sp. and *Liostrea* sp. (Figure 6.16). *Placunopsis radiata* is recorded for the first time from Bulgaria. Bivalve faunas in the *falciferum* Zone also include Entolium sp., *Pleuromya costata* and *Propeamussium pumilum*, *Coelastarte* sp, *Grammatodon* cf *insons*, *Plagiostoma* sp., and *Ctenostreon* sp. (Figure 6.16). Bivalve faunas in the *bifrons* Zone also include common *Coelastarte* sp., *Entolium* sp, Liostea sp. and *Oxytoma inequivalvis* (Figure 6.16).

Early Toarcian faunas are recorded in the ironstones of the Kiselchov Dol section (Figure 6.17). In this section bivalves found only in the *tenuicostatum* Zone include *Oxytoma inequivalvis, Goniomya hybrida, ?Modiolus* and *?Grammatodon* (Figure 6.17). *Oxytoma inequivalvis and Goniomya hybrida* do not occur after the *tenuicostatum* Zone in Bulgaria (Figure 6.19). The occurrence of *Goniomya hybrida* is recorded for the first time in Bulgaria. Bivalve fauna that are only recorded in the *falciferum* Zone include *Antiquilima* and *?Gresslya* (Figure 6.17). The *falciferum* Zone in the Kiselchov Dol section records the first occurrence of *Propeamussium pumilum* in Bulgaria (Figure 6.17). Individual, sometimes monospecific, horizons of *Entolium* are present in the *falciferum* Zone (Bed 13b, Figure 6.17). The *bifrons* Zone in this section records the first occurrence of *Grammatodon insons* and *Plagiostoma* sp.(Figure 6.17). Bivalve taxa from the early Toarcian of the Kiselchov Dol section include *Pleuromya costata, Chlamys textoria, Camptonectes auritus*, *Coelastarte* sp. and *Entolium* sp. (Figure 6.17).

The upper Toarcian bivalve record from Bulgaria comes mainly from the ironstones of the Kiselchov Dol and Dragovishtitsa sections. The first occurrence of *Pholadomya fidicula* is recorded from the *dispansum* Zone in

Bulgaria (Dragovishtitsa section, bed 14c; Figure 6.15). Many bivalves from the upper Toarcian can only be identified to genus level and include *Pinna* sp., *Chlamys* sp., *Antiquilima* sp., *Modiolu*s sp., *Plagiostoma* sp., and *Weyla* sp. (Figure 6.15).

Previous Bulgarian literature reportedly found abundant *Posidonia bronni* (now known as *Bositra buchii*) in the upper Toarcian (Shopov, 1968; Sapunov et al., 1971). However, in reviewing Bulgarian collections at Sofia University, it is evident these specimens were mis-identified and actually record the genus *Coelastarte*. The first appearance of *Bositra* in Bulgaria is from the Aalenian within the *Bositra alpina*-Etropole Formation (Sapunov and Tchoumatchenco, 1998).

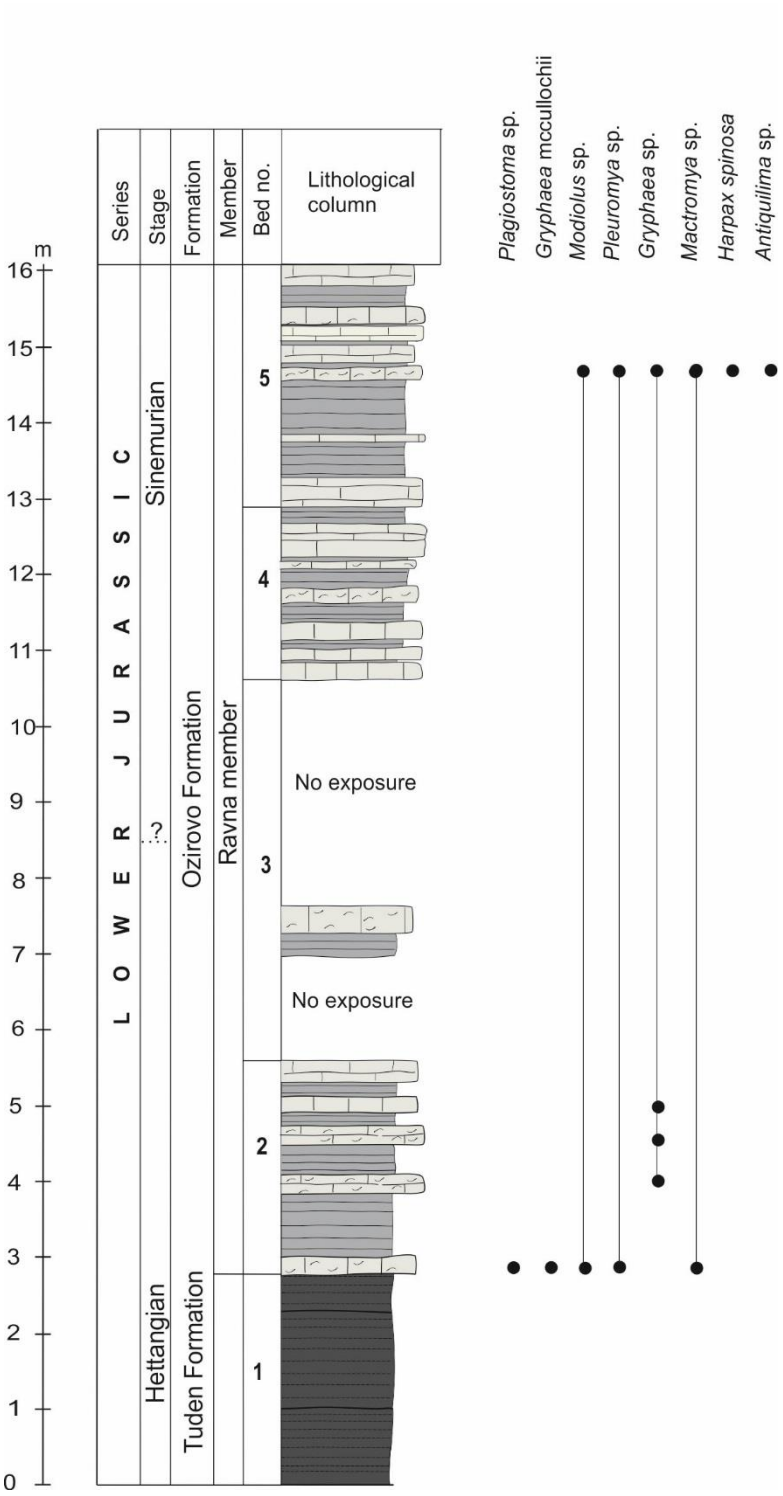

Figure 6.8 Stratigraphic log of the Vradlovtsi-1 section, showing the distribution of bivalves. Occurrence horizons from this study are shown by black dots.

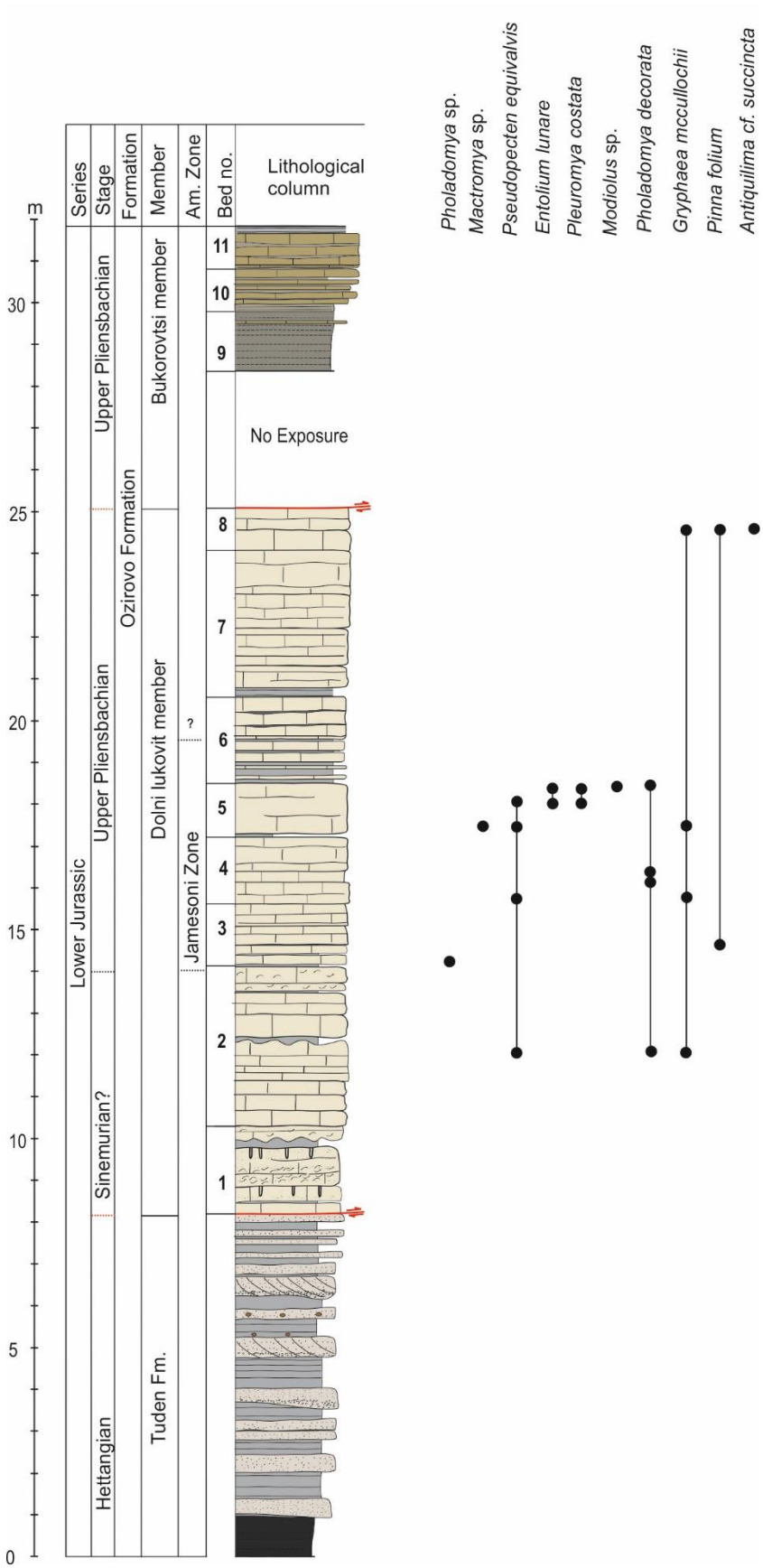

Figure 6.9 Stratigraphic log of the Vradlovtsi-2 section, showing the distribution of bivalves. Occurrence horizons from this study are shown by black dots. Am zone = Ammonite Zone.

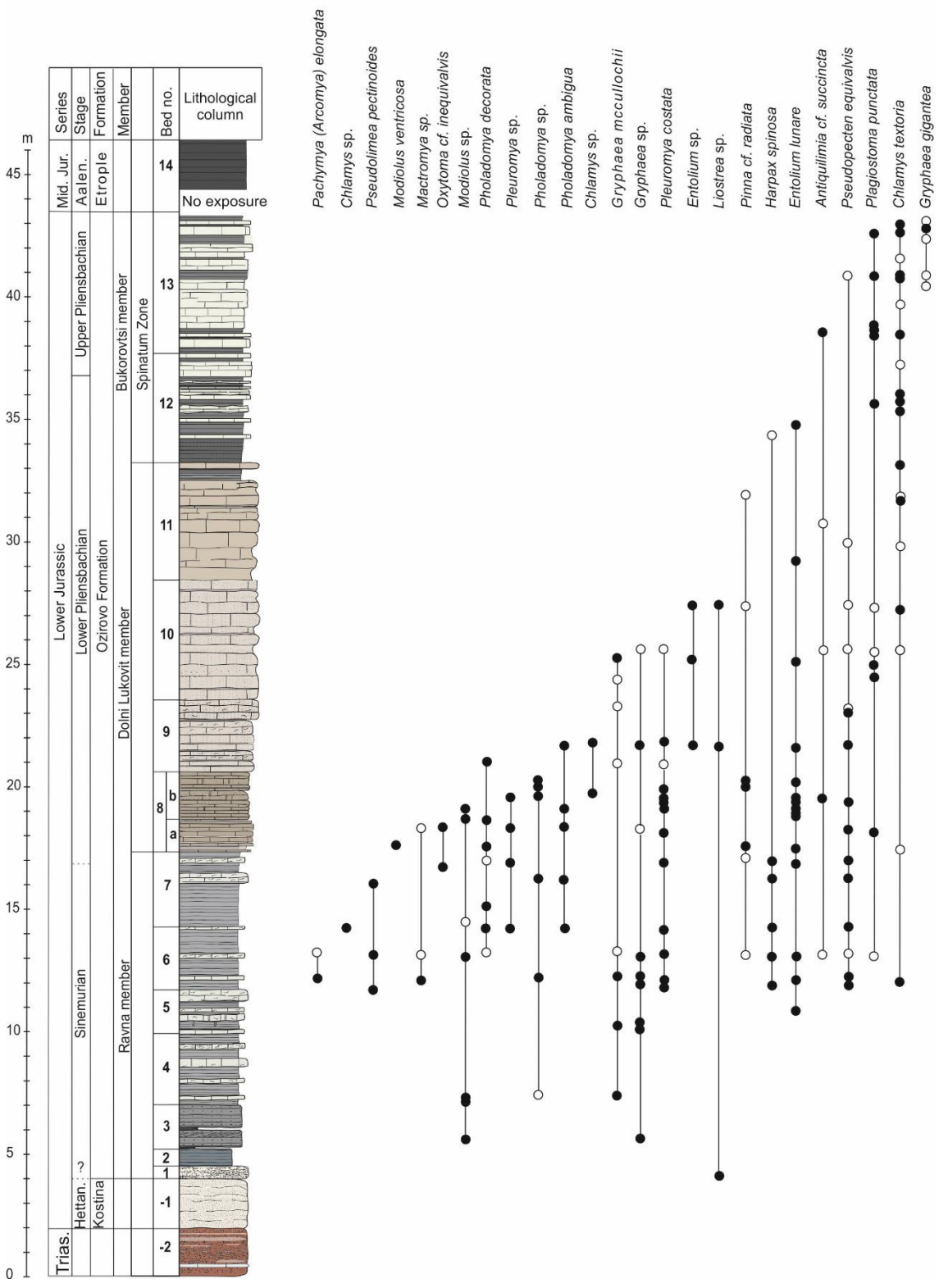

Figure 6.10 Stratigraphic log of the Ravna section, showing the distribution of bivalves. Occurrence horizons from this study are shown by black dots and additional occurrences from Shopov (1968) are shown by open circles.

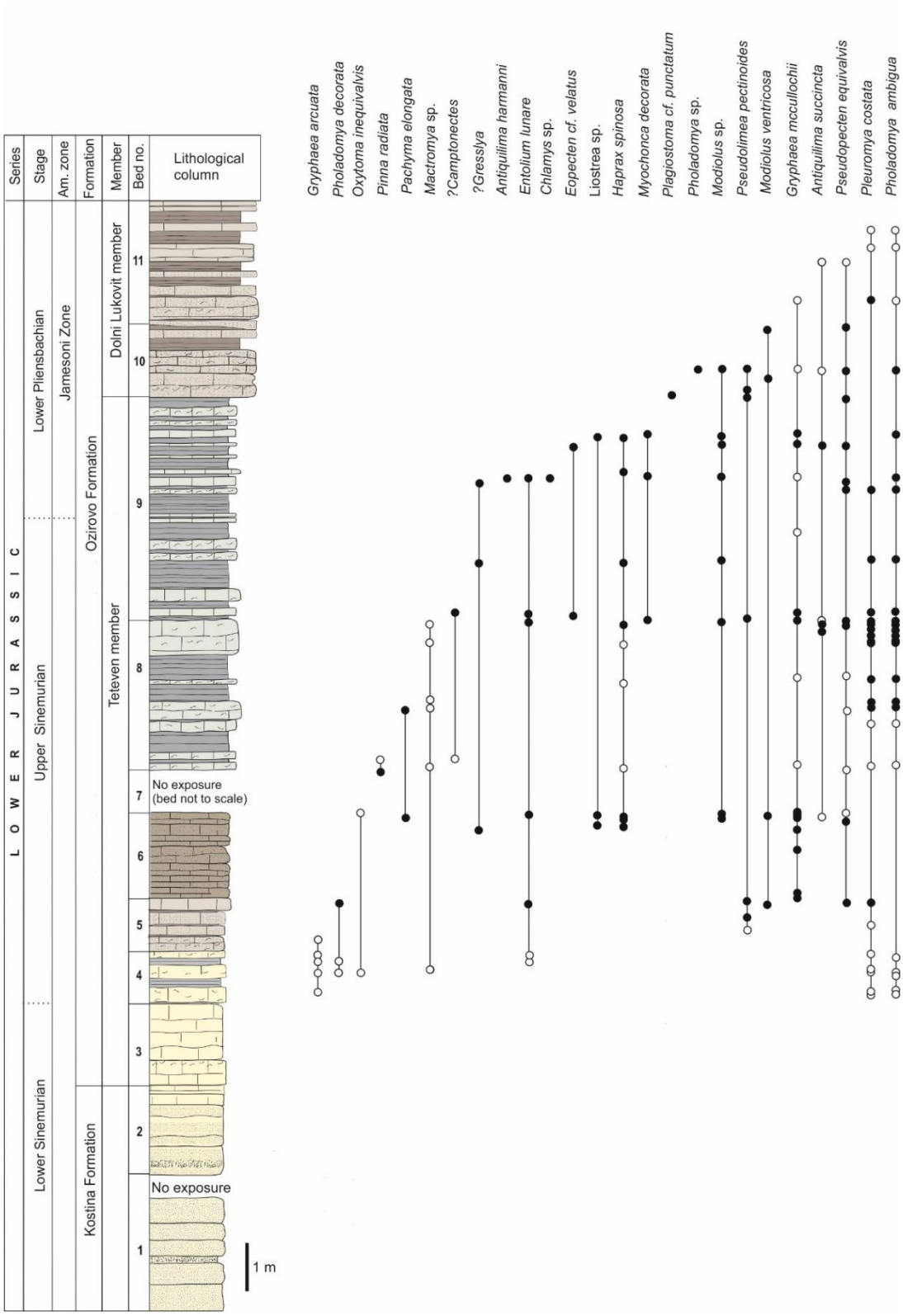

Figure 6.11 Stratigraphic log of the Teteven section, showing the distribution of bivalves. Occurrence horizons from this study are shown by black dots and additional occurrences from Shopov (1968) are shown by open circles. Am. Zone = Ammonite zone.

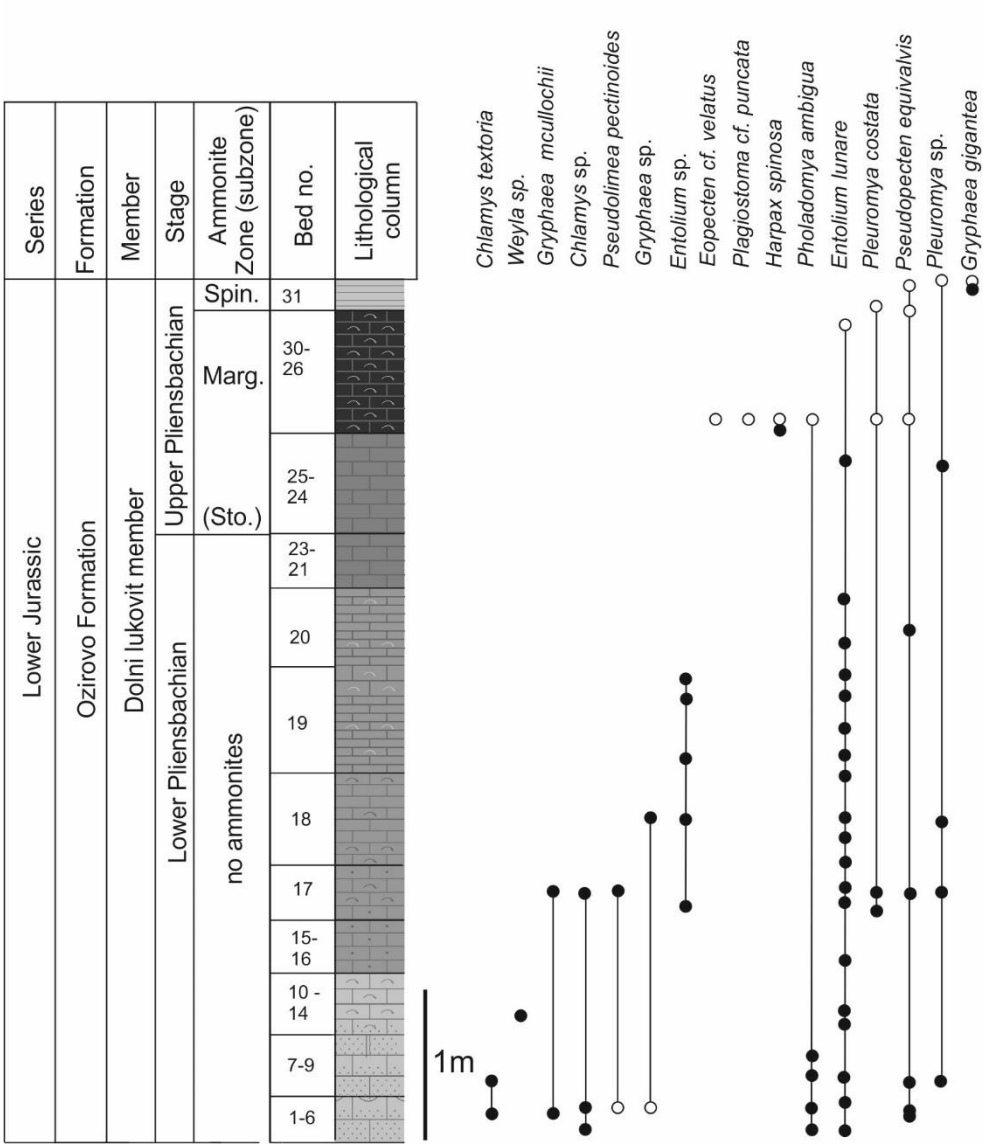

Figure 6.12 Stratigraphic log of the Brakyovtsi section, showing the distribution of bivalves. Occurrence horizons from this study are shown by black dots and additional occurrences from Shopov (1968) are shown by open circles. Ammonite Zone abbreviations: Marg= *margaritatus*. Ammonite subzone abbreviations: Sto=*Stokesi*.

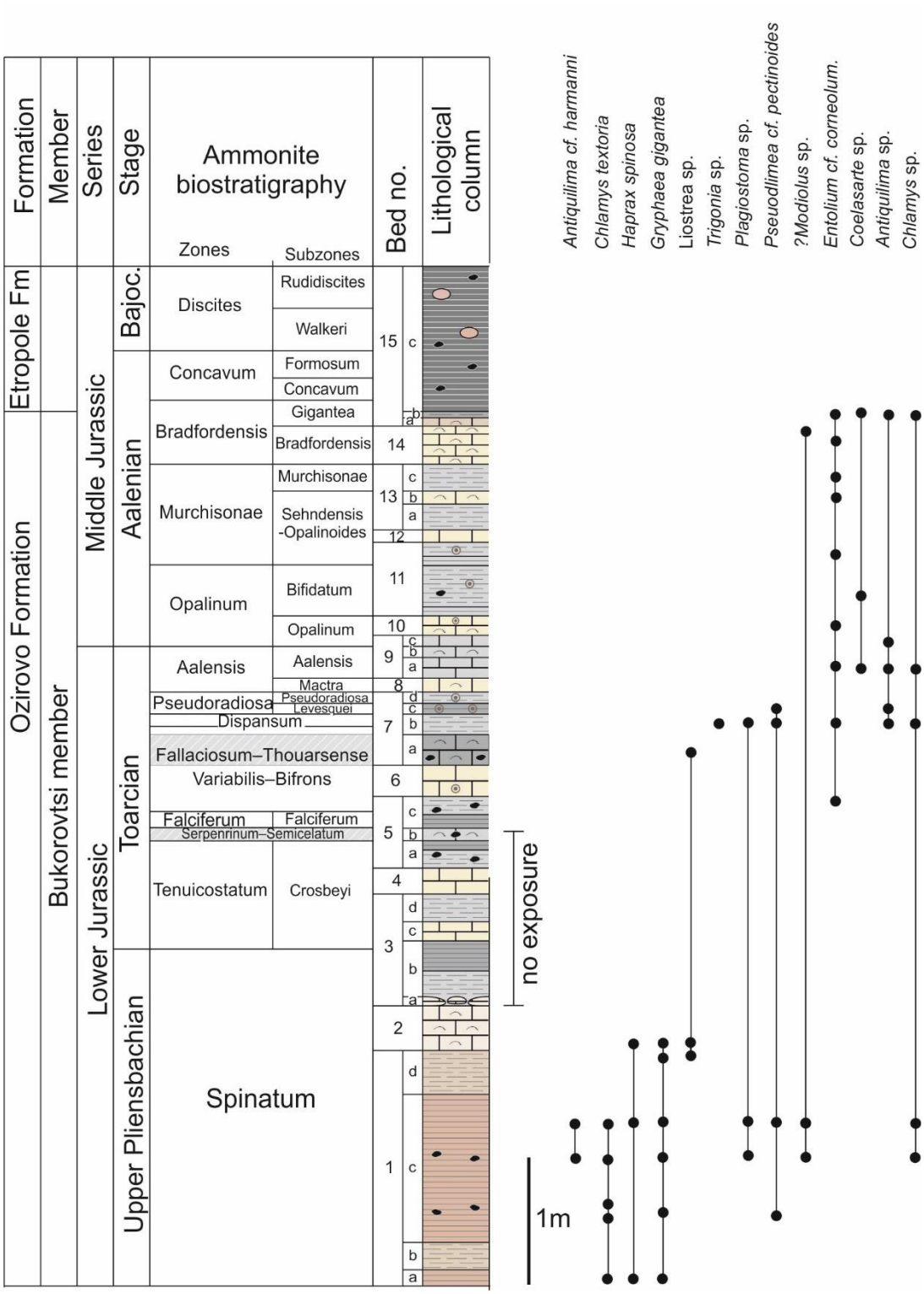

Figure 6.13 Stratigraphic log of the Dobravitsa-1 section, showing the distribution of bivalves. Occurrence horizons from this study are shown by black dots. Bajoc. = Bajocian.

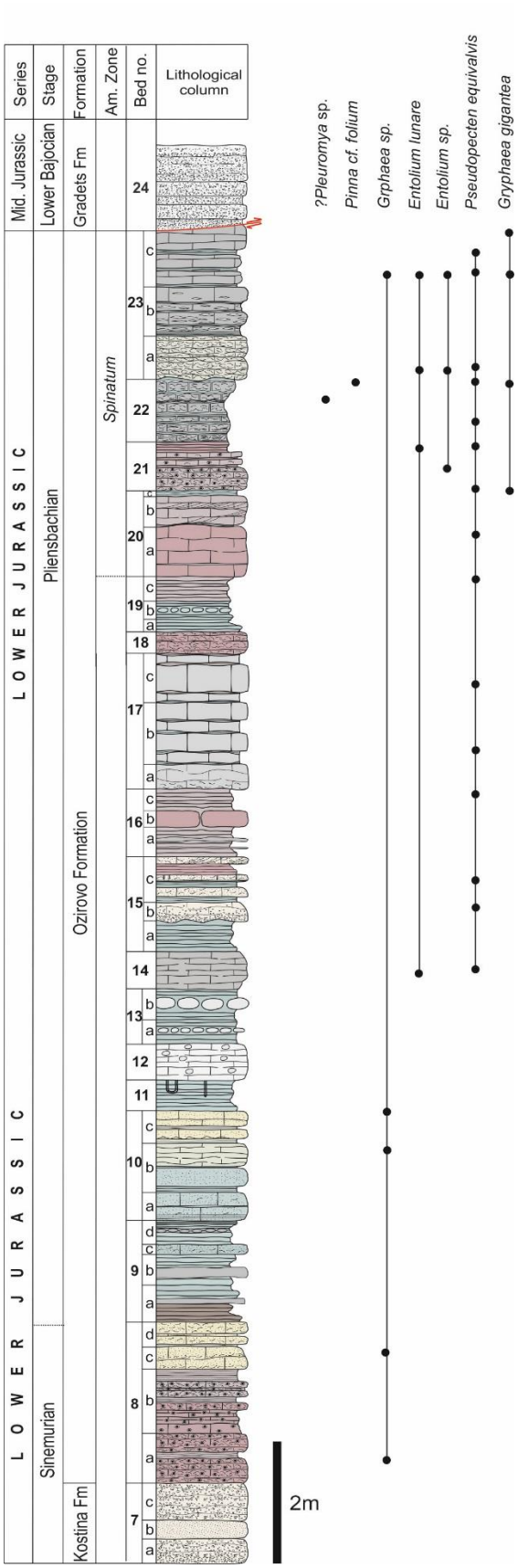

Figure 6.14 Stratigraphic log of the Balsha succession, showing the distribution of bivalves. Occurrence horizons from this study are shown by black dots. A,. zone = Ammonite zone.

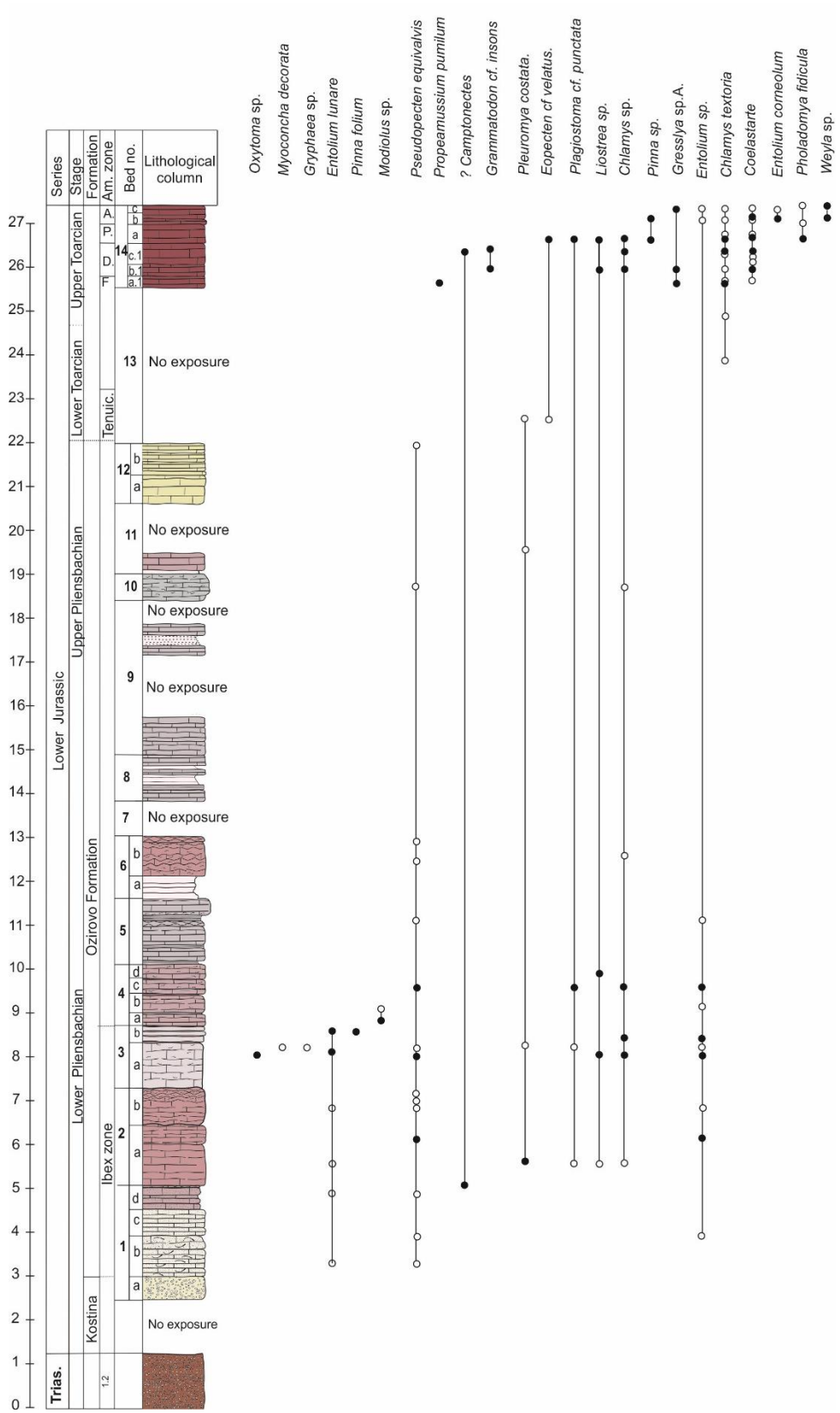

Figure 6.15 Stratigraphic log of the Dragovishtitsa section, showing the distribution of bivalves. Occurrence horizons from this study are shown by black dots and additional occurrences from Shopov (1968) are shown by open circles. Am. Zone = Ammonite Zone. F=*fallaciosum*. D=*dispansum*. P=*pseudoradiosa*. A=*aalensis*.

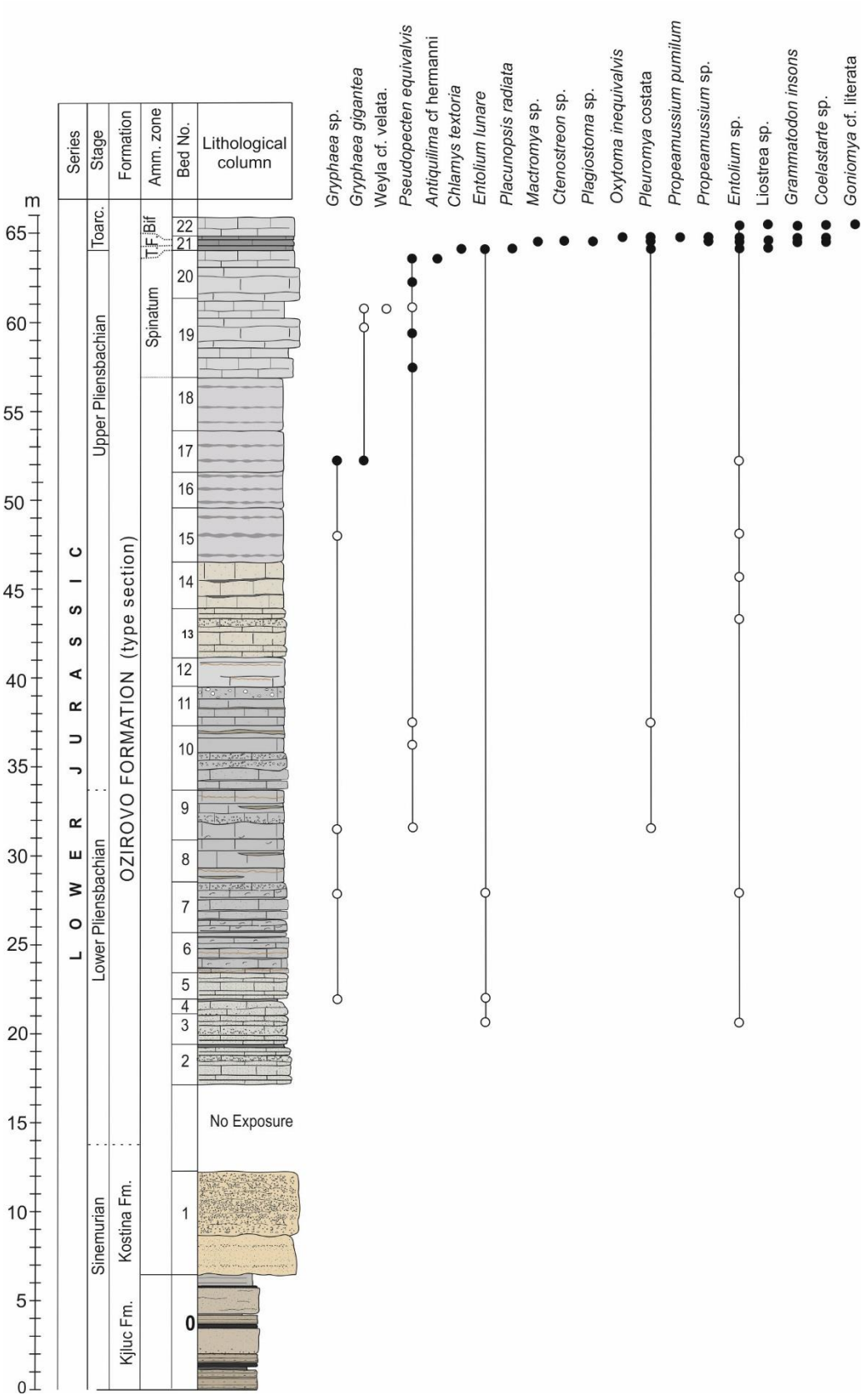

Figure 6.16 Stratigraphic log of the Gorno Ozirovo section, showing the distribution of bivalves. Occurrence horizons from this study are shown by black dots and additional occurrences from Shopov (1968) are shown by open circles. Amm. Zone = Ammonite zone. T=*tenuicostatum*. F=*falciferum*. B=*bifrons*.

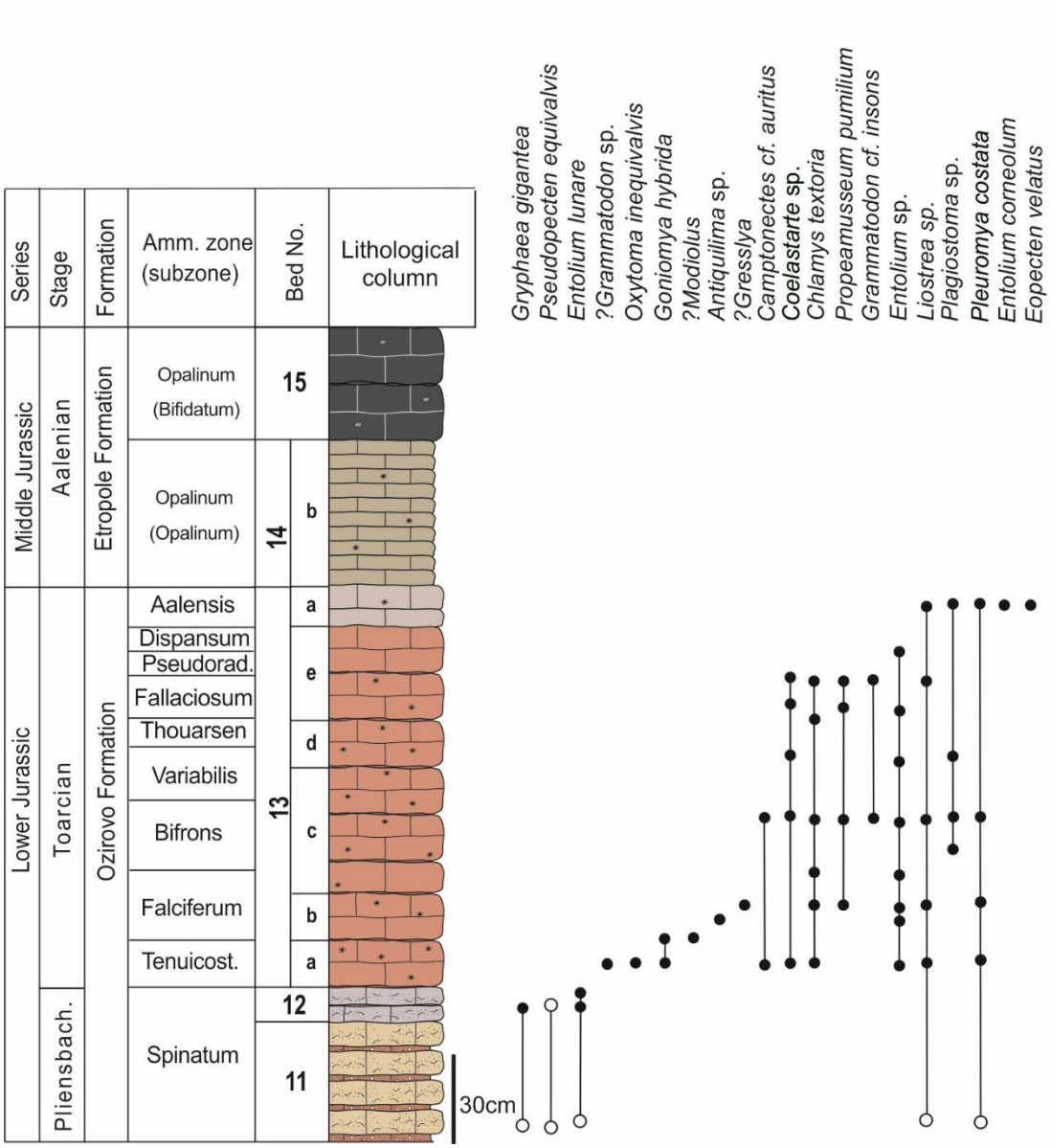

Figure 6.17 Stratigraphic log of the Kiselchov Dol section, showing the distribution of bivalves. Occurrence horizons from this study are shown by black dots and additional occurrences from Shopov (1968) are shown by open circles. Amm. Zone = Ammonite zone. Pliensbach.= Pliensbachian.

6.3.3 Early Toarcian extinction interval

The loss of bivalve species at both the Pl-To boundary and in the *tenuicostatum* Zone indicate an extinction interval in the Moesian Basin (Figure 6.19). The significant loss of bivalve fauna from the Pl-To boundary to the top of the *tenuicostatum* Zone is termed here as the 'extinction interval' (Figure 6.19). This extinction interval is considered to be a regional reflection of the globally recognised ETME.

In the Bulgarian sections, two extinction horizons are recorded during the extinction interval in Bulgaria: one at the Pl-To boundary and one at the top of the early Toarcian *tenuicostatum* Zone (Figure 6.19). A total of nine bivalve species have their last occurrence at the Pl-To boundary (extinction horizon ii; Figure 6.19), with last occurrences of *Pholadomya ambigua*, *Gryphaea gigantea, Antiquilima hermanni, Antiquilima succincta, Harpax spinosa, Pseudopecten equivalvis, Pinna radiata, Pinna folium* and *Plagiostoma punctata.* A further four species have last occurrences in the early Toarcian *tenuicostatum* Zone (extinction horizon iii; Figure 6.19), including *Goniomya hybrida, Entolium lunare, Placunopsis radiata* and *Pseudolimea* cf*. acuticostata*. *Goniomya hybrida*, *Pseudolimea pectinoides* and *Placunopsis radiata* are all single occurrence taxa in the *tenuicostatum* Zone, as part of the extinction interval (Figure 6.19).

Some bivalve taxa have only been identified to genus level, which could represent one or more species (Figure 6.19). The genera *Chamys* and *Weyla*are long-ranging taxa recorded throughout the Lower Jurassic, including occurrences within the extinction interval. Other genera occur both before and after the extinction interval, such as *Plagiostoma* and *Pleuromya* that re-appear in the following *falciferum* Zone and *Weyla*, *Modiolus* and the species *Pseudolimea pectinoides* that reappear in the upper Toarcian (Figure 6.19). However, it is not clear if these are Lazarus taxa, or the last occurrence of one species and the first occurrence of another (Fara, 2001). The genera that cannot be identified to species level are included in the range charts. However, the inclusion of these taxa causes difficulty in calculating percentages of species loss, as it is unclear how many of the genera reflect new species or species already documented. A total of 13 bivalve species are lost during the extinction interval. At genus level, five are lost during the extinction interval, out of 28 that are present prior to the extinction interval (*spinatum* Zone). This is a loss of 18% of genera, with the disappearance of *Gryphaea, Pseudopecten, Harpax, Goniomya and Placunopisis (*Figure 6.19*)*. The extinction interval in the

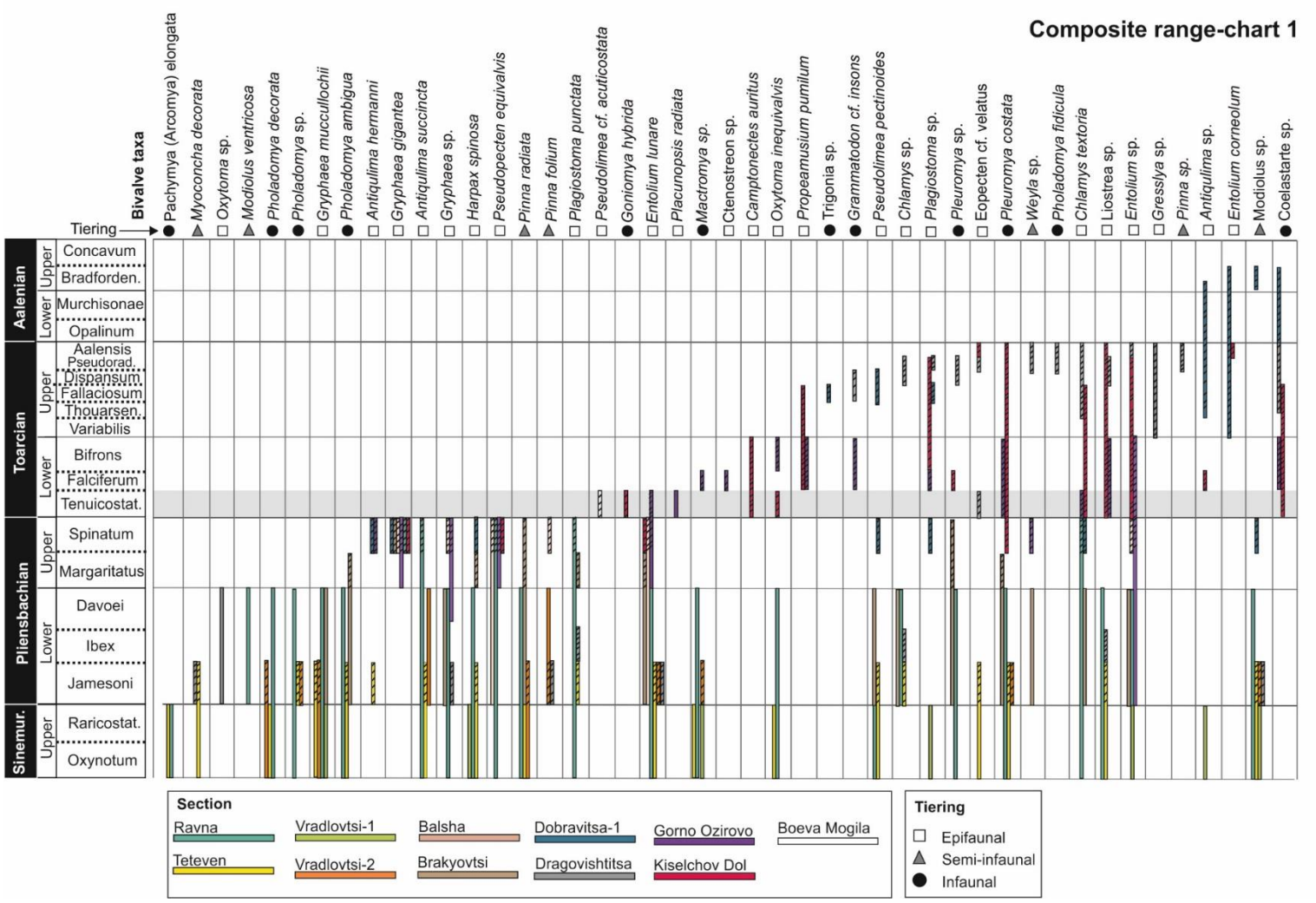

(PTO for caption)

Figure 6.18 (previous page) Composite stratigraphic range data for bivalve taxa from the Lower Jurassic of northwest and central Bulgaria. Range data are plotted against the biostratigraphic framework of Metodiev (2008). Taxa are ordered by last appearance. Bivalve occurrence plotted to sub-stage resolution, except where there is biostratigraphic control and then is plotted to ammonite zonal level (indicated by sub-horizontal shading).

Moesian Basin comprises the Pl-To boundary to the top of the early Toarcian *tenuicostatum* Zone. During this interval 5/18 genera do not continue after the extinction interval, recording a generic loss of 18%. However, all of these genera, except for *Harpax,* have global stratigraphic ranges that extend beyond the early Toarcian. The absence of these genera in the Moesian Basin following the extinction interval reflects either a local extinction, or is an artefact of sampling intensity and the genera existed, but were not found in this study. If the genera with stratigraphic ranges known to extend beyond the ETME (Damborenea, 2002a; Aberhan et al., 2011) are not taken into account a 3% generic extinction is recorded in the Moesian Basin.

The extinction recorded in the bivalves predominantly comes from bivalve occurrences within the Kiselchov Dol and Gorno Ozirovo sections, that are both record shallow marine settings in the Moesian Basin. These shallower, more proximal parts of the Moesian Basin record condensed bioclastic limestones in the early Toarcian, with bivalve assemblages predominately comprised of attached epifaunal suspension feeders. Typical assemblages including *Plagiostoma*, *Placunopsis*, *Liostrea* and *Entolium* and are often found encrusted by serpulids in both the Kiselchov Dol and Gorno Ozirovo section. Infaunal bivalves are recorded throughout the early Toarcian interval, but are not very common (Figure 6.19).

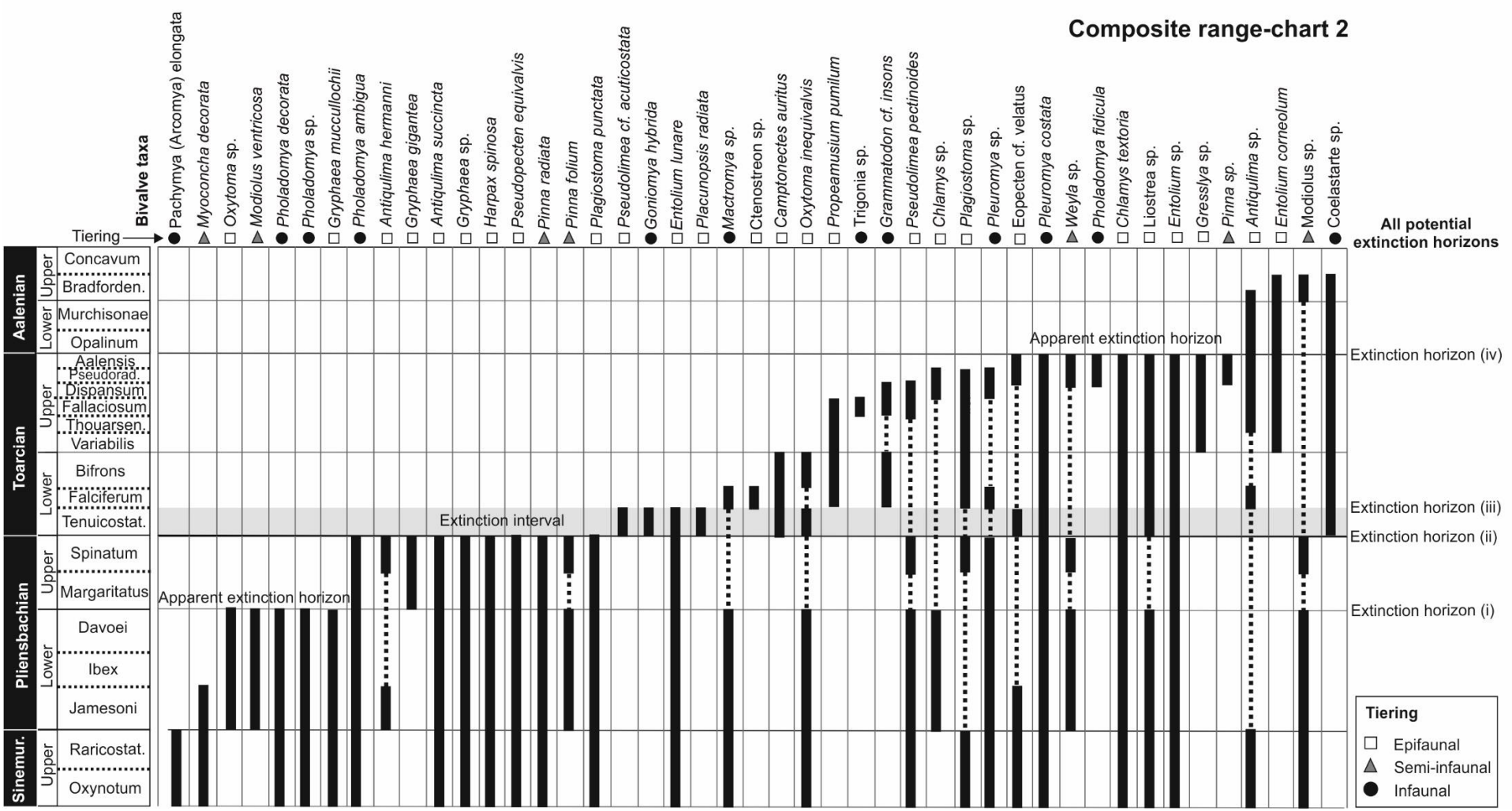

(PTO for caption)

Figure 6.19 (previous page) Composite stratigraphic range data for bivalve taxa from the Lower Jurassic of northwest and central Bulgaria, with occurrences from individual sections are combined for each bivalve taxa. Range data are plotted against the biostratigraphic framework of Metodiev (2008). Taxa are ordered by last appearance.

6.3.4 Apparent extinction intervals during the Pliensbachian and late Toarcian

The range charts show two other horizons with an apparent abrupt loss of bivalve taxa in the Moesian Basin at the lower Pliensbachian (*davoei* Zone)/upper Pliensbachian (*margaritatus* Zone) boundary (extinction horizon i; Figure 6.19) and one at the Toarcian/Aalenian boundary (horizon ii, Figure 6.19). These are considered to be artefacts, caused by poor biostratigraphic control and a lack of continuous section exposure. In the case of extinction horizon (i), a significant proportion of bivalve occurrences through the Pliensbachian can only be constrained to sub-stage level (either lower Pliensbachian or upper Pliensbachian). As a result, any taxa that occur through the lower Pliensbachian appear to terminate at the end of this sub-stage, even if their last occurrences were actually gradual. Therefore extinction horizon (i) is considered an artefact of poor biostratigraphic constraint. In the case of extinction horizon (iv), a sudden loss of taxa at the end of the Toarcian is considered to be a sampling artefact, as only one section is continuous from the Toarcian into the Aalenian.

6.3.5 Palaeobiogeographic affinity of bivalves from the Moesian Basin

There is no recognition of biogeographic patterns in bivalves during the earlier stages of the Lower Jurassic (Hettangian and Sinemurian), due to extremely low levels of emdemism following the Late Triassic mass extinction (Liu, 1995; Liu et al., 1998; Damborenea, 2002a,b). Therefore, only bivalve faunas from the Pliensbachian, Toarcian and Aalenian stages of the Moesian Basin can be attributed to a biogeographic bivalve province.

Many bivalve taxa from the Moesian Basin had a cosmopolitan distribution, as is expected from Lower Jurassic bivalves (Damborenea et al., 2013). Only a limited number of taxa can be used to attribute bivalve faunas from Bulgaria to a specific realm. *Weyla* was present in the Tethyan realm and absent from the

Boreal realm during the Pliensbachian-Toarcian interval (Liu, 1995) (Table 6.1). Additionally, *Oxytoma*, was absent from the Mediterranean province during the Pliensbachian-Toarcian interval (Liu, 1995) (Table 6.1). In Bulgaria, *Weyla* and *Oxytoma* are recorded from both the Pliensbachian and Toarcian intervals.

Based on the established realms devised for the global distribution of bivalves (Damborenea, 2017), the bivalve faunas recorded in the Moesian Basin during the Pliensbachian and Toarcian are most strongly associated with the Southern transitional province of the Tethyan realm (sensu Liu, 1995). This is also supported by the absence in Bulgaria of the genus *Hippopodium*, which was characteristic of the Boreal realm in the Pliensbachian and the genera *Pachyrisma* and *Pachymytuis*, which were characteristic of the Mediterranean province in the Tethyan realm (Liu, 1995) (Table 6.1).

Table 6.1 The occurrence of key endemic bivalve genera from the Pliensbachian-Toarcian interval of the EES. Bivalve genera recorded in Bulgaria highlighted in grey. Crosses denote where genera is present in each province and dashes indicate an absence of genera. Occurrence data indicative of biogeographic realms modified after Liu (1995), Liu et al. (1998), Damborenea, (2017). Bivalve taxa present in Bulgaria indicate an affinity with the Tethyan realm (southern Tethyan transitional province), as *Weyla* and *Oxytoma* both present.

Genera	Boreal realm	Tethyan realm (southern Tethyan transitional province)	Tethyan realm (Mediterranean Province)
Weyla	-	x	x
Oxytoma	x	x	-
Hippopodium	x	-	-
Pachyrisma	-	-	x
Pachymytuis	-	-	x

6.4 Discussion

6.4.1 Early Jurassic biotic crisis in bivalves as part of the ETME

During the Toarcian, most bivalve assemblages are present within the ‘undifferentiated’ Ozirovo Formation. Conversely, bivalves are absent or rare within the Bukorovtsi Member of the Ozirovo Formation.

Bivalves are highly facies-dependant, and this should be taken into account when studying faunal occurrences through the Lower Jurassic (Nikitin, 1886; Ortmann, 1896; Hallam, 1969; Hallam, 1971). Sedimentation in the Moesian Basin was highly diachronous and heterogeneous. Through the Lower Jurassic of the Moesian Basin, different sections represent different positions within the palaeobasin from relatively deep, to hemipelagic to inner shelf and coastal. Therefore, facies type is likely to have had some control on the bivalves present in the Moesian Basin throughout the Lower Jurassic interval.

6.4.1.1 Shallow marine extinction record in bivalves

The extinction record for bivalves is predominantly recorded from the shallower more proximal settings of the Moesian Basin (Milanovo and Boeva Mogila sections). Epifaunal bivalves are more common in both sections than infaunal bivalves, with a generally low number of infaunal bivalves recorded through the Toarcian. The low number of infaunal bivalves likely relates to the facies type.

In the Toarcian, substrate was likely too hard in the shallower parts of the basin for infauna. Firm or shell-rich substrate might have inhibited infauna, or led to a decrease in growth rates in infauna, with higher vulnerability to predetation or competition as the by-product (Kidwell and Jablonski, 1983; Oschmann, 1988; Aberhan, 1992). Enhanced substrate stability in the Moesian Basin is likely to relate to reduced sedimentation rates (Kidwell and Jablonski, 1983). Evidence for slow sedimentation rates is supported by the thin development of the early Toarcian and evidence from bivalves, that are found to be encrusted due to relatively long periods of time exposed on the sea-floor. This typical shallow marine assemblage is also different to that of the Yorkshire Coast, a previously investigated study area, as Little (1995) did not record more than two individuals *of Liostrea hisingeri* in the Whitby Mudstone Formation, and other workers did not record any oysters in the *tenuicostatum* or *falciferum* Zones (Blake and Tate, 1876; Hallam, 1976; Caswell et al., 2009).

The two main extinction horizons in Bulgaria correspond to two of the globally recognised extinction steps recorded for the ETME (Harries and Little, 1999; Caswell et al., 2009). The first at the Pl-To boundary (Figure 6.19), corresponds with extinction step 2 of Harries and Little (1999) and extinction step (i) of Caswell et al. (2009). The second at the end of the *tenuicostatum* Zone (Figure 6.19) corresponds to extinction step 4 of Harries and Little (1999) and extinction step (iii) of Caswell et al. (2009). Another extinction step has previously recorded for the mid-*semicelatum* Subzone, below the top of the *tenuicostatum*

Zone (Harries and Little, 1999; Caswell et al., 2009). It is possible more bivalve species in Bulgaria became extinct during this extinction step, but cannot be recorded to this resolution in Bulgaria, due to the condensed nature of the Toarcian sediments.

6.4.1.2 Paucity in benthic macrofauna in the deeper settings of the Moesian Basin

The absence or rarity of bivalve faunas, particularly infaunal bivalves, from deeper water, relatively distal sections (Boeva Mogila and Milanovo) through the Toarcian can be explained in three ways: 1) preservation control, 2) bottom water conditions were unsuitable (caused by changes in oxygen, temperature, salinity or nutrient supply), or 3) the substrate was unsuitable for attachment or burrowing ('soupy substrate').

Preservation control

Ammonites and most infaunal bivalves are aragonitic and therefore have a higher susceptibility to dissolution, whereas epifaunal bivalves are mainly calcitic (Kidwell and Jablonski, 1983). However, the presence of ammonites throughout the sections argues against a preservation artefact.

Unsuitable conditions

It has long been recognised that typical oxygen deficient sediments can result in a reduction in species richness (Rhoads and Morse, 1971). Anoxic conditions below or at the sediment-water interface, excluding deep and possibly shallow infaunal bivalves and resulting in a dominance of epifaunal suspension-feeders has been used to explain a paucity in bivalve faunas (Oschmann, 1988; Aberhan, 1992). A lack of benthic fauna through the Toarcian in dark grey silty marls initially appear to be lithologically similar to the temporally equivalent organic-rich 'black shales' typical of the T-OAE. However, a lack of laminated sediment and pyrite petrography, shows no evidence of oceanic anoxia in Bulgaria, with only short-lived oxygen-deficient intervals that fluctuated between oxic and dysoxic conditions. If these fluctuating redox conditions were a key control on the presence of bivalve faunas in these sections, there would likely be opportunistic fauna colonizing the sediment water interface, during re-oxygenation intervals, as seen in the Yorkshire Coast, UK (Caswell et al., 2009), SW Germany (Savrda and Bottjer, 1987; Röhl et al., 2001) and Canada (Martindale and Aberhan, 2017). Additionally, the paucity in benthic macrofauna continues through the entire Toarcian interval in Bulgaria and oxygen-deficiency

linked to the T-OAE has not been recorded into the upper Toarcian (e.g. Wignall et al., 2005; Caswell et al., 2009; Martindale and Aberhan, 2017). However, because there is some evidence for fluctuating oxygen conditions, the short-lived decreases in oxygen concentrations might partly explain absence of infaunal suspension-feeding bivalves or of all shelly benthos.

Salinity or temperature changes must be considered as a cause of the paucity in benthic macrofauna. When considering salinity, if bottom waters had become more saline, and unfavourable to benthic macrofauna, more proximal sections would be expected to show a greater change in salinity, which is not evident. Additionally, increased freshwater influx into the Moesian Basin through the Early Jurassic would not be recorded if more saline conditions prevailed. When considering the role of temperature as a main control on the lack of bivalves only in deeper water sections, there are two possible options. The first is that temperature did not play a major part, given that temperature would have increased in shallow marine environments and would undoubtedly be hotter than in the deeper bottom waters although the loss of all taxa in shallow marine waters is not recorded. This however, assumes that the thermal tolerances of all bivalve species is the same. As it is known that different groups of marine invertebrates (Song et al., 2014) have different thermal tolerances, it is also likely bivalves had different tolerances to different thermal regimes during the early Toarcian (e.g. Zakharov et al., 2006). As such, the second and more likely option is that bivalves living in shallow marine waters were more resistant to environmental extremes, such as warming, than deeper forms.

The spatial distribution of bivalves can be controlled by the availability of nutrients (Bambach, 1993). Different metabolic demands could explain the abundance of epifaunal bivalves compared to infaunal bivalves in the Dobravitsa-1 section. In a more nutrient-poor carbonate system, metabolic demands of infaunal suspension feeding bivalves were probably not fulfilled and epifaunal bivalves thus dominated. This is supported by the lack of land-derived plant remains. Also, as land-derived nutrient supply decreases in an offshore direction, this might explain why a nutrient-supply control only appears to affect the more distal facies. The differential preferences of bivalves with respect to sediment and nutrient supply is supported by Fürsich et al. (2001) and Gahr (2005), who observed that brachiopods and epifaunal bivalves dominated and infaunal bivalves were relatively rare in habitats less affected by siliciclastic supply from land on the Iberian Peninsula in the Early Jurassic. In contrast, habitats affected by a higher siliciclastic supply were dominated by infaunal deposit-feeders and suspension-feeders.

Soupy substrate

Substrate type is a key factor for bivalve distribution, and it may change regionally and locally depending on bottom conditions, sediment supply, and water movement. Soupy substrate has been termed to explain a soft substrate which is unsuitable for some benthos. This hypothesis was suggested by Jablonski and Bottjer (1983) to explain the absence or rarity of infaunal suspension-feeders in the upper Cretaceous Chalk communities and later discussed by Wignall (1993) to highlight the importance of assessing oxygen levels versus substrate control within the Oxford Clay.

In the Boeva Mogila and Milanovo sections, some bioturbation is present, however, trace fossils are generally poorly preserved possibly due to this original consistency of sediment. Poor substrate suitability is a possible explanation for the paucity of benthic macrofauna in the Boeva Mogila and Milanovo sections, and of infaunal bivalves in the Dobravitsa-1 section. This explanation could be supplemented by nutrient availability and temporary fluctuations to dysoxic conditions.

The effect of the paucity of bivalves from deeper water sections is that most of the extinction record comes from shallow-water sections. This introduces sampling bias into the extinction record from the Moesian Basin, as not all paleoenvironmental settings are equally sampled. However, the bivalve record from the Dobravitsa-1 section (relatively deeper setting) shows a similar record of bivalve losses at the Pl-To boundary to shallower water settings. This suggests the possible sampling bias between paleoenvironmental settings, in this case, does not change or effect the main extinction horizons.

6.4.2 Comparison to other global records of the ETME

6.4.2.1 The extinction interval

The highest-resolution study of the ETME comes from the Cleveland Basin (Yorkshire Coast, UK) which provides a detailed record of bivalve losses (Little, 1995; Little and Benton, 1995; Caswell et al., 2009). The Cleveland Basin was situated in the Boreal realm and the early Toarcian is recorded in predominately organic rich laminated mudstones, that record the onset of anoxic facies in the latest *semicelatum* Zone that continue through the *falciferum* Zone (Wignall, 1991). In contrast, the extinction record from the Moesian Basin situated in the eastern EES records well-oxygenated conditions throughout the early Toarcian.

At a generic-level, the 3% loss recorded in Bulgaria is slightly lower than the 5% loss in bivalves from the Cleveland Basin (UK) (Little and Benton, 1995) and 8% estimated loss at a global level (Sepkoski and Raup, 1986). This study supports previous evidence that demonstrate only a small generic loss is recorded during the early Toarcian (Little and Benton, 1995).

At a species-level, 10 out of 13 species are lost at the extinction interval in Bulgaria (for the taxa identified to species level only), giving a 76% species loss. This is similar to the 78% species loss recorded for the Cleveland Basin by Harries and Little, (1999). Many of the same bivalve species are lost in the ETME from both the Bulgarian and Yorkshire Coast record. Of the thirteen bivalve species that suffered losses in the Moesian Basin, nine also became extinct during the ETME in the Cleveland Basin (Little, 1995). These were *Gryphaea gigantea, Pholadomya ambigua, Harpax spinosa, Pinna folium, Entolium lunare, Pseudopecten equivalvis, Pseudolimea acuticostata* and *Antiquilima* sp. *(*recorded as *A. succincta and A. hermanni* in the Moesian Basin*)*. The extinction of four additional species is recorded from the Moesian Basin: *Placunposis radiata, Goniomya hybrida, Plagiostoma punctata* and *Pinna radiata* (Figure 6.19).

Overall, the number of bivalve losses recorded at the Pl-To boundary are more in Bulgaria than on the Yorkshire Coast. Some bivalves are shown to become extinct earlier in Bulgaria than on the Yorkshire Coast. For example, the extinction of *Pinna folium, Entolium lunare* and *Pseudopecten equivalvis* are recorded at the Pl-To boundary in Bulgaria, but in the *tenuicostatum* Zone on the Yorkshire Coast. This provides evidence of the Signor-Lipps effect in Bulgaria (Signor and Lipps, 1982). This effect states that the final stratigraphic occurrence of any given taxon in a particular stratigraphic succession is unlikely to be the true final occurrence of that taxon in the basin as an effect of sampling (Signor and Lipps, 1982). The overall impact of this for the ETME record is that the extinction interval in bivalves may appear more severe at the Pl-To boundary in Bulgaria than the Yorkshire Coast. Considering the Signor-Lipps effect, the Pl-To boundary marks the oldest point in time at which the extinction of bivalves in Bulgaria could have occurred, as it records the last occurrence of numerous terminal taxon (Figure 6.19).

Wignall et al. (2005) suggested that in southern Europe benthic extinctions preceded pelagic extinctions, with the majority of benthic extinctions occurring at the Pl-To boundary and the majority of pelagic extinctions occurring at the *semicelatum* Subzone horizon. Wignall et al. (2005). suggested the opposite pattern happened in NW Europe. In the Moesian Basin, the significant loss of

benthic bivalves at the Pl-To boundary more closely resemble the extinction record from southern European, such as that noted by Wignall et al. (2005). However, as it is unclear if the Pl-To boundary marks the most severe part of the extinction in Bulgaria, this is difficult to assess. Further work would also be needed to understand pelagic losses in the Moesian Basin during the ETME. In addition this distinction suggested by Wignall (2005) has been questioned in later studies (Caswell et al., 2009). A summary of Toarcian micro- and macro-fossil extinctions and decreases in relative abundance shows relatively equal losses of benthic and pelagic fauna at the Pl-To boundary and in the *semicelatum* Zone (Caswell, 2009).

On the Yorkshire Coast, infaunal bivalves suffered the most losses during the ETME, with a 100% species loss at the extinction boundary (Little and Benton, 1995). Interestingly, in the Moesian Basin there appears to be no particular selectivity against infaunal bivalves during the ETME, with infaunal bivalve taxa present throughout the extinction and post-extinction interval (Figure 6.19). In the Moesian Basin, of the 12 species that became extinct, two were deep-infaunal, two were semi-infaunal and eight were epifaunal.

The less severe impact of the ETME on infaunal bivalves from the Moesian Basin might firstly be linked to the fewer number of infaunal bivalves present in the Moesian Basin prior to the extinction interval. In particular, the presence of numerous infaunal bivalves belonging to the genera *Mesosacella*, *Palaeonucula, Eotrapezium, Nicaniella* and *Protocardia*, which were common in the Cleveland Basin (Little and Benton, 1995; Caswell et al., 2009) are not recorded in the Moesian Basin.

A similar situation is also observed elsewhere in the EES with infaunal deposit feeding nuculids recorded in southern France but not in southern Spain (Fürsich et al., 2001). Southern France is characterised by similar organic-rich mudstones that are seen across NW Europe, including the Yorkshire Coast, considered to reflect the T-OAE (Fürsich et al., 2001). Conversely, southern Spain is characterised by shallow-shelf carbonates in well-oxygenated settings, similar to Bulgaria. This highlights that the different palaeoenvironmental conditions between the Boreal and Tethyan realm has a strong control on bivalve distributions. These palaeoenvironmental conditions likely comprised differences in oxygenation, substrate consistency, turbidity and rate of sedimentation (Fürsich et al., 2001).

The differences in palaeoenvironmental conditions, particularly in oxygenation levels are also likely to contribute to the more severe losses of infaunal bivalves in the Yorkshire Coast and other NW European sections such as France and

Germany (Röhl et al., 2001), where anoxic conditions prevented bivalves from surviving on the sea-floor for prolonged periods of time (Wignall et al., 2005; Danise et al., 2013).

6.4.2.2 The post-extinction interval

Following mass extinction events, a survival interval is often recorded. The term 'survival interval' was originally defined by Kauffman and Erwin (1995) and was amongst the early attempts to define the recovery stages of mass extinction events. The survival interval is characterised by low taxonomic richness, populated by opportunistic species, with extinction and origination rates being approximately equal. In Bulgaria the significant species-level loss (at least 76%), results in a diminished record of bivalves immediately after the extinction interval. Some bivalves recorded from Bulgaria become abundant in the post-extinction interval, including *Entolium* and *Coelastarte*.

Two species of *Entolium* are common in Bulgaria: *Entolium lunare* and *Entolium corenolum.* One species (*E. lunare*) goes extinct at the Pl-To boundary, and the other (*E. corneolum*) is recorded within and after the extinction interval (Figure 6.19). This bivalve appears to have had a preference for sandy facies (Johnson, 1984), and as such is not common in the Toarcian of Yorkshire Coast. In the upper *falciferum* Zone, following the extinction interval, horizons of abundant *Entolium* are recorded from the Kiselchov Dol section (Figure 6.20). The abundance of this bivalve could be linked to the biotic crisis, representing the survival interval in the Moesian Basin. However, it is possible that they are simply opportunistic taxa that experienced a boom in abundance under normal shifting environmental conditions, not necessarily in response to a biotic crisis (such taxa are identified by Harris and Kaufmann, 1996). This interpretation may be supported by the record of *Entolium* in the upper Pliensbachian (*margaritatus* Zone) of the Moesian Basin, in which almost monospecific horizons of *Entolium lunare* are recorded prior to the ETME (beds 17 and 18; Figure 6.20).

Figure 6.20 Bedding planes with abundant *Entolium* from the late Pliensbachian (*margaritatus* Zone) of the Brakyovtsi section (left) and early Toarcian (*falciferum* Zone) of the Kiselchov Dol section (right).

Coelastarte become common during the extinction interval and may represent an opportunistic taxon that appears in the basin following the loss of infaunal bivalves *Goniomya* and *Pholadomya*. An abundance of *Astarte* in the post extinction interval is not as common elsewhere in Europe, but has been recorded as a common taxon (*Astarte* cf. *velata*) in China (Wang and Sun, 1983) and tentatively from the *bifrons* Zone in north-eastern Panthalassa (Martindale and Aberhan, 2017). Bivalves belonging to the family Astartidae are more commonly associated with lower latitudes (Damborenea, 2002a).

The abundance of *Coelastarte* and *Entolium* in the post-extinction interval might represent initial stages of recovery in the Moesian Basin. However, a progressive recovery interval in Bulgaria is not clearly recorded. For example an interval comprising severely diminished taxa, or so called ‘poorly fossiliferous interval’ (Caswell et al., 2009), with only opportunistic epifaunal bivalves, is not recorded in Bulgaria. The poorly fossiliferous interval in the Yorkshire Coast is attributed to prolonged deoxygenation of the sea-floor during the T-OAE and after, lasting into the *falciferum* Zone (Little and Benton, 1995; Caswell and Coe, 2012).

The record of infaunal bivalves in the Moesian Basin following the ETME, including *Pleuromya costata, Mactrromya* sp. and *Coelastarte* sp. suggests a relatively quick recovery (Figure 6.19). This is in contrast with NW Europe, where diversity levels did not begin to increase until the *bifrons* Zone and infaunal organisms reappeared (Riegraf, 1985; Little and Benton, 1995; Fürsich et al., 2001; Röhl et al., 2001). The re-appearance of such taxa is recorded in the Yorkshire Coast with the appearance of infaunal bivalves such as *Dacromya ovum*, co-incident with a facies change, and considered to represent recovery

through sequential refilling of functional ecologies following losses following the extinction (Bambach et al., 2007). Although high-resolution records of the recovery interval in Bulgaria are hampered by the condensed nature of the sections, it is clear the bivalve ecosystem dynamics following the extinction interval were not as drastically affected as in the NW European sections.

A faster recovery in well-oxygenated settings through the ETME has also been suggested by Gómez and Goy, (2011) who state that recovery of most of the groups was relatively rapid in the well oxygenated environments of central Spain, although no further details are provided.

The study of bivalves from the Moesian Basin demonstrates that the response of bivalve taxa following the extinction interval has different recovery times, which could be due to the differing environmental stresses on the fauna across Europe (e.g. anoxia is not always the dominant control). Bivalve assemblages from the Moesian Basin, that continues to record infaunal bivalves following the extinction interval supports that recovery could have been hindered in the Cleveland Basin due to recurrent hypoxic events (Danise et al., 2015).

A delayed recovery in benthos from the T-OAE is also recorded in north eastern Panthalassa, where the primary cause of the extinction is linked to low oxygen (Martindale and Aberhan, 2017). The delayed recovery in benthos, in contrast to pelagic ammonite records (Dera et al., 2011; Caruthers et al., 2013; Caruthers et al., 2014) is attributed to decoupling of the benthic and pelagic communities in north eastern Panthalassa during the Early Jurassic (Martindale and Aberhan, 2017). Decoupling of benthic and pelagic faunas is linked to persistent oxygen stress; there is no evidence for such decoupling in the Moesian Basin as benthos appears to recover quickly.

6.4.3 Driving mechanisms of the ETME

There is no clear consensus on the causes of the early Toarcian mass extinction, although the ultimate cause is commonly attributed to the eruption of the Karoo-Ferrar LIP. The debate is centred around two hypothesis, with most authors arguing that the ETME was caused by the wide spread of anoxia, as part of the T-OAE (e.g. Jenkyns, 1988; Little and Benton, 1995; Harries and Little, 1999; Pálfy and Smith, 2000; Vörös, 2002; Bucefalo Palliani et al., 2002; Macchioni and Cecca, 2002; Aberhan and Baumiller, 2003; Hart et al., 2003; Mattioli et al., 2004; Tremolada et al., 2005; Wignall et al., 2005; Mailliot et al., 2006; Mailliot et al., 2009). Other authors have suggested the mass extinction is predominately caused by a rapid warming event, that occurred synchronously

with the mass extinction (e.g. Gómez et al., 2008; Gómez and Arias, 2010; Joral et al., 2011).

The bivalve data set presented from Bulgaria alongside new data for palaeoenvironmental change (Chapter 4 and 5) provides additional data for testing the different hypotheses.

6.4.3.1 Role of anoxia

There is no evidence for anoxic conditions or long-term oxygen deficiency in the Moesian Basin through the Lower Jurassic; this is supported by sedimentological, biotic and geochemical records (Chapter 5).

The presence of laminations in fine-grained sediments, such as organic rich mudrocks, reflects the absence of bioturbation animals and is used as an indirect indicator of reduced oxygen conditions (Savrda and Bottjer, 1989). A lack of laminated sediments recorded in the fine-grained marls and siltstones of Bulgaria, with TOC values averaging around 0.3 wt% TOC (maximum values 0.9 wt% TOC), some degree of bioturbation in all beds, the sedimentological and biotic records indicate no reduced anoxic conditions prevailed in the Moesian Basin (Chapter 5). However, further work such as quantification of the size and intensity of burrowing would allow further discrimination of different levels of sea-floor oxygenation.

A lack of opportunistic fauna commonly associated with low-oxygen conditions (Caswell et al., 2009) is further indication of a lack of long-term oxygen deficiency in the Moesian Basin (this chapter).

Framboidal pyrite petrography indicates that in general oxygenated conditions or conditions within the upper dysoxic zone prevailed, with no substantial development of anoxia within the water column (Chapter 5). It is possible that short lived, oxygen deficient intervals in relatively deeper parts of the Moesian Basin developed. There is no evidence for the expansion of any oxygen deficient conditions into the relatively shallower carbonate shelf sections (Chapter 5) in which the extinction event in bivalves is most clearly documented (this chapter).

The bivalve record from the early Toarcian *tenuicostatum* Zone, which comprises most of the extinction interval, records taxa predominately from ooidal ironstones, and bioclastic sandy ooidal limestones considered to represent relatively shallow marine environments that were well-oxygenated during the extinction interval. In contrast, a severely diminished record of

benthic taxa is recorded from the fine-grained marls and siltstones, though to represent relatively deeper marine settings. It could be argued that oxygen deficient conditions might have developed this these parts of the basin, causing the loss in benthic taxa, and a possible cause of the extinction is overlooked. However, the sedimentological and geochemical evidence does not support this (Chapter 5) and it is likely the lack of benthic fauna in these relatively deeper parts of the shelf is controlled by other factors such as unsuitable substrate, nutrient supply and temperature sensitivity of deeper-water bivalves, rather than prevailing hypoxic conditions.

Carbon isotope stratigraphy commonly shows a broad positive $\delta^{13}C$ excursion over the T-OAE, which is also recognised in Bulgaria from biogenic calcite. The record of this positive CIE, is interpreted as a result of globally increased burial rates of organic matter in the oceans and associated with the distribution of organic-rich black shales deposited in oxygen-depleted marine waters (Jenkyns 1988). The record of the positive CIE in Bulgaria records the expression of globally spread oxygen-depleted waters in which there was widespread burial of organic matter, and does not necessarily mean all basins during this time became anoxic.

This investigation of numerous study sites within the Moesian Basin, considered to represent a range of palaeoenvironmental settings within the basin suggests that a biotic crisis is recorded in bivalves, but there is no evidence of the development of long-term oxygen deficient conditions. This means that anoxia, linked to the T-OAE cannot be considered as a driving mechanism for the biotic crisis recorded in bivalves in the Moesian Basin, considered to be a regional expression of the mass extinction event.

A key result from this study is that anoxia cannot be attributed as a mechanism driving the biotic crisis seen in bivalves during the early Toarcian. This agrees with many other studies that record a significant loss of benthic taxa as part of the ETME in the southern Tethys, in depositional settings in which anoxia is not prevalent and is either lacking or thinly developed. This includes the brachiopods faunas in the Iberian and Lusitanian Basins (Joral et al., 2018), lithiotid bivalves in Morocco (Brame et al., 2018) and trace fossils in southern Spain (Rodríguez-Tovar et al., 2017).

One argument previously made against a mass extinction event driven by anoxia for the early Toarcian event, was the restriction of the laminated anoxic black shale facies predominately to NW European basins (e.g. Gómez and Goy, 2011). Although this originally led to consideration of the T-OAE to be called a Regional Anoxic Event (e.g. McArthur et al., 2007; McArthur et al., 2008), recent

studies have recorded the prevalence of low-oxygen conditions outside of Europe, in Argentina (e.g. Al-Suwaidi et al., 2010; Al-Suwaidi et al., 2016) and Canada (Martindale and Aberhan, 2017). Although the extent of oceanic anoxia, and therefore the presence of the T-OAE, has now been recorded globally, there are records of the mass extinction event in basins which have no strong links with these prevailing low-oxygen conditions (Gómez and Goy, 2011; Brame et al., 2018). Aberhan and Fürsich, (1996) recognised that Hallam (1986) and Hallam (1987) failed to differentiate between well-oxygenated and poorly oxygenated environments during the ETME, resulting in the role of anoxia as the extinction mechanism to be somewhat overestimated. Since Hallam's work, many authors have documented the extinction event in both-well oxygenated and poorly-oxygenated conditions. However, records of the ETME from well-oxygenated settings still appear to have received less attention over the years and anoxia remains to be attributed as the main cause of the mass extinction. This particular problem for the multitude of geochemical studies that work on characterising palaeoenvironmental and climatic records of the T-OAE interval, that commonly acknowledge a link to a severe biotic crisis attributable to anoxia, commonly citing NW European studies (Hallam, 1987; Little and Benton, 1995; Wignall et al., 2005; Danise et al., 2015). Such studies from NW Europe only provide the view of the ETME from poorly-oxygenated settings and the view of the ETME from well-oxygenated settings is more rarely considered, which in some cases, can hamper the global representation of the causes of the biotic crisis and even the extent of the T-OAE.

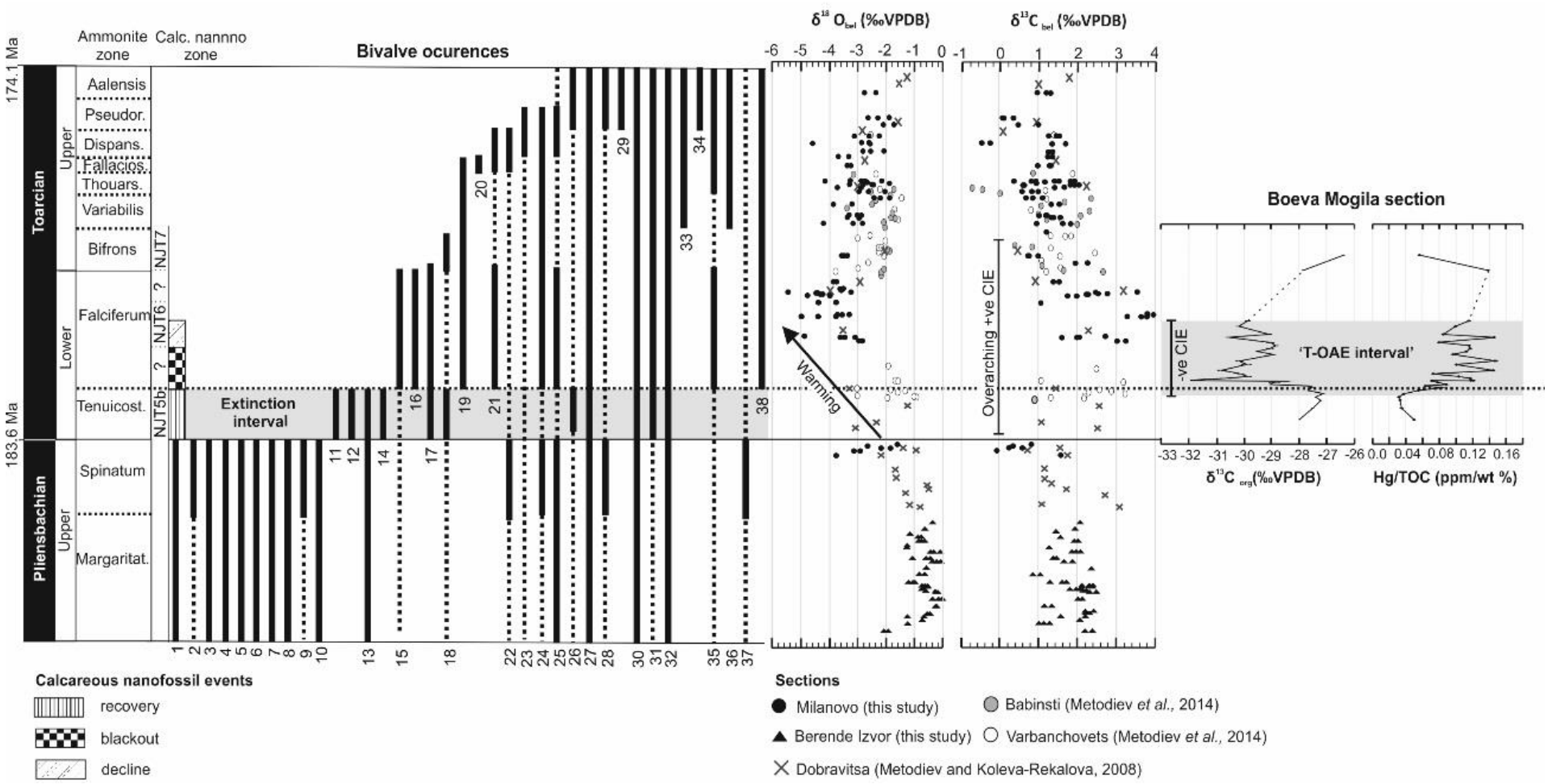

(PTO for caption)

Figure 6.21 (previous page). Composite of range data (upper Pliensbachian – upper Toarcian), calcareous nannofossil events, stable isotope trends (carbon and oxygen) and Hg/TOC records from this study. Range data plotted at ammonite zonal level, against the biostratigraphic framework of Metodiev (2008). Ages from the Geological Time Scale 2012 (Gradstein et al., 2012). Calcareous nannofossil biozones are included from the Boeva Mogila section (Chapter 3), and calacerous nannofossil events shown next to zones (Chapter 5). Bivalve range data: 1. *Pholadomya ambigua*, 2. *Antiqulima hermanni*, 3. *Gryphaea gigantea*, 4. *Antiqulima succincta*, 5. *Gryphaea* sp., 6. *Harpax spinosa*, 7. *Pseudopecten equivalvis*, 8. *Pinna radiata*, 9. *Pinna folium*, 10. *Plagiostoma punctata*, 11. *Pseudolimea* cf*. acuticostata*, 12. *Goniomya hybrida*, 13. *Entolium lunare*, 14. *Placunopsis radiata*, 15. *Mactromya* sp., 16. *Ctenostreon* sp., 17. *Camptonectes auritus*, 18. *Oxytoma inequivalvis*, 19. *Propeamuseum pumilum*, 20. *Trigonia* sp., 21. *Grammatodon* cf. *insons*, 22. *Pseudolimea pectinoides*, 23. *Chlamys* sp., 24. *Plagiostoma* sp., 25. *Pleuromya* sp., 26. *Eopecten* cf. *velatus*, 27. *Pleuromya costata*, 28. *Weyla* sp., 29. *Pholadomya fidicula*, 30. *Chlamys textoria*, 31. *Liostrea* sp., 32. *Entolium* sp., 33. *Gresslya* sp., 34. *Pinna* sp., 35. *Antiqulima* sp., 36. *Entolium corneolum*, 37. *Modiolus* sp., 38. *Coelastarte* sp. Stable isotope data for $\delta^{18}O_{bel}$ and $\delta^{13}C_{bel}$ is shown for all sections, except for belemnites from the Beledie Han sections, as belemnites are considered to be diagenetically altered (Chapter 4). $\delta^{13}C_{org}$ and Hg/TOC values are shown for the Boeva Mogila section (Chapter 5).

6.4.3.2 Role of warming

Given that oxygen depletion is an unlikely driver for the regional crisis in bivalves in the Moesian Basin, reflective of the ETME, other causative mechanisms must be assessed. An explanation for the biotic crisis in the Moesian Basin, must account for the crisis recorded in well-oxygenated settings. Other key palaeoenvironmental changes that have been considered as driving mechanisms include, but are not limited to, a rise in seawater temperature, sea level fluctuations and changing current dynamics (McArthur et al., 2000; Bailey et al., 2003; Suan et al., 2008; McArthur et al., 2008; Dera et al., 2010; Suan et al., 2010; Dera and Donnadieu, 2012). Such driving mechanisms also play a role in the ETME where anoxia is present. In the Cleveland Basin, a statistical study on how benthic communities responded to environmental change showed the onset of anoxia and the extinction horizon coincided with both a rise in temperature and sea level (Danise et al., 2015).

In the Moesian Basin, seawater temperatures, which are reflected in $\delta^{18}O_{bel,}$ indicate a progressive warming of seawater temperatures throughout the early Jurassic (*tenuicostatum-falciferum* Zone), synchronous with increased influx of freshwater into the basin (Chapter 4). The extinction interval, recording the

disappearance of many bivalve species, occurs at the start of this seawater warming trend in the Moesian Basin (Figure 6.21). However, $\delta^{18}O_{bel}$ values through the *tenuicostatum* Zone are relatively sparse, and although a general warming trend is clearly documented, high-resolution records of temperature increase through this interval are limited. Although there is a link between warming seawater temperatures and the extinction event in the Moesian Basin, temperature cannot confidently be assigned as the sole cause for the biotic crisis documented in bivalves, with more work required to understand the roles of current dynamics, nutrient supply, productivity, endemism and migration which may have all also influenced biotic crisis recorded (e.g. Aberhan and Fürsich, 1996).

6.4.3.3 The influence of sea-level changes during the extinction interval in the Moesian Basin

Although there is a long-term transgression from the Hettangian-Toarcian, there is no major facies change across the Pliensbachian-Toarcian interval in the Moesian Basin. There is evidence of a deepening in the upper Pliensbachian, represented by change from Dolni Lukovit Member to Bukorovtsi Member, which is diachronously recorded in the upper Pliensbachian. There is some indication that minor sea-level fluctuations resulted in colour changes to the sediments, seen in both the Gorno Ozirovo and Dobravitsa-1 sections that may reflect global sea-level changes. The possible transgression recorded during the late Pliensbachian that continues into the early Toarcian resembles the global sea-level curve for the NW Boreal Lower Jurassic sections (Hallam, 2001). However, expression of global sea-level changes are not simultaneously reflected in all sections. It is likely that local tectonics and subsidence dampened the effects of global sea-level rise as more proximal settings show no major synchronous lithological change at the Pl-To boundary or during the early Toarcian. Therefore. Global sea level changes may have a minor contribution to the biotic crisis in bivalves, documented in the Moesian Basin. However, the extinction horizons do not relate to a sudden change in water depth across the Moesian Basin, synchronous with the extinction. Therefore, sea level changes are unlikely to be a main driving mechanism for the ETME. This is important to note as changes in water depth have been attributed to potentially misidentifying mass extinction events, in which last occurrences are controlled by sea-level changes, causing changes in habitats, rather than species loss (Holland and Patzkowsky, 2015).

6.4.3.4 Timing of Extinction interval, Karoo-Ferrar LIP volcanism and carbon cycle perturbations

Severe climate warming during the early Toarcian has been attributed to the eruption of the Karoo-Ferrar LIP (Pálfy and Smith, 2000; Bond and Wignall, 2014). In this study, an increase in Hg values during the early Toarcian tentatively provides evidence of increased volcanism recorded in the Moesian Basin (Chapter 5). However, due to a lack of exposure and a hiatus at the Pl-To boundary in sections from the Moesian Basin the record only shows an increase in Hg/TOC values across the *tenuicostatum-falciferum* Zone boundary, at the top of the extinction interval, co-incident with the negative CIE recorded in organic carbon, as part of the 'T-OAE interval' (Figure 6.21).

The timing and causal relationships between the biotic crisis, eruptive phases of Karoo-Ferrar and the negative CIE have been widely debated, as the biotic crisis and carbonate production decrease appear to have initiated earlier than the onset of Karoo-Ferrar and the 'T-OAE' interval. However, studies are now recognising that the early Toarcian palaeoenvironmental crisis occurred in two distinct episodes that most likely related to two successive phases of intense volcanic degassing in the Karoo-Ferrar province (e.g. Suan et al., 2008). Recent work from Llanbedr (Mochras Farm), Cardigan Bay, UK has provided a high resolution stratigraphic framework which provides a new, precise correlation with the basalt lava sequence of the Karoo–Ferrar Large Igneous Province. This work has linked the Pl–To boundary and T-OAE climatic and environmental perturbations directly to this episode of major volcanic activity (Xu et al., 2018a,b). Additional evidence for perturbations at the Pl-To boundary alongside evidence of increased volcanism include recognition of a small negative CIE (Littler et al., 2010; Bodin et al., 2016; Xu et al., 2018a) and evidence of increased weathering (Percival et al., 2015). These perturbations in the carbon cycle, hydrological cycle and evidence of increased volcanic activity during both the Pl-To boundary and later, towards the top of the *tenuicostatum* Zone are considered to be of a global nature. These times of severe environmental change link to the extinction interval recognised in the Moesian Basin (Figure 6.21). This study shows the negative CIE recorded in organic matter occurs after the main extinction interval. A further negative CIE might be recorded at the Pl-To boundary, but further work is needed to constrain the palaeoenvironmental changes across the Pl-To boundary in Bulgaria.

6.4.4 Evidence for carbonate production crisis

A carbonate production crisis has been documented in the early Toarcian, characterised by the near disappearance of shallow water platforms in the early Toarcian (Sabatino et al., 2013), recording a significant drop in calcium carbonate contents in basinal successions and by a nannofossil biocalcification crisis during the T-OAE (Mattioli et al., 2004; Tremolada et al., 2005).

Calcareous nannofossils documented through the early Toarcian Boeva Mogila show a drastic decline in diversity in the *tenuicostatum* Zone, followed by an interval almost devoid of these taxa that begins just before the *tenuicostatum-falciferum* Zone boundary. This notable decrease in calcareous nannofossil abundance, termed a 'nannofossil blackout' that onsets at the top of the *tenuicostatum* Zone, coincident with the onset of the negative CIE recorded in organic matter that characterises the 'T-OAE' interval.

It is likely the sudden decrease in calcareous nannofossils represents a true decrease in abundance rather than sampling bias that may affect bivalves as the small size of the calcareous nannoplankton gives rise to more continuous preservation potential and does not present the same sampling bias problems that macrofossils do. A similar pattern is also recorded in North Yorkshire from the Jet Rock and is considered to be a response to stressful environmental conditions, rather than an extinction event, because the great majority of the species reappear (Bucefalo Palliani et al., 2002).

Increased carbon dioxide levels, as a result of flood basalt volcanism or gas hydrate dissociation, have been suggested as a possible trigger for the nannoplankton biocalcification crisis during the OAE (Mattioli et al., 2004; Tremolada et al., 2005). Exactly how changes in temperature and pCO_2 affects calcareous nannofossils is still somewhat debated, but it likely influenced by external factors such as water temperature, nutrient concentrations and salinity (Winter et al., 2006), that affect their metabolism and diversity (Spielmeyer and Pohnert, 2012; Lewandowska et al., 2012). These same triggering mechanisms may be assumed for the calcareous nannofossils, decline and blackout during the early Toarcian in the Moesian Basin.

6.4.5 Palaeobiogeographic affinity of fauna in the Moesian Basin

This study shows Pliensbachian and Toarcian bivalves in the Moesian Basin are associated with the southern Tethyan transitional province (STTP) (sensu Damborenea, 2017). The STTP, is part of the Tethyan realm and encompasses areas of western Europe including northern Spain and southern France in the Early Jurassic (Liu, 1995; Damborenea, 2017). This work, supports the studies of Radulović (2013) and Radulović et al. (2017) who attributed the Pliensbachian bivalve faunas of eastern Serbia to the Tethyan realm, although consideration of province assignment was not suggested. This study also provides the first Toarcian record of bivalve palaeobiogeographic affinity from the Moesian Basin, showing a bivalve affinity with the Tethyan realm through both the Pliensbachian and Toarcian interval. The palaeogeographic affinity of Pliensbachian and Toarcian bivalves from Bulgaria, suggested here to belong to the STTP, extends the known extent of this province further eastwards across the EES than previously known (Figure 6.22). The occurrence of a transitional zone between northwest Europe and the Mediterranean regions, is recorded by Vörös (2016) for brachiopod faunas through the Pliensbachian, who suggests the extension of this transitional unit, similar to that of the STTP, extended in a north-easterly direction through southern France, Hungary, Romania and Serbia, towards the slightly higher palaeolatitude of eastern Europe. This suggests both bivalve and brachiopod faunas showed similar transitional affinities during the Pliensbachian.

Interestingly, lithiotid bivalves are not recorded in Bulgaria. Lithiotid bivalves were a common occurrence in bivalve faunas in the Tethyan realm. These bivalves were reef formers or associated with reef environments, and characterised the ‘Lithiotis facies’, that became severely diminished during the ETME (Brame et al., 2018). The lack of these reef-forming bivalves in Bulgaria could be due to the slightly higher palaeolatitude of the Moesian Basin, as all other occurrences of Lithiotis facies are at lower palaeolatitudes (Figure 6.22) and no reefs are recorded from the Moesian Basin. Additionally, lithiotid bivalve associations most commonly form on carbonate platforms (Posenato and Masetti, 2012; Posenato et al., 2013), which did not develop in the Moesian Basin until the Late Jurassic.

The Tethyan affinity of Pliensbachian and Toarcian bivalves recorded from the Moesian Basin is in contrast to the Boreal affinities attributed to ammonites (Metodiev, 2008) and calcareous nannofossils (Chapter 3, Section 3.7.3).

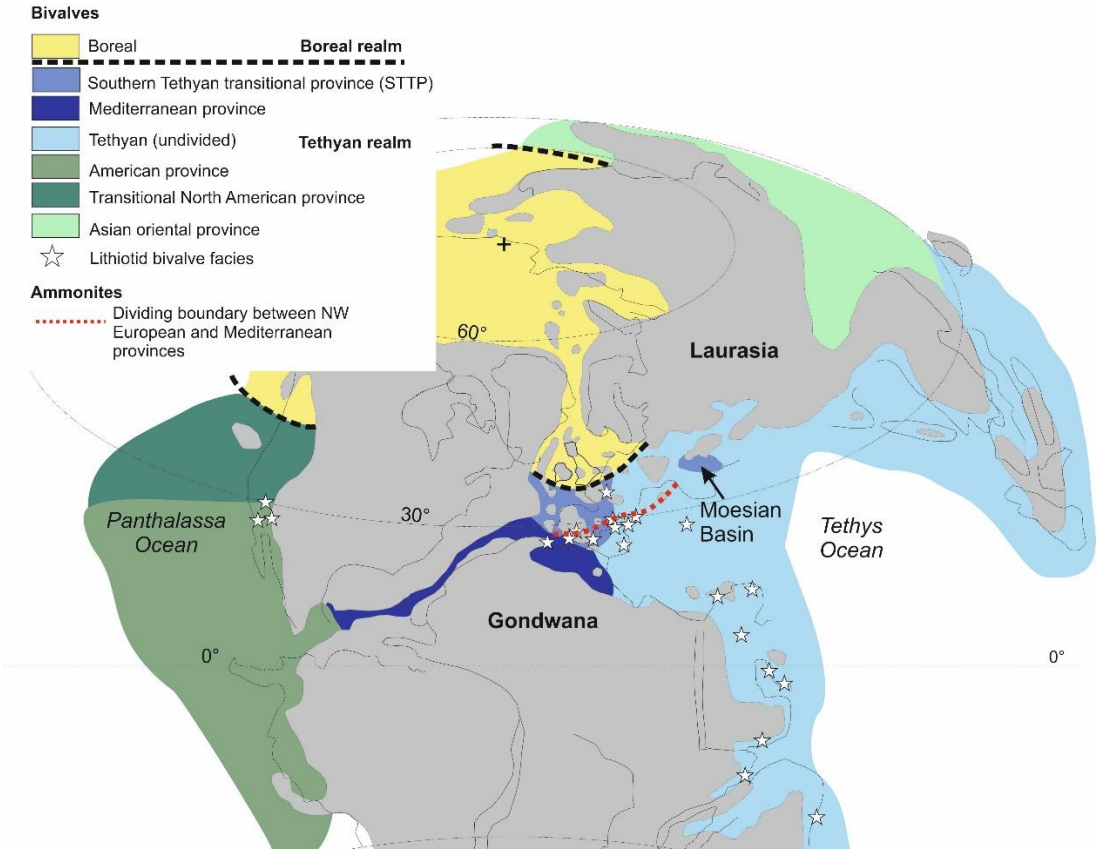

Figure 6.22 Early Jurassic bivalve marine palaeobiogeographic provinces during the Pliensbachian-Toarcian, modified after Damborenea (2017). Tethyan (undivided) shown in light blue to show regions lacking in detailed paleobiogeographic studies of bivalves that have not been assigned to a province Main divide in ammonite provinces during the Pliensbachian, between NW Europe and Mediterranean faunas modified after Dommergues et al. (2009). Base map modified after Golonka (2002).

The boundaries of provinces based on ammonites and bivalves do not always coincide and these boundaries often change depending on faunal group within a so-called broad transitional zone between the Boreal realm and Mediterranean province (Liu et al., 1998). Such discrepancies in the position of the faunal affinities between ammonites and bivalves has been noted for the Pliensbachian, with the boundary between the Boreal and Tethyan realm positioned in southern Spain for ammonites and in northern France for bivalves (Liu et al., 1998). Although such differences are noted in the western region of EES, they are poorly recognised in the eastern EES, and thus are highlighted in this study.

The distribution of faunas has been attributed to a multitude of factors by past authors and include both biotic and abiotic controls. Biotic controls suggested as an explanation for the distribution pattern of organisms include larval type, life habits, reproductive strategies, and competition (Hallam, 1975). Abiotic controls include changes in sea-level (Hallam, 1975; Hallam, 1977),

palaeogeography (Page, 2003; Dommergues et al., 2009), ocean circulation (Liu et al., 1998), salinity and seawater temperature (Neumayr, 1883; Brayard et al., 2006; Brayard et al., 2007). It is likely some combination of governing factors are responsible for the differences in faunal affinity between bivalves (Tethyan affinity), and ammonites and calcareous nannofossils (Boreal affinity). But it is clear from the work in Bulgaria that the prominent controls were different depending on the faunal group (e.g. ammonites, bivalves or calcareous nannofossils).

Since similar seawater temperatures are documented from Bulgaria as elsewhere in the EES (Chapter 4), it is unlikely this was a prominent control. This is supported by previous studies that suggest seawater temperatures were not a controlling factor for provincialism in Pliensbachian ammonites between the NW Boreal and Tethyan realms (Dommergues et al., 2009) or distribution of Early Jurassic belemnites (Doyle et al., 1994). Since no major differences in water-depth are recorded between the northern EES and southern EES, this was also an unlikely key control in causing the differences in ammonite and bivalve affinities. Additionally, physical barriers and marine connections were a key factor in the global distribution of bivalves in the Lower Jurassic. However, when considering distribution patterns of bivalves only across the EES, physical barriers play a much less significant role, as there are no major landmasses separating oceans across the EES, only scattered archipelagoes (Liu et al., 1998).

How the ammonite and bivalve taxa actually distributed themselves across the EES may have played a major part in the differences in faunal affinities in the Moesian Basin. For example, bivalves are nearly exclusively benthic, with a larval dispersal stage, whereas ammonites are nektonic and actively spread through swimming. This would imply that the distribution pattern of bivalves would have been influenced more by oceanic circulation than that of ammonites. A northward directed current has been suggested to explain the discrepancy between the Boreal and Tethyan realm boundary between ammonites and bivalves in the western EES by Liu (1995).

6.5 Conclusions

A comprehensive and up-to-date record of the stratigraphical distribution of Lower Jurassic bivalves (Sinemurian-Toarcian) is recorded in Bulgaria. This study provides one of the first detailed bivalve records from eastern Europe in which a biotic crisis is recorded in the early Toarcian (during the Pl-To boundary

to top of the *tenuicostatum* Zone), that can be recognised as part of the ETME. The spatial distribution of bivalves during the early Toarcian was likely controlled by substrate, facies type and nutrient availability. A calcareous nannofossil crisis is recorded from the top of the *tenuicostatum* Zone, co-incident with the negative CIE recorded in organic carbon. In the Bulgarian sections, a lack of organic rich mudstones (‘black shales’) and continued bioturbation through the early Toarcian interval render oxygen-deficiency an unlikely driver of the biotic crisis. Rapid warming of seawater temperatures are tentatively suggested as a key driving mechanism, triggered by the eruption of the Karoo-Ferrar LIP.

Chapter 7 Conclusions and further work

7.1 Conclusions

7.1.1 Improvements to the biostratigraphic and chemostratigraphic framework of Lower Jurassic successions in Bulgaria

New data from Bulgaria has improved parts of the Lower Jurassic biostratigraphic framework. The *ibex* Zone of the early Pliensbachian was identified for the first time in Bulgaria. In addition, the first record of Toarcian calcareous nannofossils are recorded for Bulgaria, belonging to the NJT4a, NJT5b, NJT6, NJT7a and NJT7b Zones.

New chemostratigraphic records are provided for the Pliensbachian and Toarcian. Strontium isotope and carbon isotope stratigraphy confirms the biostratigraphic dating of the Toarcian in the Milanovo section, and carbon isotopes allow major perturbations in the carbon cycle recorded from the Boeva Mogila section to be globally correlated.

7.1.2 Environmental perturbations and characterisation of the T-OAE in the Moesian Basin during the Lower Jurassic

Early Toarcian carbon isotope records from belemnites show a long-term positive isotope excursion (~ 3 ‰ positive shift), interrupted by a negative CIE recorded in organic matter (~3.5 ‰ negative shift). This is the first record of the negative CIE from the easterly edge of the EES, and the shift is of a similar magnitude to coeval global records. Methane hydrate disassociation or carbon released thermogenically from organic matter have been suggested as causes for the negative CIE, ultimately triggered by Karoo-Ferrar LIP. The cause of the overarching positive CIE is attributed to the global burial of organic rich sediments. Oxygen isotope records indicate intervals of relatively cooler seawater temperatures during the late Pliensbachian (*margaritatus* Zone and *spinatum* Zone). Oxygen isotope records also indicate a rapid increase in seawater temperatures in the Moesian Basin, alongside a likely increase in freshwater influx. This reflects the severe climate change recorded globally in the Early Jurassic.

There is no evidence for anoxia in the Moesian Basin, a setting proximal to the open ocean. This is indicated by the lack of laminated sediments and overall low TOC values (average 0.3 wt%, maximum 1 wt%). However, framboid petrography indicates short-lived oxygen deficient intervals may have intermittently developed in deeper parts of the basin throughout the Toarcian. This study indicates that the prevalent oxygen-deficient conditions, that resulted in the deposition of black shales in the basins of the EES, did not develop in the NW Tethyan shelf margin location observed in Bulgaria.

This study also highlights the need for a more careful use of the term T-OAE, which has been defined using a variety of palaeoenvironmental changes (e.g. carbon cycle perturbations, increased hydrological cycle, rapid warming) and not necessarily on the development of oxygen-depleted facies. Therefore, it is important to explain what is being defined as the 'T-OAE' in each study, so that the spatial extent and effects of oceanic anoxia can be clearly understood.

7.1.3 The ETME and causal mechanisms

A biotic crisis is recorded amongst bivalves in Bulgaria in an interval spanning the Pl-To boundary to the top of the early Toarcian *tenuicostatum* zone. This event reflects the globally documented ETME. It is here recorded for the first time in Bulgaria, and provides the most easterly record of the event amongst bivalves from the EES. The Bulgarian record is that of extinctions on a shallow marine carbonate shelf, a facies unlike those from other areas with contemporary bivalve extinctions. An extinction loss of 76% is recorded at species level, similar to that recorded in the well-known Yorkshire Coast records. In contract to the Yorkshire Coast records, there appears to be no particular selectivity against infaunal bivalves during the ETME in the Moesian Basin. The most significant loses amongst benthic bivalves in the Moesian Basin occur at the Pl-To boundary, similar to the extinction pattern observed across southern Europe.

The linked records of environmental, carbon cycle and faunal change, and volcanic activity from Bulgaria provide insight into the causal mechanisms for the extinction. Although a significant loss amongst bivalves during the ETME has in many cases been recorded to coincide with the spread of anoxia, this link is not seen in Bulgaria. As such, oxygen deficiency cannot be considered a key driving mechanism for the ETME in this part of the ocean, and other factors such as rapid warming, driven by the eruption of the Karoo-Ferrar LIP, may have played a more significant role.

There is some evidence for Karoo-Ferrar volcanic activity, indicated by enrichments in Hg in the Moesian Basin. Mercury (Hg)/total organic carbon (TOC) ratios from two sections in the Moesian Basin showed relatively elevated values at beginning and the end of the *semicelatum* Subzone (*tenuicostatum* Zone) and continuing into the *falciferum* Zone of the Toarcian. The relative enrichment in Hg does not show any correlation with redox or sedimentation rate variations during the Toarcian interval. These enrichments are similar to those reported in previous studies using Hg as a volcanic tracer in the early Toarcian, although the size of shifts is relatively smaller. However, the record of increased shifts above background levels suggests an exogenous environmental loading of Hg and subsequent enrichment in sediments.

The onset of an increased shift in Hg/TOC and negative CIE marks only the top of the extinction interval recorded in the Moesian Basin. A hiatus at the Pl-To boundary precludes understanding of possible equivalent changes that may have occurred at the start of the extinction interval. Evidence for an earlier eruptive phase of LIP volcanism has been reported for the Pl-To boundary elsewhere in the EES and this is considered to be the key driving mechanism for severe climatic change and the marine extinction in Bulgaria.

7.2 Outlook and suggestions for future work

Data generated for this thesis has raised several interesting questions that could be explored with further work.

1. **Do other marine invertebrate groups, such as brachiopods, suffer a biotic crisis in the early Toarcian in the Moesian Basin? Do they show body size changes that can provide further insight on the role of temperature related stresses?**
   Data presented in Chapter 7 record a biotic crisis in bivalves during the early Toarcian of the Moesian Basin that is considered to be a local representation of the global early Toarcian Mass extinction (ETME). Future work could determine if the ETME is also seen in other fossil groups, such as brachiopods. Brachiopod specimens have been collected bed by bed during the field seasons in this PhD study (comprising over 450 brachiopod specimens), although time constraints did not allow for taxonomic identification and further work on these samples during this PhD. This

collection could provide an initial test suite of specimens with which these questions could begin to be answered.

Recording the ranges of brachiopods through the Toarcian in Bulgaria would be interesting as the ETME represents the most severe post-Palaeozoic extinction of brachiopods, with the loss of two orders Spiriferinida and Athyridida, and a high turnover amongst the Rhynchonellida (Joral et al., 2011; Baeza-Carratalá et al., 2015; Vörös et al., 2016). Previous work on brachiopods from Bulgaria was published by Tchoumatchenco (1966), Tchoumatchenco (1972), Tchoumatchenco (1977) and Tchoumatchenco (1978), but these do not report Toarcian taxa and so the ETME cannot be assessed. The Bulgarian brachiopod record could considerably extend our understanding of the ETME in the eastern EES, allowing comparison with data from Serbia (Ruban and Vörös, 2015; Radulović et al., 2016), Turkey (Vörös and Kandemir, 2011) and the Caucasus (Ruban, 2004; Ruban, 2006).

Additionally, ongoing work has shown body size changes in brachiopods prior to the biotic crises during the ETME, in the Lusitanian Basin (Portugal) and Iberian Basin (Spain) (García Joral et al., 2018). A comparative study of body size variations in brachiopods, and potentially molluscan taxa, from the Moesian Basin could test if similar relative size changes are also recorded. Understanding size changes around the ETME interval from different palaeogeographic locations could help further test the relative roles of temperature, palaeobathymetry, and terrigenous input, which could be causing these size changes (Joral et al., 2018). This could help provide a more robust understanding of the significance of temperature related stresses during this critical early Toarcian interval.

2. **Can we further understand redox conditions in the Moesian Basin?**
   Data presented in Chapter 5 and 6 indicates long-term anoxia did not develop in the Moesian Basin during the early Toarcian and therefore was not a major contributing factor in the ETME in this part of the eastern Epicontinental Tethys. However, there were some benthic redox fluctuations in the deeper parts of the basin during the Early Jurassic, despite the bioturbated nature of the sediment. Further examination of these fluctuating redox conditions, could use additional geochemical proxies, e.g. Mo, U, V, and Zn (Algeo and Maynard, 2004). This would provide further detail on oxygen fluctuations between oxic and dysoxic conditions in the Moesian Basin that could be better indicators of redox from carbonate environments

than pyrite framboids. This would contribute to better documenting the spatial variability of palaeoenvironmental conditions during the T-OAE across the EES, in basins where anoxia is not well-developed.

3. **Improving the age model for the Lower Jurassic of the Moesian Basin**
   Although an ammonite biostratigraphic framework has been established for the Lower Jurassic and is successfully used to date Toarcian sections (Metodiev, 2008), the paucity of ammonites through the earlier stages of the Lower Jurassic (Hettangian, Sinemurian and the lower Pliensbachian) only allows for low biostratigraphic resolution of these stages. Increased sampling has provided new ammonite records (such as the first recognition of the *ibex* Zone in Bulgaria – see Chapter 3) and identification of the rarely recognised *jamesoni* Zone in Bulgaria (see also Chapter 3). An increased sampling effort for ammonites has provided additional biostratigraphic constraint for the Pliensbachian interval. However, a more robust age model for many sections is still required, and other dating methods should to be used. This could include further work on strontium isotope stratigraphy, and calcareous nannofossil and palynological biostratigraphy. This thesis has provided initial attempts at some of these dating methods (Chapter 3), with the first recognition of calcareous nannofossils from Bulgaria. Continued work on the Toarcian interval and additional work on the earlier stages of the Lower Jurassic would provide a higher resolution biostratigraphic and chemostratigraphic record for this relatively understudied part of the EES. Improved age models for the stratigraphy of the Moesian Basin would also help with understanding the basin evolution in the Early Jurassic, which is currently poorly constrained.

4. **Is there evidence for increased weathering as a response to Karoo-Ferrar LIP volcanism and climate warming in the Moesian Basin?**
   Eruption of the Karoo-Ferrar LIP is proposed to have caused abrupt environmental change caused by the eruption of large amounts of CO_2. This included global warming, which increased the hydrological cycle, enhancing continental weathering and consequent burial of large amounts of organic matter (Jenkyns, 1988).

   In the early Toarcian of the Moesian Basin this study records a positive CIE reflecting the global burial of organic matter (Chapter 4), increased Hg/TOC values postulated to link to increased volcanism (Chapter 5) and a negative $\delta^{18}O_{bel}$ trend attributed to both an increase in seawater temperatures and the

influx of freshwater run-off into the basin (Chapter 4). Further work could be done to understand changes in continental weathering rates into the Moesian Basin. Regional changes can be estimated from the osmium isotope record of seawater (e.g. Cohen et al., 1999; Cohen et al., 2004).

Osmium isotopes have been used as a proxy for continental weathering during the early Toarcian in NW Europe from the Yorkshire Coast (UK) (Cohen et al., 2004b) and Llanbedr (Mochras farm) borehole (UK) (Percival et al., 2016). These records show an increase of $^{187}Os/^{186}Os$ across both the Pl-To boundary and during the T-OAE interval. The degree to which the Yorkshire Coast record is representative of the open ocean has been questioned (McArthur et al., 2008). Records from the Llanbedr (Mochras Farm) borehole show similar trends and have been argued to record an open ocean signal (Percival et al., 2016). Nonetheless, these sections are still palaeogeographically located within the shallow marine epicontinental seaway. As the Moesian Basin is considered to be open-ocean facing and sits on the eastern edge of the EES, it would be interesting to see how the osmium isotope record compares to NW European records. This would allow further understanding between the links between volcanism, weathering and climate that were instrumental in driving episodes of environmental change. Palaeoenvironmental changes which have now been recorded during both the Pl-To boundary and the early Toarcian. Understanding records across the Pl-To boundary is particularly important for assessing the driving mechanisms for the biotic crisis in the Moesian Basin that, for bivalves, is recorded prior to the ‘T-OAE interval’ (Chapter 6).

References

Aberhan, M. 1994. Early Jurassic Bivalvia of northern Chile. Part 1. Subclasses Palaeotaxodonta, Pteriomorphia, and Isofilibranchia. *Beringeria,*. **13**(3), pp.3–115.

Aberhan, M. 2001. Bivalve palaeobiogeography and the Hispanic Corridor: time of opening and effectiveness of a proto-Atlantic seaway. *Palaeogeography, Palaeoclimatology, Palaeoecology*. **165**(3–4), pp.375–394.

Aberhan, M. 2004. *Early Jurassic Bivalvia of northern Chile. Part II. Subclass Anomalodesmata*. Würzburg.

Aberhan, M. 1992. Palökologie und zeitliche Verbreitung benthischer Faunengemeinschaften im Unterjura von Chile. *Beringeria*. **5**, pp.3–174.

Aberhan, M. and Baumiller, T.K. 2003. Selective extinction among Early Jurassic bivalves: A consequence of anoxia. *Geology*. **31**(12), p.1077.

Aberhan, M. and Fürsich, F.T. 1996. Diversity analysis of Lower Jurassic bivalves of the Andean Basin and the Pliensbachian-Toarcian mass extinction. *Lethaia*. **29**(2), pp.181–195.

Aberhan, M. and Fürsich, F.T. 2000. Mass origination versus mass extinction: the biological contribution to the Pliensbachian-Toarcian extinction event. *Journal of the Geological Society*. **157**(1), pp.55–60.

Aberhan, M., Scholz, A. and Schubert, S. 2011. Das ober-pliensbachium (domerium) der Herforderc Liasmulde - Teil 3 - Taxonomie und paläoökologie der bivalvia aus der Amaltheenton- formation (unterjura) der Herforder Liasmulde. *Geologie und Palaeontologie in Westfalen*. (80), pp.61–109.

Ait-Itto, F.Z., Price, G.D., Ait Addi, A., Chafiki, D. and Mannani, I. 2017. Bulk-carbonate and belemnite carbon-isotope records across the Pliensbachian-Toarcian boundary on the northern margin of Gondwana (Issouka, Middle Atlas, Morocco). *Palaeogeography, Palaeoclimatology, Palaeoecology*. **466**, pp.128–136.

Al-Suwaidi, A.H., Angelozzi, G.N., Baudin, F., Damborenea, S.E., Hesselbo, S.P., Jenkyns, H.C., Manceñido, M.O. and Riccardi, A.C. 2010. First record of the Early Toarcian Oceanic Anoxic Event from the Southern Hemisphere, Neuquén Basin, Argentina. *Journal of the Geological Society*. **167**(4), pp.633–636.

Al-Suwaidi, A.H., Hesselbo, S.P., Damborenea, S.E., Manceñido, M.O., Jenkyns, H.C., Riccardi, A.C., Angelozzi, G.N. and Baudin, F. 2016. The Toarcian Oceanic Anoxic Event (Early Jurassic) in the Neuquén Basin, Argentina: A Reassessment of Age and Carbon Isotope Stratigraphy. *The Journal of Geology*. **124**(2), pp.171–193.

Algeo, T.J. and Maynard, J.B. 2004. Trace-element behavior and redox facies in core shales of Upper Pennsylvanian Kansas-type cyclothems. *Chemical Geology*. **206**(3–4), pp.289–318.

Anderson, T.F. and Arthur, M.A. 1983. Stable Isotopes of Oxygen and Carbon and Their Application To Sedimentologic and Paleoenvironmental Problems *In*: *Stable Isotopes in Sedimentary Geology - SEPM Short Course*, pp.1–151.

Arias, C. 2009. Extinction pattern of marine Ostracoda across the Pliensbachian-Toarcian boundary in the Cordillera Ibérica, NE Spain: Causes and consequences. *Geobios*. **42**(1), pp.1–15.

Arkell, W.J. 1956. Jurassic geology of the World. *Journal of Paleontology*. **30**(6), pp.1376–1377.

Armendáriz, M., Rosales, I., Bádenas, B., Aurell, M., García-Ramos, J.C. and Piñuela, L. 2012. High-resolution chemostratigraphic records from Lower Pliensbachian belemnites: Palaeoclimatic perturbations, organic facies and water mass exchange (Asturian basin, northern Spain). *Palaeogeography, Palaeoclimatology, Palaeoecology*. **333–334**, pp.178–191.

Armendáriz, M., Rosales, I., Bádenas, B., Piñuela, L., Aurell, M. and García-Ramos, J.C. 2013. An approach to estimate Lower Jurassic seawater oxygen-isotope composition using δ18O and Mg/Ca ratios of belemnite calcites (Early Pliensbachian, northern Spain). *Terra Nova*. **25**(6), pp.439–445.

Baeza-Carratalá, J.F., García Joral, F., Giannetti, A. and Tent-Manclús, J.E. 2015. Evolution of the last koninckinids (Athyridida, Koninckinidae), a precursor signal of the early Toarcian mass extinction event in the Western Tethys. *Palaeogeography, Palaeoclimatology, Palaeoecology*. **429**, pp.41–56.

Bailey, T.R., Rosental, Y., McArthur, J.M., van de Schootbrugge, B. and Thirlwall, M.F. 2003. Paleoceanographic changes of the Late Pliensbachian–Early Toarcian interval: a possible link to the genesis of an Oceanic Anoxic Event. *Earth and Planetary Science Letters*. **212**(3–4), pp.307–320.

Bambach, R.K. 1993. Seafood through time: changes in biomass, energetics, and productivity in the marine ecosystem. *Paleobiology*. **19**(3), pp.372–397.

Bambach, R.K., Bush, A.M. and Erwin, D. 2007. Autoecology and the filling of ecospace: key metazoans radiation. *Palaeontology*. **50**, pp.1–22.

Barbin, V. 2000. Cathodoluminescence of Carbonate Shells: Biochemical vs Diagenetic Process *In*: *Cathodoluminescence in Geosciences* [Online]. Berlin, Heidelberg: Springer Berlin Heidelberg, pp.303–329.

Barr, S.R., Temperley, S. and Tarney, J. 1999. Lateral growth of the continental crust though deep level subduction-accretion: a re-evaluation of central Greek Rhodope. *Lithos*. **46**, pp.69–94.

Bassoulet, J.P., Elmi, S., Poisson, A., Cecca, F., Bellion, Y., Guiraud, R., Baudin, F., Dercourt, J., Ricou, L.E. and Vrielynck, B. 1993. *Mid Toarcian. Atlas Tethys paleoenvironmental maps,* pp.63-80.

Bassoulet, J.P., Lachkar, G., Baudin, F., Benshili, K., Blanc, P., Boutakiout, M., Depeche, F., Elmi, S. and Ruget, C. 1991. Stratigraphie integree dans le Toarcien du Maroc (rides sud-rifaines et moyen Atlas). *Bulletin de la Societe Geologique de France*. **162**(5), pp.825–839.

Batten, D.J. 1996. Palynofacies and palaeoenvironmental interpretation. *Palynology: principles and applications*. **3**(January 1996), pp.1011–1064.

Bedi, Y., Vasilev, E., Dabovski, C., Ergen, A., Okuyucu, C., Doğan, A., K., T.U., Ivanova, D., Boncheva, I., Lakova, I., Sachanski, V., Kuşcu, I., Tuncay, E., Demíray, G.D., H., S. and Cemal Göncüoğlu, M. 2013. New age data from the tectonostratigraphic units of the Istranca 'Massif' in NW Turkey: a correlation with SE Bulgaria. *Geologica Carpathica*. **64**(4), pp.255–277.

Bengston, P. 1988. Open nomenclature. *Palaeontology, London, UK*. **31**, pp.223– 227.

Benito, M.I. and Reolid, M. 2012. Belemnite taphonomy (Upper Jurassic, Western Tethys) part II: Fossil-diagenetic analysis including combined petrographic and geochemical techniques. *Palaeogeography, Palaeoclimatology, Palaeoecology*. **358**–**360**, pp.89–108.

Benoit, J.M., Gilmour, C.C., Mason, R.P. and Heyes, A. 1999. Sufide Controls on Bioavailability to Methylating Bacteria in Sediment Pore Waters. *Environmental Science and Technology*. **33**(6), pp.951–957.

Benoit, J.M., Mason, R.P., Gilmour, C.C. and Aiken, G.R. 2001. Constants for mercury binding by organic matter isolates from the Florida Everglades. *Geochimica et Cosmochimica Acta*. **65**(24), pp.4445–4451.

Benton, M.J. 1995. Diversficiation and Extinction in the History of Life. *Science*. **268**, pp.52–58.

Bjerrum, C.J., Surlyk, F., Callomon, J.H. and Slingerland, R.L. 2001. Numerical paleoceanographic study of the Early Jurassic Transcontinental Laurasian Seaway. *Paleoceanography*. **16**(4), pp.390–404.

Blake, J.F. and Tate., R. 1876. *The Yorkshire Lias:* (John Van Voorst, ed.). London.

Blakely, R. 2010. Europe-Paleogeographic Maps.

Blum, J.D., Sherman, L.S. and Johnson, M.W. 2014a. Mercury Isotopes in Earth and Environmental Sciences. *Annual Review of Earth and Planetary Sciences*. **42**(1), pp.249–269.

Blum, J.D., Sherman, L.S. and Johnson, M.W. 2014b. Mercury Isotopes in Earth and Environmental Sciences. *Annual Review of Earth and Planetary Sciences*. **42**(1), pp.249–269.

Bodin, S., Krencker, F.N., Kothe, T., Hoffmann, R., Mattioli, E., Heimhofer, U. and Kabiri, L. 2016. Perturbation of the carbon cycle during the late Pliensbachian – early Toarcian: New insight from high-resolution carbon isotope records in Morocco. *Journal of African Earth Sciences*. **116**(February), pp.89–104.

Bodin, S., Mattioli, E., Fröhlich, S., Marshall, J.D., Boutib, L., Lahsini, S. and Redfern, J. 2010. Toarcian carbon isotope shifts and nutrient changes from the Northern margin of Gondwana (High Atlas, Morocco, Jurassic): Palaeoenvironmental implications. *Palaeogeography, Palaeoclimatology, Palaeoecology*. **297**(2), pp.377–390.

Bončev, E. 1971. Problems of the Bulgarian geotectonics. *Tehnika*., p.202.

Bončev, E. 1986. The Balkanides – geotectonic position and development. *Geologica Balcanica, Series operum singulorum*. **1**, p.273.

Bond, D. and Grasby, S.E. 2017. On the causes of mass extinctions. *Palaeogeography, Palaeoclimatology, Palaeoecology*. **478**, pp.3–29.

Bond, D. and Wignall, P.B. 2010. Pyrite framboid study of marine Permian-Triassic boundary sections: A complex anoxic event and its relationship to contemporaneous mass extinction. *Bulletin of the Geological Society of America*. **122**(7–8), pp.1265–1279.

Bond, D., Wignall, P.B. and Racki, G. 2004. Extent and duration of marine anoxia during the Frasnian-Famennian (Late Devonian) mass extinction in Poland, Germany, Austria and France. *Geological Magazine*. **141**(2), pp.173–193.

Bond, D.P.G. and Wignall, P.B. 2014. Geological Society of America Special Papers Online First. *Volcanism, Impacts, and Mass Extinctions: Causes and Effects: Geological Society of America Special Paper 505*. **2505**(02), pp.29–55.

Bougeault, C., Pellenard, P., Deconinck, J.F., Hesselbo, S.P., Dommergues, J.-L., Bruneau, L., Cocquerez, T., Laffont, R., Huret, E. and Thibault, N. 2017. Climatic and palaeoceanographic changes during the Pliensbachian (Early Jurassic) inferred from clay mineralogy and stable isotope (C-O) geochemistry (NW Europe). *Global and Planetary Change*. **149**, pp.139–152.

Boulila, S., Galbrun, B., Huret, E., Hinnov, L.A., Rouget, I., Gardin, S. and Bartolini, A. 2014. Astronomical calibration of the Toarcian Stage: Implications for sequence stratigraphy and duration of the early Toarcian OAE. *Earth and Planetary Science Letters*. **386**, pp.98–111.

Boulila, S. and Hinnov, L.A. 2015. Comment on 'Chronology of the Early Toarcian environmental crisis in the Lorraine Sub-Basin (NE Paris Basin)' by W. Ruebsam, P. Münzberger, and L. Schwark [Earth and Planetary Science Letters 404 (2014) 273-282]. *Earth and Planetary Science Letters*. **416**, pp.143–146.

Bown, P. 1987. Taxonomy, evolution, and biostratigraphy of Late Triassic-Early Jurassic calcareous nannofossils. *Paleontological Association*. **38**.

Bown, P.R. 1998. *Calcareous nannofossil biostratigraphy*. Chapman & Hall.

Boyanov, I. and Ruseva, M. 1989. Lithostratigraphy and tectonic position of the Mesozoic rocks in the East Rhodopes. *Geologica Rhodopica*. **1**, pp.22–23.

Brame, H.M.R., Martindale, R.C., Ettinger, N.P., Debeljak, I., Vasseur, R., Lathuilière, B., Kabiri, L. and Bodin, S. 2018. Stratigraphic distribution and paleoecological significance of Early Jurassic (Pliensbachian-Toarcian) lithiotid-coral reefal deposits from the Central High Atlas of Morocco. *Palaeogeography, Palaeoclimatology, Palaeoecology*. pp.123-145.

Brand, U and Veizer, J. 1980 Carbonate diagenesis 1, trace elements.

Brand, U. and Veizer, J. 1981. Chemical Diagenesis of a Multicomponent carbonate system - 2: Stable Isotopes. *Journal of Sedimentary Petrology*. **51**(3), pp.0987–0997.

Brayard, A., Bucher, H., Escarguel, G., Fluteau, F., Bourquin, S. and Galfetti, T. 2006. The Early Triassic ammonoid recovery: Paleoclimatic significance of diversity gradients. *Palaeogeography, Palaeoclimatology, Palaeoecology*. **239**(3–4), pp.374–395.

Brayard, A., Escarguel, G. and Bucher, H. 2007. The biogeography of Early Triassic ammonoid faunas: Clusters, gradients, and networks. *Geobios*. **40**(6), pp.749–765.

Brock, T.D. 1985. Life at high temperatures. *Science*. **230**(4722), pp.132–138.

Bucefalo Palliani, R., Mattioli, E. and Riding, J.B. 2002. The response of marine phytoplankton and sedimentary organic matter to the early Toarcian (Lower Jurassic) oceanic anoxic event in northern England. *Marine Micropaleontology*. **46**(3–4), pp.223–245.

Burdige, D.J. 2007. Preservation of organic matter in marine sediments: Controls, mechanisms, and an imbalance in sediment organic carbon budgets? *Chemical Reviews*. **107**(2), pp.467–485.

Burgess, S.D., Bowring, S. a., Fleming, T.H. and Elliot, D.H. 2015. High-precision geochronology links the Ferrar large igneous province with early-Jurassic ocean anoxia and biotic crisis. *Earth and Planetary Science Letters*. **415**, pp.90–99.

Butler, I.B. and Rickard, D. 2000. Framboidal pyrite formation via the oxidation of iron (II) monosulfide by hydrogen sulphide. *Geochimica et Cosmochimica Acta*. **64**(15), pp.2665–2672.

Canfield, D.E. 1994. Factors influencing organic carbon preservation in marine sediments. *Chemical Geology*. **114**(3–4), pp.315–329.

Caruthers, A.H., Gröcke R., D. and Smith, P.L. 2011. The significance of an Early Jurassic (Toarcian) carbon-isotope excursion in Haida Gwaii (Queen Charlotte Islands), British Columbia, Canada. *Earth and Planetary Science Letters*. **307**(1–2), pp.19–26.

Caruthers, A.H., Smith, P.L. and Gröcke R., D. 2014. The Pliensbachian-Toarcian (Early Jurassic) extinction: A North American perspective.

Caruthers, A.H., Smith, P.L. and Gröcke R., D. 2013. The Pliensbachian–Toarcian (Early Jurassic) extinction, a global multi-phased event. *Palaeogeography, Palaeoclimatology, Palaeoecology*. **386**, pp.104–118.

Caswell, B. a., Coe, A.L. and Cohen, A.S. 2009. New range data for marine invertebrate species across the early Toarcian (Early Jurassic) mass extinction. *Journal of the Geological Society*. **166**(5), pp.859–872.

Caswell, B.A. and Coe, A.L. 2012. A high-resolution shallow marine record of the Toarcian (Early Jurassic) Oceanic Anoxic Event from the East Midlands Shelf, UK. *Palaeogeography, Palaeoclimatology, Palaeoecology*. **365**–**366**, pp.124–135.

Caswell, B.A. and Frid, C.L.J. 2017. Marine ecosystem resilience during extreme deoxygenation: the Early Jurassic oceanic anoxic event. *Oecologia*. **183**(1), pp.275–290.

Čatalov, G. and Černjavska, S. 1982. Palaeontological data on the Jurassic age of the rocks between the villages of Byala Voda and Kondolovo (Strandja

Mountain). *Comptes rendus de l'Académie bulgare des Sciences*. **35**(5), pp.665–668.

Černjavska, S. 1986. Lower and Middle Jurassic palynostratigraphy of Bulgaria. *Geologica Balcanica*. **16**(6), pp.21–32.

Chandler, M.A., Rind, D. and Ruedy, R. 1992. Pangean climate during the Early Jurassic: GMC simulations and the sedimentary record of paleoclimate. *Geol. Soc. Am. Bul*. **104**(May), pp.543–559.

Clémence, M.-E., Gardin, S. and Bartolini, A. 2015. New insights in the pattern and timing of the Early Jurassic calcareous nannofossil crisis. *Palaeogeography, Palaeoclimatology, Palaeoecology*. **427**, pp.100–108.

Cohen, A.S. and Coe, A.L. 2007. The impact of the Central Atlantic Magmatic Province on climate and on the Sr- and Os-isotope evolution of seawater. *Palaeogeography, Palaeoclimatology, Palaeoecology*. **244**(1–4), pp.374–390.

Cohen, A.S., Coe, A.L., Bartlett, J.M. and Hawkesworth, C.J. 1999. Precise Re–Os ages of organic-rich mudrocks and the Os isotope composition of Jurassic seawater. *Earth and Planetary Science Letters*. **167**(3–4), pp.159–173.

Cohen, A.S., Coe, A.L., Harding, S.M. and Schwark, L. 2004a. Osmium isotope evidence for the regulation of atmospheric CO2 by continental weathering. *Geology*. **32**(2), p.157.

Cohen, A.S., Coe, A.L., Harding, S.M. and Schwark, L. 2004b. Osmium isotope evidence for the regulation of atmospheric CO2 by continental weathering. *Geology*. **32**(2), p.157.

Correia, V.F., Riding, J.B., Duarte, L.V., Fernandes, P. and Pereira, Z. 2017. The palynological response to the Toarcian Oceanic Anoxic Event (Early Jurassic) at Peniche, Lusitanian Basin, western Portugal. *Marine Micropaleontology*. **137**(October), pp.46–63.

Courtillot, V.E. and Renne, P.R. 2003. On the ages of flood basalt events. *Comptes Rendus Geoscience*. **335**(1), pp.113–140.

Cox, L. R., Newell, N., Boyd, D.W., Branson, R. D., W. 1969. Part N bivalvia *In*: R. C. MOORE, ed. *Treatise on Invertebrate Paleontology*. The Geological Society of America, Inc. and The Universtiy of Kansas, pp.N385–N393.

Cox, L.R. 1994. On Pseudolimea (Arkell). *Proceedings of the Malacological Society, London*. (26), pp.74–88.

Craig, H. 1966. Isotopic Composition and Origin of the Red Sea and Salton Sea Geothermal Brines. *Science*. **154**(3756), pp.1544–1548.

Craig, H. 1965. The measurement of oxygen isotope palaeotemperatures *In*: *Stable Isotopes in Oceanographic Studies and Paleotemperatures* [Online]. Laboratorio de Geologia Nucleare, pp.161–182.

Dabovski, C., Boyanov, I., Khrischev, K., Nikolov, T., Sapunov, I.G., Yanev, Y. and Zagorchev, I.S. 2002. Structure and Alpine evolution of Bulgaria. *Geologica Balcanica*. (2–4), pp.9–15.

Dabovski, C. and Zagorchev, I.S. 2009. Geology of Bulgaria. *Geology of*

Bulgaria., pp.1–44.

Dabovski, H., Harkovska, A., Kamenov, B., Mavroudchiev, B., Stanisheva-Vassileva, G., Chounev, D. and Yanev., Y. 1989. Map of the Alpine magmatism in Bulgaria (Geodynamic ap- proach), 1: 100 000. *CIPP in Map-making, Bulgaria.*

Damborenea, S.E. 2002a. *Early Jurassic bivalves from Argentina. Part 3: Superfamilies Monotoidea, Pectinoidea, Plicatuloidea and Dimyoidea* A 265: 1-1. (Taf.;Stuttgart., ed.).

Damborenea, S.E. 1987. Early Jurassic Bivalvia of Argentina. Part II: Superfamilies Pteriacea, Buchiacea and part of Pectinacea. *Palaeontographica*. (99), pp.113–216.

Damborenea, S.E. 1993. Early Jurassic South American pectinaceans and circum-Pacific palaeobiogeography. *Palaeogeography, Palaeoclimatology, Palaeoecology*. **100**(1–2), pp.109–123.

Damborenea, S.E. 2002b. Jurassic evolution of Southern Hemisphere marine palaeobiogeographic units based on benthonic bivalves. *Geobios*. **35**, pp.51–71.

Damborenea, S.E. 2017. Revision de los bioceremas marinos globales del Jurassico segun la distribucion de los Molluscos Bivalvos. *Publicación Electrónica de la Asociación Paleontológica Argentina*. **17**(2).

Damborenea, S.E., Echevarría, J. and Ros-Franch, S. 2013. *Southern Hemisphere Palaeobiogeography of Triassic-Jurassic Marine Bivalves* [Online]. Dordrecht: Springer Netherlands.

Damborenea, S.E. and Gonzalez-Leon, C.M. 1998. *Late Triassic and Early Jurassic bivalves from Sonora, Mexico* 9 Abb., 1. Mexico.

Danise, S., Twitchett, R.J. and Little, C.T.S. 2015. Environmental controls on Jurassic marine ecosystems during global warming. *Geology*. **43**(3), pp.263–266.

Danise, S., Twitchett, R.J., Little, C.T.S. and Clémence, M.-E. 2013. The impact of global warming and anoxia on marine benthic community dynamics: an example from the Toarcian (Early Jurassic). *PloS one*. **8**(2), p.e56255.

Denison, R.E., Koepnick, R.B., Fletcher, A., Howell, M.W. and Callaway, W.S. 1994. Criteria for the retention of original seawater 87Sr86Sr in ancient shelf limestones. *Chemical Geology*. **112**(1–2), pp.131–143.

Dera, G., Brigaud, B., Monna, F., Laffont, R., Pucéat, E., Deconinck, J.-F., Pellenard, P., Joachimski, M. and Durlet, C. 2011. Climatic ups and downs in a disturbed Jurassic world. *Geology*. **39**(3), pp.215–218.

Dera, G. and Donnadieu, Y. 2012. Modeling evidences for global warming, Arctic seawater freshening, and sluggish oceanic circulation during the Early Toarcian anoxic event. *Paleoceanography*. **27**(2), n/a-n/a.

Dera, G., Neige, P., Dommergues, J.-L. and Brayard, A. 2011. Ammonite paleobiogeography during the Pliensbachian–Toarcian crisis (Early Jurassic) reflecting paleoclimate, eustasy, and extinctions. *Global and Planetary Change*. **78**(3–4), pp.92–105.

Dera, G., Neige, P., Dommergues, J.-L., Fara, E., Laffont, R. and Pellenard, P. 2010. High-resolution dynamics of Early Jurassic marine extinctions: the case of Pliensbachian-Toarcian ammonites (Cephalopoda). *Journal of the Geological Society*. **167**(1), pp.21–33.

Dera, G., Pucéat, E., Pellenard, P., Neige, P., Delsate, D., Joachimski, M., Reisberg, L. and Martinez, M. 2009. Water mass exchange and variations in seawater temperature in the NW Tethys during the Early Jurassic: Evidence from neodymium and oxygen isotopes of fish teeth and belemnites. *Earth and Planetary Science Letters*. **286**(1–2), pp.198–207.

Dommergues, J.-L., Fara, E. and Meister, C. 2009. Ammonite diversity and its palaeobiogeographical structure during the early Pliensbachian (Jurassic) in the western Tethys and adjacent areas. *Palaeogeography, Palaeoclimatology, Palaeoecology*. **280**(1–2), pp.64–77.

Dommergues, J.L., Dugué, O., Gauthier, H., Meister, C., Neige, P., Raynaud, D., Savary, X. and Trévisan, M. 2008. Les ammonites du Pliensbachien et du Toarcien basal dans la carrière de la Roche Blain (Fresnay-le-Puceux, Calvados, Basse-Normandie, France). Taxonomie, implications stratigraphiques et paléobiogéographiquees. *Revue de Paléobiologie, Genève*. **27**(1), pp.265–329.

Dommergues, J.L., Marchand, D., Sapunov, I. and Thierry, J. 1987. Les faunes d'ammonites du Jurassique bulgare: une confirmation paléobiogéographique de l'isolement relatif de la région balkano-moesienne. *Bulletin de la Société géologique de France*. **8**(3-4), pp.737–742.

Dommergues, J.L., Meister, C. and Mouterde, R. 1997. Groupe français d'étude du Jurassique. Biostratigraphie ouest-européen et méditerranéen: zonations parallèles et distribution des invertébrés et microfossiles *In*: P. Cariou, E., Hantzpergue, ed. *Bulletin du Centre de Recherche Elf Exploration Production, Mémoire*., pp.15–23.

Dončeva, M. and Ovčarova, N. 1989. Distribution and lithology of the Lower–Middle Jurassic sedimants in part of North-west Bulgaria. *Review of the Bulgarian Geological Society*. **50**(1), pp.35–45.

Doney, S.C., Ruckelshaus, M., Emmett Duffy, J., Barry, J.P., Chan, F., English, C.A., Galindo, H.M., Grebmeier, J.M., Hollowed, A.B., Knowlton, N., Polovina, J., Rabalais, N.N., Sydeman, W.J. and Talley, L.D. 2012. Climate Change Impacts on Marine Ecosystems. *Annual Review of Marine Science*. **4**(1), pp.11–37.

Doyle, P., Donovan, D.T. and Nixon, M. 1994. Phylogeny and Systematics of the Coleoidea. *the University of Kansas Paleontological Contributions*. **5**(785), pp.1532–1534.

Droser, M.L. and Bottjer, D.J. 1986. A semiquantitative field classification of ichnofabric. *Journal of Sedimentary Research*. **56**(4), pp.558–559.

Droser, M.L. and Bottjer, D.J. 1993. Trends and Patterns of Phanerozoic Ichnofabrics. *Annual Review of Earth and Planetary Sciences*. **21**(1), pp.205–225.

Duarte, L.V., Comas-Rengifo, M.J., Silva, R.L., Paredes, R. and Goy, A. 2014.

Carbon isotope stratigraphy and ammonite biochronostratigraphy across the sinemurian-pliensbachian boundary in the western Iberian margin. *Bulletin of Geosciences*. **89**(4), pp.719–736.

Duncan, R.A., Hooper, P.R., Rehacek, J., Marsh, J.S. and Duncan, A.R. 1997. The timing and duration of the Karoo igneous event, southern Gondwana. *Journal of Geophysical Research: Solid Earth*. **102**(B8), pp.18127–18138.

Dunham, R.J. 1962. Classification of carbonate rocks according to depositional textures, in HAM, W. E., ed., Classification of Carbonate Rocks: *American Association of Petroleum Geologists Memoir*. **1**, pp.108–121.

Dutton, A., Huber, B.T., Lohmann, K.C. and Zingsmeister, W.J. 2007. Hight resolution stable isotope profiles of a Dimitobelid belemnite: Implications for paleodepth habitat and Late Laastrichtian climate seasonality. *PALAIOS*. **22**(6), pp.642–650.

Elmi, S., Rulleau, L., Gabilly, J. and Mouterde, R. 1997. Toarcien. Bioestratigraphie du Jurassique ouest-européen et méditerranéen: zonations parallèles et distribution des invertébrés et microfossils P. Cariou, E., Hantzpergue, ed. *Bulletin du Centre de Recherches Exploration-Production Elf-Aquitaine*. **17**, pp.25–35.

Emili, A., Koron, N., Covelli, S., Faganeli, J., Acquavita, A., Predonzani, S. and Vittor, C. De 2011. Does anoxia affect mercury cycling at the sediment-water interface in the Gulf of Trieste (northern Adriatic Sea)? Incubation experiments using benthic flux chambers. *Applied Geochemistry*. **26**(2), pp.194–204.

Fantasia, A., Föllmi, K.B., Adatte, T., Bernárdez, E., Spangenberg, J. and Mattioli, E. 2018. The Toarcian Oceanic Anoxic Event in southwestern Gondwana: an example from the Andean Basin, northern Chile. *Journal of the Geological Society*. **175**(6), pp.883–902.

Fantasia, A., Föllmi, K.B., Adatte, T., Spangenberg, J. and Montero-Serrano, J.-C. 2018. The Early Toarcian oceanic anoxic event: Paleoenvironmental and paleoclimatic change across the Alpine Tethys (Switzerland). *Global and Planetary Change*. **162**(November 2017), pp.53–68.

Fara, E. 2001. What are Lazarus taxa? *Geological Journal*. **36**(3–4), pp.291–303.

Fauré, P. *Le Lias des Pyrénées*. Université Paul-Sabatier – Toulouse III.

Ferreira, J., Mattioli, E. and van de Schootbrugge, B. 2017. Palaeoenvironmental vs. evolutionary control on size variation of coccoliths across the Lower-Middle Jurassic. *Palaeogeography, Palaeoclimatology, Palaeoecology*. **465**, pp.177–192.

Fitzgerald, W.F., Lamborg, C.H. and Hammerschmidt, C.R. 2007. Marine biogeochemical cycling of mercury. *Chemical Reviews*. **107**(2), pp.641–662.

Fonseca, C., Mendonça Filho, J.G., Lézin, C., Duarte, L.V. and Fauré, P. 2018. Organic facies variability during the Toarcian Oceanic Anoxic Event record of the Grands Causses and Quercy basins (southern France). *International Journal of Coal Geology*. **190**(February 2017), pp.218–235.

Font, E., Adatte, T., Sial, A.N., Drude de Lacerda, L., Keller, G. and Punekar, J. 2016. Mercury anomaly, Deccan volcanism, and the end-Cretaceous mass extinction. *Geology*. **44**(2), pp.171–174.

Fourcade, E., Azéma, J., Bassoullet, J.-P., Cecca, F., Dercourt, J., Enay, R. and Guiraud, R. 1995. Paleogeography and Paleoenvironment of the Tethyan Realm During the Jurassic Breakup of Pangea *In*: *The Tethys Ocean* [Online]. Boston, MA: Springer US, pp.191–214. [Accessed 27 November 2018]. Available from: http://link.springer.com/10.1007/978-1-4899-1558-0_6.

Franceschi, M., Dal Corso, J., Posenato, R., Roghi, G., Masetti, D. and Jenkyns, H.C. 2014. Early Pliensbachian (Early Jurassic) C-isotope perturbation and the diffusion of the Lithiotis Fauna: Insights from the western Tethys. *Palaeogeography, Palaeoclimatology, Palaeoecology*. **410**, pp.255–263.

French, K.L., Sepúlveda, J., Trabucho-Alexandre, J., Gröcke R., D. and Summons, R.E. 2014. Organic geochemistry of the early Toarcian oceanic anoxic event in Hawsker Bottoms, Yorkshire, England. *Earth and Planetary Science Letters*. **390**, pp.116–127.

Fu, X., Wang, J., Feng, X., Wang, D., Chen, W., Song, C. and Zeng, S. 2016. Early Jurassic carbon-isotope excursion in the Qiangtang Basin (Tibet), the eastern Tethys: Implications for the Toarcian Oceanic anoxic event. *Chemical Geology*. **442**, pp.62–72.

Fürsich, F.T., Berndt, R., Scheuer, T. and Gahr, M.E. 2001. Comparative ecological analysis of Toarcian (Lower Jurassic) benthic faunas from southern France and east-central Spain. *Lethaia*. **34**, pp.169–199.

Gahr, M.E. 2005. Response of Lower Toarcian (Lower Jurassic) macrobenthos of the Iberian Peninsula to sea level changes and mass extinction. . **31**(2), pp.197–215.

García Joral, F., Baeza-Carratalá, J.F. and Goy, A. 2018. Changes in brachiopod body size prior to the Early Toarcian (Jurassic) Mass Extinction. *Palaeogeography, Palaeoclimatology, Palaeoecology*. **506**(June), pp.242–249.

García Joral, F., Gómez, J.J. and Goy, A. 2011. Mass extinction and recovery of the Early Toarcian (Early Jurassic) brachiopods linked to climate change in Northern and Central Spain. *Palaeogeography, Palaeoclimatology, Palaeoecology*. **302**(3–4), pp.367–380.

Gaupp, R. and Batten, D.J. 1985. Maturation of organic matter in Cretaceous strata of the Northern Calcareous Alps. *Neues Jahrbuch für Geologie und Paläontologie Monatshefte*. **3**, pp.157–175.

Gill, B.C., Lyons, T.W. and Jenkyns, H.C. 2011. A global perturbation to the sulfur cycle during the Toarcian Oceanic Anoxic Event. *Earth and Planetary Science Letters*. **312**(3–4), pp.484–496.

Glasby, G.P. and Schulz, H.D. 1999. New Types of E H , pH Diagrams to the Study of Specific Problems in Marine Geochemistry. *Aquatic Geochemistry*. **5**(1988), pp.227–248.

Golonka, J. 2007. Late Triassic and Early Jurassic palaeogeography of the

world. *Palaeogeography, Palaeoclimatology, Palaeoecology*. **244**(1–4), pp.297–307.

Golonka, J. 2004. Plate tectonic evolution of the southern margin of Eurasia in the Mesozoic and Cenozoic. *Tectonophysics*. **381**(1–4), pp.235–273.

Golonka, J. and Ford, D. 2000. Pangean (Late Carboniferous–Middle Jurassic) paleoenvironment and lithofacies. *Palaeogeography, Palaeoclimatology, Palaeoecology*. **161**(1–2), pp.1–34.

Gómez, J.J. and Arias, C. 2010. Rapid warming and ostracods mass extinction at the Lower Toarcian (Jurassic) of central Spain. *Marine Micropaleontology*. **74**(3–4), pp.119–135.

Gómez, J.J., Comas-Rengifo, M.J. and Goy, A. 2016. The hydrocarbon source rocks of the Pliensbachian (Early Jurassic) in the Asturian Basin (Northern Spain): Their relationship with the palaeoclimatic oscillations and gamma-ray response. *Journal of Iberian Geology*. **42**(3), pp.259–273.

Gómez, J.J. and Goy, A. 2011. Warming-driven mass extinction in the Early Toarcian (Early Jurassic) of northern and central Spain. Correlation with other time-equivalent European sections. *Palaeogeography, Palaeoclimatology, Palaeoecology*. **306**(3–4), pp.176–195.

Gómez, J.J., Goy, A. and Canales, M.L. 2008. Seawater temperature and carbon isotope variations in belemnites linked to mass extinction during the Toarcian (Early Jurassic) in Central and Northern Spain. Comparison with other European sections. *Palaeogeography, Palaeoclimatology, Palaeoecology*. **258**(1–2), pp.28–58.

Gong, Q., Wang, X., Zhao, L., Grasby, S.E., Chen, Z.-Q., Zhang, L., Li, Y., Cao, L. and Li, Z. 2017. Mercury spikes suggest volcanic driver of the Ordovician-Silurian mass extinction. *Scientific Reports*. **7**(1), p.5304.

Gradstein, F.M., Ogg, J.G., Schmitz, M.D. and Ogg, G. 2012. *The Geologic Time Scale 2012*. Amsrerdam; Elsevier.

Grasby, S.E., Beauchamp, B., Bond, D., Wignall, P.B. and Sanei, H. 2016. Mercury anomalies associated with three extinction events (Capitanian Crisis, Latest Permian Extinction and the Smithian/Spathian Extinction) in NW Pangea. *Geological Magazine*. **153**(2), pp.285–297.

Greene, S.E., Martindale, R.C., Ritterbush, K.A., Bottjer, D.J., Corsetti, F.A. and Berelson, W.M. 2012. Recognising ocean acidification in deep time: An evaluation of the evidence for acidification across the Triassic-Jurassic boundary. *Earth-Science Reviews*. **113**(1–2), pp.72–93.

Gröcke R., D., Hesselbo, S.P. and Findlay, D. 2007. Atypical diagenetic effects on strontium-isotope composition of Early Jurassic belemnites, Queen Charlotte Islands, British Columbia, Canada. *Canadian Journal of Earth Sciences*. **44**(2), pp.181–197.

Gröcke R., D., Hesselbo, S.P. and Jenkyns, H.C. 1999. Carbon-isotope composition of Lower Cretaceous fossil wood: Ocean-atmosphere chemistry and relation to sea-level change. *Geology*. **27**(2), pp.155–158.

Gröcke R., D., Hori, R.S., Trabucho-Alexandre, J., Kemp, D.B. and Schwark, L. 2011. An open ocean record of the Toarcian oceanic anoxic event. *Solid*

Earth. **2**(2), pp.245–257.

Guex, J., Schoene, B., Bartolini, A., Spangenberg, J., Schaltegger, U., O'Dogherty, L., Taylor, D., Bucher, H. and Atudorei, V. 2012. Geochronological constraints on post-extinction recovery of the ammonoids and carbon cycle perturbations during the Early Jurassic. *Palaeogeography, Palaeoclimatology, Palaeoecology*. **346**–**347**, pp.1–11.

Gutowska, M.A., Melzner, F., Pörtner, H.O. and Meier, S. 2010. Cuttlebone calcification increases during exposure to elevated seawater pCO2 in the cephalopod Sepia officinalis. *Marine Biology*. **157**(7), pp.1653–1663.

Hallam, a. 1996. Recovery of the marine fauna in Europe after the end-Triassic and Early Toarcian mass Extinctions. *Geological Society, London, Special Publications*. **102**(1), pp.231–236.

Hallam, a. and Wignall, P.B. 1999. Mass extinctions and sea-level changes. *Earth-Science Reviews*. **48**(4), pp.217–250.

Hallam, A. 1960. *A sedimentary and faunal study of the Blue Lias of Dorset and Glamorgan*.

Hallam, A. 1969. Faunal realms and facies in the Jurassic. *Palaeontology*. **12**(1), pp.1–18.

Hallam, A. 1977. Jurassic bivalve biogeography. *Paleobiology*. **3**(01), pp.58–73.

Hallam, A. 1975. *Jurassic Environments* [Online]. Cambridge University Press. [Accessed 8 February 2015]. Available from: https://books.google.com/books?hl=en&lr=&id=TUGq5n2lxkoC&pgis=1.

Hallam, A. 1971. Provinciality in Jurassic faunas in relation to facies and palaeogeography. *In Faunal Provinces in Space and Time*. (Geol. J. Spec. Issue 4), pp.129–152.

Hallam, A. 1987. Radiations and Extinctions in Relation to Environmental Change in the Marine Lower Jurassic of Northwest Europe. *Paleobiology*. **13**(2), pp.152–168.

Hallam, A. 1976. Stratigraphic Distribution and ecology of European Jurassic bivalves. *Lethaia*. **9**(3), pp.245–259.

Hallam, A. 1986. The Pliensbachian and Tithonian extinction events. *Nature*. **319**(6056), pp.765–768.

Hallam, A. and Wignall, P.B. 1997. *Mass extinctions and their aftermath*. UK: Oxford University Press.

Hammarlund, E.U., Dahl, T.W., Harper, D.A.T., Bond, D.P.G., Nielsen, A.T., Bjerrum, C.J., Schovsbo, N.H., Schönlaub, H.P., Zalasiewicz, J.A. and Canfield, D.E. 2012. A sulfidic driver for the end-Ordovician mass extinction. *Earth and Planetary Science Letters*. **331**–**332**, pp.128–139.

Han, Z., Hu, X., Kemp, D.B. and Li, J. 2018. Carbonate-platform response to the Toarcian Oceanic Anoxic Event in the southern hemisphere : Implications for climatic change and biotic platform demise. *Earth and Planetary Science Letters*. **489**, pp.59–71.

Harazim, D., van de Schootbrugge, B., Sorichter, K., Fiebig, J., Weug, A., Suan, G. and Oschmann, W. 2013. Spatial variability of watermass conditions

within the European Epicontinental Seaway during the Early Jurassic (Pliensbachian-Toarcian). *Sedimentology*. **60**(2), pp.359–390.

Harries, P.J. and Little, C.T.S. 1999. The early Toarcian (Early Jurassic) and the Cenomanian–Turonian (Late Cretaceous) mass extinctions: similarities and contrasts. *Palaeogeography, Palaeoclimatology, Palaeoecology*. **154**(1–2), pp.39–66.

Harris, P.J., Kauffman, E.G. and Hansen, T.A. 1996. Models for biotic survival following mass extinctions. *Geological Society, London, Special Publication*. **102**, pp.41–60.

Hart, M.B., Hylton, M.D., Oxford, M.J., Price, G.D., Hudson, W. and Smart, C.W. 2003. The search for the origin of the planktic Foraminifera. *Journal of the Geological Society*. **160**(3), pp.341–343.

Hartnett, H.E., Keil, R.G., Hedges, J.I. and Devol, A.H. 1998. Influence of oxygen exposure time on organic carbon preservation in continental margin sediments. *Nature*. **391**(6667), pp.572–574.

Hendry, J.P. and Kalin, R.M. 1997. Are oxygen and carbon isotopes of mollusc shells reliable palaeosalinity indicators in marginal marine environments? A case study from the Middle Jurassic of England. *Journal of the Geological Society*. **154**(2), pp.321–333.

Hermoso, M., Le Callonnec, L., Minoletti, F., Renard, M. and Hesselbo, S.P. 2009. Expression of the Early Toarcian negative carbon-isotope excursion in separated carbonate microfractions (Jurassic, Paris Basin). *Earth and Planetary Science Letters*. **277**(1–2), pp.194–203.

Hermoso, M., Minoletti, F., Rickaby, R.E.M., Hesselbo, S.P., Baudin, F. and Jenkyns, H.C. 2012. Dynamics of a stepped carbon-isotope excursion: Ultra high-resolution study of Early Toarcian environmental change. *Earth and Planetary Science Letters*. **319**–**320**, pp.45–54.

Hermoso, M. and Pellenard, P. 2014. Continental weathering and climatic changes inferred from clay mineralogy and paired carbon isotopes across the early to middle Toarcian in the Paris Basin. *Palaeogeography, Palaeoclimatology, Palaeoecology*. **399**.

Hesselbo, S.P., Gröcke R., D., Jenkyns, H.C., Bjerrum, C.J., Farrin, P. and Green, O.R. 2000a. Massive dissociation of gas hydrate during a Jurassic ocean anoxic event. *Nature*. **406**(July), pp.392–395.

Hesselbo, S.P., Meister, C. and Gröcke R., D. 2000. A potential global stratotype for the Sinemurian-Pliensbachian boundary (Lower Jurassic), Robin Hood's Bay, UK: Ammonite faunas and isotope stratigraphy. *Geological Magazine*. **137**(6), pp.601–607.

Hesselbo, S.P. and Jenkyns, H. 1995. *A comparison of the Hettangian to Bajocian successions of Dorset and Yorkshire* Taylor, P. Geological Society of London.

Hesselbo, S.P., Jenkyns, H.C., Duarte, L.V. and Oliveira, L.C.V. 2007. Carbon-isotope record of the Early Jurassic (Toarcian) Oceanic Anoxic Event from fossil wood and marine carbonate (Lusitanian Basin, Portugal). *Earth and Planetary Science Letters*. **253**(3–4), pp.455–470.

Hesselbo, S.P. and Pienkowski, G. 2011. Stepwise atmospheric carbon-isotope excursion during the Toarcian Oceanic Anoxic Event (Early Jurassic, Polish Basin). *Earth and Planetary Science Letters*. **301**(1–2), pp.365–372.

Heydari, E., Wade, W.J. and Hassanzadeh, J. 2001. Diagenetic origin of carbon and oxygen isotope compositions of Permian-Triassic boundary strata. *Sedimentary Geology*. **143**(3–4), pp.191–197.

Hillebrandt, A., Krystyn, L., Kürschner, W.M., Bonis, N.R., Ruhl, M., Richoz, S., Schobben, M., Urlichs, M., Bown, P.R., Kment, K., McRoberts, C.A., Simms, M. and Tomãsových, A. 2013. The Global Stratotype Section and Point (GSSP) for the base of the Jurassic system at Kuhjoch (Karwendel Mountains, Northern Calcareous Alps, Tyrol, Austria). *Episodes*. **36**(September), pp.162–198.

Himmerkus, F., Reischmann, T. and Kostopoulos, D. 2006. Late Proterozoic and Silurian basement units within the Serbo-Macedonian Massif, northern Greece: the significance of terrane accretion in the Hellenides *In*: *Tectonic development of the Eastern Mediterranean region* [Online]., pp.35–50. [Accessed 27 November 2018]. Available from: http://sp.lyellcollection.org/content/260/1/35.short.

Hodges, P. 1987. *Lower Lias (Lower Jurassic) bivlavia from South Wales and adjacent areas*. University College of Swansea.

Hodges, P. 2000. The Early Jurassic bivalvia from the Hettangian and lower Sinemurian of south-west Britain. Part 1. *Palaeontographical Society, London*. **154**.

Hoegh-Guldberg, O. 2012. The Impact of Climate Change on the. *Ecological Research*. **1523**(2010), pp.1523–1529.

Hoffmann, R., Richter, D.K., Neuser, R.D., Jöns, N., Linzmeier, B.J., Lemanis, R.E., Fusseis, F., Xiao, X. and Immenhauser, A. 2016. Evidence for a composite organic–inorganic fabric of belemnite rostra: Implications for palaeoceanography and palaeoecology. *Sedimentary Geology*. **341**, pp.203–215.

Holland, S.M. and Patzkowsky, M.E. 2015. The stratigraphy of mass extinction. *Palaeontology*. **58**(5), pp.903–924.

Horowitz, H.M., Jacob, D.J., Zhang, Y., Dibble, T.S., Slemr, F., Amos, H.M., Schmidt, J.A., Corbitt, E.S., Marais, E.A. and Sunderland, E.M. 2017. A new mechanism for atmospheric mercury redox chemistry: implications for the global mercury budget. *Atmospheric Chemistry and Physics*. **17**(10), pp.6353–6371.

Huang, C. and Hesselbo, S.P. 2014. Pacing of the Toarcian Oceanic Anoxic Event (Early Jurassic) from astronomical correlation of marine sections. *Gondwana Research*. **25**(4).

Hylton, M.D. 2000. Microfaunal investigation of the Early Toarcian (Lower Jurassic) extinction event in N. W. Europe. *Department of Geological Sciences*. **Doctor of**, p.287.

Ibarrola, G.D. 2002. Taxonomie und Palökologie der Bivalven im Mittel-und Oberjura der Keltiberischen Ketten (Spanien). *Area*.

Ikeda, M. and Hori, R.S. 2014. Effects of Karoo-Ferrar volcanism and astronomical cycles on the Toarcian Oceanic Anoxic Events (Early Jurassic). *Palaeogeography, Palaeoclimatology, Palaeoecology*. **410**, pp.134–142.

Imlay, R.W. 1965. Presidential Address Jurassic Marine Faunal Differentiation in North America. *Jornal of Paleontology*.

Immenhauser, A.M., Schreurs, G., Peters, T., Matter, A., Hauser, M. and Dumitrica, P. 1998. Stratigraphy, sedimentology and depositional environments of the Permian to uppermost Cretaceous Batain Group. *Eclogae Geologicae Helvetiae*. **91(2)**, pp.217–236.

Immenhauser, A., Schöne, B.R., Hoffmann, R. and Niedermayr, A. 2016. Mollusc and brachiopod skeletal hard parts: Intricate archives of their marine environment. *Sedimentology*. **63**(1), pp.1–59.

Izumi, K., Kemp, D.B., Itamiya, S. and Inui, M. 2018. Sedimentary evidence for enhanced hydrological cycling in response to rapid carbon release during the early Toarcian oceanic anoxic event. *Earth and Planetary Science Letters*. **481**, pp.162–170.

Izumi, K., Miyaji, T. and Tanabe, K. 2012. Early Toarcian (Early Jurassic) oceanic anoxic event recorded in the shelf deposits in the northwestern Panthalassa: Evidence from the Nishinakayama Formation in the Toyora area, west Japan. *Palaeogeography, Palaeoclimatology, Palaeoecology*. **315**–**316**, pp.100–108.

Jablonski, D. and Bottjer, D.J. 1983. Soft-Bottom Epifaunal Suspension-Feeding Assemblages in the Late Cretaceous *In*: Springer, ed. *Biotic interactions in Recent and fossil benthic communities* [Online]. Boston, pp.747–812. [Accessed 28 November 2018]. Available from: http://link.springer.com/10.1007/978-1-4757-0740-3_16.

James, N.P., Bone, Y. and Kurtis Kyser, T. 1997. Brachiopod δ18O values do reflect ambient oceanography: Lacepede Shelf, southern Australia. *Geology*. **25**(6), p.551.

James R. Frank; and Carpen, A.B. 1982. Cathodoluminescence and Composition of Calcite Cement in the Taum Sauk Limestone (Upper Cambrian), Southeast Missouri. *SEPM Journal of Sedimentary Research*. **Vol. 52**(2), pp.631–638.

Jenkyns, H., … C.J.-J. of the and 2002, undefined n.d. Chemostratigraphy of the Jurassic System: applications, limitations and implications for palaeoceanography. *pubs.geoscienceworld.org*.

Jenkyns, H.C. 2003. Evidence for rapid climate change in the Mesozoic-Palaeogene greenhouse world. *Philosophical Transactions of the Royal Society A: Mathematical, Physical and Engineering Sciences*. **361**(1810), pp.1885–1916.

Jenkyns, H.C. 2010. Geochemistry of oceanic anoxic events. *Geochemistry, Geophysics, Geosystems*. **11**(3), n/a-n/a.

Jenkyns, H.C. 1999. *Mesozoic Anoxic Events and palaeoclimate Ocean circulation and Cretaceous OAEs View project Integrated Understanding of the Early Jurassic Earth System and Timescale (JET).*

Jenkyns, H.C. 1988. The early Toarcian (Jurassic) Anoxic event:stratigraphic, sedimentary, and geochemical evidence.

Jenkyns, H.C. and Clayton, C. 1986. Black shales and carbon isotopes in pelagic sediments from the Tethyan Lower Jurassic. *Sedimentology*. **33**(1), p.87.

Jenkyns, H.C. and Clayton, C. 1997. Lower Jurassic epicontinental carbonates and mudstones from England and Wales: chemostratigraphic signals and the early Toarcian anoxic event. *Sedimentology*. **44**(4), pp.687–706.

Jenkyns, H.C., Grficke, R., Hesselbo, S.P. and Holloway, R. 2001. Nitrogen isotope evidence for water mass denitrification during the early Toarcian (Jurassic) oceanic anoxic event Stephen Abstract . Bulk sedimentary nitrogen isotope data have been generated from Lower Jurassic excursion through the exaratum Subzone. **16**(6), pp.593–603.

Jenkyns, H.C., Jones, C.E., Gröcke R., D., Hesselbo, S.P. and Parkinson, D.N. 2002. Chemostratigraphy of the Jurassic System: applications, limitations and implications for palaeoceanography. *Journal of the Geological Society*. **159**(4), pp.351–378.

Jenkyns, H.C., Jones, C.E., Gröcke R., D., Stephen, H.P. and Parkinson, D.N. 2002. Chemostratigraphy of the Jurassic System : applications , limitations and implications for palaeoceanography. *Journal of the Geological Society*. **159**, pp.351–378.

Johnson, A.L.. 1984. *The palaeobiology of the bivalve families Pectinidae and Propeamussiidae in the Jurassic of Europe*. München.

Johnson, A.L.A. 1994. Evolution of European lower Jurassic Gryphaea (Gryphaea) and contemporaneous bivalves. *Historical Biology*. **7**(2), pp.167–186.

Jones, C.E. and Jenkyns, H.C. 2001. Seawater Strontium Isotopes, Oceanic Anoxic Events, and seafloor hydrothermal activity in the Jurassic and Cretaceous. **301**, pp.112–149.

Jones, C.E., Jenkyns, H.C., Coe, A.L. and Stephen, H.P. 1994. Strontium isotopic variations in Jurassic and Cretaceous seawater. *Geochimica et Cosmochimica Acta*. **58**(14), pp.3061–3074.

Jones, C.E., Jenkyns, H.C. and Hesselbo, S.P. 1994. Strontium isotopes in Early Jurassic seawater. *Geochimica et Cosmochimica Acta*. **58**(4), pp.1285–1301.

Jones, C.E., Tarney, J., Baker, J. and Gerouki, F. 1992. Tertiary granitoids of Rhodope, northern Greece: magmatism related to extensional collapse of the Hellenic Orogen? *Tectonophysics*. **210**, pp.295–314.

Jones, D.S., Martini, A.M., Fike, D.A. and Kaiho, K. 2017. A volcanic trigger for the Late Ordovician mass extinction? Mercury data from south China and Laurentia. *Geology*. **45**(7), pp.631–634.

Jourdan, F., Féraud, G., Bertrand, H., Watkeys, M.K. and Renne, P.R. 2008. The ^{40} Ar/ ^{39} Ar ages of the sill complex of the Karoo large igneous province: Implications for the Pliensbachian-Toarcian climate change. *Geochemistry, Geophysics, Geosystems*. **9**(6).

Kafousia, N., Karakitsios, V., Mattioli, E., Kenjo, S. and Jenkyns, H.C. 2014. The Toarcian Oceanic Anoxic Event in the Ionian Zone, Greece. *Palaeogeography, Palaeoclimatology, Palaeoecology*. **393**, pp.135–145.

Kamenov, B.K., Quadt, A. Von and Peytcheva, I. 2002. New insight into petrology , geochemistry and dating of the Vejen pluton, Bulgaria. *Geochemistry, Mineralogy and Petrology*. **39**, pp.3–25.

Kaplan, M.. 1978. Calcite pseudomorphoses in Jurassic and Lower Cretaceous deposits of the northern area of eastern Siberia. *Geol. Geofiz*. **19**, pp.62–70.

Katz, M.E., Wright, J.D., Miller, K.G., Cramer, B.S., Fennel, K. and Falkowski, P.G. 2005. Biological overprint of the geological carbon cycle. *Marine Geology*. **217**(3–4), pp.323–338.

Kauffman, E. and Erwin, D. 1995. Surviving mass extinctions. *Geotimes*. **40**.

Kazmin, V.G. and Tikhonova, N.F. 2006. Evolution of Early Mesozoic back-arc basins in the Black Sea-Caucasus segment of a Tethyan active margin. *Geological Society, London, Special Publications*. **260**(1), pp.179–200.

Kearey, P. 2001. *The New Penguin Dictionary of Geology*. London: Penguin.

Kemp, D.B., Coe, A.L., Cohen, A.S. and Schwark, L. 2005. Astronomical pacing of methane release in the Early Jurassic period. *Nature*. **437**(7057), pp.396–9.

Kemp, D.B. and Izumi, K. 2014. Multiproxy geochemical analysis of a Panthalassic margin record of the early Toarcian oceanic anoxic event (Toyora area, Japan). *Palaeogeography, Palaeoclimatology, Palaeoecology*. **414**.

Kennet, J.P. and Watkins, N.. 1970. Geomagnetic Polarity Change, Volcanic Maxima and Faunal Extinction in the South Pacific. *Nature*. **227**, pp.930–943.

Kidwell, S.M. and Jablonski, D. 1983. Taphonomic Feedback Ecological consequences of shell accumulation *In*: Springer, Boston, MA, pp.195–248. [Accessed 28 November 2018]. Available from: http://link.springer.com/10.1007/978-1-4757-0740-3_5.

Koch, P.L., Zachos, J.C. and Gingerich, P.D. 1992. Correlation between isotope records in marine and continental carbon reservoirs near the Palaeocene/Eocene boundary. *Nature*. **358**(6384), pp.319–322.

Kojumdgieva, E., Nikolov, T., Sapunov, I., Tenchov, Y., Tronkov, D. and Khrischev, Kh., Chemberski, H. Tchoumatchenco, P. 1982. National Commission on Stratigraphy of Bulgaria. Stratigraphic Code of Bulgaria (lithostratigraphic units). *Review of the Bulgarian Geological Society*. **43**(3), pp.286–310.

Koleva-Rekalova, E. and Metodiev, L. 2007. Diagenetic evolution of the Toarcian Iron-Ooidal limestones and the upper Pliensbachian-Lower Bajocian hemipelagic sediments. Evidence from two sections of the western Balkan Mountains. *Comptes rendus de l'Académie bulgare des Sciences.* **10,** pp.1085–1092.

Koleva-Rekalova, E., Metodiev, L. and Mladenova, V. 2006. Cyclic model of the

Toarcian Iron Ooidal Limestone succession at the Beledie Han section, Western Balkan Mountains, Bulgaria. *Geologie Sedimentologie*. **59**(1), pp.51–56.

Kongchum, M., Hudnall, W.H. and Delaune, R.D. 2011. Relationship between sediment clay minerals and total mercury. *Journal of Environmental Science and Health - Part A Toxic/Hazardous Substances and Environmental Engineering*. **46**(5), pp.534–539.

Korte, C. and Hesselbo, S.P. 2011. Shallow marine carbon and oxygen isotope and elemental records indicate icehouse-greenhouse cycles during the Early Jurassic. *Paleoceanography*. **26**(4), pp.1–18.

Korte, C., Hesselbo, S.P., Ullmann, C. V., Dietl, G., Ruhl, M., Schweigert, G. and Thibault, N. 2015. Jurassic climate mode governed by ocean gateway. *Nature Communications*. **6**, p.10015.

Korte, C., Jones, P.J., Brand, U., Mertmann, D. and Veizer, J. 2008. Oxygen isotope values from high-latitudes: Clues for Permian sea-surface temperature gradients and Late Palaeozoic deglaciation. *Palaeogeography, Palaeoclimatology, Palaeoecology*. **269**(1–2), pp.1–16.

Kozhoukharova, E.S. 1996. New data for the geologic position of the Precambrian ophiolitic association in the Rhodope massif. *Comptes Rendus de L'Academie Bulgare des Sciences*. **49**, pp.57–60.

Krencker, F.N., Bodin, S., Hoffmann, R., Suan, G., Mattioli, E., Kabiri, L., Föllmi, K.B. and Immenhauser, A. 2014. The middle Toarcian cold snap: Trigger of mass extinction and carbonate factory demise. *Global and Planetary Change*. **117**, pp.64–78.

Krencker, F.N., Bodin, S., Suan, G., Heimhofer, U., Kabiri, L. and Immenhauser, A. 2015. Toarcian extreme warmth led to tropical cyclone intensification. *Earth and Planetary Science Letters*. **425**.

Kronberg, P., Meyer, W. and Pilger, A. 1970. Geologie der Rila-Rhodope-Masse zwischen Strimon und Nestos (Nordgriechenland). *Beihtrage Geologisches Jahrbuch*. **88**(133–180).

Kump, L.R. and Arthur, M.A. 1999. Interpreting carbon-isotope excursions: Carbonates and organic matter. *Chemical Geology*. **161**(1), pp.181–198.

Lewandowska, A.M., Breithaupt, P., Hillebrand, H., Hoppe, H.G., Jürgens, K. and Sommer, U. 2012. Responses of primary productivity to increased temperature and phytoplankton diversity. *Journal of Sea Research*. **72**, pp.87–93.

Li, Q., McArthur, J.M. and Atkinson, T.C. 2012. Lower Jurassic belemnites as indicators of palaeo-temperature. *Palaeogeography, Palaeoclimatology, Palaeoecology*. **315**–**316**, pp.38–45.

Li, Q., McArthur, J.M., Doyle, P., Janssen, N., Leng, M.J., Müller, W. and Reboulet, S. 2013. Evaluating Mg / Ca in belemnite calcite as a palaeo-proxy. . **388**, pp.98–108.

Liao, W., Wang, Y., Kershaw, S., Weng, Z. and Yang, H. 2010. Shallow-marine dysoxia across the Permian–Triassic boundary: Evidence from pyrite framboids in the microbialite in South China. *Sedimentary Geology*. **232**(1–

2), pp.77–83.

Little, C.T.S. 1995. *The Pliensbachian–Toarcian (Lower Jurassic) Extinction Event*. University of Bristol.

Little, C.T.S. and Benton, M.J. 1995. Early Jurassic mass extinction: A global long-term event. *Geology*. **23**(6), p.495.

Littler, K., Hesselbo, S.P. and Jenkyns, H.C. 2010. A carbon-isotope perturbation at the Pliensbachian-Toarcian boundary: Evidence from the lias group, NE England. *Geological Magazine*. **147**(2), pp.181–192.

Liu, C. 1995. Jurassic bivalve palaeobiogeography of the proto-Atlantic and the application of multivariate analysis methods to palaeobiogeography. *Beringeria*. **16**, pp.3–123.

Liu, C., Heinze, M. and Fürsich, F.T. 1998. Bivalve provinces in the Proto-Atlantic and along the southern margin of the Tethys in the Jurassic. *Palaeogeography, Palaeoclimatology, Palaeoecology*. **137**, pp.127–151.

Lohmann, K.C. 1988. Geochemical Patterns of Meteoric Diagenetic Systems and Their Application to Studies of Paleokarst *In*: *Paleokarst* [Online]. New York, NY: Springer New York, pp.58–80. [Accessed 16 October 2018]. Available from: http://link.springer.com/10.1007/978-1-4612-3748-8_3.

Lyons, T.W. and Severmann, S. 2006. A critical look at iron paleoredox proxies: New insights from modern euxinic marine basins. *Geochimica et Cosmochimica Acta*. **70**(23), pp.5698–5722.

Macchioni, F. and Cecca, F. 2002. Biodiversity and biogeography of middle–late liassic ammonoids: implications for the early Toarcian mass extinction. *Geobios*. **35**(SUPPLEMENT), pp.165–175.

Mailliot, S., Mattioli, E., Bartolini, A., Baudin, F., Pittet, B. and Guex, J. 2009. Late Pliensbachian-Early Toarcian (Early Jurassic) environmental changes in an epicontinental basin of NW Europe (Causses area, central France): A micropaleontological and geochemical approach. *Palaeogeography, Palaeoclimatology, Palaeoecology*. **273**(3–4), pp.346–364.

Mailliot, S., Mattioli, E., Guex, J. and Pittet, B. 2006. The Early Toarcian anoxia, a synchronous event in the Western Tethys? An approach by quantitative biochronology (Unitary Associations), applied on calcareous nannofossils. *Palaeogeography, Palaeoclimatology, Palaeoecology*. **240**(3–4), pp.562–586.

Marshall, J.D. 1992. Climatic and oceanographic isotopic signals from the carbonate rock record and their preservation. *Geological Magazine*. **129**(2), pp.143–160.

Martindale, R. and Aberhan, M. 2017. Response of macrobenthic communities to the Toarcian Oceanic Anoxic Event in northeastern Panthalassa (Ya Ha Tinda, Alberta, Canada). *Palaeogeography, Palaeoclimatology, Palaeoecology*. **478**, pp.103–120.

Martindale, R.C. 2012. *Paleoecology of upper Triassic reef ecosystems and their demise at the Triassic-Jurassic extinction, a potential ocean acidification event*.

Martinez, M. and Dera, G. 2015. Orbital pacing of carbon fluxes by a ∼9-My

eccentricity cycle during the Mesozoic. *Proceedings of the National Academy of Sciences*. **112**(41), pp.12604–12609.

Marwick, J. 1953. Divisions and faunas of the Hokonui System (Triassic and Jurassic). *New Zealand Geological Survey Paleontological Bulletin*. **21**, pp.1–141.

Mattioli, E. and Erba, E. 1999. Synthesis of calcareous n annofossil events in tethyan lower and middle Jurassic successions. *Rivista Italiana di Paleontologia e Stratigrafia*. **105**(3), pp.343–376.

Mattioli, E., Pittet, B., Petitpierre, L. and Mailliot, S. 2009. Dramatic decrease of pelagic carbonate production by nannoplankton across the Early Toarcian anoxic event (T-OAE). *Global and Planetary Change*. **65**(3–4), pp.134–145.

Mattioli, E., Pittet, B., Suan, G. and Mailliot, S. 2008. Calcareous nannoplankton changes across the early Toarcian oceanic anoxic event in the western Tethys. *Paleoceanography*. **23**(3), n/a-n/a.

Mattioli, E., Pittet, B., Young, J.R. and Bown, P.R. 2004. Biometric analysis of Pliensbachian-Toarcian (Lower Jurassic) coccoliths of the family Biscutaceae: Intra- and interspecific variability versus palaeoenvironmental influence. *Marine Micropaleontology*. **52**(1–4), pp.5–27.

McArthur, J.M., Algeo, T.J., van de Schootbrugge, B., Li, Q. and Howarth, R.J. 2008. Basinal restriction, black shales, Re-Os dating, and the Early Toarcian (Jurassic) oceanic anoxic event. *Paleoceanography*. **23**(4), n/a-n/a.

McArthur, J.M., Donovan, D.T., Thirlwall, M.F., Fouke, B.W. and Mattey, D. 2000. Strontium isotope profile of the early Toarcian (Jurassic) oceanic anoxic event, the duration of ammonite biozones, and belemnite palaeotemperatures. *Earth and Planetary Science Letters*. **179**(2), pp.269–285.

McArthur, J.M., Doyle, P., Leng, M.J., Reeves, K., Williams, C.T., Garcia-Sanchez, R. and Howarth, R.J. 2007. Testing palaeo-environmental proxies in Jurassic belemnites: Mg/Ca, Sr/Ca, Na/Ca, δ18O and δ13C. *Palaeogeography, Palaeoclimatology, Palaeoecology*. **252**(3–4), pp.464–480.

McArthur, J.M., Howarth, R.J. and Bailey, T.R. 2001. Strontium Isotope Stratigraphy: LOWESS Version 3: Best Fit to the Marine Sr-Isotope Curve for 0–509 Ma and Accompanying Look-up Table for Deriving Numerical Age. *The Journal of Geology*. **109**(2), pp.155–170.

McArthur, J.M., Mutterlose, J., Price, G.D., Rawson, P.., Ruffell, A. and Thirlwall, M.F. 2004. Belemnites of Valanginian, Hauterivian and Barremian age: Sr-isotope stratigraphy, composition (87Sr/86Sr, δ13C, δ18O, Na, Sr, Mg), and palaeo-oceanography. *Palaeogeography, Palaeoclimatology, Palaeoecology*. **202**(3–4), pp.253–272.

McArthur, J.M., Steuber, T., Page, K.N. and Landman, N.H. 2016. Sr-Isotope Stratigraphy : Assigning Time in the Campanian , Pliensbachian. Taorcian, and Valnginian. . **124**, pp.569–586.

McArthur, J.M. and Wignall, P.B. 2007. Comment on “Non-uniqueness and interpretation of the seawater 87Sr/86Sr curve” by Dave Waltham and

Darren R. Gröcke (GCA, 70, 2006, 384–394). *Geochimica et Cosmochimica Acta*. **71**(13), pp.3382–3386.

McElwain, J.C., Wade-Murphy, J. and Hesselbo, S.P. 2005. Changes in carbon dioxide during an oceanic anoxic event linked to intrusion into Gondwana coals. *Nature*. **435**(7041), pp.479–482.

McElwain, J.C., Wade-Murphy, J. and Hesselbo, S.P. 2005. Changes in carbon dioxide during an oceanic anoxic event linked to intrusion into Gondwana coals. *Nature*. **435**(7041), pp.479–482.

Meister, C., Dommergues, J.L., Dommergues, C., Lachkar, N. and El Hariri, K. 2011. Les ammonites du Pliensbachien du jebel Bou Rharraf (Haut Atlas oriental, Maroc). *Géobios*. **44**, pp.117.

Meister, C. and Böhm, F. 1993. Austroalpine Liassic Ammonites from the Adnet Formation (Northern Calcareous Alps). *Jahrbuch der Geologischen Bundesanstalt*. **136**(1), pp.163–211.

Metodiev, L. 2000. Etude de la limite Toarcian-Aalenien et stratigraphie de L'aalenien dans quelques coupes de mont balkan occidental et central en Bulgarie. *Strata*. **10**(1), pp.117–121.

Metodiev, L. 2002. Grammoceras, Pseudogrammoceras et Podagrosites (Grammoceratinae, Ammonitina) du Toarcien superieur dans la region du Balkan (Bulgarie). Taxonomie et biostratigraphie. *Geologica Balcanica*. **32**(2–4), pp.165–189.

Metodiev, L. 2003a. Les Dactylioceratidae (Ammonitina) - Criteres morphologiques taxonomiques. Implications sur les representants de la Familie du Toarcien en Bulgarie. *Geologie Paleontologie*. **56**(10), pp.69–74.

Metodiev, L. 2006. New data about the ammonite genus Pseudolioceras Buckman, 1889 (Harpoceratinae, Ammonitina) from the Toarcian of the Balkan Mountains (Bulgaria). *Geologie Paleontologie, Comptes rendus de l'Académie bulgare des Sciences*. **59**(7), pp.767–774.

Metodiev, L. 2003b. Notes on the Status and application of the Upper Toarcian Haugia variabilis Zone in Bulgaria. *Geologica Balcanica*. **33**, pp.110–111.

Metodiev, L. 2008. The ammonite zones of the Toarcian in Bulgaria - new evidence, subzonation and correlation with the standard zones and subzones in North-West Europe. *Geologie Stratigraphie, Comptes rendus de l'Académie bulgare des Sciences*. **61**(1), pp.87–132.

Metodiev, L. 1997. Toarcian and Aalenian ammonites in a part of the Western Stara Planina Mts., Bulgaria (taxonomy, stratigraphy). *Geologica Balcanica*. **27**(2–4), pp.3–31.

Metodiev, L., Ivanova, D. and Koleva-Rekalova, E. 2005. Biostratigraphy of the Toarcian in the section at the village of Beledie Han (Western Balkan Mts), Bulgaria *In*: *Geologie Stratigraphie*., pp.39–46.

Metodiev, L. and Koleva-Rekalova, E. 2003. Cathodoluminescence test of belemnite rostra - first condition for precise isotope and chemical analyses: an example from the Toarcian at the section near the village of Beledie Han (Western Balkan Mts), Bulgaria. *C.R. Acad. Bulg. Sci.* **56**, pp.61–66.

Metodiev, L. and Koleva-Rekalova, E. 2008. Stable isotope records (δ18O and δ13C) of Lower-Middle Jurassic belemnites from the Western Balkan mountains (Bulgaria): Palaeoenvironmental application. *Applied Geochemistry*. **23**(10), pp.2845–2856.

Metodiev, L. and Koleva-Rekalova, E.K. 2005. Preservational features of the Upper Pliensbachian-Lower Bajocian belemnite rostra from two clayey-limestone successions of the west Balkan Mts (Bulgaria). Taphonomic and sedimentological evidence. *C. R. Acad. Bulg. Sci.* **58**, pp.705–710.

Metodiev, L. and Sapunov, I.G. 1999. Representatives of the Toarcian ammonite genera Osperleioceras Krimholz, 1957 and Phlyseogrammoceras Buckman. 1901 in Bulgaria. *Geologica Balcanica*. **31**(3–4), pp.59–70.

Metodiev, L., Savov, I.P., Gröcke R., D., Wignall, P.B., Newton, R.J., Andreeva, P. V and Koleva-Rekalova, E. 2014. Paleoenvironmental conditions recorded by 87Sr/86Sr, δ13C and δ18O in late Pliensbachian–Toarcian (Jurassic) belemnites from Bulgaria. *Palaeogeography, Palaeoclimatology, Palaeoecology*. **409**, pp.98–113.

Metodiev, L., Savov, I.P. and Koleva-Rekalova, E. 2012. 87Sr/86Sr isotope systematics on belemnites from the Pliensbachian of West Bulgaria *In*: *Bulgarian Geological Society National Conference*., pp.86–87.

Meyer, K.M. and Kump, L.R. 2008. Oceanic Euxinia in Earth History: Causes and Consequences. *Annual Review of Earth and Planetary Sciences*. **36**(1), pp.251–288.

Middelburg, J.J., Vlug, T., Jaco, F. and van der Nat, W.A. 1993. Organic matter mineralization in marine systems. *Global and Planetary Change*. **8**(1–2), pp.47–58.

Miguez-Salas, O., Rodríguez-Tovar, F.J. and Duarte, L.V. 2017. Selective incidence of the toarcian oceanic anoxic event on macroinvertebrate marine communities: a case from the Lusitanian basin, Portugal. *Lethaia*. **50**(4), pp.548–560.

Monteiro, F.M., Pancost, R.D., Ridgwell, A. and Donnadieu, Y. 2012. Nutrients as the dominant control on the spread of anoxia and euxinia across the Cenomanian-Turonian oceanic anoxic event (OAE2): Model-data comparison. *Paleoceanography*. **27**(4), pp.1–17.

Montero-Serrano, J.-C., Föllmi, K.B., Adatte, T., Spangenberg, J., Tribovillard, N., Fantasia, A. and Suan, G. 2015. Continental weathering and redox conditions during the early Toarcian Oceanic Anoxic Event in the northwestern Tethys: Insight from the Posidonia Shale section in the Swiss Jura Mountains. *Palaeogeography, Palaeoclimatology, Palaeoecology*. **429**, pp.83–99.

Morbey, S.J. 1978. Late Triassic and Early Jurassic subsurface palynostratigraphy in northwestern Europe. *Palinologia*. **1**, pp.355–365.

Nachev, I. 1975a. Diagenetic glauconites in Bulgaria. *Palaeontology, Stratigraphy and Lithology*. **1**, pp.85–100.

Nachev, I. 1960. Jurassic sedimentary iron ore in the Troyan-Teteven region. *Bulletin of the Geological Institute*. **8**, pp.47–103.

Nachev, I. 1968. Lithology and geochemistry of sedimentary iron ore in Toarcian and Lower Bajocian in the Balkan Area. *Geol. Inst., Acad. Bulg. Sci., Jub. Geol.*, pp.221–231.

Nachev, I. 1975b. On the origin of sedimentary glauconites. Palaeontology, Stratigraphy and Lithology. *Palaeontology, Stratigraphy and Lithology*. **2**, pp.73–81.

Nachev, I. 1974. Regularities in the distribution of the components in the Jurassic iron ores in Bulgaria. *Bulletin of the Geological Institute, Series Stratigraphy and Lithology*. **23**, pp.131–141.

Nachev, I. 1973. Structure and geochemical features of iron ores of Sinemurian–Pliensbachian age in Bulgaria. *Comptes rendus de l'Académie bulgare des Sciences*. **26**(10), pp.1383–1386.

Neuendorf, K. and Jackson, J. 2005. *Glossary of Geology* 5th editio. Alexandria: Am. Geol. Inst.,.

Neumayr, M. 1885. Die geographische Verbreitung der Juraformation. *Denkschriften der Österreichischen Akademie der Wissenschaften, Mathematisch-Naturwissenschaftliche Klasse*. **50**, pp.57–142.

Neumayr, M. 1883. Über klimatische Zonen während der Jura- und Kreidezeit. Denkschriften der kaiserlichen Akademie der Wissenschaften, Wien. *Mathematisch-naturwissenschaftlichen Classe*. **47**(1), pp.277–310.

Neumeister, S., Gratzer, R., Algeo, T.J., Bechtel, A., Gawlick, H.J., Newton, R.J. and Sachsenhofer, R.F. 2015. Oceanic response to Pliensbachian and Toarcian magmatic events: Implications from an organic-rich basinal succession in the NW Tethys. *Global and Planetary Change*. **126**, pp.62–83.

Newton, R.J., Reeves, E.P., Kafousia, N., Wignall, P.B., Bottrell, S. and Sha, J.G. 2011. Low marine sulfate concentrations and the isolation of the European epicontinental sea during the Early Jurassic. *Geology*. **39**(1), pp.7–10.

Nielsen, J.K. and Shen, Y. 2004. Evidence for sulfidic deep water during the Late Permian in the East Greenland Basin. *Geology*. **32**(12), p.1037.

Nikitin, S. 1886. Über die Beziehungen zwischen der russischen und der westeuropäischen Juraformation. *Neues Jahrb. für Min*.

Nikolov, T. and Sapunov, I. 2002. *Stratigraphic Code of Bulgaria (second revised and expanded edition). National Commission on Stratigraphy of Bulgaria.* Sofia: Bulgarian Academy of Sciences Academic Press.

Nunn, E. V. and Price, G.D. 2010. Late Jurassic (Kimmeridgian-Tithonian) stable isotopes (??18O, ??13C) and Mg/Ca ratios: New palaeoclimate data from Helmsdale, Northeast Scotland. *Palaeogeography, Palaeoclimatology, Palaeoecology*. **292**(1–2), pp.325–335.

O'Neil, J.R., Clayton, R.N. and Mayeda, T.K. 1969. Oxygen Isotope Fractionation in Divalent Metal Carbonates. *The Journal of Chemical Physics*. **51**(12), pp.5547–5558.

Ohno, T. and Hirata, T. 2007. Simultaneous Determination of Mass-dependent Isotopic Fractionation and Radiogenic Isotope Variation of Strontium in

Geochemical Samples by Multiple Collector-ICP-Mass Spectrometry. *Analytical Sciences*. **23**(11), pp.1275–1280.

Ortmann, A. 1896. An examination of the arguments given by Neumayr for the existence of climatic zones in Jurassic times. *American Journal of Science*. **1**(4), pp.257–270.

Oschmann, W. 1988. Upper Kimmeridgian and Portlandian marine macrobenthic associations from southern England and northern France. *Facies*. **18**(1), pp.49–82.

Owens, J.D., Gill, B.C., Jenkyns, H.C., Bates, S.M., Severmann, S., Kuypers, M.M.M., Woodfine, R.G. and Lyons, T.W. 2013. Sulfur isotopes track the global extent and dynamics of euxinia during Cretaceous Oceanic Anoxic Event 2. *Proceedings of the National Academy of Sciences*. **110**(46), pp.18407–18412.

Page, K.N. 2003. The Lower Jurassic of Europe: its subdivision and correlation. *Geological Survey of Denmark and Greenland Bulletin*. **1**, pp.23–59.

Pálfy, J., Demény, A., Haas, J., Hetényi, M., Orchard, M.J. and Veto, I. 2001. Carbon isotope anomaly and other geochemical changes at the Triassic-Jurassic boundary from a marine section in Hungary. *Geology*. **29**(11), p.1047.

Pálfy, J. and Smith, P.L. 2000. Synchrony between Early Jurassic extinction, oceanic anoxic event, and the Karoo-Ferrar flood basalt volcanism. *Geology*. **28**(8), p.747.

Palliani, R.B. and Riding, J.B. 1999. Relationships between the early Toarcian anoxic event and organic-walled phytoplankton in central Italy. *Marine Micropaleontology*. **37**(2), pp.101–116.

Palmer, M.R. and Edmond, J.M. 1989. The strontium isotope budget of the modern ocean. *Earth and Planetary Science Letters*. **92**(1), pp.11–26.

Pancost, R.D., Crawford, N., Magness, S., Turner, A., Jenkyns, H.C. and Maxwell, J.R. 2004. Further evidence for the development of photic-zone euxinic conditions during Mesozoic oceanic anoxic events. *Journal of the Geological Society*. **161**(3), pp.353–364.

Paredes, R. 2014. Bivalvos del Jurásico Inferior de la colección Suárez Vega depositada en el Museo del Jurásico de Asturias (MUJA), España. *Bol. R. Soc. Esp. Hist. Nat. Sec. Geol.,*. **108**, pp.53–79.

Paredes, R. 2014. Síntese dos bivalves citados para o Pliensbaquiano (Jurássico Inferior) da Bacia Lusitânica (Portugal). *Comunicações Geológicas*. **101**, pp.521–525.

Paredes, R., Comas-Rengifo, M.J., Damborenea, S.E., Duarte, L.V. and Goy, A. 2015. Migrants from the Americas : the early Jurassic pectinid Weyla restricted distribution in Iberian Peninsula platforms. . (October).

Payne, J.L. and Clapham, M.E. 2012. End-Permian Mass Extinction in the Oceans: An Ancient Analog for the Twenty-First Century? *Annual Review of Earth and Planetary Sciences*. **40**(1), pp.89–111.

Pearce, C.R., Cohen, A.S., Coe, A.L. and Burton, K.W. 2008. Molybdenum isotope evidence for global ocean anoxia coupled with perturbations to the

carbon cycle during the Early Jurassic. *Geology*. **36**(3), p.231.

Pearce, C.R., Parkinson, I.J., Gaillardet, J., Charlier, B.L.A., Mokadem, F. and Burton, K.W. 2015. Reassessing the stable (δ 88/86 Sr) and radiogenic (87 Sr/ 86 Sr) strontium isotopic composition of marine inputs. *Geochimica et Cosmochimica Acta*. **157**, pp.125–146.

Percival, L.M.E., Cohen, A.S., Davies, M.K., Dickson, A.J., Hesselbo, S.P., Jenkyns, H.C., Leng, M.J., Mather, T. a., Storm, M.S. and Xu, W. 2016. Osmium isotope evidence for two pulses of increased continental weathering linked to Early Jurassic volcanism and climate change. *Geology*. **44**(9).

Percival, L.M.E., Ruhl, M., Hesselbo, S.P., Jenkyns, H.C., Mather, T. a. and Whiteside, J.H. 2017. Mercury evidence for pulsed volcanism during the end-Triassic mass extinction. *Proceedings of the National Academy of Sciences*.

Percival, L.M.E., Witt, M.L.I., Mather, T. a., Hermoso, M., Jenkyns, H.C., Hesselbo, S.P., Al-Suwaidi, A.H., Storm, M.S., Xu, W. and Ruhl, M. 2015. Globally enhanced mercury deposition during the end-Pliensbachian extinction and Toarcian OAE: A link to the Karoo–Ferrar Large Igneous Province. *Earth and Planetary Science Letters*. **1**, pp.1–14.

Peti, L., Thibault, N., Clémence, M.-E., KORTE, C., Dommergues, J.-L., Bougeault, C., Pellenard, P., Jelby, M.E. and Ullmann, C. V. 2017. Sinemurian–Pliensbachian calcareous nannofossil biostratigraphy and organic carbon isotope stratigraphy in the Paris Basin: Calibration to the ammonite biozonation of NW Europe. *Palaeogeography, Palaeoclimatology, Palaeoecology*. **468**, pp.142–161.

Petrova, S., Rabrenović, D., Lakova, I., Koleva-Rekalova, E., Ivanova, D., Metodiev, L. and Malešević., N. 2012. Biostratigraphy and microfacies of the pelagic carbonates across the Jurassic/Cretaceous boundary in eastern Serbia (Stara Planina–Poreč Zone). *Geologica Balcanica*. **41**(1–3), pp.53–76.

Pittet, B., Suan, G., Lenoir, F., Duarte, L.V. and Mattioli, E. 2014. Carbon isotope evidence for sedimentary discontinuities in the lower Toarcian of the Lusitanian Basin (Portugal): Sea level change at the onset of the Oceanic Anoxic Event. *Sedimentary Geology*. **303**, pp.1–14.

Podlaha, O.G., Mutterlose, J. and Veizer, J. 1998. Preservation of ??18O and ??13C in belemnite rostra from the Jurassic/Early Cretaceous successions. *American Journal of Science*. **298**(4), pp.324–347.

Posenato, R., Bassi, D. and Avanzini, M. 2013. Bivalve pavements from shallow-water black-shales in the Early Jurassic of northern Italy: A record of salinity- and oxygen-depleted environmental dynamics. *Palaeogeography, Palaeoclimatology, Palaeoecology*. **369**, pp.262–271.

Posenato, R. and Masetti, D. 2012. Environmental control and dynamics of Lower Jurassic bivalve build-ups in the Trento Platform (Southern Alps, Italy). *Palaeogeography, Palaeoclimatology, Palaeoecology*. **361**–**362**, pp.1–13.

Poulton, S.W. and Canfield, D.E. 2005. Development of a sequential extraction

procedure for iron: Implications for iron partitioning in continentally derived particulates. *Chemical Geology*. **214**(3–4), pp.209–221.

Price, G. 1999. The evidence and implications of polar ice during the Mesozoic. *Earth-Science Reviews*. **48**(3), pp.183–210.

Price, G.D., Fozy, I. and Pálfy, J. 2016. Carbon cycle history through the Jurassic-Cretaceous boundary: A new global δ13C stack. *Palaeogeography, Palaeoclimatology, Palaeoecology*. **451**, pp.46–61.

Price, G.D. and Sellwood, B.W. 1997. 'Warm' palaeotemperatures from high Late Jurassic palaeolatitudes (Falkland Plateau): Ecological, environmental or diagenetic controls? *Palaeogeography, Palaeoclimatology, Palaeoecology*. **129**(3–4), pp.315–327.

Pyle, D.M. and Mather, T.A. 2003. The importance of volcanic emissions for the global atmospheric mercury cycle. *Atmospheric Environment*. **37**(36), pp.5115–5124.

Quesada, S., Robles, S. and Rosales, I. 2005. Depositional architecture and transgressive-regressive cycles within Liassic backstepping carbonate ramps in the Basque-Cantabrian basin, northern Spain. *Journal of the Geological Society*. **162**(3), pp.531–548.

Radulović, B. V. 2013. Lower Jurassic bivalves of eastern Serbia. *Beringeria*. **43**, pp.3–61.

Radulović, B. V., Radulovic, V. and Ruban, D.A. 2017. Bivalves from the tectonic units of eastern Serbia in the context of the Pliensbachian (Early Jurassic) palaeobiogeography of Europe. *Palaeogeography, Palaeoclimatology, Palaeoecology*. **466**, pp.1–6.

Radulović, B. V., Radulovic, V. and Ruban, D.A. 2016. Similarity of Early and Middle Jurassic brachiopods between the Danubian and Getic tectonic units of eastern Serbia. *Palaeogeography, Palaeoclimatology, Palaeoecology*. **443**(July 2016), pp.230–236.

Raup, D.M. 1994. The role of extinction in evolution. *Proceedings of the National Academy of Sciences*. **91**(15), pp.6758–6763.

Reolid, M., Emanuela, M., Nieto, L.M. and Rodríguez-Tovar, F.J. 2014. The Early Toarcian Oceanic Anoxic Event in the External Subbetic (Southiberian Palaeomargin, Westernmost Tethys): Geochemistry, nannofossils and ichnology. *Palaeogeography, Palaeoclimatology, Palaeoecology*. **411**.

Reolid, M., Rodríguez-Tovar, F.J., Marok, a. and Sebane, A. 2012. The Toarcian oceanic anoxic event in the Western Saharan Atlas, Algeria (North African paleomargin): Role of anoxia and productivity. *Geological Society of America Bulletin*. **124**(9–10), pp.1646–1664.

Rexfort, A. and Mutterlose, J. 2006. Stable isotope records from Sepia officinalis-a key to understanding the ecology of belemnites? *Earth and Planetary Science Letters*. **247**(3–4), pp.212–221.

Rhoads, D.C. and Morse, J.W. 1971. *Evolutionary and ecologic significance of oxygen-deficient marine basins* [Online]. [Accessed 16 November 2018]. Available from: https://onlinelibrary.wiley.com/doi/pdf/10.1111/j.1502-

3931.1971.tb01864.x.

Richter, D.K., Neuser, R.D., Schreuer, J., Gies, H. and Immenhauser, A. 2011. Radiaxial-fibrous calcites: A new look at an old problem. *Sedimentary Geology*. **239**(1–2), pp.23–36.

Riegraf, W. 1985. Mikrofauna, biostratigraphie und fazies im unteren Toarcium südwestdeutschlans und vergeiche mit benachbarten gebieten. *Tübinger Mikropaläontologische Mitteilungen*. **3**, pp.1–232.

Rodríguez-Tovar, F.J., Miguez-Salas, O. and Duarte, L.V. 2017. Toarcian Oceanic Anoxic Event induced unusual behaviour and palaeobiological changes in Thalassinoides tracemakers. *Palaeogeography, Palaeoclimatology, Palaeoecology*. **485**, pp.46–56.

Rodríguez-Tovar, F.J. and Reolid, M. 2013. Environmental conditions during the Toarcian Oceanic Anoxic Event (T-OAE) in the westernmost Tethys: influence of the regional context on a global phenomenon. *Bulletin of Geosciences*. **88**(4), pp.697–712.

Rodríguez-Tovar, F.J. and Uchman, A. 2010. Ichnofabric Evidence for the Lack of Bottom Anoxia During the Lower Toarcian Oceanic Anoxic Event in the Fuente De La Vidriera Section, Betic Cordillera, Spain. *Palaios*. **25**(9), pp.576–587.

Rogov, M.A. and Zakharov, V.A. 2010. Jurassic and Lower Cretaceous glendonite occurences and their implication for Arctic paleoclimate reconstructions and stratigraphy . *Earth Science Frontiers*. **17**, pp.345–347.

Röhl, H.J., Schmid-Röhl, A., Oschmann, W., Frimmel, A. and Schwark, L. 2001. The Posidonia Shale (Lower Toarcian) of SW-Germany: an oxygen-depleted ecosystem controlled by sea level and palaeoclimate. *Palaeogeography, Palaeoclimatology, Palaeoecology*. **165**(1–2), pp.27–52.

Rosales, I., Barnolas, A., Goy, A., Sevillano, A., Armendáriz, M. and López-García, J.M. 2018. Isotope records (C-O-Sr) of late Pliensbachian-early Toarcian environmental perturbations in the westernmost Tethys (Majorca Island, Spain). *Palaeogeography, Palaeoclimatology, Palaeoecology*. **497**(February), pp.168–185.

Rosales, I., Quesada, S. and Robles, S. 2004. Paleotemperature variations of Early Jurassic seawater recorded in geochemical trends of belemnites from the Basque-Cantabrian basin, northern Spain. *Palaeogeography, Palaeoclimatology, Palaeoecology*. **203**(3–4), pp.253–275.

Rosales, I., Quesada, S. and Robles, S. 2001. Primary and diagenetic isotopic signals in fossils and hemipelagic carbonates: The Lower Jurassic of northern Spain. *Sedimentology*. **48**(5), pp.1149–1169.

Rosales, I., Robles, S. and Quesada, S. 2004. Elemental and Oxygen Isotope Composition of Early Jurassic Belemnites: Salinity vs. Temperature Signals. *Journal of Sedimentary Research*. **74**, pp.342–354.

Rosales, I., Robles, S. and Quesada, S. 2005. Oxygen isotope , Mg / Ca and Sr / Ca records of Lower Jurassic belemnite shells : implications for the interpretation of the isotopic record of old fossils and changes of ancient seawater paleotemperature. . **7**.

Rothschild, L.J. 2001. Life in Extreme Environments. *Ad Astra*. **14**(September 2000), pp.1092–1101.

Ruban, D.A. 2004. Diversity dynamics of Early – Middle Jurassic brachiopods of Caucasus , and the Pliensbachian – Toarcian mass extinction. . **49**(2), pp.275–282.

Ruban, D.A. 2006. Taxonomic diversity dynamics of the Jurassic bivalves in the Caucasus: Regional trends and recognition of global patterns. *Palaeogeography, Palaeoclimatology, Palaeoecology*. **239**, pp.63–74.

Ruban, D.A. and Vörös, A. 2015. Palaeobiogeographical affinity of the early Pliensbachian (Early Jurassic) brachiopod assemblage of the Northern Caucasus (Russia): A new evidence. *Palaeogeography, Palaeoclimatology, Palaeoecology*. **430**, pp.11–20.

Ruebsam, W., Mayer, B. and Schwark, L. 2019. Cryosphere carbon dynamics control early Toarcian global warming and sea level evolution. *Global and Planetary Change*. **172**, pp.440–453.

Ruebsam, W., Müller, T., Kovács, J., Pálfy, J. and Schwark, L. 2018. Environmental response to the early Toarcian carbon cycle and climate perturbations in the northeastern part of the West Tethys shelf. *Gondwana Research*. **59**, pp.144–158.

Ruebsam, W., Münzberger, P. and Schwark, L. 2014. Chronology of the Early Toarcian environmental crisis in the Lorraine Sub-Basin (NE Paris Basin). *Earth and Planetary Science Letters*. **404**, pp.273–282.

Ruhl, M., Hesselbo, S.P., Hinnov, L.A., Jenkyns, H.C., Xu, W., Riding, J.B., Storm, M.S., Minisini, D., Ullmann, C. V. and Leng, M.J. 2016. Astronomical constraints on the duration of the Early Jurassic Pliensbachian Stage and global climatic fluctuations. *Earth and Planetary Science Letters*. **455**, pp.149–165.

Ruvalcaba Baroni, I., Pohl, A., van Helmond, N.A.G.M., Papadomanolaki, N.M., Coe, A.L., Cohen, A.S., van de Schootbrugge, B., Donnadieu, Y. and Slomp, C.P. 2018. Ocean Circulation in the Toarcian (Early Jurassic): A Key Control on Deoxygenation and Carbon Burial on the European Shelf. *Paleoceanography and Paleoclimatology*. **33**(9), pp.994–1012.

Sabatino, N. 2013. Carbon-isotope record and palaeoenvironmental changes during the early Toarcian oceanic anoxic event in shallow-marine carbonates of the Adriatic Carbonate Platform in Croatia. . **150**, pp.1085–1102.

Sabatino, N., Neri, R., Bellanca, A., Jenkyns, H.C., Baudin, F., Parisi, G. and Masetti, D. 2009. Carbon-isotope records of the Early Jurassic (Toarcian) oceanic anoxic event from the Valdorbia (Umbria-Marche Apennines) and Monte Mangart (Julian Alps) sections: palaeoceanographic and stratigraphic implications. *Sedimentology*. **56**(5), pp.1307–1328.

Sabatino, N., Vlahović, I., Jenkyns, H.C., Scopelliti, G., Neri, R., Prtoljan, B. and Velić, I. 2013. Carbon-isotope record and palaeoenvironmental changes during the early toarcian oceanic anoxic event in shallow-marine carbonates of the adriatic carbonate platform in Croatia. *Geological Magazine*. **150**, pp.1085–1102.

Saelen, G. 1989. Diagenesis and construction of the belemnite rostrum. *Palaeontology*. **32**(4), pp.765–798.

Saelen, G., Doyle, P. and Talbot, M.R. 1996. Stable-Isotope Analyses of Belemnite Rostra from the Whitby Mudstone Fm., England: Surface Water Conditions during Deposition of a Marine Black Shale. *PALAIOS*. **11**(2), p.97.

Sælen, G., Tyson, R. V., Telnæs, N. and Talbot, M.R. 2000. Contrasting watermass conditions during deposition of the Whitby Mudstone (Lower Jurassic) and Kimmeridge Clay (Upper Jurassic) formations, UK. *Palaeogeography, Palaeoclimatology, Palaeoecology*. **163**(3–4), pp.163–196.

Sanei, H., Grasby, S.E. and Beauchamp, B. 2012. Latest Permian mercury anomalies. *Geology*. **40**(1), pp.63–66.

Sapunov, I.., Tchoumatchenco, P., Baburkov, I.., Bakalova, D.., Dodekova, L.., Zheleva, C.., Nikolova, M.. and Černjavska, S. 1986. The Jurassic System in the new boreholes in the area of Provadija. *Review of the Bulgarian Geological Society*. **47**(2), pp.103–120.

Sapunov, I. and Stephanov, J. 1964. The stages, substages, ammonite zones and subzones of the Lower and Middle Jurassic in the Western and Central Balkan Range (Bulgaria). *Colloque du Jurassique, Luxembourg*., pp.705–718.

Sapunov, I. and Tchoumatchenco, P. 1991. A revision of the Jurassic formal lithostratigraphic units in Bulgaria introduced prior to 1990. *Review of the Bulgarian Geological Society*. **52**(2), pp.56–66.

Sapunov, I. and Tchoumatchenco, P. 1988. Bulgarian experience in Lower Jurassic biozonation based on different fossil groups – a retrospection *In*: *Symp. on Jurassic Stratigraphy, Lisboa*., pp.699–715.

Sapunov, I. and Tchoumatchenco, P. 1987a. Geological development of North-east Bulgaria during the Jurassic. *Palaeontology, Stratigraphy and Lithology*. **24**(3–59).

Sapunov, I. and Tchoumatchenco, P. 1987b. *Jurassic System stratigraphy* (H. Bokov, P. and Chemberski, ed.). Sofia, pp.58-64.

Sapunov, I. and Tchoumatchenco, P. 1986. Revision of the Bulgarian formal lithostratigraphic units related to the Jurassic System, introduced prior to 1985. *Review of the Bulgarian Geological Society*. **47**(1), pp.35–50.

Sapunov, I. and Tchoumatchenco, P. 1998. The Jurassic geological sites in North-West Bulagria. *Geologica Balcanica*. **28**(3–4), pp.137–142.

Sapunov, I., Tchoumatchenco, P., Atanasov, A. and Marinkov, A. 1991. Central North Bulgaria during the Jurassic. *Geologica Balcanica*. **21**(5), pp.3–68.

Sapunov, I., Tchoumatchenco, P., Bărdarov, S.., Vavilova, M., Dodekova, L., Kitov, P. and Černjavska, S. 1986. Stratigraphy of the Jurassic rocks from the borehole sections between the villages of Resen, Veliko Tărnovo Area and Konak, Tărgovište area. . **47**(3), pp.26–42.

Sapunov, I., Tchoumatchenco, P. and Shopov, V. 1971. Concerning certain features of the palaeogeography of the Teteven Area in the Early Jurassic.

Bulletin of the Geological Institute, Series Stratigraphy and lithology. **20**, pp.33–62.

Sapunov, I., Tchoumatchenco, P. and Shopov, V. 1967. Stratigraphie et paléoecologie du Jurassique inférieur dans une partie du Bulgarie occidentale. *Annuaire de l'Université de Sofia, Faculté de géologie et géographie, Livre 1, géologie*. **67**, pp.101–149.

Sapunov, I., Tchoumatchenco, P. and Shopov, V. 1996. The Lower Jurassic in the Troyan Region and the south-eastern part of the Teteven Region, Central Balkanids (brachiopod-, bivalve- and ammonite stratigraphy and palaeotectonics). *Geologica Balcanica*. **26**(3), pp.3–19.

Sapunov, I.G. 1961. Ammonites from the Liassic family Liparoceratidae in Bulgaria. *Travaux sur la géologie de Bulgarie, Série Paléontologie*. **3**, pp.39–70.

Sapunov, I.G. 1971. Concerning the nature of the Early-Middle Jurassic depressions in Bulgaria. *Comptes rendus de l'Académie bulgare des Sciences*. **24**(9), pp.1223–1226.

Sapunov, I.G. 1983. Introduction in the stratigraphy of the sediments of Mesozoic Eratem: Jurassic System *In*: P. Atanasov, A. and Bokov, ed. *Geology and oil and gas perspectives of the Moesian Platform in Central North Bulgaria.* Sofia: Tehnika, pp.18–28.

Sapunov, I.G. 1979. *Les fossiles de Bulgarie. Jurassique supérieur, Ammonoidea* III. (V. Tzankov, ed.). Sofia: Bulgarian Academy of Sciences Academic Press, pp. 263.

Sapunov, I.G. 1964. Notes on the boundary between the Lower and Middle Jurassic and on the stage term Aalenian *In*: *Colloque du Jurassique, Luxembourg*. Luxembourg, pp.221–228.

Sapunov, I.G. 1969. On the age of the iron ores of the Ponor-Gradets Jurassic strip (Western Balkan Range). *Comptes rendus de l'Académie bulgare des Sciences*. **22**(7), pp.807–810.

Sapunov, I.G. 1959. Stratigraphic and palaeontological studies of the Toarcian in the vicinity of the town of Teteven (Central Balkan Range). *Travaux sur la géologie de Bulgarie*. **1**, pp.17–49.

Sapunov, I.G. 1968. The ammonite zones of the Toarcian in Bulgaria. *Bulletin of the Geological Institute, Series Palaeontology*. **17**, pp.133–165.

Sapunov, I.G. 1999. The Jurassic in the south-eastern part of Bulgaria (stratigraphy, geodynamics, facies and palaeogeographic evolution). *Geologica Balcanica*. **29**(1–2), pp.19–59.

Sapunov, I.G. 1963. Toarcian ammonites of the family Dactylioceratidae from Western Bulgaria. *Travaux sur la géologie de Bulgarie, Série Paléontologie*. **5**, pp.109–147.

Sapunov, I.G. and Metodiev, L. 2007. Main features of the Jurassic in Bulgaria. *Comptes Rendus de L'Academie Bulgare des Sciences*. **60**(2), pp.169–178.

Sapunov, I.G. and Metodiev, L. 2007a. Main features of the Jurassic in Bulgaria. *Comptes rendus de l'Académie bulgare des Sciences*. **60**(2),

pp.169–178.

Sapunov, I.G. and Metodiev, L. 2007b. The Hettangian-Pliensbachian ammonite zones and subzones in Bulgaria–a retrospection and correlation with the standard zones and subzones in North-western Europe. *Comptes rendus de l'Académie bulgare des Sciences*. **60**(9), pp.991–1000.

Sapunov, I.G., Tchoumatchenco, P. and Černjavska, S. 1990. The Kotel Formation and other olistostrome formations in East Stara Planina and Eleno-Tvurditsa Stara Planina (relations, age and distribution). *Geologica Balcanica*. **20**(3), pp.55–56.

Saunders, A. and Reichow, M. 2009. Chinese Science Bulletin The Siberian Traps and the End-Permian mass extinction: a critical review. *Chinese Science Bulletin*. **54**(1), pp.20–37.

Savrda, C.E. and Bottjer, D.J. 1989. Anatomy and Implications of Bioturbated Beds in 'Black Shale' Sequences: Examples from the Jurassic Posidonienschiefer (Southern Germany). *PALAIOS*. **4**(4), p.330.

Savrda, C.E. and Bottjer, D.J. 1987. Trace fossils as indicators of bottom-water redox conditions in ancient marine environments *In*: *New concepts in the use of biogenic sedimentary structures for paleoenvironmental interpretation: volume and guidebook* [Online]., pp.3–26. [Accessed 28 November 2018]. Available from: http://archives.datapages.com/data/pac_sepm/067/067001/pdfs/3.pdf.

Scaife, J.D., Ruhl, M., Dickson, A.J., Mather, T.A., Jenkyns, H.C., Percival, L.M.E., Hesselbo, S.P., Cartwright, J., Eldrett, J.S., Bergman, S.C. and Minisini, D. 2017. Sedimentary Mercury Enrichments as a Marker for Submarine Large Igneous Province Volcanism? Evidence From the Mid-Cenomanian Event and Oceanic Anoxic Event 2 (Late Cretaceous). *Geochemistry, Geophysics, Geosystems*. **18**(12), pp.4253–4275.

Schlanger, S.O. and Jenkyns, H.C. 1976. Cretaceous Oceanic Anoxic Events: Causes and Consquences. *Geologie en Mijnbouw*. **55**, pp.179–184.

Schlegelmilch, R. 1998. *Die Belemniten des süddeutschen Jura* [Online].

Schmid-Röhl, A., Röhl, H.J., Oschmann, W., Frimmel, A. and Schwark, L. 2002. Palaeoenvironmental reconstruction of Lower Toarcian epicontinental black shales (Posidonia Shale, SW Germany): global versus regional control. *Geobios*. **35**(1), pp.13–20.

Schobben, M., Ullmann, C. V., Leda, L., Korn, D., Struck, U., Reimold, W.U., Ghaderi, A., Algeo, T.J. and KORTE, C. 2016. Discerning primary versus diagenetic signals in carbonate carbon and oxygen isotope records: An example from the Permian–Triassic boundary of Iran. *Chemical Geology*. **422**, pp.94–107.

Scholz, F., McManus, J. and Sommer, S. 2013. The manganese and iron shuttle in a modern euxinic basin and implications for molybdenum cycling at euxinic ocean margins. *Chemical Geology*. **355**, pp.56–68.

van de Schootbrugge, B., McArthur, J.M., Bailey, T.R., Rosenthal, Y., Wright, J.D. and Miller, K.G. 2005. Toarcian oceanic anoxic event: An assessment of global causes using belemnite C isotope records. *Paleoceanography*. **20**(3), pp.1–10.

Schouten, S. 2000. Stable Carbon isotopic composition of Early Toarcian Carbon. (January), pp.1–22.

Seilacher, A. 1964. *Sedimentological classification and nomenclature of trace fossils*.

Sell, B., Ovtcharova, M., Guex, J., Bartolini, A., Jourdan, F., Spangenberg, J., Vicente, J.-C. and Schaltegger, U. 2014. Evaluating the temporal link between the Karoo LIP and climatic–biologic events of the Toarcian Stage with high-precision U–Pb geochronology. *Earth and Planetary Science Letters*. **408**, pp.48–56.

Şengör, A. 2011. Tectonic evolution of the Mediterranean: a dame with four husbands. *Trabajos de geología*. **50**, pp.45–50.

Sepkoski, J.J.J. and Raup, D.M. 1986. Periodicity in marine extinction events.

Shackleton, N.J. and Kennett, J.P. 1975. Paleotemperature History of the Cenozoic and the Initiation of Antarctic Glaciation: Oxygen and Carbon Isotope Analyses in DSDP Sites 277, 279 and 281 *In*: *Initial Reports of the Deep Sea Drilling Project, 29* [Online]. U. S. Government Printing Office, pp.743–755. [Accessed 28 November 2018]. Available from: https://ci.nii.ac.jp/naid/10010291201/.

Sholupov, S.E. and Ganeyev, A.A. 1995. Zeeman atomic absorption spectrometry using high frequency modulated light polarization. *Spectrochimica Acta Part B: Atomic Spectroscopy*. **50**(10), pp.1227–1236.

Shopov, V. 1975. Bivalve fauna of the Hettangian in Bulgaria. *Palaeontology, Stratigraphy and Lithology*. **1**, pp.53–70.

Shopov, V. 1970. Bivalvian zones in the lower Jurassic in Bulgaria. *Bulletin of the Geological Institute, Series Stratigraphy and lithology*. **19**, pp.15–39.

Shopov, V. 1974a. Genus Gryphaea Lamarck (Bivalvia) representatives from the Lower Jurassic in Bulgaria. *Bulletin of the Geological Institute, Series Palaeontology*. **23**, pp.57–74.

Shopov, V. 1968a. *Lower Jurassic Bulgaria Shopov thesis*. University of Sofia.

Shopov, V. 1968b. *Lower Jurassic Bulgaria Shopov Thesis*. University of Sofia.

Shopov, V. 1969. Notes on the Hettangian and Sinemurian in the Central and Western Balkanides and the Kraishte. *Bulletin of the Geological Institute, Series Stratigraphy and lithology*. **18**, pp.21–30.

Shopov, V. 1974b. Stratigraphic range and biostratinomy of some Lower Jurassic Pectinacea (Bivalvia) from Bulgaria. *Bulletin of the Geological Institute, Series Palaeontology*. **23**, pp.75–80.

Sial, A.N., Lacerda, L.D., Ferreira, V.P., Frei, R., Marquillas, R.A., Barbosa, J.A., Gaucher, C., Windmöller, C.C. and Pereira, N.S. 2013. Mercury as a proxy for volcanic activity during extreme environmental turnover: The Cretaceous-Paleogene transition. *Palaeogeography, Palaeoclimatology, Palaeoecology*. **387**, pp.153–164.

Signor, P.W. and Lipps, J.H. 1982. Sampling bias, gradual extinction patterns and catastrophes in the fossil record *In*: *Geological implications of impacts of large asteroids and comets on the Earth* [Online]., pp.291–296.

Silva, R.L. and Duarte, L. V. 2015. Organic matter production and preservation in the Lusitanian Basin (Portugal) and Pliensbachian climatic hot snaps. *Global and Planetary Change*. **131**, pp.24–34.

Silva, R.L., Duarte, L.V., Comas-Rengifo, M.J., Mendonça Filho, J.G. and Azerêdo, A.C. 2011. Update of the carbon and oxygen isotopic records of the Early-Late Pliensbachian (Early Jurassic, ~187Ma): Insights from the organic-rich hemipelagic series of the Lusitanian Basin (Portugal). *Chemical Geology*. **283**(3–4), pp.177–184.

Song, H., Wignall, P.B., Tong, J., Bond, D.P.G., Song, H., Lai, X., Zhang, K., Wang, H. and Chen, Y. 2012. Geochemical evidence from bio-apatite for multiple oceanic anoxic events during Permian–Triassic transition and the link with end-Permian extinction and recovery. *Earth and Planetary Science Letters*. **353**–**354**, pp.12–21.

Spaeth, C., Hoefs, J. and Vetter, U. 1971. Some aspects of isotopic composition of belemnites and related paleotemperatures. *Bulletin of the Geological Society of America*. **82**(11), pp.3139–3150.

Spielmeyer, A. and Pohnert, G. 2012. Influence of temperature and elevated carbon dioxide on the production of dimethylsulfoniopropionate and glycine betaine by marine phytoplankton. *Marine Environmental Research*. **73**, pp.62–69.

Stampfli, G.M. and Borel, G.D. 2002. A plate tectonic model for the Paleozoic and Mesozoic constrained by dynamic plate boundaries and restored syntetic ocean isochrons. *Earth and Planetary Science Letters*. **196**, pp.17–33.

Stampfli, G.M., Hochard, C., Vérard, C., Wilhem, C. and VonRaumer, J. 2013. The formation of Pangea. *Tectonophysics*. **593**, pp.1–19.

Stevens, G.R. 1967. Upper Jurassic Fossils From Ellsworth Land, West Antarctica, and Notes on Upper Jurassic Biogeography of the South Pacific Region. *New Zealand Journal of Geology and Geophysics*. **10**(2), pp.345–393.

Stevens, G.R. and Clayton, R.N. 1971. Oxygen isotope studies on Jurassic and Cretaceous belemnites from New Zealand and their biogeographic significance. *New Zealand Journal of Geology and Geophysics*. **14**(4), pp.829–897.

Stoyanova-Vergilova, M. 1979. An attempt for belemnite zonal subdivision of the Lower Jurassic sediments in Bulgaria. *Annuaire de l'Université de Sofia, Faculté de géologie et géographie*. **70**, pp.161–192.

Stramma, L., Johnson, G.C., Sprintall, J. and Mohrholz, V. 2008. Expanding Oxygen-Minimum Zones in the Tropical Oceans. *Science*. **320**, pp.655–658.

Suan, G., Mattioli, E., Pittet, B., Lécuyer, C., Suchéras-Marx, B., Duarte, L.V., Philippe, M., Reggiani, L. and Martineau, F. 2010. Secular environmental precursors to Early Toarcian (Jurassic) extreme climate changes. *Earth and Planetary Science Letters*. **290**(3–4), pp.448–458.

Suan, G., Mattioli, E., Pittet, B., Lécuyer, C., Suchéras-Marx, B., Duarte, L.V., Philippe, M., Reggiani, L. and Martineau, F. 2010. Secular environmental

precursors to Early Toarcian (Jurassic) extreme climate changes. *Earth and Planetary Science Letters*. **290**(3–4), pp.448–458.

Suan, G., Mattioli, E., Pittet, B., Mailliot, S. and Lécuyer, C. 2008. Evidence for major environmental perturbation prior to and during the Toarcian (Early Jurassic) oceanic anoxic event from the Lusitanian Basin, Portugal. *Paleoceanography*. **23**(1), n/a-n/a.

Suan, G., Nikitenko, B.L., Rogov, M., Baudin, F., Spangenberg, J., Knyazev, V.G., Glinskikh, L.A., Goryacheva, A.A., Adatte, T., Riding, J.B., Föllmi, K.B., Pittet, B., Mattioli, E. and Lécuyer, C. 2011. Polar record of Early Jurassic massive carbon injection. *Earth and Planetary Science Letters*. **312**(1–2), pp.102–113.

Suan, G., Rulleau, L., Mattioli, E., Suchéras-Marx, B., Rousselle, B., Pittet, B., Vincent, P., Martin, J.E., Léna, A., Spangenberg, J. and Föllmi, K.B. 2013. Palaeoenvironmental significance of Toarcian black shales and event deposits from southern Beaujolais, France. *Geological Magazine*. **150**.

Suan, G., Schöllhorn, I., Schlögl, J., Segit, T., Mattioli, E., Lécuyer, C. and Fourel, F. 2018. Euxinic conditions and high sulfur burial near the European shelf margin (Pieniny Klippen Belt, Slovakia) during the Toarcian oceanic anoxic event. *Global and Planetary Change*. **170**, pp.246–259.

Suan, G., van de Schootbrugge, B., Adatte, T., Fiebig, J. and Oschmann, W. 2015. Calibrating the magnitude of the Toarcian carbon cycle perturbation. *Paleoceanography*. **30**(5), pp.495–509.

Svensen, H., Corfu, F., Polteau, S., … Ø.H.-E. and P. and 2012, undefined n.d. Rapid magma emplacement in the Karoo large igneous province. *Elsevier*.

Svensen, H., Planke, S., Chevallier, L., Malthe-Sørenssen, A., Corfu, F. and Jamtveit, B. 2007a. Hydrothermal venting of greenhouse gases triggering Early Jurassic global warming. *Earth and Planetary Science Letters*. **256**(3–4), pp.554–566.

Svensen, H., Planke, S., Chevallier, L., Malthe-Sørenssen, A., Corfu, F. and Jamtveit, B. 2007b. Hydrothermal venting of greenhouse gases triggering Early Jurassic global warming. *Earth and Planetary Science Letters*. **256**(3–4), pp.554–566.

Tchoumatchenco, P. 1978. Brachiopodes du Jurassique moyen des environs du village de Dolni Lom, District de Vidin (Bulgarie du Nord-ouest). *Annuaire de l'Université de Sofia, Faculté de géologie et géographie, Livre 1, géologie*. **69**, pp.193–232.

Tchoumatchenco, P. 1977. Les biozones de brachiopodes du Jurassique moyen en Bulgarie. *Geologica Balcanica,*. **7**(1), pp.97–108.

Tchoumatchenco, P. 1988. Reconstruction stratigraphique et paléogéographique du Jurassique inférieur et moyen à partir des olistolithes inclus dans la Formation de Kotel (Stara Planina orientale, Bulgarie). *Geologica Balcanica*. **18**(6), pp.3–28.

Tchoumatchenco, P. 1966. Tetrarhynchia dunrobinensis (Rollier) un brachiopode du Jurassique inférieur près du v. Komštica, District de Godeč. *Travaux sur la géologie de Bulgarie, Série Paléontologie*. **8**, pp.11–19.

Tchoumatchenco, P. 1972. Thanatocoenoses and biotopes of Lower Jurassic brachiopods in central and western Bulgaria. *Palaeogeography, Palaeoclimatology and Palaeoecology*. **12**, pp.227–242.

Tchoumatchenco, P. and Černjavska, S. 1989. The Jurassic System in East Stara Planina. I. Stratigraphy. *Geologica Balcanica*. **19**(4), pp.33–65.

Tchoumatchenco, P. and Černjavska, S. 1990. The Jurassic System in East Stara Planina. II. Palaeogeographic and palaeotectonic evolution. *Geologica Balcanica*. **20**(3), pp.17–58.

Tchoumatchenco, P., Nikolov, T. and Sapunov, I. 1989. Outline of the Jurassic and Early Cretaceous tectonic evolution of Bulgaria. *Comptes rendus de l'Académie bulgare des Sciences*. **42**(112), pp.99–102.

Tchoumatchenco, P., Rabrenovic, D., Radulović, B. V. and Radulovic, V. 2006. Trans-border (south-east Serbia/west Bulgaria) correlations of the Jurassic sediments: Infra-Getic Unit. *Geoloski anali Balkanskog poluostrva*. (67), pp.19–33.

Tchoumatchenco, P., Rabrenovic, D., Radulovic, V., Malesevic, N. and Radulović, B. V. 2011. Trans-border (north-east Serbia/north-west Bulgaria) correlations of the Jurassic lithostratigraphic units. *Geoloski anali Balkanskog poluostrva*. (72), pp.1–20.

Tchoumatchenco, P., Rabrenovic, D., Radulovic, V., Mmalesevic, N. and Radulović, B. V. 2008. Trans-border (south-eastern Serbia/south-western Bulgaria) correlations of the Jurassic sediments: the Getic and Supra-Getic units. *Annales Geologiques de la Peninsule Balkanique*. **69**, pp.1–12.

Tchoumatchenco, P. and Sapunov, I. 1994. Intraplate tectonics in the Bulgarian part of the Moesian Platform during the Jurassic. *Geologica Balcanica*. **24**(3), pp.3–12.

Tchoumatchenco, P., Zagorchev, I., Yaneva, M., Budurov, K. and Koleva-Rekalova, E. 2006. The Triassic and Jurassic of East Stara Planina (Bulgaria), Tulcea Zone (North Dobrogea, Romania) and South Crimea (Gorniy Krim, Ukraine). Essay of Correlation. *Comptes rendus de l'Académie bulgare des Sciences*. **59**(12), p.1265.

Them, T.R., Gill, B.C., Caruthers, A.H., Gröcke R., D., Tulsky, E.T., Martindale, R., Poulton, T.P. and Smith, P.L. 2017. High-resolution carbon isotope records of the Toarcian Oceanic Anoxic Event (Early Jurassic) from North America and implications for the global drivers of the Toarcian carbon cycle. *Earth and Planetary Science Letters*. **459**, pp.118–126.

Them, T.R., Gill, B.C., Selby, D., Gröcke R., D., Friedman, R.M. and Owens, J.D. 2017. Evidence for rapid weathering response to climatic warming during the Toarcian Oceanic Anoxic Event. *Scientific Reports*. **7**(1), p.5003.

Them, T.R., Jagoe, C.H., Caruthers, A.H., Gill, B.C., Grasby, S.E., Gröcke R., D., Yin, R. and Owens, J.D. 2019. Terrestrial sources as the primary delivery mechanism of mercury to the oceans across the Toarcian Oceanic Anoxic Event (Early Jurassic). *Earth and Planetary Science Letters*. **507**, pp.62–72.

Thibault, N., Ruhl, M., Ullmann, C. V., KORTE, C., Kemp, D.B., Gröcke R., D. and Hesselbo, S.P. 2017. The wider context of the Lower Jurassic Toarcian

oceanic anoxic event in Yorkshire coastal outcrops, UK. *Proceedings of the Geologists' Association*.

Thibodeau, A.M., Ritterbush, K., Yager, J.A., West, A.J., Ibarra, Y., Bottjer, D.J., Berelson, W.M., Bergquist, B.A. and Corsetti, F.A. 2016. Mercury anomalies and the timing of biotic recovery following the end-Triassic mass extinction. *Nature Communications*. **7**(1), p.11147.

Thierry, J. 2000. Middle Toarcian *In*: J. Dercourt, M. Gaetani, B. Vrielynck, E. Barrier, B. Biju-Duval, M.-F. Brunet, J. P. Cadet, S. Crasquin and M. Sandulescu, eds. *Atlas Peri-Tethys Paleogeographical Maps*. Paris, p.8.

Todaro, S., Rigo, M., Randazzo, V. and Di Stefano, P. 2018. The end-Triassic mass extinction: A new correlation between extinction events and δ 13 C fluctuations from a Triassic-Jurassic peritidal succession in western Sicily. *Sedimentary Geology*. **368**, pp.105–113.

Trecalli, A., Spangenberg, J., Adatte, T., Föllmi, K.B. and Parente, M. 2012. Carbonate platform evidence of ocean acidification at the onset of the early Toarcian oceanic anoxic event. *Earth and Planetary Science Letters*. **357**–**358**, pp.214–225.

Tremolada, F., van de Schootbrugge, B. and Erba, E. 2005. Early Jurassic schizosphaerellid crisis in Cantabria, Spain: Implications for calcification rates and phytoplankton evolution across the Toarcian oceanic anoxic event. *Paleoceanography*. **20**(2), pp.1–11.

Tyson, R. V. 2005. The" productivity versus preservation" controversy: cause, flaws, and resolution. *SEPM special publicatication*. **88**, p.17.

Uhlig, V. 1911. Die marinen Reiche des Jura und der Unterkreide. *Mitteilungen der Geologischen Gesellschaft in Wien*. **4**(3), pp.229–448.

Ullmann, C. V. 2013. *Isotopic and elemental proxies in mollusc and brachiopod calcite: diagenesis, vital effects and climatic trends*. University of Copenhagen.

Ullmann, C. V., Campbell, H.J., Frei, R., Hesselbo, S.P., Pogge von Strandmann, P.A.E. and KORTE, C. 2013. Partial diagenetic overprint of Late Jurassic belemnites from New Zealand: Implications for the preservation potential of ??7Li values in calcite fossils. *Geochimica et Cosmochimica Acta*. **120**, pp.80–96.

Ullmann, C. V., Campbell, H.J., Frei, R. and Korte, C. 2014. Geochemical signatures in Late Triassic brachiopods from New Caledonia. *New Zealand Journal of Geology and Geophysics*. **57**(4), pp.420–431.

Ullmann, C. V. and Korte, C. 2015a. Diagenetic alteration in low-Mg calcite from macrofossils: a review. *Geological Quarterly*. **59**(1), pp.3–20

Ullmann, C. V., Frei, R., Korte, C. and Hesselbo, S.P. 2015b. Chemical and isotopic architecture of the belemnite rostrum. *Geochimica et Cosmochimica Acta*. **159**, pp.231–243.

Ullmann, C. V., Campbell, H.J., Frei, R. and Korte, C. 2015c. Oxygen and carbon isotope and Sr/Ca signatures of high-latitude Permian to Jurassic calcite fossils from New Zealand and New Caledonia. *Gondwana Research*.

Ullmann, C. V., Frei, R., Korte, C. and Lüter, C. 2017. Element/Ca, C and O isotope ratios in modern brachiopods: Species-specific signals of biomineralization. *Chemical Geology*. **460**.

Ullmann, C. V., Hesselbo, S.P. and Korte, C. 2013. Tectonic forcing of early to middle jurassic seawater Sr/Ca. *Geology*. **41**(12), pp.1211–1214.

Ullmann, C. V., Thibault, N., Ruhl, M., Hesselbo, S.P. and KORTE, C. 2014. Effect of a Jurassic oceanic anoxic event on belemnite ecology and evolution. *Proceedings of the National Academy of Sciences*. **111**(28), pp.10073–10076.

Ullmann, C. V., Wiechert, U. and KORTE, C. 2010. Oxygen isotope fluctuations in a modern North Sea oyster (Crassostrea gigas) compared with annual variations in seawater temperature: Implications for palaeoclimate studies. *Chemical Geology*. **277**(1–2), pp.160–166.

Urey, H.C., Lowenstam, H.A., Epstein, S. and McKinney, C.R. 1951. Measurement of Paleotemperatures and Temperatures and the Southeastern United States. *Bulletin of the geological society of America*. **62**(April), pp.399–416.

V., S. 1966. New data about the biozone of Pseudopecten aequivalvis (J. Sowerby). *Comptes rendus de l'Académie bulgare des Sciences*. **19**(11), pp.1083–1085.

Valdes, P.J., Sellwood, B. and Price, G. 1995. Modelling Late Jurassic Milankovitch climate variations, Orbital Forcing Timescales and Cyclostratigraphy. *Spec. Pub. Geol. Soc. Lond*. **85**, pp.115–132.

Valls, J., Comas-Rengifo, M.J. and Goy, A. 2004. Bivalvos del Pliensbachiense en la Sección de lmonacid de la Cuba. (Cordillera Ibérica, España). *Coloquios de Paleontología*. **54**, pp.145–178.

Vance, D., Teagle, D.A.H. and Foster, G.L. 2009. Variable Quaternary chemical weathering fluxes and imbalances in marine geochemical budgets. *Nature*. **458**(7237), pp.493–496.

Veizer, J. 1974. Chemical diagenesis of belemnite shells and possible consequences for paleotemperature determinations. *N. Jb. Geol. Paläont. Abh.* **147**(1), pp.91–111.

Veizer, J., Ala, D., Azmy, K., Bruckschen, P., Buhl, D., Bruhn, F., Carden, G. a. F., Diener, A., Ebneth, S., Godderis, Y., Jasper, T., Korte, C., Pawellek, F., Podlaha, O.G. and Strauss, H. 1999. 87Sr/86Sr, δ13C and δ18O evolution of Phanerozoic seawater. *Chemical Geology*. **161**(1–3), pp.59–88.

Veizer, J. and Compston, W. 1974. 87Sr/86Sr composition of seawater during the Phanerozoic. *Geochimica et Cosmochimica Acta*. **38**(9), pp.1461–1484.

Veizer, J., Fritz, P. and Jones, B. 1986. Geochemistry of brachiopods: Oxygen and carbon isotopic record of Paleozoic oceans. *Geochimica et Cosmochimica Acta*. **50**, pp.1679–1696.

Vogt, P.R. 1972. Evidence for global synchronism in mantle plume convection, and possible significance for geology. *Nature*. **240**(5380), pp.338–342.

Vörös, A. 2016. Early Jurassic (Pliensbachian) brachiopod biogeography in the western Tethys: The Euro-Boreal and Mediterranean faunal provinces

revised. *Palaeogeography, Palaeoclimatology, Palaeoecology*. **457**, pp.170–185.

Vörös, A. 1993. Jurassic microplate movements and brachiopod migrations in the western part of the Tethys. *Palaeogeography, Palaeoclimatology, Palaeoecology*. **100**(1–2), pp.125–145.

Vörös, A. 2002. Victims of the Early Toarcian anoxic event: The radiation and extinction of Jurassic Koninckinidae (Brachiopoda). *Lethaia*. **35**, pp.345–357.

Vörös, A. and Kandemir, R. 2011. A new Early Jurassic brachiopod fauna from the Eastern Pontides (Turkey). *Neues Jahrbuch für Geologie und Paläontologie - Abhandlungen*. **260**(3), pp.343–363.

Vörös, A., Kocsis, Á.T. and Pálfy, J. 2016. Demise of the last two spire-bearing brachiopod orders (Spiriferinida and Athyridida) at the Toarcian (Early Jurassic) extinction event. *Palaeogeography, Palaeoclimatology, Palaeoecology*. **457**(July), pp.233–241.

Wang, Y.G. and Sun, D.L. 1983. A survey of the Jurassic System of China. *Canadian Journal of Earth Sciences*. **20**(11), pp.1646–1656.

Wei, H., Chen, D., Wang, J., Yu, H. and Tucker, M.E. 2012. Organic accumulation in the lower Chihsia Formation (Middle Permian) of South China : Constraints from pyrite morphology and multiple geochemical proxies. *Palaeogeography, Palaeoclimatology, Palaeoecology*. **353**–**355**, pp.73–86.

Westermann, G.E.G. 2000. Marine faunal realms of the Mesozoic: review and revision under the new guidelines for biogeographic classification and nomenclature. *Palaeogeography, Palaeoclimatology, Palaeoecology*. **163**(1–2), pp.49–68.

Wierzbowski, H. and Joachimski, M. 2007. Reconstruction of late Bajocian–Bathonian marine palaeoenvironments using carbon and oxygen isotope ratios of calcareous fossils from the Polish Jura Chain (central Poland). *Palaeogeography, Palaeoclimatology, Palaeoecology*. **254**(3–4), pp.523–540.

Wierzbowski, H. and Joachimski, M. 2009. Stable Isotopes, Elemental Distribution, and Growth Rings of Belemnopsid Belemnite Rostra: Proxies for Belemnite Life Habitat. *Palaios*. **24**(6), pp.377–386.

Wierzbowski, H. and Rogov, M. 2011. Reconstructing the palaeoenvironment of the Middle Russian Sea during the Middle-Late Jurassic transition using stable isotope ratios of cephalopod shells and variations in faunal assemblages. *Palaeogeography, Palaeoclimatology, Palaeoecology*. **299**(1–2), pp.250–264.

Wignall, P.B. 1993. Distinguishing between oxygen and substrate control in fossil benthic assemblages. *Journal of the Geological Society*. **150**, pp.193–196.

Wignall, P.B. 2001. Large igneous provinces and mass extinctions. *Earth-Science Reviews*. **53**(1–2), pp.1–33.

Wignall, P.B. 2007. The End-Permian mass extinction - How bad did it get?

Geobiology. **5**(4), pp.303–309.

Wignall, P.B. 2005. The Link between Large and Mass Extinctions. , pp.293–297.

Wignall, P.B., Hallam, a., Newton, R.J., Sha, J.G., Reeves, E.P., Mattioli, E. and Crowley, S. 2006. An eastern Tethyan (Tibetan) record of the Early Jurassic (Toarcian) mass extinction event. *Geobiology*. **4**(3), pp.179–190.

Wignall, P.B., Newton, R. and Brookfield, M.E. 2005. Pyrite framboid evidence for oxygen-poor deposition during the Permian–Triassic crisis in Kashmir. *Palaeogeography, Palaeoclimatology, Palaeoecology*. **216**(3–4), pp.183–188.

Wignall, P.B. and Newton, R.J. 1998. Pyrite framboid diameter as a measure of oxygen deficiency in ancient mudrocks. *American Journal of Science*. **298**(7), pp.537–552.

Wignall, P.B., Newton, R.J. and Little, C.T.S. 2005. The timing of paleoenvironmental change and cause-and-effect relationships during the early Jurassic mass extinction in Europe. *American Journal of Science*. **305**(10), pp.1014–1032.

Wilkin, R.T., Barnes, H.L. and Brantley, S.L. 1996. The size distribution of framboidal pyrite in modern sediments: An indicator of redox conditions. *Geochimica et Cosmochimica Acta*. **60**(20), pp.3897–3912.

Winter, A., Jordan, R.W. and Roth, P.H. 2006. Biogeography of living coccolithophores in ocean waters *In*: *Coccolithophores* [Online]. Cambridge University Press, pp.161–177. [Accessed 16 November 2018]. Available from: https://ci.nii.ac.jp/naid/10016579063/.

Wood and D., G. 1996. Chapter 3. Palynological techniques-processing and microscopy. In. Jasonius, J. and McGregor, D. C. eds., Palynology: Principles and Application. *American Association of Stratigraphic Palynologists Foundation*. **1**, pp.29–50.

Woodfine, R.G., Jenkyns, H.C., Sarti, M., Baroncini, F. and Violante, C. 2008. The response of two Tethyan carbonate platforms to the early Toarcian (Jurassic) oceanic anoxic event: environmental change and differential subsidence. *Sedimentology*. **55**(4), pp.1011–1028.

Xu, W., Ruhl, M., Hesselbo, S.P., Riding, J.B. and Jenkyns, H.C. 2017. Orbital pacing of the Early Jurassic carbon cycle, black-shale formation and seabed methane seepage. *Sedimentology*. **64**(1), pp.127–149.

Xu, W., Ruhl, M., Jenkyns, H.C., Hesselbo, S.P., Riding, J.B., Selby, D., Naafs, B.D.A., Weijers, J.W.H., Pancost, R.D., Tegelaar, E.W. and Idiz, E.F. 2017. Carbon sequestration in an expanded lake system during the Toarcian oceanic anoxic event. *Nature Geoscience*. **10**(2), pp.129–134.

Xu, W., Mac Niocaill, C., Ruhl, M., Jenkyns, H.C., Riding, J.B. and Hesselbo, S.P. 2018a. Magnetostratigraphy of the Toarcian Stage (Lower Jurassic) of the Llanbedr (Mochras Farm) Borehole, Wales: basis for a global standard and implications for volcanic forcing of palaeoenvironmental change. *Journal of the Geological Society*. **175**(4), pp.594–604.

Xu, W., Ruhl, M., Jenkyns, H.C., Leng, M.J., Huggett, J.M., Minisini, D.,

Ullmann, C. V., Riding, J.B., Weijers, J.W.H., Storm, M.S., Percival, L.M.E., Tosca, N.J., Idiz, E.F., Tegelaar, E.W. and Hesselbo, S.P. 2018b. Evolution of the Toarcian (Early Jurassic) carbon-cycle and global climatic controls on local sedimentary processes (Cardigan Bay Basin, UK). *Earth and Planetary Science Letters*. **484**, pp.396–411.

Zagorchev, I., Ch., D. and Nikolov, T. 2009. Mesozoic geology *In*: *Geology of Bulgaria. Part II*. Sofia: Drinov Academic Press, p.766.

Zakharov, V. a., Shurygin, B.N., Il'ina, V.I. and Nikitenko, B.L. 2006. Pliensbachian-Toarcian biotic turnover in north Siberia and the Arctic region. *Stratigraphy and Geological Correlation*. **14**(4), pp.399–417.

Ziegler, P. 1990. Geological atlas of western and central Europe. *Geological Society of London*.

Zlatarski, G. 1908. Le système jurassique en Bulgarie. *Ann. Univ. Sofia*. **3**, pp.148–224.

Appendices

Appendix A. Supplementary material from Chapter 3
Appendix B. Supplementary material from Chapter 4
Appendix C. Supplementary material from Chapter 5
Appendix D. Supplementary material from Chapter 6

Appendix A. Strontium isotope values ($^{87}Sr/^{86}Sr$).

Sample number	Stratigraphic height (m)	$^{87}Sr/^{86}Sr$	Std err (abs)
Milanovo section			
Mv.P10.30	-0.13	0.70721591	±4.396561e-006
Mv.P12.200	0.0	0.70720747	±3.561602e-006
Mv.P18.1	0.08	0.70722261	±3.354481e-006
Mv.P18.2	0.08	0.70718195	±3.710826e-006
Mv.P18.3	0.08	0.70712793	±3.764618e-006
Mv.2.5	1.51	0.70719812	±3.850755e-006
Mv.2.12	1.58	0.70731314	±4.432086e-006
Mv.2.40	1.86	0.70724151	±3.767770e-006
Mv.2.60	2.06	0.70727074	±3.898067e-006
Mv.2.72	2.18	0.70726718	±3.187097e-006
Mv.2.73	2.19	0.70726698	±7.334623e-006
Mv.2.90	2.36	0.70725848	±3.596316e-006
Mv.3.5	2.21	0.70722972	±3.258892e-006
Mv.4.5	2.86	0.70727419	±3.470807e-006
Mv.5.10	3.11	0.70728782	±3.063551e-006
Mv.5.30	3.31	0.70729705	±6.345891e-006
Mv.5.35	3.36	0.70729306	±4.008946e-006
Mv.6.5	3.37	0.70727921	±3.514108e-006
Mv.6.80	3.39	0.70728472	±4.516125e-006
MV.7.10	3.63	0.70729998	±5.736645e-006
MV.7.26	3.79	0.70731234	±3.710826e-006
MV.7.35	3.88	0.70731067	±3.657451e-006
Mv.8.10	3.93	0.70732089	±4.742355e-006
Mv.7.80	4.33	0.70729806	±3.764618e-006

Sample number	Stratigraphic height (m)	$^{87}Sr/^{86}Sr$	Std err (abs)
Vradlovtsi-2 section			
Vd.1.base	5.71	0.70722473	±5.696577e-006
Vd.1.15.1	5.86	0.70722398	±3.763233e-006
Vd.1.120	6.61	0.70734253	±5.659263e-006
Vd.1.100	6.81	0.70740647	±6.325247e-006
Vd.2.60	8.41	0.70736934	±4.252565e-006
Vd.2.190	9.71	0.70731481	±4.825644e-006
Vd.2.130	10.27	0.70734984	±4.235345e-006
Vd.2.15	11.52	0.70729528	±5.624477e-006
Vd.3.100	12.67	0.70729579	±4.056317e-006
Vd.4.7	13.24	0.70727535	±4.262015e-006
Vd.4.50.1	13.67	0.70729677	±4.836217e-006
Vd.5.95	15.66	0.70738555	±4.349983e-006
Standards and reference material			
YCB ref	-	0.70709921	±3.254357e-006
YCB ref	-	0.70708354	±3.900681e-006
YCB ref	-	0.70710413	±6.787839e-006
YCB ref	-	0.70709576	±3.265732e-006
YCB ref	-	0.70712354	±8.381091e-006
YCB ref	-	0.70708556	±3.696694e-006
YCB ref	-	0.70710326	±4.393214e-006
B7 std	-	0.70830775	±3.856451e-005
B7 std	-	0.70833612	±3.697198e-005
B7 std	-	0.70835389	±3.679781e-005
B7 std	-	0.70830089	±8.426561e-005
B7 std	-	0.70833262	±1.096682e-006
JLS-1 std	-	0.70782404	±6.371272e-006

Sample number	Stratigraphic height (m)	$^{87}Sr/^{86}Sr$	Std err (abs)
JLS-1 std	-	0.70786012	±8.489412e-006
JLS-1 std	-	0.70790595	±4.119119e-006

Appendix B.1. Key element concentrations. LOQ = Limit of quantification. LOD = Limit of detection.

Sample number (belemnite sample)	Stratigraphic height (m)	Ca (%)	Mg (ppm)	Sr (ppm)	Fe (ppm)	Mn (ppm)
Milanovo section						
MV.P10.30 (Sr)	-0.13	40.09	2729	1374	219	30
MV.P10.30 (1)	-0.13	40.21	2548	1292	199	25
MV.P12.200 (Sr)	0.00	41.47	2690	1390	96	<LOQ
MV.P12.200 (1)	0.00	37.66	2530	1239	133	<LOQ
MV.P12.200 (2)	0.00	34.24	2302	1083	188	<LOQ
MV.P18.1 (Sr)	0.08	36.97	1438	883	152	21
MV.P18.1 (1)	0.08	38.40	1491	916	139	21
MV.P18.1 (2)	0.08	39.23	1579	973	146	22
MV.P18.2 (Sr)	0.14	39.74	1695	1171	90	22
MV.P18.2 (1)	0.14	38.52	1654	1152	117	22
MV.P18.3 (Sr)	0.18	39.46	1401	991	60	<LOQ
MV.P18.3 (1)	0.18	39.38	1435	1052	115	<LOQ
MV.2.5 (Sr)	1.51	39.01	2741	1333	82	<LOQ
MV.2.5 (1)	1.51	39.38	2660	1350	78	<LOQ
MV.2.5 (2)	1.51	39.83	2720	1328	68	<LOQ
MV.2.10 (Sr)	1.56	38.54	2273	1202	48	<LOD
MV.2.10 (1)	1.56	39.58	2812	1444	73	<LOQ
MV.2.10 (2)	1.56	38.71	2398	1277	28	<LOD
MB.2.10 (3)	1.56	31.81	1975	1085	32	<LOD
MV.2.12 (Sr)	1.58	38.50	2640	1018	173	34
MV.2.12 (1)	1.58	41.84	2953	1202	135	32
MV.2.40.1 (Sr)	1.86	38.37	2909	1170	76	<LOQ
MV.2.40.1 (1)	1.86	40.01	2975	1169	58	<LOQ
MV.2.40.1 (2)	1.86	38.39	2905	1177	66	<LOQ
MV.2.40.1 (3)	1.86	38.50	2946	1160	128	37
MV.2.40.2 (Sr)	1.89	37.86	2611	1166	256	35
MV.2.40.2 (1)	1.89	39.03	2699	1253	85	18
MV.2.40.2 (2)	1.89	39.34	2737	1336	39	<LOQ
MV.2.40.2 (3)	1.89	38.70	2373	1192	173	30
MV.2.60 (Sr)	2.06	38.42	2327	1189	184	25
MV.2.60 (1)	2.06	40.09	2462	1151	188	56
MV.2.60 (2)	2.06	40.38	2352	1157	187	33
MV.2.70 (Sr)	2.16	39.42	2781	1153	202	40
MV.2.70 (1)	2.16	39.09	2636	1119	151	33
MV.2.70 (2)	2.16	39.92	2927	1106	219	44
MV.2.72 (Sr)	2.18	31.32	2406	963	118	22

Sample number (belemnite sample)	Stratigraphic height (m)	Ca (%)	Mg (ppm)	Sr (ppm)	Fe (ppm)	Mn (ppm)
MV.2.72 (1)	2.18	38.37	2927	1109	178	28
MV.2.72 (2)	2.18	38.97	2900	1202	94	20
MV.2.73 (Sr).1	2.19	39.46	2836	1124	-	22
MV.2.73 (Sr).2	2.19	39.22	2849	1132	-	22
MV.2.73 (1)	2.19	38.96	3060	1162	163	23
MV.2.73 (2)	2.19	38.21	2887	1105	87	<LOQ
MV.3.5 (Sr)	2.21	38.62	3315	1167	117	<LOQ
MV.3.5 (1)	2.21	38.79	2561	1208	303	28
MV.3.5 (2)	2.21	38.55	3069	1121	78	<LOQ
MV.3.5 (3)	2.21	38.79	2671	1252	40	<LOQ
MV.2.90 (Sr)	2.36	38.56	2791	1212	118	<LOQ
MV.2.90 (1)	2.36	38.79	2827	1228	168	28
MV.2.90 (2)	2.36	39.72	2991	1213	79	<LOQ
MV.2.120 (Sr)	2.66	37.38	3384	1353	36	<LOQ
MV.2.120 (1)	2.66	42.65	4081	1576	103	<LOQ
MV.2.120 (2)	2.66	41.10	4068	1509	74	36
MV.4.5 (Sr)	2.86	39.33	2344	1192	113	<LOQ
MV.4.5 (1)	2.86	38.85	2336	1201	71	<LOQ
MV.4.5 (2)	2.86	39.03	2285	1189	192	29
MV.4.5 (3)	2.86	39.16	2371	1187	167	28
MV.5.10.1 (Sr)	3.11	38.77	2173	1233	49	<LOQ
MV.5.10.1 (1)	3.11	36.98	2095	1314	50	<LOD
MV.5.10.1 (2)	3.11	41.96	2363	1523	36	<LOD
MV.5.10.1 (3)	3.11	41.75	2499	1476	49	<LOD
MV.5.10.2 (Sr)	3.16	41.80	2786	1443	93	<LOQ
MV.5.10.2 (1)	3.16	39.39	2201	1199	93	<LOQ
MV.5.10.2 (2)	3.16	41.63	2894	1463	81	<LOQ
MV.5.10.2 (3)	3.16	40.11	2686	1421	77	<LOQ
MV.5.10.3 (Sr)	3.17	41.22	2511	1479	-	<LOD
MV.5.10.3 (1)	3.17	40.96	2356	1436	59	<LOQ
MV.5.10.3 (2)	3.17	40.45	2301	1430	53	23
MV.5.10.3 (3)	3.17	41.73	2385	1440	94	<LOQ
MV.2.180 (Sr)	3.26	39.02	2176	1067	94	<LOQ
MV.2.180 (1)	3.26	38.65	2113	1156	98	<LOQ
MV.2.180 (2)	3.26	40.33	2224	1175	163	27
MV.5.30 (Sr)	3.31	41.14	2417	1287	127	<LOQ
MV.5.30 (1)	3.31	38.87	2172	1177	101	22
MV.5.30 (2)	3.31	40.81	2303	1333	15	<LOD
MV.5.30 (3)	3.31	40.80	2417	1422	47	<LOD

Sample number (belemnite sample)	Stratigraphic height (m)	Ca (%)	Mg (ppm)	Sr (ppm)	Fe (ppm)	Mn (ppm)
MV.6.5 (Sr)	3.36	40.67	2202	1346	107	<LOD
MV.6.5 (1)	3.36	40.54	2345	1345	189	<LOD
MV.6.5 (2)	3.36	40.22	2368	1294	185	23
MV.6.5 (3)	3.36	37.84	2289	1210	91	<LOQ
MV.6.8 (Sr)	3.39	42.17	2815	1452	135	<LOQ
MV.6.8 (1)	3.39	40.07	2621	1368	284	39
MV.6.8 (2)	3.39	36.19	2568	1276	55	<LOD
MV.5.40 (Sr)	3.41	38.45	2093	1187	-	22
MV.5.40 (1)	3.41	40.23	2098	1274	-	<LOD
MV.5.40 (2)	3.41	42.52	2422	1315	-	<LOD
MV.5.40 (3)	3.41	40.56	2366	1274	-	<LOD
MV.6.10 (Sr)	3.41	41.00	2363	1385	42	<LOD
MV.6.10 (1)	3.41	40.64	2400	1335	65	<LOQ
MV.6.10 (2)	3.41	40.93	2379	1353	99	<LOQ
MV.6.11 (Sr)	3.42	39.65	2698	1477	113	<LOQ
MV.6.11 (1)	3.42	39.49	2651	1462	159	<LOQ
MV.5.42 (Sr)	3.43	40.73	2305	1235	212	21
MV.5.42 (1)	3.43	40.89	2366	1267	117	<LOQ
MV.5.42 (2)	3.43	42.00	2292	1266	85	<LOQ
MV.5.43 (Sr)	3.44	41.09	2179	1255	73	<LOQ
MV.5.43 (1)	3.44	41.39	2244	1352	147	21
MV.5.43 (2)	3.44	40.66	2070	1364	25	<LOD
MV.5.43 (3)	3.44	42.07	2091	1321	110	21
MV.6.13 (Sr)	3.44	39.97	2822	1480	61	<LOD
MV.6.13 (1)	3.44	40.58	2828	1416	42	<LOD
MV.6.13 (2)	3.44	41.55	3015	1582	42	<LOQ
MV.6.13 (3)	3.44	40.23	2820	1501	59	<LOQ
MV.2.210 (Sr)	3.56	39.11	2383	1233	82	<LOQ
MV.2.210 (1)	3.56	38.73	2341	1221	85	<LOQ
MV.2.210 (2)	3.56	34.81	2441	1117	147	<LOQ
MV.2.210 (3)	3.56	38.61	2315	1202	-	<LOQ
MV.7.10 (Sr)	3.63	40.82	3058	1632	73	<LOQ
MV.7.10 (1)	3.63	40.36	2998	1574	123	<LOQ
MV.7.10 (2)	3.63	40.26	3158	1530	477	76
MV.7.14 (Sr)	3.67	42.10	2617	1557	56	<LOD
MV.7.14 (1)	3.67	42.68	2606	1561	36	<LOD
MV.7.14 (2)	3.67	27.51	1675	1015	21	<LOD
MV.7.14 (3)	3.67	41.62	2596	1520	42	<LOD
MV.7.20 (Sr)	3.73	43.50	2709	1532	85	<LOQ

Sample number (belemnite sample)	Stratigraphic height (m)	Ca (%)	Mg (ppm)	Sr (ppm)	Fe (ppm)	Mn (ppm)
MV.7.20 (1)	3.73	41.17	2539	1386	65	<LOQ
MV.7.20 (2)	3.73	40.54	2671	1542	252	<LOQ
MV.7.21 (Sr)	3.74	41.53	2335	1238	59	<LOQ
MV.7.21 (1)	3.74	40.31	2581	1269	152	<LOQ
MV.7.21 (2)	3.74	41.62	2518	1192	191	48
MV.7.26 (Sr)	3.79	40.37	2676	1481	35	<LOD
MV.7.26 (1)	3.79	41.35	2555	1509	600	<LOD
MV.7.26 (2)	3.79	41.69	2521	1481	193	<LOD
MV.7.26 (3)	3.79	41.56	2802	1516	129	<LOD
MV.7.35 (Sr)	3.88	40.49	1404	1263	96	<LOQ
MV.7.35 (2)	3.88	40.17	1440	1214	156	27
MV.7.35 (1)	3.88	39.42	1390	1173	154	31
MV.8.10 (Sr)	3.93	40.65	1912	1291	177	27
MV.8.10 (1)	3.93	40.65	1913	1300	130	<LOQ
MV.8.10 (2)	3.93	40.33	2044	1325	86	<LOD
MV.8.10 (3)	3.93	40.08	2272	1443	120	<LOQ
MV.7.80 (Sr)	4.3	40.43	2828	1565	72	<LOQ
MV.7.80 (1)	4.33	40.30	2850	1550	74	<LOQ
MV.7.80 (2)	4.33	40.44	2648	1486	40	<LOD
MV.7.80 (3)	4.33	37.55	2411	1378	72	<LOQ
Berende Izvor section						
BI.1 (2)	1.50	41.10	2294	1467	1005	<LOQ
BI.1 (3)	1.50	41.53	2324	1493	927	<LOQ
BI.1b (1)	1.50	38.80	3298	1612	455	<LOQ
BI.1b (2)	1.50	42.69	3954	1787	1212	24
BI.1b (3)	1.50	30.06	2796	1236	486	<LOQ
BI.2a (1)	2.28	39.94	2373	1027	431	<LOQ
BI.2a (2)	2.28	41.73	2570	1149	831	<LOQ
BI.2a (3)	2.28	42.72	2542	1260	1015	<LOQ
BI.2 (1)	2.40	39.09	1949	1022	368	<LOQ
BI.2 (2)	2.40	44.19	2391	1218	1136	<LOQ
BI.2 (3)	2.40	40.78	2133	1107	1008	<LOQ
BI.3 (1)	3.24	43.02	2790	1475	1486	20
BI.3 (2)	3.24	43.53	2955	1444	575	<LOQ
BI-3 (3)	3.24	42.25	2775	1398	938	<LOQ
BI.3a (1)	3.42	45.88	2905	1634	871	<LOD
BI.3b (1)	4.25	-	-	-	-	<LOD
BI.3b (2)	4.25	-	-	-	-	<LOD
BI.3b (3)	4.25	-	-	-	-	<LOD

Sample number (belemnite sample)	Stratigraphic height (m)	Ca (%)	Mg (ppm)	Sr (ppm)	Fe (ppm)	Mn (ppm)
BI.4 (1)	4.73	-	-	-	-	<LOD
BI.5 (1)	5.23	37.25	2090	1238	-	<LOD
BI.5 (2)	5.23	43.46	2522	1468	143	<LOQ
BI.6 (1)	5.55	41.29	2384	1347	773	<LOQ
BI.6 (2)	5.55	43.14	2621	1558	339	<LOQ
BI.6 (3)	5.55	35.08	1987	1177	590	<LOD
BI.6b (1)	5.74	42.80	1579	1224	1100	<LOD
BI.6b (2)	5.74	43.95	1697	1270	175	<LOD
BI.6b (3)	5.74	45.80	1727	1305	273	<LOD
BI.6a (1)	7.19	42.29	2198	1411	232	<LOD
BI.6a (2)	7.19	45.47	2251	1462	191	<LOD
BI.6a (3)	7.19	44.60	2270	1475	778	<LOD
BI.6c (1)	7.38	47.67	2518	1504	249	<LOQ
BI.6c (2)	7.38	45.64	2496	1470	556	<LOQ
BI.6c (3)	7.38	45.29	2548	1479	1494	<LOQ
BI.7 (1)	7.53	45.31	3424	1092	824	<LOQ
BI.7 (2)	7.53	46.88	3210	1148	757	<LOQ
BI.7a (1)	7.99	48.17	2464	1635	253	<LOD
BI.7a (2)	7.99	46.20	2129	1543	597	<LOQ
BI.8 (1)	8.95	45.61	3047	1466	764	<LOD
BI.8 (2)	8.95	45.76	3136	1351	877	<LOQ
BI.8 (3)	8.95	44.88	2866	1304	1021	<LOD
BI.9 (1)	9.71	45.65	1943	1261	447	<LOD
BI.9 (3)	9.71	48.29	1919	1338	178	<LOD
BI.10 (1)	10.94	46.48	2743	1290	716	<LOD
BI.10 (2)	10.94	46.83	2887	1317	692	<LOQ
BI.10 (3)	10.94	47.56	3262	1353	744	<LOD
BI.11 (1)	12.09	45.13	2417	1233	481	<LOQ
BI.11 (2)	12.09	47.52	2891	1178	282	<LOQ
BI.11 (3)	12.09	46.36	2578	1192	439	<LOQ
BI.11a (1)	12.59	-	-	-	536	<LOQ
BI.12 (1)	13.13	45.84	2580	1357	-	<LOQ
BI.12 (2)	13.13	46.68	2562	1347	1169	<LOQ
BI.13 (1)	13.59	44.49	2469	1457	1144	<LOQ
BI.13 (2)	13.59	49.34	2724	1557	130	<LOQ
BI.13a (1)	13.88	49.48	2987	1554	1821	<LOD
BI.13a (2)	13.88	50.85	2996	1686	376	<LOD
BI.13a (3)	13.88	48.01	3043	1626	656	<LOD
BI.14 (1)	14.66	47.10	1632	1128	810	<LOD
BI.14 (2)	14.66	48.09	1651	1127	224	<LOD

Sample number (belemnite sample)	Stratigraphic height (m)	Ca (%)	Mg (ppm)	Sr (ppm)	Fe (ppm)	Mn (ppm)
BI.15 (1)	15.75	32.92	2042	1214	328	<LOD
BI.15 (2)	15.75	40.60	2487	1522	111	<LOD
BI.15 (3)	15.75	41.25	2723	1627	196	<LOD
BI.16 (1)	16.77	40.17	2828	1425	1063	<LOQ
BI.16 (2)	16.77	41.11	2879	1572	1222	<LOD
BI.17 (2)	17.01	-	-	-	630	<LOD
BI.17 (3)	17.01	39.65	2361	1327	646	<LOD
BI.17a (1)	17.21	38.41	2889	1310	-	<LOQ
BI.17a (2)	17.21	40.63	3067	1426	186	<LOQ
BI.17a (3)	17.21	41.08	2977	1465	359	<LOQ
BI.17b (1)	17.52	37.36	2160	1278	379	<LOQ
BI.17b (2)	17.52	38.38	2253	1283	448	<LOQ
BI.17b (3)	17.52	40.29	2448	1326	388	<LOQ
BI.17c (1)	17.79	38.01	2501	1410	588	<LOQ
BI.17c (2)	17.79	39.83	2710	1518	153	<LOQ
BI.17c (3)	17.79	37.00	2600	1441	262	<LOQ
BI.18 (1)	18.27	36.13	2212	1127	918	<LOQ
BI.18 (2)	18.27	39.45	2642	1270	368	<LOD
BI-18 (3)	18.27	41.94	2712	1373	377	<LOD
BI.20 (1)	20.53	37.24	1990	1169	188	<LOQ
BI.20 (2)	20.53	37.80	2074	1160	225	<LOQ
BI.21 (1)	21.47	31.44	2225	1117	1348	<LOQ
BI.22 (1)	22.49	35.63	2256	1215	351	<LOD
BI.22 (2)	22.49	37.41	2455	1389	471	<LOD
BI.22 (3)	22.49	36.70	2656	1446	658	<LOD
BI.23 (1)	22.98	33.14	1927	1082	366	<LOD
BI.23 (2)	22.98	37.76	2157	1253	275	<LOD
BI.24 (1)	23.95	36.48	2420	1337	331	<LOD
BI.24 (2)	23.95	37.32	2433	1396	86	<LOD
BI.24 (3)	23.95	35.63	2553	1338	133	<LOD
BI.25 (1)	26.44	36.27	2322	1115	338	<LOQ
BI.26 (1)	28.42	35.33	2322	1260	350	<LOD
BI.26 (2)	28.42	40.49	2569	1451	218	<LOQ
BI.26 (3)	28.42	35.01	2230	1300	410	<LOD
BI.27 (1)	29.38	35.25	2342	1098	337	<LOD
BI.27 (2)	29.38	35.01	2126	1091	423	<LOQ
BI.27a (1)	30.36	35.77	2346	1119	458	<LOD
BI.28 (1)	31.36	34.22	2197	1194	514	<LOD
BI.29 (1)	33.02	-	-	-	365	<LOQ
Vradlovtsi-2 section						

Sample number (belemnite sample)	Stratigraphic height (m)	Ca (%)	Mg (ppm)	Sr (ppm)	Fe (ppm)	Mn (ppm)
Vd.1.base Sr	0.00	41.05	2109	1333	103	<LOQ
Vd.1.base (1)	0.00	41.08	1960	1360	139	<LOQ
Vd.1.base (2)	0.00	41.12	2049	1480	134	<LOQ
Vd.1.base (3)	0.00	39.34	2126	1290	153	<LOQ
Vd.11.5.1 Sr	0.15	40.58	2379	1382	179	<LOQ
Vd.11.5.1 (1)	0.15	41.08	2344	1351	178	<LOQ
Vd.11.5.1 (2)	0.15	46.50	2786	1511	0	22
Vd.11.5.1 (3)	0.15	41.06	2368	1391	186	<LOQ
Vd.11.5.2 Sr	0.15	40.23	2984	1431	147	<LOQ
Vd.11.5.2 (1)	0.15	40.78	2514	1351	179	<LOQ
Vd.11.5.2 (2)	0.15	41.32	2576	1462	120	<LOQ
Vd.11.5.2 (3)	0.15	40.63	2483	1316	141	<LOQ
Vd.1.160 Sr	0.50	43.29	2283	1381	86	<LOQ
Vd.1.160 (1)	0.50	42.37	2187	1377	118	<LOQ
Vd.1.160 (2)	0.50	44.82	2378	1430	265	<LOQ
Vd.1.160 (3)	0.50	40.99	2174	1306	370	27
Vd.1.120 Sr	0.90	43.73	1921	1203	87	<LOQ
Vd.1.120 (1)	0.90	42.94	1765	1283	112	<LOQ
Vd.1.120 (2)	0.90	40.98	1760	1234	128	<LOD
Vd.1.120 (3)	0.90	40.83	1821	1207	376	<LOQ
Vd.1.100 Sr	1.10	39.40	2045	1276	300	<LOQ
Vd.1.100 (1)	1.10	40.64	2062	1305	78	<LOQ
Vd.1.100 (2)	1.10	41.93	2001	1254	81985	36
Vd.1.100 (3)	1.10	43.22	2043	1197	72	42
Vd.260 Sr	2.70	45.28	2483	1464	184	<LOQ
Vd.260 (1)	2.70	41.97	2435	1447	154	<LOQ
Vd.260 (2)	2.70	42.16	2534	1401	93	<LOQ
Vd.2.60 (3)	2.70	43.00	2472	1431	110	<LOQ
Vd.2.190 Sr	4.00	44.74	1814	1473	72	<LOD
Vd.2.190 (1)	4.00	43.66	1620	1395	57	<LOD
Vd.2.190 (2)	4.00	43.37	1614	1426	60	<LOD
Vd.2.190 (3)	4.00	43.88	1789	1456	68	<LOD
Vd.2.130 Sr	4.66	42.68	3165	1200	-	<LOQ
Vd.2.130 (1)	4.66	42.76	2806	1275	-	<LOQ
Vd.2.130 (2)	4.66	42.43	2787	1233	-	<LOQ
Vd.2.130 (3)	4.66	42.63	3011	1311	-	<LOQ
Vd.2.15 Sr	5.81	42.72	2765	1709	-	19
Vd.2.15 (1)	5.81	44.25	2586	1682	-	<LOQ
Vd.2.15 (2)	5.81	45.47	2636	1814	-	<LOQ
Vd.2.15 (3)	5.81	43.17	2792	1663	-	21

Sample number (belemnite sample)	Stratigraphic height (m)	Ca (%)	Mg (ppm)	Sr (ppm)	Fe (ppm)	Mn (ppm)
Vd.3 base.1 Sr	5.97	43.61	2606	1546	155	<LOQ
Vd.3 base.1 (1)	5.97	42.83	2442	1348	269	22
Vd.3 base.1 (2)	5.97	43.37	2544	1467	174	<LOQ
Vd.3 base.1 (3)	5.97	43.29	2515	1472	279	21
Vd.3 base.2 Sr	5.99	38.83	2271	1232	59	<LOD
Vd.3 base.2 (1)	5.99	44.33	2606	1416	51	<LOD
Vd.3 base.2 (2)	5.99	42.95	2643	1503	56	<LOD
Vd.3 base.2 (3)	5.99	43.48	2710	1481	43	<LOD
Vd.3.100 Sr	6.96	44.68	2781	1607	33	<LOD
Vd.3.100 (1)	6.96	43.95	1852	1244	37	<LOD
Vd.3.100 (2)	6.96	83.81	3622	2531	0	<LOD
Vd.3.100 (3)	6.96	42.80	2494	1354	93	<LOQ
Vd.3.40 Sr	7.06	42.91	2770	1415	99	<LOQ
Vd.3.40 (1)	7.06	43.11	2674	1486	36	<LOD
Vd.3.40 (2)	7.06	42.76	2891	1361	80	<LOQ
Vd.3.10 Sr	7.36	43.15	2815	1233	90	<LOQ
Vd.3.10 (1)	7.36	42.77	2985	1232	77	<LOQ
Vd.3.10 (2)	7.36	42.83	2785	1194	95	<LOQ
Vd.3.10 (3)	7.36	43.10	2967	1245	53	<LOD
Vd.47 Sr	7.53	42.98	1501	1136	40	<LOD
Vd.47 (1)	7.53	43.15	1620	1113	72	<LOQ
Vd.47 (2)	7.53	40.89	1616	1073	55	<LOQ
Vd.450.2 Sr	7.9	44.41	2805	1351	91	<LOQ
Vd.450.2 (1)	7.9	43.24	2811	1297	84	<LOQ
Vd.450.2 (2)	7.9	35.33	2027	1159	43	<LOQ
Vd.450.2 (3)	7.9	42.94	2711	1260	94	23
Vd.450.1 Sr	7.96	43.00	2844	1546	49	<LOD
Vd.450.1 (1)	7.96	42.92	3490	1609	47	<LOD
Vd.450.1 (2)	7.96	43.81	3588	1633	50	<LOD
Vd.450.1 (3)	7.96	43.93	2976	1469	35	<LOD
Vd.520 Sr	9.25	40.37	3145	1144	109	<LOQ
Vd.520 (1)	9.25	40.85	3166	1143	107	<LOQ
Vd.520 (2)	9.25	39.71	3112	1095	130	<LOQ
Vd.520 (3)	9.25	43.08	3687	1224	-	<LOD
Vd.6.base Sr	9.46	43.19	2499	1478	233	67
Vd.6.base (1)	9.46	44.62	2816	1641	93	<LOD
Vd.6. base (2)	9.46	44.01	2630	1602	89	<LOQ
Vd.6. base (3)	9.46	45.47	2755	1621	91	<LOQ
Vd.5.95.1 Sr	9.95	42.68	2315	1632	106	<LOQ
Vd.5.95.1 (1)	9.95	42.91	1879	1453	88	<LOQ

Sample number (belemnite sample)	Stratigraphic height (m)	Ca (%)	Mg (ppm)	Sr (ppm)	Fe (ppm)	Mn (ppm)
Vd.5.95.1 (2)	9.95	41.17	1994	1467	137	<LOQ
Vd.5.95.2 Sr	9.99	41.92	2160	1501	66	<LOQ
Vd.5.95.2 (1)	9.99	41.77	1713	1267	78	<LOQ
Vd.5.95.2 (2)	9.99	41.88	1731	1311	57	<LOQ
Vd.6.55 Sr	10.95	45.35	2689	1729	102	<LOQ
Vd.6.55 (1)	10.95	44.49	2757	1732	73	<LOD
Vd.6.55 (2)	10.95	42.96	2286	1520	353	25
Vd.6.60 Sr	11.00	43.10	2528	1427	77	<LOQ
Vd.6.60 (1)	11.00	42.97	2635	1443	54	<LOD
Vd.6.60 (2)	11.00	43.31	2693	1420	65	<LOD
Vd.6.60 (3)	11.00	42.37	2620	1487	61	<LOD
Vd.6.70 Sr	11.10	41.55	2610	1396	54	<LOD
Vd.6.70 (1)	11.10	43.16	2601	1397	61	<LOD
Vd.6.70 (2)	11.10	43.67	2980	1506	73	<LOQ
Vd.6.70 (3)	11.10	43.65	2589	1206	120	<LOQ
Vd.6.95 Sr	11.35	43.78	2902	1708	107	<LOQ
Vd.6.95 (1)	11.35	42.97	2807	1683	81	<LOQ
Vd.6.95 (2)	11.35	42.59	2696	1545	115	<LOQ
Vd.6.68 Sr	11.86	42.20	2448	1315	202	<LOQ
Vd.6.68 (1)	11.86	43.82	2671	1227	116	<LOQ
Vd.6.68 (3)	11.86	41.83	2481	1244	272	23
Vd.6.30 Sr	12.24	42.72	2234	1513	-	<LOQ
Vd.6.30 (1)	12.24	43.07	2150	1420	-	18
Vd.6.30 (2)	12.24	42.77	2183	1430	-	24
Vd.6.25 (1)	12.29	43.34	2224	1245	-	41
Vd.6.25 (2)	12.29	44.33	2202	1343	-	31
Vd.6.70 Sr	11.84	43.43	2164	1340	-	26
Vd.6.70 (1)	11.84	42.97	2736	1418	-	<LOQ
Vd.6.70 (2)	11.84	42.21	2854	1339	-	<LOQ
Vd.6.70 (3)	11.84	43.00	2584	1619	-	<LOQ
Vd.7.23 Sr	12.77	43.81	2583	1195	112	<LOQ
Vd.7.23 (1)	12.77	43.03	2901	1534	103	<LOQ
Vd.7.23 (2)	12.77	43.38	3270	1383	66	<LOQ
Vd.7.40 Sr	12.94	43.41	2645	1395	256	<LOD
Vd.7.40 (1)	12.94	42.57	2445	1363	147	<LOQ
Vd.7.40 (2)	12.94	42.78	2340	1464	125	<LOQ
Vd.7.40 (3)	12.94	42.70	3147	1234	221	<LOQ
Vd.7.85 Sr	13.39	43.32	2850	1316	120	<LOQ
Vd.7.85 (1)	13.39	44.40	1924	1399	215	<LOQ
Vd.7.85 (2)	13.39	43.33	1903	1267	150	<LOQ

Sample number (belemnite sample)	Stratigraphic height (m)	Ca (%)	Mg (ppm)	Sr (ppm)	Fe (ppm)	Mn (ppm)
Vd.7.85 (3)	13.39	43.95	1807	1351	97	<LOQ
Vd.7.90 Sr	13.44	44.56	1724	1320	219	<LOQ
Vd.7.90 (1)	13.44	42.30	2118	999	225	<LOQ
Vd.7.90 (2)	13.44	43.31	2310	977	471	<LOQ
Vd.7.90 (3)	13.44	43.54	2697	1084	188	34
VD.7.35 (1)	15.71	44.07	2277	1155	198	<LOQ
VD.7.35 (2)	15.71	43.75	2309	1213	170	<LOQ
Vd.8.15 Sr	16.21	43.90	2894	1277	293	<LOQ
Vd.8.15 (1)	16.21	43.34	2501	1437	183	<LOQ
Vd.8.15 (2)	16.21	43.68	2481	1436	182	<LOQ
Vd.8.15 (3)	16.21	42.93	2261	1366	828	<LOQ
Vd.8.25 Sr	16.31	43.33	2415	1279	242	68
Vd.8.25 (1)	16.31	43.09	2865	1510	353	18
Vd.8.25 (2)	16.31	42.85	3003	1425	117	24
Vd.8.25 (3)	16.31	43.23	3058	1550	96	<LOQ
Vd.8.35 Sr	16.41	44.31	3218	1585	1150	<LOQ
Vd.8.35 (1)	16.41	41.73	3250	1521	193	82
Vd.8.35 (2)	16.41	42.35	2471	1543	222	<LOQ
Vd.8.35 (3)	16.41	43.24	2542	1441	247	19
Vd.8.52 Sr	16.64	42.55	2800	1120	640	<LOQ
Vd.8.52 (1)	16.64	42.39	2440	1115	106	36
Vd.8.52 (2)	16.64	42.93	2573	1176	209	<LOQ
Vd.8.35 Sr	16.86	42.32	2263	1413	150	21
Vd.8.35 (1)	16.86	41.11	2828	1152	103	<LOQ
Vd.8.35 (2)	16.86	39.49	2571	1150	83	<LOQ
Vd.8.35 (3)	16.86	41.75	2799	1119	292	<LOQ
Vd.8.100 Sr	17.06	44.11	2647	1119	121	<LOQ
Vd.8.100 (1)	17.06	43.48	2502	1445	91	<LOQ
Vd.8.100 (2)	17.06	42.05	2475	1462	172	<LOQ
Vd.8.100 (3)	17.06	42.81	2310	1350	212	<LOQ
Vd.8 .top Sr	17.21	39.79	2466	1247	126	23
Vd.8 .top (1)	17.21	39.89	3091	1260	188	<LOQ
Vd.8. top (2)	17.21	41.87	3137	1320	366	26
Vd.8 .top (3)	17.21	41.73	3076	1363	286	52
Vd.9.25 Sr	20.62	41.11	3033	1286	105	39
Vd.9.25 (1)	20.62	41.80	3567	1334	82	<LOQ
Vd.9.25 (2)	20.62	41.68	3375	1394	94	<LOQ
Vd.9.25 (3)	20.62	41.40	2956	1325	76	<LOQ
Vd.9.35 Sr	20.72	41.83	3735	1531	114	<LOQ

Sample number (belemnite sample)	Stratigraphic height (m)	Ca (%)	Mg (ppm)	Sr (ppm)	Fe (ppm)	Mn (ppm)
Vd.9.35 (1)	20.72	42.31	2949	1287	154	<LOQ
Vd.9.35 (2)	20.72	41.35	2993	1171	159	<LOQ
Vd.9.35 (3)	20.72	40.94	2878	1248	459	32
Vd.9.45.1 Sr	20.82	41.07	2935	1194	132	22
Vd.9.45.1 (1)	20.82	40.07	3072	1208	90	<LOQ
Vd.9.45.1 (2)	20.82	40.91	2973	1261	90	<LOQ
Vd.9.45.1 (3)	20.82	41.08	3003	1307	95	<LOQ
Vd.9.40 Sr	21.41	41.96	3040	1306	217	<LOQ
Vd.9.40 (1)	21.41	40.66	3388	1562	178	22
Vd.9.40 (2)	21.41	38.76	3253	1494	175	22
Vd.9.26 Sr	21.55	39.96	3361	1542	86	21
Vd.9.26 (1)	21.55	40.71	3003	1333	84	<LOQ
Vd.9.26 (2)	21.55	40.89	2892	1284	109	<LOQ
Vd.9.26 (3)	21.55	39.92	2959	1293	88	<LOQ
Vd.9.10 Sr	21.71	40.52	2884	1265	220	<LOQ
Vd.9.10 (1)	21.71	40.97	2488	1038	253	27
Vd.9.10 (2)	21.71	40.52	2508	1058	285	30
Vd.9.10 (3)	21.71	41.14	2426	1033	-	36
Vd.10. base Sr	21.81	40.49	2520	1073	-	29
Vd.10. base (2)	21.81	40.08	2508	1059	84	<LOQ
Vd.10.18 Sr	21.99	39.90	2414	1108	274	<LOQ
Vd.10.18 (1)	21.99	40.59	3588	1393	124	43
Vd.10.18 (2)	21.99	41.25	3310	1505	348	<LOQ
Vd.10.18 (3)	21.99	40.47	3427	1355	116	70
Vd.10.25 Sr	22.06	40.37	3139	1412	79	<LOQ
Vd.10.25 (1)	22.06	40.60	2847	1184	63	<LOQ
Vd.10.25 (2)	22.06	42.36	2814	1230	59	<LOQ
Vd.10.25 (3)	22.06	42.22	2919	1237	80	<LOQ
Vd.10.28 Sr	22.09	42.13	2625	1236	100	<LOQ
Vd.10.28 (2)	22.09	42.01	2598	1318	104	<LOQ
Vd.10.40 Sr	22.21	41.81	2520	1239	452	<LOQ
Vd.10.40 (1)	22.21	41.96	3184	1224	2198	34
Vd.10.40 (2)	22.21	41.11	3399	1026	119	447
Vd.10.47 Sr	22.28	43.07	3009	1196	55	<LOQ
Vd.10.47 (1)	22.28	43.42	3183	1306	62	<LOQ
Vd.10.47 (2)	22.28	43.39	3080	1339	91	<LOQ
Vd.10.55 Sr	22.36	43.71	3413	1323	54	<LOQ
Vd.10.55 (1)	22.36	44.64	2345	1209	108	<LOQ
Vd.10.55 (2)	22.36	41.98	2421	1140	61	<LOQ

Sample number (belemnite sample)	Stratigraphic height (m)	Ca (%)	Mg (ppm)	Sr (ppm)	Fe (ppm)	Mn (ppm)
Vd.10.59 Sr	22.40	42.99	2322	1191	91	<LOQ
Vd.10.59 (1)	22.40	42.83	2917	1323	108	<LOQ
Vd.10.59 (2)	22.40	43.89	3009	1275	97	<LOQ
Vd.10.60 Sr	22.41	43.48	3368	1383	73	<LOQ
Vd.10.60 (1)	22.41	43.83	2530	1336	94	<LOQ
Vd.10.60 (2)	22.41	44.54	2569	1310	242	<LOQ
Vd.10.66 Sr	22.47	44.23	2368	1212	84	43
Vd.10.66 (1)	22.47	44.17	2398	1240	59	<LOQ
Vd.10.66 (2)	22.47	43.86	2511	1204	97	<LOQ
Vd.10.66 (3)	22.47	44.23	2620	1186	0	<LOQ
Vd.10.26 Sr	22.69	44.46	2446	1266	83	<LOQ
Vd.10.26 (1)	22.69	43.11	3058	1161	93	<LOQ
Vd.10.26 (2)	22.69	43.86	3008	1224	59	<LOQ
Vd.10.26 (3)	22.69	43.37	3306	1284	45	<LOQ
Vd.10.15 Sr	22.80	44.27	3307	1309	102	<LOQ
Vd.10.15 (1)	22.80	42.81	2434	1140	101	<LOQ
Vd.10.15 (2)	22.80	44.19	2376	1169	69	<LOQ
Vd.10.14 Sr	22.81	44.03	2316	1239	56	<LOQ
Vd.10.14 (1)	22.81	43.94	2419	1273	65	<LOQ
Vd.10.14 (2)	22.81	42.78	2558	1289	46	<LOQ
Vd.10.12 Sr	22.83	42.30	2270	1197	87	<LOQ
Vd.10.12 (1)	22.83	40.84	2492	1100	96	<LOQ
Vd.10.12 (2)	22.83	42.76	2205	1066	90	19
Vd.10.10 Sr	22.85	42.28	2612	1100	105	<LOQ
Vd.10.10 (1)	22.85	43.49	2406	1096	73	<LOQ
Vd.10.10 (2)	22.85	35.83	1944	901	105	<LOQ
Vd.10.5 Sr	22.90	42.96	2446	1106	114	<LOQ
Vd.10.5 (1)	22.90	43.61	3067	1312	100	<LOQ
Vd.10.5 (2)	22.90	42.75	2753	1153	83	<LOQ
Vd.10.5 (3)	22.90	42.01	2818	1337	122	<LOQ
Vd.11. base.1 Sr	22.95	41.04	2660	1042	67	<LOQ
Vd.11. base.1 (1)	22.95	42.34	2932	1324	57	<LOQ
Vd.11. base.1 (2)	22.95	42.75	2956	1310	71	<LOQ
Vd.11. base.3 Sr	23.00	42.99	2954	1330	64	<LOQ
Vd.11. base.3 (1)	23.00	42.39	-	-	-	<LOQ
Vd.11. base.3 (2)	23.00	42.39	2100	927	100	28
Vd.11. base.3 (3)	23.00	42.21	2426	1125	-	<LOQ
Vd.11. base.2 Sr	23.00	44.46	2490	1166	229	<LOQ
Vd.11. base.2 (1)	22.97	42.16	2635	1205	84	<LOQ
Vd.11. base.2 (2)	22.97	42.56	2829	1225	81	<LOQ

Sample number (belemnite sample)	Stratigraphic height (m)	Ca (%)	Mg (ppm)	Sr (ppm)	Fe (ppm)	Mn (ppm)
Vd.11. base.2 (3)	22.97	42.75	2611	1208	127	<LOQ
Vd.11.15 Sr	23.10	43.69	1989	1006	74	<LOQ
Vd.11.15 (1)	23.10	43.19	1945	1030	77	<LOQ
Vd.11.15 (2)	23.10	42.64	2008	945	127	<LOQ
Vd.11.23 Sr	23.18	43.11	2647	1068	107	<LOQ
Vd.11.23 (1)	23.18	42.97	3152	1213	213	<LOQ
Vd.11.23 (2)	23.18	45.31	2747	1123	433	44
Vd.11.70 Sr	23.65	43.12	2464	1301	111	<LOQ
Vd.11.70 (1)	23.65	43.52	2296	1249	102	<LOQ
Vd.11.70 (2)	23.65	43.87	2237	1305	80	<LOQ
Vd.11.75 Sr	23.70	43.37	2710	1337	44	<LOQ
Vd.11.75 (1)	23.70	43.14	2734	1324	79	<LOQ
Vd.11.75 (2)	23.70	43.96	2495	1260	0	<LOQ
Vd.11.93 (1)	23.88	45.76	2327	905	113	<LOQ
Vd.11.93 (2)	23.88	41.37	2139	824	105	<LOQ
Vd.11.93 (3)	23.88	41.27	2114	817	93	<LOQ
Boeva Mogila section						
Te.28 (Sr)	0.05	35.31	1699	1152	57	14
Te.28 (1)	0.05	35.47	1715	1204	21	<LOQ
Te.28 (2)	0.05	34.42	1626	1109	26	7
Te.28 (3)	0.05	36.30	1724	1197	19	<LOQ
Te.26 (Sr)	0.65	35.00	1582	1142	60	21
Te.26 (1)	0.65	35.63	1743	1132	139	35
Te.26 (2)	0.65	34.85	1606	1091	54	15
Te.26 (3)	0.65	35.34	1676	1128	67	23
Te.25 (Sr)	0.75	36.16	1894	1256	19	<LOQ
Te.25 (1)	0.75	35.64	1868	1243	18	<LOQ
Te.25 (2)	0.75	35.88	1859	1247	19	5
Te.25 (3)	0.75	35.86	1970	1257	28	7
Te.24 (Sr)	0.80	36.93	2262	1396	35	14
Te.24 (1)	0.80	37.24	2448	1487	196	51
Te.24 (2)	0.80	36.11	2014	1543	587	147
Te.24 (3)	0.80	35.56	2584	1438	345	65
Te-23 (Sr)	0.90	36.35	1907	1300	183	25
Te.23 (1)	0.90	36.77	1784	1229	84	19
Te.23 (2)	0.90	36.35	1885	1309	49	10
Te.23 (3)	0.90	36.19	1667	1134	83	18
Te.1 (Sr)	1.05	36.32	1628	1021	73	18
Te.1 (1)	1.05	29.21	1155	780	70	22

Sample number (belemnite sample)	Stratigraphic height (m)	Ca (%)	Mg (ppm)	Sr (ppm)	Fe (ppm)	Mn (ppm)
Te.1 (2)	1.05	35.56	1478	1009	84	31
Te.1 (3)	1.05	36.41	1286	919	143	45
Te.2 (Sr)	1.10	36.17	1900	1281	37	13
Te.2 (1)	1.10	35.96	2050	1344	24	10
Te.2 (2)	1.10	36.76	1919	1293	32	14
Te.2 (3)	1.10	37.20	1976	1289	30	15
Te.3 (Sr)	1.15	36.21	1992	1219	335	91
Te.3 (1)	1.15	35.92	1994	1184	67	23
Te.3 (2)	1.15	35.31	1827	1178	203	77
Te.3 (3)	1.15	34.60	1770	1179	167	63
Te.4 (Sr)	1.22	36.86	2039	1249	27	12
Te.4 (1)	1.22	34.78	2018	1214	26	12
Te.4 (2)	1.22	37.37	2126	1260	22	12
Te.4 (3)	1.22	38.18	2108	1273	23	12
Te.21 (Sr)	4.40	36.82	3720	1369	196	153
Te.21 (1)	4.40	36.99	3928	1417	112	101
Te.21 (2)	4.40	37.75	4320	1507	29	14
Te.21 (3)	4.40	35.19	3710	1306	96	78
Te.22a (Sr)	4.80	34.32	2687	1269	704	433
Te.22a (1)	4.80	36.18	2903	1277	350	232
Te.22a (2)	4.80	36.62	2804	1281	360	259
Te.22a (3)	4.80	33.77	3083	1170	72	42
Te.22b (Sr)	4.80	36.22	4685	1401	30	16
Te.22b (1)	4.80	36.49	4284	1385	29	15
Te.22b (2)	4.80	36.09	4016	1430	27	13
Te.22b (3)	4.80	35.55	3858	1396	37	15
Te.22c (Sr)	4.80	36.78	4189	1372	536	294
Te.22c (1)	4.80	35.86	3907	1352	280	213
Te.22c (2)	4.80	36.60	4305	1483	353	177
Te.22c (3)	4.80	37.12	4022	1439	50	30
Diagenetically altered calcite ‘bad bits’						
Te.22 x1	4.8	-	-	-	-	-
Te.1 x2	1.05	-	-	-	-	-
Te.26 x3	0.65	-	-	-	-	-
Te.21 x4	4.4	-	3224	13801	262	1786
Te.28 x5	0.05	-	-	-	-	-
Mv.7.10 x1	3.63	-	-	-	-	-
Mv.2.180 x2	3.26	-	2684	13147	208	490
Mv.5.25 x3	3.31	-	2630	12916	279	913

Sample number (belemnite sample)	Stratigraphic height (m)	Ca (%)	Mg (ppm)	Sr (ppm)	Fe (ppm)	Mn (ppm)
Mv.2.60 x4	2.06	-	2527	12817	203	696
Mv.2.73 x5	2.19	-	2895	11423	1021	2076
Bl.17a x1	17.21	-	2442	11970	159	232
Bl.7a x2	7.99	-	2519	13235	723	365
Bl.10 x3	10.94	-	2827	13769	283	119
Bl.10 x4	10.94	-	-	-	-	-
Bl.2 x5	2.40	-	-	-	-	-
Vd.7.90 x1	13.44	-	1889	8094	2329	1622
Vd.11.base x2	22.95	-	-	-	-	-
Vd.8.top x3	17.21	-	2308	11289	673	850
Vd.6.60 x4	11.0	-	-	-	-	-
Vd.9.45 x5	20.82	-	-	-	-	-

Appendix B.2 Stable isotope data, estimated palaeotemperatures and CL alteration type.

Sample number (subsample)	Stratigraphic height (m)	CL alteration type	$\delta^{13}C_{bel}$ rel. PBD	$\delta^{18}O_{bel}$ rel. PBD	Palaeotemperature (°C)
Milanovo section					
MV.P10.30 (1)	-0.13	5	1.64	-3.76	28.40
MV.P12.200 (1)	0.00	5	-0.02	-3.11	25.31
MV.P12.200 (2)	0.00	5	-0.06	-2.89	24.30
MV.P18.1 (1)	0.08	5	0.61	-2.15	20.91
MV.P18.1 (2)	0.08	5	0.28	-1.82	19.49
MV.P18.2 (1)	0.14	5	0.37	-2.63	23.09
MV.P18.3 (1)	0.18	4	0.74	-1.58	18.46
MV.2.5 (1)	1.51	4	3.05	-2.82	23.96
MV.2.5 (2)	1.51	4	3.27	-2.95	24.58
MV.2.10 (1)	1.56	4	1.64	-3.45	26.95
MV.2.10 (2)	1.56	4	2.03	-3.60	27.65
MB.2.10 (3)	1.56	4	1.35	-3.36	26.52
MV.2.12 (1)	1.58	5	2.75	-4.86	33.91
MV.2.40.1 (1)	1.86	4	3.67	-4.95	34.37
MV.2.40.1 (2)	1.86	4	3.81	-3.75	28.38
MV.2.40.1 (3)	1.86	4	2.07	-3.07	25.14
MV.2.40.2 (1)	1.89	3	3.99	-3.54	27.35
MV.2.40.2 (2)	1.89	3	3.97	-3.29	26.18
MV.2.40.2 (3)	1.89	3	3.82	-3.71	28.17
MV.2.60 (1)	2.06	4	1.09	-4.37	31.43
MV.2.60 (2)	2.06	4	1.12	-3.75	28.35
MV.2.70 (1)	2.16	4	2.01	-3.97	29.44
MV.2.70 (2)	2.16	4	1.78	-4.75	33.35

Sample number (subsample)	Stratigraphic height (m)	CL alteration type	$\delta^{13}C_{bel}$ rel. PBD	$\delta^{18}O_{bel}$ rel. PBD	Palaeotemperature (°C)
MV.2.72 (1)	2.18	4	2.26	-4.22	30.68
MV.2.72 (2)	2.18	4	2.31	-4.30	31.08
MV.2.73 (1)	2.19	4	2.57	-4.44	31.76
MV.2.73 (2)	2.19	4	2.80	-4.42	31.66
MV.3.5 (1)	2.21	4	3.55	-3.56	27.43
MV.3.5 (2)	2.21	4	2.50	-5.44	36.93
MV.3.5 (3)	2.21	4	3.58	-3.22	25.83
MV.2.90 (1)	2.36	5	1.56	-3.73	28.25
MV.2.90 (2)	2.36	5	1.42	-3.84	28.81
MV.2.120 (1)	2.66	4	2.29	-3.53	27.30
MV.2.120 (2)	2.66	4	1.98	-3.59	27.61
MV.4.5 (1)	2.86	3	0.79	-3.45	26.93
MV.4.5 (2)	2.86	3	0.77	-3.38	26.58
MV.4.5 (3)	2.86	3	1.03	-3.55	27.39
MV.5.10.1 (1)	3.11	3	0.99	-4.19	30.53
MV.5.10.1 (2)	3.11	3	1.86	-3.15	25.51
MV.5.10.1 (3)	3.11	3	1.66	-2.81	23.91
MV.5.10.2 (1)	3.16	4	1.36	-6.46	42.47
MV.5.10.2 (2)	3.16	4	1.42	-3.34	26.38
MV.5.10.2 (3)	3.16	4	1.60	-2.94	24.50
MV.5.10.3 (1)	3.17	4	1.26	-2.84	24.07
MV.5.10.3 (2)	3.17	4	1.05	-3.29	26.15
MV.5.10.3 (3)	3.17	4	1.23	-2.99	24.78
MV.2.180 (1)	3.26	5	1.57	-3.19	25.70
MV.2.180 (2)	3.26	5	1.36	-3.85	28.84
MV.5.30 (1)	3.31	4	0.72	-2.19	21.12

Sample number (subsample)	Stratigraphic height (m)	CL alteration type	$\delta^{13}C_{bel}$ rel. PBD	$\delta^{18}O_{bel}$ rel. PBD	Palaeotemperature (°C)
MV.5.30 (2)	3.31	4	0.90	-1.86	19.65
MV.5.30 (3)	3.31	4	1.14	-2.41	22.10
MV.6.5 (1)	3.36	3	1.03	-2.02	20.35
MV.6.5 (2)	3.36	3	0.87	-2.61	23.01
MV.6.5 (3)	3.36	3	0.62	-2.94	24.52
MV.6.8 (1)	3.39	4	1.45	-3.70	28.12
MV.6.8 (2)	3.39	4	1.70	-2.84	24.06
MV.5.40 (1)	3.41	2	1.96	-2.78	23.77
MV.5.40 (2)	3.41	2	2.08	-3.28	26.14
MV.5.40 (3)	3.41	2	1.85	-2.50	22.49
MV.6.10 (1)	3.41	3	0.65	-2.82	23.99
MV.6.10 (2)	3.41	3	0.67	-2.44	22.21
MV.6.11 (1)	3.42	3	1.00	-1.86	19.68
MV.5.42 (1)	3.43	4	1.20	-2.77	23.74
MV.5.42 (2)	3.43	4	1.12	-2.63	23.08
MV.5.43 (1)	3.44	4	0.98	-2.88	24.23
MV.5.43 (2)	3.44	4	0.86	-2.13	20.84
MV.5.43 (3)	3.44	4	0.41	-3.25	25.96
MV.6.13 (1)	3.44	4	1.56	-4.13	30.21
MV.6.13 (2)	3.44	4	1.86	-2.82	23.95
MV.6.13 (3)	3.44	4	1.71	-2.72	23.50
MV.2.210 (1)	3.56	3	1.32	-3.23	25.87
MV.2.210 (2)	3.56	3	1.02	-3.35	26.44
MV.7.10 (1)	3.63	4	1.40	-3.30	26.20
MV.7.10 (2)	3.63	4	1.28	-3.67	27.96
MV.7.14 (1)	3.67	3	1.29	-2.53	22.65

Sample number (subsample)	Stratigraphic height (m)	CL alteration type	$\delta^{13}C_{bel}$ rel. PBD	$\delta^{18}O_{bel}$ rel. PBD	Palaeotemperature (°C)
MV.7.14 (2)	3.67	3	1.40	-2.06	20.55
MV.7.14 (3)	3.67	3	1.29	-2.80	23.89
MV.7.20 (1)	3.73	4	1.39	-4.58	32.49
MV.7.20 (2)	3.73	4	1.73	-2.55	22.74
MV.7.21 (1)	3.74	4	-0.19	-2.58	22.85
MV.7.21 (2)	3.74	4	-0.41	-2.85	24.12
MV.7.26 (1)	3.79	3	1.50	-2.23	21.28
MV.7.26 (2)	3.79	3	1.30	-2.58	22.89
MV.7.26 (3)	3.79	3	1.57	-3.10	25.28
MV.7.35 (2)	3.88	3	1.03	-1.70	18.94
MV.7.35 (1)	3.88	3	0.52	-2.08	20.64
MV.8.10 (1)	3.93	3	0.12	-1.87	19.70
MV.8.10 (2)	3.93	3	0.16	-2.27	21.49
MV.8.10 (3)	3.93	3	0.40	-2.62	23.03
MV.7.80 (1)	4.33	3	1.35	-2.33	21.75
MV.7.80 (2)	4.33	3	1.01	-2.33	21.73
MV.7.80 (3)	4.33	3	1.24	-2.74	23.60
Berende Izvor section					
BI.1 (2)	1.50	-	1.08	-0.77	15.06
BI.1 (3)	1.50	-	0.79	-0.77	15.04
BI.1b (1)	1.50	-	1.67	-0.98	15.91
BI.2a (1)	2.28	-	0.90	-1.52	18.20
BI.2a (2)	2.28	-	0.56	-1.47	17.96
BI.2a (3)	2.28	-	1.03	-1.18	16.75
BI.2 (1)	2.40	-	1.04	-1.33	17.39
BI.2 (2)	2.40	-	0.96	-1.32	17.35

Sample number (subsample)	Stratigraphic height (m)	CL alteration type	$\delta^{13}C_{bel}$ rel. PBD	$\delta^{18}O_{bel}$ rel. PBD	Palaeotemperature (°C)
BI.2 (3)	2.40	-	1.03	-1.18	16.75
BI.3 (1)	3.24	-	1.83	-1.48	18.03
BI.3 (3)	3.24	-	1.72	-1.61	18.58
BI.3a (1)	3.42	-	0.23	-1.80	19.38
BI.3b (1)	4.25	-	2.13	-1.17	16.70
BI.3b (2)	4.25	-	2.15	-1.24	16.99
BI.3b (3)	4.25	-	1.89	-1.32	17.33
BI.4 (1)	4.73	-	0.81	-1.76	19.23
BI.5 (1)	5.23	-	1.62	-0.79	15.16
BI.5 (2)	5.23	-	1.48	-1.27	17.13
BI.6 (1)	5.55	-	1.10	-1.28	17.18
BI.6 (2)	5.55	-	1.61	-0.80	15.19
BI.6 (3)	5.55	-	1.44	-1.10	16.42
BI.6b (1)	5.74	-	1.16	-0.40	13.58
BI.6b (2)	5.74	-	1.09	-0.53	14.08
BI.6b (3)	5.74	-	1.16	-0.33	13.30
BI.6a (1)	7.19	-	1.60	-0.70	14.78
BI.6a (2)	7.19	-	1.53	-0.49	13.91
BI.6a (3)	7.19	-	1.59	-0.49	13.91
BI.6c (1)	7.38	-	0.88	-1.12	16.50
BI.6c (2)	7.38	-	1.22	-1.21	16.86
BI.6c (3)	7.38	-	1.06	-1.19	16.81
BI.7 (1)	7.53	-	0.42	-1.60	18.53
BI.7 (2)	7.53	-	-0.04	-1.66	18.78
BI.7a (1)	7.99	-	1.84	-0.60	14.38
BI.7a (2)	7.99	-	1.69	-0.79	15.13

Sample number (subsample)	Stratigraphic height (m)	CL alteration type	$\delta^{13}C_{bel}$ rel. PBD	$\delta^{18}O_{bel}$ rel. PBD	Palaeotemperature (°C)
BI.8 (1)	8.95	-	2.48	-1.46	17.92
BI.8 (2)	8.95	-	2.01	-1.69	18.93
BI.8 (3)	8.95	-	2.20	-1.17	16.70
BI.9 (1)	9.71	-	1.86	-0.36	13.42
BI.9 (3)	9.71	-	1.90	-0.20	12.78
BI.10 (1)	10.94	-	2.43	-1.91	19.86
BI.10 (2)	10.94	-	2.41	-2.02	20.36
BI.10 (3)	10.94	-	2.24	-2.02	20.38
BI.11 (1)	12.09	-	1.20	-1.19	16.80
BI.11 (2)	12.09	-	1.10	-1.18	16.73
BI.11 (3)	12.09	-	1.34	-1.20	16.84
BI.11a (1)	12.59	-	2.11	-0.67	14.66
BI.12 (1)	13.13	-	1.62	-0.61	14.41
BI.12 (2)	13.13	-	1.64	-1.20	16.83
BI.13 (1)	13.59	-	2.36	-0.49	13.92
BI.13 (2)	13.59	-	2.25	-0.44	13.74
BI.13a (1)	13.88	-	2.24	-0.61	14.41
BI.13a (2)	13.88	-	2.48	-0.65	14.56
BI.13a (3)	13.88	-	2.26	-0.36	13.41
BI.14 (1)	14.66	-	1.22	-0.20	12.78
BI.14 (2)	14.66	-	1.40	-0.17	12.65
BI.15 (1)	15.75	-	2.06	-0.31	13.19
BI.15 (2)	15.75	-	2.17	-0.09	12.34
BI.15 (3)	15.75	-	2.16	0.02	11.91
BI.16 (1)	16.77	-	2.36	-0.20	12.76
BI.16 (2)	16.77	-	2.52	-0.14	12.53

Sample number (subsample)	Stratigraphic height (m)	CL alteration type	$\delta^{13}C_{bel}$ rel. PBD	$\delta^{18}O_{bel}$ rel. PBD	Palaeotemperature (°C)
Bl.17 (2)	17.01	-	2.27	-0.22	12.84
Bl.17 (3)	17.01	-	2.21	-0.55	14.18
Bl.17a (1)	17.21	-	1.86	-0.69	14.72
Bl.17a (2)	17.21	-	2.02	-0.71	14.79
Bl.17a (3)	17.21	-	2.11	-0.64	14.54
Bl.17b (1)	17.52	-	2.43	-0.50	13.96
Bl.17b (2)	17.52	-	2.31	-0.48	13.87
Bl.17b (3)	17.52	-	2.15	-0.58	14.30
Bl.17c (1)	17.79	-	2.16	-0.66	14.60
Bl.17c (2)	17.79	-	2.37	-0.57	14.26
Bl-17c (3)	17.79	-	2.43	-0.54	14.11
Bl.18 (1)	18.27	-	1.35	-0.99	15.98
Bl.18 (2)	18.27	-	1.77	-1.15	16.62
Bl.18 (3)	18.27	-	1.66	-0.93	15.70
Bl.20 (1)	20.53	-	1.11	-0.78	15.08
Bl.20 (2)	20.53	-	0.92	-0.60	14.35
Bl.21 (1)	21.47	-	2.40	-0.54	14.11
Bl.22 (1)	22.49	-	1.70	-0.32	13.25
Bl.22 (2)	22.49	-	1.92	-0.17	12.67
Bl.22 (3)	22.49	-	1.72	-0.05	12.17
Bl.23 (1)	22.98	-	1.44	-1.03	16.13
Bl.23 (2)	22.98	-	1.52	-0.53	14.07
Bl.24 (1)	23.95	-	1.91	-0.38	13.47
Bl.24 (2)	23.95	-	2.01	-0.05	12.18
Bl.24 (3)	23.95	-	2.13	-0.31	13.19
Bl.25 (1)	26.44	-	1.33	-1.21	16.88

Sample number (subsample)	Stratigraphic height (m)	CL alteration type	$\delta^{13}C_{bel}$ rel. PBD	$\delta^{18}O_{bel}$ rel. PBD	Palaeotemperature (°C)
BI.26 (1)	28.42	-	1.97	-0.73	14.89
BI.26 (2)	28.42	-	2.06	-0.78	15.08
BI.26 (3)	28.42	-	2.08	-0.60	14.36
BI.27 (1)	29.38	-	1.60	-0.84	15.34
BI.27 (2)	29.38	-	1.63	-0.72	14.87
BI.27a (1)	30.36	-	1.50	-1.13	16.53
BI.28 (1)	31.36	-	1.99	-0.59	14.34
BI.29 (1)	33.02	-	2.13	-0.32	13.24
Vradlovtsi-2 section					
Vd.1.base (1)	0.00	3	0.83	-1.45	17.87
Vd.1.base (2)	0.00	3	1.12	-1.34	17.41
Vd.1.base (3)	0.00	3	0.80	-1.06	16.24
Vd.1.15.1 (1)	0.15	4	1.35	-1.59	18.47
Vd.1.15.1 (2)	0.15	4	1.18	-1.37	17.53
Vd.1.15.1 (3)	0.15	4	1.18	-1.19	16.79
Vd.1.15.2 (1)	0.15	4	1.18	-2.08	20.63
Vd.1.15.2 (2)	0.15	4	1.16	-1.93	19.98
Vd.1.15.2 (3)	0.15	4	1.06	-2.03	20.40
Vd.1.160 (1)	0.50	-	0.37	-1.76	19.24
Vd.1.160 (2)	0.50	-	0.01	-2.48	22.42
Vd.1.160 (3)	0.50	-	-0.40	-2.47	22.35
Vd.1.120 (1)	0.90	-	-0.01	-0.93	15.71
Vd.1.120 (2)	0.90	-	0.17	-0.99	15.94
Vd.1.120 (3)	0.90	-	-0.34	-2.42	22.13
Vd.1.100 (1)	1.10	2	0.48	-1.19	16.79
Vd.1.100 (2)	1.10	2	0.71	-0.70	14.76

Sample number (subsample)	Stratigraphic height (m)	CL alteration type	$\delta^{13}C_{bel}$ rel. PBD	$\delta^{18}O_{bel}$ rel. PBD	Palaeotemperature (°C)
Vd.1.100 (3)	1.10	2	0.39	-0.70	14.78
Vd.2.60 (1)	2.70	3	1.35	-1.85	19.60
Vd.2.60 (2)	2.70	3	1.29	-1.56	18.34
Vd.2.60 (3)	2.70	3	1.37	-1.24	16.98
Vd.2.190 (1)	4.00	-	0.69	-1.09	16.35
Vd.2.190 (2)	4.00	-	0.85	-1.46	17.94
Vd.2.190 (3)	4.00	-	0.79	-1.42	17.78
Vd.2.130 (1)	4.66	-	-0.10	-2.02	20.38
Vd.2.130 (2)	4.66	-	0.13	-1.97	20.15
Vd.2.130 (3)	4.66	-	0.26	-1.86	19.66
Vd.2.15 (1)	5.81	-	2.48	-1.02	16.07
Vd.2.15 (2)	5.81	-	2.82	-1.46	17.93
Vd.2.15 (3)	5.81	-	2.56	-1.76	19.22
Vd.3.base.1 (1)	5.97	-	0.37	-2.02	20.34
Vd.3 base.1 (2)	5.97	-	0.75	-1.81	19.42
Vd.3 base.1 (3)	5.97	-	0.95	-1.75	19.19
Vd.3 base.2 (1)	5.99	3	1.14	-1.66	18.79
Vd.3 base.2 (2)	5.99	3	1.22	-1.51	18.13
Vd.3 base.2 (3)	5.99	3	1.14	-1.29	17.21
Vd.3.100 (1)	6.96	-	-0.20	-1.32	17.35
Vd.3.100 (2)	6.96	-	-0.35	-1.28	17.16
Vd.3.100 (3)	6.96	-	1.41	-1.72	19.05
Vd.3.40 (1)	7.06	-	0.52	-1.24	17.00
Vd.3.40 (2)	7.06	-	0.37	-1.52	18.18
Vd.3.10 (1)	7.36	-	0.41	-1.83	19.53
Vd.3.10 (2)	7.36	-	0.62	-1.82	19.47

Sample number (subsample)	Stratigraphic height (m)	CL alteration type	$\delta^{13}C_{bel}$ rel. PBD	$\delta^{18}O_{bel}$ rel. PBD	Palaeotemperature (°C)
Vd.3.10 (3)	7.36	-	0.45	-1.73	19.10
Vd.4.7 (1)	7.53	-	-1.73	-0.79	15.12
Vd.4.7 (2)	7.53	-	-1.39	-0.60	14.38
Vd.4.50.2 (1)	7.9	-	1.32	-1.81	19.44
Vd.4.50.2 (2)	7.9	-	2.12	-1.27	17.13
Vd.4.50.2 (3)	7.9	-	1.14	-1.88	19.74
Vd.4.50.1 (1)	7.96	-	2.54	-1.06	16.26
Vd.4.50.1 (2)	7.96	-	2.18	-1.31	17.29
Vd.5.20 (1)	9.25	2	1.35	-1.89	19.77
Vd.5.20 (2)	9.25	2	1.13	-1.85	19.62
Vd.5.20 (3)	9.25	2	1.21	-1.79	19.36
Vd.6 base (1)	9.46	-	2.04	-1.48	18.01
Vd.6 base (2)	9.46	-	2.06	-1.22	16.90
Vd.6 base (3)	9.46	-	1.91	-1.65	18.76
Vd.5.95.1 (1)	9.95	-	0.94	-1.70	18.97
Vd.5.95.1 (2)	9.95	-	0.76	-1.64	18.69
Vd.5.95.2 (1)	9.99	-	0.61	-1.99	20.24
Vd.5.95.2 (2)	9.99	-	0.55	-2.18	21.06
Vd.6.55 (1)	10.95	-	2.21	-0.83	15.31
Vd.6.55 (2)	10.95	-	2.12	-1.36	17.49
Vd.6.60 (1)	11.00	3	1.32	-1.51	18.13
Vd.6.60 (2)	11.00	3	1.47	-1.64	18.71
Vd.6.60 (3)	11.00	3	1.42	-1.43	17.82
Vd.6.70 (1)	11.10	-	2.37	-1.60	18.55
Vd.6.70 (2)	11.10	-	2.04	-1.73	19.11
Vd.6.70 (3)	11.10	-	2.79	-0.66	14.59

Sample number (subsample)	Stratigraphic height (m)	CL alteration type	$\delta^{13}C_{bel}$ rel. PBD	$\delta^{18}O_{bel}$ rel. PBD	Palaeotemperature (°C)
Vd.6.95 (1)	11.35	-	1.54	-2.01	20.30
Vd.6.95 (2)	11.35	-	1.41	-1.19	16.79
Vd.6.68 (1)	11.86	-	1.47	-1.85	19.62
Vd.6.68 (2)	11.86	-	1.42	-2.33	21.74
Vd.6.68 (3)	11.86	-	0.79	-2.57	22.84
Vd.6.30 (1)	12.24	4	1.71	-1.24	20.35
Vd.6.30 (2)	12.24	4	1.45	-1.46	16.98
Vd.6.25 (1)	12.29	3	1.64	-1.13	16.53
Vd.6.25 (2)	12.29	3	1.49	-1.47	17.98
Vd.6.70 (1)	11.84	-	0.73	-1.87	19.70
Vd.6.70 (2)	11.84	-	1.25	-1.17	16.70
Vd.6.70 (3)	11.84	-	1.20	-1.14	16.56
Vd.7.23 (1)	12.77	4	1.32	-1.55	18.33
Vd.7.23 (2)	12.77	4	1.78	-0.89	15.53
Vd.7.40 (1)	12.94	-	1.82	-1.09	16.36
Vd.7.40 (2)	12.94	-	0.81	-1.45	17.90
Vd.7.40 (3)	12.94	-	1.02	-1.53	18.23
Vd.7.85 (1)	13.39	-	1.66	-0.92	15.66
Vd.7.85 (2)	13.39	-	1.70	-0.73	14.87
Vd.7.85 (3)	13.39	-	1.79	-0.56	14.20
Vd.7.90 (1)	13.44	4	1.66	-2.10	20.72
Vd.7.90 (2)	13.44	4	1.71	-2.02	20.35
Vd.7.90 (3)	13.44	4	1.68	-2.02	20.34
VD.7.35 (1)	15.71	-	1.67	-1.49	18.08
VD.7.35 (2)	15.71	-	1.43	-1.92	19.90
Vd.8.15 (1)	16.21	3	1.53	-2.42	22.14

Sample number (subsample)	Stratigraphic height (m)	CL alteration type	$\delta^{13}C_{bel}$ rel. PBD	$\delta^{18}O_{bel}$ rel. PBD	Palaeotemperature (°C)
Vd.8.15 (2)	16.21	3	1.18	-1.74	19.13
Vd.8.15 (3)	16.21	3	1.29	-2.52	22.60
Vd.8.25 (1)	16.31	-	1.00	-1.78	19.30
Vd.8.25 (2)	16.31	-	1.15	-1.53	18.22
Vd.8.25 (3)	16.31	-	1.31	-1.27	17.15
Vd.8.35 (1)	16.41	-	0.63	-2.14	20.87
Vd.8.35 (2)	16.41	-	1.32	-1.25	17.06
Vd.8.35 (3)	16.41	-	0.59	-2.10	20.71
Vd.8.52 (1)	16.64	-	-0.10	-1.24	17.00
Vd.8.52 (2)	16.64	-	0.45	-1.28	17.16
Vd.8.35 (1)	16.86	-	1.72	-1.46	17.93
Vd.8.35 (2)	16.86	-	0.48	-2.07	20.58
Vd.8.35 (3)	16.86	-	1.58	-1.86	19.67
Vd.8.100 (1)	17.06	4	1.42	-1.48	18.04
Vd.8.100 (2)	17.06	4	1.16	-1.61	18.57
Vd.8.100 (3)	17.06	4	1.40	-1.48	18.00
Vd.8 top (1)	17.21	4	1.48	-1.13	16.53
Vd.8 top (2)	17.21	4	1.41	-1.48	18.02
Vd.8 top (3)	17.21	4	1.41	-1.03	16.10
Vd.9.25 (1)	20.62	2	2.40	-1.88	19.75
Vd.9.25 (2)	20.62	2	2.50	-1.52	18.17
Vd.9.25 (3)	20.62	2	2.15	-1.38	17.58
Vd.9.35 (1)	20.72	-	1.20	-0.28	13.09
Vd.9.35 (2)	20.72	-	1.30	-0.32	13.23
Vd.9.35 (3)	20.72	-	0.83	-0.13	12.48
Vd.9.45.1 (1)	20.82	-	1.14	-1.03	16.13

Sample number (subsample)	Stratigraphic height (m)	CL alteration type	$\delta^{13}C_{bel}$ rel. PBD	$\delta^{18}O_{bel}$ rel. PBD	Palaeotemperature (°C)
Vd.9.45.1 (2)	20.82	-	1.01	-1.17	16.70
Vd.9.45.1 (3)	20.82	-	1.04	-1.09	16.38
Vd.9.40 (1)	21.41	4	2.60	-1.04	16.18
Vd.9.40 (2)	21.41	4	2.58	-0.92	15.67
Vd.9.26 (1)	21.55	-	1.70	-0.63	14.49
Vd.9.26 (2)	21.55	-	2.03	-0.85	15.39
Vd.9.26 (3)	21.55	-	2.02	-0.75	14.96
Vd.9.10 (1)	21.71	4	1.00	-1.04	16.18
Vd.9.10 (2)	21.71	4	0.59	-1.44	17.86
Vd.9.10 (3)	21.71	4	0.93	-1.11	16.47
Vd.10 base (2)	21.81	-	0.97	-0.62	14.43
Vd.10.18 (1)	21.99	-	2.34	-1.01	16.05
Vd.10.18 (2)	21.99	-	2.41	-1.28	17.16
Vd.10.18 (3)	21.99	-	2.07	-1.06	16.26
Vd.10.25 (1)	22.06	-	1.33	-0.90	15.61
Vd.10.25 (2)	22.06	-	1.17	-0.70	14.77
Vd.10.25 (3)	22.06	-	1.59	-0.70	14.76
Vd.10.28 (2)	22.09	-	0.92	-0.68	14.69
Vd.10.40 (1)	22.21	-	0.75	-1.86	19.64
Vd.10.40 (2)	22.21	-	0.80	-1.22	16.90
Vd.10.47 (1)	22.28	-	1.90	-0.72	14.85
Vd.10.47 (2)	22.28	-	1.40	-1.45	17.88
Vd.10.55 (1)	22.36	4	1.21	-0.81	15.22
Vd.10.55 (2)	22.36	4	1.30	-0.30	13.16
Vd.10.59 (1)	22.40	-	1.26	-1.02	16.06
Vd.10.59 (2)	22.40	-	1.22	-0.95	15.79

Sample number (subsample)	Stratigraphic height (m)	CL alteration type	$\delta^{13}C_{bel}$ rel. PBD	$\delta^{18}O_{bel}$ rel. PBD	Palaeotemperature (°C)
Vd.10.60 (1)	22.41	-	1.61	-0.25	12.98
Vd.10.60 (2)	22.41	-	1.58	-0.12	12.46
Vd.10.66 (1)	22.47	-	2.17	-0.94	15.74
Vd.10.66 (2)	22.47	-	1.99	-1.06	16.23
Vd.10.66 (3)	22.47	-	2.19	-0.83	15.29
Vd.10.26 (1)	22.69	-	1.63	-1.72	19.06
Vd.10.26 (2)	22.69	-	1.27	-1.54	18.28
Vd.10.26 (3)	22.69	-	1.25	-1.47	17.97
Vd.10.15 (1)	22.80	-	0.77	-0.52	14.03
Vd.10.15 (2)	22.80	-	0.97	-0.27	13.03
Vd.10.14 (1)	22.81	-	1.30	-0.44	13.70
Vd.10.14 (2)	22.81	-	1.42	-0.30	13.15
Vd.10.12 (1)	22.83	-	1.56	-0.82	15.27
Vd.10.12 (2)	22.83	-	0.34	-0.81	15.20
Vd.10.10 (1)	22.85	-	2.83	3.03	1.43
Vd.10.10 (2)	22.85	-	1.19	-0.60	14.36
Vd.10.5 (1)	22.90	4	0.83	-1.22	16.93
Vd.10.5 (2)	22.90	4	1.42	-0.69	14.73
Vd.10.5 (3)	22.90	4	0.67	-1.22	16.93
Vd.11 base.1 (1)	22.95	4	1.71	-1.81	19.42
Vd.11 base.1 (2)	22.95	4	1.74	-1.89	19.79
Vd.11 base.3 (1)	23.00	-	1.67	-0.79	15.12
Vd.11 base.3 (2)	23.00	-	1.18	-0.76	15.01
Vd.11 base.3 (3)	23.00	-	0.89	-0.41	13.61
Vd.11 base.2 (1)	22.97	-	0.91	-0.81	15.21
Vd.11 base.2 (2)	22.97	-	1.15	-0.41	13.60

Sample number (subsample)	Stratigraphic height (m)	CL alteration type	$\delta^{13}C_{bel}$ rel. PBD	$\delta^{18}O_{bel}$ rel. PBD	Palaeotemperature (°C)
Vd.11.15 (1)	23.10	-	1.06	-0.52	14.05
Vd.11.15 (2)	23.10	-	0.55	-0.72	14.86
Vd.11.23 (1)	23.18	5	0.73	-0.90	15.59
Vd.11.23 (2)	23.18	5	1.00	-1.06	16.25
Vd.11.70 (2)	23.65	-	1.22	-0.17	12.66
Vd.11.75 (2)	23.70	-	1.82	-0.78	15.11
Vd.11.93 (2)	23.88	4	0.51	-0.36	13.40
Boeva Mogila section					
Te.28 (1)	0.05	2	-	-	-
Te.28 (2)	0.05	2	-	-	-
Te.28 (3)	0.05	2	-	-	-
Te.26 (1)	0.65	4	-	-	-
Te.26 (2)	0.65	4	-	-	-
Te.26 (3)	0.65	4	-	-	-
Te.25 (1)	0.75	4	-	-	-
Te.25 (2)	0.75	4	-	-	-
Te.25 (3)	0.75	4	-	-	-
Te.24 (1)	0.80	3	-	-	-
Te.24 (2)	0.80	3	-	-	-
Te.24 (3)	0.80	3	-	-	-
Te.23 (1)	0.90	3	-	-	-
Te.23 (2)	0.90	3	-	-	-
Te.23 (3)	0.90	3	-	-	-
Te.1 (1)	1.05	3	-	-	-
Te.1 (2)	1.05	3	-	-	-
Te.1 (3)	1.05	3	-	-	-

Sample number (subsample)	Stratigraphic height (m)	CL alteration type	$\delta^{13}C_{bel}$ rel. PBD	$\delta^{18}O_{bel}$ rel. PBD	Palaeotemperature (°C)
Te.2 (1)	1.10	2	-	-	-
Te.2 (2)	1.10	2	-	-	-
Te.2 (3)	1.10	2	-	-	-
Te.3 (1)	1.15	2	-	-	-
Te.3 (2)	1.15	2	-	-	-
Te.3 (3)	1.15	2	-	-	-
Te.4 (1)	1.22	2	-	-	-
Te.4 (2)	1.15	2	-	-	-
Te.4 (3)	1.22	2	-	-	-
Te.21 (1)	4.40	3	-	-	-
Te.21 (2)	4.40	3	-	-	-
Te.21 (3)	4.40	3	-	-	-
Te.22a (1)	4.80	4	-	-	-
Te.22a (2)	4.80	4	-	-	-
Te.22a (3)	4.80	4	-	-	-
Te.22b (1)	4.80	3	-	-	-
Te.22b (2)	4.80	3	-	-	-
Te.22b (3)	4.80	3	-	-	-
Te.22c (1)	4.80	-	-	-	-
Te.22c (2)	4.80	-	-	-	-
Te.22c (3)	4.80	-	-	-	-
Ravna section					
Rv.4.ii	2.85	5	-	-	-
Rv.4.ix	5.60	6	-	-	-
Rv.6.v	9.6	5	-	-	-
Rv.8.125	18.55	5	-	-	-

Sample number (subsample)	Stratigraphic height (m)	CL alteration type	$\delta^{13}C_{bel}$ rel. PBD	$\delta^{18}O_{bel}$ rel. PBD	Palaeotemperature (°C)
Rv.8.180	19.10	5	-	-	-
Rv.11.40	28.50	5	-	-	-
Rv.11.20	28.70	4	-	-	-
Rv.12.2	33.30	5	-	-	-
Rv.12.L4.30	36.0	4	-	-	-
Rv.12.M4.1	36.10	4	-	-	-
Rv.12.M5	36.11	4	-	-	-
Rv.13.26	38.10	4	-	-	-
Rv.13.27	38.11	6	-	-	-
Rv.13.130	39.40	4	-	-	-
Rv.15.11	41.11	5	-	-	-
Rv.15.26	41.26	5	-	-	-
Rv.15.115	42.15	4	-	-	-
Rv.16.10	44.06	4	-	-	-
Balsha section					
B.8.70	12.34	6	-	-	-
B.8.140	13.04	4	-	-	-
B.8.180	13.44	5	-	-	-
B.9a	14.64	6	-	-	-
B.9.80	14.85	5	-	-	-
B.9.10	15.55	6	-	-	-
B.10.45	17.6	5	-	-	-
B.10.baseC	15.65	5	-	-	-
B.14.08	19.90	3	-	-	-
B.15.45	21.97	5	-	-	-
B.16.23	21.75	4	-	-	-

Sample number (subsample)	Stratigraphic height (m)	CL alteration type	$\delta^{13}C_{bel}$ rel. PBD	$\delta^{18}O_{bel}$ rel. PBD	Palaeotemperature (°C)
B.16.120	22.7	5	-	-	-
B.16.5	22.57	5	-	-	-
B.17.10	24.72	5	-	-	-
B.18.20	25.02	5	-	-	-
B.19.50	25.67	4	-	-	-
B.20.c	27.60	5	-	-	-
B.21.60	28.22	4	-	-	-
B.21.23	28.17	5	-	-	-
B.22.143	29.80	6	-	-	-
B.22.190	20.27	5	-	-	-
B.22.1	29.36	5	-	-	-
B.23.60	29.97	6	-	-	-
B.23.1	31.66	6	-	-	-
Dragovishtitsa section					
Dg.2a	6.34	4	-	-	-
Dg.4.20	9.20	5	-	-	-
Dg.5.80	11.2	5	-	-	-
Dg.6.100	12.93	4	-	-	-
Vradlovtsi-1 section					
Vd.1.5.195	14.8	3	-	-	-
Teteven section					
Tv.5.vii.1	8.20	5	-	-	-
Tv.5.vii.2	8.20	5	-	-	-
Brakyovtsi section					
By.10.2	8.25	5	-	-	-
Dobravitsa-1 section					

Sample number (subsample)	Stratigraphic height (m)	CL alteration type	$\delta^{13}C_{bel}$ rel. PBD	$\delta^{18}O_{bel}$ rel. PBD	Palaeotemperature (°C)
Do.20a	6.80	4	(Metodiev and Kovela-Rekalova, 2008)		
Do.20	6.65	3	(Metodiev and Kovela-Rekalova, 2008)		
Do.19s	6.40	3	(Metodiev and Kovela-Rekalova, 2008)		
Do.18a	5.10	3	(Metodiev and Kovela-Rekalova, 2008)		
Do.17a	4.55	4	(Metodiev and Kovela-Rekalova, 2008)		
Do.16	4.45	5	(Metodiev and Kovela-Rekalova, 2008)		
Do.15b	4.40	3	(Metodiev and Kovela-Rekalova, 2008)		
Do.14	3.90	4	(Metodiev and Kovela-Rekalova, 2008)		
Do.13c	3.60	4	(Metodiev and Kovela-Rekalova, 2008)		
Do.12	3.40	3	(Metodiev and Kovela-Rekalova, 2008)		
Do.12a	2.90	5	(Metodiev and Kovela-Rekalova, 2008)		
Do.11	2.70	3	(Metodiev and Kovela-Rekalova, 2008)		
Do.10	2.65	2	(Metodiev and Kovela-Rekalova, 2008)		
Do.9	2.45	2	(Metodiev and Kovela-Rekalova, 2008)		
Do.7	2.00	5	(Metodiev and Kovela-Rekalova, 2008)		
Do.6b	1.80	2	(Metodiev and Kovela-Rekalova, 2008)		
Do.6a	1.60	5	(Metodiev and Kovela-Rekalova, 2008)		
Do.5	1.40	3	(Metodiev and Kovela-Rekalova, 2008)		
Do.4a	1.35	2	(Metodiev and Kovela-Rekalova, 2008)		
Dobravitsa-1 section					
Do.4	1.24	3	(Metodiev and Kovela-Rekalova, 2008)		
Do.2a	0.85	4	(Metodiev and Kovela-Rekalova, 2008)		
Do.2	0.70	4	(Metodiev and Kovela-Rekalova, 2008)		
Do.1c	0.60	3	(Metodiev and Kovela-Rekalova, 2008)		
Do.1b	0.55	2	(Metodiev and Kovela-Rekalova, 2008)		
Do.1	0.40	3	(Metodiev and Kovela-Rekalova, 2008)		

Sample number (subsample)	Stratigraphic height (m)	CL alteration type	$\delta^{13}C_{bel}$ rel. PBD	$\delta^{18}O_{bel}$ rel. PBD	Palaeotemperature (°C)
Do.1ds	0.10	3	(Metodiev and Kovela-Rekalova, 2008)		
Do.0	0.05	3	(Metodiev and Kovela-Rekalova, 2008)		
Beledie Han section					
Be.26	4.30	3	(Metodiev and Kovela-Rekalova, 2008)		
Be.25	4.00	2	(Metodiev and Kovela-Rekalova, 2008)		
Be.24	3.39	2	(Metodiev and Kovela-Rekalova, 2008)		
Be.23a	3.95	3	(Metodiev and Kovela-Rekalova, 2008)		
Be.22	3.70	3	(Metodiev and Kovela-Rekalova, 2008)		
Be.21	3.65	3	(Metodiev and Kovela-Rekalova, 2008)		
Be.20	3.64	3	(Metodiev and Kovela-Rekalova, 2008)		
Be.19a	3.44	2	(Metodiev and Kovela-Rekalova, 2008)		
Be.19	3.43	3	(Metodiev and Kovela-Rekalova, 2008)		
Be.18	3.42	2	(Metodiev and Kovela-Rekalova, 2008)		
Be.18a	2.42	2	(Metodiev and Kovela-Rekalova, 2008)		
Be.17	3.41	2	(Metodiev and Kovela-Rekalova, 2008)		
Be.16b	3.4	3	(Metodiev and Kovela-Rekalova, 2008)		
Be.16a	3.39	3	(Metodiev and Kovela-Rekalova, 2008)		
Be.16a*	3.38	3	(Metodiev and Kovela-Rekalova, 2008)		
Be.16	3.25	3	(Metodiev and Kovela-Rekalova, 2008)		
Be.15	3.21	3	(Metodiev and Kovela-Rekalova, 2008)		
Beledie Han section					
Be.14	3.19	2	(Metodiev and Kovela-Rekalova, 2008)		
Be.13	3.00	3	(Metodiev and Kovela-Rekalova, 2008)		
Be.12	295	2	(Metodiev and Kovela-Rekalova, 2008)		
Be.11	2.88	2	(Metodiev and Kovela-Rekalova, 2008)		
Be.10a	2.75	2	(Metodiev and Kovela-Rekalova, 2008)		

Sample number (subsample)	Stratigraphic height (m)	CL alteration type	$\delta^{13}C_{bel}$ rel. PBD	$\delta^{18}O_{bel}$ rel. PBD	Palaeotemperature (°C)
Be.10	2.69	2	(Metodiev and Kovela-Rekalova, 2008)		
Be.9	2.63	2	(Metodiev and Kovela-Rekalova, 2008)		
Be.8	2.55	2	(Metodiev and Kovela-Rekalova, 2008)		
Be.7a	2.44	2	(Metodiev and Kovela-Rekalova, 2008)		
Be.7	2.40	2	(Metodiev and Kovela-Rekalova, 2008)		
Be.6	2.30	2	(Metodiev and Kovela-Rekalova, 2008)		
Be.5	2.20	2	(Metodiev and Kovela-Rekalova, 2008)		
Be.4	2.05	2	(Metodiev and Kovela-Rekalova, 2008)		
Be.3	1.90	2	(Metodiev and Kovela-Rekalova, 2008)		
Be.2	1.67	2	(Metodiev and Kovela-Rekalova, 2008)		
Be.1	1.66	2	(Metodiev and Kovela-Rekalova, 2008)		
Be.0	1.54	2	(Metodiev and Kovela-Rekalova, 2008)		

Appendix C.1. Framboid data. strat.= stratigraphic, N= number of framboids, Sd= standard deviation, Min= minimum, Max= maximum, ox= oxidised, not ox.= not oxidised. Presv.=preservation, ox.= oxidised, not ox.= not oxidised, NF =no framboids recorded.

Sample	Strat. height (m)	N	Mean	Sd	Min.	Max.	Framboid abundance	Presv.
Mv.4	1.00	105	5.95	1.91	3.00	14.00	Common	ox.
Mv.5	1.00	102	7.70	3.65	2.50	17.50	Common	ox.
Mv.6	2.15	103	6.89	2.37	4.50	14.00	Common	ox.
Mv.7v	1.90	127	7.00	2.08	2.50	14.50	Common	ox.
Mv.8	2.00	100	8.89	3.83	3.00	22.50	Common	ox.
Mv.9	2.36	24	9.31	1.65	5.00	12.00	Rare	ox.
Mv.10	2.40	89	10.48	3.66	5.50	25.00	Common	ox.
Mv.11	2.50	93	10.30	3.76	5.00	20.50	Common	ox.
Mv.12	2.76	118	6.65	2.37	2.50	14.50	Common	ox.
Mv.13	3.01	100	9.36	3.38	5.00	26.00	Common	ox.
Mv.14	3.16	100	8.74	3.83	3.50	23.00	Common	ox.
Mv.15	3.31	81	7.53	2.45	4.00	14.00	Common	ox.
Mv.16	3.35	100	8.20	2.20	3.50	13.00	Common	ox.
Mv.17	3.56	100	7.88	2.72	3.5	15.5	Common	ox.
Mv.18	3.83	102	6.20	2.85	3.00	21.00	Common	ox.
Mv.19	3.93	100	7.35	2.91	3.50	20.00	Common	ox.
Mv.20	3.94	101	8.98	3.68	4.00	26.00	Common	ox.
Mv.21	2.25	26	6.90	2.50	4.50	14.00	Rare	ox.
Te.1	1.05	100	7.50	2.42	3.00	17.00	Common	ox.
Te.2	1.10	108	8.05	2.64	3.50	15.00	Common	ox.
Te.3	1.15	4	7.00	0.41	6.50	8.00	Rare	ox.
Te.4	1.20	100	8.61	3.77	4.00	27.00	Common	ox.

Sample	Strat. height (m)	N	Mean	Sd	Min.	Max.	Framboid abundance	Presv.
Te.5	1.25	102	6.89	2.17	3.50	14.00	Common	not ox.
Te.6	1.30	107	5.79	2.71	2.50	21.00	Common	ox.
Te.7	1.35	100	7.62	2.65	6.50	8.00	Common	ox.
Te.7a	1.40	100	8.22	4.59	3.50	25.00	Common	ox.
Te.8	1.50	103	6.46	1.72	3.50	11.00	Common	ox.
Te.9	1.60	103	6.61	2.25	4.00	17.00	Common	ox.
Te.10	1.80	102	8.61	3.43	4.00	23.00	Common	ox.
Te.11	1.90	119	7.66	3.42	4.00	24.00	Common	ox.
Te.12	2.10	112	9.29	3.82	4.00	21.00	Common	ox.
Te.13	2.20	107	9.39	3.64	3.50	24.00	Common	ox.
Te.14	2.30	101	10.19	4.12	4.00	21.00	Common	ox.
Te.15	2.40	100	8.62	2.74	4.00	18.00	Common	ox.
Te.16	2.50	100	7.92	2.25	4.00	15.00	Common	ox.
Te.18	2.75	104	6.08	3.12	2.50	21.00	Common	ox.
Te.19	3.00	100	7.71	3.71	3.50	21.00	Common	ox.
Te.20	3.20	105	7.39	2.54	4.00	18.00	Common	ox.
Te.21	4.40	100	8.79	2.62	4.00	15.00	Common	ox.
Te.22	4.80	100	10.01	4.66	4.00	23.00	Common	ox.
Te.23	0.90	100	7.42	3.24	4.00	23.00	Common	ox.
Te.24	0.80	100	7.21	2.59	3.50	24.00	Common	not ox.
Te.25	0.75	100	7.42	2.48	3.50	17.00	Common	ox.
Te.26	0.65	100	7.03	2.95	3.50	17.00	Common	not ox.
Te.27	0.35	101	6.95	2.22	3.00	14.00	Common	not ox.
Te.28	0.05	101	6.37	1.73	3.00	14.00	Common	not ox.
Db.2.1	1.40	118	8.98	4.15	4.00	27.00	Common	ox.
Db.3a	1.60	144	7.05	3.66	2.00	20.00	Common	ox.

Sample	Strat. height (m)	N	Mean	Sd	Min.	Max.	Framboid abundance	Presv.
Db.3c	2.10	118	5.78	2.41	2.00	13.50	Common	ox.
Db 5a.1	2.3	140	8.96	3.29	3.50	27.50	Common	ox.
Db.5a.2	2.35	39	11.17	4.93	3.00	20.00	Rare	ox.
Db.5b	2.60	100	6.45	1.78	3.00	9.50	Common	not ox.
Db.5c	2.75	156	7.76	2.83	2.50	23.00	Common	ox.
Db.7b.2	3.25	17	11.35	4.87	4.50	23.50	Rare	ox.
Db.10	3.80	100	6.07	2.12	2.50	16.50	Common	not ox.
Db.11	4.10	109	7.65	2.12	3.00	12.50	Common	ox.
Db.13c	4.60	100	6.55	2.06	3.00	13.50	Common	not ox.
Db.14	4.90	102	6.67	3.32	2.50	27.00	Common	not ox.
Db.15c	5.50	100	6.71	2.27	3.00	16.50	Common	not ox.
Rv.4i	2.85	24	9.31	1.65	5.00	12.00	Rare	ox.
Rv.4v	4.00	139	6.21	2.89	2.50	24.00	Common	ox.
Rv.5iv	6.60	111	8.13	4.20	3.00	25.00	Common	ox.
Rv.6v	9.10	118	6.67	2.26	3.00	14.50	Common	ox.
Kd.1	1.35	NF	NF	NF	NF	NF	Absent	NF
Kd.2	1.75	NF	NF	NF	NF	NF	Absent	NF
Kd.3	2.05	NF	NF	NF	NF	NF	Absent	NF
Kd.4	2.30	NF	NF	NF	NF	NF	Absent	NF
Kd.5	2.50	NF	NF	NF	NF	NF	Absent	NF
Kd.6	2.80	NF	NF	NF	NF	NF	Absent	NF
Go.19	1.15	NF	NF	NF	NF	NF	Absent	NF
Go.20	0.75	NF	NF	NF	NF	NF	Absent	NF
Go.1	1.50	NF	NF	NF	NF	NF	Absent	NF
Go.2	2.20	NF	NF	NF	NF	NF	Absent	NF
Go.3	2.80	NF	NF	NF	NF	NF	Absent	NF

Appendix C.2. Sedimentary geochemistry.

Sample (bulk rock)	Stratigraphic height (m)	δ^{13}Corg VPDB	TOC (wt %)	Hg (ppb)	TOC/Hg (ppm)
Milanovo section					
Mv.4 (1)	1	-22.551795	0.2167491	20.1	0.092734
Mv.4 (2)	1	-27.43919	0.2638774	19.6	0.074277
Mv.4 (3)	1	-27.590077	0.220297	19.8	0.089879
Mv.5 (1)	1.1	-26.931923	0.2575463	20.5	0.079597
Mv.5 (2)	1.1	-26.942183	0.2747885	19.9	0.072419
Mv.5 (3)	1.1	-27.174492	0.2384838	19.4	0.081347
Mv.6 (1)	2.15	-25.852858	0.2855809	30.2	0.105749
Mv.6 (2)	2.15	-26.198487	0.2819671	30.2	0.107105
Mv.6 (3)	2.15	-26.061522	0.3079072	30.2	0.098081
Mv.6 (4)	2.15	-26.298332	-	-	-
Mv.7 (1)	1.9	-26.351077	0.3244402	35.1	0.108186
Mv.7 (2)	1.9	-26.686661	0.2883792	35.1	0.121715
Mv.7 (3)	1.9	-	0.2382287	35.1	0.147337
Mv.8 (1)	2	-26.184895	0.2314562	32.5	0.140415
Mv.8 (2)	2	-26.482346	0.2207818	32.5	0.147204
Mv.9 (1)	2.36	-26.394852	0.2834491	34	0.119951
Mv.9 (2)	2.36	-26.519292	0.2734213	34	0.12435
Mv.9 (3)	2.36	-	0.3216623	34	0.105701
Mv.10 (1)	2.4	-26.401946	0.205415	33	0.16065
Mv.10 (2)	2.4	-26.673655	0.1992159	33	0.165649
Mv.11 (1)	2.5	-26.736342	0.2460101	34.3	0.139425
Mv.11 (2)	2.5	-26.695575	0.2331822	34.3	0.147095
Mv.12 (1)	2.76	-27.139903	0.2276558	26.1	0.114647
Mv.12 (2)	2.76	-27.161814	0.2181824	26.1	0.119625
Mv.13 (1)	3.01	-26.975505	0.27304	31.4	0.115001
Mv.13 (2)	3.01	-26.891712	0.239272	31.4	0.131231
Mv.14 (1)	3.16	-26.870317	0.2597533	31.5	0.121269
Mv.14 (2)	3.16	-27.06728	0.2516953	31.5	0.125151

Sample (bulk rock)	Stratigraphic height (m)	δ^{13}Corg VPDB	TOC (wt %)	Hg (ppb)	TOC/Hg (ppm)
Mv.14 (3)	3.16	-26.945074	-	-	-
Mv.14 (4)	3.16	-26.639824	-	-	-
Mv.15 (1)	3.31	-27.233765	0.3023383	31.9	0.105511
Mv.15 (2)	3.31	-26.915488	0.274316	31.9	0.116289
Mv.16 (1)	3.35	-27.442186	0.3034795	29.1	0.095888
Mv.16 (2)	3.35	-27.290693	0.2832714	29.1	0.102728
Mv.17 (1)	3.56	-27.425547	0.2847943	30.1	0.10569
Mv.17 (2)	3.56	-27.514904	0.2823071	30.1	0.106621
Mv.18 (1)	3.83	-27.616342	0.142359	21.1	0.148217
Mv.19 (1)	3.93	-27.614365	0.166824	20.8	0.124682
Mv.19 (2)	3.93	-27.455311	-	-	-
Mv.20 (1)	3.94	-27.41363	0.1492365	21.9	0.146747
Mv.20 (2)	3.94	-27.458596	-	-	-
Boeva Mogila section					
Te.1 (1)	1.05	-27.576351	0.3202	26.5	0.082761
Te.1 (2)	1.05	-27.565384	-	-	-
Te.1 (3)	1.05	-27.549135	-	-	-
Te.1 (3)	1.05	-27.309409	-	-	-
Te.2 (1)	1.1	-27.67772	0.3563481	22.5	0.063141
Te.2 (2)	1.1	-27.626537	-	-	-
Te.2 (3)	1.1	-27.54197	-	-	-
Te.3 (1)	1.15	-29.040607	0.3380964	29.9	0.088436
Te.3 (2)	1.15	-29.008134	-	-	-
Te.4 (1)	1.2	-29.049557	0.3400587	26.5	0.077928
Te.4 (2)	1.2	-29.003726	-	-	-
Te.4 (3)	1.2	-28.737088	-	-	-
Te.4 (4)	1.2	-28.874235	-	-	-
Te.5 (1)	1.25	-28.403871	0.2979119	21.1	0.070826
Te.5 (2)	1.25	-28.570313	-	-	-
Te.6 (1)	1.3	-32.289122	0.9859419	116.5	0.118161

Sample (bulk rock)	Stratigraphic height (m)	δ^{13}Corg VPDB	TOC (wt %)	Hg (ppb)	TOC/Hg (ppm)
Te.6 (2)	1.3	-31.517691	0.9859419	118.8	0.120494
Te.7 (1)	1.35	-30.825808	0.5540425	64.9	0.117139
Te.7 (2)	1.35	-30.528915	-	-	-
Te.7a (1)	1.4	-29.998628	0.4193568	43.1	0.102776
Te.7a (2)	1.4	-29.759359	-	-	-
Te.8 (1)	1.5	-30.204654	0.5599293	40.6	0.072509
Te.8 (2)	1.5	-30.019693	-	-	-
Te.9 (1)	1.6	-30.930376	0.4747937	68.6	0.144484
Te.9 (2)	1.6	-30.670215	-	-	-
Te.10 (1)	1.8	-30.04003	0.3943872	39.5	0.100155
Te.10 (2)	1.8	-29.755349	-	-	-
Te.11 (1)	1.9	-30.273258	0.2406519	35.5	0.147516
Te.11 (2)	1.9	-30.073943	0.2406519	35.2	0.146269
Te.12 (1)	2.1	-28.875878	0.2406519	23.2	0.096405
Te.12 (2)	2.1	-28.957339	-	-	-
Te.13 (1)	2.2	-29.525195	0.3056586	34.3	0.112217
Te.13 (2)	2.2	-29.508936	-	-	-
Te.14 (1)	2.3	-29.168058	0.2659344	31.1	0.116946
Te.14 (2)	2.3	-28.958843	-	-	-
Te.15 (1)	2.4	-28.898946	0.2386833	27.6	0.115634
Te.15 (2)	2.4	-28.785418	-	-	-
Te.16 (1)	2.5	-29.131843	0.3280291	26.2	0.079871
Te.16 (2)	2.5	-28.947725	-	-	-
Te.17 (1)	2.65	-30.586903	0.4756624	69.2	0.145481
Te.17 (2)	2.65	-30.473972	-	-	-
Te.18 (1)	2.75	-29.194761	0.341006	28.9	0.084749
Te.18 (2)	2.75	-29.027403	-	-	-
Te.19 (1)	3	-30.252938	0.5297885	52.6	0.099285
Te.19 (2)	3	-30.148077	-	-	-
Te.20 (1)	3.2	-29.925434	0.4095479	47.4	0.115737

Sample (bulk rock)	Stratigraphic height (m)	δ^{13}Corg VPDB	TOC (wt %)	Hg (ppb)	TOC/Hg (ppm)
Te.20 (2)	3.2	-29.781238	-	-	-
Te.21 (1)	4.4	-27.769568	0.3139603	43.4	0.138234
Te.21 (2)	4.4	-27.736893	-	-	-
Te.22 (1)	4.8	-26.286999	0.2989122	16.7	0.055869
Te.22 (2)	4.8	-26.273816	-	-	-
Te.23 (1)	0.9	-27.606219	0.3724248	20.50.	0.055045
Te.23 (2)	0.9	-27.847098	-	-	-
Te.24 (1)	0.8	-27.116934	0.3989853	15	0.037595
Te.25 (1)	0.75	-27.401745	0.4532015	14.3	0.031553
Te.26 (1)	0.65	-27.226931	0.3558296	11.7	0.032881
Te.27 (1)	0.35	-27.542388	0.3184558	11	0.034542
Te.28 (1)	0.05	-28.006313	0.4166776	20.7	0.049679

Appendix D.1. Integrated bivalve taxa synonomised from Shopov (1986)

Reported taxa	Literature source (Shopov, 1968)	Taxa synonymy	Literature source
Pinna secxostata (Terquem&Piette, 1936)	p.528, pl.2, figs. 1.,2,3. BAN J-2867	*Pinna (Pinna) similis* (Chapuis&Dewalque)	Hodges (1987)
Pinna hartmanni (Zieten)	p.528, pl.2, fig.4. BAN J-1964	*Pinna (Pinna) radiata* (Münster)	Personal obsv. Sofia museum collections
Pinna semistriata (Tarquem)	p.528, pl.2, fig. 5. BAN J-1870	Pinna (Pinna) folium (Young&Bird)	Radulovic (2014)
Pinna dumortieri (Rollier)	p.528, pl.2, figs. 6,7. BAN J-4105	*Pinna (Pinna) radiata* (Münster)	Personal obsv. Sofia museum collections
Chlamys falgeri (Merian)	p.531, pl.3, figs.10,11. BAN J-2574, BAN-2646	*Chlamys (Ch.) valoniensis* (Defrance)	Johnson (1984)
Chlamys dispar (Terquem)	p.531 pl.3, figs.14,15,16. BAN J-2076	*Chlamys (Ch.) valoniensis* (Defrance)	Johnson (1984)
Chlamys trigeri (Oppel)	p.531 pl.3, figs,12,13. BAN J-2734, BAN-2582	*Chlamys (Ch.) textoria* (Scholtheim)	Johnson (1984)
Jurapecten (Jurapecten) priscus (Scholtheim)	p.533, pl.4, figs.3,4. BAN J-1160, BAN J-1430	*Pseudopecten (Ps.) equivalvis* (J. Sowerby)	Johnson (1984)

Reported taxa	Literature source (Shopov, 1968)	Taxa synonymy	Literature source
Jurapecten (Jurapecten) acutiradiatus (Münster)	p.533, pl.4, fig,5. BAN J-4010	*Pseudopecten (Ps.) equivalvis* (J. Sowerby)	Johnson (1984)
Jurapecten (Jurapecten) thiollierei (Martin)	p.533, pl.4, fig,6. BAN J-2461	*Pseudopecten (Ps.) dentautus* (J.Sowerby)	Johnson (1984)
Jurapecten (Jurapecten) julianus (Dumortier)	p.533, pl.4, fig,7. BAN J-1805	*Pseudopecten (Ps.) veyrasensis* (Dumortier)	Johnson (1984)
Jurapecten (Euthymeipecten) barbatus (Römer)	p.533, pl.4, fig,9. BAN J-2941	*Pseudopecten (Echinopecten) barbaratus* (J.Sowerby)	Johnson (1984)
Jurapecten (Euthymeipecten) aequiplicatus (Terquem)	pl.4, p.533, figs, 9,10. BAN J-2499	*Pseudopecten (Ps.) dentautus* (J.Sowerby)	Johnson (1984)
Pseudopecten aequivalvis (J.Sowerby)	p.533, pl.4, fig.12. BAN J-1647. P.534, pl.5, fig.1. BAN J-1647.	*Pseudopecten (Ps.) equivalvis* (J.Sowerby)	Johnson (1984)
Pseudopecten acuticostatus (Lamarck)	p.533, pl.4, fig.13. BAN J-2275. P534, pl.5, fig.2. J-2275.	*Pseudopecten (Ps.) equivalvis* (J.Sowerby)	Johnson (1984)
Entolium cingulatus (Goldfuss)	p.536, pl.6, fig.9. BAN J-2804	*Entolium (E.) corneolum* (Young&Bird)	Johnson (1984)

Reported taxa	Literature source (Shopov, 1968)	Taxa synonymy	Literature source
Entolium calvus (Goldfuss)	p.536, pl.6, figs.10,11. BAN J-2981, BAN J-2967	*Entolium (E.) lunare* (Rofmer)	Johnson (1984)
Entolium frontalis (Dumortier)	p.538, pl.7, figs. 1,2. BAN J-2695, BAN J-2932	*Entolium (E.) lunare* (Rofmer)	Johnson (1984)
Entolium disciformis (Schübler)	p.538, pl.7, figs. 3,4. BAN J-2932, BAN J-2874	*Entolium (E.) lunare* (Rofmer)	Johnson (1984)
Entolium hehli (D'Orbigny)	p.538, pl.7, figs. 5,6. BAN J-2695, BAN J-2112, BAN J-2223	*Entolium (E.) lunare* (Rofmer)	Johnson (1984)
Variamussium pumilus (Lamarck)	p.538, pl.7, figs. 7,8,9. BAN J-2392, BAN J-1992	*Propeamusium (P.) pumilus* (Lamarck)	Johnson (1984)
Plicatula pectinoides (Lamarck)	p.540, pl.8, figs. 1,2,3. BAN J-4795	*Harpax spinosa*	Damborenea (2002)
Plicatula spinosa (J.Sowerby)	p.540, pl.8, figs. 4,5,6. BAN J-4788, BAN J-4790	*Harpax spinosa*	Damborenea (2002)
Posidonia bronni (Voltz)	p.540, pl.8, figs. 9, 10, 11. BAN J-4714, BAN J-1757, BAN J-4724	Mis-identified from *Astarte*	N/A
Plagiostoma gigantea (J.Sowerby)	p.540, pl.8, fig. 12. BAN J-2307	*Plagiostoma giganteum* (J.Sowerby)	Aberhan (2011)

Reported taxa	Literature source (Shopov, 1968)	Taxa synonymy	Literature source
Plagiostoma amoena (Terquem)	p.540, pl.8, fig. 15. BAN J-2437	*Plagiostoma punctata* (J.Sowerby)	Hodges (1987)
Plagiostoma praecursor (Quenstedt)	p.540, pl.8, figs. 16,17. BAN J-4077	*Plagiostoma giganteum* (J.Sowerby)	Hodges (1987)
Pseudolimea hettangiensis (Terquem)	p.542, pl.9, fig. 6. BAN J-4064, BAN J-1890	*Pseudolimea pectinoides* (J.Sowerby)	Pers. Comms.
Antiquilima harmanni (Voltz)	p.542, pl.9, figs. 9,10. BAN J-4108	*Antiquilima (Antiquilima) succincta* (Scholtheim)	Aberhan (1998)
Ctenestreon pectiniformis (Scholtheim)	p.542, pl.9, fig. 11. BAN J-2702	*Ctenestreon* sp.	Personal Observation at Sofia University Collection
Liogryphaea arcuata (Lamarck)	p.543, pl.10, figs. 1,2,3,4,5 6,7. BAN J-6042, BAN J-6038	*Gryphaea arcuata* (Lamarck)	Hallam (1968); Nori and Lathuilière (2003)
Liogryphaea obliquata (J.Sowerby)	p.543, pl.10, figs. 9,10. BAN J-1191	*Gryphaea arcuata* (Lamarck)	Hallam (1968); Nori and Lathuilière (2003)
Liogryphaea cymbium (Lamarck)	p.545, pl.12, figs. 1,2,3,4. BAN J-4814, BAN J-4822	*Gryphaea mccullochii* (J.Sowerby)	Hallam (1968)

Reported taxa	Literature source (Shopov, 1968)	Taxa synonymy	Literature source
Liogryphaea subsportelloides (Charles& Maubeuge)	p.548, pl.15, figs. 1,2. BAN J-1283	*Gryphaea arcuata* (Lamarck)	Hallam (1968); Nori and Lathuilière (2003)
Liogryphaea gigantea (J.Sowerby)	p.546, pl.13, figs. 1,2,3,4. BAN J-1304, BAN J-1234. p.547, pl.14, figs. 1,2,3,4. BAN J-1217, BAN J-1243	*Gryphaea gigantea* (J.Sowerby)	Hallam (1968)
Liogryphaea obliqua (Goldfuss)	p.549, pl.16, figs. 1,2,3,4. BAN J-1284	*Gryphaea arcuata* (Lamarck)	Hallam (1968)
Liogryphaea sportella (Dumortier)	p.551, pl.17, figs. 1,2,3,4,5,6,7,8,9, 10. BAN J-1095, BAN J-6046, BAN J-1273, BAN J-1170 p.552, pl.18, figs. 1,2,3. BAN J-1167	*Gryphaea sportella* (Dumortier)	Hallam (1968)
Liogryphaea sportella bisulcate subsp.nov.	p.552, pl.18, figs. 4,5,6,7,8,9,10. BAN J-6060, BAN J-1172	*Gryphaea sportella* (Dumortier)	Hallam (1968)

Reported taxa	Literature source (Shopov, 1968)	Taxa synonymy	Literature source
Arcomya elongata (Agassiz)	p.560, pl.24, figs. 6,7,8. BAN J-4370	*Pachymya (Arcomya) elongata* (Agassiz)	Hodges (1987)
Pholadomya idea (D'Orbigny)	p.556, pl.21, figs. 1,2,3,4,5. BAN J-1649, BAN J'-4472 p.557, pl.22, figs. 1,2,3. BAN J-4472	*Pholadomya ambigua* (J.Sowerby)	Radulovic (2013)
Pholadomya fraasi (D'Orbigny)	p.557, pl.22, figs. 4,5,6. BAN J-4493 p.559, pl.23, fig.1. BAN J-4493	*Pholadomya ambigua* (D'Orbigny)	Aberhan (2011)
Pholadomya voltzi (Agassiz)	p.559, pl.23, figs. 9,10,11. BAN J-4466 p.560, pl.24, fig. 1. BAN J-4466	*Pholadomya ambigua* (J.Sowerby)	Radulovic (2013)
Pleuromya unioides (Römer)	p.561, pl.25, figs. 1,2,3,4. BAN J-4554	*Pleuomya costata* (Young&Bird)	Aberhan (2011)
Pleuromya alundi (Brongniart)	p.561, pl.25, figs. 5,6,7,8. BAN J-4181	*Pleuomya costata* (Young&Bird)	Aberhan (2011)
Pleuromya striatula (Agassiz)	p.561, pl.25, fig. 9. BAN J-4655 p.563, pl.26, figs. 1,2,3. BAN J-4655	*Pleuomya costata* (Young&Bird)	Aberhan (2011)

Reported taxa	Literature source (Shopov, 1968)	Taxa synonymy	Literature source
Pleuromya triangulata (Trauth)	p.563, pl.26, figs. 4,5,6,7. BAN J-4460	*Pleuomya costata* (Young&Bird)	Aberhan (2011)
Pleuromya cf. jurassioides (Chapuis)	p.563, pl.26, fig. 8. BAN J-4463	*Pleuomya costata* (Young&Bird)	Aberhan (2011)
Pleuromya galathea (Agassiz)	p.563, pl.26, figs. 9,10,11,12. BAN J-4665	*Gresslya galathea* (Young&Bird)	Hodges (1987)
Pleuromya elongata (Münster)	p.563, pl.26, figs. 13,14. BAN J-4650	*Pleuomya costata* (Young&Bird)	Aberhan (2011)

Reported taxa	Literature source (Shopov, 1968)	Taxa not integrated into this study from Shopov (1968)
Mytilus (Falcimytilus) minutus (Goldfuss)	p.527, pl. 1, fig. 3. BAN J-4759	*Cannot be verified, not integrated into this study*
Mytilus (Falcimytilus) rugosa (Römer)	p.527, pl. 1, figs. 4,5,6. BAN J-4758, BAN J-4757	*Cannot be verified, not integrated into this study*
Mytilus (Falcimytilus) psilonoti (Quenstedt)	p.527, pl. 1, fig. 7. BAN J-4756	*Cannot be verified, not integrated into this study*
Modiolus amplor (Stur)	p.527, pl. 1, figs. 8,9,10,11. BAN J-4750	*Cannot be verified, not integrated into this study*

Reported taxa	Literature source (Shopov, 1968)	Taxa not integrated into this study from Shopov (1968)
Modiolus thiollierei (Dumortier)	p.527, pl. 1, figs. 12,13,14,15. BAN J-4749	*Cannot be verified, not integrated into this study*
Modiolus morrisi (Oppel)	p.527, pl. 1, fig. 17. BAN J-1165	*Cannot be verified, not integrated into this study*
Modiolus hillanus (J.Sowerby)	p.527, pl. 1, figs. 20,21. BAN J-4332	*Cannot be verified, not integrated into this study*
Modiolus subparallelus (Chapuis&Dewalque)	p.527. pl.1, fig. 23. BAN J-1090	*Cannot be verified, not integrated into this study*
Arcomytilus semistriatus sp.nov,	p.527. pl.1, figs. 23,34,25,26. BAN J-4752; BAN J-1150, BAN J-1162, BAN-J 1164	*Cannot be verified, not integrated into this study*
Cardinia concinna (J.Sowerby)	p.554, pl.19, fig. 11. BAN J-1226	*Cannot be verified, not integrated into this study*
Cardinia copides (De Ryckholt)	p.555, pl.20, fig. 1. BAN J-1468	*Cannot be verified, not integrated into this study*
Cardinia cf. *crassiuscula* (J.Sowerby)	p.555, pl.20, fig. 2. BAN J-1769	*Cannot be verified, not integrated into this study*
Cardinia cf. *angustiplexa* (Chapuis & Dewalque)	p.555, pl.20, fig. 3. BAN J-1763	*Cannot be verified, not integrated into this study*
Cardinia cf. *depressa* (Zieten)	p.555, pl.20, fig. 4. BAN J-1777	*Cannot be verified, not integrated into this study*
Cardinia gibba (Chapuis & Dewalque)	p.555, pl.20, fig. 5. BAN J-4241	*Cannot be verified, not integrated into this study*
Cardinia hybrida (J.Sowerby)	p.555, pl.20, fig. 6. BAN J-1470	*Cannot be verified, not integrated into this study*

Reported taxa	Literature source (Shopov, 1968)	Taxa not integrated into this study from Shopov (1968)
Cardinia listeri (J.Sowerby)	p.555, pl.20, figs. 7,8. BAN J-1756, BAN J-1761	*Cannot be verified, not integrated into this study*
Gervillia acuminata (Terquem)	p.531, pl.3, figs.1,2. BAN J-1806	*Species not found in this study, not integrated*
Gervillia reinchardti (Terquem & Piette)	p.531, pl.3, fig.3. BAN J-2604	*Species not found in this study, not integrated*
Gervillia oblonga (Moore)	p.531, pl.3, fig.4. BAN J-1865	*Species not found in this study, not integrated*
Isognomon cf. *infraliassicus* (Quenstedt)	p.531, pl.3, figs. 6,7. BAN J-1988, BAN-1816	*Species not found in this study, not integrated*
Parallelodon hettangiensis (Terquem)	p.527, pl. 1, figs.1,2. BAN J-1395	*Species not found in this study, not integrated*
Oxytoma sinemuriensis (D'Orbigny)	p.534, pl.5, figs.6,7. BAN J-2261, BAN J-2260	*Species not found in this study, not integrated*
Oxytoma cygnipes (Yound&Bird)	p.534, pl.5, fig.8. BAN J-1481	*Species not found in this study, not integrated*
Plicatula acuminata (Terquem & Piette)	p.540, pl.8, fig. 7. BAN J-1713	*Cannot be verified, not integrated into this study*
Plicatula cf. *hettangiensis* (Terquem)	p.540, pl.8, fig. 8. BAN J-4783	*Cannot be verified, not integrated into this study*
Jurapecten (Jurapecten) humberti (Dumortier)	p.533, pl.4, fig,8. BAN J-1680	*Cannot be verified, not integrated into this study*
Plagiostoma jauberti (Dumortier)	p.542, pl.9, fig. 1. BAN J-2258	*Cannot be verified, not integrated into this study*

Reported taxa	Literature source (Shopov, 1968)	Taxa not integrated into this study from Shopov (1968)
Liogryphaea regularis (Deshayes)	p.544, pl.11, figs. 1,2,3. BAN J-4800	*Cannot be verified, not integrated into this study*
Liogryphaea ovalis (Zieten)	p.544, pl.11, fig. 4. BAN J-4853	*Cannot be verified, not integrated into this study*
Liogryphaea geyeri (Trauth)	p.544, pl.11, figs. 5,6. BAN J-6023, BAN J-6012	*Cannot be verified, not integrated into this study*
Myoconcha scabra (Terquem & Piette)	p.554, pl.19, fig. 9. BAN J-4763	*Cannot be verified, not integrated into this study*

Appendix D.2 All bivalve taxa

Section	Bed no.(height)	Genus	Species
Teteven	5(vii)	*Pseudopecten*	*equivalvis*
Teteven	5(vii)	*Entolium*	*lunare*
Teteven	5(vii)	*Pseudopecten*	*equivalvis*
Teteven	5(vii)	*Pseudopecten*	*equivalvis*
Teteven	5(vii)	*Pseudopecten*	*equivalvis*
Teteven	5(vii)	*Modiolus*	*ventricosa*
Teteven	5(vii)	*Pseudopecten*	*equivalvis*
Teteven	5(vii)	*Pseudopecten*	*equivalvis*
Teteven	5(vii)	*Pseudopecten*	*equivalvis*
Teteven	5(vii)	*Pleuromya*	*costata*
Teteven	5(vii)	*Pseudopecten*	*equivalvis*
Teteven	5(vii)	*Pseudopecten*	*equivalvis*
Teteven	5(vii)	*Pseudopecten*	*equivalvis*
Teteven	5(vii)	*Pseudopecten*	*equivalvis*
Teteven	5(vii)	*Entolium*	*lunare*
Teteven	5(vii)	*Pseudolimea*	sp. indet
Teteven	5(vii)	*Pseudolimea*	sp. indet
Teteven	5(vii)	*Pseudopecten*	*equivalvis*
Teteven	5(vii)	*Pseudopecten*	*equivalvis*
Teteven	5(vii)	*Pseudopecten*	*equivalvis*
Teteven	5(vii)	*Entolium*	*lunare*
Teteven	5(vii)	*Pseudopecten*	*equivalvis*
Teteven	5(vii)	*Pseudopecten*	*equivalvis*
Teteven	5(vii)	*Gryphaea*	sp. indet
Teteven	5(vii)	*Gryphaea*	sp. indet
Teteven	5(vii)	*Gryphaea*	sp. indet

Section	Bed no.(height)	Genus	Species
Teteven	5(vii)	*Gryphaea*	sp. indet
Teteven	5(vii)	*Gryphaea*	sp. indet
Teteven	5(vii)	*Gryphaea*	sp. indet
Teteven	5(vii)	*Gryphaea*	sp. indet
Teteven	5(vii)	*Gryphaea*	sp. indet
Teteven	5(vii)	*Gryphaea*	sp. indet
Teteven	5(vii)	*Gryphaea*	sp. indet
Teteven	5(vii)	*Entolium*	*lunare*
Teteven	5(vii)	*Entolium*	*lunare*
Teteven	5(vii)	*Entolium*	*lunare*
Teteven	5(vii)	*Entolium*	*lunare*
Teteven	5(vii)	*Pseudopecten*	*equivalvis*
Teteven	5(vii)	*Pseudopecten*	*equivalvis*
Teteven	5(vii)	*Chlamys*	sp. indet
Teteven	6 (↑100cm)	*Gryphaea*	sp. indet
Teteven	6 (↑140cm)	*Gryphaea*	sp. indet
Teteven	6 (↑170cm)	*Pseudopecten*	equivalvis
Teteven	6 (↑170cm)	*Modiolus*	sp. indet
Teteven	6 (↑170cm)	*Gryphaea*	sp. indet
Teteven	6 (↑185cm)	*Entolium*	*lunare*
Teteven	6 (↑185cm)	*Modiolus*	sp. indet
Teteven	6 (↑185cm)	*Harpax*	*spinosa*
Teteven	6 (↑183cm)	*?Gresslya*	sp. indet
Teteven	6 (↑183cm)	*Harpax*	*spinosa*
Teteven	6 (↑183cm)	*Harpax*	*spinosa*
Teteven	6 (↑183cm)	*Harpax*	*spinosa*
Teteven	6 (↑183cm)	*Harpax*	*spinosa*

Section	Bed no.(height)	Genus	Species
Teteven	6 (↑183cm)	*Harpax*	*spinosa*
Teteven	6 (↑185cm)	*Modiolus*	sp. indet
Teteven	6 (↑185cm)	*Gryphaea*	sp. indet
Teteven	6 (↑185cm)	*Gryphaea*	sp. indet
Teteven	6 (↑180cm)	*Gryphaea*	sp. indet
Teteven	6 (↑180cm)	*Gryphaea*	sp. indet
Teteven	6 (↑180cm)	*Gryphaea*	sp. indet
Teteven	6 (↑180cm)	*Gryphaea*	sp. indet
Teteven	6 (↑10cm)	*Gryphaea*	sp. indet
Teteven	6 (↑10cm)	*Gryphaea*	sp. indet
Teteven	6 (↑10cm)	*Gryphaea*	sp.indet
Teteven	6 (top)	*?Pachyma*	sp. indet
Teteven	7 (↑20cm)	*Gryphaea*	sp. indet
Teteven	7 (↑20cm)	*Gryphaea*	sp. indet
Teteven	7 (↑160cm)	*Oyster*	sp. et gen. indet
Teteven	7 (↑160cm)	*Harpax*	*spinosa*
Teteven	7 (↑160cm)	*Harpax*	*spinosa*
Teteven	8 (top)	*Pleuromya*	*costata*
Teteven	8 (top)	*Gryphaea*	sp. indet
Teteven	8(vi)	*Pleuromya*	*costata*
Teteven	8 (top)	*Pleuromya*	*costata*
Teteven	8(vi)	*Pachmya*	*elongata*
Teteven	8 (top)	*Pleuromya*	*costata*
Teteven	8 (top)	*Pleuromya*	*costata*
Teteven	8 (top)	*Pleuromya*	*costata*
Teteven	8 (top)	*Pleuromya*	*costata*
Teteven	8 (top)	*Pleuromya*	*costata*

Section	Bed no.(height)	Genus	Species
Teteven	8 (top)	*Pleuromya*	*costata*
Teteven	8 (top)	*Pleuromya*	*costata*
Teteven	8 (top)	*Pleuromya*	*costata*
Teteven	8 (top)	*Pleuromya*	*costata*
Teteven	8 (top)	*Pleuromya*	*costata*
Teteven	8 (top)	*Pleuromya*	*costata*
Teteven	8 (top)	*Pleuromya*	*costata*
Teteven	8(vi)	*Pleuromya*	*costata*
Teteven	8 (top)	*Pleuromya*	*costata*
Teteven	8(vi)	*Pleuromya*	*costata*
Teteven	8 (top)	*Pleuromya*	*costata*
Teteven	8 (top)	*Pleuromya*	*costata*
Teteven	8 (top)	*Pleuromya*	*costata*
Teteven	8 (top)	*Pleuromya*	*costata*
Teteven	8(vi)	*Pleuromya*	*costata*
Teteven	8(vi)	*Pleuromya*	*costata*
Teteven	8 (top)	*Pleuromya*	*costata*
Teteven	8 (top)	*Pleuromya*	*costata*
Teteven	8(vi)	*Pleuromya*	*costata*
Teteven	8(vi)	*Pleuromya*	*costata*
Teteven	8 (top)	*Pleuromya*	*costata*
Teteven	8(vi)	*Pleuromya*	*costata*
Teteven	8(vi)	*Pleuromya*	*costata*
Teteven	8(vi)	*Pleuromya*	*costata*
Teteven	8(vi)	*Pleuromya*	*costata*
Teteven	8(vi)	*Pholadomya*	*ambigua*
Teteven	8(vi)	*Pholadomya*	*ambigua*

Section	Bed no.(height)	Genus	Species
Teteven	8(vi)	*Pholadomya*	*ambigua*
Teteven	8(vi)	*Pholadomya*	*ambigua*
Teteven	8(vi)	*Pholadomya*	*ambigua*
Teteven	8(vi)	*Pholadomya*	*ambigua*
Teteven	8 (top)	*Antiquilimea*	*succincta*
Teteven	8 (top)	*Antiquilimea*	*succincta*
Teteven	8(vi)	*Pholadomya*	*ambigua*
Teteven	8(vi)	*Pholadomya*	*ambigua*
Teteven	8(vi)	*Pholadomya*	*ambigua*
Teteven	8(vi)	*Pholadomya*	*ambigua*
Teteven	8(vi)	*Pholadomya*	*ambigua*
Teteven	8(vi)	*Pholadomya*	*ambigua*
Teteven	8(vi)	*Pholadomya*	*ambigua*
Teteven	8 (vi)	*Pleuromya*	*costata*
Teteven	8 (vi)	*Pleuromya*	*costata*
Teteven	8 (top)	*Pholadomya*	*ambigua*
Teteven	8 (top)	*Pholadomya*	*ambigua*
Teteven	8 (top)	*Pholadomya*	*ambigua*
Teteven	8 (top)	*Pholadomya*	*ambigua*
Teteven	8 (top)	*Pholadomya*	*ambigua*
Teteven	8 (top)	*Pholadomya*	*ambigua*
Teteven	8 (top)	*Pholadomya*	*ambigua*
Teteven	8 (top)	*Pholadomya*	*ambigua*
Teteven	8 (top)	*Pholadomya*	*ambigua*
Teteven	8 (top)	*Pholadomya*	*ambigua*
Teteven	8 (top)	*Pholadomya*	*ambigua*
Teteven	8 (top)	*Gryphaea*	sp.indet

Section	Bed no.(height)	Genus	Species
Teteven	8 (top)	*Pseudopecten*	*equivalvis*
Teteven	8 (top)	*Pseudopecten*	*equivalvis*
Teteven	8 (top)	*Pholadomya*	sp. indet
Teteven	8 (top)	*Pholadomya*	sp. indet
Teteven	8 (top)	*Myoconcha*	*decorata*
Teteven	8 (top)	*Entolium*	*lunare*
Teteven	8 (top)	*Pleuromya*	*costata*
Teteven	8 (top)	*Pleuromya*	*costata*
Teteven	8 (top)	*Pleuromya*	*costata*
Teteven	8 (vi)	*Pleuromya*	*costata*
Teteven	8 (↓110cm)	*Pholadomya*	*ambigua*
Teteven	8 (↓110cm)	*Pleuromya*	*costata*
Teteven	8 (↓110cm)	*Pleuromya*	*costata*
Teteven	8 (↓110cm)	*Pleuromya*	*costata*
Teteven	8 (↓110cm)	*Pleuromya*	*costata*
Teteven	8 (↓110cm)	*Pleuromya*	*costata*
Teteven	8 (↓110cm)	*Pleuromya*	*costata*
Teteven	8 (↓110cm)	*Pleuromya*	*costata*
Teteven	8 (↓110cm)	*Pleuromya*	*costata*
Teteven	8 (↓110cm)	*Pleuromya*	*costata*
Teteven	8 (↓110cm)	*Pleuromya*	*costata*
Teteven	8 (↓110cm)	*Pleuromya*	*costata*
Teteven	8 (↓110cm)	*Pholadomya*	*ambigua*
Teteven	8 (↓110cm)	*Pholadomya*	*ambigua*
Teteven	8 (↓110cm)	*Pholadomya*	*ambigua*
Teteven	8 (↓110cm)	*Pseuolimea*	*pectinoides*
Teteven	8 (vi)	*Pleuromya*	*costata*

Section	Bed no.(height)	Genus	Species
Teteven	8 (vi)	*Pleuromya*	*costata*
Teteven	8 (vi)	*Pleuromya*	*costata*
Teteven	8 (vi)	*Pleuromya*	*costata*
Teteven	8 (vi)	*Pleuromya*	*costata*
Teteven	9 (↑270cm)	*Pleuromya*	*costata*
Teteven	9 (↑270cm)	*Harpax*	*spinosa*
Teteven	9 (↑270cm)	*Pseudopecten*	*equivalvis*
Teteven	9 (↓70cm)	*Myoconcha*	*decorata*
Teteven	9 (↓70cm)	*Oyster*	sp. et gen. indet
Teteven	9 (↑270cm)	*Harpax*	*spinosa*
Teteven	9 (↑270cm)	*Harpax*	*spinosa*
Teteven	9 (↑270cm)	*Harpax*	*spinosa*
Teteven	9 (↑270cm)	*Harpax*	*spinosa*
Teteven	9 (↑270cm)	*Harpax*	*spinosa*
Teteven	9 (↑270cm)	*Harpax*	*spinosa*
Teteven	9 (↑270cm)	*Harpax*	*spinosa*
Teteven	9 (↑270cm)	*Harpax*	*spinosa*
Teteven	9 (ii)	*?Camptonectes*	sp. indet
Teteven	9 (↓70cm)	*Entolium*	*lunare*
Teteven	9 (ii)	*Antiqulima*	sp. indet
Teteven	9 (ii)	*Pholadomya*	*ambigua*
Teteven	9 (ii)	*Pleuromya*	*costata*
Teteven	9 (ii)	*Pleuromya*	*costata*
Teteven	9 (ii)	*Pleuromya*	*costata*
Teteven	9 (ii)	*Pholadomya*	*ambigua*
Teteven	9 (ii)	*Pholadomya*	*ambigua*
Teteven	9 (ii)	*Pleuromya*	*costata*

Section	Bed no.(height)	Genus	Species
Teteven	9 (ii)	*Pleuromya*	*costata*
Teteven	9 (ii)	*Pleuromya*	*costata*
Teteven	9 (ii)	*Pleuromya*	*costata*
Teteven	9 (ii)	*Pleuromya*	*costata*
Teteven	9 (ii)	*Pholadomya*	*ambigua*
Teteven	9 (ii)	*Pholadomya*	*ambigua*
Teteven	9 (ii)	*Pholadomya*	*ambigua*
Teteven	9 (ii)	*Eopecten*	cf. *velatus*
Teteven	9 (ii)	*Entolium*	*lunare*
Teteven	9 (ii)	*Pleuromya*	*costata*
Teteven	9 (ii)	*Pholadomya*	*ambigua*
Teteven	9 (ii)	*Pholadomya*	*ambigua*
Teteven	9 (ii)	*Pholadomya*	*ambigua*
Teteven	9 (ii)	*Pholadomya*	*ambigua*
Teteven	9 (↑40cm)	*Gryphaea*	*mccullocchii*
Teteven	9 (↑120cm)	*Pleuromya*	*costata*
Teteven	9 (↑120cm)	*Pleuromya*	*costata*
Teteven	9 (↑120cm)	*?Gresslya*	sp. indet
Teteven	9 (↑120cm)	*Modiolus*	sp. indet
Teteven	9 (↑120cm)	*Pholadomya*	*ambigua*
Teteven	9 (↑120cm)	*Pleuromya*	*costata*
Teteven	9 (↑120cm)	*Modiolus*	sp. indet
Teteven	9 (↑120cm)	*Harpax*	*spinosa*
Teteven	9 (↓170cm)	*Pholadomya*	*ambigua*
Teteven	9 (↓170cm)	*?Gresslya*	sp. indet
Teteven	9 (↓170cm)	*Entolium*	*lunare*
Teteven	9 (↓170cm)	*Entolium*	*lunare*

Section	Bed no.(height)	Genus	Species
Teteven	9 (↓170cm)	*Chlamys*	sp. indet
Teteven	9 (↓170cm)	*Chlamys*	sp. indet
Teteven	9 (↓170cm)	*Pholadomya*	*ambigua*
Teteven	9 (↓170cm)	*Antiquilima*	*harmanni*
Teteven	9 (↓170cm)	*Modiolus*	sp. indet
Teteven	9 (↓170cm)	*Myochonca*	*decorata*
Teteven	9 (↓70cm)	*Pseudopecten*	*equivalvis*
Teteven	9 (↓70cm)	*Pseudopecten*	*equivalvis*
Teteven	9 (↓70cm)	*Pseudopecten*	*equivalvis*
Teteven	9 (↓70cm)	*Pseudopecten*	*equivalvis*
Teteven	9 (↓70cm)	*Harpax*	*spinosa*
Teteven	9 (↓70cm)	*Gryphaea*	sp. indet
Teteven	9 (↓70cm)	*Modiolus*	sp. indet
Teteven	9 (↓156cm)	*Harpax*	*spinosa*
Teteven	9 (↓156cm)	*Harpax*	*spinosa*
Teteven	9 (↓156cm)	*Harpax*	*spinosa*
Teteven	9 (↓156cm)	*Harpax*	*spinosa*
Teteven	9 (↓156cm)	*Harpax*	*spinosa*
Teteven	9 (↓156cm)	*Harpax*	*spinosa*
Teteven	9 (↓100cm)	*Gryphaea*	sp. indet
Teteven	9 (↓100cm)	*Modiolus*	sp. indet
Teteven	9 (↓100cm)	*Eopecten*	cf. *velatus*
Teteven	9 (↓100cm)	*Pseudopecten*	*equivalvis*
Teteven	9 (↓20cm)	*Chlamys*	*textoria*
Teteven	10 (base)	*Plagiostoma*	cf. *punctata*
Teteven	10 (base)	*Pseudopecten*	*equivalvis*
Teteven	10 (base)	*Pseudolimea*	*pectinoides*

Section	Bed no.(height)	Genus	Species
Teteven	10 (base)	*Pseudolimea*	*pectinoides*
Teteven	10 (↑70cm)	*Pseudolimea*	*pectinoides*
Teteven	10 (↑70cm)	*Pholadomya*	cf. *decorata*
Teteven	10 (↑70cm)	*Modiolus*	*ventricosa*
Teteven	10 (top)	*Modiolus*	*ventricosa*
Teteven	10 (top)	*Pseudopecten*	*equivalvis*
Teteven	10 (top)	*Pseudopecten*	*equivalvis*
Teteven	10 (top)	*Pseudopecten*	*equivalvis*
Teteven	10 (top)	*Pseudopecten*	*equivalvis*
Teteven	10 (top)	*Pseudopecten*	*equivalvis*
Teteven	11 (↑50cm)	*Pleuromya*	*costata*
Teteven	12 (↑50cm)	*Pleuromya*	*costata*
Teteven	13 (↑50cm)	*Pleuromya*	*costata*
Teteven	14 (↑50cm)	*Pleuromya*	*costata*
Balsha	8a	*Pseudopecten*	*equivalvis*
Balsha	8a	*Pseudopecten*	*equivalvis*
Balsha	8a	*Pseudopecten*	*equivalvis*
Balsha	8c	*Pseudopecten*	*equivalvis*
Balsha	10b	*Pseudopecten*	*equivalvis*
Balsha	10c	*Pseudopecten*	*equivalvis*
Balsha	14	*Pseudopecten*	*equivalvis*
Balsha	15b	*Pseudopecten*	*equivalvis*
Balsha	15b	*Pseudopecten*	*equivalvis*
Balsha	15c	*Pseudopecten*	*equivalvis*
Balsha	16c	*Pseudopecten*	*equivalvis*
Balsha	17b	*Pseudopecten*	*equivalvis*
Balsha	17c	*Pseudopecten*	*equivalvis*

Section	Bed no.(height)	Genus	Species
Balsha	19c	*Pseudopecten*	*equivalvis*
Balsha	19c	*Pseudopecten*	*equivalvis*
Balsha	19c	*Pseudopecten*	*equivalvis*
Balsha	20a	*Pseudopecten*	*equivalvis*
Balsha	20c	*Pseudopecten*	*equivalvis*
Balsha	20c	*Pseudopecten*	*equivalvis*
Balsha	20c	*Gryphaea*	*gigantea*
Balsha	20c	*Gryphaea*	*gigantea*
Balsha	20c	*Gryphaea*	*gigantea*
Balsha	20c	*Pseudopecten*	*equivalvis*
Balsha	21	*Pseudopecten*	*equivalvis*
Balsha	21	*Pseudopecten*	*equivalvis*
Balsha	21	*Pseudopecten*	*equivalvis*
Balsha	21	*Pseudopecten*	*equivalvis*
Balsha	21	*Entolium*	*lunare*
Balsha	22.1	*Pseudopecten*	*equivalvis*
Balsha	22.1	*Pseudopecten*	*equivalvis*
Balsha	22.1	*Gryphaea*	*gigantea*
Balsha	22.1	*?Pleuromya*	sp. indet
Balsha	22.1	*Pseudopecten*	*equivalvis*
Balsha	23a	*Pseudopecten*	*equivalvis*
Balsha	23a	*Pseudopecten*	*equivalvis*
Balsha	23a	*Entolium*	*lunare*
Balsha	23a	*Entolium*	*lunare*
Balsha	23a	*Entolium*	sp. indet
Balsha	23a	*Pinna*	cf. *folium*
Balsha	23c.1	*Pseudopecten*	*equivalvis*

Section	Bed no.(height)	Genus	Species
Balsha	23c.1	*Pseudopecten*	*equivalvis*
Balsha	23c.1	*Entolium*	*lunare*
Balsha	23c.1	*Entolium*	*lunare*
Balsha	23c.2	*Pseudopecten*	*equivalvis*
Balsha	23c.3	*Gryphaea*	*gigantea*
Balsha	23c.3	*Gryphaea*	*gigantea*
Balsha	23c.3	*Entolium*	*lunare*
Balsha	23c.3	*Entolium*	*lunare*
Balsha	23c.3	*Entolium*	*lunare*
Balsha	23c.3	*Entolium*	sp. indet
Balsha	23c.3	*Entolium*	sp. indet
Balsha	23c.3	*Entolium*	sp. indet
Balsha	23c.3	*Entolium*	sp. indet
Balsha	23c.3	*Entolium*	sp. indet
Kiselchov Dol	12	*Entolium*	*lunare*
Kiselchov Dol	12	*Entolium*	*lunare*
Kiselchov Dol	12	*Gryphaea*	*gigantea*
Kiselchov Dol	13a (↑10cm)	*Entolium*	sp. indet
Kiselchov Dol	13a (↑10cm)	*Entolium*	sp. indet
Kiselchov Dol	13a (↑10cm)	*Pleuromya*	*costata*
Kiselchov Dol	13a (↑10cm)	*Entolium*	sp. indet
Kiselchov Dol	13a (↑10cm)	*Entolium*	sp. indet
Kiselchov Dol	13a (↑10cm)	*Pleuromya*	*costata*
Kiselchov Dol	13a (↑10cm)	*Entolium*	sp. indet
Kiselchov Dol	13a (↑10cm)	*Entolium*	sp. indet
Kiselchov Dol	13a (↑10cm)	*Entolium*	sp. indet
Kiselchov Dol	13a (↑10cm)	*Entolium*	sp. indet

Section	Bed no.(height)	Genus	Species
Kiselchov Dol	13a (↑10cm)	*Entolium*	sp. indet
Kiselchov Dol	13a (↑10cm)	*Entolium*	sp. indet
Kiselchov Dol	13a (↑10cm)	*Entolium*	sp. indet
Kiselchov Dol	13a (↑10cm)	*Entolium*	sp. indet
Kiselchov Dol	13a (↑10cm)	*Goniomya*	*hybrida*
Kiselchov Dol	13a (↑10cm)	*Entolium*	sp. indet
Kiselchov Dol	13a (↑10cm)	*Entolium*	sp. indet
Kiselchov Dol	13a (↑10cm)	*Entolium*	sp. indet
Kiselchov Dol	13a (↑10cm)	*Entolium*	sp. indet
Kiselchov Dol	13a (↑10cm)	*Entolium*	sp. indet
Kiselchov Dol	13a (↑10cm)	*Entolium*	sp. indet
Kiselchov Dol	13a (↑10cm)	*Goniomya*	*hybrida*
Kiselchov Dol	13a (↑10cm)	*Entolium*	sp. indet
Kiselchov Dol	13a (↑10cm)	*Entolium*	sp. indet
Kiselchov Dol	13a (↑10cm)	*Entolium*	sp. indet
Kiselchov Dol	13a (↑10cm)	*Entolium*	sp. indet
Kiselchov Dol	13a (↑10cm)	*Entolium*	sp. indet
Kiselchov Dol	13a (↑10cm)	*Entolium*	sp. indet
Kiselchov Dol	13a (↑10cm)	*Entolium*	sp. indet
Kiselchov Dol	13a (↑10cm)	*Entolium*	sp. indet
Kiselchov Dol	13a (↑10cm)	*Entolium*	sp. indet
Kiselchov Dol	13a (↑10cm)	*Entolium*	sp. indet
Kiselchov Dol	13a (↑10cm)	*Entolium*	sp. indet
Kiselchov Dol	13a (↑10cm)	*Entolium*	sp. indet
Kiselchov Dol	13a (↑10cm)	*Entolium*	sp. indet
Kiselchov Dol	13a (↑10cm)	*Entolium*	sp. indet
Kiselchov Dol	13a (↑10cm)	*Entolium*	sp. indet

Section	Bed no.(height)	Genus	Species
Kiselchov Dol	13a (↑10cm)	*Entolium*	sp. indet
Kiselchov Dol	13a (↑10cm)	*Entolium*	sp. indet
Kiselchov Dol	13a (↑10cm)	*Entolium*	sp. indet
Kiselchov Dol	13a (↑10cm)	*Entolium*	sp. indet
Kiselchov Dol	13a (↑10cm)	*Entolium*	sp. indet
Kiselchov Dol	13a (↑10cm)	*Entolium*	sp. indet
Kiselchov Dol	13a (↑10cm)	*Entolium*	sp. indet
Kiselchov Dol	13a (↑10cm)	*?Coelastarte*	sp. indet
Kiselchov Dol	13a (↑10cm)	*?Grammatodon*	sp. indet
Kiselchov Dol	13a (↑10cm)	*Oxytoma*	sp. indet
Kiselchov Dol	13a (↑10cm)	*Camptonectes*	cf. auritus
Kiselchov Dol	13a (↑10cm)	*Coelastarte*	sp. indet
Kiselchov Dol	13a (↑10cm)	*?Gresslya*	sp. indet
Kiselchov Dol	13a (↑10cm)	*Goniomya*	*hybrida*
Kiselchov Dol	13a (↑10cm)	*Entolium*	sp. indet
Kiselchov Dol	13a (↑10cm)	*Chlamys*	*textoria*
Kiselchov Dol	13b (base)	*?Modiolus*	sp. indet
Kiselchov Dol	13b (base)	*Goniomya*	*hybrida*
Kiselchov Dol	13b (↑5cm)	*Chlamys*	cf. *textoria*
Kiselchov Dol	13b (↑5cm)	*Chlayms*	cf. *textoria*
Kiselchov Dol	13b (↑5cm)	*Propeamuseum*	*pumilum*
Kiselchov Dol	13b (↑5cm)	*?Gresslya*	sp. indet
Kiselchov Dol	13b (↑5cm)	*Antiquilimea*	sp. indet
Kiselchov Dol	13b (↑10cm)	*Entolium*	cf. *corneolum*
Kiselchov Dol	13b (↑10cm)	*Entolium*	cf. *corneolum*
Kiselchov Dol	13b (↑10cm)	*Entolium*	cf. *corneolum*
Kiselchov Dol	13b (↑10cm)	*Entolium*	cf. *corneolum*

Section	Bed no.(height)	Genus	Species
Kiselchov Dol	13b (↑10cm)	*Entolium*	cf. *corneolum*
Kiselchov Dol	13b (↑10cm)	*Entolium*	cf. *corneolum*
Kiselchov Dol	13b (↑10cm)	*Entolium*	cf. *corneolum*
Kiselchov Dol	13b (↑10cm)	*Entolium*	cf. *corneolum*
Kiselchov Dol	13b (↑10cm)	*Entolium*	cf. *corneolum*
Kiselchov Dol	13b (↑10cm)	*Entolium*	cf. *corneolum*
Kiselchov Dol	13b (↑10cm)	*Entolium*	cf. *corneolum*
Kiselchov Dol	13b (↑10cm)	*Entolium*	cf. *corneolum*
Kiselchov Dol	13b (↑10cm)	*Entolium*	cf. *corneolum*
Kiselchov Dol	13b (↑10cm)	*Entolium*	cf. *corneolum*
Kiselchov Dol	13b (↑10cm)	*Entolium*	cf. *corneolum*
Kiselchov Dol	13b (↑10cm)	*Entolium*	cf. *corneolum*
Kiselchov Dol	13b (↑10cm)	*Entolium*	cf. *corneolum*
Kiselchov Dol	13b (↑10cm)	*Entolium*	cf. *corneolum*
Kiselchov Dol	13b (↑10cm)	*Entolium*	cf. *corneolum*
Kiselchov Dol	13b (↑10cm)	*Entolium*	cf. *corneolum*
Kiselchov Dol	13b (↑10cm)	*Entolium*	cf. *corneolum*
Kiselchov Dol	13b (↑10cm)	*Entolium*	cf. *corneolum*
Kiselchov Dol	13b (↑10cm)	*Entolium*	cf. *corneolum*
Kiselchov Dol	13b (↑10cm)	*Entolium*	cf. *corneolum*
Kiselchov Dol	13b (↑10cm)	*Entolium*	cf. *corneolum*
Kiselchov Dol	13b (↑10cm)	*Antiquilimea*	sp. indet
Kiselchov Dol	13b (↑10cm)	*?Gresslya*	sp. indet
Kiselchov Dol	13b (↑10cm)	*Entolium*	cf. *corneolum*
Kiselchov Dol	13b (↑10cm)	*Entolium*	cf. *corneolum*
Kiselchov Dol	13b (↑10cm)	*Entolium*	cf. *corneolum*
Kiselchov Dol	13b (↑10cm)	*Entolium*	cf. *corneolum*

Section	Bed no.(height)	Genus	Species
Kiselchov Dol	13b (↑10cm)	*Entolium*	cf. *corneolum*
Kiselchov Dol	13b (↑10cm)	*Entolium*	cf. *corneolum*
Kiselchov Dol	13b (↑10cm)	*Entolium*	cf. *corneolum*
Kiselchov Dol	13b (↑10cm)	*Entolium*	cf. *corneolum*
Kiselchov Dol	13b (↑10cm)	*Entolium*	cf. *corneolum*
Kiselchov Dol	13b (↑10cm)	*Entolium*	cf. *corneolum*
Kiselchov Dol	13b (↑10cm)	*Entolium*	cf. *corneolum*
Kiselchov Dol	13b (↑10cm)	*Entolium*	cf. *corneolum*
Kiselchov Dol	13b (↑10cm)	*Entolium*	cf. *corneolum*
Kiselchov Dol	13b (↑10cm)	*Entolium*	cf. *corneolum*
Kiselchov Dol	13b (↑10cm)	*Entolium*	cf. *corneolum*
Kiselchov Dol	13b (↑10cm)	*Entolium*	cf. *corneolum*
Kiselchov Dol	13b (↑10cm)	*Entolium*	cf. *corneolum*
Kiselchov Dol	13b (↑10cm)	*Chlamys*	sp. indet
Kiselchov Dol	13b (↑10cm)	*Chlamys*	sp. indet
Kiselchov Dol	13b (↑10cm)	*Entolium*	cf. *corneolum*
Kiselchov Dol	13b (↑10cm)	*Entolium*	cf. *corneolum*
Kiselchov Dol	13b (↑10cm)	*Entolium*	cf. *corneolum*
Kiselchov Dol	13b (↑10cm)	*Entolium*	cf. *corneolum*
Kiselchov Dol	13b (↑10cm)	*Entolium*	cf. *corneolum*
Kiselchov Dol	13b (↑10cm)	*Entolium*	cf. *corneolum*
Kiselchov Dol	13b (↑10cm)	*?Gresslya*	sp. indet
Kiselchov Dol	13b (↑10cm)	*Entolium*	cf. *corneolum*
Kiselchov Dol	13b (↑10cm)	*Entolium*	cf. *corneolum*
Kiselchov Dol	13b (↑10cm)	*Entolium*	cf. *corneolum*
Kiselchov Dol	13b (↑10cm)	*Entolium*	cf. *corneolum*
Kiselchov Dol	13b (↑10cm)	*Entolium*	cf. *corneolum*

Section	Bed no.(height)	Genus	Species
Kiselchov Dol	13b (↑10cm)	*Entolium*	cf. *corneolum*
Kiselchov Dol	13b (↑10cm)	*Entolium*	cf. *corneolum*
Kiselchov Dol	13b (↑10cm)	*Entolium*	cf. *corneolum*
Kiselchov Dol	13b (↑10cm)	*Entolium*	cf. *corneolum*
Kiselchov Dol	13b (↑10cm)	*Entolium*	cf. *corneolum*
Kiselchov Dol	13b (↑10cm)	*Entolium*	cf. *corneolum*
Kiselchov Dol	13b (↑10cm)	*Entolium*	cf. *corneolum*
Kiselchov Dol	13b (↑10cm)	*Entolium*	cf. *corneolum*
Kiselchov Dol	13b (↑10cm)	*Entolium*	cf. *corneolum*
Kiselchov Dol	13b (↑10cm)	*Entolium*	cf. *corneolum*
Kiselchov Dol	13b (↑10cm)	*Entolium*	cf. *corneolum*
Kiselchov Dol	13b (↑10cm)	*Entolium*	cf. *corneolum*
Kiselchov Dol	13b (↑10cm)	*Entolium*	cf. *corneolum*
Kiselchov Dol	13b (↑10cm)	*Entolium*	cf. *corneolum*
Kiselchov Dol	13b (↑10cm)	*Entolium*	cf. *corneolum*
Kiselchov Dol	13b (↑10cm)	*Chlamys*	*textoria*
Kiselchov Dol	13b (↑10cm)	*Entolium*	cf. *corneolum*
Kiselchov Dol	13b (↑10cm)	*Entolium*	cf. *corneolum*
Kiselchov Dol	13b (↑10cm)	*Entolium*	cf. *corneolum*
Kiselchov Dol	13b (↑10cm)	*Entolium*	cf. *corneolum*
Kiselchov Dol	13b (↑10cm)	Oyster	gen. et sp. indet
Kiselchov Dol	13b (↑10cm)	Oyster	gen. et sp. indet
Kiselchov Dol	13b (↑10cm)	Oyster	gen. et sp. indet
Kiselchov Dol	13b (↑10cm)	Oyster	gen. et sp. indet
Kiselchov Dol	13b (↑10cm)	*Entolium*	cf. *corneolum*
Kiselchov Dol	13b (↑10cm)	*Entolium*	cf. *corneolum*
Kiselchov Dol	13b (↑10cm)	*Entolium*	cf. *corneolum*

Section	Bed no.(height)	Genus	Species
Kiselchov Dol	13b (↑10cm)	*Entolium*	cf. *corneolum*
Kiselchov Dol	13b (↑10cm)	*Entolium*	cf. *corneolum*
Kiselchov Dol	13b (↑10cm)	*Entolium*	cf. *corneolum*
Kiselchov Dol	13b (↑10cm)	*Entolium*	cf. *corneolum*
Kiselchov Dol	13b (↑10cm)	*Entolium*	cf. *corneolum*
Kiselchov Dol	13b (↑10cm)	*Entolium*	cf. *corneolum*
Kiselchov Dol	13b (↑10cm)	*Entolium*	cf. *corneolum*
Kiselchov Dol	13b (↑15cm)	*Entolium*	cf. *corneolum*
Kiselchov Dol	13b (↑15cm)	*Entolium*	cf. *corneolum*
Kiselchov Dol	13b (↑15cm)	*Entolium*	cf. *corneolum*
Kiselchov Dol	13b (↑15cm)	*Entolium*	cf. *corneolum*
Kiselchov Dol	13b (↑15cm)	*Entolium*	cf. *corneolum*
Kiselchov Dol	13b (↑15cm)	*Entolium*	cf. *corneolum*
Kiselchov Dol	13b (↑15cm)	*Entolium*	cf. *corneolum*
Kiselchov Dol	13b (↑15cm)	*Entolium*	cf. *corneolum*
Kiselchov Dol	13b (↑15cm)	*Entolium*	cf. *corneolum*
Kiselchov Dol	13b (↑15cm)	*Entolium*	cf. *corneolum*
Kiselchov Dol	13b (↑15cm)	*Entolium*	cf. *corneolum*
Kiselchov Dol	13b (↑15cm)	*Entolium*	cf. *corneolum*
Kiselchov Dol	13b (↑15cm)	*Entolium*	cf. *corneolum*
Kiselchov Dol	13b (↑15cm)	*Entolium*	cf. *corneolum*
Kiselchov Dol	13b (↑15cm)	*Entolium*	cf. *corneolum*
Kiselchov Dol	13b (↑15cm)	*Entolium*	cf. *corneolum*
Kiselchov Dol	13b (↑15cm)	*Entolium*	cf. *corneolum*
Kiselchov Dol	13b (↑15cm)	*Entolium*	cf. *corneolum*
Kiselchov Dol	13b (↑15cm)	*Entolium*	cf. *corneolum*
Kiselchov Dol	13b (↑15cm)	*Entolium*	cf. *corneolum*

Section	Bed no.(height)	Genus	Species
Kiselchov Dol	13b (↑15cm)	*Entolium*	cf. *corneolum*
Kiselchov Dol	13b (↑15cm)	*Entolium*	cf. *corneolum*
Kiselchov Dol	13b (↑15cm)	*Entolium*	cf. *corneolum*
Kiselchov Dol	13b (↑15cm)	*Entolium*	cf. *corneolum*
Kiselchov Dol	13b (↑15cm)	*Chlayms*	*textoria*
Kiselchov Dol	13c (↑30cm)	*Chlayms*	*textoria*
Kiselchov Dol	13c (↑30cm)	*Plagiostoma*	sp. indet
Kiselchov Dol	13c (↑30cm)	*Plagiostoma*	sp. indet
Kiselchov Dol	13c (↑30cm)	*Entolium*	sp. indet
Kiselchov Dol	13c (↑25cm)	*Chlayms*	*textoria*
Kiselchov Dol	13c (↑25cm)	*Chlamys*	*textoria*
Kiselchov Dol	13c (↑35cm)	*Chlayms*	*textoria*
Kiselchov Dol	13c (↑35cm)	*Coelastarte*	sp. indet
Kiselchov Dol	13c (↑35cm)	*Oyster*	gen. et sp. indet
Kiselchov Dol	13c (↑35cm)	*Plagiostoma*	sp. indet
Kiselchov Dol	13c (↑35cm)	*Plagiostoma*	sp. indet
Kiselchov Dol	13c (↑35cm)	*Entolium*	cf. *corneolum*
Kiselchov Dol	13c (↑35cm)	Oyster	gen. et sp. indet
Kiselchov Dol	13c (↑35cm)	*Chlamys*	*textoria*
Kiselchov Dol	13c (↑35cm)	*Coelastarte*	sp. indet
Kiselchov Dol	13c (↑35cm)	*Entolium*	cf. *corneolum*
Kiselchov Dol	13c (↑35cm)	Oyster	gen. et sp. indet
Kiselchov Dol	13c (↑35cm)	*?Grammatodon*	sp. indet
Kiselchov Dol	13c (↑35cm)	*Chlamys*	*textoria*
Kiselchov Dol	13c (↑35cm)	*Plagiostoma*	sp.indet
Kiselchov Dol	13c (↑35cm)	Oyster	gen. et sp. indet
Kiselchov Dol	13c (↑35cm)	*Entolium*	cf. *corneolum*

Section	Bed no.(height)	Genus	Species
Kiselchov Dol	13c (↑35cm)	*Coelastarte*	sp. indet
Kiselchov Dol	13c (↑35cm)	*Coelastarte*	sp. indet
Kiselchov Dol	13c (↑35cm)	*Plagiostoma*	sp. indet
Kiselchov Dol	13c (↑35cm)	*Entolium*	cf. *corneolum*
Kiselchov Dol	13c (↑35cm)	*Plagiostoma*	sp. indet
Kiselchov Dol	13c (↑35cm)	*Coelastarte*	sp. indet
Kiselchov Dol	13c (↑35cm)	*Entolium*	cf. *corneolum*
Kiselchov Dol	13c (↑35cm)	*Camptonectes*	cf. *auritus*
Kiselchov Dol	13c (↑35cm)	*Chlamys*	*textoria*
Kiselchov Dol	13c (↑35cm)	*Propeamuseum*	*pumilum*
Kiselchov Dol	13c (↑35cm)	*Chlamys*	*textoria*
Kiselchov Dol	13c (↑35cm)	*Coelastarte*	sp. indet
Kiselchov Dol	13c (↑35cm)	Oyster	gen. et sp. indet
Kiselchov Dol	13c (↑35cm)	*Propeamuseum*	cf. *pumilum*
Kiselchov Dol	13c (↑35cm)	*Entolium*	*corneolum*
Kiselchov Dol	13c (↑35cm)	*Plagiostoma*	sp. indet
Kiselchov Dol	13c (↑35cm)	Oyster	gen. et sp. indet
Kiselchov Dol	13c (↑35cm)	*Coelastarte*	sp. indet
Kiselchov Dol	13c (↑35cm)	Oyster	gen. et sp. indet
Kiselchov Dol	13c (↑35cm)	Oyster	gen. et sp. indet
Kiselchov Dol	13c (↑35cm)	*?Gresslya*	sp. indet
Kiselchov Dol	13c (↑35cm)	*Coelastarte*	sp. indet
Kiselchov Dol	13c (↑35cm)	Oyster	gen. et sp. indet
Kiselchov Dol	13c (↑35cm)	*Entolium*	sp. indet
Kiselchov Dol	13c (↑35cm)	*Coelastarte*	sp. indet
Kiselchov Dol	13c (↑35cm)	?Gresslya	sp. indet
Kiselchov Dol	13c (↑35cm)	*Entolium*	sp. indet

Section	Bed no.(height)	Genus	Species
Kiselchov Dol	13c (↑35cm)	*Plagiostoma*	sp. indet
Kiselchov Dol	13c (↑35cm)	*Entolium*	cf. *corneolum*
Kiselchov Dol	13c (↑35cm)	*Chlamys*	*textoria*
Kiselchov Dol	13c (↑35cm)	Oyster	gen. et sp. indet
Kiselchov Dol	13c (↑35cm)	*Entolium*	sp. indet
Kiselchov Dol	13c (↑35cm)	*Coelastarte*	sp. indet
Kiselchov Dol	13c (↑35cm)	*Propeamuseum*	cf. *pumilum*
Kiselchov Dol	13c (↑35cm)	*Entolium*	sp. indet
Kiselchov Dol	13d (↑10cm)	*Plagiostoma*	sp. indet
Kiselchov Dol	13d (↑10cm)	*Entolium*	sp. indet
Kiselchov Dol	13d (↑10cm)	*Coelastarte*	sp. indet
Kiselchov Dol	13e (↑5cm)	*Chlamys*	*textoria*
Kiselchov Dol	13e (↑10cm)	*Coelastarte*	sp. indet
Kiselchov Dol	13e (↑10cm)	*Propeamuseum*	*pumilum*
Kiselchov Dol	13e (↑10cm)	Oyster	gen. et sp. indet
Kiselchov Dol	13e (↑10cm)	Oyster	gen. et sp. indet
Kiselchov Dol	13e (↑10cm)	Oyster	gen. et sp. indet
Kiselchov Dol	13e (↑10cm)	*Chlamys*	sp. indet
Kiselchov Dol	13e (↑10cm)	*Coelastarte*	sp. indet
Kiselchov Dol	13e (↑15cm)	*Grammatodon*	sp. indet
Kiselchov Dol	13e (↑20cm)	*?Entolium*	sp. indet
Kiselchov Dol	13e (↑20cm)	*Entolium*	sp. indet
Kiselchov Dol	13e (↑20cm)	*Entolium*	sp. indet
Kiselchov Dol	13e (↑20cm)	*Propeamuseum*	cf. *pumilum*
Kiselchov Dol	13e (↑20cm)	*Coelastarte*	sp. indet
Kiselchov Dol	13c (↑35cm)	*Entolium*	cf. *corneolum*
Kiselchov Dol	13c (↑35cm)	*Entolium*	cf. *corneolum*

Section	Bed no.(height)	Genus	Species
Kiselchov Dol	13c (↑35cm)	*Entolium*	cf. *corneolum*
Kiselchov Dol	13c (↑35cm)	*Entolium*	cf. *corneolum*
Kiselchov Dol	13c (↑35cm)	*Entolium*	cf. *corneolum*
Kiselchov Dol	13c (↑35cm)	Entolium	cf. corneolum
Kiselchov Dol	14a (↑10cm)	*?Plagiostoma*	sp. indet
Kiselchov Dol	14a (↑10cm)	*?Eopecten*	sp. indet
Kiselchov Dol	14a (↑10cm)	Oyster	gen. et sp. indet
Kiselchov Dol	14a (↑10cm)	Oyster	gen. et sp. indet
Kiselchov Dol	14a (↑10cm)	*Entolium*	sp. indet
Kiselchov Dol	14a (↑10cm)	*?Gresslya*	sp. indet
Kiselchov Dol	14a (↑10cm)	*?Gresslya*	sp. indet
Kiselchov Dol	14a (↑10cm)	*?Gresslya*	sp. indet
Kiselchov Dol	14a (↑10cm)	*?Gresslya*	sp. indet
Kiselchov Dol	14a (↑10cm)	*?Gresslya*	sp. indet
Kiselchov Dol	14a (↑10cm)	*Entolium*	cf. *corneolum*
Kiselchov Dol	14a (↑10cm)	*?Gresslya*	sp. indet
Kiselchov Dol	14a (↑10cm)	*?Gresslya*	sp. indet
Kiselchov Dol	14a (↑10cm)	*?Gresslya*	sp. indet
Kiselchov Dol	14a (↑10cm)	*?Gresslya*	sp. indet
Kiselchov Dol	14a (↑10cm)	*?Gresslya*	sp. indet
Kiselchov Dol	14a (↑10cm)	*Entolium*	cf. *corneolum*
Kiselchov Dol	14a (↑10cm)	*Entolium*	cf. *corneolum*
Kiselchov Dol	14a (↑10cm)	*Entolium*	cf. *corneolum*
Kiselchov Dol	14a (↑10cm)	*Entolium*	cf. *corneolum*
Kiselchov Dol	14a (↑10cm)	*Entolium*	cf. *corneolum*
Kiselchov Dol	14a (↑10cm)	*Entolium*	cf. *corneolum*
Kiselchov Dol	14a (↑10cm)	*Entolium*	cf. *corneolum*

Section	Bed no.(height)	Genus	Species
Kiselchov Dol	14a (↑10cm)	*Entolium*	cf. *corneolum*
Gorno Ozirovo	20	*Pseudopecten*	*equivalvis*
Gorno Ozirovo	20	*Antiquilimea*	sp. indet
Gorno Ozirovo	20	*Pseudopecten*	*equivalvis*
Gorno Ozirovo	20	*Pseudopecten*	*equivalvis*
Gorno Ozirovo	20	*Pseudopecten*	*equivalvis*
Gorno Ozirovo	0.21	*?Entolium*	sp. indet
Gorno Ozirovo	21	*Propeamussium*	*pumilum*
Gorno Ozirovo	21	*Propeamussium*	*pumilum*
Gorno Ozirovo	21	*Propeamussium*	sp. indet
Gorno Ozirovo	21	*Placunopisis*	*radiata*
Gorno Ozirovo	21	Oyster	gen. et sp. indet
Gorno Ozirovo	21	*Propeamussium*	*pumilum*
Gorno Ozirovo	21	*Propeamussium*	*pumilum*
Gorno Ozirovo	21	*Pleuromya*	*costata*
Gorno Ozirovo	21	*Pleuromya*	*costata*
Gorno Ozirovo	21	*Chlamys*	*textoria*
Gorno Ozirovo	21	*Entolium*	sp. indet
Gorno Ozirovo	21	*Entolium*	sp. indet
Gorno Ozirovo	21	*Entolium*	sp. indet
Gorno Ozirovo	21	*Entolium*	sp. indet
Gorno Ozirovo	21	*Entolium*	sp. indet
Gorno Ozirovo	21	*Entolium*	sp. indet
Gorno Ozirovo	21	*Entolium*	sp. indet
Gorno Ozirovo	21	*Entolium*	sp. indet
Gorno Ozirovo	21	*Entolium*	sp. indet
Gorno Ozirovo	21	*Propeamussium*	*pumilum*

Section	Bed no.(height)	Genus	Species
Gorno Ozirovo	21	*Propeamussium*	sp. indet
Gorno Ozirovo	21	*Propeamussium*	sp. indet
Gorno Ozirovo	21	*Entolium*	sp. indet
Gorno Ozirovo	21	*Coelastarte*	sp. indet
Gorno Ozirovo	21	*Entolium*	sp. indet
Gorno Ozirovo	21	Oyster	gen. et sp. indet
Gorno Ozirovo	21	*Coelastarte*	sp. indet
Gorno Ozirovo	21	*Entolium*	sp. indet
Gorno Ozirovo	21	*Entolium*	sp. indet
Gorno Ozirovo	21	*Mactromya*	sp. indet
Gorno Ozirovo	21	*?Gresslya*	sp. indet
Gorno Ozirovo	21	*Propeamussium*	*pumilum*
Gorno Ozirovo	21	*Propeamussium*	*pumilum*
Gorno Ozirovo	21	*Coelastarte*	sp. indet
Gorno Ozirovo	21	*Plagiostoma*	sp. indet
Gorno Ozirovo	21	*Entolium*	sp. indet
Gorno Ozirovo	21	*Entolium*	sp. indet
Gorno Ozirovo	21	Oyster	gen. et sp. indet
Gorno Ozirovo	21	*Entolium*	sp. indet
Gorno Ozirovo	21	*Entolium*	sp. indet
Gorno Ozirovo	21	*Entolium*	sp.indet
Gorno Ozirovo	21	*Propeamussium*	*pumilum*
Gorno Ozirovo	21	*?Entolium*	sp. indet
Gorno Ozirovo	21	*Pleuromya*	*costata*
Gorno Ozirovo	21	*Grammatodon*	cf. *insons*
Gorno Ozirovo	21	*Coelastarte*	sp. indet
Gorno Ozirovo	21	*Coelastarte*	sp. indet

Section	Bed no.(height)	Genus	Species
Gorno Ozirovo	21	*Plagiostoma*	sp. indet
Gorno Ozirovo	21	*Propeamussium*	*pumilum*
Gorno Ozirovo	21	*Propeamussium*	*pumilum*
Gorno Ozirovo	21	*Plagiostoma*	sp. indet
Gorno Ozirovo	21	*Grammatodon*	cf. *insons*
Gorno Ozirovo	21	*Grammatodon*	cf. *insons*
Gorno Ozirovo	21	*Grammatodon*	cf. *insons*
Gorno Ozirovo	21	*Grammatodon*	cf. *insons*
Gorno Ozirovo	21	*Coelastarte*	sp. indet
Gorno Ozirovo	21	*Coelastarte*	sp. indet
Gorno Ozirovo	21	*Grammatodon*	cf. *insons*
Gorno Ozirovo	21	*Chlamys*	*textoria*
Gorno Ozirovo	21	Oyster	gen. et sp. indet
Gorno Ozirovo	21	*Ctenostreon*	sp. indet
Gorno Ozirovo	21	*Entolium*	sp. indet
Gorno Ozirovo	21	*Coelastarte*	sp. indet
Gorno Ozirovo	21	*Coelastarte*	sp. indet
Gorno Ozirovo	21	*Coelastarte*	sp. indet
Gorno Ozirovo	21	*Coelastarte*	sp. indet
Gorno Ozirovo	21	*Coelastarte*	sp. indet
Gorno Ozirovo	21	*Propeamusium*	sp. indet
Gorno Ozirovo	21	*Propeamusium*	*pumilum*
Gorno Ozirovo	21	*Propeamusium*	sp. indet
Gorno Ozirovo	21	*Oxytoma*	*inequivalvis*
Gorno Ozirovo	21	*Coelastarte*	sp. indet
Gorno Ozirovo	21	*Coelastarte*	sp. indet
Gorno Ozirovo	21	*Coelastarte*	sp. indet

Section	Bed no.(height)	Genus	Species
Gorno Ozirovo	21	*Coelastarte*	sp. indet
Gorno Ozirovo	21	*Grammatodon*	cf. *insons*
Gorno Ozirovo	21	*Grammatodon*	cf. *insons*
Gorno Ozirovo	21	*Coelastarte*	sp. indet
Gorno Ozirovo	21	*Coelastarte*	sp. indet
Gorno Ozirovo	21	*Coelastarte*	sp. indet
Gorno Ozirovo	21	*Coelastarte*	sp. indet
Gorno Ozirovo	21	*Coelastarte*	sp. indet
Gorno Ozirovo	21	*Coelastarte*	sp. indet
Gorno Ozirovo	21	*Coelastarte*	sp. indet
Gorno Ozirovo	21	*Coelastarte*	sp. indet
Gorno Ozirovo	21	*Coelastarte*	sp. indet
Gorno Ozirovo	21	*Pleuromya*	*costata*
Gorno Ozirovo	21	*Entolium*	sp. indet
Gorno Ozirovo	21	*Coelastarte*	sp. indet
Gorno Ozirovo	21	*Grammatodon*	cf. *insons*
Gorno Ozirovo	21	*Coelastarte*	sp. indet
Gorno Ozirovo	21	*Coelastarte*	sp. indet
Gorno Ozirovo	21	*Pleuromya*	*costata*
Gorno Ozirovo	21	*Coelastarte*	sp. indet
Gorno Ozirovo	21	*Coelastarte*	sp. indet
Gorno Ozirovo	21	*Goniomya*	cf. *literata*
Gorno Ozirovo	21	*Grammatodon*	cf. *insons*
Gorno Ozirovo	21	*Coelastarte*	sp. indet
Gorno Ozirovo	21	*Coelastarte*	sp. indet
Gorno Ozirovo	21	*Coelastarte*	sp. indet
Gorno Ozirovo	21	*Grammatodon*	cf. *insons*
Gorno Ozirovo	21	*Coelastarte*	sp. indet

Section	Bed no.(height)	Genus	Species
Gorno Ozirovo	21	*Coelastarte*	sp. indet
Gorno Ozirovo	21	*Coelastarte*	sp. indet
Gorno Ozirovo	21	*Coelastarte*	sp. indet
Gorno Ozirovo	21	*Coelastarte*	sp. indet
Gorno Ozirovo	21	*Coelastarte*	sp. indet
Gorno Ozirovo	21	*Coelastarte*	sp. indet
Gorno Ozirovo	21	*Coelastarte*	sp. indet
Gorno Ozirovo	21	*Coelastarte*	sp. indet
Gorno Ozirovo	21	*Coelastarte*	sp. indet
Gorno Ozirovo	21	*Coelastarte*	sp. indet
Gorno Ozirovo	21	*Grammatodon*	cf. *insons*
Gorno Ozirovo	21	*Grammatodon*	cf. *insons*
Gorno Ozirovo	21	*Entolium*	sp. indet
Gorno Ozirovo	22	*Coelastarte*	sp. indet
Gorno Ozirovo	22	*Coelastarte*	sp. indet
Gorno Ozirovo	22	*Coelastarte*	sp. indet
Gorno Ozirovo	22	*Coelastarte*	sp. indet
Gorno Ozirovo	22	*Coelastarte*	sp. indet
Gorno Ozirovo	22	*Coelastarte*	sp. indet
Gorno Ozirovo	22	*Coelastarte*	sp. indet
Gorno Ozirovo	22	*Grammatodon*	cf. *insons*
Gorno Ozirovo	22	*Grammatodon*	cf. *insons*
Gorno Ozirovo	22	Oyster	gen. et sp. indet
Gorno Ozirovo	22	*Goniomya*	cf. *literata*
Gorno Ozirovo	22	*Entolium*	sp. indet
Gorno Ozirovo	22	*Grammatodon*	cf. *insons*
Gorno Ozirovo	22	*Entolium*	sp. indet

Section	Bed no.(height)	Genus	Species
Gorno Ozirovo	22	*Entolium*	sp. indet
Gorno Ozirovo	22	*Entolium*	sp. indet
Gorno Ozirovo	22	*Entolium*	sp. indet
Gorno Ozirovo	22	Pectinid	gen. et sp. indet
Gorno Ozirovo	22	*Entolium*	sp. indet
Gorno Ozirovo	22	*Coelastarte*	sp. indet
Vradlovtsi-1	2 (i)	*Pleuromya*	sp. indet
Vradlovtsi-1	2 (i)	*Pleuromya*	sp. indet
Vradlovtsi-1	2 (i)	*Pleuromya*	sp. indet
Vradlovtsi-1	2 (i)	*Modilous*	sp. indet
Vradlovtsi-1	2 (i)	*Modilous*	sp. indet
Vradlovtsi-1	2 (i)	*Modilous*	sp. indet
Vradlovtsi-1	2 (i)	*Modilous*	sp. indet
Vradlovtsi-1	2 (i)	*Mactromya*	sp. indet
Vradlovtsi-1	2 (i)	*Mactromya*	sp. indet
Vradlovtsi-1	2 (i)	*Gryphaea*	*mccullochii*
Vradlovtsi-1	2 (i)	*Gryphaea*	*mccullochii*
Vradlovtsi-2	2 (i)	*Gryphaea*	*mccullochii*
Vradlovtsi-3	2 (i)	*Gryphaea*	*mccullochii*
Vradlovtsi-4	2 (i)	*Gryphaea*	*mccullochii*
Vradlovtsi-5	2 (i)	*Plagiostoma*	sp. indet
Vradlovtsi-6	2 (iii)	*Gryphaea*	*mccullochii*
Vradlovtsi-6	2 (iii)	*Gryphaea*	*mccullochii*
Vradlovtsi-6	2 (iv)	*Gryphaea*	*mccullochii*
Vradlovtsi-1	5 (↑195cm)	*Pleuromya*	sp. indet
Vradlovtsi-1	5 (↑195cm)	*Pleuromya*	sp. indet
Vradlovtsi-1	5 (↑195cm)	*Pleuromya*	sp. indet

Section	Bed no.(height)	Genus	Species
Vradlovtsi-1	5 (↑195cm)	*Pleuromya*	sp. indet
Vradlovtsi-1	5 (↑195cm)	*Pleuromya*	sp. indet
Vradlovtsi-1	5 (↑195cm)	*Pleuromya*	sp. indet
Vradlovtsi-1	5 (↑195cm)	*Harpax*	*spinosa*
Vradlovtsi-1	5 (↑195cm)	*Pholadomya*	sp. indet
Vradlovtsi-1	5 (↑195cm)	*Cardinia*	sp. indet
Vradlovtsi-1	5 (↑195cm)	*Antiqulima*	*succincta*
Vradlovtsi-1	5 (↑195cm)	*Pseudolimea*	cf. *pectinoides*
Vradlovtsi-1	5 (↑195cm)	*Mactromya*	cf. *cardinoides*
Vradlovtsi-1	5 (↑60cm)	*Mactromya*	sp. indet
Vradlovtsi-1	5 (↑60cm)	*Modiolus*	sp. indet
Vradlovtsi-1	5 (↑60cm)	*Modiolus*	sp. indet
Vradlovtsi-1	5 (↑60cm)	*Entolium*	sp. indet
Vradlovtsi-2	2 (↑195cm)	*Gryphaea*	*mccullochii*
Vradlovtsi-2	2 (↑195cm)	*Pseudopecten*	*equivalvis*
Vradlovtsi-2	2 (↑195cm)	*Gryphaea*	*mccullochii*
Vradlovtsi-2	2 (↑195cm)	*Gryphaea*	*mccullochii*
Vradlovtsi-2	2 (↑195cm)	*Pholadomya*	*decorata*
Vradlovtsi-2	3 (base)	*Pinna*	*folium*
Vradlovtsi-2	3 (base)	*Pinna*	*folium*
Vradlovtsi-2	3 (base)	*Pinna*	*folium*
Vradlovtsi-2	3 (base)	*Pinna*	*folium*
Vradlovtsi-2	3 (base)	*Pholadomya*	sp. indet
Vradlovtsi-2	3 (base)	*Pholadomya*	sp. indet
Vradlovtsi-2	3 (base)	*Pholadomya*	sp. indet
Vradlovtsi-2	3 (base)	*Pholadomya*	*ambigua*
Vradlovtsi-2	3 (base)	*Gryphaea*	*mccullochii*

Section	Bed no.(height)	Genus	Species
Vradlovtsi-2	4 (base)	*Pseudopecten*	*equivalvis*
Vradlovtsi-2	2 (↑50cm)	*Pholadomya*	*decorata*
Vradlovtsi-2	4 (↑70cm)	*Pholadomya*	*decorata*
Vradlovtsi-2	5 (↑20cm)	*Gryphaea*	*mccullochii*
Vradlovtsi-2	5 (↑20cm)	*Mactromya*	sp. indet
Vradlovtsi-2	5 (↑20cm)	*Mactromya*	sp. indet
Vradlovtsi-2	5 (↑20cm)	*Pseudopecten*	*equivalvis*
Vradlovtsi-2	5 (↓60cm)	*Pseudopecten*	*equivalvis*
Vradlovtsi-2	5 (↓60cm)	*Entolium*	*lunare*
Vradlovtsi-2	5 (↓60cm)	*Pleuromya*	*costata*
Vradlovtsi-2	5 (↑140cm)	*Modiolus*	sp. indet
Vradlovtsi-2	5 (↑140cm)	*Pholadomya*	cf. *decorata*
Vradlovtsi-2	5 (↑140cm)	*Entolium*	*lunare*
Vradlovtsi-2	5 (↑140cm)	*Pleuromya*	*costata*
Vradlovtsi-2	6	*Pinna*	sp. indet
Vradlovtsi-2	6	*Gryphaea*	*mccullochii*
Vradlovtsi-2	6	*Gryphaea*	*mccullochii*
Vradlovtsi-2	6	*Antiquilima*	cf. *succincta*
Vradlovtsi-2	6	*Antiquilima*	cf. *succincta*
Vradlovtsi-2	6	*Antiquilima*	cf. *succincta*
Vradlovtsi-2	6	*Antiquilima*	cf. *succincta*
Vradlovtsi-2	6	*Antiquilima*	cf. *succincta*
Vradlovtsi-2	6	*Antiquilima*	cf. *succincta*
Beledie Han	4 (↑80cm)	*Chlamys*	sp. indet
Beledie Han	4 (↑80cm)	*Chlamys*	sp. indet
Beledie Han	4 (↑90cm)	*Chlamys*	sp. indet
Beledie Han	4 (↑120cm)	Infaunal	sp. indet

Section	Bed no.(height)	Genus	Species
Beledie Han	4 (↑140cm)	*Entolium*	sp. indet
Beledie Han	4 (↑140cm)	*Entolium*	sp. indet
Beledie Han	4 (↑140cm)	*Entolium*	sp. indet
Beledie Han	4 (↑140cm)	*Entolium*	sp. indet
Beledie Han	4 (↑150cm)	*Entolium*	sp. indet
Beledie Han	4 (↑150cm)	*Entolium*	sp. indet
Beledie Han	4 (↑160cm)	Pectenid	gen. et sp. indet
Beledie Han	4 (↑160cm)	Pectenid	gen. et sp. indet
Beledie Han	5	*Entolium*	sp. indet
Beledie Han	11	*Entolium*	*corneolum*
Beledie Han	11	*Entolium*	*corneolum*
Beledie Han	12	*Ctenestron*	sp. indet
Boeva Mogila	4	*Pseudolimea*	cf. *acuticostata*
Boeva Mogila	4	*Pseudolimea*	cf. *acuticostata*
Dobravitsa-1	1d	Oyster	gen. et sp. indet
Dobravitsa-1	1a	*Chlamys*	*textoria*
Dobravitsa-1	1a	*Plicatula*	*spinosa*
Dobravitsa-1	1a	*Gryphaea*	*gigantea*
Dobravitsa-1	1c	*Antiquilima*	cf. *harmanni*
Dobravitsa-1	1c	*Antiquilima*	cf. *harmanni*
Dobravitsa-1	1c	Pectinid	gen. et sp. indet
Dobravitsa-1	1c	*Chlamys*	*textoria*
Dobravitsa-1	1c	*Chlamys*	*textoria*
Dobravitsa-1	1c	Pectinid	gen. et sp. indet
Dobravitsa-1	1c	Pectinid	gen. et sp. indet
Dobravitsa-1	1c	Pectinid	gen. et sp. indet
Dobravitsa-1	1c	*?Modiolus*	sp. indet

Section	Bed no.(height)	Genus	Species
Dobravitsa-1	1c	*Chlamys*	sp. indet
Dobravitsa-1	1c	*Chlamys*	*textoria*
Dobravitsa-1	1c	*Chlamys*	*textoria*
Dobravitsa-1	1c	*Chlamys*	*textoria*
Dobravitsa-1	1c	*Chlamys*	*textoria*
Dobravitsa-1	1c	*Plagiostoma*	sp. indet
Dobravitsa-1	1c	*Chlamys*	sp. indet
Dobravitsa-1	1c	*Pseudolimea*	sp. indet
Dobravitsa-1	1c	*?Modiolus*	sp. indet
Dobravitsa-1	1c	*Chlamys*	sp. indet
Dobravitsa-1	1c	*Chlamys*	sp. indet
Dobravitsa-1	1c	*Plagiostoma*	sp. indet
Dobravitsa-1	1c	*Antiquilima*	cf. *harmanni*
Dobravitsa-1	1c	*Chlamys*	*textoria*
Dobravitsa-1	1c	*Chlamys*	*textoria*
Dobravitsa-1	1c	*Pseudolimea*	cf. *pectinoides*
Dobravitsa-1	1c	*Harpax*	*spinosa*
Dobravitsa-1	1c	*Harpax*	cf. *spinosa*
Dobravitsa-1	1c	*Pseudopecten*	*equivalvis*
Dobravitsa-1	1c	*Chlamys*	*textoria*
Dobravitsa-1	1c	*Chlamys*	*textoria*
Dobravitsa-1	1c	*Gryphaea*	*gigantea*
Dobravitsa-1	1c	*Gryphaea*	*gigantea*
Dobravitsa-1	1c	*Gryphaea*	*gigantea*
Dobravitsa-1	1	*Gryphaea*	*gigantea*
Dobravitsa-1	2	*Gryphaea*	*gigantea*
Dobravitsa-1	2	*Gryphaea*	*gigantea*

Section	Bed no.(height)	Genus	Species
Dobravitsa-1	2	*Gryphaea*	*gigantea*
Dobravitsa-1	2	*Gryphaea*	*gigantea*
Dobravitsa-1	2	*Gryphaea*	*gigantea*
Dobravitsa-1	2	*Gryphaea*	*gigantea*
Dobravitsa-1	2	Oyster	gen. et sp. indet
Dobravitsa-1	2	*Harpax*	*spinosa*
Dobravitsa 1	5c	*Enotlium*	sp. indet
Dobravitsa 1	5c	*Enotlium*	sp. indet
Dobravitsa 1	5c	Oyster	gen. et sp. indet
Dobravitsa 1	5c	Oyster	gen. et sp. indet
Dobravitsa-1	7a	Oyster	gen. et sp. indet
Dobravitsa-1	7b	*Antiquilima*	sp. indet
Dobravitsa-1	7b	*Plagiostoma*	sp. indet
Dobravitsa-1	7b	Pectinid	gen. et sp. indet
Dobravitsa-1	7b	*Chlamys*	sp. indet
Dobravitsa-1	7b	*Entolium*	cf. *corneolum*
Dobravitsa-1	7b	*Entolium*	cf. *corneolum*
Dobravitsa-1	7b	*Chlamys*	sp. indet
Dobravitsa-1	7b	*Entolium*	cf. *corneolum*
Dobravitsa-1	7b	*Pseudolimea*	cf. *pectinoides*
Dobravitsa-1	7b	*Plagiostoma*	sp. indet
Dobravitsa-1	7b	*Entolium*	cf. *corneolum*
Dobravitsa-1	7b	*Trigonia*	sp. indet
Dobravitsa-1	7b	*Entolium*	cf. *corneolum*
Dobravitsa-1	7b	*Entolium*	cf. *corneolum*
Dobravitsa-1	7b	*Entolium*	cf. *corneolum*
Dobravitsa-1	7c	*Antiquilima*	sp. indet

Section	Bed no.(height)	Genus	Species
Dobravitsa-1	7c	*Pseudolimea*	cf. *pectinoides*
Dobravitsa-1	9c	*Antiquilima*	sp. indet
Dobravitsa-1	9c	*?Placunopisis*	sp. indet
Dobravitsa-1	9c	*?Placunopisis*	sp. indet
Dobravitsa-1	9a	*Antiquilima*	sp. indet
Dobravitsa-1	9a	*Coelastarte*	sp. indet
Dobravitsa 1	9a	*Chlamys*	sp. indet
Dobravitsa 1	9a	*Entolium*	cf. *corneolum*
Dobravitsa 1	9a	*Entolium*	cf. *corneolum*
Dobravitsa 1	9a	*Entolium*	cf. *corneolum*
Dobravitsa-1	10	*Entolium*	cf. *corneolum*
Dobravitsa-1	11	*Entolium*	cf. *corneolum*
Dobravitsa 1	11 (top)	*Entolium*	cf. *corneolum*
Dobravitsa-1	13b	*Entolium*	cf. *corneolum*
Dobravitsa 1	13b	*Entolium*	cf. *corneolum*
Dobravitsa 1	13b	*Entolium*	cf. *corneolum*
Dobravitsa 1	13b	*Entolium*	cf. *corneolum*
Dobravitsa-1	13c	*Entolium*	cf. *corneolum*
Dobravitsa-1	13c	*Entolium*	cf. *corneolum*
Dobravitsa-1	14	*Entolium*	cf. *corneolum*
Dobravitsa-1	14	*Entolium*	cf. *corneolum*
Dobravitsa-1	14	*?Modiolus*	sp. indet
Dobravitsa-1	14	*Entolium*	cf. *corneolum*
Dobravitsa-1	14	*Chlamys*	sp. indet
Dobravitsa-1	14	*Entolium*	cf. *corneolum*
Dobravitsa-1	14	*Coelastarte*	sp. indet
Dobravitsa-1	14	*Entolium*	cf. *corneolum*

Section	Bed no.(height)	Genus	Species
Dobravitsa-1	14	*Entolium*	cf. *corneolum*
Dobravitsa-1	15	*Entolium*	cf. *corneolum*
Dobravitsa-1	15	*Entolium*	cf. *corneolum*
Dobravitsa-1	15	*Coelastarte*	sp. indet
Dobravitsa-1	15	*Entolium*	cf. *corneolum*
Dobravitsa-1	15	*Entolium*	cf. *corneolum*
Dobravitsa-1	15	*Entolium*	cf. *corneolum*
Dobravitsa-1	15	*Entolium*	cf. *corneolum*
Dobravitsa-1	15	*Entolium*	cf. *corneolum*
Dobravitsa-1	15	*Entolium*	cf. *corneolum*
Dobravitsa-1	15	*Entolium*	cf. *corneolum*
Dobravitsa-1	15	*Entolium*	cf. *corneolum*
Dobravitsa 1	15a	*Chlamys*	sp. indet
Dobravitsa 1	15a	*Chlamys*	sp. indet
Dobravitsa 1	15a	*Antiquilimea*	sp. indet
Brakyovtsi	2	*Pseudopecten*	*equivalvis*
Brakyovtsi	2	*Pseudopecten*	*equivalvis*
Brakyovtsi	2	*Entolium*	*lunare*
Brakyovtsi	2	*Pholadomya*	*ambigua*
Brakyovtsi	2	*Oxytoma*	sp. indet
Brakyovtsi	2	*Pseudolimea*	sp. indet
Brakyovtsi	4	*Pholadomya*	*ambigua*
Brakyovtsi	4	*Gryphaea*	*mcullochii*
Brakyovtsi	4	*Chlamys*	*textoria*
Brakyovtsi	4	*Pseudopecten*	*equivalvis*
Brakyovtsi	4	*Pseudopecten*	*equivalvis*
Brakyovtsi	4	*Pseudopecten*	*equivalvis*

Section	Bed no.(height)	Genus	Species
Brakyovtsi	4	*Pseudopecten*	*equivalvis*
Brakyovtsi	5	*Chlamys*	sp. indet
Brakyovtsi	5	*Pseudopecten*	*equivalvis*
Brakyovtsi	5	*Pseudopecten*	*equivalvis*
Brakyovtsi	5	*Chlamys*	sp. indet
Brakyovtsi	5	*Pseudopecten*	*equivalvis*
Brakyovtsi	5	*Pseudopecten*	*equivalvis*
Brakyovtsi	5	*Pseudopecten*	*equivalvis*
Brakyovtsi	5	*Entolium*	*lunare*
Brakyovtsi	5	*Pseudopecten*	*equivalvis*
Brakyovtsi	5	*Pseudopecten*	*equivalvis*
Brakyovtsi	7	*Pseudopecten*	*equivalvis*
Brakyovtsi	7	*Pleuromya*	*costata*
Brakyovtsi	7	*Pleuromya*	*costata*
Brakyovtsi	7	*Pleuromya*	*costata*
Brakyovtsi	7	*Chlamys*	*textoria*
Brakyovtsi	7	*Entolium*	*lunare*
Brakyovtsi	7	*Entolium*	*lunare*
Brakyovtsi	7	*Entolium*	*lunare*
Brakyovtsi	7	*Pseudopecten*	*equivalvis*
Brakyovtsi	7	*Pleuromya*	*costata*
Brakyovtsi	7	*Pleuromya*	*costata*
Brakyovtsi	7	*Pleuromya*	*costata*
Brakyovtsi	8	*Pseudopecten*	*equivalvis*
Brakyovtsi	10	*Entoium*	*lunare*
Brakyovtsi	10	*Entoium*	*lunare*
Brakyovtsi	10	*Weyla*	sp. indet

Section	Bed no.(height)	Genus	Species
Brakyovtsi	11	*Entoium*	*lunare*
Brakyovtsi	15	*Entoium*	*lunare*
Brakyovtsi	15	*Pseudopecten*	*equivalvis*
Brakyovtsi	15	*Pseudopecten*	*equivalvis*
Brakyovtsi	15	*Pseudopecten*	*equivalvis*
Brakyovtsi	17	*Entoium*	*lunare*
Brakyovtsi	17	*Pleuromya*	*costata*
Brakyovtsi	17	*Entoium*	*lunare*
Brakyovtsi	17	*Pleuromya*	*costata*
Brakyovtsi	17	*Pseudopecten*	*equivalvis*
Brakyovtsi	17	*Pleuromya*	sp. indet
Brakyovtsi	17	*Pleuromya*	sp. indet
Brakyovtsi	17	*Pseudopecten*	*equivalvis*
Brakyovtsi	17	*Pseudopecten*	*equivalvis*
Brakyovtsi	17	*Entolium*	*lunare*
Brakyovtsi	17	*Entolium*	sp. indet
Brakyovtsi	17	*Entolium*	sp. indet
Brakyovtsi	17	*Pseudolimea*	sp. indet
Brakyovtsi	17	*Entolium*	*lunare*
Brakyovtsi	17	*Entolium*	*lunare*
Brakyovtsi	17	*Entolium*	*lunare*
Brakyovtsi	17	*Entolium*	*lunare*
Brakyovtsi	17	*Entolium*	*lunare*
Brakyovtsi	17	*Entolium*	*lunare*
Brakyovtsi	17	*Entolium*	*lunare*
Brakyovtsi	17	*Pseudopecten*	*equivalvis*
Brakyovtsi	17	*Gryphaea*	*gigantea*

Section	Bed no.(height)	Genus	Species
Brakyovtsi	17	*Pleuromya*	*costata*
Brakyovtsi	17	*Entolium*	*lunare*
Brakyovtsi	17	*Entolium*	*lunare*
Brakyovtsi	17	*Entolium*	*lunare*
Brakyovtsi	17	*Entolium*	*lunare*
Brakyovtsi	17	*Entolium*	*lunare*
Brakyovtsi	17	*Entolium*	*lunare*
Brakyovtsi	17	*Entolium*	*lunare*
Brakyovtsi	17	*Entolium*	*lunare*
Brakyovtsi	18	*Entolium*	*lunare*
Brakyovtsi	18	*Entolium*	*lunare*
Brakyovtsi	18	*Entolium*	*lunare*
Brakyovtsi	18	*Entolium*	*lunare*
Brakyovtsi	18	*Entolium*	*lunare*
Brakyovtsi	18	*Entolium*	*lunare*
Brakyovtsi	18	*Entolium*	*lunare*
Brakyovtsi	18	*Gryphaea*	sp. indet
Brakyovtsi	18	*Pleuromya*	*coasta*
Brakyovtsi	18	*Entolium*	*lunare*
Brakyovtsi	18	*Entolium*	*lunare*
Brakyovtsi	18	*Entolium*	*lunare*
Brakyovtsi	19	*Pseudopecten*	*equivalvis*
Brakyovtsi	19	*Pseudopecten*	*equivalvis*
Brakyovtsi	19	*Entolium*	*lunare*
Brakyovtsi	20	*Entolium*	*lunare*
Brakyovtsi	20	*Entolium*	*lunare*
Brakyovtsi	21	*Gryphaea*	*gigantea*

Section	Bed no.(height)	Genus	Species
Brakyovtsi	25	*Pseudopecten*	*equivalvis*
Brakyovtsi	25	*Entolium*	*lunare*
Brakyovtsi	25	*Entolium*	*lunare*
Brakyovtsi	25	*Pseudopecten*	*equivalvis*
Brakyovtsi	25	*Entolium*	*lunare*
Brakyovtsi	25	*Entolium*	*lunare*
Brakyovtsi	25	*Entolium*	*lunare*
Brakyovtsi	25	*Entolium*	*lunare*
Brakyovtsi	26	*Harpax*	*spinosa*
Brakyovtsi	26	*Gryphaea*	*gigantea*
Ravna	1	Oyster	gen. et sp. indet
Ravna	1	Oyster	gen. et sp. indet
Ravna	3 (↑30cm)	*Gryphaea*	sp. indet
Ravna	3 (↑30cm)	*Pseudopecten*	*equivalvis*
Ravna	3 (↑30cm)	*Pseudopecten*	*equivalvis*
Ravna	3 (↑30cm)	*Pseudopecten*	*equivalvis*
Ravna	4(i)	*Pseudopecten*	*equivalvis*
Ravna	4(i)	*Pseudopecten*	*equivalvis*
Ravna	4(ii)	*Gryphaea*	*mccullochii*
Ravna	5i	*Gryphaea*	sp. indet
Ravna	5(ii)	*Gryphaea*	sp. indet
Ravna	5(ii)	*Gryphaea*	sp. indet
Ravna	5(ii)	*Gryphaea*	*muccullochii*
Ravna	5(ii)	*Gryphaea*	*muccullochii*
Ravna	5v	*Entolium*	*lunare*
Ravna	6 (i)	*Gryphaea*	sp. indet
Ravna	6 (i)	*Entolium*	*lunare*

Section	Bed no.(height)	Genus	Species
Ravna	6 (i)	*Gryphaea*	sp. indet
Ravna	6 (i)	*Harpax*	*spinosa*
Ravna	6 (i)	*Harpax*	*spinosa*
Ravna	6 (i)	*Harpax*	*spinosa*
Ravna	6 (i)	*Pseudolimea*	*pectinoides*
Ravna	6 (i)	*Pholadomya*	cf. *decorata*
Ravna	6 (i)	*Pseudopecten*	*equivalvis*
Ravna	6 (i)	*Pleuromya*	*costata*
Ravna	6 (i)	*Pleuromya*	*costata*
Ravna	6 (i)	*Mactromya*	sp. indet
Ravna	6 (i)	*Mactromya*	sp. indet
Ravna	6 (ii)	*Gryphaea*	sp. indet
Ravna	6 (ii)	*Gryphaea*	sp. indet
Ravna	6 (ii)	*Entolium*	*lunare*
Ravna	6 (ii)	*Gryphaea*	sp. indet
Ravna	6 (ii)	*Pholadomya*	sp. indet
Ravna	6 (ii)	*Pseudopecten*	*equivalvis*
Ravna	6 (ii)	*Pseudopecten*	*equivalvis*
Ravna	6 (ii)	*Gryphaea*	*mccullochii*
Ravna	6 (ii)	*Pholadomya*	sp. indet
Ravna	6 (ii)	*Pleuromya*	*costata*
Ravna	6 (ii)	*Chlamys*	*textoria*
Ravna	6 (ii)	*Chlamys*	*textoria*
Ravna	6 (ii)	*Chlamys*	*textoria*
Ravna	6 (ii)	*Pleuromya*	*costata*
Ravna	6iv	*Harpax*	*spinosa*
Ravna	6iv	*Harpax*	*spinosa*

Section	Bed no.(height)	Genus	Species
Ravna	6iv	*Harpax*	*spinosa*
Ravna	6iv	*Harpax*	*spinosa*
Ravna	6iv	*Pholadomya*	sp. indet
Ravna	6iv	*Pholadomya*	sp. indet
Ravna	6iv	*Pholadomya*	sp. indet
Ravna	6iv	*Pholadomya*	sp. indet
Ravna	6iv	*Pholadomya*	sp. indet
Ravna	6iv	*Pholadomya*	sp. indet
Ravna	6iv	*Pholadomya*	sp. indet
Ravna	6iv	*Pleuromya*	*costata*
Ravna	6iv	*Pleuromya*	*costata*
Ravna	6iv	*Pleuromya*	*costata*
Ravna	6iv	*Pleuromya*	*costata*
Ravna	6iv	*Pleuromya*	*costata*
Ravna	6iv	*Pleuromya*	*costata*
Ravna	6iv	*Pseudolimea*	*pectinoides*
Ravna	6iv	*Gryphaea*	*mccullochii*
Ravna	6iv	*Gryphaea*	*mccullochii*
Ravna	6iv	*Modiolus*	sp. indet
Ravna	6iv	*Entolium*	*lunare*
Ravna	6vi	*Harpax*	*spinosa*
Ravna	6vi	*Harpax*	*spinosa*
Ravna	6vi	*Harpax*	*spinosa*
Ravna	6vi	*Chlamys*	sp. indet
Ravna	6vi	*Harpax*	*spinosa*
Ravna	6vi	*Harpax*	*spinosa*
Ravna	6vi	*Harpax*	*spinosa*

Section	Bed no.(height)	Genus	Species
Ravna	6vi	*Harpax*	*spinosa*
Ravna	6vi	*Harpax*	*spinosa*
Ravna	6vi	*Harpax*	*spinosa*
Ravna	6vi	*Pseudopecten*	*equivalvis*
Ravna	6vi	*Pseudopecten*	*equivalvis*
Ravna	6vi	*Pleuromya*	*coastata*
Ravna	6vi	*Pleuromya*	*coastata*
Ravna	6vi	*Pleuromya*	sp. indet
Ravna	6 (top)	*Pholadomya*	sp. indet
Ravna	6 (top)	*Pholadomya*	sp. indet
Ravna	6 (top)	*Pholadomya*	sp. indet
Ravna	6 (top)	*Pholadomya*	sp. indet
Ravna	6 (top)	*Pholadomya*	sp. indet
Ravna	7(ii)	*Pseudolimea*	sp. indet
Ravna	7(ii)	*Oxytoma*	cf. *inequivalvis*
Ravna	7(ii)	*Harpax*	*spinosa*
Ravna	7(ii)	*Harpax*	*spinosa*
Ravna	7(ii)	*Harpax*	*spinosa*
Ravna	7(ii)	*Harpax*	*spinosa*
Ravna	7(ii)	*Harpax*	*spinosa*
Ravna	7(ii)	*Harpax*	*spinosa*
Ravna	7(ii)	*Harpax*	*spinosa*
Ravna	7(ii)	*Harpax*	*spinosa*
Ravna	7(ii)	*Harpax*	*spinosa*
Ravna	7(ii)	*Harpax*	*spinosa*
Ravna	7(ii)	*Harpax*	*spinosa*
Ravna	7(ii)	*Harpax*	*spinosa*

Section	Bed no.(height)	Genus	Species
Ravna	7(ii)	*Harpax*	*spinosa*
Ravna	7(ii)	*Harpax*	*spinosa*
Ravna	7(ii)	*Harpax*	*spinosa*
Ravna	7(ii)	*Harpax*	*spinosa*
Ravna	7(ii)	*Harpax*	*spinosa*
Ravna	7(ii)	*Harpax*	*spinosa*
Ravna	7(ii)	*Harpax*	*spinosa*
Ravna	7(ii)	*Pseudolimea*	*pectinoides*
Ravna	7(ii)	*Pseudopecten*	*equivalvis*
Ravna	7(ii)	*Pseudopecten*	*equivalvis*
Ravna	7(ii)	*Pseudopecten*	*equivalvis*
Ravna	7(ii)	*Pseudolimea*	*pectinoides*
Ravna	7(ii)	*Pseudolimea*	*pectinoides*
Ravna	7(ii)	*Pholadomya*	*ambigua*
Ravna	7(ii)	*Pholadomya*	*ambigua*
Ravna	7(ii)	*Pseudopecten*	*equivalvis*
Ravna	7(ii)	*Pholadomya*	sp. indet
Ravna	7(ii)	*Pleuromya*	*costata*
Ravna	7(ii)	*Pleuromya*	*costata*
Ravna	7(iv)	*Oxytoma*	cf. *inequivalvis*
Ravna	7(iv)	*Oxytoma*	sp. indet
Ravna	7(iv)	*Oxytoma*	Cf. *cignipes*
Ravna	7(iv)	*Harpax*	*spinosa*
Ravna	7(iv)	*Harpax*	*spinosa*
Ravna	7(iv)	*Harpax*	*spinosa*
Ravna	7(iv)	*Harpax*	*spinosa*
Ravna	7(iv)	*Harpax*	*spinosa*

Section	Bed no.(height)	Genus	Species
Ravna	7(iv)	*Oxytoma*	sp. indet
Ravna	7(iv)	*Pseudopecten*	*equivalvis*
Ravna	7(iv)	*Pinna*	*radiata*
Ravna	7(iv)	*Pinna*	*radiata*
Ravna	7 (↑75cm)	*Pholadomya*	cf. *decorata*
Ravna	8a (top)	*Entolium*	*lunare*
Ravna	8a (top)	*Pseudopecten*	*equivalvis*
Ravna	8a (top)	*Pseudopecten*	*equivalvis*
Ravna	8a (top)	*Pseudopecten*	*equivalvis*
Ravna	8a (top)	*Pseudopecten*	*equivalvis*
Ravna	8a (top)	*Pseudopecten*	*equivalvis*
Ravna	8a (top)	*Pleuromya*	sp. indet
Ravna	8a (top)	*Pleuromya*	*costata*
Ravna	8a (top)	*Pleuromya*	*costata*
Ravna	8a (top)	*Pleuromya*	*costata*
Ravna	8a (top)	*Pholadomya*	cf. *decorata*
Ravna	8a (top)	*Pholadomya*	cf. *decorata*
Ravna	8a (top)	*Pholadomya*	sp. indet
Ravna	8a (top)	*Pholadomya*	sp. indet
Ravna	8a (top)	*Pholadomya*	sp. indet
Ravna	8a (top)	*Pholadomya*	*ambigua*
Ravna	8a (top)	*Pholadomya*	*ambigua*
Ravna	8a (top)	*Pholadomya*	*ambigua*
Ravna	8a (top)	*Pholadomya*	*ambigua*
Ravna	8a (top)	*Pholadomya*	*ambigua*
Ravna	8a (top)	*Pholadomya*	*ambigua*
Ravna	8a (top)	*Plagiostoma*	*punctata*

Section	Bed no.(height)	Genus	Species
Ravna	8a (↑30cm)	*Modiolus*	*ventricosa*
Ravna	8a (↑30cm)	*Entolium*	*lunare*
Ravna	8a (↑30cm)	*Pholadomya*	cf. *decorata*
Ravna	8a (↑30cm)	*Modiolus*	*ventricosa*
Ravna	8a (↑30cm)	*Modiolus*	*ventricosa*
Ravna	8a (↑30cm)	*Pholadomya*	cf. *decorata*
Ravna	8b (↑10cm)	*Entolium*	*lunare*
Ravna	8b (↑10cm)	*Entolium*	*lunare*
Ravna	8b (↑10cm)	*?Camptonectes*	sp. indet
Ravna	8b (↑40cm)	*Pleuromya*	*costata*
Ravna	8b (↑40cm)	*Pholadomya*	*ambigua*
Ravna	8b (↑40cm)	*Entolium*	*lunare*
Ravna	8b (↑40cm)	*Modiolus*	sp.indet
Ravna	8b (↑60cm)	*Entolium*	*lunare*
Ravna	8b (↑60cm)	*Pleuromya*	*costata*
Ravna	8b (↑60cm)	*Pseudopecten*	*equivalvis*
Ravna	8b (↑60cm)	*Pseudopecten*	*equivalvis*
Ravna	8b (↑150cm)	*Pholadomya*	sp. indet
Ravna	8b (↑150cm)	*Pholadomya*	sp. indet
Ravna	8b (↑150cm)	*Pleuromya*	*costata*
Ravna	8b (↑150cm)	*Pleuromya*	*costata*
Ravna	8b (↑150cm)	*Pinna*	cf. *radiata*
Ravna	8b (↑180cm)	*Pinna*	cf. *radiata*
Ravna	8b (↑180cm)	*Pholadomya*	sp. indet
Ravna	8b (↑180cm)	*Entolium*	*lunare*
Ravna	8 (↓100cm)	*Pleuromya*	sp. indet
Ravna	8 (↓100cm)	*Pholadomya*	sp. indet

Section	Bed no.(height)	Genus	Species
Ravna	8 (↓100cm)	*Pholadomya*	sp. indet
Ravna	8 (↓100cm)	*Pholadomya*	sp. indet
Ravna	8 (↓100cm)	*Pleuromya*	*costata*
Ravna	8 (↓100cm)	*Pleuromya*	*costata*
Ravna	8 (↓100cm)	*Pleuromya*	*costata*
Ravna	8 (↓100cm)	*Pleuromya*	sp. indet
Ravna	8 (↓100cm)	*?Pleuromya*	sp. indet
Ravna	8 (↓100cm)	*?Pleuromya*	sp. indet
Ravna	8 (↓100cm)	*Pholadomya*	sp. indet
Ravna	8 (↓100cm)	*Pseduopecten*	*equivalvis*
Ravna	8 (↓100cm)	*Chlamys*	sp. indet
Ravna	8 (↓100cm)	*Antiqulimea*	cf. *succincta*
Ravna	8 (↓100cm)	*Antiqulimea*	cf. *succincta*
Ravna	8 (↓100cm)	*Entolium*	*lunare*
Ravna	8 (↓100cm)	*Pholadomya*	sp. indet
Ravna	8 (↓100cm)	*Pholadomya*	sp. indet
Ravna	8 (↓100cm)	*Pholadomya*	sp. indet
Ravna	8 (↓100cm)	*Pholadomya*	sp. indet
Ravna	8 (↓100cm)	*Antiquilimea*	cf. *succincta*
Ravna	8 (↓100cm)	*Antiquiliema*	cf. *succincta*
Ravna	8 (↓100cm)	*Entolium*	*lunare*
Ravna	8 (↓100cm)	*Entolium*	*lunare*
Ravna	8 (↓100cm)	*Entolium*	*lunare*
Ravna	8 (↓100cm)	*Pleuromya*	*costata*
Ravna	8 (↓100cm)	*Pleuromya*	*costata*
Ravna	8 (↓100cm)	*Pleuromya*	*costata*
Ravna	8 (↓100cm)	*Pleuromya*	*costata*

Section	Bed no.(height)	Genus	Species
Ravna	8 (↓100cm)	*Pleuromya*	*costata*
Ravna	8 (↓100cm)	*Pleuromya*	*costata*
Ravna	8 (↓100cm)	*Pleuromya*	*costata*
Ravna	8 (base)	*Modiolus*	sp. indet
Ravna	8 (base)	*Entolium*	sp. indet
Ravna	8 (base)	*Entolium*	sp. indet
Ravna	8	*Pinna*	*radiata*
Ravna	9 (↑40cm)	*Pholadomya*	*decorata*
Ravna	9 (↑40cm)	*Pholadomya*	*decorata*
Ravna	9 (↑40cm)	*Pinna*	sp. indet
Ravna	9 (↓40cm)	*Pseudopecten*	*equivalvis*
Ravna	9 (↑100cm)	*Pleuromya*	*costata*
Ravna	9 (↑100cm)	*Pleuromya*	*costata*
Ravna	9 (↓150cm)	*Pholadomya*	sp. indet
Ravna	9 (↓190cm)	*Pseudopecten*	*equivalvis*
Ravna	9 (↓190cm)	*Pseudopecten*	*equivalvis*
Ravna	9 (↓190cm)	Oyster	gen. et sp. indet
Ravna	9 (↓190cm)	*Gryphaea*	sp. indet
Ravna	9 (↓190cm)	*Pholadomya*	*ambigua*
Ravna	9 (↓190cm)	*Pholadomya*	*ambigua*
Ravna	9 (↓190cm)	*Chlamys*	sp. indet
Ravna	9 (↓190cm)	*Entolium*	*lunare*
Ravna	10 (↑20cm)	*Plagiostoma*	*punctata*
Ravna	10 (↓100cm)	Oyster	gen. et sp. indet
Ravna	10 (↓100cm)	*Chlamys*	*textoria*
Ravna	10 (↓100cm)	*Chlamys*	*textoria*
Ravna	10 (↓100cm)	*Pseudopecten*	*equivalvis*

Section	Bed no.(height)	Genus	Species
Ravna	10 (↓100cm)	Oyster	gen. et sp. indet
Ravna	10 (↓100cm)	*Entolium*	sp. indet
Ravna	10 (↑170cm)	*Plagiostoma*	*punctata*
Ravna	10 (↑170cm)	*Plagiostoma*	*punctata*
Ravna	10 (↑170cm)	*Entolium*	*lunare*
Ravna	10 (↑170cm)	*Plagiostoma*	*punctata*
Ravna	10 (↑170cm)	*Gryphaea*	*mccullochii*
Ravna	10 (↑170cm)	*Gryphaea*	*mccullochii*
Ravna	11 (↑140cm)	*Chlamys*	sp. indet
Ravna	11 (↑140cm)	*Chlamys*	*textoria*
Ravna	11 (↑140cm)	*Antiquilima*	cf. *succincta*
Ravna	12 (↑320cm)	*Chlamys*	*textoria*
Ravna	12 (↑10cm)	*Chlamys*	*textoria*
Ravna	12 (m3)	*Entolium*	*lunare*
Ravna	12 (↑250cm)	*Chlamys*	*textoria*
Ravna	12 (↑250cm)	*Chlamys*	*textoria*
Ravna	12 (↑250cm)	*Chlamys*	*textoria*
Ravna	12 (↑250cm)	*Chlamys*	*textoria*
Ravna	12 (L4)	*Chlayms*	*textoria*
Ravna	12 (L4)	*Plagiostoma*	*punctata*
Ravna	12 (L4)	*Plagiostoma*	*punctata*
Ravna	12 (L4)	*Plagiostoma*	*punctata*
Ravna	12 (L4)	*Chlamys*	*textoria*
Ravna	12 (L4)	*Chlamys*	*textoria*
Ravna	12 (M4)	*Chlamys*	*textoria*
Ravna	12 (M4)	*Chlamys*	*textoria*
Ravna	12 (M4)	*Chlamys*	*textoria*

Section	Bed no.(height)	Genus	Species
Ravna	12 (M4)	*Chlamys*	*textoria*
Ravna	12 (M2)	*Plagiostoma*	*punctata*
Ravna	12 (M2)	*Plagiostoma*	*punctata*
Ravna	13 (↑40cm)	*Plagiostoma*	*punctata*
Ravna	13 (↑40cm)	*Plagiostoma*	*punctata*
Ravna	13 (↑320cm)	*Chlamys*	*textoria*
Ravna	13 (↑320cm)	*Chlamys*	*textoria*
Ravna	13 (↑320cm)	*Chlamys*	*textoria*
Ravna	13 (↑320cm)	*Chlamys*	*textoria*
Ravna	13 (↑100cm)	*Plagiostoma*	*punctata*
Ravna	13 (↑100cm)	*Plagiostoma*	*punctata*
Ravna	13 (↑100cm)	*Antiquilima*	*succincta*
Ravna	13 (↑100cm)	*Antiquilima*	*succincta*
Ravna	13 (↑100cm)	*Chlamys*	*textoria*
Ravna	13 (↑100cm)	*Chlamys*	*textoria*
Ravna	13 (↑100cm)	*Chlamys*	*textoria*
Ravna	13 (↑130cm)	*Chlamys*	*textoria*
Ravna	13 (↑130cm)	*Chlamys*	*textoria*
Ravna	13 (↑140cm)	*Chlamys*	*textoria*
Ravna	13 (↑140cm)	*Chlamys*	*textoria*
Ravna	13 (↑140cm)	*Chlamys*	*textoria*
Ravna	13 (↑140cm)	*Plagiostoma*	sp. indet
Ravna	13 (↑140cm)	*Plagiostoma*	sp. indet
Ravna	13 (↑140cm)	*Plagiostoma*	sp. indet
Ravna	13 (↑140cm)	*Chlamys*	*textoria*
Ravna	13 (↑140cm)	*Plagiostoma*	*punctata*
Ravna	13 (top)	*Plagiostoma*	*punctata*

Section	Bed no.(height)	Genus	Species
Ravna	13 (top)	*Plagiostoma*	*punctata*
Ravna	13 (top)	*Plagiostoma*	*punctata*
Ravna	13 (top)	*Plagiostoma*	*punctata*
Ravna	13 (top)	*Plagiostoma*	*punctata*
Ravna	13 (top)	*Chlamys*	*textoria*
Ravna	13 (top)	*Chlamys*	*textoria*
Ravna	13 (top)	*Chlamys*	*textoria*
Ravna	13 (top)	*Chlamys*	*textoria*
Ravna	13 (top)	*Chlamys*	*textoria*
Ravna	13 (top)	*Chlamys*	*textoria*
Ravna	13 (top)	*Chlamys*	*textoria*
Ravna	13 (top)	*Chlamys*	*textoria*
Ravna	13 (top)	*Gryphaea*	*gigantea*
Ravna	13 (top)	*Chlamys*	*textoria*
Ravna	13 (top)	*Pleuromya*	*costata*
Ravna	13 (top)	*Pseudopecten*	*equivalvis*
Dragovishtitsa	1d	*?Camptonectes*	sp. indet
Dragovishtitsa	1d	*?Camptonectes*	sp. indet
Dragovishtitsa	1d	*Entolium*	*lunare*
Dragovishtitsa	2a	*Pholadomya*	sp. indet
Dragovishtitsa	2a	*Entolium*	*lunare*
Dragovishtitsa	2a	*Pseudopecten*	*equivalvis*
Dragovishtitsa	2a	*Pseudopecten*	*equivalvis*
Dragovishtitsa	3 (↓70cm)	Oyster	gen. et sp. indet
Dragovishtitsa	3 (↓70cm)	*Chlamys*	sp. indet
Dragovishtitsa	3 (↓70cm)	*Chlamys*	sp. indet
Dragovishtitsa	3 (↓70cm)	*Chlamys*	sp. indet

Section	Bed no.(height)	Genus	Species
Dragovishtitsa	3 (↓70cm)	*Psedopecten*	*equivalvis*
Dragovishtitsa	3 (↓70cm)	*Entolium*	*lunare*
Dragovishtitsa	3 (↓70cm)	*Entolium*	*lunare*
Dragovishtitsa	3 (↓70cm)	*Oxytoma*	sp. indet
Dragovishtitsa	3(top)	*Chlamys*	sp. indet
Dragovishtitsa	3(top)	*Chlamys*	sp. indet
Dragovishtitsa	3(top)	*Entolium*	sp. indet
Dragovishtitsa	3(top)	*Entolium*	sp. indet
Dragovishtitsa	3(top)	*Entolium*	sp. indet
Dragovishtitsa	3(top)	*Entolium*	*lunare*
Dragovishtitsa	3(top)	*Entolium*	*lunare*
Dragovishtitsa	3(top)	*Pinna*	cf. *folium*
Dragovishtitsa	4	Pecten	gen. et sp. indet
Dragovishtitsa	4	Pecten	gen. et sp. indet
Dragovishtitsa	4	Oyster	gen. et sp. indet
Dragovishtitsa	4 (↓165cm)	*Plagiostoma*	cf. *punctata*
Dragovishtitsa	4 (↓165cm)	*Chlamys*	*textoria*
Dragovishtitsa	4 (↓165cm)	*Pseudopecten*	*equivalvis*
Dragovishtitsa	5	*Entolium*	*lunare*
Dragovishtitsa	14a.1	*?Camptonectes*	sp. indet
Dragovishtitsa	14a.1	*Gresslya*	sp. A
Dragovishtitsa	14b.1	*Chlamys*	*textoria*
Dragovishtitsa	14b.1	*Coelastarte*	sp. indet
Dragovishtitsa	14b.1	*Coelastarte*	sp. indet
Dragovishtitsa	14b.1	*Coelastarte*	sp. indet
Dragovishtitsa	14b.1	Anomaldesmatin	gen. et sp. indet
Dragovishtitsa	14b.1	Oyster	gen. et sp. indet

Section	Bed no.(height)	Genus	Species
Dragovishtitsa	14b.1	Oyster	gen. et sp. indet
Dragovishtitsa	14b.1	Oyster	gen. et sp. indet
Dragovishtitsa	14b.1	*Coelastarte*	sp. indet
Dragovishtitsa	14b.1	*Coelastarte*	sp. indet
Dragovishtitsa	14b.1	*Coelastarte*	sp. indet
Dragovishtitsa	14b.1	*Gresslya*	sp. A
Dragovishtitsa	14b.1	*Chlamys*	sp. indet
Dragovishtitsa	14b.1	*Grammatodon*	cf. *insons*
Dragovishtitsa	14c.1	*Chlamys*	sp. indet
Dragovishtitsa	14c.1	*Coelastarte*	sp. indet
Dragovishtitsa	14c.1	*Chlamys*	*textoria*
Dragovishtitsa	14c.1	*Chlamys*	sp. indet
Dragovishtitsa	14c.1	*Coelastarte*	sp. indet
Dragovishtitsa	14c.1	*Coelastarte*	sp. indet
Dragovishtitsa	14c.1	*?Camptonectes*	sp. indet
Dragovishtitsa	14c.1	*Grammatodon*	cf. *insons*
Dragovishtitsa	14a	*Chlayms*	*textoria*
Dragovishtitsa	14a	*Chlayms*	*textoria*
Dragovishtitsa	14a	*Chlayms*	*textoria*
Dragovishtitsa	14a	*Chlayms*	*textoria*
Dragovishtitsa	14a	*Chlayms*	*textoria*
Dragovishtitsa	14a	*Chlayms*	sp. indet
Dragovishtitsa	14a	*Chlayms*	*textoria*
Dragovishtitsa	14a	*Chlayms*	*textoria*
Dragovishtitsa	14a	*Chlayms*	*textoria*
Dragovishtitsa	14a	*Chlayms*	*textoria*
Dragovishtitsa	14a	*Chlayms*	*textoria*

Section	Bed no.(height)	Genus	Species
Dragovishtitsa	14a	*Chlayms*	*textoria*
Dragovishtitsa	14a	*Chlayms*	*textoria*
Dragovishtitsa	14a	*Chlayms*	*textoria*
Dragovishtitsa	14a	*Chlayms*	*textoria*
Dragovishtitsa	14a	*Chlayms*	*textoria*
Dragovishtitsa	14a	*Coelastarte*	sp. indet
Dragovishtitsa	14a	*Chlayms*	*textoria*
Dragovishtitsa	14a	*Chlayms*	*textoria*
Dragovishtitsa	14a	Anomaldesmatin	gen. et sp. indet
Dragovishtitsa	14a	Oyster	gen. et sp. indet
Dragovishtitsa	14a	*Plagiostoma*	cf. *punctata*
Dragovishtitsa	14a	*Plagiostoma*	cf. *punctata*
Dragovishtitsa	14a	*Eopecten*	sp. indet
Dragovishtitsa	14a	*Pholadomya*	cf. *fidicula*
Dragovishtitsa	14a	*Entolium*	cf. *corneolum*
Dragovishtitsa	14b	*Pinna*	sp. indet
Dragovishtitsa	14b	*Weyla*	cf. *alata*
Dragovishtitsa	14b	*Coelastarte*	sp. indet
Dragovishtitsa	14b	*Coelastarte*	sp. indet
Dragovishtitsa	14b	*Propeamusium*	*pumilum*
Dragovishtitsa	14b	*Weyla*	cf. *alata*
Dragovishtitsa	14b	*Weyla*	cf. *alata*
Dragovishtitsa	14b	*Weyla*	cf. *alata*
Dragovishtitsa	14b	*Weyla*	cf. *alata*
Dragovishtitsa	14b	*Weyla*	cf. *alata*
Dragovishtitsa	14b	*Weyla*	cf. *alata*
Dragovishtitsa	14c	*Weyla*	cf. *alata*

Section	Bed no.(height)	Genus	Species
Dragovishtitsa	14c	*Weyla*	cf. *alata*
Dragovishtitsa	14c	*Chlamys*	*textoria*
Dragovishtitsa	14c	*Chlamys*	*textoria*
Dragovishtitsa	14c	*Chlamys*	*textoria*
Dragovishtitsa	14c	*Chlamys*	*textoria*
Dragovishtitsa	14c	*Chlamys*	*textoria*
Dragovishtitsa	14c	*Chlamys*	*textoria*
Dragovishtitsa	14c	*Chlamys*	*textoria*